Metal-organic coordination polymers based on mixed ligands

Inaugural-Dissertation

zur Erlangung des Doktorgrades
der Mathematisch-Naturwissenschaftlichen Fakultät
der Heinrich-Heine-Universität Düsseldorf

vorgelegt von

Anas Tahli
aus Syrien, Homs

Düsseldorf, March 2015

Aus dem Institut für Anorganische Chemie und Strukturchemie

der Heinrich-Heine-Universität Düsseldorf

Gedruckt mit der Genehmigung der Mathematisch-Naturwissenschaftlichen Fakultät der Heinrich-Heine-Universität Düsseldorf

Referent: Prof. Dr. Ch. Janiak

Korreferent: Prof. Dr. Ch. Ganter

Tag der mündlichen Prüfung: 28.05.2014

Die vorliegende Arbeit wurde in der Zeit von November 2010 bis März 2015 am Institut für Anorganische Chemie und Strukturchemie, Abteilung für Bioanorganische Chemie, MOFs, Nanos und Katalyse, der Heinrich-Heine-Universität Düsseldorf im Arbeitskreis von **Prof. Dr. Christoph Janiak** durchgeführt.

Publikationen:

A. Tahli, J. K. Maclaren, I. Boldog, C. Janiak, *Inorganica Chimica Acta*, 2011, **374**, 506-513.

Vortrag:

A. Tahli, L. Xing, C. Heering, G. Makhloufi, I. Boldog, H. Than, A. Khutia, C. Janiak, „*MOFs mit Azol- und Azolat-Carboxylat-Liganden*", **2012**, 8. Koordinationschemie-Treffen, Univ. Dortmund, Deutschland.

Teilnahme an Tagungen:

02/2012	8. Koordinationschemie-Treffen	Univ. Dortmund, Deutschland
10/2012	Japanese-German Symposium on Coordination Programming	Univ. Münster, Deutschland

Teilnahme an Seminar:

04/2014	„Gute Wissenschaftliche Praxis für Promovierende" „Good Scientific Practice for Doctoral Researchers"	Univ. Düsseldorf, Deutschland

Selbstständigkeitserklärung

Hiermit versichere ich an Eides statt, dass die vorgelegte Dissertation (Metal-organic coordination polymers based on mixed ligands) von mir selbstständig verfasst und unter ausschließlicher Verwendung der angegebenen Literatur und Hilfsmittel gemäß der (Gute wissenschaftliche Praxis für Promovierende) an der Heinrich-Heine-Universität Düsseldorf erstellt wurde.

Bisher habe ich keine erfolglosen Promotionsversuche unternommen und diese Dissertation nicht an einer anderen Fakultät vorgelegt.

Düsseldorf, den 30.03.2015

Anas Tahli

For my family, my country and friends

Table of contents

1 Acknowledgements

I am extremely grateful to Prof. Dr. Christoph Janiak, my thesis supervisor, for suggesting the research problem and for his valuable guidance, support and encouragement, the chance he gave me to work in many disciplines in an excellent working environment and to develop independent thinking, which lead to the successful completion of this work.

I would like to thank Prof. Dr. Christian Ganter for being my co-referee and co-examiner.

I sincerely thank the Al-Furat University and Ministry of Higher Education in Syria for the financial support (scholarship) during my study in Germany (Language, diploma recognition-Master equivalent statements and PhD).

I am extremely thankful to Dr. Reda El Shaarawy, Abdul Hadi Al-Dmairi, Mhyeddeen Halawa, Ahmad Sarakbi, Dr. Ishtvan Boldog and Hamza Al-Qasmi for their help, support inspiring discussions, their ideas and encouragement.

For the measurement of NMR spectroscopy I am grateful to Peter Behm, Roland Thoma and Beate Rau.

For the measurement of mass spectroscopy I am grateful to Ralf Bürgel und Dr. Peter Tommes

For the measurement of FT-IR spectroscopy I am grateful to Birgit Tommes.

I am extremely thankful Tian Zhao for his help with gas adsorption measurement, his friendship and his kindness.

I would like to thank Dr. Harold Tanh Jeazet for his help with the thermogravimetric analysis and powder X-ray diffraction measurements.

I wish to thank Christian Heering, Anna Christin Kautz and Vera Vasylyeva for single crystal X-ray measurements.

For his support and teaching of single-crystal X-ray analysis, I am grateful to Dr. Guido J. Reiß, Anne-Christine Chamayou, Sladjana B. Novaković and Christian Heering, who helped me to solve and refine problematic structures after X-ray single crystal measurements.

I deeply express my sincere thanks to Dr. Reda El Shaarawy and Abdul Hadi Al-Dmairi for their kind support at the initial stage of my research career and for the proof reading of my thesis.

I would like to thank Axel Mund, Dietmar Frunzke and Annette Ricken for technical assistance, kindness and general help.

I would like also to express my grateful thanks to my students who worked with me in my laboratory, Ümit Köc and Leif Römer. Thanks for their contribution to the experiments of this work.

I would like to thank all the students I had the pleasure and the honor to supervise in the practice lab (Praktikum für Anorganische, Analytische und Allgemeine Chemie) during the four years, when I was an assistant in this practice lab. Of course it is not possible to enumerate all the names, but I will keep a very good memory of this practical teaching lab. The first bachelor students group of the summer semester 2011 is particularly acknowledged.

My thanks go to all my colleagues for their help and friendship but also for the good laughing moments in the laboratory and the general good work atmosphere in our group: Dr. Christian Vollmer, Dr. Dorothea Marquardt, Dr. Anupam Khutia, Lei Xing, Martin Wickenheiser, Roland Thoma, Kai Schütte, Christina Rutz, Hajo Meyer, Raquel Marcos Esteban, Gamall Makhloufi, Anna Christin Kautz, Annika Herbst, Sebastian Glomb, Dr. Ines Dumsch, Subarna Dey, Janina Dechnik, Laure Cuignet, Irina Gruber, Maximilian Klopotowski, Sandra Nießing, Susann Wegner and Vasile Lozan.

A lot of special thanks go to: Tian Zhao, Dr. Reda El Shaarawy, Dr. Harold Tanh Jeazet, Francis Bijou and Christian Heering for their kindness, help and friendship during these long writing days and also the last past years.

I want to thank the whole work groups of Prof. Ganter: Abdelaziz Makhloufi, Markus Jonek, Michaela Wahl, Sebastian Appel, Hannes Buhl, Kathrin Verlinden, Björn Hildebrandt, Julia Faßbender and Markus Braun.

I express my sincere thanks to all my friends for their love, care and support at different stages of my life.

I owe a lot to my parents, my sisters and brothers, my uncles and cousin with his family members, who encouraged and helped me at every stage of my personal and academic life, and longed to see this achievement come true.

2 List of abbreviations and units

Abbrevation	Name
tr	*1*,*2*,*4*-triazole
btre	1,2-bis(1,2,4-triazol-4-yl) ethane
btrip	1,2-bis(1,2,4-triazol-4-yl)propane
btrb	1,4-bis(1,2,4-triazol-4-yl) butane
3pytr	3-(1,2,4-triazol-4-yl) pyridine, 4-(pyrid-3-yl)-1,2,4-triazole
4pytr	4-(1,2,4-triazol-4-yl) pyridine, 4-(pyrid-4-yl)-1,2,4-triazole
btr	4,4`-bis(1,2,4-triazol-4-yl)
dm-H_2aip	4,6-dimethyl-5-amino isophthalic acid
atr	*4*-amino-1,2,4-triazole
5H_2iptr	5-(1,2,4-triazol-4-yl)isophthalic acid
H_2aip	5-amino isophthalic acid
abs.	absolute
OAc^-	acetate-ion
CH_3CN	acetonitril
Å	Angstrom
ATR	attenuated total reflection
H_3btt	benzene-1,3,5-tri(1H-tetrazol-5-yl)
H_3btc	benzene-1,3,5-tricarboxylic acid, trimesic acid
H_2ipdt	benzene-1,3-di(1H-tetrazol-5-yl)
H_2ip	benzene-1,3-dicarboxylic acid, isophthalic acid
H_2bdt	benzene-1,4-di(1H-tetrazol-5-yl)
H_2bdc	benzene-1,4-dicarboxylic acid, terephthalic acid
br	broad signal (NMR, IR band)
calc.	calculated
δ	chemical shift in (ppm)
ca.	circa
d	day(s), doublet (NMR), pore diameter
DMSO-d_6	deuterated dimethyl sulfoxide
D_2O	deuterium oxide
DCM	dicholoromethane, methylene dichloride
DMSO	dimethyl sulfoxide
DUT	dresden University of Technology
F(000)	effective number of electrons in the unit cell
EI	electron impact
EA	elemental analysis
eq	equivalent

Abbrevation	Name
EtOH	ethanol
Et	ethyl
HKUST	Hongkong University of Science and Technology
h	hour(s)
IR	infrared spectroscopy
IRMOF	isoreticular metal-organic framework
K	Kelvin
MS	mass spectrometry
MIL	Matériaux de l'Institut Lavoisier
MHz	megahertz
m.p.	melting point
MOF	Metal-Organic Framework
MFU	Metal-Organic Framework Ulm
MeOH	methanol
Me	methyl
min	minute(s)
m	multiplet (NMR), medium (IR band), meta
DEF	*N,N`*-diethylformamid
DMA	*N,N`*-dimethylacetamide
DMF	*N,N`*-dimethylmethanamide, *N,N`*-dimethylformamide
NMR	nuclear magnetic resonance spectroscopy
Z	number of formula units in the unit cell
obs.	observed
ppm	part per million
PCP	Porous coordination polymer
PXRD	powder X-ray diffraction
p.a.	pro analysis
*p*TosOH	*p*-Toluensulfonic acid
q	quartet (NMR)
rac	racemic mixture, racemate
m/z	ratio of mass to charge
SBU	secondary building unit
sh	shoulder (IR band)
SCXRD	single crystal X-ray diffraction
s	singlet (NMR), strong (IR band)
Tab.	table
T	temperature
TGA	thermo gravimetric analysis
Et_3N	triethylamine
t	triplet (NMR), time

Abbrevation	Name
α, β, γ	unit cell angles
a, b, c	unit cell axes
UiO	universitetet i Oslo
vs	very strong (IR band)
vw	very weak (IR band)
w	weak (IR band)
Hts	Hydrothermal synthesis
Sts	Solvothermal synthesis

3 Zusammenfassung

Es wurden neue Syntheserouten zu gemischt-Donor Azol-Carboxylat-Liganden mit der Einheit 4-(3,5-Dicarboxyl-1,2,4-triazol-4-yl)aromat durchgeführt, um damit eine neue Generation von Koordinationspolymeren zu erhalten.

Die 1H-Tetrazol-enthaltenen Liganden Benzol-1,4-di(1H-tetrazol-5-yl) (H_2bdt) und Benzol-1,3-di(1H-tetrazol-5-yl) (H_2ipdt), die 1,2,4-Triazol-enthaltenen Liganden 4,4`-bis(1,2,4-triazol) (btr), 1,2-Bis(1,2,4-triazol-4-yl)propan (btrip), 3-(1,2,4-Triazol-4-yl)pyridin (3pytr), 4-(1,2,4-triazol-4-yl)pyridin (4pytr) und der gemischt-Donor Ligand 5-(1,2,4-triazol-4-yl)isophthalsäure ($5H_2$iptr) wurden synthetisiert und verwendet, um neue Koordinationspolymere mit gemischten Carboxylat- und Tetrazolat-Liganden oder Carboxylat- und Triazol-Liganden zu erhalten.

Die Verbindungen 2D-$[Cu_3(\mu_6\text{-btc})(\mu\text{-btc})(\mu\text{-atr})(H_2O)_5]_n$ **24** und 1D-$\{[Cd_2(\mu_2\text{-btc})_2(atr)_2(H_2O)_4][Cd(H_2O)_6]\cdot 2H_2O\}_n$ **25** wurden unter Hydrothermalsynthese bei 125 °C aus $CuCl_2\cdot 2H_2O$ (für **24**) und $Cd(OAc)_2\cdot 2H_2O$ (für **25**) mit 4,4`-Bis(1,2,4-triazol-4-yl) (btr) und Benzol-1,3,5-tricarbonsäure ($H_3$btc) in einem 2:3:1 molaren Verhältnis erhalten. Eine $Et_3N/H_2O$ Lösung wurde als Base verwendet, um $H_3$btc zu deprotonieren. Der 4,4`-bis-(1,2,4-triazol-4-yl) (btr) Ligand wurde nicht mehr vollständig, sondern als 4-Amino-1,2,4-triazol (atr) Zersetzungsprodukt in den Strukturen gefunden. Wahrscheinlich wurde ein Triazolring bei 125 °C thermisch unter Bildung dieses atr-Verbindung zersetzt.

Die Verbindung 2D-$[Cd(\mu_3\text{-Hbtc})(H_2O)_2]_n$ **26** wurde unter identischer Hydrothermalreaktion wie für Verbindungen **24** und **25** erhalten, aber bei höherer Temperatur von 140 °C. Unter dieser Bedingung wurde der btr Ligand vollständig thermisch zersetzt und nicht mehr in der Struktur gefunden.

Die Verbindung 1D-$[Zn_3(\mu_3\text{-btc})(\mu_2\text{-btc})(H_2O)_{12}]_n$ (aus verschiedenen Zinksalze als **35**, **36**, **37** und **38**) wurde nach 30 min bei Raumtemperatur über die Reaktion von $Zn(NO_3)_2\cdot 4H_2O$, $Zn(ClO_4)_2\cdot 6H_2O$, $ZnCl_2$ und $ZnBr_2$ mit btr und H_3btc in Lösung erhalten. Eine Et_3N/H_2O Lösung wurde als Base verwendet, um H_3btc zu deprotonieren. 1D-$[Co_3(\mu_3\text{-btc})(\mu_2\text{-btc})(H_2O)_{12}]_n$ **39** wurden unter Hydrothermalsynthese bei 150 °C aus $Co(NO_3)_2\cdot 6H_2O$ mit Benzol-1,4-bis(1H-tetrazol-5-yl) (H_2bdt) und H_3btc erhalten. Eine NH_3/H_2O Lösung wurde als Base verwendet, um Tetrazol- und Carboxyl-Liganden (H_2bdt, H_3btc) zu deprotonieren.

Die Verbindungen 3D-$\{[Cu_4(\mu\text{-OH})_2(\mu\text{-bdc})_2(\mu_4\text{-}rac\text{-btrip})_3](NO_3)_2(H_2O)_{10}\}_n$ **16**, 3D-$\{[Cu_4(\mu_4\text{-Cl})(\mu_4\text{-}rac\text{-btrip})_4(H_2O)_4](BF_4/ClO_4/OH)_7\cdot xH_2O\}_n$ **17** und 3D-$\{[Cu(\mu_4\text{-}rac\text{-btrip})(SO_4)]\cdot\sim H_2O\}_n$ **18**

wurden unter Hydrothermalsynthese bei 125 °C aus $Cu(NO_3)_2 \cdot 2.5H_2O$ (für **16**), $Cu(BF_4)_2 \cdot 6H_2O$ (für **17**) oder $CuSO_4$ (für **18**) mit racemischem 1,2-bis(1,2,4-triazol-4-yl)propan (*rac*-btrip) und Benzol-1,4-dicarbonsäure (H_2bdc) erhalten. Eine NH_3/H_2O Lösung wurde als Base verwendet, um H_2bdc zu deprotonieren.

Die Verbindung 3D-$\{[Cu(CH_3CN)_4][Cu_3(\mu_6\text{-btc})_2]_2(NO_3/O_2CCH_3)\cdot(H_2O,\ CH_3CN)_x\}_n$ wurde unter Hydrothermalsynthese bei 125 °C aus $Cu(NO_3)_2 \cdot 2.5H_2O$ (für **33**) oder $Cu(OAc)_2 \cdot H_2O$ (für **34**) mit *rac*-btrip und H_3btc erhalten. Eine Et_3N/H_2O Lösung wurde als Base verwendet, um H_3btc zu deprotonieren.

Die Verbindungen 2D-$\{[Cu_2(\mu\text{-}Br)_2(\mu_4\text{-}rac\text{-btrip})]\cdot H_2O/MeOH\}_n$ **27**, 3D-$\{[Cu_2(\mu_4\text{-}rac\text{-btrip})_2]SO_4 \cdot xH_2O\}_n$ **28** and 3D-$\{[Cu(\mu_4\text{-}rac\text{-btrip})]CH_3COO \cdot xH_2O\}_n$ **29** wurden unter Solvothermalsynthese bei 125 °C aus $CuBr_2$ (für **27**), $CuSO_4 \cdot 5H_2O$ (für **28**) oder $Cu(OAc)_2 \cdot H_2O$ (für **29**) mit *rac*-btrip und H_3btc erhalten. Eine Et_3N/H_2O Lösung wurde als Base verwendet, um H_3btc zu deprotonieren. In zweiten Schritt der Synthese, wurde DMSO jeder Probe zugegeben. Die Proben wurden wieder auf 140 °C erwärmt. Bei der Verwendung von anderen Metallsalze wie $Cu(NO_3)_2 \cdot 2.5H_2O$ (für **30**), $Cu(BF_4)_2 \cdot 6H_2O$ (für **31**) und $CuCl_2$ (für **32**) wurden weitere Kristalle unter identischen Solvothermalreaktionen erhalten, aber diese Produkte wurden nicht weiter über Einkristall-Röntgenstrukturanalyse untersucht, weil in den vorherigen Produkten **27-29** nur der *rac*-btrip Ligand mit den Cu-Atomen koordiniert.

Die homochiralen Kristalle mit enantiomorphen Strukturen 2D-$\{[Zn(\mu\text{-Hbtc})(\mu\text{-}R\text{-btrip})]\cdot H_2O\}_n$ **19** und 2D-$\{[Zn(\mu\text{-Hbtc})(\mu\text{-}S\text{-btrip})]\cdot H_2O\}_n$ **20** wurden durch spontane Racematspaltung als racemisches Konglomerat unter Hydro- oder Solvothermal- (H_2O/CH_3OH) Reaktion aus $Zn(NO_3)_2 \cdot 6H_2O$ (für **19**) oder $ZnBr_2$ (für **20**) mit *rac*-btrip und H_3btc bei 125°C oder 140°C erhalten. Eine Et_3N/H_2O Lösung wurde als Base verwendet, um H_3btc zu deprotonieren. Identische Verbindungen wurden unter gleicher Hydrothermalsreaktion erhalten, wenn andere Zinksalze verwendet wurden, wie $ZnCl_2$ (für **21**), $Zn(ClO_4)_2 \cdot 6H_2O$ (für **22**) und $Zn(OAc)_2 \cdot 2H_2O$ (für **23**).

Es wurde bemerkt, dass die dritte Carboxylgruppe im $Hbtc^{2-}$ Liganden in den Verbindungen **19** und **20** protoniert bleibt, und nicht an die Zinkatome koordiniert. Deswegen wurden andere aromatische Dicarboxyl-Liganden verwendet, wie Isophthalsäure (H_2ip), 5-Amino-isophthalsäure (H_2aip) und 4,6-Dimethyl-5-amino-isophthalsäure (dm-H_2aip), um ähnliche (chirale) Strukturen wie **19/20** unter gleichen Reaktionsbedingungen zu erhalten. Aber die IR- und ^{1}H NMR Spectren der erhaltenen Kristallen zeigten, dass entweder nur der *rac*-btrip oder nur der Carboxylligand mit den Zinkatomen koordiniert, wie in Verbindung 2D-$[Zn(\mu_3\text{-aip})(H_2O)]_n$ **40**.

4 Abstract

Synthesis routes for the new combined multi-dentate azole-carboxylate 4-(3,5-dicarboxyl-1,2,4-triazol-4-yl)aromatic ligand (Scheme 4.2.3.1) have been developed to obtain a new generation of coordination polymers.

The 1H-tetrazole derivative ligands benzene-1,4-di(1H-tetrazol-5-yl) H_2bdt and benzene-1,3-di(1H-tetrazol-5-yl) H_2ipdt, the 1,2,4-triazole derivative ligands 4,4`-bis(1,2,4-triazole) (btr), 1,2-bis(1,2,4-triazol-4-yl)propane (btrip), 3-(1,2,4-triazol-4-yl)pyridine (3pytr), 4-(1,2,4-triazol-4-yl)pyridine (4pytr) and the combined multi-dentate ligand 5-(1,2,4-triazol-4-yl)isophthalic acid ($5H_2$iptr) have been synthesized and used to obtain new coordination polymers with mixed-ligand systems of carboxylate and tetrazolate ligands or carboxylate and triazol ligands.

Compounds 2D-$[Cu_3(\mu_6\text{-btc})(\mu\text{-btc})(\mu\text{-atr})(H_2O)_5]_n$ **24** or 1D-$\{[Cd_2(\mu_2\text{-btc})_2(atr)_2(H_2O)_4][Cd(H_2O)_6]\cdot 2H_2O\}_n$ **25** are obtained from the hydrothermal reaction at 125 °C of $CuCl_2\cdot 2H_2O$ or $Cd(OAc)_2\cdot 2H_2O$, 4,4`-bis(1,2,4-triazol-4-yl) (btr) and benzene-1,3,5-tricarboxylic acid ($H_3$btc) in approximately 2:3:1 molar ratio with $Et_3N/H_2O$ solution used as base to deprotonate the carboxylate groups of $H_3$btc. The 4,4`-bis-(1,2,4-triazol-4-yl) (btr) ligand is not completely incorporated into the structure at 125°C probably due to the thermal decomposition of one triazole ring to form 4-amino-1,2,4-triazole (atr) ligand.

The compound 2D-$[Cd(\mu_3\text{-Hbtc})(H_2O)_2]_n$ **26** is obtained from the identical hydrothermal reaction for compounds **24** and **25** but at higher temperature 140 °C. Under these conditions the btr ligand is completely thermally decomposed and not incorporated into the product.

Compoound 1D-$[Zn_3(\mu_3\text{-btc})(\mu_2\text{-btc})(H_2O)_{12}]_n$ (from different starting materials as **35**, **36**, **37** and **38**) is obtained after 30 min at room temperature *via* the reaction of a solution of $Zn(NO_3)_2\cdot 4H_2O$, $Zn(ClO_4)_2\cdot 6H_2O$, $ZnCl_2$ or $ZnBr_2$, 4,4`-bis(1,2,4-triazol-4-yl) (btr) and benzene-1,3,5-tricarboxylic acid (H_3btc) where triethylamine (Et_3N) is used as base to deprotonate the carboxyl groups of (H_3btc). 1D-$[Co_3(\mu_3\text{-btc})(\mu_2\text{-btc})(H_2O)_{12}]_n$ **39** is obtained from the hydrothermal reaction of $Co(NO_3)_2\cdot 6H_2O$, 1,4-bis(1H-tetrazol-5-yl)benzene (H_2bdt) and benzene-1,3,5-tricarboxylic acid (H_3btc) at 150°C with ammonia solution (NH_3/H_2O) as base to deprotonate the tetrazole and carboxyl groups of both ligands (H_2bdt, H_3btc).

Compounds 3D-$\{[Cu_4(\mu\text{-OH})_2(\mu\text{-bdc})_2(\mu_4\text{-}rac\text{-btrip})_3](NO_3)_2\ (H_2O)_{10}\}_n$ **16**, 3D-$\{[Cu_4(\mu_4\text{-Cl})(\mu_4\text{-}rac\text{-btrip})_4(H_2O)_4](BF_4/ClO_4/OH)_7\cdot xH_2O\}_n$ **17** and 3D-$\{[Cu(\mu_4\text{-}rac\text{-btrip})(SO_4)]\cdot\sim H_2O\}_n$ **18** are obtained from the hydrothermal reaction of an aqueous solution of $Cu(NO_3)_2\cdot 2.5H_2O$ (for **16**), $Cu(BF_4)_2\cdot 6H_2O$ (for **17**) or $CuSO_4$ (for **18**), an aqueous solution racemic 1,2-bis(1,2,4-triazol-

4-yl)propane (*rac*-btrip) and benzene-1,4-dicarboxylic acid (H_2bdc) at 125°C with NH_3 solution used as base to deprotonate the H_2bdc ligand.

3D-$\{[Cu(CH_3CN)_4][Cu_3(\mu_6\text{-btc})_2]_2(NO_3/O_2CCH_3)\cdot(H_2O,\ CH_3CN)_x\}_n$ is obtained from the hydrothermal reaction of an aqueous solution of $Cu(NO_3)_2\cdot 2.5H_2O$ (for **33**) or $Cu(OAc)_2\cdot H_2O$ (for **34**), *rac*-btrip ligand and H_3btc ligand at 125°C with Et_3N solution used as base to deprotonate the H_3btc ligand.

Compounds 2D-$\{[Cu_2(\mu\text{-Br})_2(\mu_4\text{-}rac\text{-btrip})]\cdot H_2O/MeOH\}_n$ **27**, 3D-$\{[Cu_2(\mu_4\text{-}rac\text{-btrip})_2]SO_4\cdot xH_2O\}_n$ **28** and 3D-$\{[Cu(\mu_4\text{-}rac\text{-btrip})]\ CH_3COO\cdot xH_2O\}_n$ **29** are obtained from the solvothermal reaction of $CuBr_2$ (for **27**), $CuSO_4\cdot 5H_2O$ (for **28**) or $Cu(OAc)_2\cdot H_2O$ (for **29**), the *rac*-btrip and H_3btc ligand at 125°C with Et_3N used as base to deprotonate the H_3btc ligand. In a second step of the synthesis, DMSO was added to each sample. The samples were heated again at 140°C. Crystalline products were also obtained through the same solvothermal reaction using other copper salts such as $Cu(NO_3)_2\cdot 2.5H_2O$ (for **30**), $Cu(BF_4)_2\cdot 6H_2O$ (for **31**) and $CuCl_2$ (for **32**). Yet these products were not investigated by single crystal X-ray diffraction because the previous products **27-29** showed that only the *rac*-btrip ligand was coordinated with copper atoms.

The homochiral crystals with the enantiomorphous structures 2D-$\{[Zn(\mu\text{-Hbtc})(\mu\text{-}R\text{-btrip})]\cdot H_2O\}_n$ **19** and 2D-$\{[Zn(\mu\text{-Hbtc})(\mu\text{-}S\text{-btrip})]\cdot H_2O\}_n$ **20** are obtained by spontaneous resolution as a racemic conglomerate from the hydro- or solvothermal (H_2O/CH_3OH) reaction of $Zn(NO_3)_2\cdot 6H_2O$ (for **19**) or $ZnBr_2$ (for **20**), the *rac*-btrip and H_3btc ligand at 125°C or 140°C with Et_3N used as base to deprotonate the H_3btc ligand. The same products were also obtained through the hydrothermal reaction using other zinc salts such as $ZnCl_2$ (for **21**), $Zn(ClO_4)_2\cdot 6H_2O$ (for **22**) and $Zn(OAc)_2\cdot 2H_2O$ (for **23**).

It was noted that in the structure of compound **19** and **20** the third carboxyl group of the $Hbtc^{2-}$ ligand stayed protonated and was not coordinated to a zinc atom. Therefore, other aromatic dicarboxylic acids like isophthalic acid (H_2ip), 5-amino isophthalic acid (H_2aip) and 4,6-dimethyl-5-aminoisophthalic acid (dm-H_2aip) were used to try to obtain the same structure of **19/20** under the identical reaction conditions. But IR- and ^{1}H NMR spectra from the obtained crystals showed, that only either the *rac*-btrip or the carboxylic ligand was coordinated with zinc atoms as shown for compound 2D-$[Zn(\mu_3\text{-aip})(H_2O)]_n$ **40**.

5 Introduction

5.1 Definition of porous coordination polymers

Metal-organic coordination polymers or porous coordination polymers (PCPs), also known as metal-organic frameworks (MOFs) [1] are infinitely extended 1D, 2D or 3D-metal-ligand networks with metal atoms or metal clusters as nodes, which are connected with polydentate bridging organic ligands as linkers *via* coordination bonds, and often contain pores with large BET surface areas independent of pore size, channel size, and topologies of 3D-networks [2].

5.2 Prototypical bridging ligands

The used ligands in the construction of coordination polymers have to bridge between metal ions/clusters. This requires usually polydentate ligands with two or more donor atoms/groups. Anions or negatively charged bridging ligands such as carboxylates or tetrazolate are necessary for the charge balance of the metal cations, which typically function as nodes in the framework. Such PCPs mostly contain either neutral or cationic frameworks. Carboxylate or tetrazolate ligands with suitable spacers, such as benzene or hydrogen-carbon chains, are frequent choices for the synthesis of metal–organic networks. Benzene-1,4-dicarboxylic acid H_2bdc (terephthalate, linear ligand) [3], benzene-1,3-dicarboxylic acid H_2ip (isophthalate, V-angle ligand) [4] and benzene-1,3,5-tricarboxylic acid H_3btc (trimesic acid, trigonal ligand) (Figure 4.2.1) [5] have been extensively used as bridging ligands in the synthesis of 1D-, 2D- and 3D-metal organic coordination polymers. Tetrazolate ligands, such as benzene-1,4-di(1H-tetrazol-5-yl) H_2bdt, benzene-1,3-di(1H-tetrazol-5-yl) H_2ipdt and benzene-1,3,5-tri(1H-tetrazol-5-yl) H_3btt, have also been used as bridging ligands in the synthesis of 1D-, 2D- and 3D-PCPs. The coordination possibilities of the tetrazolate ring with metal ions will be shown in Scheme 4.2.2.2 & 4.2.2.3. Rigid bridging linkers, as aromatic carboxylate or tetrazolate ligands, are important for thermally stable and robust porous frameworks that retain the porous structure after removing the guest molecules from their pores. In the case of neutral bridging ligands, anions from the original metal salt are coordinated/bridged with metal ions for charge balance, examples being Cl^-, NO_3^-, SO_4^{2-}, BF_4^-, etc. Generally, N- and O-donor atoms of bridging ligands feature often in the

construction of coordination polymers. Common ligands used in the fabrication of metal coordination polymers are shown in Figure 4.2.1.

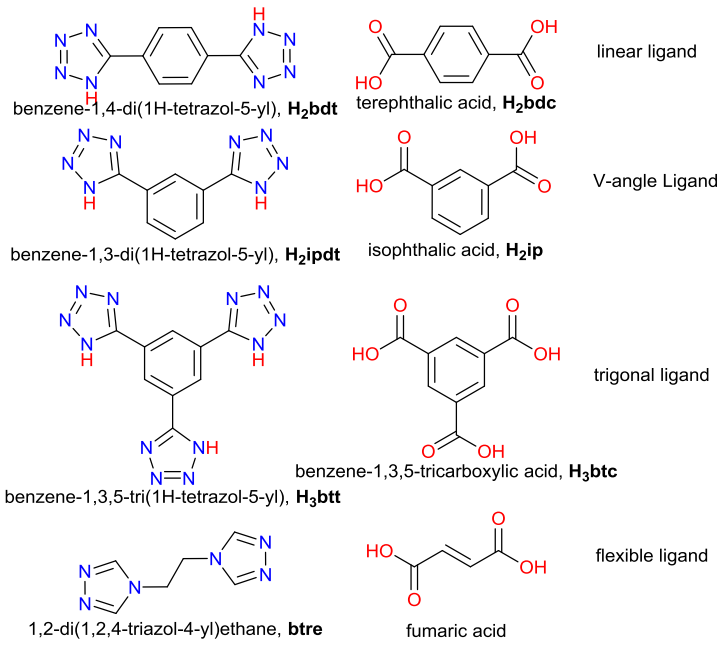

Figure 4.2.1: Examples of linear, V-angle, trigonal and flexible bridging ligands of used carboxylate, tetrazolate and traizole ligands for PCPs.

5.2.1 Introduction to 1,2,4-triazole derivative ligands

Synthesis of new multi-dentate organic ligands which could be utilized for the building of porous coordination polymers is not easy. They have to be stable in different reaction conditions of PCP synthesis and to have the ability to bridge at least between two metal atoms or secondary building units (SBUs). The structure of the organic ligands, secondary building units (SBUs), geometry of metal atoms, π-π interactions and hydrogen bonds have great influence on the topology of the coordination polymers. The topology of a series of porous supramolecular architecture from metal-organic coordination materials with various crystal structures depends on the choice of multi-dentate bridging ligands and the coordination geometries of metal ions [6]. The assembly of porous materials from organic molecules and metal-ion secondary building units is of great interest, to design new generations of open supramolecular architectures [7] due to their interesting features such as physical, mechanical properties and their applications [8]. The design of coordination polymers is an important area of research with several potential applications in various areas such as catalysis, conductivity, magnetic, gas storage, porosity, non-linear optics and other

different applications [1],[74],[9]. Benzene carboxylic acid ligands (Figure 4.2.1) are commonly used as motif-controlling functional elements in crystal engineering for the synthesis of porous coordination polymers. They can form different SBUs (Fig. 4.2.1.1) with metal ions *via* their carboxylate groups with additional hydrogen-bonding and π-π interactions.

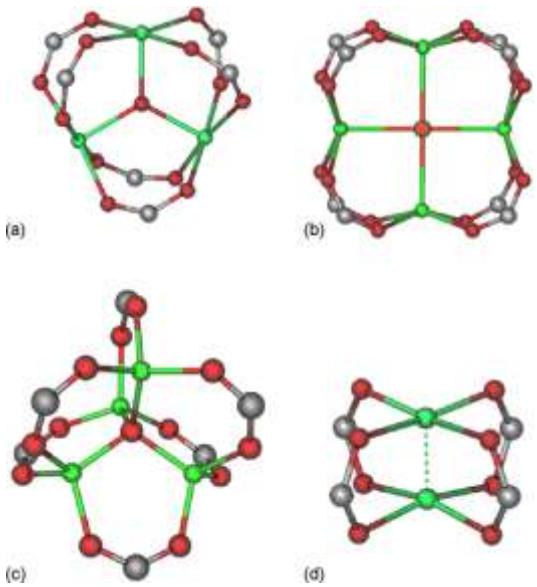

Figure 4.2.1.1: Structural representations of some SBUs of carboxylate groups (a) trigonal planar, (b) square planar, (c) tetrahedral, (d) tetragonal paddlewheel. (Figure was taken from ref. [48], Copyright, 2009 Elsevier B. V. All rights reserved.)

Examples of prototypical rigid and bridging carboxylic acids are terephthalic acid (H_2bdc) [10], isophthalic acid (H_2ip) [11] and benzene-1,3,5-tricarboxylic acid (H_3btc) (Figure 4.2.1). The latter has a 3-fold molecular symmetry and forms a 2D honeycomb network through hydrogen-bonded between adjacent carbouxyl groups in its solid-state structure [12]. Functionalized benzene-1,3,5-tricarboxylic acid such as monomethyl esterification benzene-1,3,5-tricarboxylic acid [13], its protonated forms [14] and its metal complexes [15] were already employed as unique building blocks in crystal engineering.

1,2,4-Triazole derivatives (Scheme 4.2.1.1) are very interesting ligands because they combine the coordination geometry of pyrazoles and imidazoles with their donor atoms (N1 and N2) and can form different interesting SBUs. Some posible different SBUs that could be designed by 1,2,4-triazole derivatives are presented in Scheme 4.2.1.2. A comparison between the tetranuclear SBU formed by carboxyl groups and triazole rings is presented in Figure 4.2.1.2. These SBUs should lead to porous coordination polymer in order to make the coordination network interesting for possible applications.

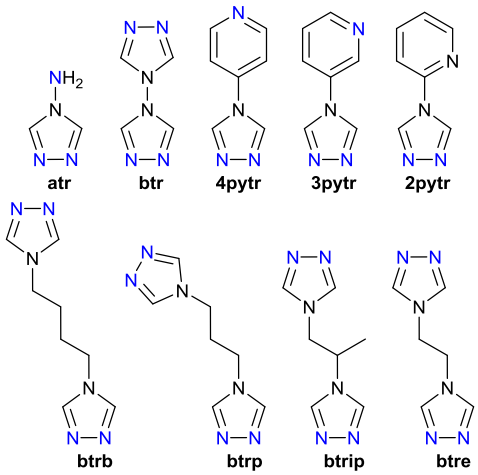

Scheme 4.2.1.1: The structure of different 1,2,4-triazole derivative ligands (see the list of abbreviations and units). Potential metal coordinating N atoms are depicted in blue.

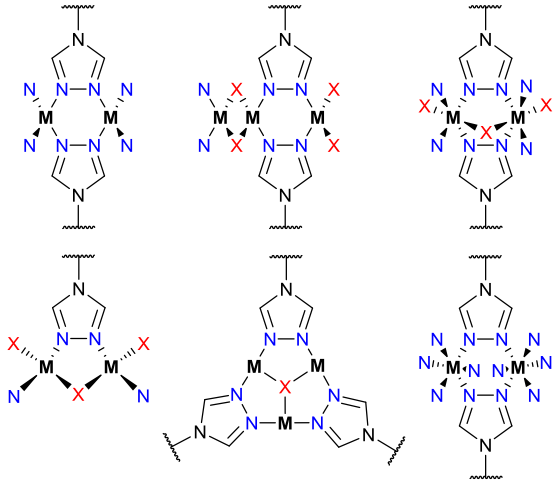

Scheme 4.2.1.2: Some different secondary building units of 1,2,4-triazole ligands. X can be Cl, Br, O, OH, NO_3, SO_4, ClO_4, H_2O, etc.

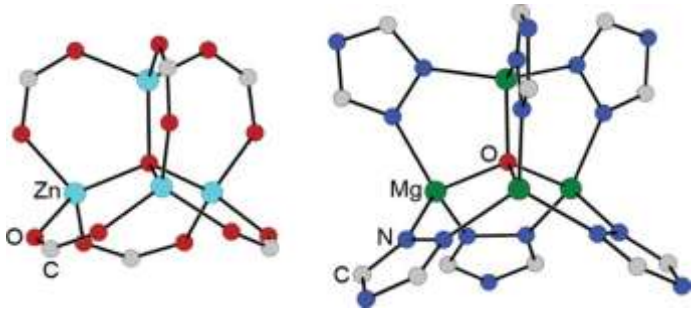

Fig. 4.2.1.2: A tetranuclear SBU of carboxylate groups (left) and triazole rings (right). (Figure was reprinted with permission from ref. [16], Copyright 2006 American Chemical Society).

The smallest triazole ligand shown and also used here in this work is 4-(1,2,4-triazol-4-yl)-amine (atr) (Scheme 4.2.1.1), which mostly bridges the metal ions *via* N1,N2 of the 1,2,4-triazole ring (Scheme 4.2.1.3) and give molecular complexes [17], polynuclear complexes [18], inorganic-organic [19] and metal-organic networks [20] of different dimensions also of mixed ligands.

Another common triazole ligand is 4,4'-bis(1,2,4-triazole) (btr) (Scheme 4.2.1.1), a symmetric 1,2,4-triazole derivative, which can bridge the metal atoms through its donor atoms (N1, N2) of a single triazole ring or from two different 1,2,4-triazole rings (N1, N1'). So the 4,4'-bis(1,2,4-triazole) ligand has different coordination possibilities with metal atoms (Scheme 4.2.1.3), which may lead to the formation of polynuclear complexes, one-, two- and three-dimensional inorganic organic coordination polymers [21]. Noteworthy, most of the metal-btr complexes and coordination polymers were obtained at ambient temperature.

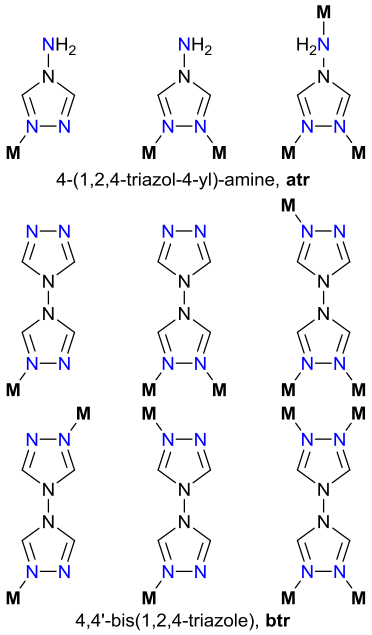

Scheme 4.2.1.3: The different coordination possibilities between 4-(1,2,4-triazol-4-yl)-amine (atr) or 4,4'-bis(1,2,4-triazole) (btr) and metal atoms.

Other examples for aromatic 1,2,4-triazole derivative ligands are 4-(pyrid-*n*-yl)-1,2,4-triazole (*n* = 2, 3, 4), which can also coordinate with metal atoms in different coordination modes (Scheme 4.2.1.4) to form molecular or polynuclear complexes or one-, two-, and three-dimensional inorganic-organic coordination polymers with helical chains or layered networks [22].

The bent ligand 1,2-bis(1,2,4-triazol-4-yl)ethane (btre) can assume cis- and trans-orientations (Scheme 4.2.1.5) and has previously been used for the build-up of polynuclear complexes and several 1D-, 2D-, and 3D-coordination compounds with different metal ions and mixed-ligand system [132],[23].

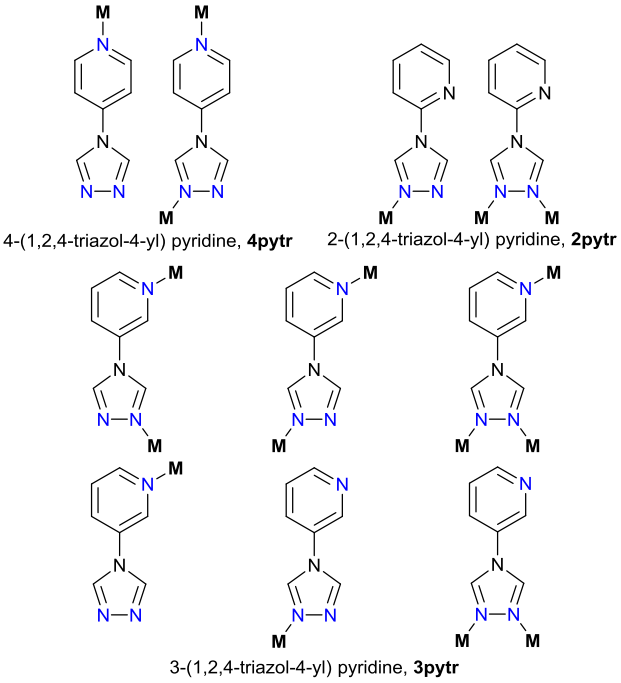

Scheme 4.2.1.4: Possible different coordination modes of 4-(pyrid-*n*-yl)-1,2,4-triazole (*n* = 2, 3, 4) with metal atoms.

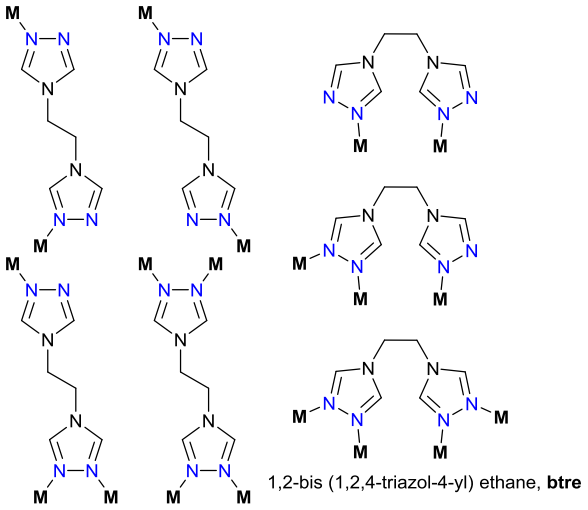

Scheme 4.2.1.5: Some of the different possibility orientation (cis and trans conformations) and the coordination modes between 1,2-bis(1,2,4triazol-4-yl)-ethane (btre) and metal atoms.

An interesting example for a combined carboxylate-triazole ligand is 5-(1,2,4-triazol-4-yl)-isophthalic acid ($5H_2$iptr), which has been previously been used for molecular, polynuclear complexes and several 1D-, 2D-, and 3D-coordination frameworks with different metal ions, especially in the co-working group of Prof. Dr. Krautscheid, Sun and Ueyama [24] (Scheme 4.2.1.6).

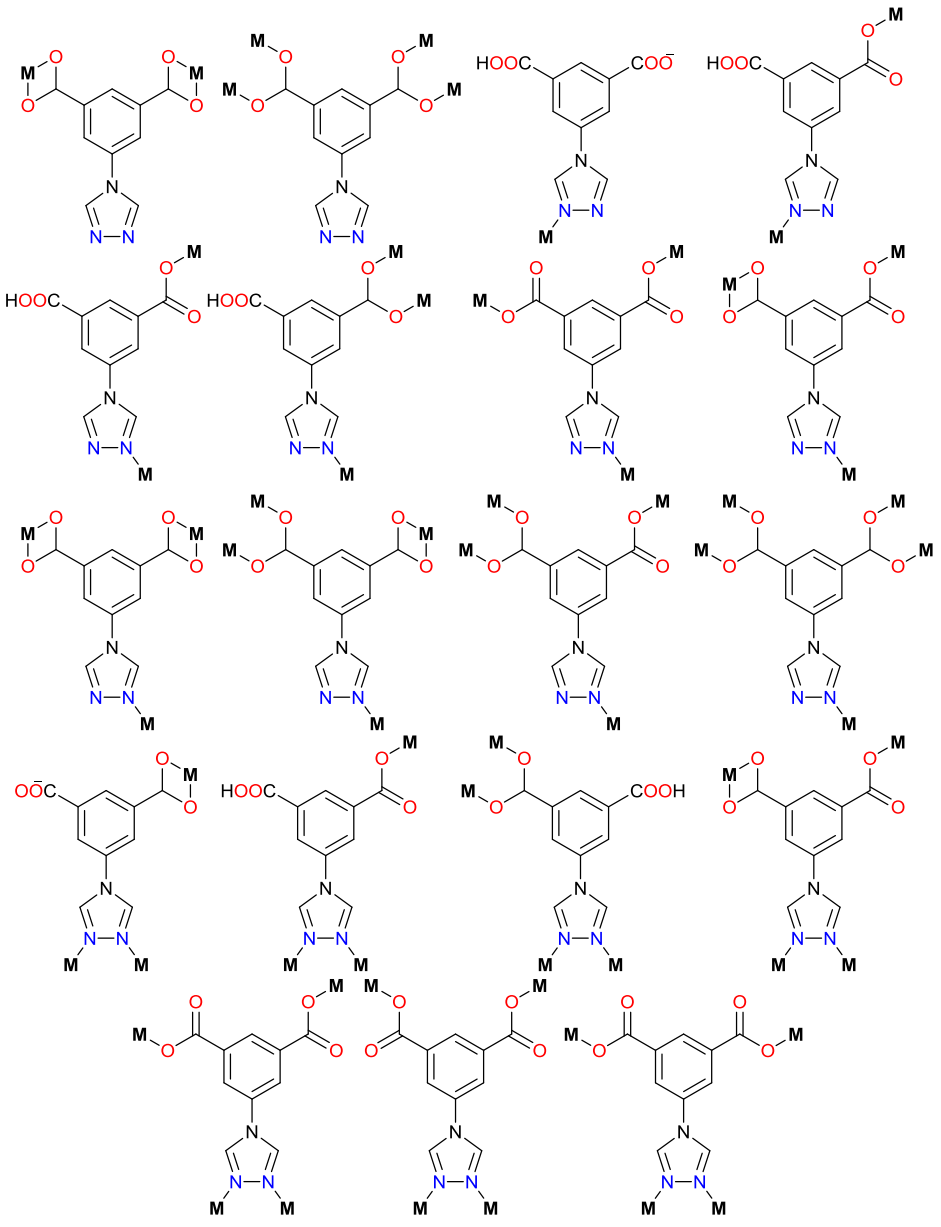

Scheme 4.2.1.5: The different coordination possibilities of singly- and doubly-deprotonated 5-(1,2,4-triazol-4-yl)isophthalic acid ($5H_2$iptr) with metal atoms.

In the following we describe some examples of coordination polymers based on 5-(1,2,4-triazol-4-yl)-isophthalic acid ($5H_2$iptr = H_2L) from the co-working group of Prof. Dr. Krautscheid, Sun and Ueyama.

The sovothermal reaction of $Cu(SO_4)_2 \cdot 5H_2O$ with 5-(1,2,4-triazol-4-yl)-isophthalic acid ($5H_2$iptr = H_2L) produced the 3D-porous coordination polymers 3D-$\{[Cu_3(\mu_3\text{-}OH)(\mu_3\text{-}SO_4)]_4[Cu_2(H_2O)_2]_3(\mu_6\text{-}L)_{12}]\}_n$ (Figure 4.2.1.3) [24a]. The crystal structure has two structural motifs, a trinuclear hydroxy bridged copper unit and a paddle wheel unit. Both the sulfate ion and the hydroxy group, which reside on the 3-fold axis, bridge the three copper ions. While the trinuclear hydroxy bridged copper unit represents a six-connected nodal point, the paddle wheel unit acts as four connected nodal point. By linkage through the three-connecting L^{2-} ligand with SBUs, a 3D-framework of twf-d topology with 66% solvent accessible pore volume is built up. The single cage consists of 6 paddle-wheel units $[Cu_2(H_2O)_2]$, 8 trinuclear hydroxyl solfate bridged copper unit $[Cu_3(\mu_3\text{-}OH)(\mu_3\text{-}SO_4)]$, and 24 5-triazolyl isophthalate ions. As shown in Figures 4.2.1.3.

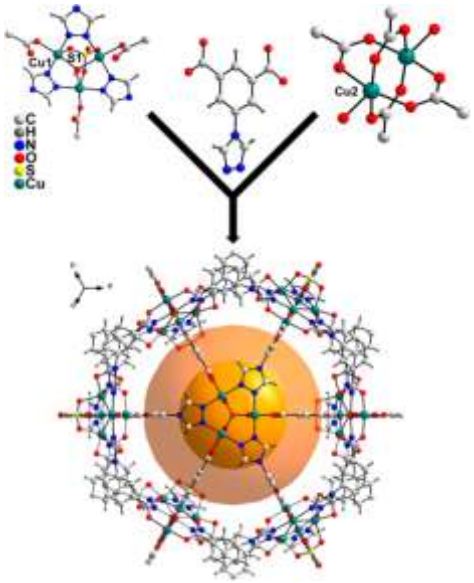

Figure 4.2.1.3: representation of ligand, SBUs and single cage of 3D-$\{[Cu_3(\mu_3\text{-}OH)(\mu_3\text{-}SO_4)]_4[Cu_2(H_2O)_2]_3(\mu_6\text{-}L)_{12}]\}_n$. (Figure was reproduced from ref. [24a], Copyright American Chemical Society 2012).

A ligand 5-(1,2,4-triazol-4-yl)-isophthalic acid ($5H_2$iptr = H_2L) with N- and O-donors was successfully applied to construct a series of coordination complexes 3D-$[Cu_3\text{-}(\mu_3\text{-}OH)_2(HL)_4]_n$ (1), $[Co(HL)_2(H_2O)_4]\cdot 3H_2O$ (2), $[Ni(HL)_2(H_2O)_4]\cdot 3H_2O$ (3), 3D-$[Mn(HL)_2]_n$ (4), 3D-$\{[Cu_2(L)_2(\mu\text{-}OH_2)_2]\cdot 3H_2O\}_n$ (5), 3D-$\{[Co_2(L)_2(\mu\text{-}OH_2)_2]\cdot 3H_2O\}_n$ (6), 3D-$\{[Ni_2(L)_2(\mu\text{-}OH_2)_2]\cdot 3H_2O\}_n$ (7), and

3D-{[Mn(L)(μ-OH_2)]·$2H_2O$}$_n$ (8) under hydrothermal conditions [24h] (Figure 4.2.1.4). The results revealed that the reaction pH and the metal center play important role in determining the structures of the complexes. By adjusting the reaction pH, H_2L ligand is partially deprotonated to give HL^- form in 1-4 and completely deprotonated L^{2-} form in 5-8. The structural analyses revealed that complex 1 is a 3D-(3,3,5,6)-connected network, while 2 and 3 are discrete mononuclear complexes which are extended by hydrogen bonds to form 3D network. The 3D-(3,6)-connected network of 4 is defined as a metal-organic replica of anatase (ant) net. Complexes 5-7 are isostructural and display 3D-(4,5)-connected network, and 8 is a binodal 3D-(4,6)-connected net. As shown in Figures 4.2.1.4.

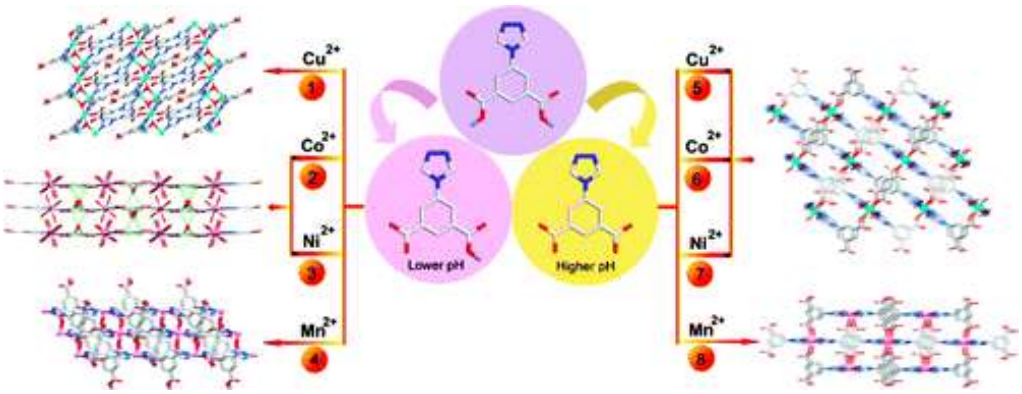

Figure 4.2.1.4: Abstract graphic of a series of coordination complexes based on 5-(1,2,4-triazol-4-yl)-isophthalic acid (5H_2iptr = H_2L) and different metal centers independent on pH reaction. (Figure was reprinted from ref. [24h], Copyright American Chemical Society 2011).

The sovothermal reaction of $Zn(NO_3)_2·6H_2O$ with 5-(1,2,4-triazol-4-yl)-isophthalic acid (5H_2iptr = H_2L) produced the 2D-coordination polymers 2D-[Zn(L)(H_2O)]$_n$ (Figure 4.2.1.5) [24f]. The coordination environment around the Zn(II) atom in 2D-[Zn(L)(H_2O)]$_n$ is depicted as a tetrahedral sphere surrounded by two O atoms from two L^{2-} ligands, one N atom from the third L^{2-} and one aqua ligand (Figure. 4.2.1.5a). Each L^{2-} ligand connect three Zn(II) atoms and form a 2D-**hcb** network (Figure 4.2.1.5b). This 2D network is heavily undulated, which allows another one to interpenetrate in a parallel mode. Hydrogen bonds can be detected to hold these two networks together and further link the interpenetrating layers to result in a 3D-supramolecular network as shown in Figure 4.2.1.5c and d.

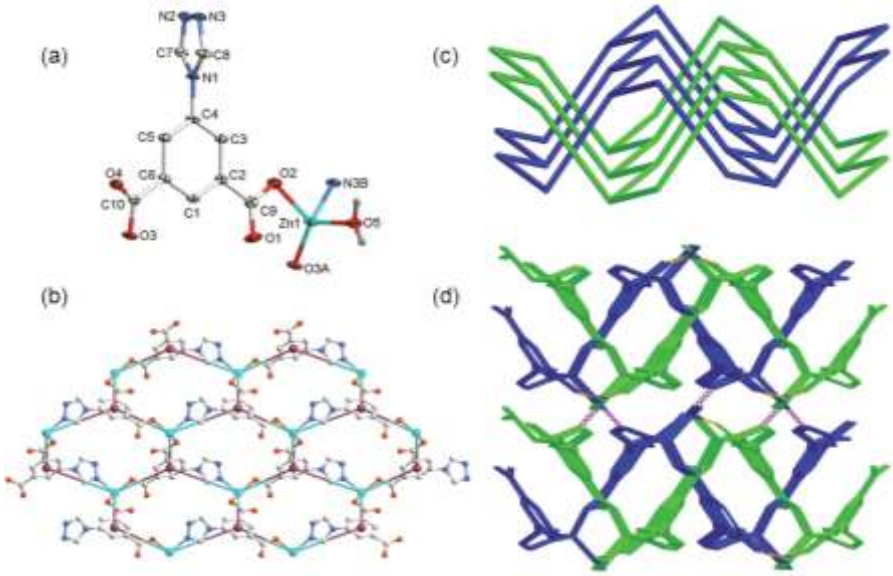

Figure 4.2.1.5: (a) Coordination environment of Zn(II) atom in 2D-$[Zn(L)(H_2O)]_n$ with the ellipsoids drawn at the 30% probability level. The hydrogen atoms except for the coordinated water molecule are omitted for clarity. (b) The single 2D-**hcb** layer structure. (c) The side view of the 2-fold interpenetrating network. (d) The 3D-supramolecular network with hydrogen bonds indicated by dashed lines. (Figure was reproduced from ref. [24f], Copyright The Royal Society of Chemistry 2012).

5.2.2 Introduction of 1H-tetrazole derivative ligands

5-Substituted 1H-tetrazole derivative ligands (Scheme 4.2.2.1) are very interesting ligands because they combine the coordination geometry of pyrazoles, triazoles, imidazoles and carboxylate groups with their donor atoms.

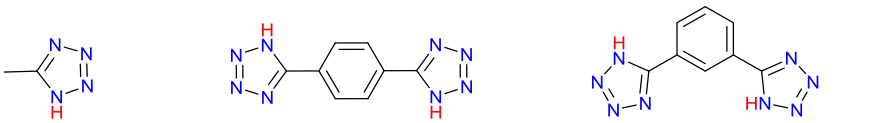

5-methyl-1H-tetrazole, **5met** benzene-1,4-di(1H-tetrazol-5-yl), **H_2bdt** benzene-1,3-di(1H-tetrazol-5-yl), **H_2ipdt**

Scheme 4.2.2.1: Examples of different 5-substituted 1H-tetrazole derivatives.

1H-Tetrazole ligands can build different secondary building units (SBUs) similar to triazole rings and carboxylate groups. A comparison between different SBUs from carboxylate groups and tetrazolate rings is presented in Scheme 4.2.2.2. The SBUs in porous coordination polymer of tetrazolate ligands are larger than from triazole and carboxylate

ligands. Carboxylate groups and tetrazolate rings can also build planar tetranuclear secondary building units as shown in Figure 4.2.2.1.

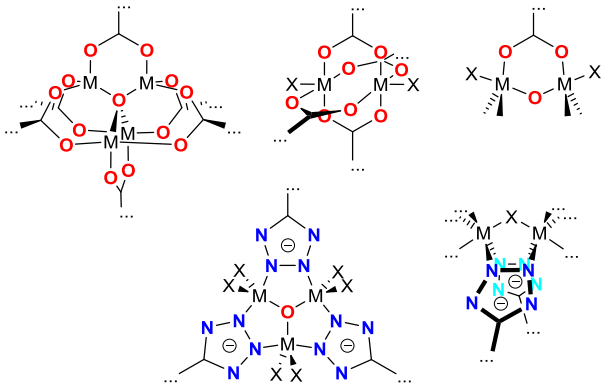

Scheme 4.2.2.2: A comparison between different SBUs from carboxylate groups and tetrazolate rings.

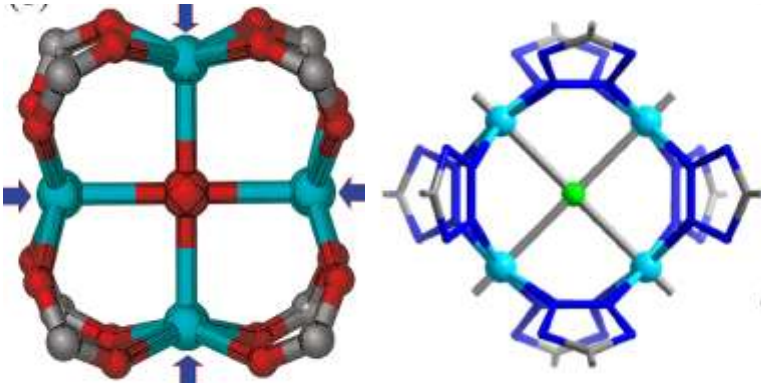

Fig. 4.2.2.1: Tetranuclear SBUs from carboxylate groups [25] (left) and triazole rings [26] (right). The arrows in the carboxylate SBU are for axial or terminal ligands. (Figure reprinted from [25],[26], Copyright 2009 American Chemical Society (left) and The Royal Society of Chemistry 2014 (right)).

5-Substituted 1H-tetrazolate derivative ligands are known from previous work to coordinate to metal atoms in different modes (Scheme 4.2.2.3) and build molecular or polynuclear complexes, and 1D-, 2D-, and 3D-coordination frameworks [27] [28].

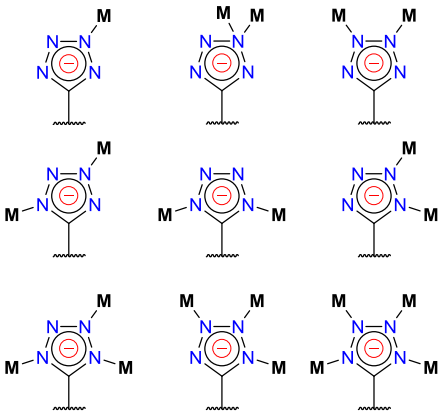

Scheme 4.2.2.3: The different coordination possibilities of a tetrazolate ring with metal ions.

The 1H-tetrazole/~ate ligands depicted in Figure 4.2.1 have not been previously described together with benzene carboxylate ligands as mixed-ligand coordination polymers. Unfortunately, in this work, several attempts through different synthesis conditions to obtain coordination polymers with a mixed carboxylate/tetrazole ligand system were unsuccessful, because either only the tetrazolate or carboxylate ligand coordinated to the metal atoms (see section 7.5).

5.2.3 Introduction to combined 3,5-dicarboxyl-triazol-4-yl derivate ligands

Synthesis of new combined multi-dentate organic ligands for the building of porous coordination polymers PCPs is a challenge. It is advantageous, that the coordinating groups carry a negative charge and the donor atoms are close to each other, which will lead to more stable PCPs and large multinuclear secondary building units SBUs with many metal atoms. 3,5-Dicarboxyl-triazol-4-yl derived ligands are a new generation of multi-dentate ligands, which have not been synthesized. The structures of such ligands are shown in Scheme 4.2.3.1.

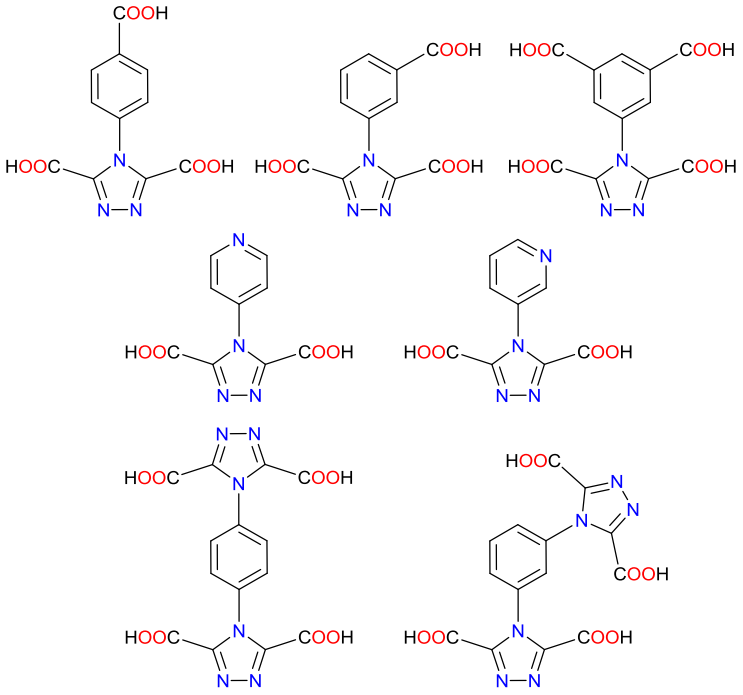

Scheme 4.2.3.1: Structure of combined multi-dentate 3,5-dicarboxyl-triazol-4-yl derived ligands.

3,5-Dicarboxyl-triazol-4-yl derivate ligands could be very important for very stable porous MOFs, because the 3,5-dicarboxyl-triazol-4-yl part of these new combined multi-dentate ligands can coordinate with many metal atoms in different coordination modes and build large multinuclear SBUs. Scheme 4.2.3.2 shows some binding positions and graph set of possible coordination modes.

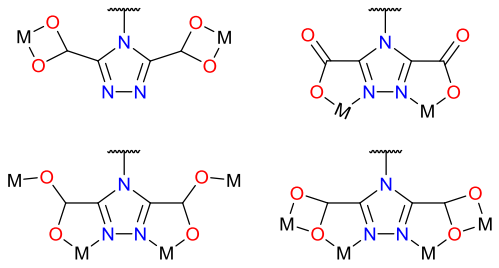

Scheme 4.2.3.2: Some binding positions and graph set of possible coordination modes of the 3,5-dicarboxyl-triazol-4-yl part of combined multi-dentate ligands.

The new multi-dentate 3,5-dicarboxyl-triazol-4-yl derivate ligands could be obtained from the reaction of an aromatic primary amine via 3,5-dimethyltriazol-4-yl derivates, where both methyl groups would then be oxidized by $KMnO_4$ to obtain the desired product (Scheme 4.2.3.3).

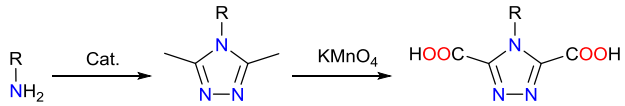

Scheme 4.2.3.3: General synthesis to obtain new combined multi-dentate ligands.

There are different methods to obtain 3,5-dimethyltriazol-4-yl derivates. Aromatic primary amine react under suitable reaction conditions with diacetylhydrazine [29], 2,5-disubstituted-1,3,4-oxadiazoles [88] or *N,N`*-dimethyl acetamide azine, DMAA [88] as shown in Scheme 4.2.3.4. Mr Gamall Makhloufi has tried in his Diploma work to obtain the 3,5-dimethyltriazol-4-yl derivate ligands through the first and second method, but he did not get the desired ligands [30]. Mr. Leif Römer has tried in his Bachelor work to obtain 3,5-dimethyltriazol-4-yl derivates through the third method [31]. Unfortunately, the reaction failed to yield any 3,5-disubstituted-1,2,4-triazol-4-yl derivate, but instead the acetamide derivative was obtained.

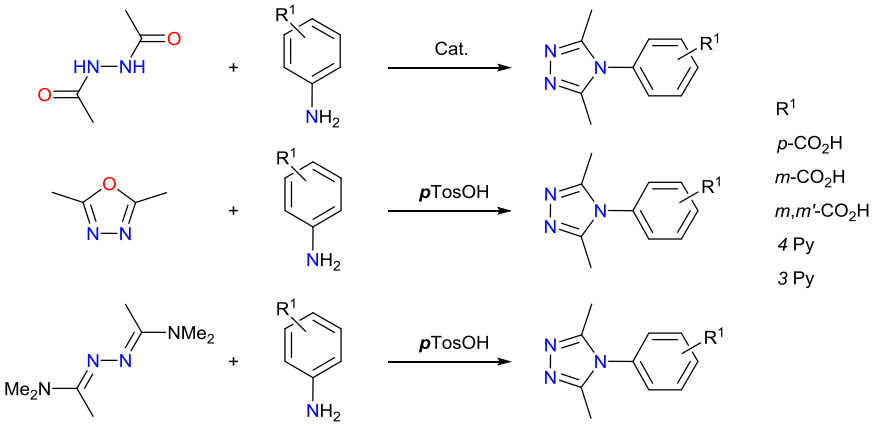

Scheme 4.2.3.4: Different methods for the synthesis of 3,5-dimethyltriazol-4-yl derivates [29],[88].

For the oxidation of both methyl groups of 3,5-dimethyl-1,2,4-triazole derivates it is possible to use $KMnO_4$ as oxidant in basic solution as shown in Scheme 4.2.3.5 to obtain 3,5-dicarboxyltriazol-4-yl derivates [32].

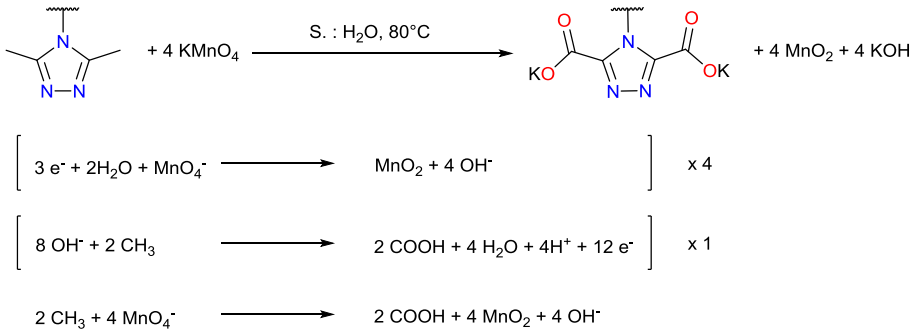

Scheme 4.2.3.5: Oxidation reaction of methyl groups of 3,5-dimethyl-1,2,4-triazole derivates [32].

A more sophisticated approach to the synthesis of 3,5-disubstituted-1,2,4-triazoles is the reaction of 2,5-disubstituted-1,3,4-oxadiazoles with respective primary amines (Scheme 4.2.3.4). 2,5-Dimethyl-1,3,4-Oxadiazoles can be obtained through different pathways either through the reaction of 5-methyl-tetrazoles with acetic anhydrides or acetyl chloride [88],[33], or by the reaction of diacetylhydrazine with thionyl chloride or acetic anhydride [29]. The last method is the reaction of acetylhydrazide with triethyl orthoacetate [88],[34] (Scheme 4.2.3.6).

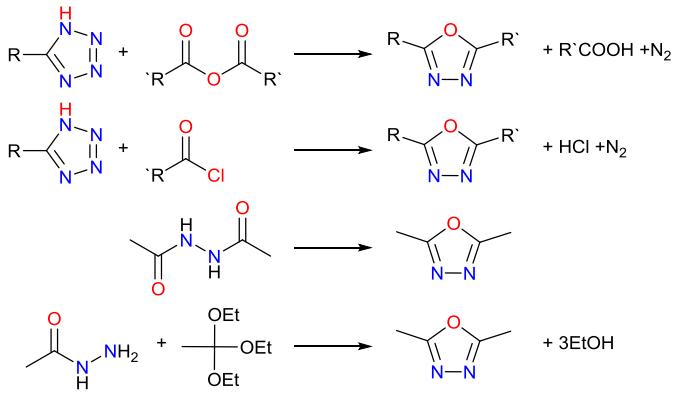

Scheme 4.2.3.6: Different syntheses of 2,5-dimethyl-1,3,4-oxadiazoles [29],[33],[34],[88].

Mr Leif Römer has tried in his Bachlor work to obtain 2,5-dimethyl-1,3,4-oxadiazole through the reaction of 5-methyl-tetrazole with acetic acid anhydride (Scheme 4.2.3.7). But the reaction did not yield any product [31]. From the dissertation of Dr. Jörg Linke [35] it was noticed that the reaction yields 2,5-disubstituted-1,3,4-oxadiazole, when 5-pyridyl-tetrazole was used for the synthesis. Probably, there are resonance formula between the phenyl and the tetrazole ring, which make the bonds between the nitrogen atoms in the tetrazole ring weak. So, when acetic acid anhydride reacts with the tetrazole ring in 5-pyridyl-tetrazole the

product 2-pyridyl-5-methyl-1,3,4-oxadiazole is formed. Mr Gamall Makhloufi has tried in his diplom work [30] to obtain 2,5-dimethyl-1,3,4-oxadiazole through the reaction of acetyl hydrazide with triethyl orthoacetate (Scheme 4.2.3.7), which yielded a red oil. 2,5-Dimethyl-1,3,4-oxadiazole was hygroscopic and not easy to obtain as a pure product, as Dr. Jörg Linke has written in his dissertation [35].

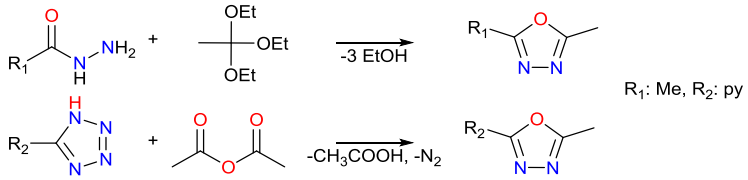

Scheme 4.2.3.7: Attempted syntheses of 2,5-disubstituted-1,3,4-oxadiazoles [88].

Dr. Jana K. Maclaren has synthesized 1,2,4-triazole derivates through the same reaction [162a]. The reactions were carried out under inert conditions. Triethyl orthoformate (2 eq) and monoformylhydrazine (1 eq) were dissolved in dried methanol. After refluxing the mixture for 2 h, the amine was slowly added to the reaction mixture (1eq, one amino group). After 4 h of refluxing, the solvent was removed under vacuum. Pink oil to white-pink milky residue was obtained. The white-pink milky residue was dissolved in methanol and diethyl ether was added into the solution. The product was precipitated and filtered, washed with acetonitrile or dichloromethane and recrystallized in isopropanol or ethanol.

2,5-Dimethyl-1,3,4-oxadiazole as the simplest 1,3,4-oxadiazole was obtained on a molar scale in 85% optimised yield from acetyl hydrazine and triethyl orthoacetate following the known reaction procedure [34],[36]. The proposed mechanism for this reaction is shown in Scheme 4.2.3.8.

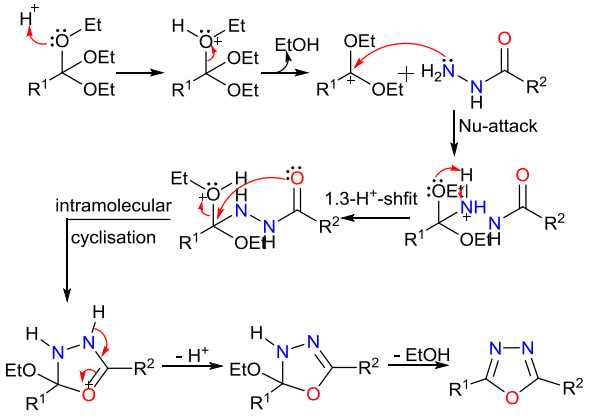

Scheme 4.2.3.8: The proposed mechanism for the synthesis of 2,5-dimethyl-1,3,4-oxadiazole from acetyl hydrazine and triethyl orthoacetate [37].

Eventually the synthesis of the 1,2,4-triazoles was performed by applying a modified method of Meyer, who achieved the triazole synthesis by the condensation of 2,5-dialkyl- or 2-alkyl-5-arylsubstituted-1,3,4-oxadiazoles and highly reactive primary amines such as aniline and methyl amine. [38] In our case, the reactivity of the amines used was not sufficient to lead to the formation of triazoles; hence, we improved the reaction by the addition of *p*-toluene sulfonic acid to enable the reaction (Scheme 4.2.3.9).

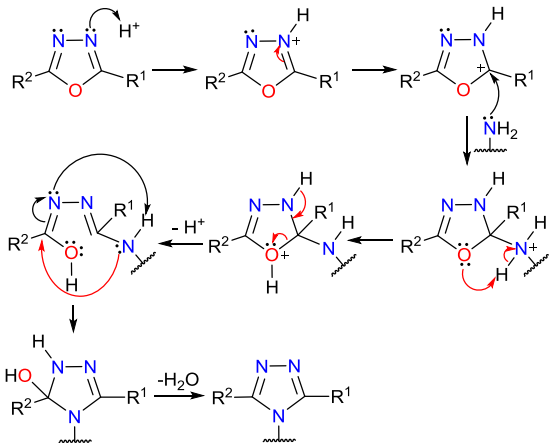

Scheme 4.2.3.9: The proposed mechanism for synthesis of 3,5-disubstituted-1,2,4-triazoles from 2,5-disubstituted-1,3,4-oxadiazoles and primary amines.

5.3 Topologies of coordination polymers

In principle, coordination polymer could be obtained through the reaction of polydentate bridging ligand with a metal ion, which has more than one labile site. An infinite extended 1D coordination polymer chain, 2D coordination network or 3D metal organic framework can arise, depending on the nature of the used polydentate ligands and geometry of metal ions. For example, using metal ions which can function as 4-connected nodes and linear linkers lead to building of an extended 2D coordination network or 3D metal organic framework as shown in Figure 4.3.1.

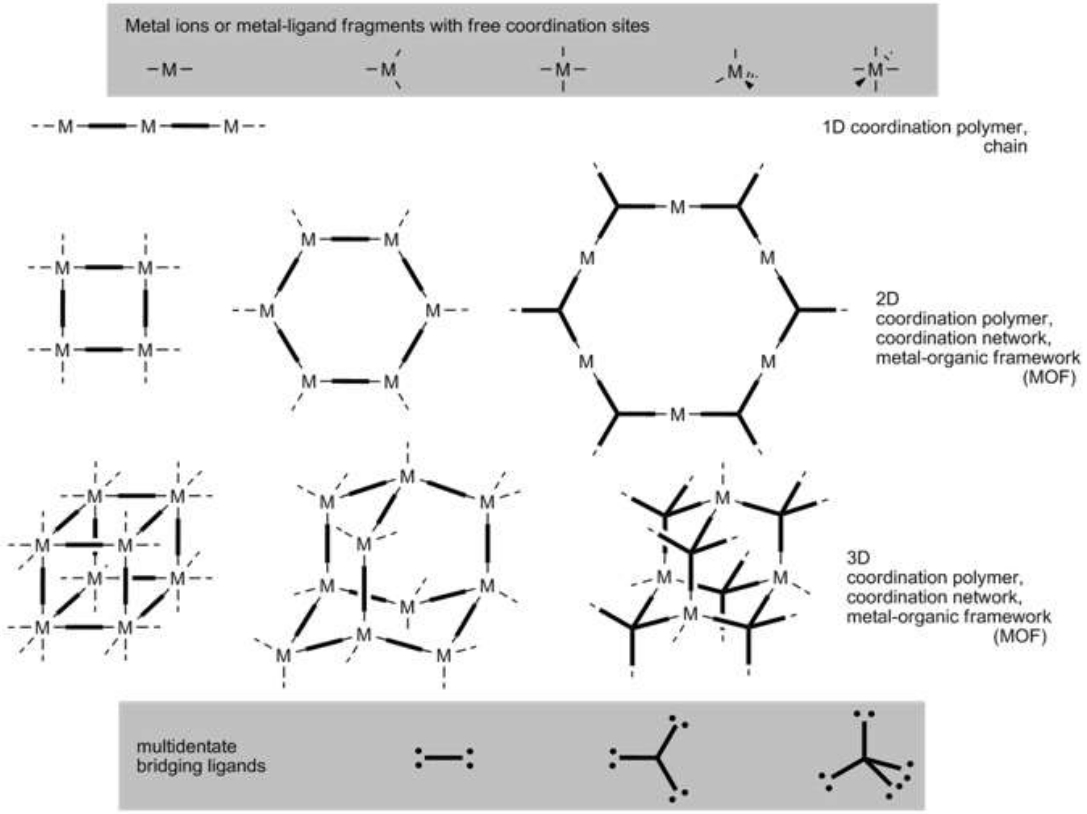

Figure 4.3.1: Schematic presentation of topologies for the construction of typical porous coordination polymers (PCPs/MOFs) from molecular building blocks and metal ions. (Figure was reprinted from ref. [1c],[39], Copyright The Royal Society of Chemistry and the Centre National de la Recherche Scientifique 2010 and The Royal Society of Chemistry 2003)

5.4 Coordination polymers constructed from SBUs

PCPs can be controlled by the coordination geometry of the metal ions or metal clusters, the shape and flexibility of bridging organic linkers, and the size of guest inside their pores. Network topologies were introduced to describe the characteristic attribute connectivity of the frameworks, which are usually simplified as reticular structure resource. In general, the coordination geometry and positions of polynuclear clusters have more directionality and selectivity compared with single metal ions. Therefore, using polynuclear metal clusters as secondary building units SBUs to construct PCPs usually gives more simple control over node-to-node orientation which lead to selective network topologies [40]. For example, high-symmetry metal-carboxylate clusters can have a SBU, such as $M_2(COO)_4L_2$ (L is an axially coordinate terminal or bridging ligand). The paddle-wheel $M_2(COO)_4L_2$ clusters can act as square-planar 4-connected nodes to form the 3D highly symmetric porous network [$Cu_3(\mu_6$-btc$)_2(H_2O)_3$] (HKUST-1), with a (3,4)-connected **bor** topology (Fig. 4.4.1a) [41] and as 6-

connected nodes to form the 3D unsymmetrical **pcu** network, $M_2(bdc)_2(bpy)_2$ (bpy is a linear bipyridyl-type ligand, M = Zn, Fig. 4.4.1b) [42]. Furthermore, $M_3(\mu_3\text{-}O/OH)(RCOO)_6L_3$ trinuclear clusters can be used as symmetrical trigonal-prismatic 6-connected nodes. Example are found in MIL-101 [43] and MIL-100 [44] (Fig. 4.4.1c–d), In addition, many high-nuclearity SBUs can also be interlinked by bridging organic ligands to form interesting PCPs.

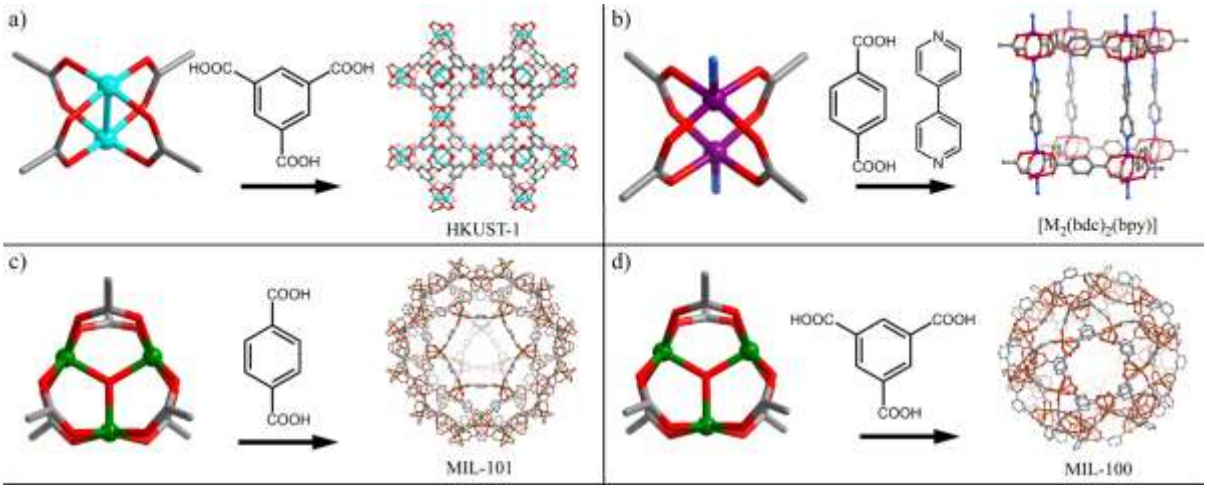

Figure 4.4.1: Presentation shows some typical porous coordination polymers PCPs (right) constructed from polynuclear metal clusters (left) as SBUs and polydentate bridging organic ligands as linkers (middle) (Figure was reproduced from ref. [45], Copyright 2015 Published by Elsevier B.V.).

5.5 Topological entanglement in PCPs structure

Complexity arises when one considers the dimensionality of the starting building blocks versus that of the resulting final architecture. Polycatenation is defined by an increase in the dimensionality of the final architecture over the dimensionality of the building blocks. On the contrary, in interpenetration there is no change in dimensionality. This distinction is therefore truly topological rather than just semantic [46]. A further criterion for polycatenation is that, unlike interpenetration, each distinct building block is never interlaced with all the others in the array. In interpenetration, it is possible to define a degree of interpenetration, because there are always a finite number of interpenetrated components. This is impossible for polycatenated arrays where there are an infinite number of entangled components [47] (Fig. 4.5.1). The important topological differences between interpenetration and polycatenation are summarized in Table 4.5.1.

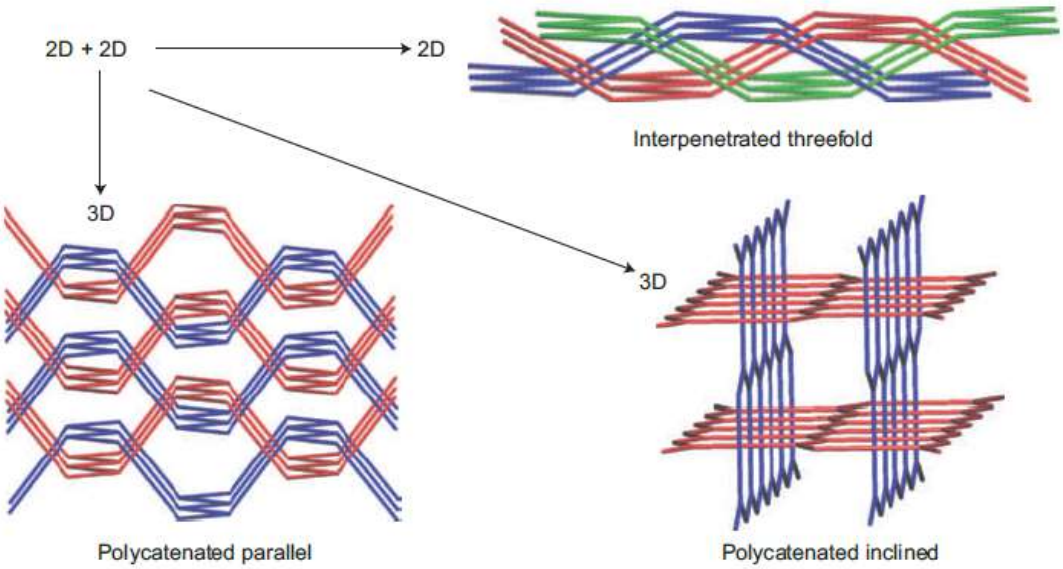

Figure 4.5.1: Topologically distinct entanglements of hexagonal layers. Two different modes of polycatenation are shown, which both result in an increase in dimensionality, versus interpenetration in which the dimensionality remains the same. (Figure was reprinted from ref. [47a], Copyright 2010 Macmillan Publishers Limited. All rights reserved).

Table 4.5.1: Topological differences between interpenetration and polycatenation [47].

Interpenetration	**Polycatenation**
same dimensionality of the interpenetrating coordination networks (parallel nets)	increased dimensionality of the interpenetrated coordination network
components either 2D- or 3D-nets	components either 0D-, 1D- or 2D-nets
degree of entangled motifs is finite (n-fold)	degree of entangled motifs is infinite
each motif is interlaced with all the others	each motif is never interlaced with all the others

5.6 Synthetic conditions and methods for coordination polymers

Syntheses of coordination polymers have been usually carried out by combining polydentate organic linkers and metal salts in solution under different reaction conditions in order to obtain crystalline products susceptible to single crystal X-ray diffraction for their structure elucidation. The reactants are mixed in highly polar solvents such as water, dialkyl formamides (DMF, DEF), dimethyl sulfoxide (DMSO), acetonitrile or a mixture of solvents [48]. The most important parameters to influence the crystallization of coordination polymers are temperature, reaction time, the concentrations of metal salt and ligand, the extent of

solubility of the reactants in the solvent, solvent mixtures, the pH of the solution and molar ratios of starting materials. The characteristics of the ligand (bond angles, ligand length, bulkiness, chirality, donor groups, flexible, solubility in solvent, thermal stability, etc.) play an important role in the topology and structure of the resultant framework. Additionally, the geometries and coordination number of metal ions also influence the structure of the coordination polymers. H-bonds and π–π interactions play important roles in the stability of the resulting coordination networks. Anions have an effect to neutralize the positive charges of metal ions. The metal–ligand network materials are mostly synthesized in solution through solvent evaporation, solvent diffusion or through the hydro- or solvo-thermal method [49] from molecular building blocks. Reviews, which describe the synthesis and characterization of MOFs/PCPs have been previously published [50].

The use of PCPs in industrial applications is envisioned and sought due to their characteristic properties. Requirements of the PCPs that must be fulfilled for a possible application include permanent porosity, thermal and chemical stability, as well as sustainability. Laboratory syntheses, which were established in the search of new PCPs, must also be adapted. From there, the following problems should be taken into account: (1) availability and cost of the starting materials, (2) synthesis conditions (low temperature, ambient pressure), (3) workup procedure, (4) activation process, (5) necessity of obtaining high yields, (5) avoiding large amount of impurities, and (6) using only small amounts of solvents [51]. The most detailed structural information will be obtained from single crystal X-ray crystallography. Therefore, synthesis of metal organic coordination polymer is strongly directed toward obtaining X-ray quality single crystals. Because, without knowing the crystal structure, it is very hard to interpret any observed properties.

5.7 Coordination polymers based on mixed ligands

In the following we describe examples of mixed-ligand coordination polymers from the work of others. The chosen examples contain nitrogen and carboxylate ligands which are similar to the ligands which are used in this thesis.

2D-{[Zn(H_2bpz)(bdc)]·1/2(H_2bpz)}$_n$ [52] (H_2bpz = 3,3`,5,5`-tetramethyl-4,4`-bipyrazole; H_2bdc = terephthalic acid) has been isolated from the hydrothermal reaction of $ZnSO_4$, H_2bpz and H_2bdc. The Zn(II) ions are coordinated by two nitrogen atoms from two H_2bpz and two oxygen atoms from two bdc^{2-}. Combination of H_2bpz, bdc^{2-} and Zn(II) centers lead to two different 1D-zigzag chains. One chain is extended by H_2bpz along ***c***, whereas the other is led by bdc^{2-} along ***a*** within a two-dimensional (4,4) network as demonstrated in Figure 4.7.1.

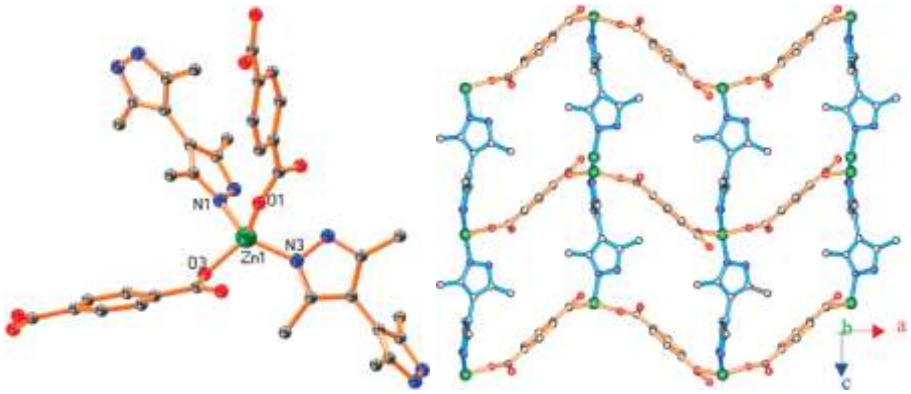

Figure 4.7.1: The coordination environment around the Zn(II) center (left), two types of zigzag chain assembly from H_2bpz or bdc^{2-} and Zn(II) atoms. (Figure was reproduced from ref. [52], Copyright 2007 American Chemical Society).

2D-$[Zn(Hbtc)(H_2mdp)]_n$ [53] has been synthesized under hydrothermal condition. The zinc atom is coordinated to two oxygen atoms from two different trimesic acid ($Hbtc^{2-}$) groups and two nitrogen atoms from two different H_2mdp molecules. Interestingly, only two carboxylate groups of trimesic acid are coordinated to the metal centre while the third remains protonated. $[Zn(Hbtc)(H_2mdp)]_n$ reveals 2D (4,4) rhombohedral nets oriented parallel to the ***ab*** plane. Both Hbtc and H_2mdp molecules are helically arranged on the ***ab*** plane, while Hbtc molecules are linked to every alternate node of two parallel helical strands of H_2mdp molecules. As illustrated in Figure 4.7.2, the twisted grids adopt a bowl-like shape and interdigitate. This coupled with the steric bulk of the methyl groups of H_2mdp rules out the possibility of interpenetration.

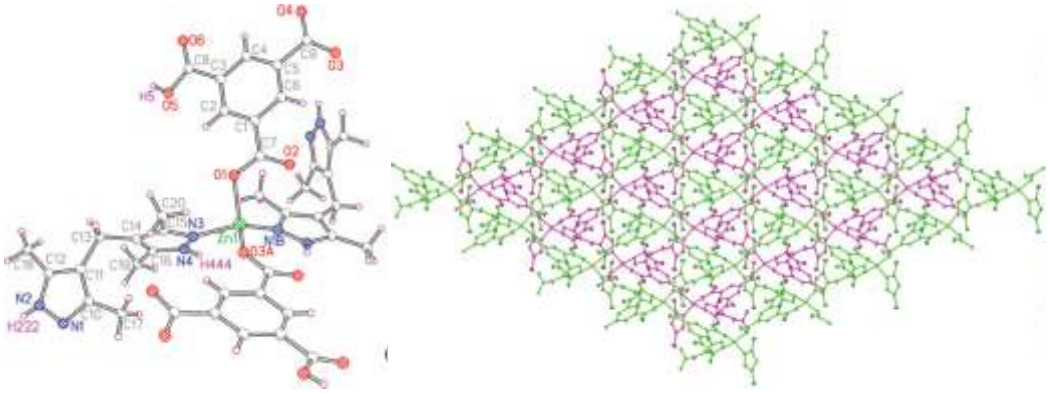

Figure 4.7.2: Coordination environment of Zn(II) (left). Crystal packing of 2D-$[Zn(Hbtc)(H_2mdp)]_n$ showing the formation of a non-interpenetrating (4,4) network. Two different networks (green and pink) are shown to highlight the offset stacking of (4,4) nets. (Figure was taken from ref. [53], Copyright The Royal Society of Chemistry 2008).

2D-{Co(H_2mdp)(Hbtc)}$_n$ [54] (H_2mdp methylenebis(3,5-dimethylpyrazole), H_3btc = benzene-1,3,5-tricarboxylic acid) has been isolated under hydrothermal condition. Co(II) is coordinated by two nitrogen atoms from two different H_2mdp ligands, and two oxygen atoms from two different $Hbtc^{2-}$ ligands. Such 2D-{Co(H_2mdp)(Hbtc)}$_n$ is isostructure to last example 2D-[Zn(Hbtc)(H_2mdp)]$_n$. Two kinds of 1D helical chains: one is composed of H_2mdp ligands and the other is constructed from $Hbtc^{2-}$ ligands, which constitute a 2D (4,4) helical layers with small rhombic open windows parallel to the ***ab*** plane as shown in Figure 4.7.3.

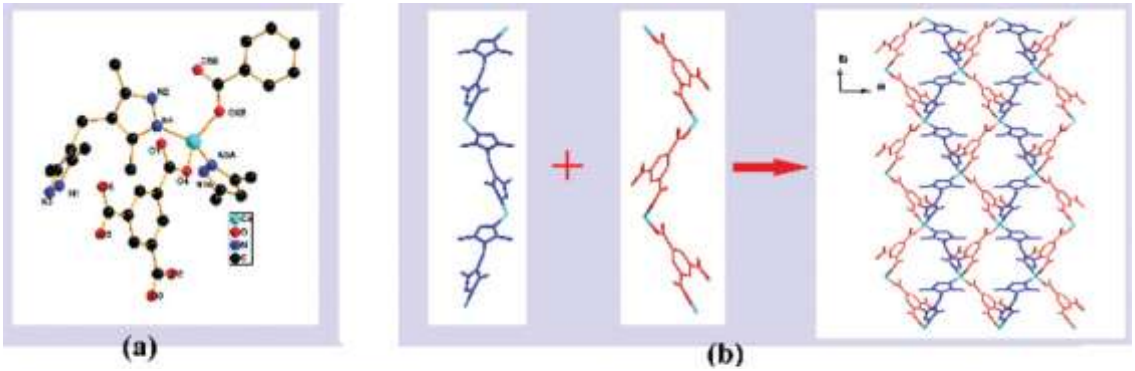

Figure 4.7.3: (a) Coordination environment of Co(II). (b) View of a helical layer with small open windows. (Figure was reprinted from ref. [54], Copyright The Royal Society of Chemistry 2013).

The hydrothermal reaction of Ni(NO_3)$_2$·6H_2O with benzene-1,3,5-tricarboxylic acid (H_3btc) and 1,2-bis(1,2,4-triazol-4-yl)ethane (btre) produced the mixed-ligand coordination polymers (MOFs) 3D-{[Ni_3(μ_3-btc)$_2$(μ_4-btre)$_2$(μ-H_2O)$_2$]·~22H_2O} (**1`**) (Fig. 4.7.4, left) [23f]. This compounds features a trinuclear SBU within the 3D-framework. Each btre ligand connects four nickel atoms and each btc^{3-} ligand bridges between three symmetry related Ni1 atoms. Also, the Ni atoms and the btre ligands form parallelepipedic 4,4 nets parallel to ***bc*** (Fig. 4.7.4, bottom). Careful control of the dehydration procedure (freeze-drying) for **1`** allowed for a solid-state reaction with single-crystal-to-single-crystal structural transformations in obtaining the largely dehydrated product 3D-{[$Ni_3$($\mu_2$-btc)$_2$($\mu_4$-btre)$_2$($\mu$-$H_2O$)$_2$($H_2O$)$_2$] 4$H_2O$} (**2`**) (Fig. 4.7.4, right). The freeze-dried crystal product retains the trinuclear nickel unit with its bridging aqua and btre-ligands (Fig. 1b). The main difference between **1`** and **2`** in the Ni_3 unit is the replacement of one of the three coordinating btc^{3-} ligands on Ni1 in **1`** by a terminal aqua ligand in **2`**. In the transformation from **1`** to **2`** the unit cell volume is reduced to about ~60% as shown in Figure 4.7.4.

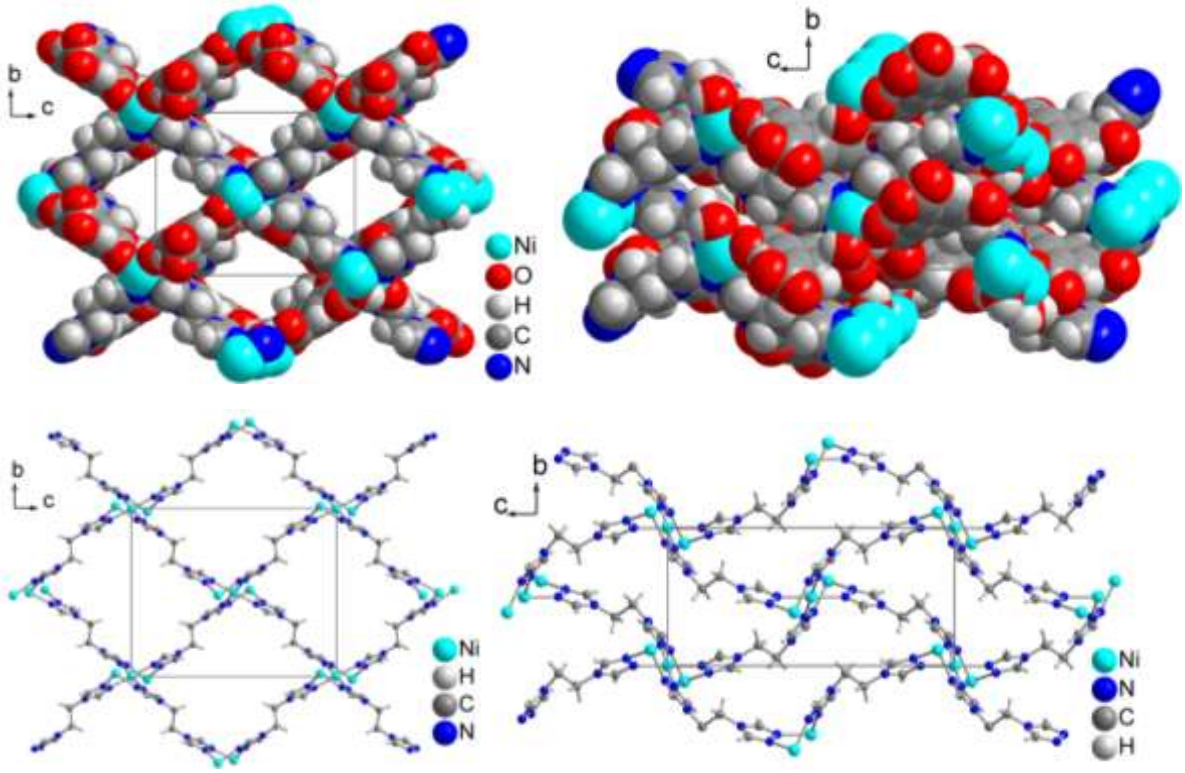

Figure 4.7.4: Space-filling packing diagram without water of crystallization in the channels omitted for **1`** (left, up), for **2`** (right, up). Packing analysis {Ni-btre}-nets for **1`** (left, bottom) for **2`** (right, bottom). Note the shortening of the *b*-axis to 61% in comparison to the *b*-axis of structure **1`**. (Figure was reprinted from ref. [23f], Copyright The Royal Society of Chemistry 2008).

The hydrothermal reaction of $Co(OAc)_2 \cdot 4H_2O$ with Adamantane-1,3-dicarboxylic acid (H_2adc) and 4,4`-bipyrazole (H_2bpz) produced the mixed-ligand coordination polymers 2D-$\{[Co(Hadc)_2(\mu\text{-}H_2bpz)_2] \cdot 2H_2O\}_n$ [55] (Figure 4.7.5). The Co^{2+} coordination environment comprises four pyrazole N-atom donors in the equatorial planes and two carboxylate O atoms in axial positions. The H_2bpz ligands act as bitopic connectors, while the $Hadc^-$ anion represents a monodentate carboxylate ligand retaining a noncoordinated neutral carboxylic acid group. The metal-bipyrazole parts of structure exist in the form of 2D square-grid networks, which are parallel to the **bc** plane. The singly charged $Hadc^-$ anions are accommodated on both axial sides of these layers (Figure 4.7.5)

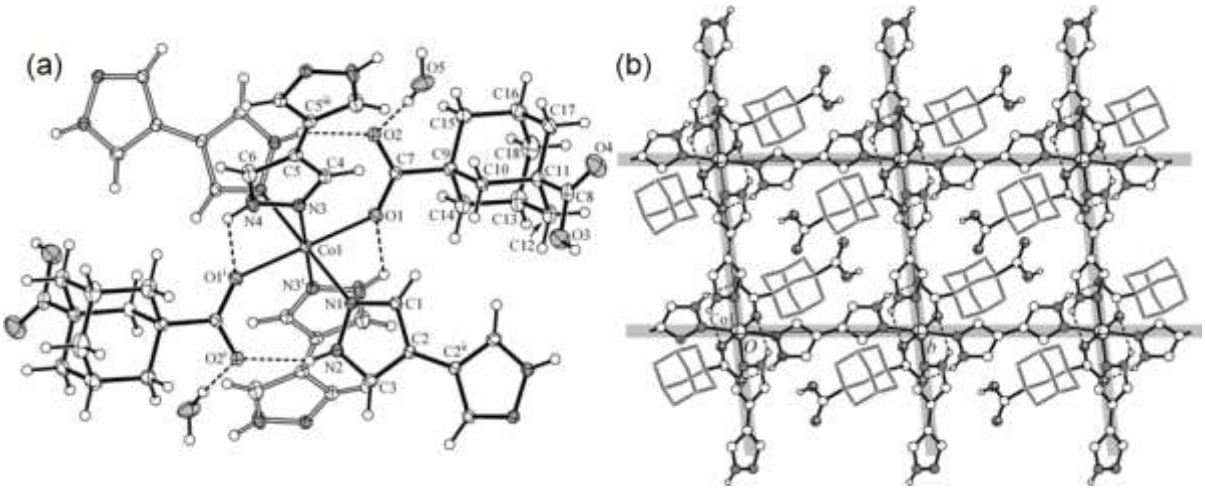

Figure 4.7.5: (a) Coordination environment of Co(II) with atom labeling of the asymmetric unit. (b) A packing diagram of 2D square-grid coordination network showing the accommodating of the $Hadc^-$ anions. (Figure was reproduced from ref. [55], Copyright 2013 International Union of Crystallography)

The hydrothermal reaction of $Cd(NO_3)_2 \cdot 4H_2O$ with 5-sodiumsulfoisophthalic acid ($NaSO_3$-H_2ip) and 1,2-bis(1,2,4-triazol-4-yl)ethane (btre) produced the mixed-ligand coordination polymers 3D-$\{[Cd_3(btre)_2(SO_3\text{-}ip)_2] \cdot 4H_2O\}_n$ [23a] (Figure 4.7.6). Each Cd(II) atom is six-coordinated by four oxygen atoms and two nitrogen atoms from two btre ligands in a distorted octahedral geometry. The SO_3-ip ligands exhibit a 5-connected mode, bridge five Cd(II) atoms and extend to form the 2D-$[Cd_3(SO_3\text{-}ip)_2]_n$ network. Each btre ligand shows a 3-connected mode, bridges three Cd(II) atoms and adopts a gauche-conformation. The 3-connected btre ligands link adjacent 2D-$[Cd_3(SO_3\text{-}ip)_2]_n$ and extend to form a 3D-$[Cd_3(btre)_2(SO_3\text{-}ip)_2]_n$ network. Topologically, each Cd1 atom connects three SO_3-ip and two btre ligands and is 5-connected. Each Cd2 atom coordinates four SO_3-ip and two btre ligands and is 6-connected. The SO_3-ip and btre ligands are 5- and 3-connected, respectively. Therefore the 3D-$[Cd_3(btre)_2(SO_3\text{-}ip)_2]_n$ shows a (3,5,5,6)-connected 3D-network (Figure 4.7.6).

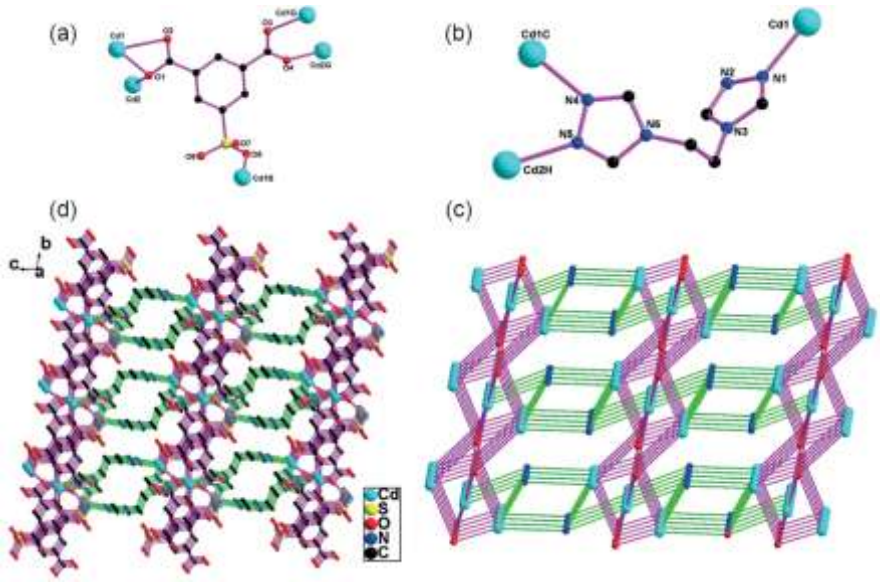

Fig. 4.7.6: (a) The 5-connected SO_3-ip ligand. (b) The 3-connected btre ligand. (d) The 3D-$[Cd_3(btre)_2(SO_3\text{-ip})_2]_n$ network. (c) Schematic of the (3,5,5,6)-connected 3D network. The red and blue balls exhibit the 5-connected SO_3-ip and 3-connected btre ligands, respectively. The turquoise balls show the 5- and 6-connected Cd(II) atoms. (Figure was reproduced from ref. [23a], Copyright The Royal Society of Chemistry 2014)

The hydrothermal reaction of $Co(OAc)_2{\cdot}4H_2O$ with 4-amino-3,5-bis(4-pyridyl)-1,2,4-triazole (bpt) and benzene-1,3,5-tricarboxylic acid (H_3btc) produced the mixed-ligand coordination polymers 2D-$[Co(bpt)(Hbtc)(H_2O)]_n$ [5d] (Figure 4.7.7). The coordination sphere of each central Co(II) atom is provided by four oxygen atoms and two nitrogen atoms from two (Hbtc), one aqua, and two (bpt) ligands, displaying a distorted octahedral geometry. Carboxylate groups of Hbtc bridge the Co(II) centers in chelating bidentate and monodentate coordination modes, to produce wavelike 1D-polymeric chains, which are further extended by exo-bidentate bpt connectors to produce a greatly corrugated 2D-(4,4)-network. The Hbtc moieties, located up and down each 2D array, insert into the lateral voids of the adjacent networks to produce an unusual interdigitated tactic motif (Figure 4.7.7).

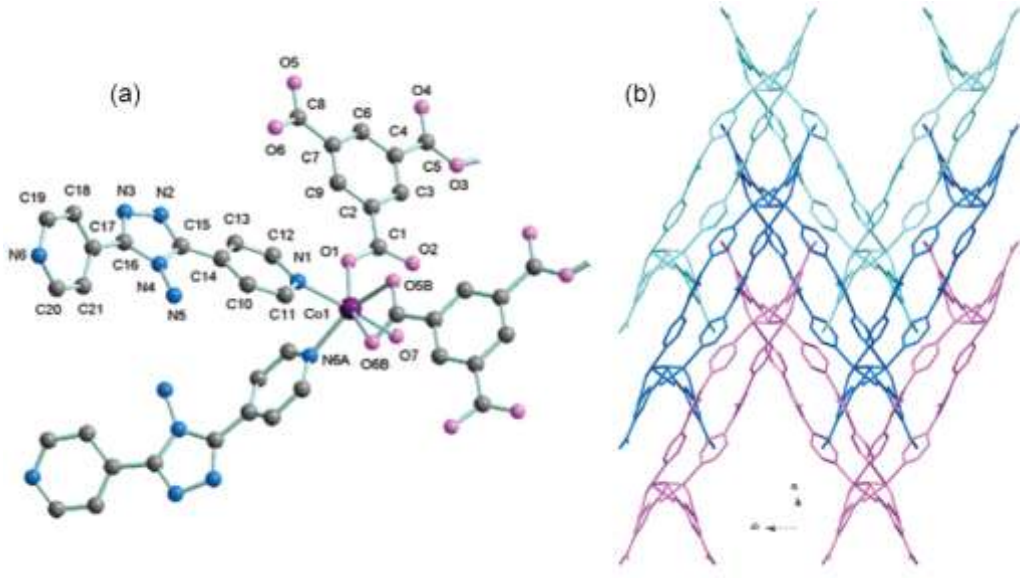

Figure 4.7.7: (a) Coordination environment of Co(II) with atom labeling of the asymmetric unit. (b) A packing diagram of three 2D corrugated coordination network showing the interdigitation of the 2D nets. (Figure was reproduced from ref. [5d], Copyright 2006 American Chemical Society)

Hydrothermal reaction of $ZnSO_4 \cdot 7H_2O$ with 1,3,5-benzenetricarboxylic acid (H_3btc) and 2,6-bis(1,2,4-triazolyl)pyridine (btp) afforded a novel 2D-$\{[Zn_3(btc)_2(btp)_2(H_2O)_2] \cdot 4H_2O\}_n$ [56] (Figure 4.7.8). Zn(1) atom coordinates to two triazole nitrogen atoms and two carboxylate oxygen atoms in a distorted tetrahedral coordination environment. Zn(2) atom coordinates to a N atom of triazole, a O(1w) of water and two O atoms of carboxylate in a distorted trigonal-pyramidal coordination environment. Carboxyl groups of (btc) are all deprotonated and coordinated to three Zn(II) atoms in a monodentate mode. (btp) acts as a bidentate bridging ligand links two Zn(II) atoms through two triazole N atoms. Both multidentate ligands assembled with Zn(II) atoms forms a 2D-polymeric network. Interestingly, this network contains two kinds of molecular squares and a rectangle. One square is constructed by four bpt edges, the other square is constructed by four btc edges. A rectangle is formed by two bpt edges and two btc edges and held between four squares. Further research found that three networks interpenetrate to each other (Figure 4.7.8).

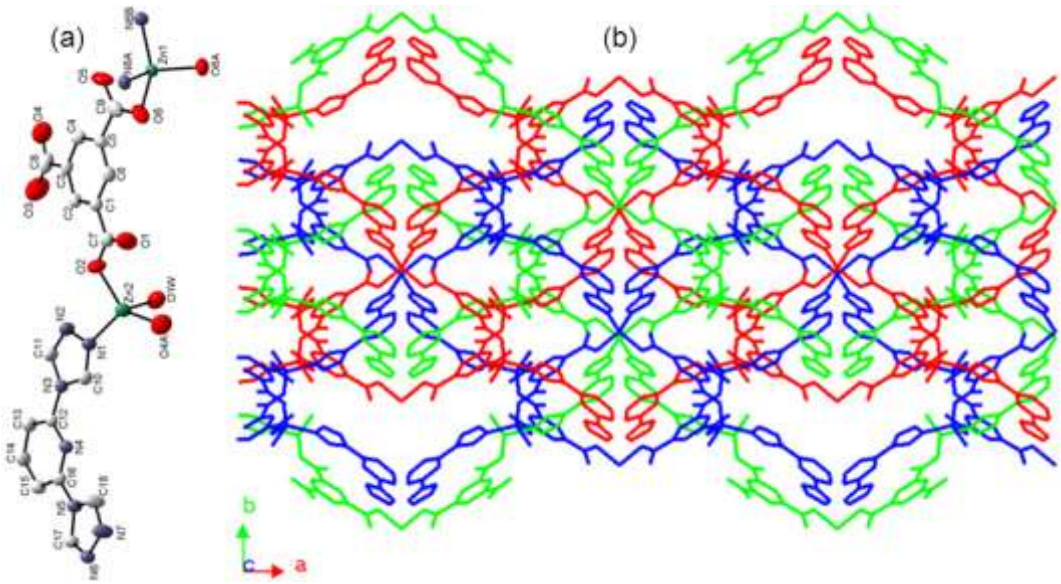

Figure 4.7.8: (a) Coordination environment of Zn(II) with atom labeling of the asymmetric unit. (b) A packing diagram of three 2D interpenetrating coordination networks showing the molecular squares and a rectangle of the 2D nets. (Figure was reproduced from ref. [56], Copyright 2007 Elsevier B.V. All rights reserved.)

The hydrothermal reaction of zinc acetate hydrate with 3,3`,5,5`-tetramethyl-4,4`-bipyrazole (me4bpz) and benzene-1,3-dicarboxylic acid (isophthalic acid) (H_2ip) produced the mixed-ligand coordination polymers 3D-[Zn(μ–ip)(μ–me4bpz)]$_n$ [57] (Figure 4.7.9). The cations are coordinated tetrahedrally by two bipyrazole ligands and two carboxylate ligands.The connection of the metal centers by carboxylate anions leads to formation of zigzag chains along the crystallographic ***c*** direction. These chains are linked together by (me$_4$bpz) ligands in ***b*** direction, where metal atoms and (me4bpz) form right-handed helices in ***b*** direction. This is connection arts lead to form 3D-(6,4)-nets with diamondoid topology. Three of these nets interpenetrate each other; each translated one unit cell edge length in the crystallographic ***a*** direction (Figure 4.7.9).

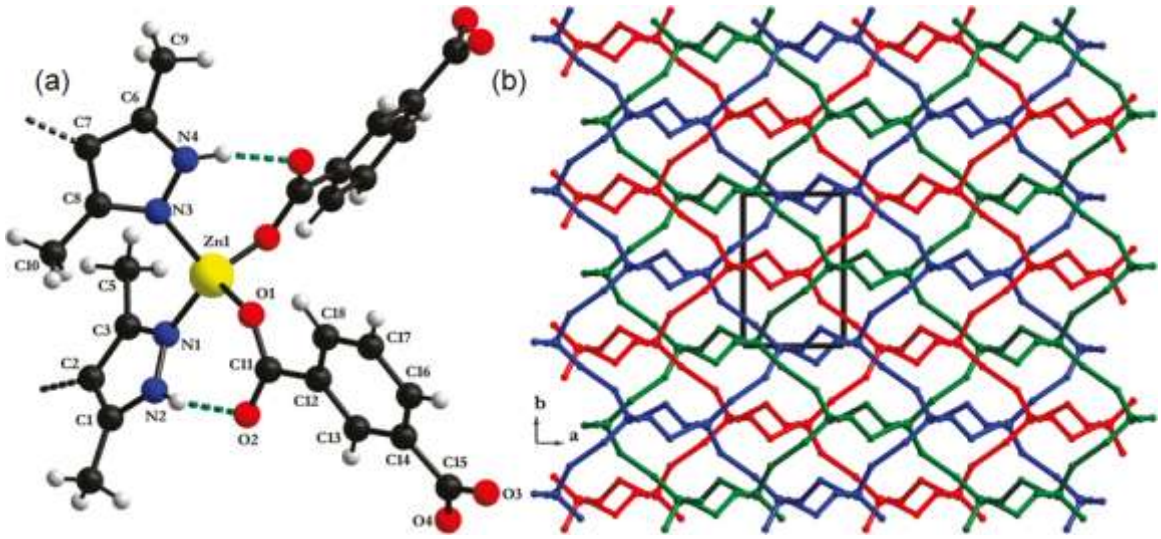

Figure 4.7.9: (a) Coordination environment of Zn(II) with atom labeling of the asymmetric unit. (b) A packing diagram of three 3D interpenetrating coordination networks along ***c*** axis. (Figure was reproduced from ref. [57], Copyright 2009 American Chemical Society)

Different groups have used differing terminology to describe the types of MOF based on mixed linkers or metals. For example, mixed-ligand MOFs have been termed MIXMOFs by Baiker and co-workers [58], multivariate MOFs (MTV-MOFs) by Yaghi and co-workers [59] and coordination co-polymers by Matzger and co-workers [60]. Andrew D. Burrows [61] has been introduced the term mixed-component MOFs (MC-MOFs) as an over-arching term for all of the mixed-ligand and mixed metal MOFs described and summarized the categories in Figure 4.7.10. His review concerns the formation of MOFs containing either mixed ligands or mixed metals. Many of these mixed-ligand or mixed-metal MOFs are solid solutions, in which the proportions of the ligands or metals can be adjusted or even controlled. These MC-MOFs can be prepared directly, using more than one ligand or metal in the synthesis, or formed by post-synthetic modification. A second class of MC-MOFs has core–shell structures, and these can be prepared through epitaxial growth of one MOF on the surface of another or post-synthetic modification of the crystal surfaces [61] as shown in Figure 4.7.10.

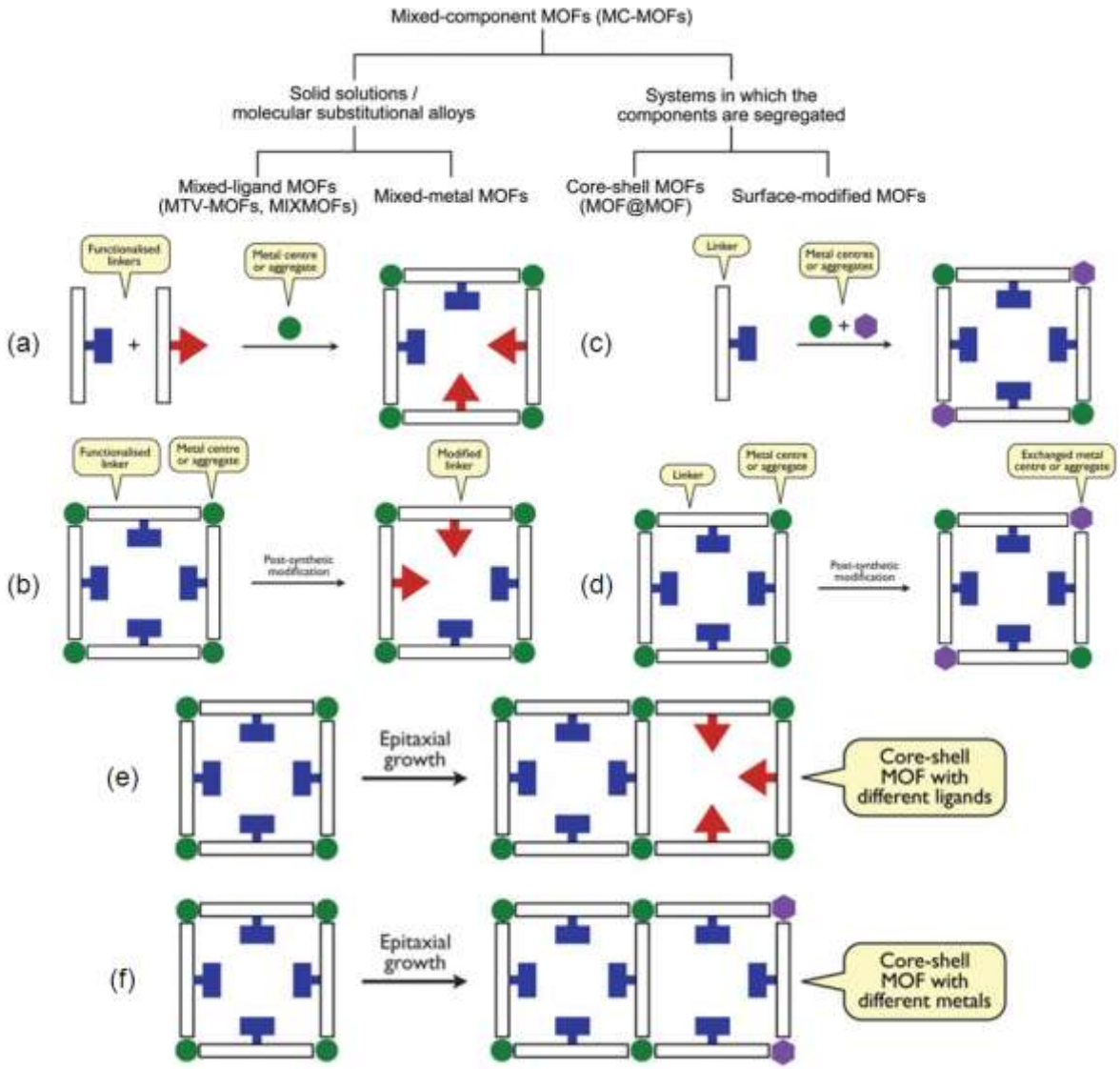

Figure 4.7.10: The different categories of mixed-component MOFs (up) and schematic representation to generate MC-MOF by using (a) isosteric ligands with different substituents, (b) post-synthetic modification, (c) different metal centres, (d) post-synthetic substitution of some of the metal centres, (e) core–shell approach with different ligands and (f) core–shell approach with different metals. (Figure was reproduced from ref. [61], Copyright, The Royal Society of Chemistry 2011)

Fang and co-workers [62] summarized a number of MOFs adapting the acid–acid, acid–base and base–base mixed ligand strategy and also the influence of the solvent, pH conditions, metal ions and synthetic route on the assembly.

Zheng and co-workers [63] introduced in their review some factors influencing the assembly of metal organic coordination polymers such as positional isomerism, substituents and spacers of organic ligands, the coordination mode with metal centers, SBUs, solvents, metal ions and so on that have prominent influence on the formation, structure and properties of MOFs. But the control of the product structure still remains a challenge in this field due to the

fact that the self-assembly process is affected by other various external physical or chemical factors including counterions [64], template, temperature [65], pressure, solvent [66], pH value, etc.

Zeng and co-workers [67] presented review to highlight the use of the concept of mixed organic ligands, where two or more organic ligands have independent roles in the development of different structural topologies, from a range of materials from some selected typical examples mainly focus on the critical role of matching mixed ligands of different sizes, shapes, and coordination features and the resulting 3D structures of cluster based MOFs, pillared-layer, rod-spacer, special interpenetrated system, and some related pillared-bilayer and interdigitated structures. These compounds not only show interesting structure arrays and various crystal to crystal transformations but also show a unique performance in magnetism, iodine enrichment and controlled release, heterogeneous catalysis, luminescence sensing and other properties. A number of parameters needed to be taken into account at the synthesis, for example, the solubility of ligands, competition of ligands to coordination with metal ions, thermodynamic and dynamic equilibrium, crystal growth and others. When additional complementary organic ligands such as a polycarboxylate or a small polydentate chelating ligand like lactate, glycolate, or 3-hydroxypicolinate was introduced, it found that the one metal node changes to more complex SBUs having 0D polynuclear clusters, 1D chains or rods or 2D layers. Connecting these SBUs by linear linkers like pyridine-carboxylate results in structures of polynuclear cluster-spacer [68], rod-spacer MOFs [69], and pillared-layer [70] as shown in Figure 4.7.11. Apparently, the advances made towards mixed ligand MOFs would be helpful for gaining a better understanding and extending the synthetic chemistry of MOFs [67].

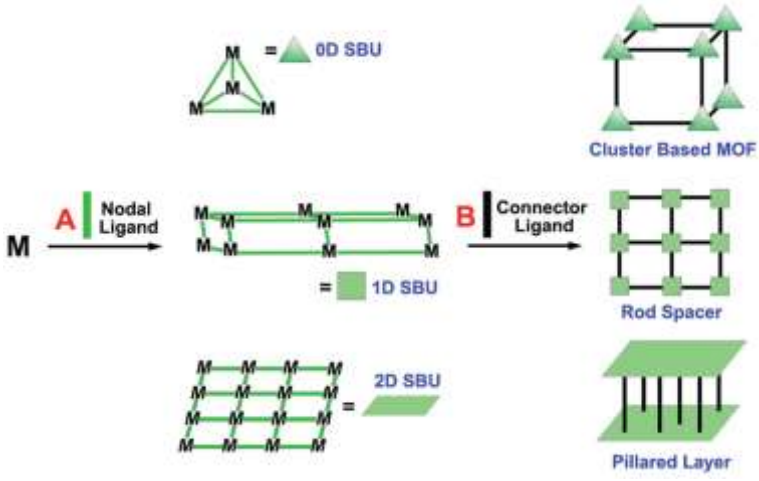

Figure 4.7.11: Concept of mixed organic ligand MOFs. (Scheme was reprinted from ref. [67], Copyright, The Royal Society of Chemistry 2015)

5.8 Multifunctional properties of coordination polymers

Porous coordination polymers (PCPs) or metal-organic frameworks (MOFs) are crystalline materials [71] with designable or tunable porosity (nano/microporous material, solvent control, anion control etc.) [72], and structural variability (architecture, interpenetration, noncovalent interactions, helices, chirality of linkers, etc.) [73]. Therefore PCPs have a great interest for potential applications [74] (Figure 4.8.1) [1]. Metal-organic coordination polymers could be used for gas storage [75], separation processes [76], reversible host guest interactions [77], sensor technology [78], catalysis [79], luminescence [80], non-linear optics (NLO, frequency doubling) [81], ionic or electronic conductivity [82], magnetism [83] and low temperature heating and cooling through reversible water de- and adsorption [84]. Interesting applications of metal organic coordination polymers are presented in Figure 4.8.1.

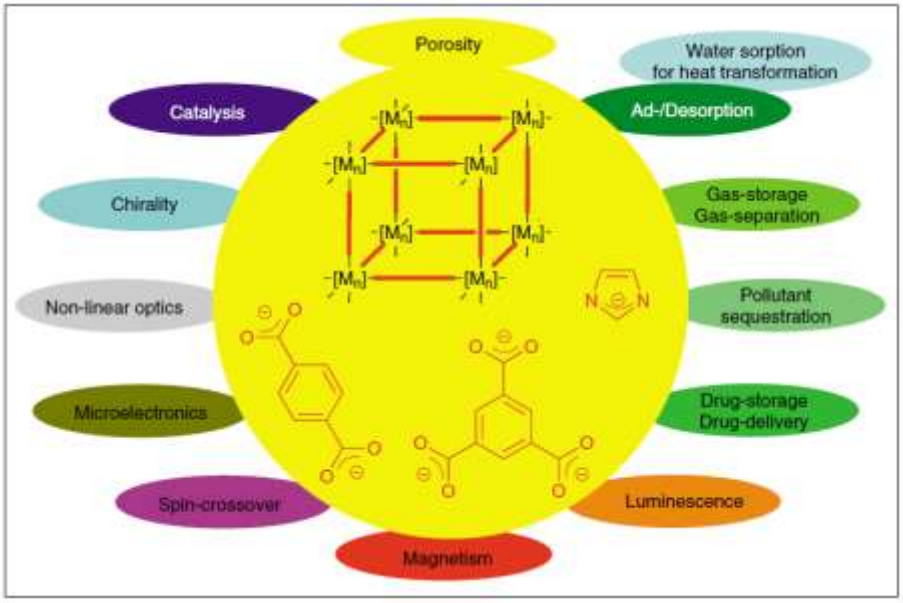

Figure 4.8.1: Presentation of multifunctional properties of coordination polymers (PCPs/MOFs) with prototypical linkers. (Figure was reprinted from ref. [1a,c] [84d], Copyright Schweizerische Chemische Gesellschaft).

6 Objectives of the work (Tasks)

One aim of the present work was to synthesize new coordination polymers with combined multidentate azole-carboxylate ligands, and – if successful – to study their properties such as thermal stability and magnetism and their applications as for heat transformation, gas storage, etc. Hitherto not used 4-(3,5-dicarboxyl-1,2,4-triazol-4-yl)aromatic ligands (Scheme 5.1) directed our attention towards synthesizing them and utilizing them for the formation of new coordination polymers.

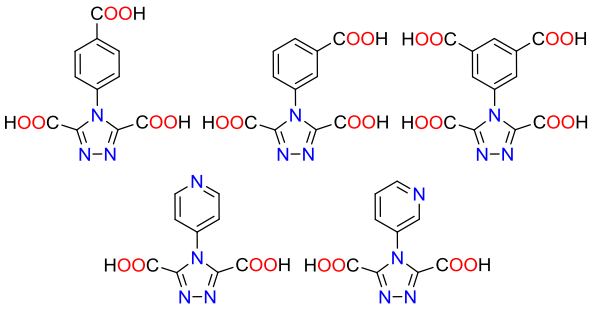

Scheme 5.1: Structure of targeted new combined multidentate azole-(protonated)carboxylate 4-(3,5-dicarboxyl-1,2,4-triazol-4-yl)aromatic ligands.

The preparation of new coordination polymers by using a mixture of ligands (Scheme 5.2) was another aim of this work. The composition of coordination polymers by using mixture of ligands are difficult to foresee and to obtain, because only one of both ligands may be coordinated with the metal ions.

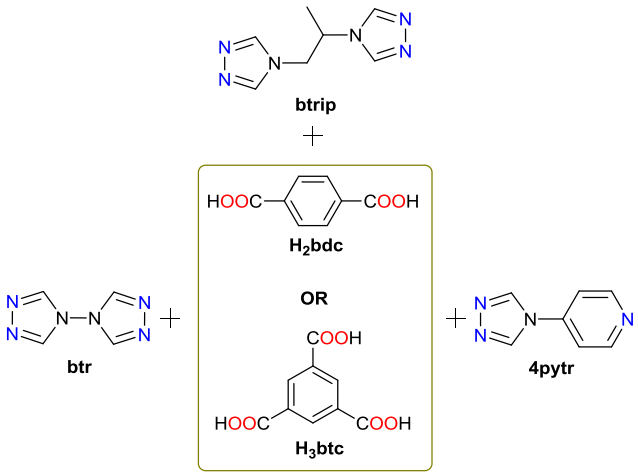

Scheme 5.2: Used triazole and protonated carboxyl ligands for the preparation of new mixed-ligand coordination polymers.

In all cases, an aim was to investigate the obtained compounds for their structures and properties. As part of the structures the supramolecular interactions like the hydrogen-bonding networks should be analyzed for their contribution to the crystal packing.

Crystallography has become the most important method of structure determination, for this reason, suitable crystals for single crystal X-ray analysis should be obtained. In addition, new compounds should by characterized and analyzed by elemental analysis, FT-IR, NMR, thermogravimetric analyis and powder X-ray diffraction.

7 Results and discussion

7.1 Synthesis of ligands

7.1.1 Synthesis of 1,2,4-triazole derivative ligands

Three different chemical ways can be used to obtain 1,2,4-triazole ligands with one or two triazole rings (Scheme 6.1.1.1). In the first route, the reaction was carried out by heating the amino component and diformylhydrazine to 160-190 °C for 10-30 min [85]. In the second route, the amino component was reacted with monoformylhydrazine and orthoformate in dried methanol [23g],[86]. While in the third route, the amino component was reacted with *N,N`*-dimethylformamide azine using *p*-toluene sulfonic acid monohydrate as a catalyst in dried organic solvent at 120-150 °C [22a],[87],[88].

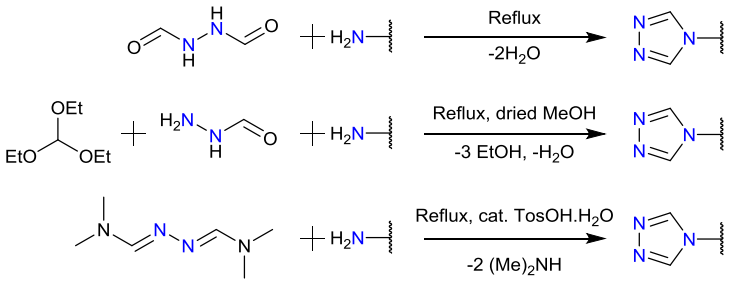

Scheme 6.1.1.1: Possibile synthesis routes to 1,2,4-triazole ligands.

In this thesis, the ligands 4,4`-bis(1,2,4-triazole) (btr), 1,2-bis(1,2,4-triazol-4-yl)propane (btrip), 3-(1,2,4-triazol-4-yl)pyridine (3pytr), 4-(1,2,4-triazol-4-yl)pyridine (4pytr), and 5-(1,2,4-triazol-4-yl)isophthalic acid ($5H_2$iptr) were synthesized according to the third method in Scheme 6.1.1.1 [87a]. All reactions were carried out under inert conditions.

First *N,N`*-dimethylformamide azine was synthesized from thionyl chloride, $SOCl_2$, *N,N`*-dimethylformamide, DMF, and hydrazine monohydrate, $N_2H_4.H_2O$ according to Scheme 6.1.1.2 [87a].

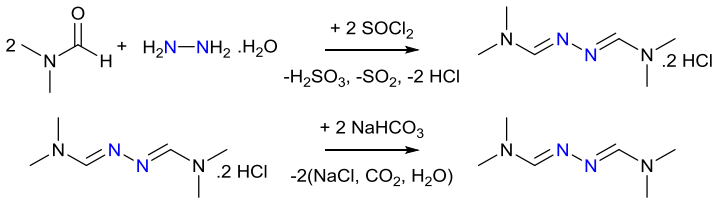

Scheme 6.1.1.2: Synthese of *N,N`*-dimethylformamide azine.

The reaction mechanism of *N,N`*-dimethylformamide azine dihydrochloride formation involves the reaction of the amide with phosphorus oxychloride or thionyl chloride to produce an electrophlic iminium cation [89]. The electrophilic action of both nitrogen atoms of hydrazine react *via* a Vilsmeier complex and produce the unstable iminium ion, which then decomposes to give *N,N`*-dimethylformamide azine dihydrochloride (Scheme 6.1.1.3).

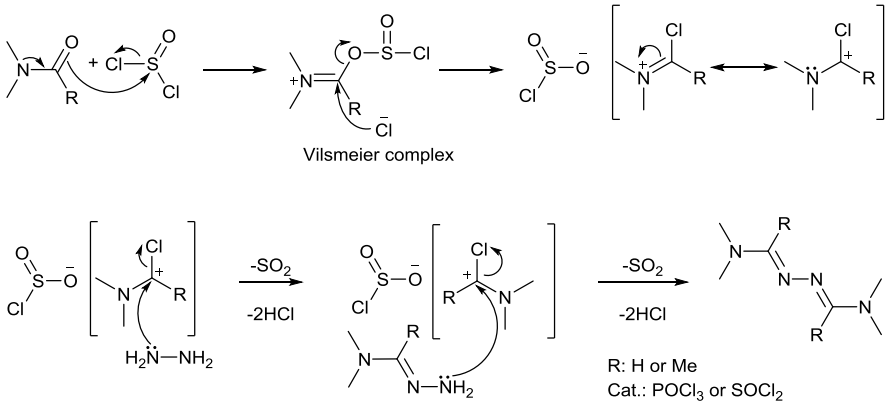

Scheme 6.1.1.3: The mechanism of *N,N`*-dimethylformamide azine dihydrochloride formation.

N,N`-dimethylformamide azine, the mono- or diamino substrate and *p*-toluenesulfonic acid monohydrate as a catalyst were reacted to the triazole derivative according to Scheme 6.1.1.4.

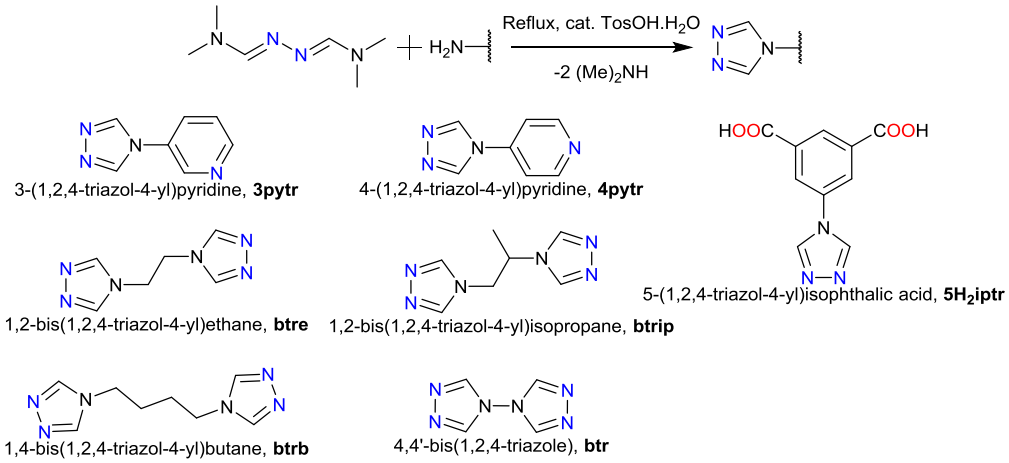

Scheme 6.1.1.4: General synthesis of different 1,2,4-triazol derivative ligands used in this work.

In the suggested mechanism the heterocyclization of substituted 1,2,4-triazol-4-yl compounds through the reaction of *N,N`*-dimethylformamide azine, DMFA with primary amines is catalysed by acid. It is assumed, that in the first step the DMFA molecule is protonated to form a quaternary ammonium transition state which further reacts with a primary amine. The resulting quaternary ammonium compound eliminates Me_2NH and undergoes an intramolecular cyclization. The elimination of a second molecule of Me_2NH with the subsequent elimination of a proton leads to the formation of the targeted 1,2,4-triazoles (Scheme 6.1.1.5) [90].

1,2-Bis(1,2,4-triazol-4-yl)propane (btrip) is chiral ligand. For basic studies on the btrip coordination chemistry the ligand was synthesized as the racemate here from *rac*-1,2-diaminopropane. We just note for follow-up studies that chiral metal-organic frameworks MOFs are of interest in catalysis and material chemistry [91].

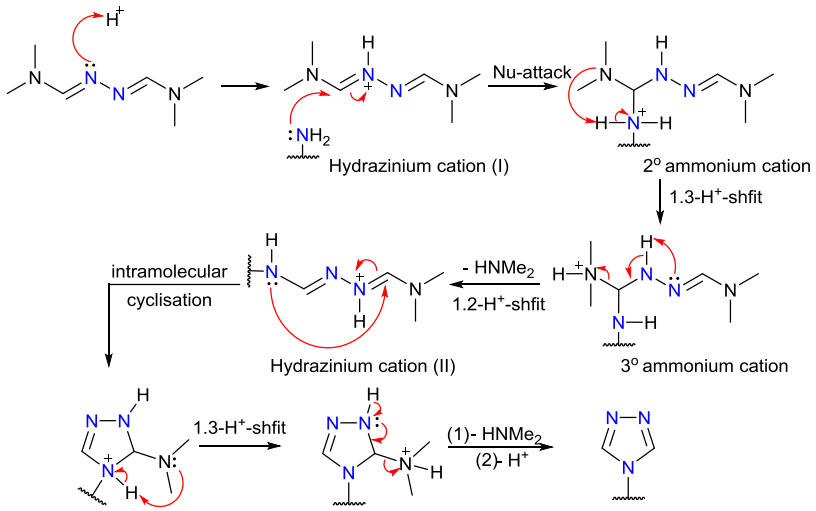

Scheme 6.1.1.5: The mechanism of hetrocyclisation reaction of substituted 1,2,4-triazol-4-yl ligands [90].

7.1.2 Synthesis of 1H-tetrazole derivative ligands

Different possible reactions under different conditions (reflux, hydro-, solvothermal reaction and microwave), catalysts and solvents allow to obtain different 5-substituted 1H-tetrazole ligands with one or two 1H-tetrazole rings, when sodium azide NaN_3 is used as reagent [92] [93]. 5-Substituted 1H-tetrazole derivatives can be prepared in good yields from alkyl and aryl nitrile derivatives according to the general procedure shown in Scheme 6.1.2.1, where the primary nitrile component is stirred under reflux with sodium azide and amonium chloride in a molar ratio of 1:1:1 with triethylamine (Et_3N) as a catalyst and solvent for a time dependent on the reactivity of the nitrile derivative. A high reaction temperature and long reaction time are effective to obtain higher yield.

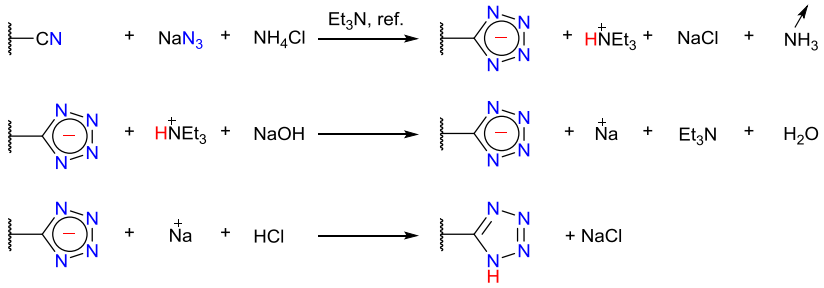

Scheme 6.1.2.1: General synthesis of 5-substituted 1H-tetrazole derivatives used in this work.

The general mechanism for the reaction appears to be a nucleophilic attack of azide ion on the carbon of the nitrile group, followed by ring closure of the imino azide to form the tetrazole ring. Apparently, a charge ($+\delta$) on the nitrile carbon is necessary for the azide ion attack since conditions which enhance or favor such a charge increase the rate of reaction. The reaction has been found to be subject to general acid catalysis. Coordination of a Lewis acid with the nitrile carbon or proton with the nitrile nitrogen would generate a charge ($+\delta$) on the nitrile carbon and make the nucleophilic attack of the azide ion possible. It is likely that a (triethyl)ammonium cation $[Et_3NH]^+$ or $[NH_4]^+$ could provide the necessary charge ($+\delta$) on the nitrile carbon to activate the nitrile towards azide addition while allowing for the use of only one equivalent of azide salt in these reactions (Scheme 6.1.2.2). Hydrazoic acid, amine hydrazides and Lewis acids, such as BF_3, $AlCl_3$ more than double the yield of 5-substituted tetrazole from substituted nitrile. The solubility of the azide salt also influences the rate of reaction [94],[95].

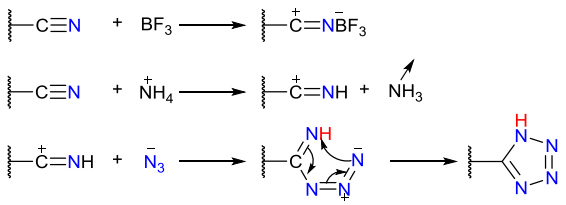

Scheme 6.1.2.2: General reaction mechanism for the formation of 5-substituted 1H-tetrazole derivatives [94],[95].

7.1.3 Synthesis of new combined 3,5-dicarboxyl-triazol-4-yl derivate ligands

3,5-Dimethyl-1,2,4-triazol-4-yl derivates can obtain from the reaction of *N,N`*-dimethylacetamide azine, DMAA with primary aromatic amines (Scheme 6.1.3.1). *N,N`*-dimethylacetamide azine, was synthesized under same reaction conditions as *N,N`*-dimethylformamide azine, DMFA by using either $SOCl_2$ or $POCl_3$ as catalysts. It was noticed that DMAA is hygroscopic (Scheme 6.1.3.2) [88],[96].

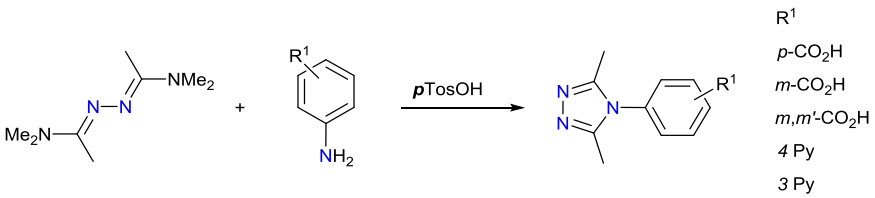

Scheme 6.1.3.1: Synthesis of 3,5-dimethyltriazol-4-yl derivates from DMAA [88],[29].

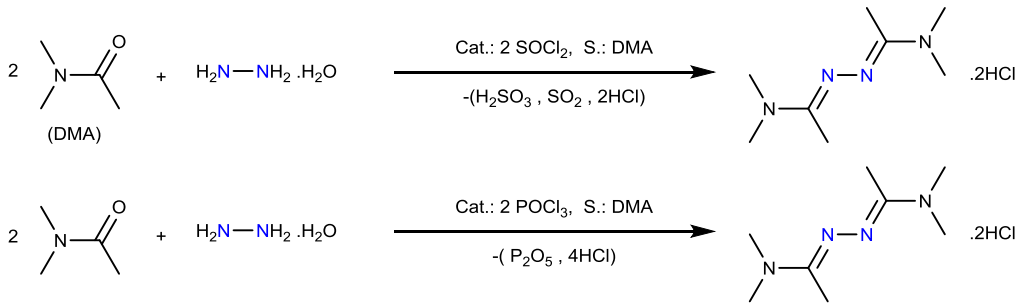

Scheme 6.1.3.2: Synthesis of *N,N`*-dimethylacetamide azine, DMAA.

Interestingly, the reaction between *N,N`*-dimethylformamide azine and the amino component in presence of a catalytic amount of *p*-toluenesulfonic acid, *p*TosOH, depends upon the structure of substrates and reaction conditions. Under extra dry conditions the reaction of

N,N`*-dimethylformamide azine, DMFA or *N,N`-dimethylacetamide azine, DMAA with Ar-NH_2 catalyzed by *p*TosOH leads to the co-crystallization of the corresponding 4-substituted-1,2,4-triazoles [87a,c],[88],[90],[96] *via* a transamination reaction. The proposed multi-step mechanism depicted in Scheme 6.1.3.3 for this transamination reaction involves: (i) Protonation of the DMFA or DMAA molecule by *p*TosOH to give the corresponding hydrazinium cation (I). (ii) Nucleophilic attack by a primary amine at the α-position to the hydrazinium moiety. (iii) 1,3 proton-transfer through the N-C-N fragment of the secondary ammonium cation to form the tertiary ammonium cation. (iv) The resulting tertiary ammonium cation eliminates a molecule of Me_2NH to give the hydrazinium cation (II) which further undergoes an intramolecular cyclisation. (v) The further elimination of a second molecule of Me_2NH with the subsequent elimination of a proton leads to the formation of the targeted 1,2,4-triazoles (Scheme 6.1.3.3). The suggested mechanism is in line with the reaction of amidines with primary amines, catalysed by acid [90].

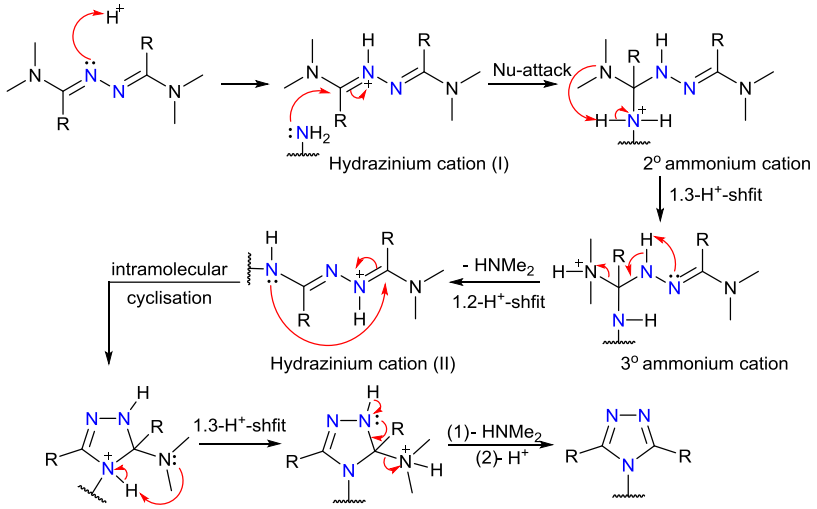

Scheme 6.1.3.3: Proposed mechanism for the synthesis of 3,5-disubstituted-1,2,4-triazol-4-yl derivates from DMAA or DMFA and primary amines [90].

Unfortunately, the reaction of DMAA with a pyridyl amine or carboxyl-substituted aryl amine mediated by *p*-toluenesulfonic acid monohydrate, *p*TosOH·H_2O failed to yield any 3,5-disubstituted-1,2,4-triazol-4-yl derivate, regardless of the reaction conditions, but instead the acetamide derivative was obtained (Scheme 6.1.3.4).

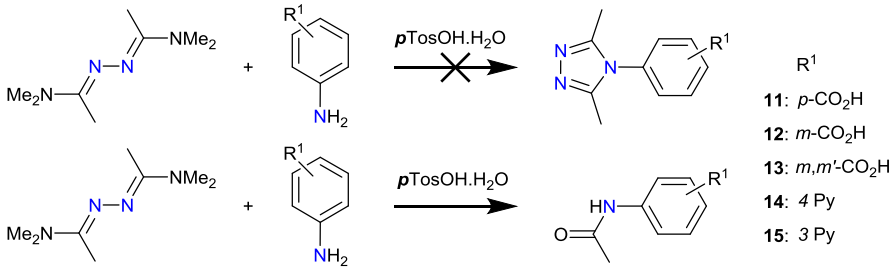

Scheme 6.1.3.4: Reaction synthesis of acetamide derivatives.

This can be attributed to the competitive nucleophic attack in the hydrazinium cation (II) between a water molecule and the aromatic amine. The nucleophilicity of a nucleophile depends on the "availability" of the non-bonded pair of electrons (NBEs) for attack at an electrophilic center. Thus electronic, represented in electron-withdrawing substituents (C=N and aromatic moiety) and steric factors reduce the nucleophilicity of the amino component and hinder its nucleophic attack in the hydrazinium cation (II). Consequently prevent the intramolecular cyclisation. The proposed mechanism for such reaction is illustrated in Scheme 6.1.3.5.

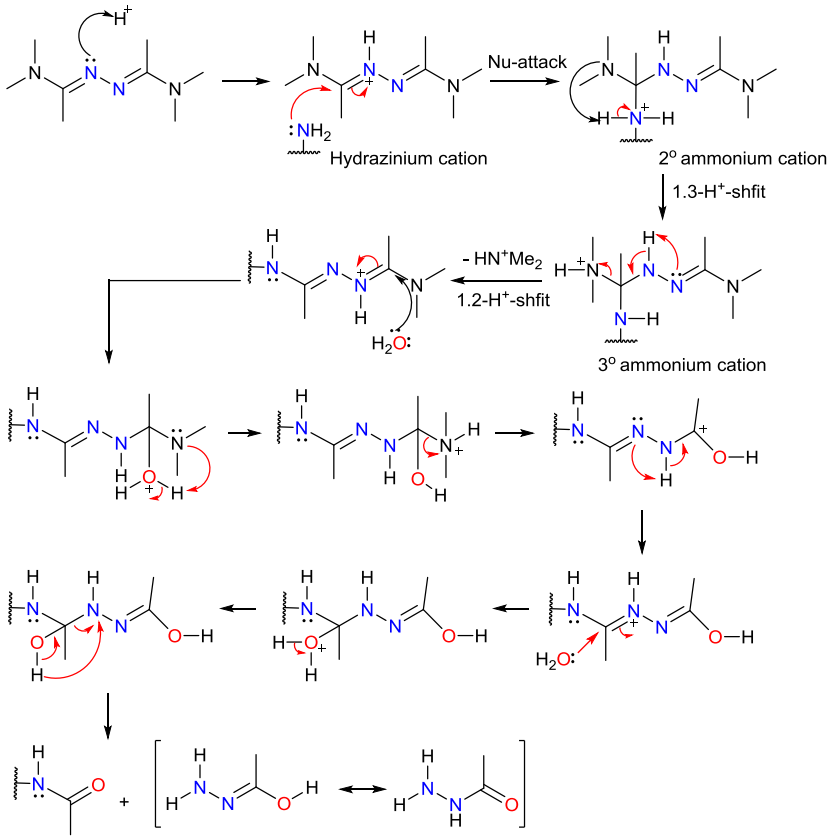

Scheme 6.1.3.5: Proposed mechanism of the competitive nucleophic attack in the hydrazinium cation (II) between a water molecule and the aromatic amine, when the reaction yields acetamide derivatives [87a,c],[88],[90],[96].

Dr. Daniel Lässig has reported in his publication (Scheme 6.1.3.6) [88] that it is possible to obtain 3,5-dimethyl-1,2,4-triazol-4-yl derivates from the reaction of *N,N`*-dimethylacetamide azine, DMAA with a primary aromatic amine by using *p*-toluenesulfonic acid, *p*TosOH as catalyst under inert reaction conditions. But Dr. Jörg Linke has written in his Thesis [35, page 15-17], that 3,5-disubstituted-1,2,4-triazol-4-yl derivates can be obtained from the reaction of 2,5-disubstituted-1,3,4-oxadiazole with primary aromatic amine by using *p*-toluenesulfonic acid *p*TosOH as catalysis under inert conditions. In this work, when the primary aromatic amine was reacted with *N,N`*-dimethylacetamide azine under inert conditions using *p*-toluenesulfonic acid monohydrate *p*TosOH.H_2O as catalyst acetamide derivatives were obtained. Probably, one has to dry the catalyst in order to obtain 3,5-dimethyl-1,2,4-triazol-4-yl derivates, because it was noticed that DMAA was hygroscopic and the previously proposed mechanism (Scheme 6.1.3.6) explained, why the reaction yielded to acetamide derivatives and not 3,5-dimethyl-1,2,4-triazol-4-yl derivates, if the reaction mixture contained some water.

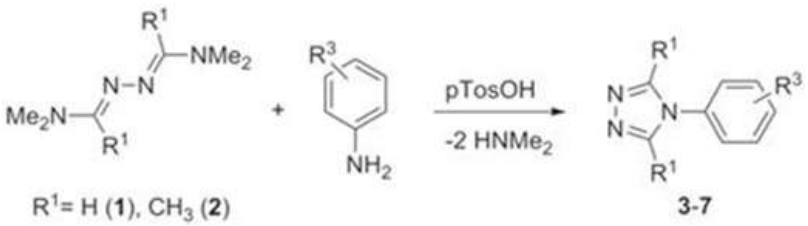

R^1	R^3	Pro-duct	compound	yield in %	Mp. in °C (decomp.)
H	p-CO_2H	**3**	H(trz-pba)	70	327
H	m-CO_2H	**4**	H(trz-mba)	65	264
H	m,m'-CO_2H	**5**	(H_2NMe_2)H(trz-ia)	45	238
CH_3	p-CO_2H	**6**	H(Me_2trz-pba)	77	322
CH_3	m-CO_2H	**7**	H(Me_2trz-mba)	81	257

Scheme 6.1.3.6: General reaction for the synthesis of 3,5-disubstituted-1,2,4-triazol-4-yl derivate ligands. Equation and Table are taken from Ref. [88].

7.2 Coordination polymers with mixed-ligands constructed from 1,2-bis(1,2,4-triazol-4-yl)propane or 4-amino(1,2,4-triazol-4-yl) and carboxylate ligands

7.2.1 Introduction

The preparation of new coordination polymers by using a mixture of ligands, cannot be easily predicted because there are different possible results as one or both ligands may be coordinated to metal ions with or without solvent molecules. Therefore the formation of single crystals and their characterization through NMR- and IR-spectrometry was very important before stucture determination. The coordination polymers with the used carboxylate ligands were already known. The different possible results are show in Scheme 6.2.1.1.

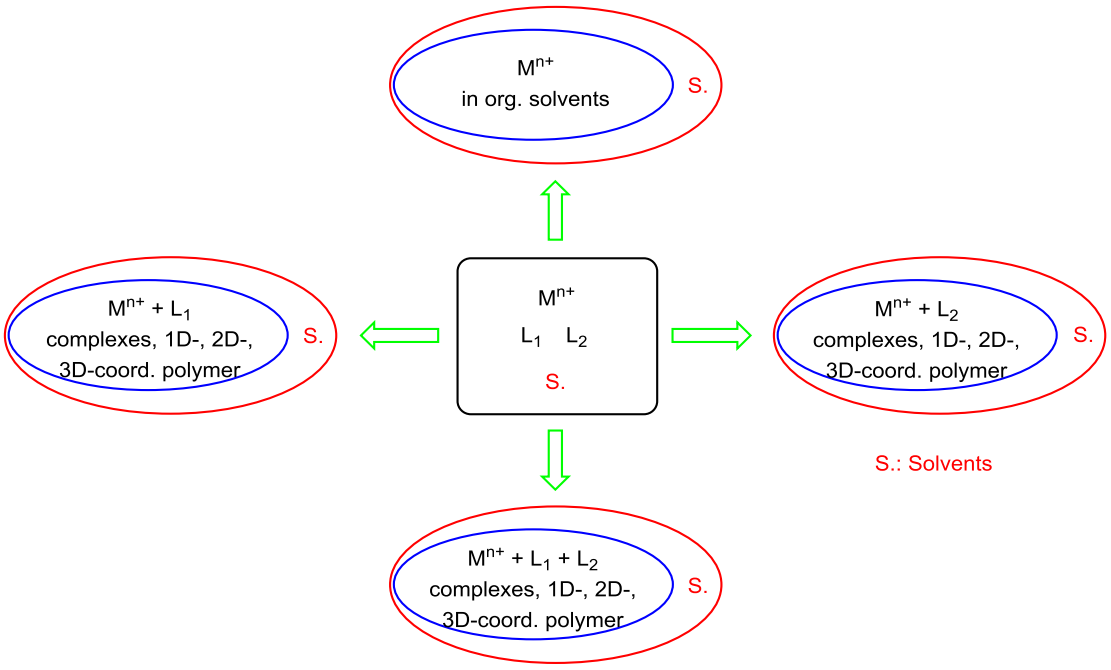

Schema 6.2.1.1: Different possible results of prepared coordination polymers by using a mixture of ligands.

7.2.2 Structure analysis and characterization of 3D-{[Cu_4(μ-OH)$_2$(μ-bdc)$_2$(μ$_4$-*rac*-btrip)$_3$] (NO_3)$_2$(H_2O)$_{10}$}$_n$ (16)

An aqueous solution of copper(II) nitrate hydrate, racemic 1,2-bis(1,2,4-triazol-4-yl)propane (*rac*-btrip) and benzene-1,4-dicarboxylic acid (H_2bdc) were mixed in a glass tube. NH_3 was used as base to deprotonate H_2bdc. The sample was heated in a programmable heating oven to 125°C. Blue single crystals albeit no phase pure (Figure 6.2.2.1) were obtained from the hydrothermal reaction. The resulting crystals were filtered, washed with mother liquor and then with *ca.* 20 ml of methanol. The reaction was repeated several times and found reproducible. Freshly prepared crystals were small and light blue, but after *ca.* two months in mother liquor the crystals were grown in size with color deepening (Figure 6.2.2.1). Freshly single crystals were manually separated and used for the subsequent characterization and analysis.

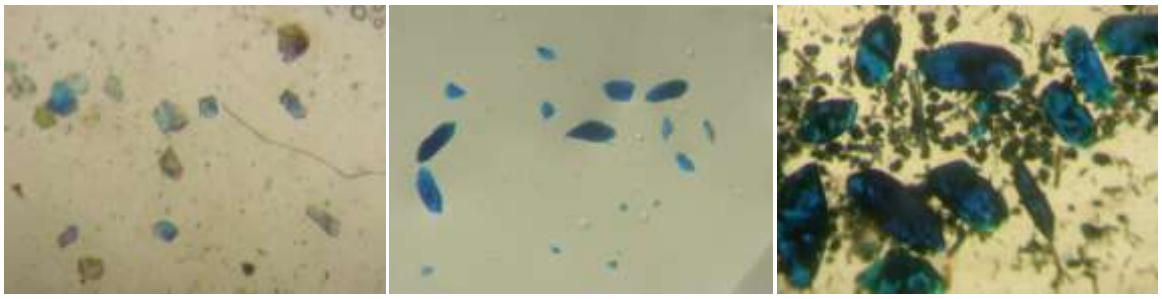

Fig. 6.2.2.1: Crystals images of **16** freshly formed (left) and after more than one month in the mother liquor (right).

Proton NMR analysis of a sample of **16** digested in NaOD/D_2O gave a molar btrip : bdc ratio close to 3:2 (see below). Single-crystal X-ray structure analysis revealed a novel 3D coordination polymer of formula 3D-{[Cu_4(μ-OH)$_2$(μ-bdc)$_2$(μ$_4$-*rac*-btrip)$_3$]·(NO_3)$_2$(H_2O)$_{10}$}$_n$ **16** which crystallizes in the monoclinic crystal system, with the centrosymmetric space group *C 2/m* with two formula units (Z = 2) per unit cell. One copper atom, half of a bdc^{2-} anion, two halves of both *R*- and *S*-configured btrip ligand and a bridging hydroxido ligand form the asymmetric unit of the cationic network (hence space group Z = 8).

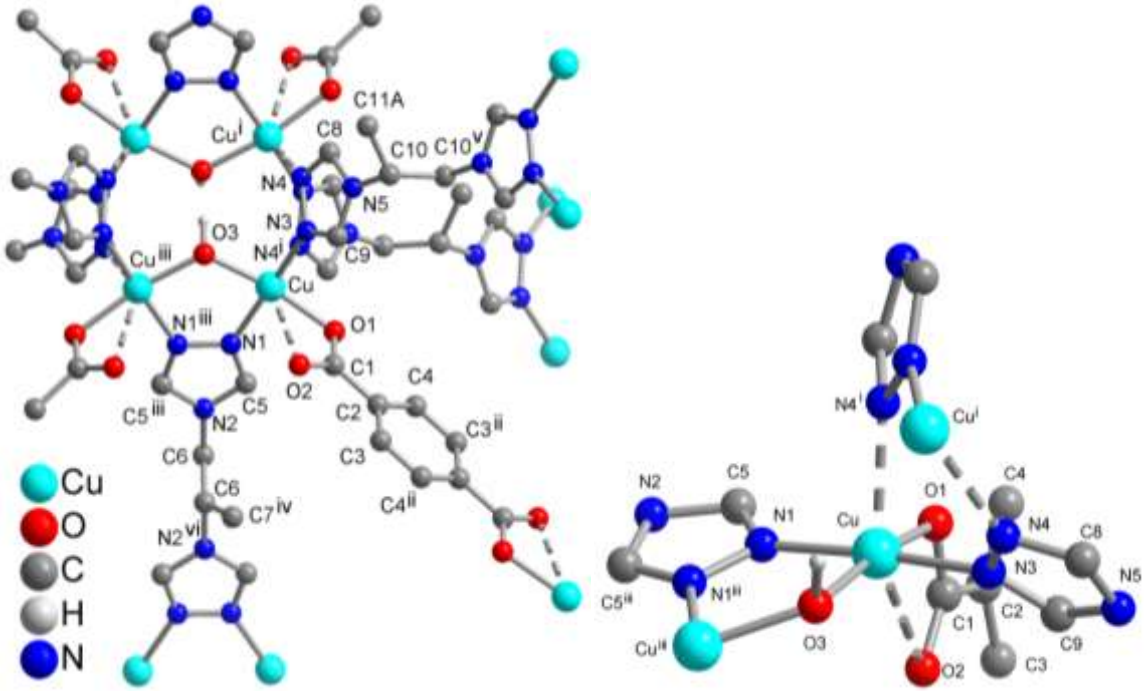

Figure 6.2.2.2: Left: Extended building unit of the cationic network in **16**. Only one position of the symmetry-disordered methyl groups is shown. Right: Jahn-Teller distorted Cu coordination sphere. Hydrogen atoms are omitted for clarity except on the bridging hydroxido ligand. Symmetry transformations : i = -x+1,y,-z+1; ii = -x+1/2,-y+1/2,-z; iii = x,-y+1,z; iv = -x+1,-y+1,-z; v = -x+1/2,-y+1/2,-z+1; vi = -x+1,y,-z.

The Cu coordination sphere is essentially square pyramidal (τ = 0.13) [97] with a long sixth contact from the second carboxylate oxygen atom. Thus, the carboxylate group approaches a chelating coordination to Cu (Fig. 6.2.2.2, right).

Table 6.2.2.1: Selected bond lengths [Å] and angles [°] for **16**.

Cu-N1	2.012(2)	N3-Cu-N4^{i}	89.89(8)
Cu-N3	1.9842(19)	O1-Cu-N1	89.20(8)
Cu-N4^{i}	2.327(2)	O1-Cu-N4^{i}	86.63(7)
Cu-O1	1.9880(16)	O3-Cu-N1	86.89(8)
Cu-O2	2.716(2)	O3-Cu-N3	90.83(8)
Cu-O3	1.9189(10)	O3-Cu-N4^{i}	104.82(8)
O1-C1	1.275(3)	O3-Cu-O1	168.13(8)
C1-O2	1.244(4)	N3-Cu-O1	92.35(8)
N1-Cu-N4^{i}	94.12(8)	N3-Cu-N1	175.78(8)

Symmetry transformations used to generate equivalent atoms: i = -x+1,y,-z+1.

The structure consists of a tetranuclear SBU in which the four Cu^{+2} cations form a rectangle and are bridged by two hydroxido ligands above and below the frame of the rectangle, and six triazole rings of *rac*-btrip ligands above and below outside of the rectangle (Fig. 6.2.2.3). Each hydroxido and triazole ring bridges between two Cu^{+2} atoms. The distances between Cu atoms in the SBU vary from 3.9024 Å (bridged by btrip ligand type A-blue), 3.3970 Å (bridged by btrip ligand type C-yellow and hydroxido ligand) to 5.1738 Å (diagonal). Each carboxylate group of bdc^{2-} ligand is coordinated with one Cu atom (Fig. 6.2.2.2, 6.2.2.3 and 6.2.2.4).

In the right part of Fig. 6.2.2.2 it is shown that, each Cu(II) ion is coordinated to three nitrogen atoms (N1, N3 and N4) from three separate *R*- or *S*-btrip ligands, one to two oxygen atoms (O1 and O2) of the carboxylate groups of bdc^{2-} ligand and one oxygen atom (O3) of hydroxido (Figure 6.2.2.2). The bond Cu-N4 and especially the contact Cu-O2 is longer than the other Cu-ligand bonds in this structure. Selected bond lengths and angles are summarized in (Table 6.2.2.1).

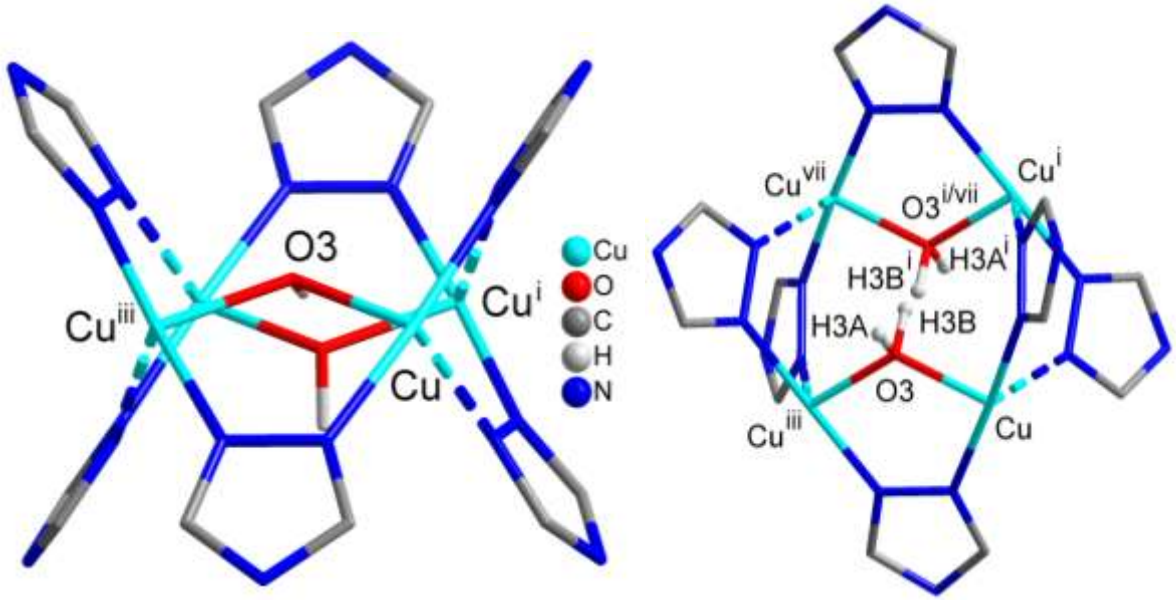

Fig 6.2.2.3: Tetranuclear SBU with the Cu_4 rectangle, the copper-bridging triazolyl and hydroxido groups. Carboxylate groups are not shown for clarity. The H atom on the hydroxido ligand was calculated disordered over two positions using AFIX 23 with half occupancy each. Otherwise, the (O)H atoms on the two bridging OH ligands would point at each other because of their symmetry relationship. Details of the H-bond contact are given in Table 6.2.2.2. Symmetry transformations : i = -x+1,y,-z+1; iii = x,-y+1,z; vii = -x+1, -y+1, -z+1.

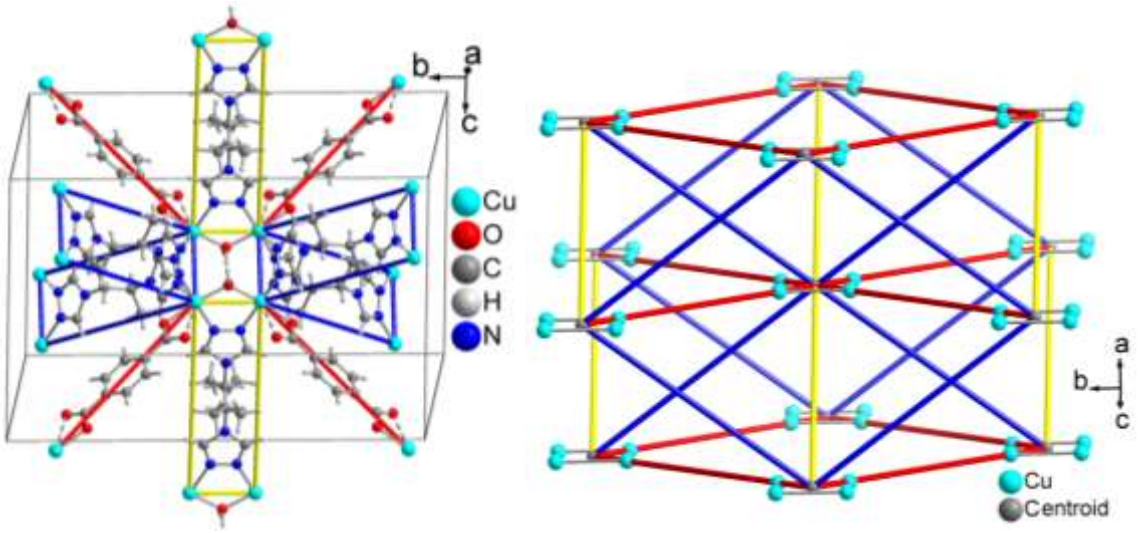

Figure 6.2.2.4: Left: Full bridging ligands around a $Cu_4(\mu\text{-}OH)_2$ SBU 3D-{$[Cu_4(\mu\text{-}OH)_2(\mu\text{-}bdc)_2(\mu_4\text{-}rac\text{-}btrip)_3]\cdot(NO_3)_2(H_2O)_{10}\}_n$ in **16**. The different ligand connection types are color coded for topological Cu-Cu contacts (ligand type A blue, type B red and type C yellow). Right: Network topology of the uninodal 10-c net showing the 10-connectivity around a central $Cu_4(\mu\text{-}OH)_2$ SBU to its neighbors.

There are two independent bis(triazolyl)propene ligands in the structure. Both ligands sit on a special position. For ligand A-blue (N3-N4-C8-N5-C9-C10-C11) the special position bisecting the C10-$C10^{v}$ bond (cf. Fig. 6.2.2.2) is a two-fold axis. Hence, the methyl group C11 is disordered over two positions. For ligand C-yellow (N1-C5-N2-N6-C7) this is a mirror plane and a two-fold axis. Hence, the methyl group C7 is disordered over four positions and was refined with a PART command. As both *rac*-btrip ligands have a disorder in the position of their methyl group; it is therefore not possible to assign an individual chirality to each ligand. Each btrip and each bdc ligand bridges to a neighboring tetranuclear SBU. Thus, the SBU is a 10-coordinated node (see also below for the assignment of the network topology). Fig. 6.2.2.4 depicts the two different btrip ligands either as type A-blue or as type C-yellow and the bdc ligand as type B-red. It can be noted that from the stoichiometric ratios of bdc : btrip = 1 : 1 and 1 : 2 offered during synthesis the two ligands are incorporated in a 1 : 1.5 ratio in this mixed-ligand coordination network. Examination of the 3D-network of 3D-{$[Cu_4(\mu\text{-}OH)_2(\mu\text{-}bdc)_2(\mu_4\text{-}rac\text{-}btrip)_3]\cdot(NO_3)_2(H_2O)_{10}\}_n$ **16**, then highlights the bridging action of the three different ligands between the tetranuclear SBUs by color. The four blue btrip ligands (type A) are arranged *cis* to each other, above and below the plane of the Cu atoms in the tetranuclear SBU. Four red lines of the bdc^{2-} ligands are in the equatorial sites (type B) and two yellow btrip ligands (type C) are arranged *trans* to each other, above and below the Cu_4 plane (Fig. 6.2.2.4).

The topology of this 3D mixed-ligand framework is a 10-c uninodal (Cu_4 taken as metal node) net of type bct [98], 10/3/t1 or sqc8 with the point symbol ($3^{12}.4^{28}.5^5$) [99] as analyzed by the program package TOPOS 4.0 (vertex symbol [3.3.3.3.3.3.3.3.3.3.3.3.4.4.4.4.4.4.4.4.4(2).4(2).4(2).4(2).4(2).4(2).4(2).4(2).*.*.*.]. [100], [101] The 10-connected network topoloy of the Cu_4 nodes is depicted in Fig. 6.2.2.4.

The μ-connectivity of nitrogen atoms (N3 and N4) of *rac*-btrip ligands (type A-blue) with Cu atoms of $Cu_4(\mu\text{-}OH)_2$ lead to Cu-btrip-zigzag chains in **a** axis direction. The interchain distance between two Cu-atoms of the 1D zigzag chain is Cu···Cu = 16.183 Å and the shortest distance is Cu···Cu = 10.9907 Å. These zigzag chains are connected to each other *via* SBUs in **b** axis direction, so that a layer from zigzag chains and SBUs are built, which are stacked parallel to **ab** plane with an interlayer distance 8.1186 Å of their neighboring planes (dihedral between two planes is 0.00°) as shown in (Fig. 6.2.2.5, right). The alternating layers of zigzag chains have the opposite zigzag chain direction. This leads to **ABAB…** layers parallel to the **ab** lattice plane.

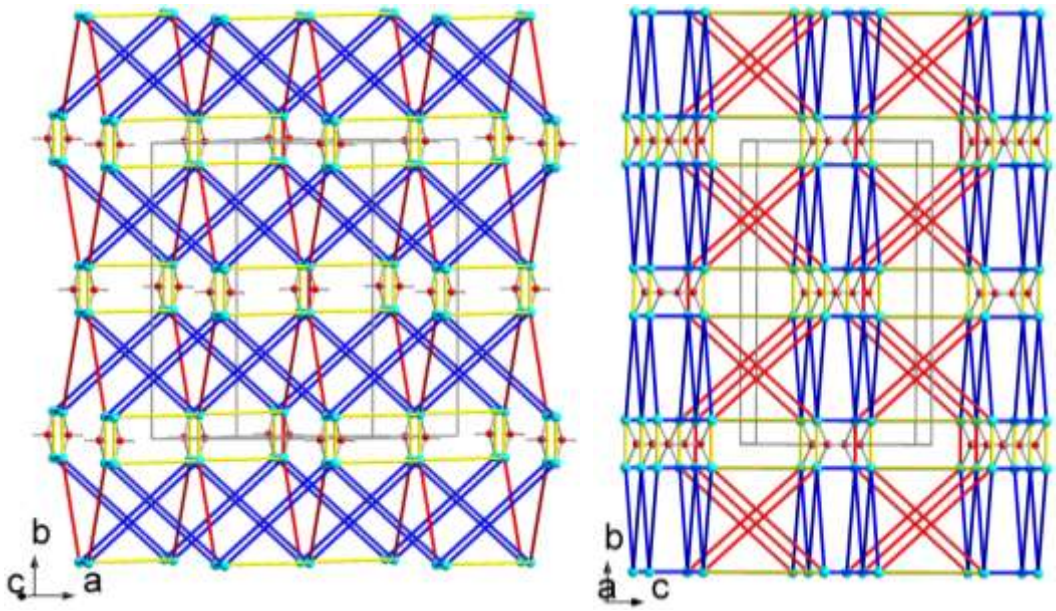

Fig. 6.2.2.5: The network of **16** viewed along the **c**-axis (left) and **a**-axis (right) The infinite 1D zigzag chains of *rac*-btrip ligands (type A) and $Cu_4(\mu\text{-}OH)_2$ are orientated in the **a** axis direction, the other infinite 1D corrugated chains of bdc^{2-} ligands (type B) and $Cu_4(\mu\text{-}OH)_2$ are orientated in the **b** axis direction. (For connectivity color codes see Fig. 6.2.2.4).

The 3D network of **16** contains rhombic channels along the crystallographic **c** axis. These rhombic channels are filled with nitrate anions and lattice water molecules as shown in (Fig.

6.2.2.6). Yet, the nitrate anions and crystal water molecules could not be clearly located in the X-ray structure analysis because of their high disorder. Hence, the channel content was removed with the SQUEEZE option (see below). Between the two hydroxo ligands of $Cu_4(\mu\text{-}OH)_2$ there are H-bonds which lead to a more stable SBU. Details of this hydrogen bond are given in Table 6.2.2.2.

Table 6.2.2.2: Details of hydrogen bond in **16** (Å, °).

D-H···A	**d(D-H)**	**d(H···A)**	**d(D···A)**	**<(D-H···A)**
O3-H3B···O3^{i}	0.99	1.75	2.724(4)	167

Symmetry transformations used to generate equivalent atoms: i = -x+1,-y+1,-z+1.

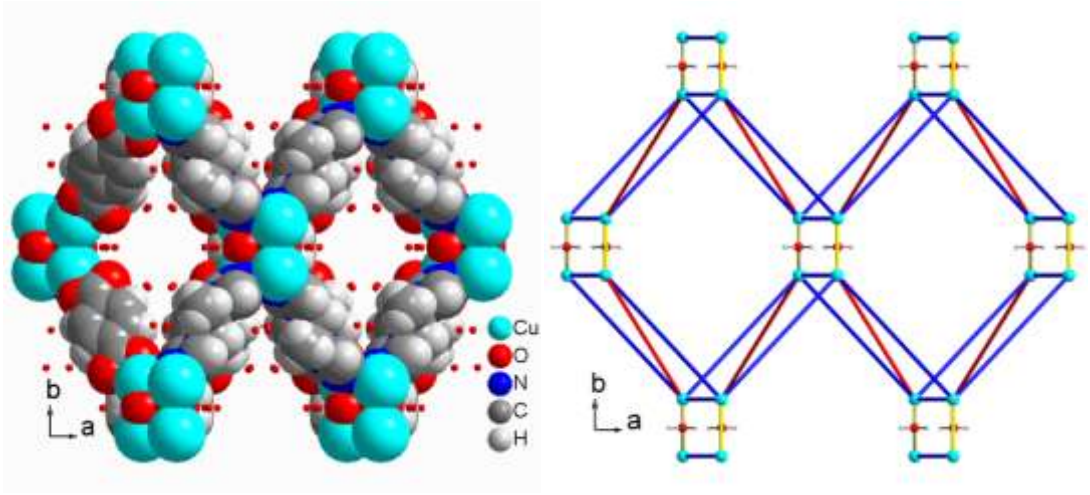

Fig. 6.2.2.6: The network of **16** along the **c** axis showed the canals in space filling mode (left), which formed due to the connectivity of different ligands with secondary building units (right). The channels are occupied by nitrate anions and solvent molecules (red dots). The Cu-Cu connectivity is showed in red for bdc^{2-}, blue and yellow for *rac*-btrip (ref. Fig. 6.2.2.4).

Overall, six SBUs, six *rac*-btrip ligands (blau and yellow) and four bdc ligands define the six vertices and ten edges of an octahedral cage (Figure 6.2.2.7) with distances between the centroid…centroid vertices = 16.183, 21.670 and 24.066 Å. Each octahedral cage shares its vertices and edges with eight other neighboring octahedral cavities, defining a 3D-network structure identical to the sodium halide structure (NaCl) or isopolyanions like $[W_6O_{19}]^{2-}$, $[Ta_6O_{19}]^{8-}$ [102], where tetrahedral holes are occupied between vertex-sharing octahedral cavities (Figure 6.2.2.8). Topologically, each SBU can be simplified as a 10-connected unit,

and the ligand as a linker. So that a 3D-framework is defined as 3D-(2,10)-connected network.

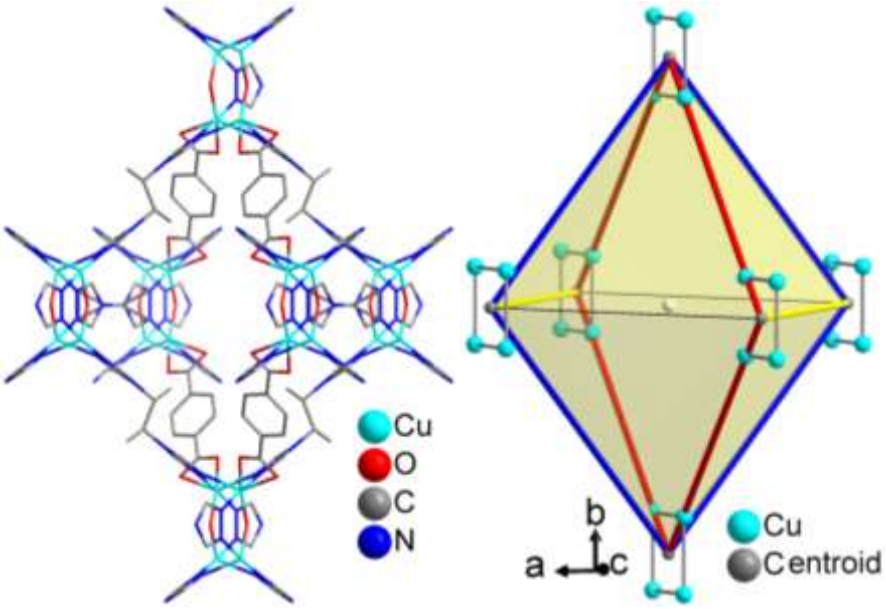

Figure 6.2.2.7: Representation of the octahedral cage in compound **16** without guest molecules and hydrogen atoms not shown for clarity. Ligands and SBUs are showing in stick model.

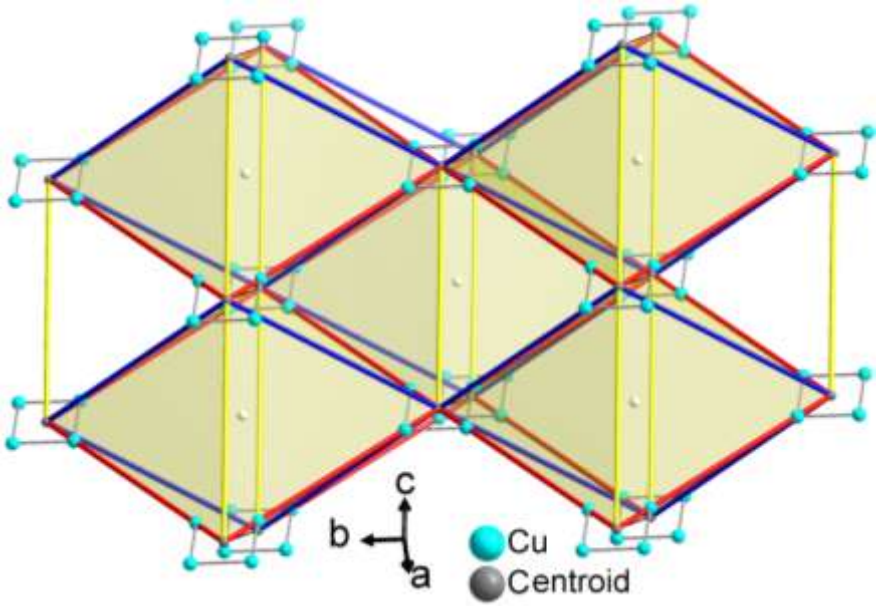

Figure 6.2.2.8: Representation of five octahedral cavities in compound **16**, which share their edges and vertices. Tetrahedral holes are formed between neighboring shared octahedral cavities. Guest molecules, anions and H-atoms are omitted for clarity.

The phase purity of the 3D coordination polymer, 3D-{$[Cu_4(\mu\text{-}OH)_2(\mu\text{-}bdc)_2(\mu_4\text{-}rac\text{-}btrip)_3]\cdot(NO_3)_2(H_2O)_{10}\}_n$ **16**, is not readily confirmed by the comparison of the measured and simulated PXRD pattern (Fig. 6.2.2.9). A reason for difference between the measured and simulated PXRD pattern could be, that there are different crystal phases in the sample and crystal deterioration upon removal from mother liquor and drying. The sample was dried in vacuum for *ca.* 0.5 h at temperature 40 °C before PXRD measurement in Figure 6.2.2.9, middle, and was not completely dried after washing with methanol in Fig. 6.2.2.9, top.

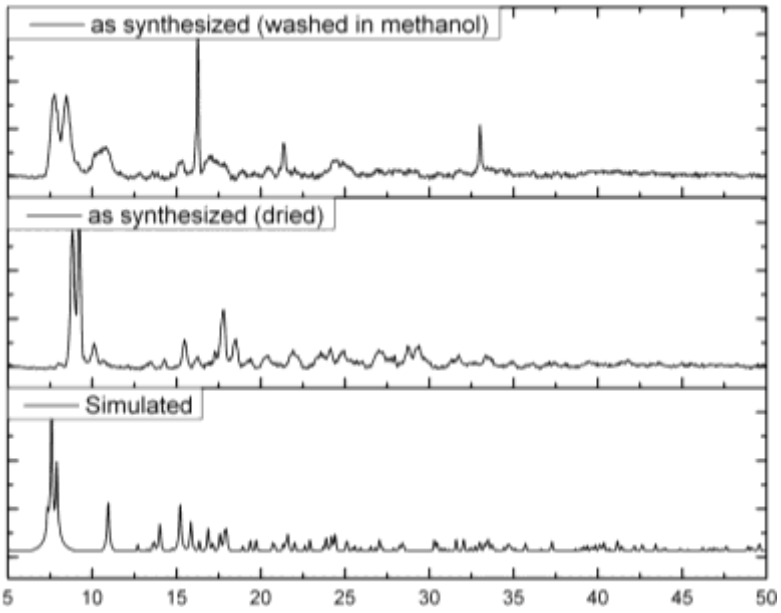

Fig. 6.2.2.9: Combination of the experimental powder X-ray diffractogram of compound **16** (top and middle) at Cu-Kα wavelength 1.54184 Å with the theoretical pattern calculated from the single crystal data (bottom). The measured PXRD is smoothed and baseline corrected.

For **16** a total of 672 electrons per potential solvent accessible void volume of 2110 $Å^3$ in the unit cell (4211.9(16) $Å^3$) with formula unit 3D-$[Cu_4(\mu\text{-}OH)_2(O_2C\text{-}C_6H_4\text{-}CO_2)_2(N_3C_2H_2\text{-}C_3H_6\text{-}C_2H_2N_3)_3]$ and Z = 2 was squeezed. PLATON [103] calculates a total potential solvent area volume of 2115.3 $Å^3$ per unit cell volume of 4211.9 $Å^3$ [50.2%]. The void area also contains the nitrate anions. One nitrate anion has 32 electron. Four nitrate anions per unit cell then account for 128 electrons leaving about 544 electrons for solvent molecules. If the solvent molecules are taken as mostly H_2O molecules with 10 electrons each, then about 54 crystal water molecules reside in the unit cell. This translates into 27 solvent water molecules per Cu_4 formula unit.

For the formula $[Cu_4(\mu\text{-}OH)_2(O_2C\text{-}C_6H_4\text{-}CO_2)_2(N_3C_2H_2\text{-}C_3H_6\text{-}C_2H_2N_3)_3](NO_3)_2$ = C37 H40 Cu4 N20 O16 with M = 1275.03 g/mol an amount of 27 H2O = 27 x 18 g/mol = 486 g/mol then corresponds to 486 : (1275.03 + 486) = 27.6 wt% of crystal water.

Most of this solvent of crystallization is easily lost upon drying in air at room temperature or 40°C preceding the elemental and thermogravimetric analysis (TGA) (see below). Only about 10 wt% is lost from the sample in TGA up to about 100°C. 10 wt% corresponds to ca. 144 : (1275+144) or 8 out of 27 crystal water molecules. Most likely, these are the solvating water molecules for the nitrate anion.

N_2 adsorption study: The potential permanent porosity was studies by gas sorption measurement. The porosity and BET surface area was evaluated by N_2 adsorption at 77 K. For activation the sample of **16** was heated at 130 °C under vacuum for 4 h to free the pores from solvent molecules (degassed). The result reveal an isotherm of type III accompanied by a type-H2 hysteresis loop [127] according to the International Union of Pure and Applied Chemistry (IUPAC). This type of isotherms is distinctive of mesoporous materials. This class of isotherm is characteristic of weak adsorbate-adsorbent interactions. The weak interactions between the adsorbate and the adsorbent lead to low uptakes at low relative pressures. The adsorbate-adsorbate interaction, which is much stronger, becomes the driving force of the adsorption process, resulting in accelerated uptakes at higher relative pressure [127], while the H2-type hysteresis is generally associated to regular pores with interconnecting channels [128]. Capillary condensation gives rise to a hysteresis loop [104]. Furthermore, the experimental data were fitted using the Barrett, Joyner and Halenda (BJH) model [129] to give the pore size distribution (PSD) curve (Figure 6.2.2.10) in the mesoporous region. A Brunauer–Emmett–Teller (BET) calculation [130] gives the low BET surface area for **16** equal to 74 m^2/g; and the Langmuir method gives the surface area of mesopores equal to 330 m^2/g. Moreover, the total pore volume is calculated and found to be 0.096 cm^3/g according to the amount adsorbed at a relative pressure P/P_0 of 0.95. The low value of BET surface area for **16** is due to collapse of the framework (see changes in the PXRD) and that the pores are still occupied by NO_3^- anions to neutralize the positively charged 3D-framework. PXRD pattern were measured before and after N_2 adsorption to check structure stability upon activation (Figure 6.2.2.11). Crystal images as synthesized and activated are shown in Figure 6.2.2.12.

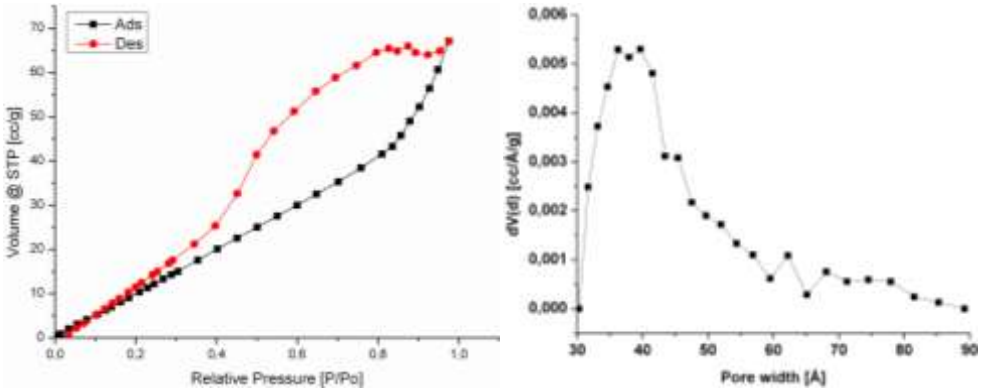

Fig. 6.2.2.10: Nitrogen adsorption-desorption isotherms at 77 K of **16** (left). The BJH pore-size distributions (right).

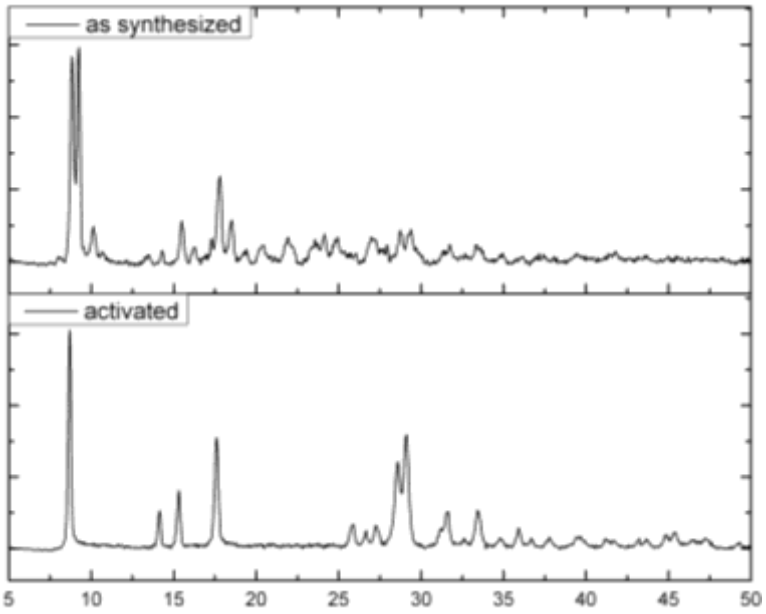

Fig. 6.2.2.11: Combination of the experimental powder X-ray diffractograms for compound **16** as synthesized (top) and activated (bottom) at Cu-Kα wavelength 1.54184 Å. The measured PXRD curves are smoothed and baseline corrected.

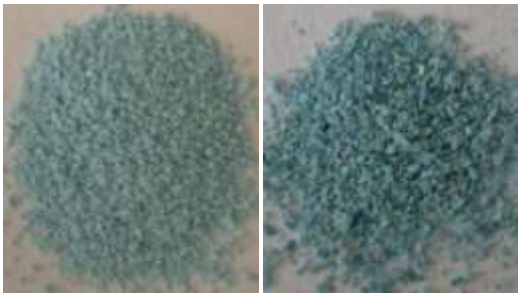

Fig. 6.2.2.12: Images of sample **16** as synthesized (left) activated (right).

The elemental analysis data for the complex is consistent with the proposed formula ($C_{37}H_{40}Cu_4N_{20}O_{16}$ + 10 x H_2O) of 3D-{[Cu_4(μ-OH)$_2$(O_2C-C_6H_4-CO_2)$_2$($N_3C_2H_2$-C_3H_6-$C_2H_2N_3$)$_3$] (NO_3)$_2$(H_2O)$_{10}$}$_n$ **16** 3D coordination polymer. Notably, the sample was dried in vacuum furnace for *ca.* 3 h at temperature 40 °C before CHN measurement; therefore probably the pre-dried compound contains more solvent molecules in their channels.

To examine the thermal stability of 3D-{[Cu_4(μ-OH)$_2$(μ-bdc)$_2$(μ$_4$-*rac*-btrip)$_3$]·(NO_3)$_2$(H_2O)$_{10}$}$_n$, TG-DTG experiment of **16** was carried out in the temperature range 27-600 °C under a flow of nitrogen gas 10 ml/min with a heating rate of 5 °C/min and sample mass 7.72 mg. Ten lattice water molecules were released at temperature 186°C (obs. 12.35%, calc. 12.37%). The dehydrated 3D-{[Cu_4(μ-OH)$_2$(μ-bdc)$_2$(μ$_4$-*rac*-btrip)$_3$] (NO_3)$_2$}$_n$ is thermally stable up to ~200°C and then the complex begins to decompose in multi weight loss steps on further heating. The next step appears at temperature 250 °C, and corresponds to the loss of three *rac*-btrip ligands, N_2O_5 gas from two nitrate anions and water molecule from two bridged hydroxido ligands of the tetranuclear secondary building unit of (Cu_4(μ-OH)$_2$) (obs. 45.49%, calc. 45.38%). The next weight loss stage starts at temperature 480°C, due to the loss of two bdc ligands (obs. 22.80%, calc. 22.55%). The final residual the black precipitate is mostly assigned to 4(Cu_2O) (obs. 19.24%, calc. 19.66%). It is clear from TGA profile, that the compound **16** is thermally stable up to ~200°C, after that it decomposes by losing ligands in multi steps. (Figure 6.2.2.13).

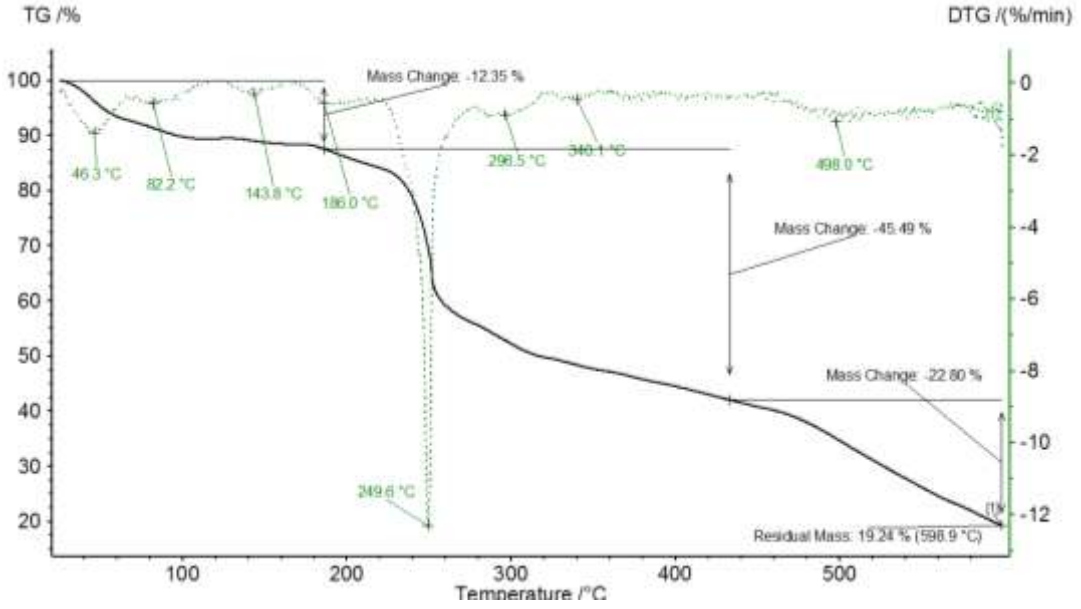

Fig. 6.2.2.13: The experimental TGA and DTG curves for the decomposition of **16**, in N_2 atmosphere, gas flow 10 ml/min at a heating rate of 5 °C/min and sample mass 7.72 mg. Common presentation of the TGA curve (black) together with the DTG curve (red, dotted line). (The image is generated by the instrument's software).

The comparison between the FT-IR spectra (ATR) of 3D-{[Cu_4(μ-OH)$_2$(μ-bdc)$_2$(μ$_4$-*rac*-btrip)$_3$]·(NO_3)$_2$(H_2O)$_{10}$}$_n$ **16** and the mixture of the *rac*-btrip and H_2bdc ligands, shows, that both spectra are mostly identical, which were confirmed by their bands width and position matching. The characteristic bands of the coordinated carboxylate group (C=O) of bdc ligand and triazole ring (C=N) of *rac*-btrip ligand appearing at 1567 cm^{-1} for the asymmetric stretching vibration and 1500 cm^{-1} for the symmetric stretching vibration. The other characteristic bands of the carboxylate group (C-O) of bdc ligand and triazole ring (C-N) of *rac*-btrip ligand appearing at 1291 cm^{-1} for the asymmetric stretching vibration and 1209 cm^{-1} for the symmetric stretching vibration [105],[106],[107]. The absence of characteristic band of protonated carboxyl group (COOH) of H_2bdc proves that, the carboxylate group is completely deprotonated [105],[108]. Band at 3610 cm^{-1} are attributed O–H stretching vibrations of μ-coordinated water of SBU. The weak sharp bands at 3101 and 3007 cm^{-1} are attributed C–H stretching vibrations of *rac*-btrip ligand. Band at 734 cm^{-1}, in the fingerprint region, for **16** is due to 1,4-disubstituted benzene [109]. Band at 645 cm^{-1} is attributed to triazole ring of *rac*-btrip ligand. This comparison of FT-IR spectra is presented in Figure 6.2.2.14.

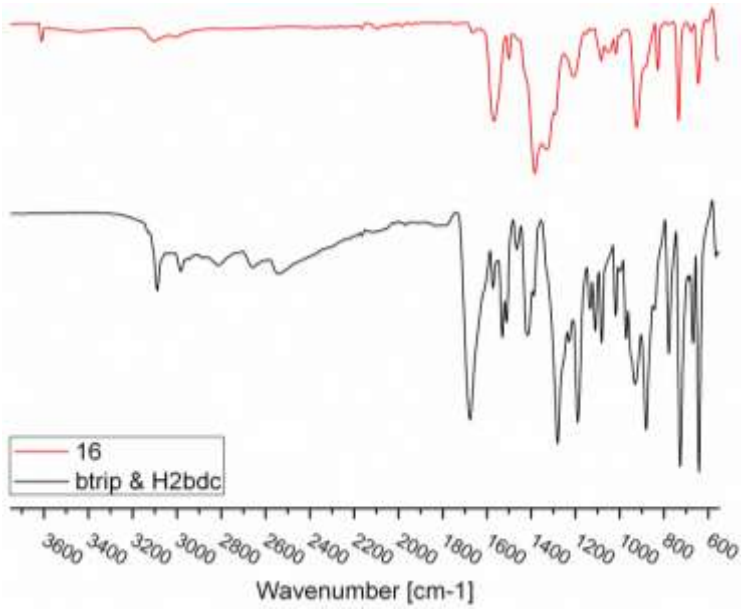

Fig. 6.2.2.14: IR Spectra (ATR) for comparison between the compound **16** and the mixture of *rac*-btrip and H_2bdc ligands in range 550-3750 cm^{-1}.

When the NMR samples are prepared, an excess of NaCN was added to each sample to change the magnetic properties of copper atoms from paramagnetic to diamagnetic by forming the Cu(I) d^{10} complex $Na_3[Cu(CN)_4]$ in the deuterated solvent. After centrifugation, the pipette-separated supernatant was measured. The ^{1}H NMR spectrum of 3D-{[Cu_4(μ-

$OH)_2(\mu\text{-bdc})_2(\mu_4\text{-}rac\text{-btrip})_3]\cdot(NO_3)_2(H_2O)_{10}\}_n$ **16** shows that, both *rac*-btrip and bdc ligands are built into the compound. But there are problems associated with dissolving the network in deuterated NMR solvents. The peaks expected for the four equivalent protons of the benzene ring in bdc ligand did not appear in the ^{1}H NMR spectrum, when the sample was dissolved in DMSO-d_6 *via* heating in an ultrasonic bath at 50°C. On the other hand, the peaks of the four protons of the two different triazole rings in the *rac*-btrip ligand did not show in the ^{1}H NMR spectrum, if a mixture of NaOD/D_2O was used as a solvent again by heating at 50°C and using ultrasonic bath for 15-30 min. The former is explained by the still present coordination of bdc^{2-} to Cu in DMSO-d_6 which apparently was only able to displace and solubilize the btrip ligand. In the latter case, the slightly acidic C-H protons on the triazolyl ring are exchanged by C-D in NaOD/D_2O as was proven by measuring the H_2bdc ligand in DMSO-d_6 and btrip ligand in NaOD/D_2O. (Figure 6.2.2.15a,b). The integration between CH_3- of btrip for three protons and four protons of bdc^{2-} show, that molar btrip : bdc ratio between both ligands in compound for a proton is close to 0.33:0.21~3:2.

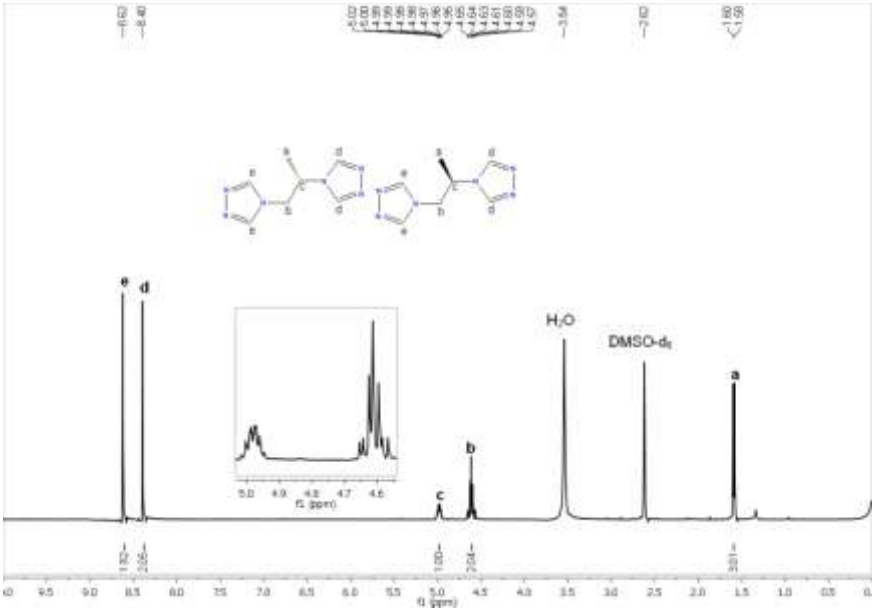

Fig. 6.2.2.15a: ^{1}H NMR Spectrum (500 MHz) of compound **16** in DMSO-d_6.

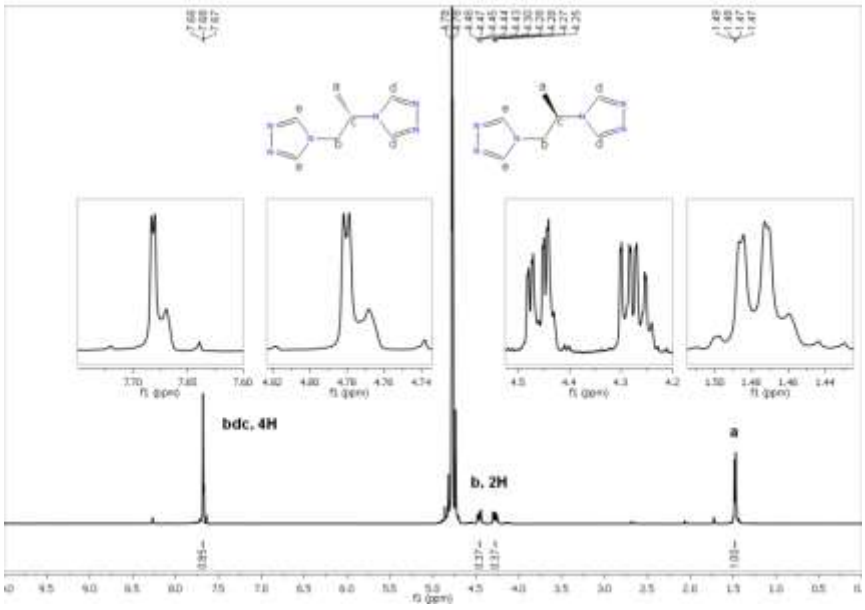

Fig. 6.2.2.15b: ^{1}H NMR Spectrum (500 MHz) of compound **16** in NaOD/D_2O.

7.2.3 Structure analysis and characterization of 2D-{[Zn(μ-Hbtc)(μ-*R*-btrip)] $(H_2O)\}_n$ (19)

Colorless single crystals (Figure 6.2.3.1) were obtained from the hydrothermal reaction of an aqueous solution of zinc(II) nitrate hydrate, a solution of the *rac*-btrip ligand and a solution of H_3btc ligand. The latter was deprotonated by using Et_3N (3 eq. to H_3btc) as base. The solutions were mixed in a glass tube and then placed in a programmable furnace at 125°C or 140°C. The resulting crystals were filtered and washed with the mother liquor. The reaction was repeated several times and found to be reproducible. The crystals are insoluble in water and organic solvents such as ethanol or methanol. The single crystal X-ray structure was measured after more than one month of synthesis when crystals kept in mother liquor.

Fig. 6.2.3.1: Crystal images of different batches of the reaction between $Zn(NO_3)_2$, *rac*-btrip and H_3btc/Et_3N in (MeOH/H_2O); **19** (left), **19-1** (middle) and **19-2** (right).

Proton NMR of a sample digested in NaOD/D_2O gave a molar ratio of the btrip and btc ligand of 1:1 (see below). From the single-crystal X-ray structure the compound was identified as the novel compound 2D-{[Zn(μ-Hbtc)(μ-*R*-btrip)]·H_2O}$_n$ **19** which crystallized in the orthorhombic crystal system with the non-centrosymmetric space group $P\ 2_12_12_1$ (Flack parameter 0.005(8)) [110]. The asymmetric unit consists of one Zn atom, one $Hbtc^{2-}$ anion and one (here *R*)-btrip ligand. There are four formula units in the unit cell (Z = 4). The 2D coordination polymer is overall neutral. The Zn(II) ions are pseudo-tetrahedrally coordinated to two nitrogen atoms (N1 and N4) from two btrip ligands and two oxygen atoms (O1 and O5) from two carboxylate groups of two $Hbtc^{2-}$ ligands (Figure 6.2.3.2, Table 6.2.3.1). The Zn atom has a distorted tetrahedral coordination sphere with the angles around the metal center varying from 99.30 to 131.26° and distances from 1.989 to 2.036 Å. There are additional longer metal contacts of 2.65 Å to each of the second carboxylate oxygen atom.

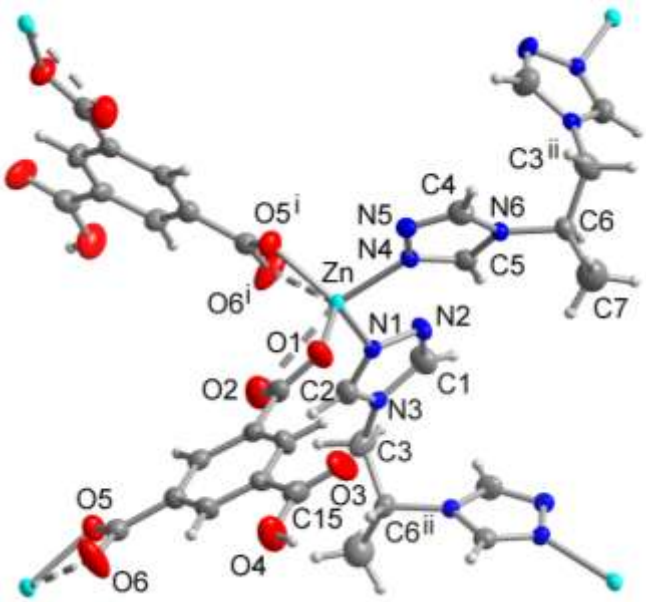

Fig. 6.2.3.2: Coordination environment of Zn(II) ion in 2D-{[Zn(μ-Hbtc)(μ-*R*-btrip)]·H_2O}$_n$ **19** also showing the bridging action of the ligands in this extended asymmetric unit. Symmetry operations: i = -x, y+1/2,-z+1/2, ii = 2-x, y-1/2,-z+1/2. The crystal water molecule is omitted for clarity.

Table 6.2.3.1: Selected bond lengths [Å] and angles [°] for **19**.

Zn-O1	1.989(3)	O1-Zn-O5^{i}	102.68(11)
Zn-O5^{i}	1.996(3)	O1-Zn-N1	112.68(13)
Zn-N1	2.005(3)	O5^{i}-Zn-N1	131.26(11)
Zn-N4	2.036(3)	O1-Zn-N4	99.30(12)
Zn-O2	2.649	O5^{i}-Zn-N4	105.22(12)
Zn-O6^{i}	2.652	N1-Zn-N4	101.08(13)

Symmetry transformations used to generate equivalent atoms: i = -x, y+1/2,-z+1/2.

Only two carboxylate groups of the H_3btc ligand are deprotonated and coordinate to the metal center while the third one remains protonated and non-coordinated. This is also confirmed by FT-IR spectra. A strong absorption band at 1691 cm^{-1} in the FT-IR spectra confirms the presence of a protonated carboxylic group. The hydrogen atom attached to O4 of the non-coordinated carboxylate group was located crystallographically. The shorter bond length of C15–O3 (1.217 Å) compared to C15–O4 (1.315 Å) is consistent with the C=O double bond character of the C15–O3 bond. Remarkably, the single crystal structure reveals a case of spontaneous resolution. A racemic mixture of the btrip ligand was used in the synthesis. Yet, the individual crystal contains only one of the two enantiomers. In the absence of inversion symmetry elements in the space group $P\ 2_12_12_1$ and with a Flack parameter of 0.005(8) [110] the crystal is homochiral (enantiopure) with all btrip ligands of the same *R* or *S* configuration. The overall ensemble of the crystals in a batch can be expected to be racemic, that is, to contain crystals of *R*- and *S*-configured btrip ligands, respectively, in equal amounts.[111]. The structure in the next section 7.2.4 will show the enantiomorph with the *S*-ligand (see below). Accordingly and different from the structure of 3D-$\{[Cu_4(\mu\text{-}OH)_2(\mu\text{-}bdc)_2(\mu_4\text{-}rac\text{-}btrip)_3]\cdot(NO_3)_2(H_2O)_{10}\}_n$ **16** the methyl group on the btrip ligand is not disordered here.

Zn(II) ions are bridged both by $Hbtc^{2-}$ ligands *via* carboxylate groups, and by the btrip ligands through one of the adjacent N atoms (Figure 6.2.3.2). This gives rise to a 2D 4,4-net with Zn atoms as the nodes (Fig. 6.2.3.3). The 4,4-net lie parallel to the *ab* plane and can also be constructed by parallel chains of {Zn(Hbtc)} and chains of {Zn(btrip)} which run along the *b* direction and alternate along *a* (Fig. 6.2.3.3). One can also consider the parallel chains of {Zn(Hbtc)} crosslinked by the btrip ligands and *vice versa*. Besides the enantiomeric ligand there is a higher element of chirality in this homochiral structure namely the formation of helical chains of {Zn(Hbtc)} and of {Zn(btrip)} along *b*. These chains are of *P* helicity or right-handed in the investigated crystal with the *R* configured btrip ligand (Fig. 6.2.3.4).

In the 4,4-net the Zn nodes form rhombic, almost square windows. The area of the rhombic windows within sheet can be defined by Zn-Zn distances of 9.264 Å and 9.534 Å along the btrip and Hbtc sides, respectively, and of 12.605 and 13.890 Å along the diagonal with different Zn-Zn-Zn angles of $(Zn\text{-}Zn\text{-}Zn)_{Hbtc\text{-}Hbtc}$ = 82.76°, $(Zn\text{-}Zn\text{-}Zn)_{btrip\text{-}btrip}$ = 85.74° and $(Zn\text{-}Zn\text{-}Zn)_{btrip\text{-}Hbtc}$ = 95.27°. These openings are large enough so that a second 4,4-net, only related by symmetry, can interweave. The nets run parallel to each other so that a 2D→2D interpenetration results [47].

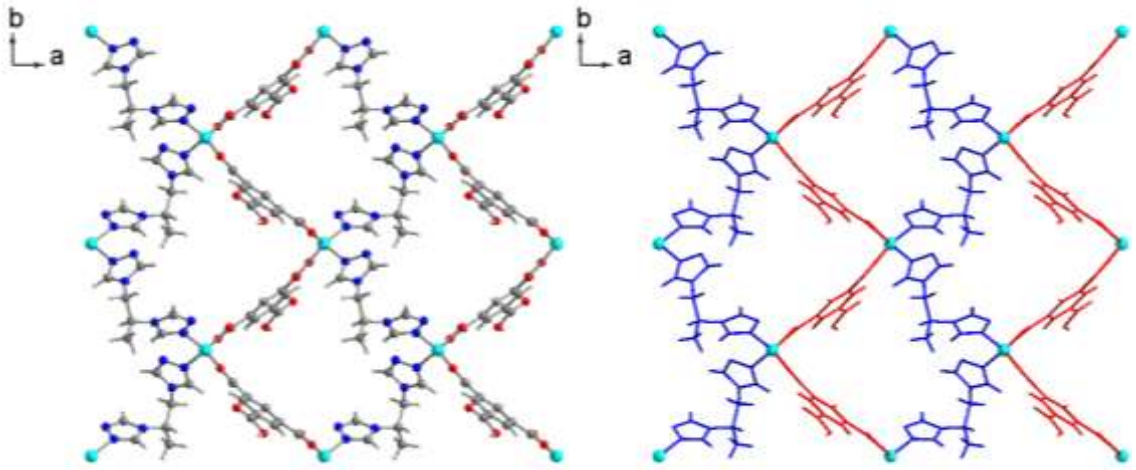

Fig. 6.2.3.3: 2D (4,4) nets of **19** showing the formation of small rhombic windows within the network, which are formed via connection of alternating 1D-chains of bridging Hbtc (red) and bridging btrip (blue). The lattice water molecules are omitted for clarity.

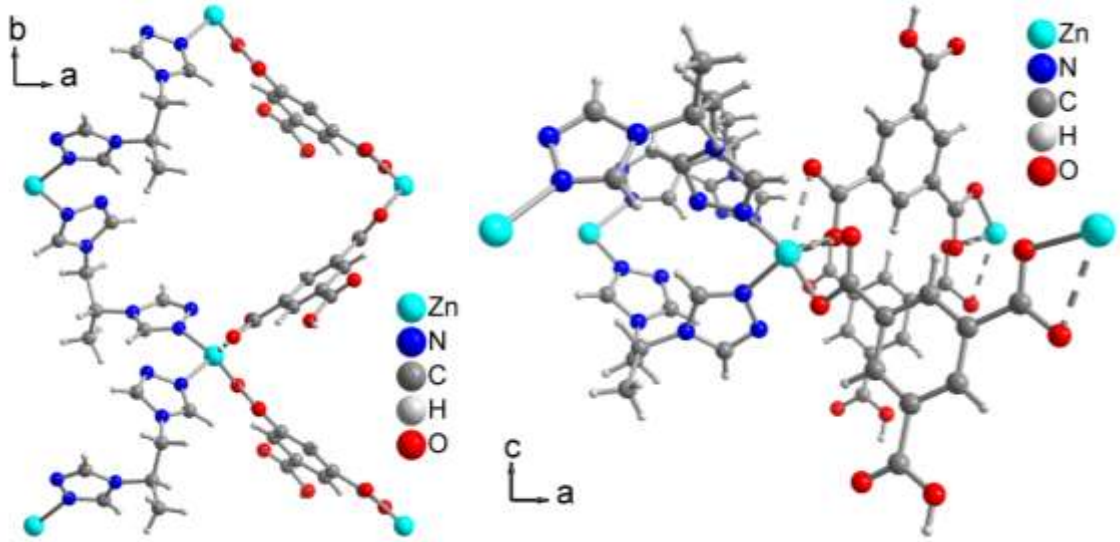

Fig. 6.2.3.4: A neighboring single {Zn(Hbtc)} and {Zn(btrip)} chain along *b* and their *P* helicity or right-handedness when viewed along *b* in a central projection.

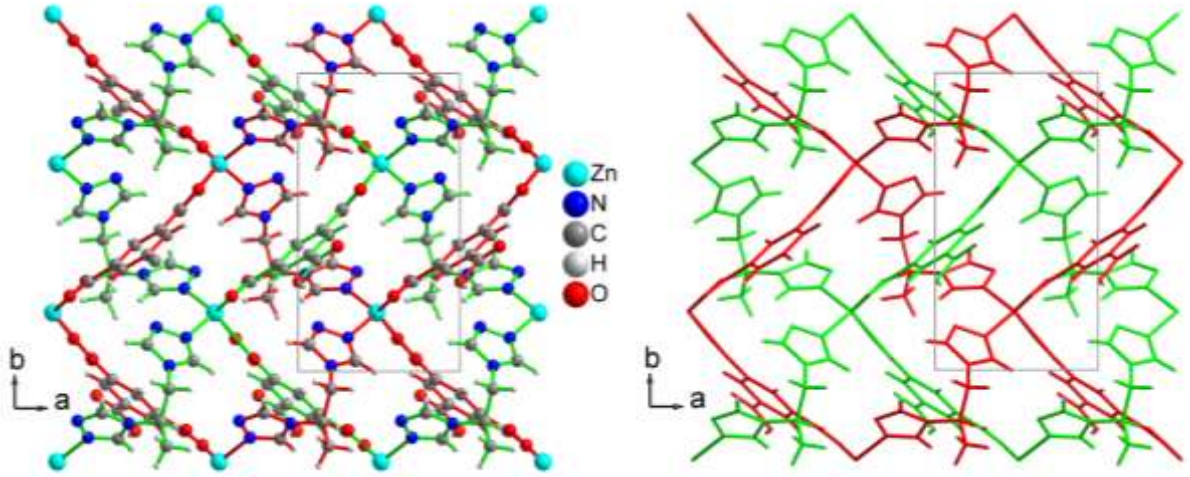

Fig. 6.2.3.5: Interpenetration of two 2D rhombic (4,4)-networks (red and green) in the crystal structure of 2D-{[Zn(μ-Hbtc)(μ-*R*-btrip)]·H_2O}$_n$ **19**. The lattice water molecules are omitted for clarity.

The interpenetrated 2D rhombic (4,4) nets are oriented parallel to the **ab** lattice plane (Figure 6.2.3.5) and stacked in the **c** crystallographic axis direction. They are orientated as **ABAB…** layers along **c** crystallographic axis direction (Figure 6.2.3.6). The lattice water molecules are placed between the neighboring interpenetrated layers. Neighboring interpenetrated 2D (4,4) layers are connected to each other *via* hydrogen bonds between a protonated carboxylic group and a coordinated carboxylate group (Fig. 6.2.3.6). Possibly, there are other hydrogen bonds between lattice water molecules in the structure, but a determination of the hydrogen atoms of the water molecules was not possible.

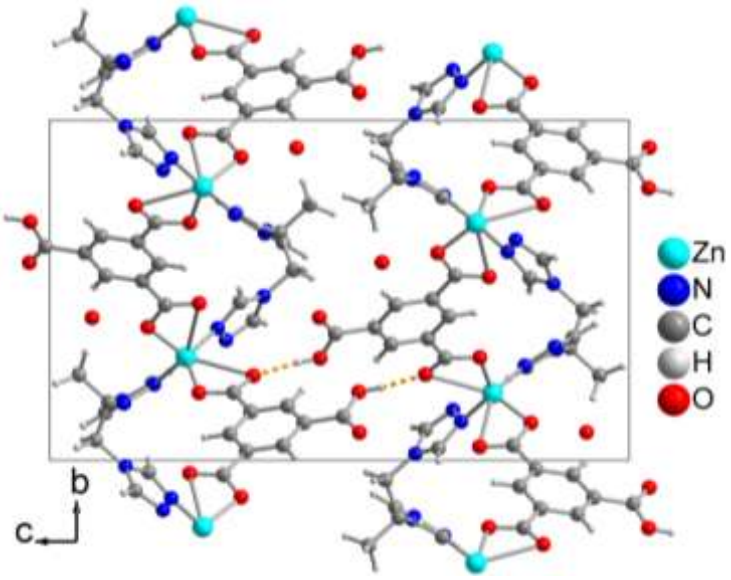

Fig. 6.2.3.6: 3D supramolecular structure of **19** with neighboring interpentrated [47] 4,4-nets connected by inter-planar hydrogen bonds (yellow dotted line).

Table 6.2.3.2: Details of hydrogen bond in **19** (Å, °).

D-H···A	d(D-H)	d(H···A)	d(D···A)	<(D-H···A)
O4-H4···O6^{v}	0.86	1.73	2.587(3)	174(4)

Symmetry transformation used to generate equivalent atoms: v = x+1/2,-y+1/2,-z+1.

The good phase purity of the chiral coordination polymer, 2D-{[Zn(μ-Hbtc)(μ-*R*-btrip)]·H_2O}$_n$, is confirmed by the comparison of the measured and simulated PXRD pattern, which is calculated from the obtained x-ray single crystal structure data for the zinc compound. A typical agreement between measured and simulated PXRD patterns is presented in Figure 6.2.3.7.

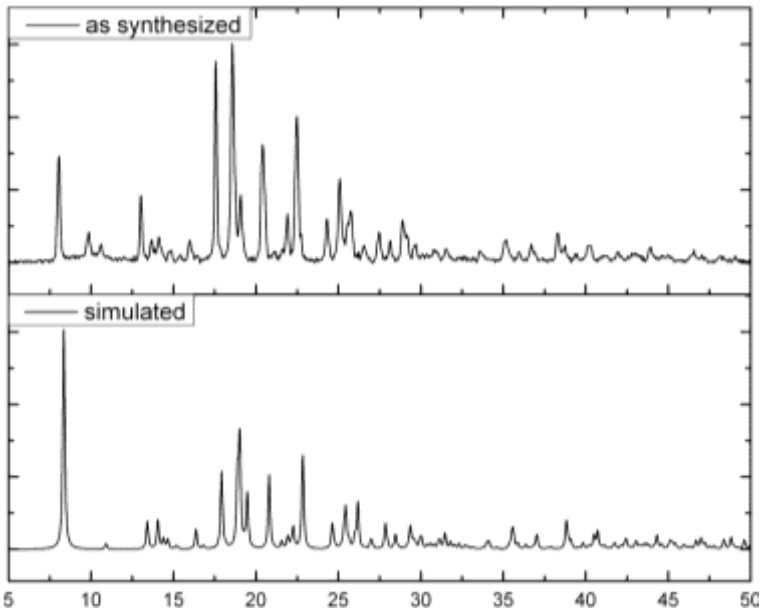

Fig. 6.2.3.7: Combination of the experimental powder X-ray pattern of zinc compound **19** (top) at Cu-Kα wavelength 1.54184 Å with the theoretical pattern, which is calculated from the obtained single crystal data (bottom). The measured PXRD pattern is smoothed and baseline corrected.

The elemental analysis data for the complex is consistent with the proposed formula ($C_{16}H_{16}N_6O_7Zn$) of 2D-{[Zn(μ-Hbtc)(μ-*R*-btrip)]·H_2O}$_n$ **19** (see Experimental Section 10.2.3).

To examine the thermal stability of 2D-{[Zn(μ-Hbtc)(μ-*R*-btrip)]·H_2O}$_n$, TG-DTG curves experiments of **19** were carried out in the temperature range 27-600 °C under a flow of nitrogen gas 10 ml/min with a heating rate of 5 °C/min and sample mass 8.11 mg. The lattice water molecules were released in the temperature range of 71-101 °C (obs. 5.44%, calc.

3.83%). Decomposition of the dehydrated 2D-[Zn(μ-Hbtc)(μ-*R*-btrip)]$_n$ continues from 100 °C on as indicated by the steady weight loss. The loss of the btrip ligand appears to be complete at 368 °C (obs. 37.76%, calc. 37.93%). The next weight loss up to 600 °C corresponded to decomposition of the Hbtc ligand (obs. 35.48%, calc. 37.06%). The final residual mass is assigned to $Zn(OH)_2$ (obs. 20.95%, calc. 21.16%) (Figure 6.2.3.8).

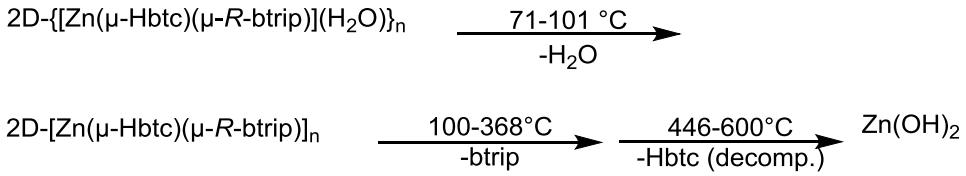

Scheme 6.2.3.1: Decomposition reaction of **19** through thermal stability measurement.

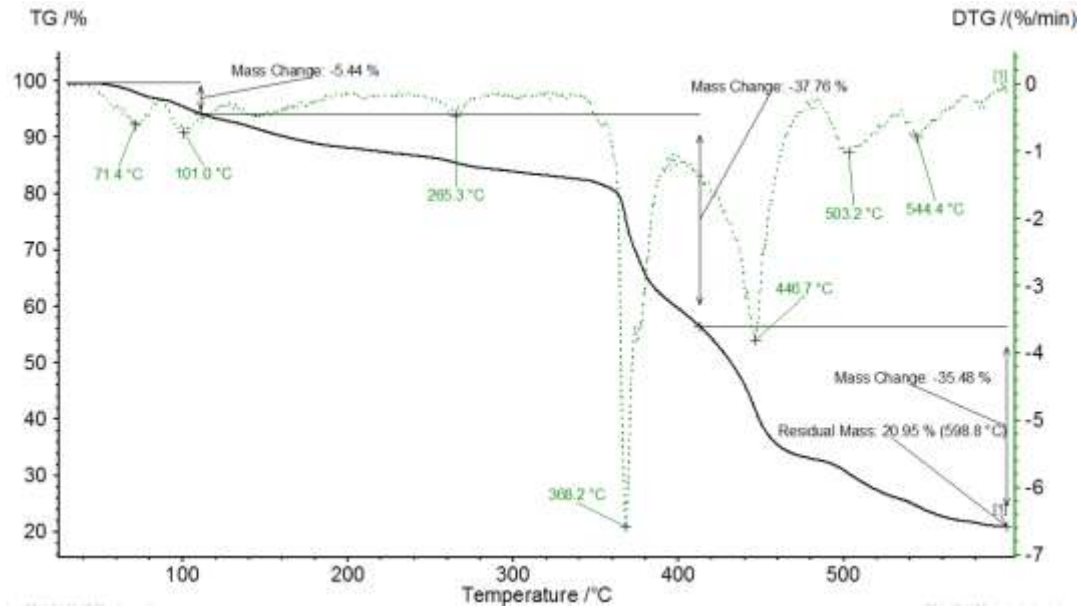

Fig. 6.2.3.8: The experimental TGA and DTG curves for the decomposition of **19**, in N_2 atmosphere, gas flow 10 ml/min at a heating rate of 5 °C/min in temperature range 27-600 °C and sample mass 8.11 mg. Common presentation of the TGA curve (black) together with the DTG curve (red, dotted line). (The image is generated by the instrument's software).

The comparison between the FT-IR spectra (ATR) of 2D-{[Zn(μ-Hbtc)(μ-*R*-btrip)]·H_2O}$_n$ **19** and the mixture of btrip and H_3btc ligands, shows, that both spectra are mostly identical, which were confirmed by their bands width and position matching. The characteristic bands of the coordinated carboxylate group of Hbtc ligand and triazole ring of *rac*-btrip ligand appearing at 1630 and 1437 cm^{-1} for the asymmetric stretching vibration and 1592 and 1380

cm^{-1} for the symmetric stretching vibration [105], [106], [107]. The characteristic band of protonated carboxyl group (COOH) of Hbtc ligand is observed at 1689 and 1259 cm^{-1} [105], [108]. The weak sharp band at 3113 cm^{-1} is attributed (C–H) stretching vibrations of *rac*-btrip ligand and the weakly band at 3643 cm^{-1} are attributed (O–H) stretching vibrations of protonated carboxyl group and lattice water, which indicate the presence of inter-layer hydrogen bonding in the lattice at 2485, 2056 cm^{-1} [112]. Bands at 736, and 684 cm^{-1}, in the fingerprint region, for **19** are due to 1,3,5-trisubstituted benzene [109]. Band at 640 cm^{-1} is due to triazole ring of *rac*-btrip ligand. The comparison of FT-IR spectra is presented in Figure 6.2.3.9.

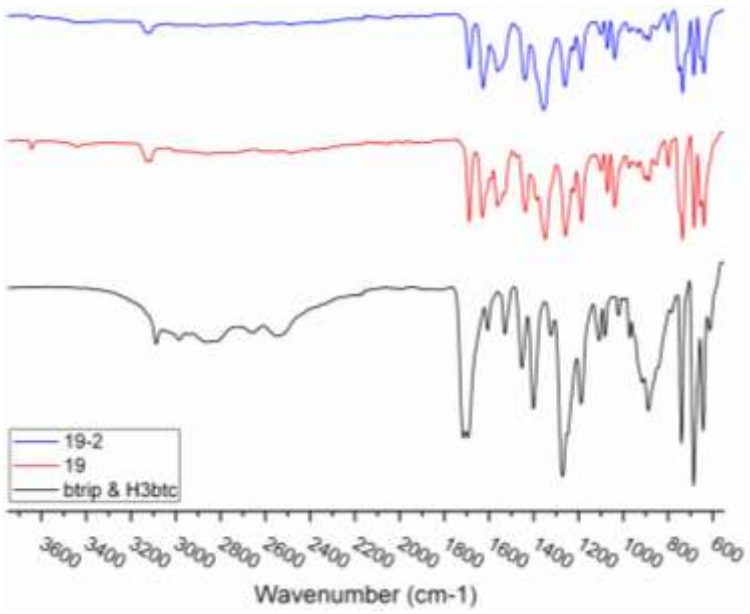

Fig. 6.2.3.9: IR Spectra (ATR) for comparison between the compounds **19-2** (140 °C), **19** (125 °C) in two different temperature and the mixture of *rac*-btrip and H_3btc ligands in range 550-3675 cm^{-1}.

When the NMR-samples are prepared, only the pipette-separated supernatant was measured after centrifugation. The ^{1}H-NMR spectrum of 2D-{[Zn(μ-Hbtc)(μ-*R*-btrip)]·H_2O}$_n$ shows that both *rac*-btrip and $Hbtc^{2-}$ ligands are built into the compound. But there are problems associated with using of the deuterated NMR solvent. The peaks expected for the three protons of benzene ring in H_3btc ligand are not seen in the ^{1}H-NMR spectrum, when the sample is partly dissolved in DMSO-d_6 *via* heating in an ultrasonic bath at 50°C. On the other hand, the peaks of four protons of the two different triazole rings in *rac*-btrip ligand did not show in the ^{1}H-NMR spectrum, if a mixture of NaOD/D_2O is used as a solvent for the crystals of complex 2D-{[Zn(μ-Hbtc)(μ-*R*-btrip)]·H_2O}$_n$ by heating again at 50 °C and using an ultrasonic bath for 15-30 min. (Figure 6.2.3.10). The former is explained by the still present

coordination of $Hbtc^{2-}$ to Zn in DMSO-d_6 which apparently was only able to displace and solubilize the btrip ligand. An insoluble residue remained in DMOS-d_6 which is assigned to a Zn-(Hbtc) adduct. The residue was removed by centrifugation and only the clear pipette-separated supernatant was measured. In the latter case, the slightly acidic C-H protons on the triazolyl ring are exchanged by C-D in NaOD/D_2O as was proven by measuring the H_3btc ligand in DMSO-d_6 and the btrip ligand in NaOD/D_2O. (Figure 6.2.3.10). The integration between CH_3- of btrip and three protons of $Hbtc^{2-}$ show, that molar ratio between the btrip and btc ligand in compound is 1:1 as found in structure.

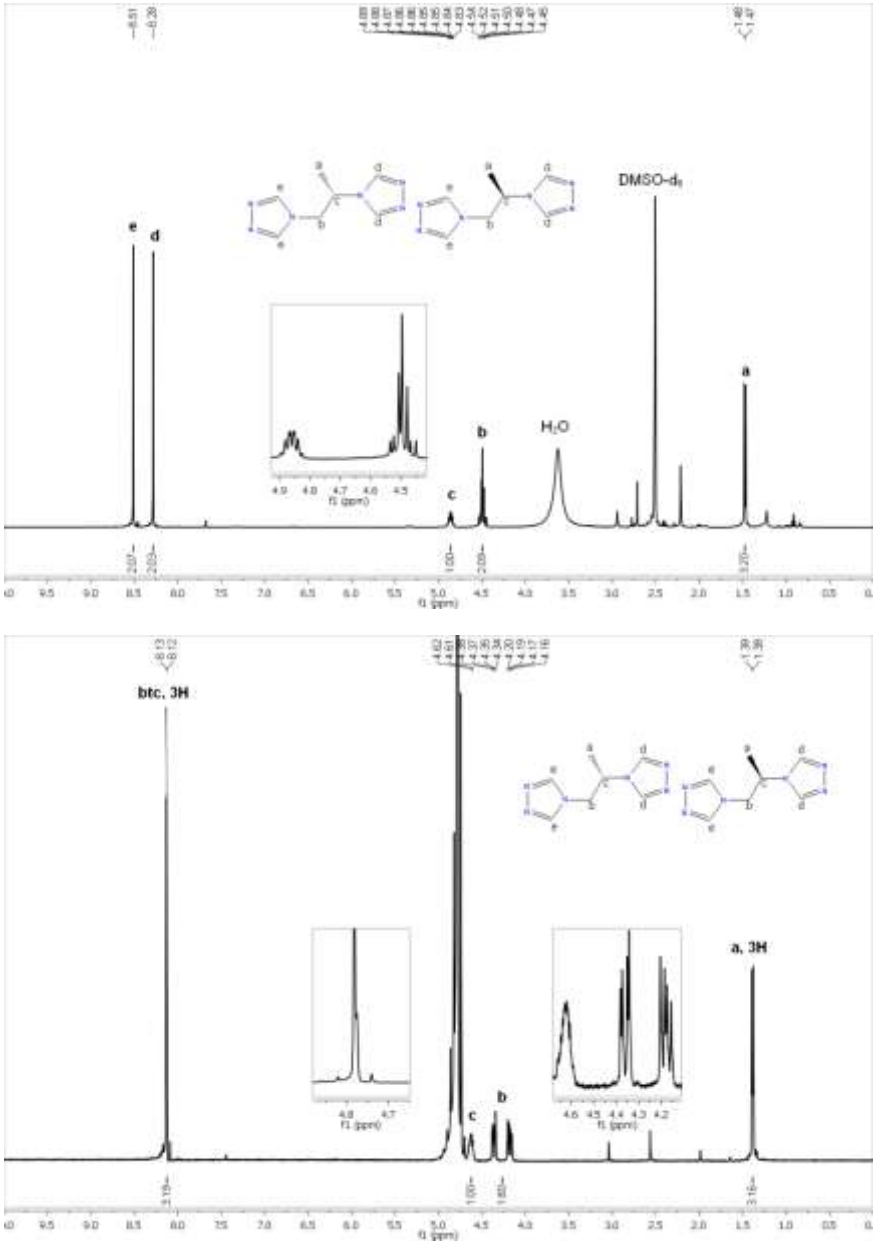

Fig. 6.2.3.10: ^{1}HNMR Spectrum (500 MHz) of compound **19** in two different solvents DMSO-d_6 (top) and in NaOD/D_2O (bottom).

7.2.4 Structure analysis and characterization of 2D-{[Zn(μ-Hbtc)(μ-*S*-btrip)]·H_2O}$_n$ (20)

The structure described in this section represents the enantiomorph to the previous structure presented in section 7.2.3, 2D-{[Zn(μ-Hbtc)(μ-*R*-btrip)]·H_2O}$_n$ **19**. Here the structure with the *S*-btrip ligand was obtained. This lends support to the assumption that only the single crystal is homochiral (enantiopure) with all btrip ligands of the same *R* or *S* configuration. Whereas, the overall ensemble of the crystals in a batch can be expected to be racemic, that is, to contain crystals of *R*- and *S*-configured btrip ligands, respectively, in equal amounts. The same synthetic procedure used for **19** (section 7.2.3) was followed to prepare the enantiomorphous title compound except by using $ZnBr_2$ instead of $Zn(NO_3)_2$ as zinc salt. Colorless single crystals (Figure 6.2.4.1) were again obtained from the hydrothermal reaction. The crystallographic data set was measured *ca.* one month after their synthesis with the crystals kept in mother liquor.

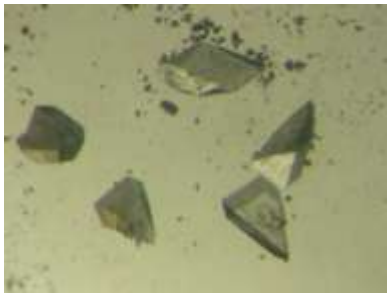

Fig. 6.2.4.1: Crystals image of **20**.

Compound 2D-{[Zn(μ-Hbtc)(μ-*S*-btrip)]·H_2O}$_n$ **20** has the same, just enantiomorphous structure as compound **19**. Thus, the molecular structure does not have to be discussed in detail again. Fig. 6.2.4.2 shows the coordination environment around zinc, Table 6.2.4.1 lists the relevant bond lengths and angles.

Table 6.2.4.1: Selected bond lengths [Å] and angles [°] for **20**.

Zn-O1	1.986(3)	O1-Zn-O5^{i}	103.17(12)
Zn-O5^{i}	2.000(2)	O1-Zn-N1	112.86(13)
Zn-N1	2.005(3)	O5^{i}-Zn-N1	131.59(12)
Zn-N4	2.040(3)	O1-Zn-N4	99.36(13)
Zn-O2	2.646(9)	O5^{i}-Zn-N4	104.08(11)
Zn-O6^{i}	2.628(7)	N1-Zn-N4	100.85(12)

Symmetry transformations used to generate equivalent atoms: i = -x+2, y-1/2,-z+3/2.

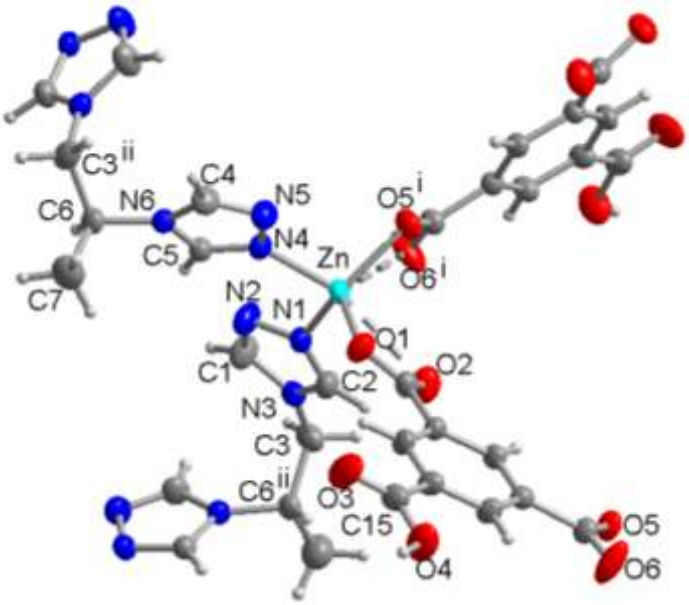

Fig. 6.2.4.2: Coordination environment of Zn(II) ion in 2D-{[Zn(μ-Hbtc)(μ-*S*-btrip)]·H_2O}$_n$ **20**. Symmetry operations for **20**: i = 2-x, y-1/2,-z+3/2, ii = -x, y+1/2,-z+3/2. Notice, that lattice water molecules are omitted for clarity.

The difference between both structures is that the chiral btrip ligand is now found in the *S*-configuration. Consequently, the helical chains of {Zn(Hbtc)} and of {Zn(btrip)} along *b* are now of *M* helicity or left-handed in the investigated crystal with the *S* configured btrip ligand (Fig. 6.2.4.3).

Table 6.2.4.2: Details of hydrogen bond for **20** (Å, °).

D-H···A	**d(D-H)**	**d(H···A)**	**d(D···A)**	**<(D-H···A)**
O4-H4···O6^{v}	0.79	1.81	2.596	177

Symmetry transformation used to generate equivalent atoms: v = x-1/2,-y+3/2,-z+1.

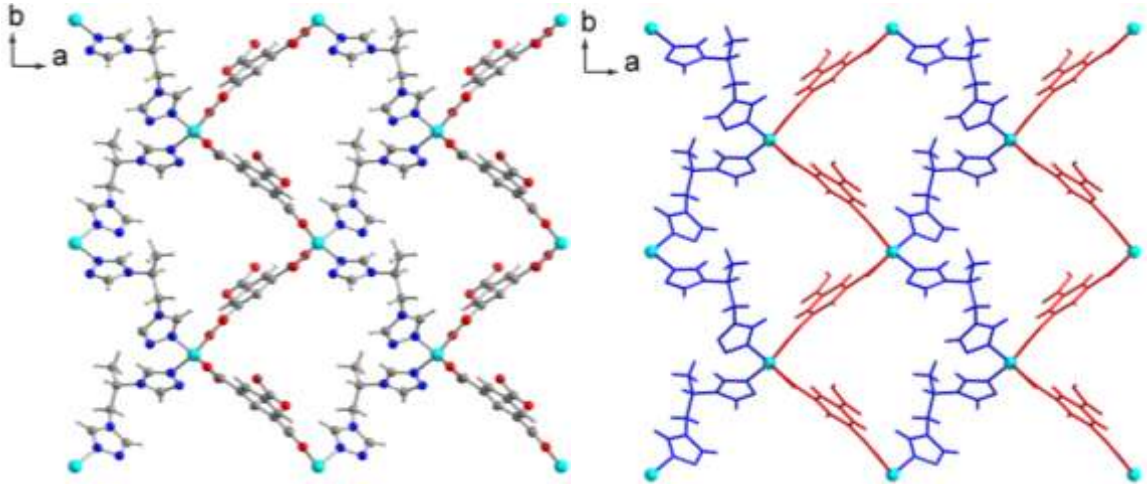

Fig. 6.2.4.3: representation one of 2D (4,4) net of **20** showing the formation small rhombic windows within the helical network, which are formed via connection of two different 1D- chains of Hbtc-bridging (red) and btrip-bridging (blue). The lattice water molecules are omitted for clarity.

The phase purity of the 2D-{[Zn(μ-Hbtc)(μ-*S*-btrip)]·H_2O}$_n$ chiral coordination polymer is confirmed by the positively matching the measured and simulated PXRD pattern presented in Figure 6.2.4.4.

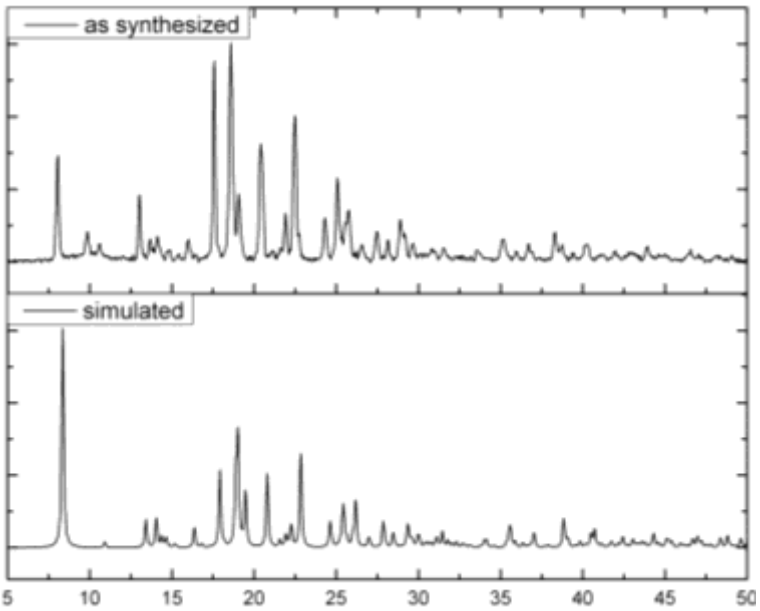

Fig. 6.2.4.4: Combination of the experimental powder X-ray diffraction of compound **20** (top) at wavelength 1.54184 Å with the theoretical pattern, which is calculated obtained from the single x-ray crystal data (bottom). The measured PXRD pattern is smoothed and baseline corrected.

The comparison between the FT-IR spectra (ATR) of the chiral coordination polymer, 2D-{[Zn(μ-Hbtc)(μ-*S*-btrip)]·H_2O}$_n$ **20**, and the mixture of free ligands, btrip and H_3btc, shows, that

both spectra are mostly identical, which were confirmed by their bands width and position matching. The comparison of FT-IR spectra is presented in Figure 6.2.4.5. The FT-IR spectrum for compound **20** is identical to the one of the enantiomorphous compound **19** and was discussed in last section 7.2.3.

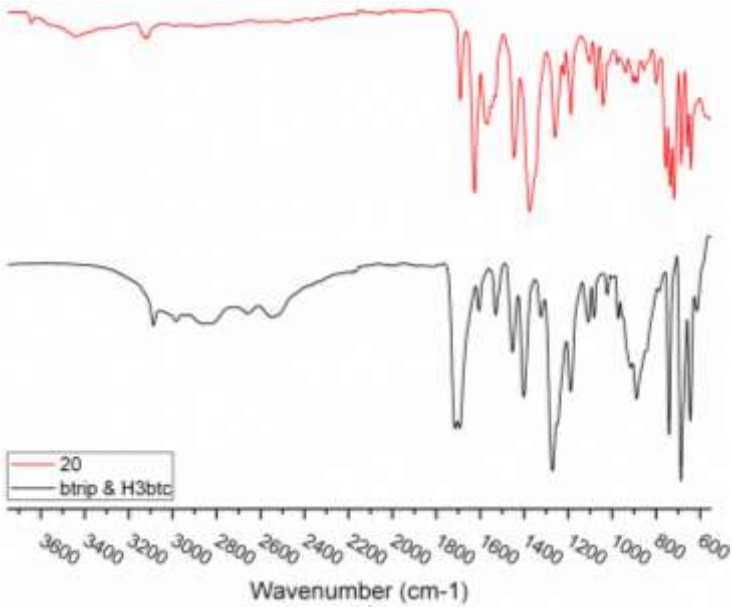

Fig. 6.2.4.5: IR Spectra (ATR) for comparison between the compound **20** and the mixture of btrip and H_3btc ligands in range 500-3675 cm^{-1}.

To examine the thermal stability of the chiral coordination polymer, 2D-{[Zn(μ-Hbtc)(μ-*S*-btrip)]·H_2O}$_n$, TG-DTG experiments of **20** were carried out in the temperature range 27-600 °C under a flow of nitrogen gas, 30 ml/min, with a heating rate of 10 °C/min and sample mass 7.57 mg. The experimental TGA and DTG curves for the decomposition of **20** are presented in Figure 6.2.4.6. TGA and DTG curves for **20** show identical curves for **19**, where were discussed in last section 7.2.3.

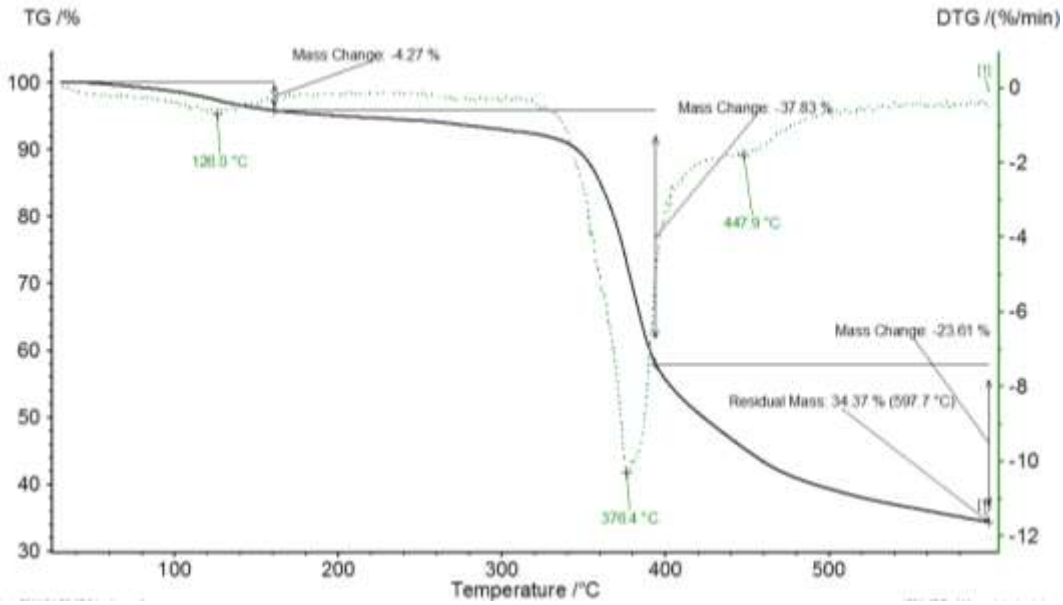

Fig. 6.2.4.6: The experimental TGA and DTG curves for the decomposition of **20**, in N_2 atmosphere, gas flow 30 ml/min at a heating rate of 10 °C/min in temperature range 27-600 °C and sample mass 7.57 mg. Common presentation of the TGA curve (black) together with the DTG curve (red, dotted line). (The image is generated by the instrument's software).

7.2.4.1 Data analysis and characterization of same compound with other Zn-salts

The same compound 2D-{[Zn(μ-Hbtc)(μ-btrip)]·H_2O}$_n$ as in the previous sections 7.2.3 and 7.2.4 were obtained as colorless crystals by the same synthetic procedure but using other zinc salts such as $Zn(ClO_4)_2·6H_2O$, $ZnCl_2$ or $Zn(OAc)_2.2H_2O$. A single crystal x-ray diffraction analyses for these other crystals was not carried out anymore because it had already been noticed, that the anions of the zinc salts ($Zn(NO_3)_2·6H_2O$ and $ZnBr_2$) were not included in the structures. Therefore, PXRD pattern, TG analysis only for $ZnCl_2$-compound, IR and NMR-spectra for the all Zn-compounds were measured to chemical and structural identity.

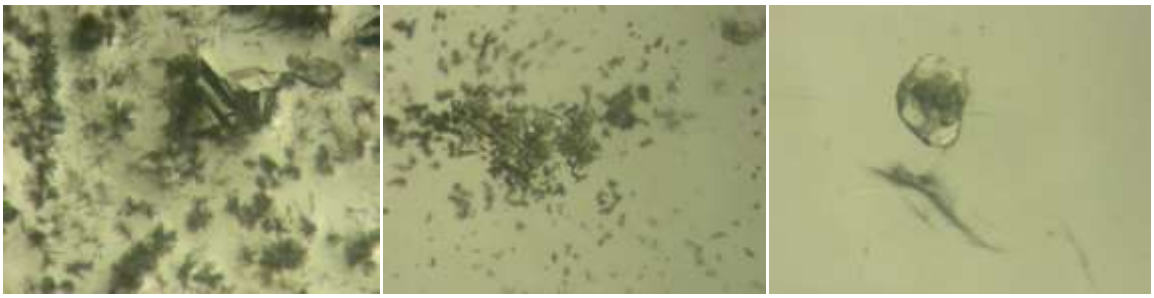

Fig. 6.2.4.1.1: Crystals images of **22** (left), **21** (middle) and **23** (right).

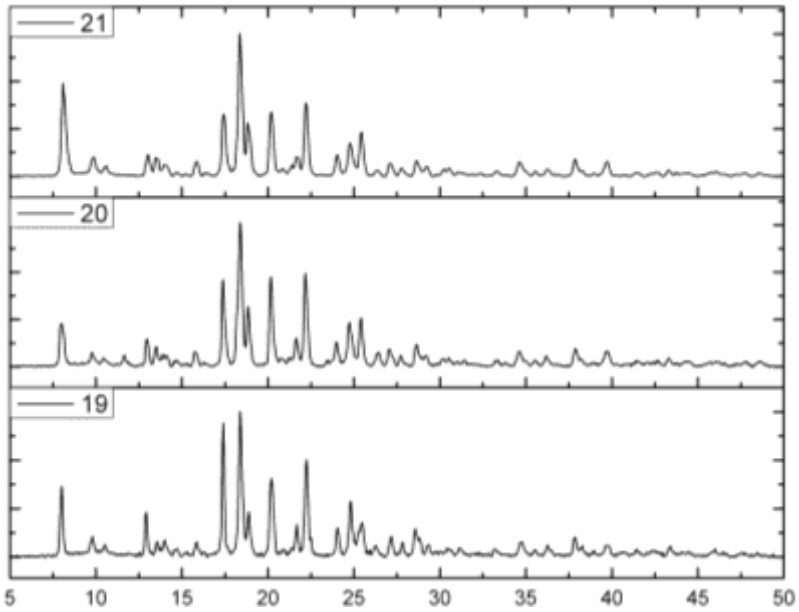

Fig. 6.2.4.1.2: Combination of the experimental powder X-ray diffractogram of zinc compounds at Cu-Kα wavelength 1.54184 Á. The measured PXRDs are smoothed and baseline corrected.

The fully matching PXRD patterns in Fig. 6.2.4.1.2 of the products from different zinc salts show that all isolated compounds are isostructural.

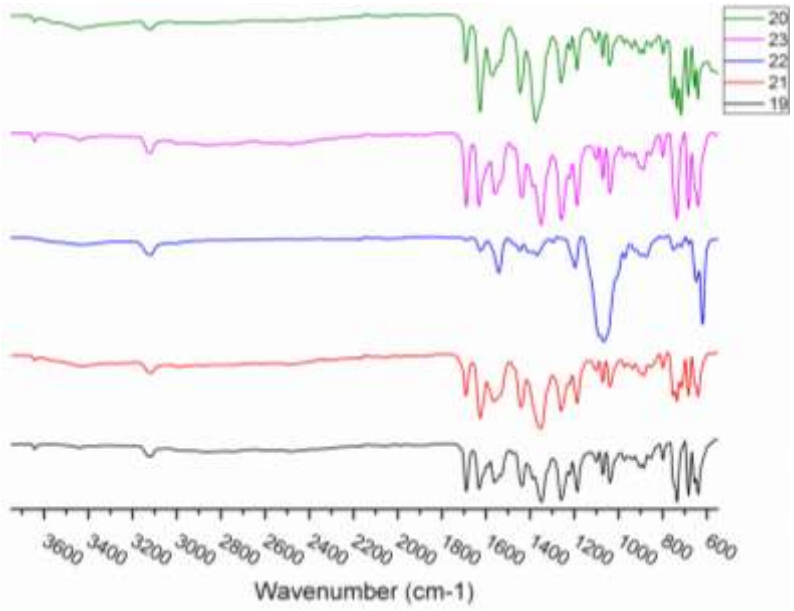

Fig. 6.2.4.1.3: IR Spectra (ATR) for comparison different compounds **19**, **21**, **22**, **23** and **20** to each other in range 550-3750 cm^{-1}.

The infrared spectra in Fig. 6.2.4.1.3 of zinc compounds show very similar patterns in the fingerprint region, thereby, supporting the chemical identity. For the product from $Zn(ClO_4)_2 \cdot 6H_2O$, it was not easy to separate the colorless target crystals from the co-precipitate, therefore, the IR-spectra contains an additional strong band at ~1100 cm^{-1}.

The ^{1}H-NMR spectra of zinc compounds show that, the *rac*-btrip ligand was included in the compound (Fig. 6.2.4.1.4). The ^{1}H-NMR spectra of other zinc compounds were measured only in DMSO-d_6 so that the signals of the btc ligand could not be detected. The phenomenon of not observing the btc protons was discussed in the previous section 7.2.3.

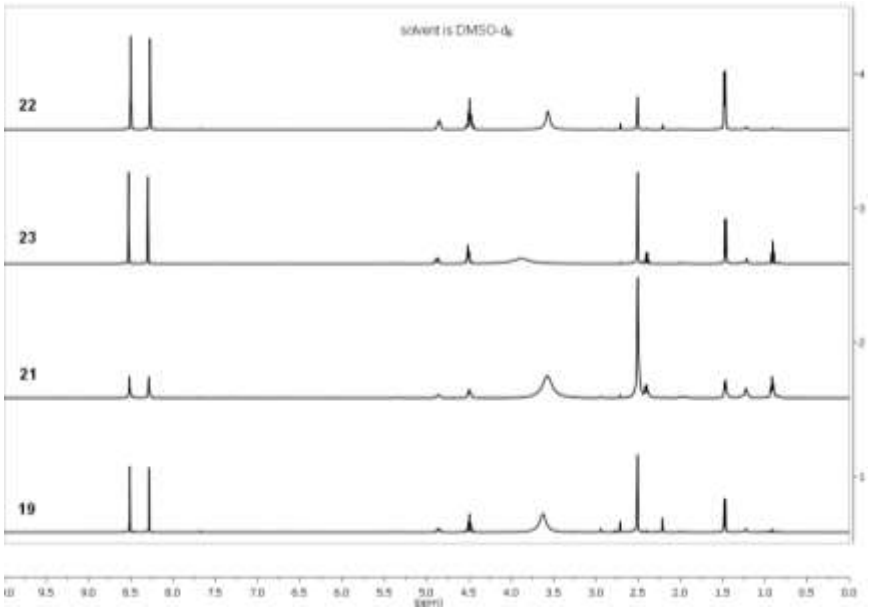

Fig. 6.2.4.1.4: ^{1}H NMR Spectrum (500 MHz) of zinc compounds in DMSO-d_6 showing the signals of the btrip ligand (see Fig. 6.2.2.15a,b for assignment).

7.2.5 Structure analysis and characterization of 2D-$[Cu_3(\mu_6\text{-btc})(\mu\text{-btc})(\mu\text{-atr})(H_2O)_5]_n$ (24)

This compound has been synthesized by Mr. Ümit Köc in his Diploma work [113]. Blue crystals (Fig. 6.2.5.1) of formula 2D-$[Cu_3(\mu_6\text{-btc})(\mu\text{-btc})(\mu\text{-atr})(H_2O)_5]_n$ **24**, are obtained from the hydrothermal reaction, at 125 °C, of copper(II) chloride hydrate, 4,4`-bis(1,2,4-triazol-4-yl) (btr) and benzene-1,3,5-tricarboxylic acid (H_3btc) in approximately 2:3:1 molar ratio. An Et_3N/H_2O solution was used as base to deprotonate the carboxylate groups of H_3btc. The resulting single crystals were separated from the precipitate and washed with the mother liquor. The reaction was repeated several times and found to be reproducible. The light blue prismatic crystals were obtained after two weeks of their synthesis. They are soluble in water, ethanol and methanol.

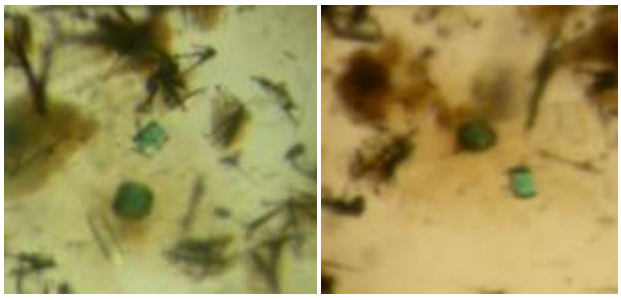

Fig. 6.2.5.1: Crystal images of **24** after about three weeks.

This compound crystallizes in the orthorhombic crystal system with the *Cmca* space group, and the crystallographic asymmetric unit consists of two different Cu(II) ions with two 2/3 btc ligands, 1/2 atr ligand and three coordinated aqua ligands. The 4,4`-bis-(1,2,4-triazol-4-yl) (btr) ligand is not completely incorporated into the structure probably due to the thermal decomposition of one triazole ring during the hydrothermal reaction at 125 °C. The obtained 2D-network polymer, 2D-$[Cu_3(\mu_6\text{-btc})(\mu\text{-btc})(\mu\text{-atr})(H_2O)_5]_n$, is as seen before in reference [114] which was synthesized using different conditions (Scheme 6.2.5.1). The extended asymmetric unit of 2D-$[Cu_3(\mu_6\text{-btc})(\mu\text{-btc})(\mu\text{-atr})(H_2O)_5]_n$ in ball-stick model is represented in Figure 6.2.5.2. Selected bond lengths and angles are summarized in (Table 6.2.5.1).

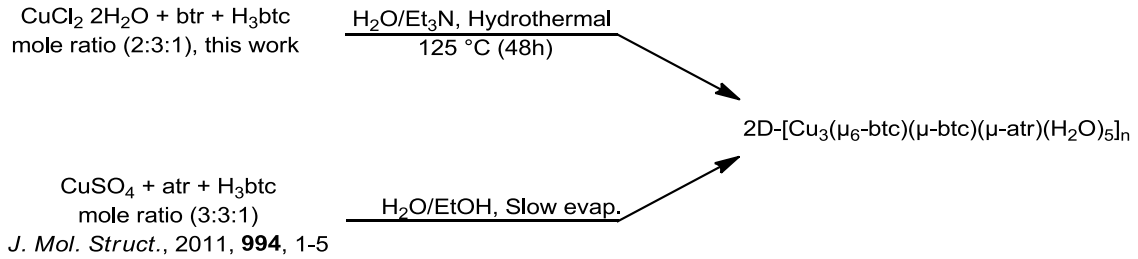

Scheme 6.2.5.1: Synthesis of 2D-$[Cu_3(\mu_6\text{-btc})(\mu\text{-btc})(\mu\text{-atr})(H_2O)_5]_n$ **24** in different conditions.

The structure of **24** contains 2D waved metal-ligands layers parallel to **ac** lattice plane, which involve two different types of coordination mode for btc^{3-} anions, where all carboxylic groups are deprotonated and coordinated to two different Cu(II) centers in different coordination environments.

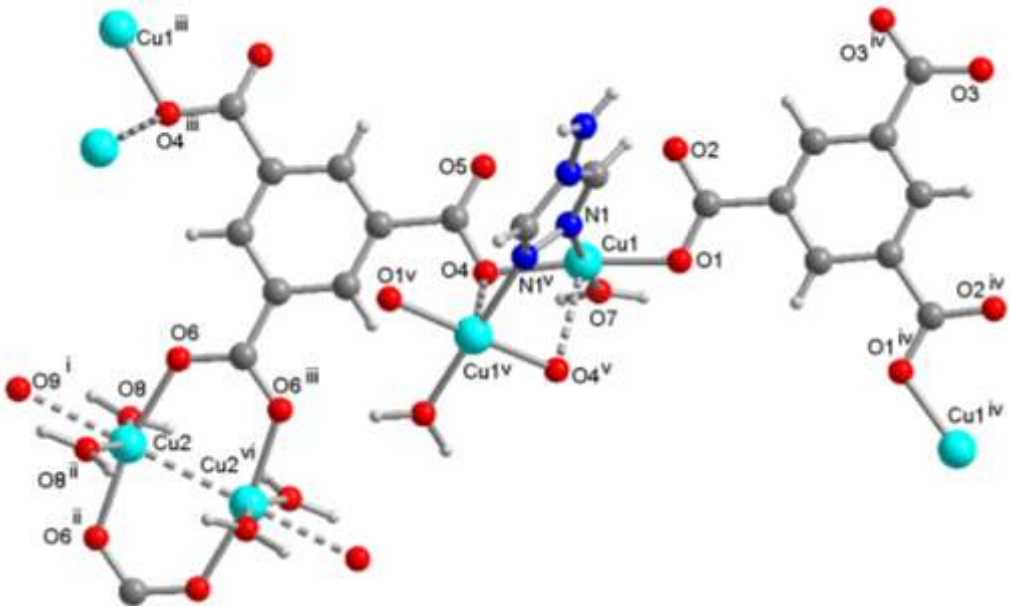

Fig. 6.2.5.2: Coordination environment of Cu(II) ions for compound 2D-$[Cu_3(\mu_6\text{-btc})(\mu\text{-btc})(\mu\text{-atr})(H_2O)_5]_n$ **24** shows the bridging action of the ligands and two different metal clusters. Symmetry operations: i = 1-x, 1/2-y, -1/2+z; ii = x, -y, -z; iii = 1-x, y, z; iv = -x, y, z; v = 1/2-x, y, 1/2-z; vi = 1-x, -y, -z.

The structure is not described further here, because it has already been reported in ref. [114]. Only a Figure for the section of the packing diagram is shown in Fig. 6.2.5.3.

Table 6.2.5.1: Selected bond lengths [Å] and angles [°] for **24**.

Cu1-O1	1.929(8)	O1-Cu1-N1	91.7(4)
Cu1-O4	1.969(8)	O1-Cu1-O4^{v}	100.1(3)
Cu1-O4^{v}	2.470(9)	O4-Cu1-O7	91.4(4)
Cu1-O7	1.947(9)	O4-Cu1-N1	89.9(4)
Cu1-N1	2.014(9)	O4-Cu1-O4^{v}	74.8(3)
Cu2-O6	2.019(13)	O6-Cu2-O8	89.5(5)
Cu2-O8	1.885(12)	O6-Cu2-O9^{i}	96.1(5)
Cu2-O9^{i}	2.460(4)	O6-Cu2-O6^{ii}	167.9(8)
Cu2-Cu2^{vi}	2.7147(13)	O6-Cu2-O8^{ii}	93.3(5)
O1-Cu1-O4	174.4(4)	O8-Cu2-O9^{i}	76.6(5)
O1-Cu1-O7	87.4(4)	O8-Cu2-O8^{ii}	153.1(9)

Symmetry transformations used to generate equivalent atoms: i = 1-x, 1/2-y, -1/2+z; ii = x, -y, -z; v = 1/2-x, y, 1/2-z; vi = 1-x, -y, -z.

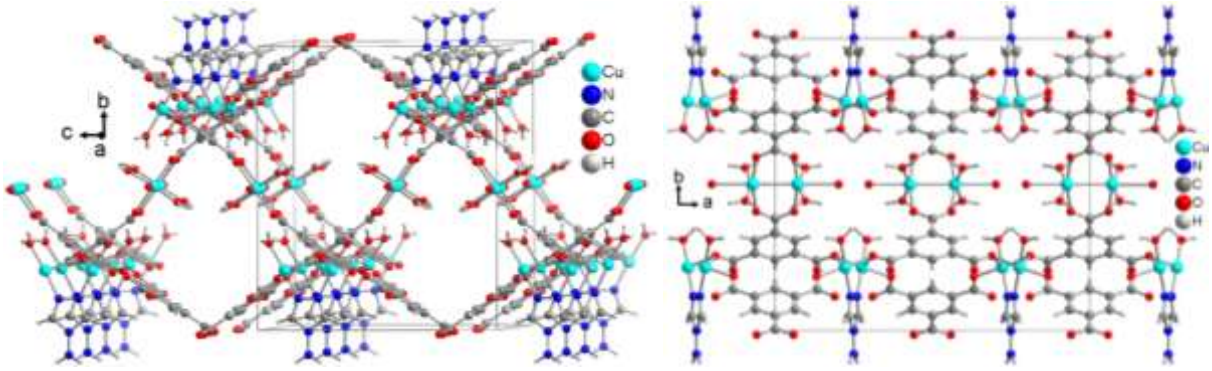

Fig. 6.2.5.3: 2D-net of **24** showing the formation of 1D-chains of bridging atr and btc ligands with Cu1-atoms along **a** axis within the network (left), which are connected *via* paddlewheel SBU of Cu2-atoms and two carboxylate groups of btc ligands (right).

The 2D-waved layers are polycatenated with two adjacent 2D-layers, above and below along ***b*** axis, which lead to formation of a 3D-polycatenated network [47] (Figure 6.2.5.4).

The comparison of the measured and simulated PXRD patterns, which is calculated from obtained x-ray single crystal structure data for the copper compound, is represented in Figure 6.2.5.5 which shows that both PXRD patterns differ. Some peaks were missed in measured PXRD pattern. This could be attributed to drying of the crystals in vacuum furnace for *ca.* 3h at temperature 40°C before PXRD measurement.

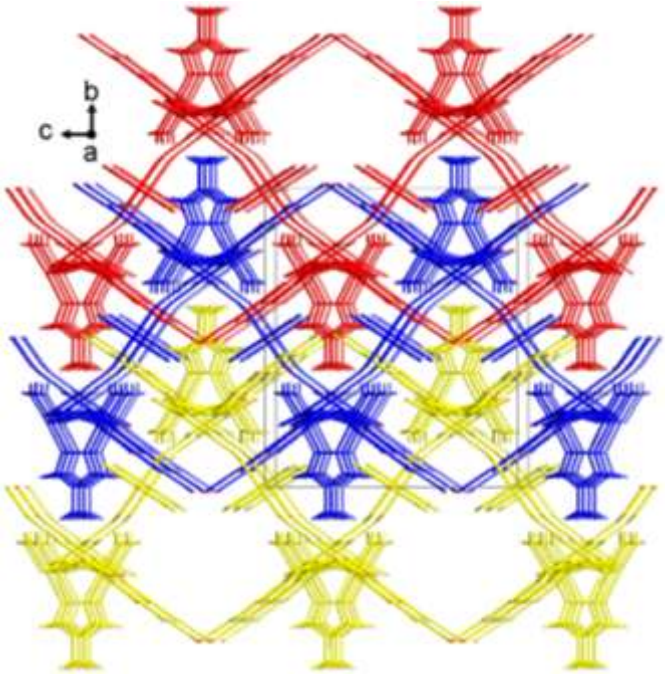

Fig. 6.2.5.4: Interpenetration of three 2D-networks (red, blue and yellow) in the crystal structure lead to form 3D supramolecular structure of polycatenated 2D-nets.

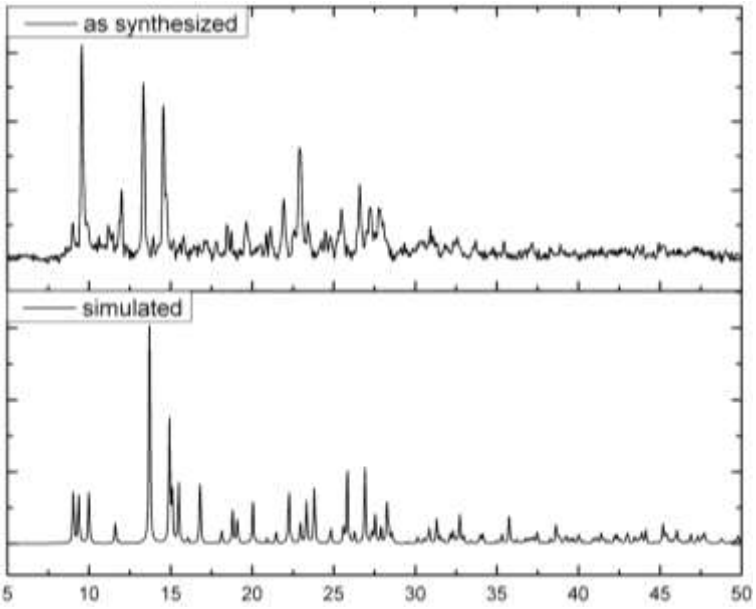

Fig. 6.2.5.5: Combination of the experimental powder X-ray diffractogram of compound **24** (top) at Cu-Kα wavelength 1.54184 Á with the theoretical pattern calculated from the single crystal data-new measurement (bottom). The measured PXRD is smoothed and baseline corrected.

NaCN was added to sample before ^{1}H NMR measurement. After centrifugation, the pipette-separated supernatant was measured. In Figure 6.2.5.6 the signal of the two protons of the

triazole ring in the atr ligand appears in the ^{1}H NMR spectrum at 9.17 ppm and the signal for the amino group is observed at 6.27 ppm. The signals at 8.37 and 8.12 ppm are assigned to three protons of the benzene ring in the btc ligand. Signals for residual Et_3N appeared at 0.92 and 2.41 ppm, where the crystals were washed with mother liquor and Et_3N was used to deprotonate the H_3btc ligand. Mostly, $[Et_3NH]^+$ CN^- was formed in deuterated NMR solvent after NaCN addition. The integration ratio between signal of for three protons for btc ligand and signal of two protons for triazole ring of atr ligand is not clear, because, it was not easy to separate single crystals from precipitate (see Figure 6.2.5.1).

The comparison between the FT-IR spectra (ATR) of compound **24** and the mixture of atr and H_3btc ligands (Figure 6.2.5.7) shows that both ligands are coordinated with Cu-atoms. The multiple weak broad peaks around 3374, 3304 and 3128 cm^{-1}, which can be assigned to the O–H/N–H stretching vibrations of aqua ligands and amino group of atr ligand [112]. The absence of a peak at *ca* 1715 cm^{-1} in **24** indicates the full deprotonation of H_3btc ligand. Additionally, the asymmetric and symmetric stretching vibrations of the carboxylate group [105] are observed at 1622, 1568, and 1434, 1366, 1340 cm^{-1}, which reveal the different binding modes of carboxylate group in **24**. Bands at 747, and 724 cm^{-1}, in the fingerprint region, for **24** are due to 1,3,5-trisubstituted benzene [105]. Furthermore, the band at 620 cm^{-1} can be assigned to the vibration mode of the triazole ring of atr ligand [115]. Thus, the IR and ^{1}H NMR spectra are in agreement with its single-crystal X-ray diffraction.

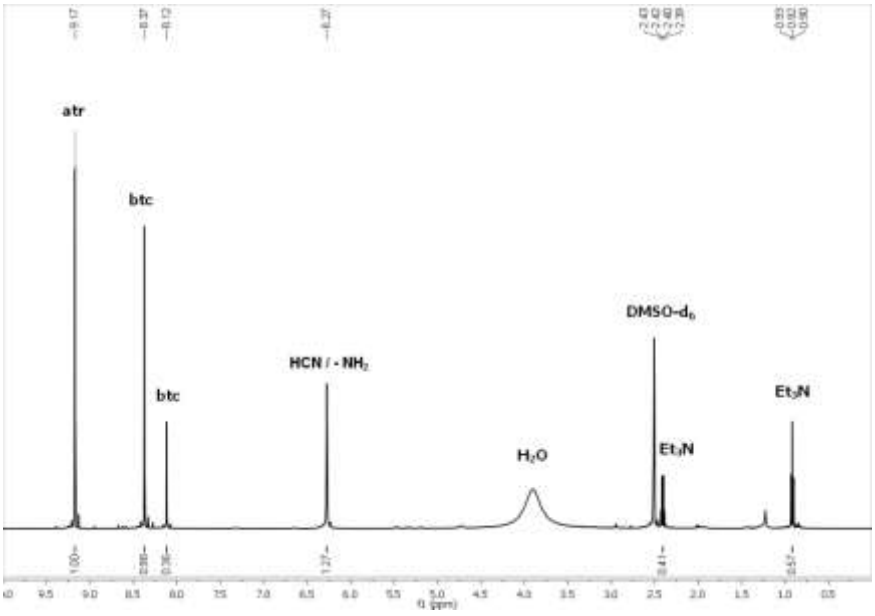

Fig. 6.2.5.6: ^{1}H NMR Spectrum (500 MHz) of **24** in DMSO-d_6.

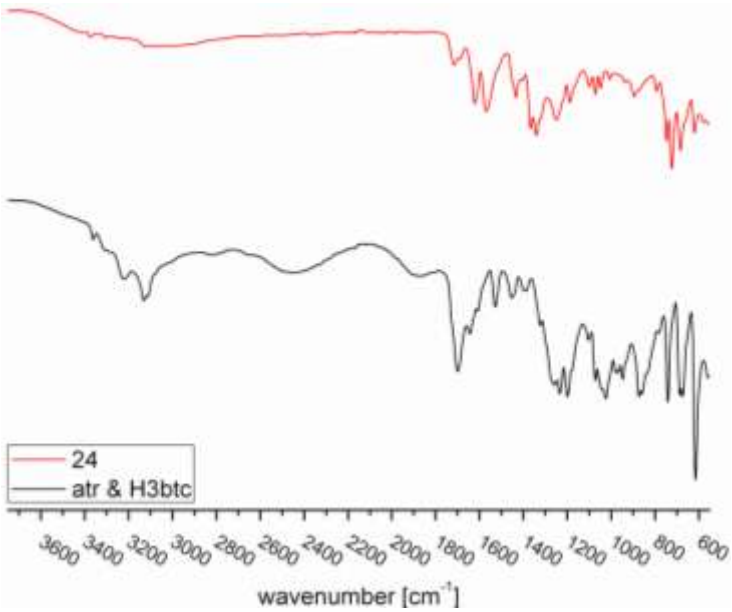

Fig. 6.2.5.7: IR Spectra (ATR) for comparison between the compound **24** and the mixture of ligands atr and H_3btc in range 550-3750 cm^{-1}.

7.2.6 Structure analysis and characterization of 1D-{[$Cd_2(\mu_2$-btc$)_2$(atr$)_2(H_2O)_4$][$Cd(H_2O)_6$]·$2H_2O$}$_n$ (25)

This compound has been synthesized by Mr. Ümit Köc in his Diploma work [113]. Colorless crystals (Fig. 6.2.6.1) of formula 1D-{[$Cd_2(\mu_2$-btc$)_2$(atr$)_2(H_2O)_4$][$Cd(H_2O)_6$]·$2H_2O$}$_n$ **25**, are obtained from the hydrothermal reaction of $Cd(OAc)_2.2H_2O$, 4,4`-bis(1,2,4-triazol-4-yl) (btr) and benzene-1,3,5-tricarboxylic acid (H_3btc) in approximately 1:3:1 molar ratio. Et_3N/H_2O solution was used as base to deprotonate the carboxylate groups of H_3btc. The synthesis is almost identical to compound 2D-[$Cd(\mu_3$-Hbtc$)(H_2O)_2]_n$ **26**. Except, that the synthesis was carried out at lower temperature 125 °C instead of 140 °C. The reaction was repeated several times and found reproducible. The crystals are soluble in water and ethanol.

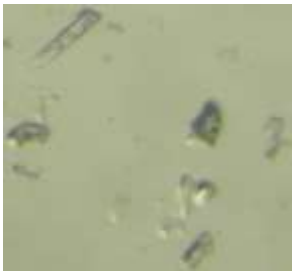

Fig. 6.2.6.1: Colorless crystals of 1D-{[$Cd_2(\mu_2$-btc$)_2$(atr$)_2(H_2O)_4$][$Cd(H_2O)_6$]·$2H_2O$}$_n$ **25**.

This compound crystallizes in the monoclinic crystal system with the *P* 2_1/c space group and the crystallographic asymmetric unit consists of Cd1(II) ions with ligands (btc, atr and H_2O) and half cationic aqua complex of Cd2(II) ions and lattice water molecule. The ligand 4,4`-bis(1,2,4-triazol-4-yl) (btr) is not completely incorporated into the structure probably due to decomposition of one triazole ring by heating to 125°C. The extended asymmetric unit of 1D-$\{[Cd_2(\mu_2\text{-btc})_2(atr)_2(H_2O)_4][Cd(H_2O)_6]\cdot 2H_2O\}_n$ with 50% thermal ellipsoids for non-hydrogen atoms is represented in Figure 6.2.6.2.

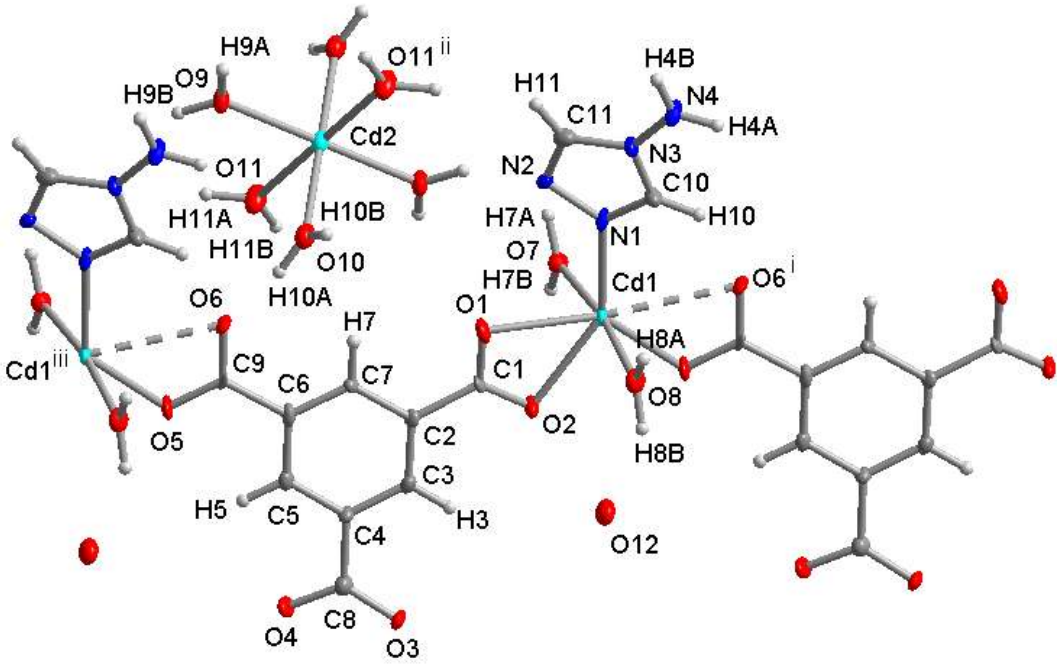

Figure 6.2.6.2: The extended asymmetric unit of 1D-$\{[Cd_2(\mu_2\text{-btc})_2(atr)_2(H_2O)_4][Cd(H_2O)_6]\cdot 2H_2O\}_n$ **25** with 50% thermal ellipsoids for non-hydrogen atoms showing the full coordination environment of the cadmium atoms. Symmetry transformation: i = x+1, y, z; ii = -x+1, -y+1, -z+1; iii = x-1, y, z.

The Cd1 atom is coordinated in a distorted pentagonal bipyramidal fashion by one nitrogen atom of 4-amino-1,2,4-triazol-4-yl (atr) and six oxygen atoms; two of them belong to axial aqua ligands. The other O atoms belong to two fully deprotoneted btc^{3-} benzene-tricarboxylate anions, two of their carboxylate groups are bonded *via* bidentate chelating carboxylate groups (O1-Cd-O2 and O5-Cd-O6), whilst the third carboxylate group stays without coordination. The O-atoms of btc^{3-} and N-atom of atr ligands are located in the equatorial plane. The Cd-O6 is longer than other Cd-O bonds, their lengths vary in the range 2.261(5)-2.762(8) Å. The atr ligand coordinates with Cd1 through N1-atom of its triazol ring while the other N-atoms remain without coordination. The btc^{3-} anions coordinate with two Cd1 atoms in bidentate chelating mode while the third carboxylate group being

uncoordinated to form extended 1D-anionic chains. Each Cd2 atom has slightly distorted octahedral environment with six water molecules, which lead cationic aqua-complexes between anionic chains (Fig. 6.2.6.3). Such the positive charges of the aqua-complexes neutralize the negative charges of the chains and the structure is overall neutral. The structural representation of **25** with atom labeling is shown in Fig. 6.2.6.2. Selected bond lengths and angles are summarized in Table 6.2.6.1.

Table 6.2.6.1: Selected bond lengths [Å] and angles [°] for **25**.

Cd1-N1	2.252(6)	$O5^{i}$-Cd1-O2	84.43(16)
Cd1-O1	2.413(5)	O8-Cd1-O2	89.39(18)
Cd1-O2	2.354(5)	O7-Cd1-O2	82.45(17)
Cd1-$O5^{i}$	2.261(5)	N1-Cd1-O1	88.02(17)
Cd1-$O6^{i}$	2.762(8)	$O5^{i}$-Cd1-O1	139.38(16)
Cd1-O7	2.327(5)	O8-Cd1-O1	90.35(18)
Cd1-O8	2.303(5)	O7-Cd1-O1	84.87(17)
Cd2-O9	2.273(5)	O2-Cd1-O1	54.95(16)
Cd2-O10	2.301(5)	$O9^{II}$-Cd2-O9	179.998(1)
Cd2-O11	2.264(5)	O10-Cd2-$O10^{ii}$	180.0(2)
N1-Cd1-$O5^{i}$	132.59(18)	$O11^{ii}$-Cd2-O11	179.999(2)
N1-Cd1-O8	90.6(2)	O11-Cd2-$O9^{II}$	92.35(18)
$O5^{I}$-Cd1-O8	88.52(18)	O11-Cd2-O9	87.66(18)
N1-Cd1-O7	95.81(19)	$O11^{II}$-Cd2-O10	94.1(2)
$O5^{I}$-Cd1-O7	90.82(17)	O11-Cd2-O10	85.9(2)
O8-Cd1-O7	171.84(17)	$O9^{II}$-Cd2-O10	93.13(18)
N1-Cd1-O2	142.96(17)	O9-Cd2-O10	86.87(18)

Symmetry transformations used to generate equivalent atoms: i = x+1, y, z; ii = -x+1, -y+1, -z+1.

The infinite anionic chains are stacked parallel to each other, so that there are significant π-π interactions [116] between the adjacent benzene rings of the btc ligands and the neighboring triazole rings of atr ligands. The centroid–centroid distance of adjacent benzene rings is 3.7264(6) Å and for neighboring triazole rings it is 3.5985(6) Å, which is shown in Figure 6.2.6.3. The remaining spaces between the neighboring anionic chains are occupied by cationic aqua-Cd2 complexes and lattice water molecules as shown in Figure 6.2.6.4.

Furthermore, the structure of compound **25** contains unusual strong hydrogen bonding (Table 6.2.6.2) between the aqua ligands of cationic complexes and anionic chains. The π-π interactions between adjacent anionic chains and the hydrogen bonds between cationic

complexes and anionic chains with lattice water molecules build a 3D superamolecular network as shown in Figure 6.2.6.5.

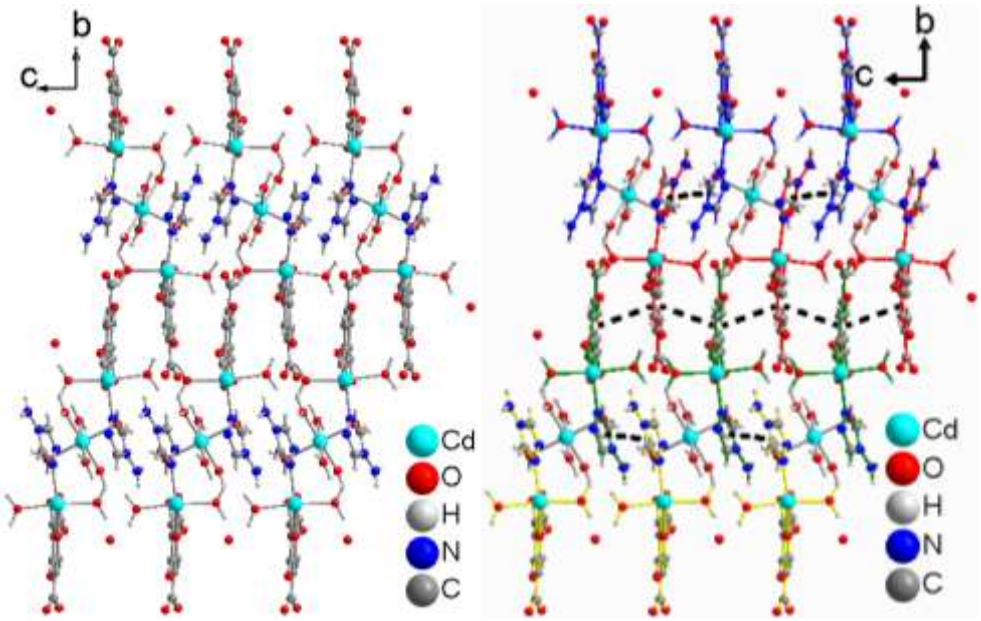

Figure 6.2.6.3: Packing diagram of **25** shows the alternating cationic complexes and anionic chains in ball-stick representation (left), in different color (right). The π-π interactions between neighboring benzene rings and between adjacent triazole rings are shown as black dashed lines.

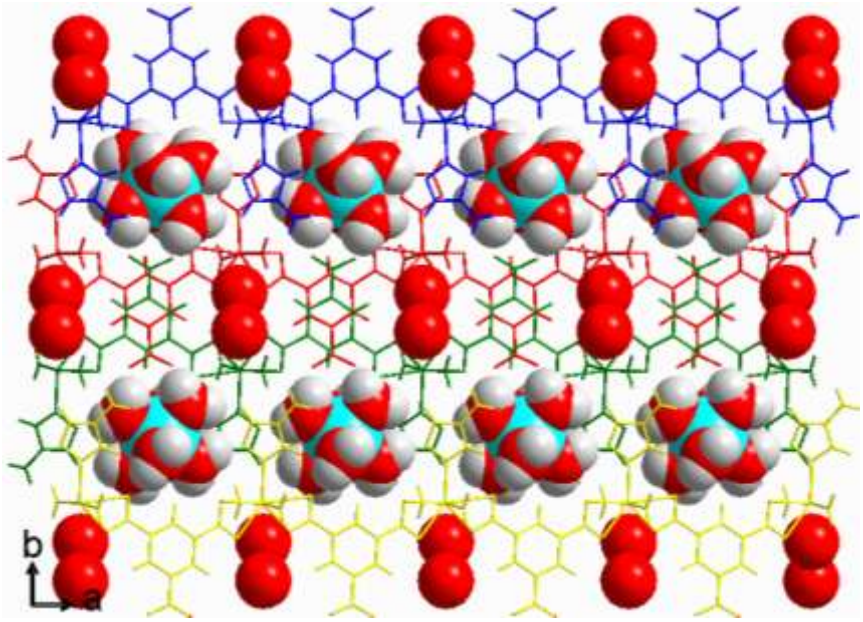

Figure 6.2.6.4: The Packing diagram of **25** showing the cationic complexes and lattice water molecules in space-filling and anionic chains in wires.

Table 6.2.6.2: Details of hydrogen bond in **25** (Å, °).

D-H…A	d(D-H)	d(H…A)	d(D…A)	<(D-H…A)
O7-H7A…N4^{iv}	0.95	2.31	3.126(8)	143
O7-H7B…O12^{i}	0.95	2.07	2.684(7)	121
O8-H8A…O11^{v}	0.95	2.42	3.288(7)	152
O8-H8B…O12^{v}	0.95	2.07	2.714(7)	124
O9-H9B…N2^{ii}	0.95	2.00	2.891(8)	156
O9-H9A…O3^{vi}	0.95	1.84	2.788(7)	177
O10-H10A…O6	0.91	1.87	2.746(7)	160
O10-H10B…N4^{vii}	0.95	2.32	2.810(8)	111
O11-H11B…O4^{viii}	0.95	1.70	2.636(7)	172
N4-H4A…O10^{vii}	0.88	1.98	2.810(8)	156
N4-H4B…O1^{vii}	0.88	2.19	2.851(8)	131

Symmetry transformation used to generate equivalent atoms: i = x+1, y, z; ii= -x+1, -y+1, -z+1; iv = -x+2, -y+1, -z+1; v = x+1, y, z+1; vi = -x+1, y+1/2, -z+3/2; vii = -x+2, -y+1, -z+2; viii = x, -y+1/2, z-1/2.

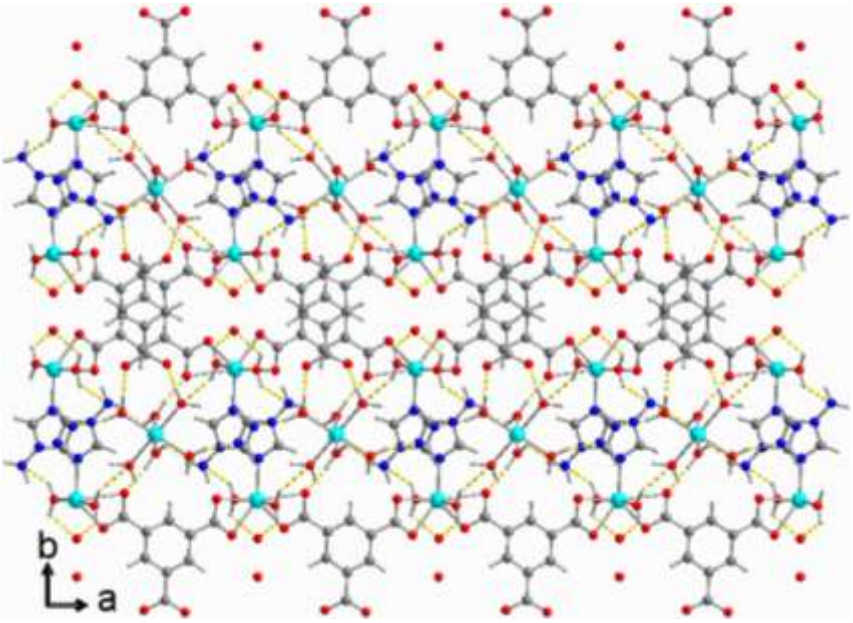

Figure 6.2.6.5: Packing diagram of **25** showing the H bonds as yellow dashed lines between cationic complexes and anionic chains in ball-stick representation.

The comparison of the measured and simulated PXRD pattern, shows that both PXRD patterns differ substantially in their peaks position and relative intensity. As reason for this case is probably that the unit cell parameter was changed, when the crystals were dried in vacuum furnace for *ca*. 3h at temperature 40°C before PXRD measurement.

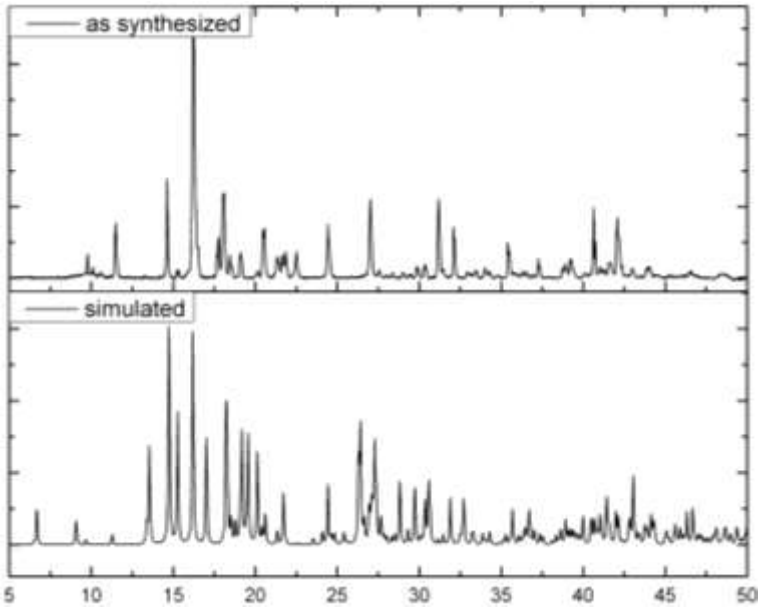

Figure 6.2.6.6: Combination of the experimental powder X-ray diffractogram of compound **25** (top) at Cu-Kα wavelength 1.54184 Å with the theoretical pattern calculated from the single crystal data (bottom). The measured PXRD is smoothed and baseline corrected.

For ^{1}H NMR measurement of compound **25**, the sample was dissolved in DMSO-d_6 *via* heating in an ultrasonic bath at 50°C then NaCN was added to sample and after centrifugation, the pipette-separated supernatant was measured. The ^{1}H NMR spectrum of compound **25** (Figure 6.2.6.7) shows both atr and btc ligands signals. The signal due to two protons of the triazole ring in the atr ligand appears at 9.17 ppm and the signal for amino group is observed at 6.30 ppm. The signal for the three protons of the benzene ring in the btc ligand is noted at 8.36 ppm. Signals for residual Et_3N appear at 0.91 and 2.40 ppm. The integration ratio between signal for three protons of btc ligand and the signal for two protons of the triazole ring of the atr ligand show that the molar ratio between both ligands for one proton is close to 0.56:0.50~1:1. Thus, the ^{1}H NMR spectrum is in agreement with the single crystal X-ray structure.

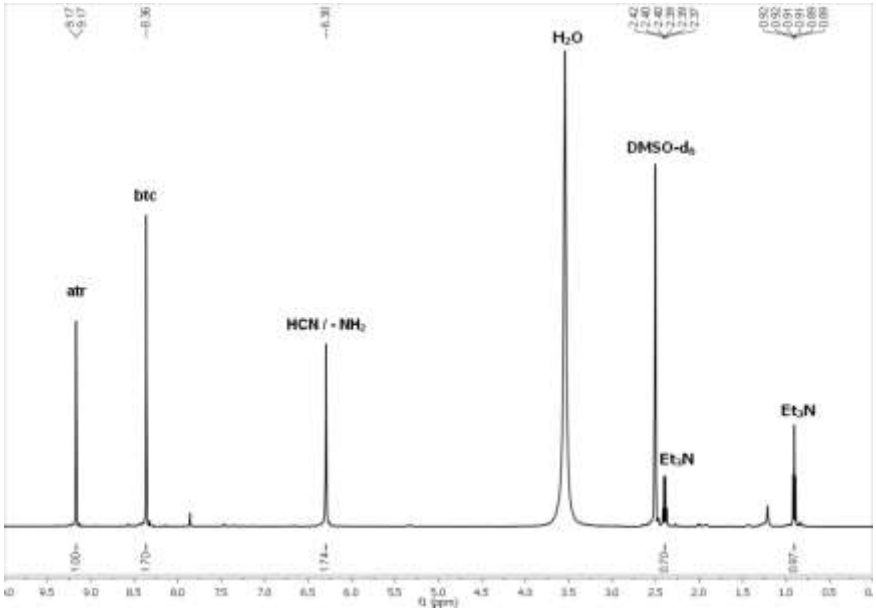

Fig. 6.2.6.7: ^{1}H NMR Spectrum (500 MHz) of **25** in DMSO-d_6.

The comparison between the FT-IR spectra (ATR) of compound **25** and the mixture of atr and H_3btc ligands (Figure 6.2.6.8) shows that both ligands are coordinated to Cd-ions. The multiple weak broad peaks around 3257, 3208, 3136 and 3103 cm^{-1}, which can be assigned to the O–H/N–H stretching vibrations of aqua ligands and amino group of atr ligand [112]. The absence of a peak at ca 1700 cm^{-1} in **25**, respectively indicate the full deprotonation of H_3btc ligand. Additionally, the asymmetric and symmetric stretching vibrations of the carboxylate group [105] are observed at 1648, 1606, and 1430, 1363 cm^{-1}, which reveal the different binding modes of carboxylate group in **25**. Thus, the IR spectrum is in agreement with its single-crystal X-ray diffraction. Bands at 754, and 727 cm^{-1}, in the fingerprint region, for **25** are due to 1,3,5-trisubstituted benzene [109], [112]. Furthermore, the band at 611 cm^{-1} can be assigned to the vibration mode of the triazole ring of atr ligand [115].

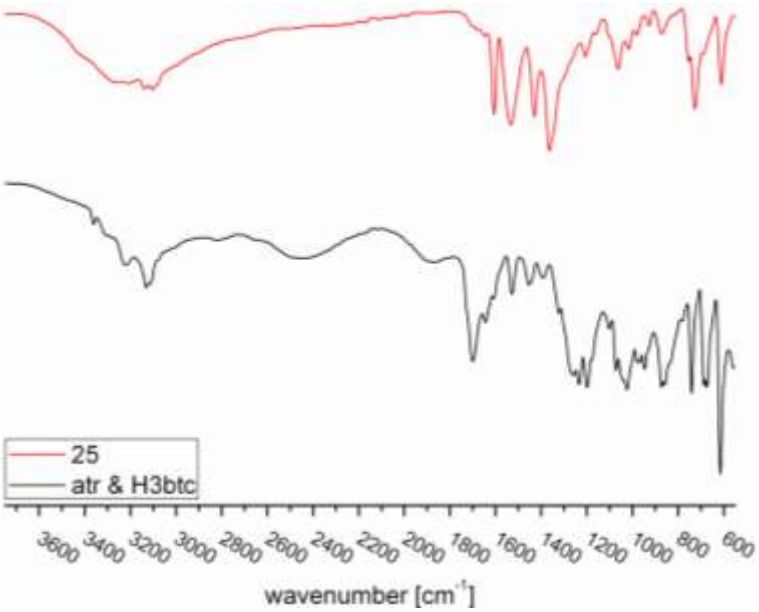

Fig. 6.2.6.8: IR Spectra (ATR) for comparison between the compound **25** and the mixture of ligands atr and H_3btc in range 550-3750 cm^{-1}.

7.3 Coordination polymers with 1,2-bis(1,2,4-triazol-4-yl)propane

7.3.1 Structure analysis and characterization of 3D-{[$Cu_4(\mu_4\text{-}Cl)(\mu_4\text{-}$*rac*-btrip$)_4(H_2O)_4$] ($BF_4/ClO_4/OH)^-_7 \cdot xH_2O\}_n$ (17)

Blue, square plate single crystals of compound **17** (Figure 6.3.1.1) were obtained by the same hydrothermal reaction condition that were used to synthesize the coordination polymer **16**, but by using copper(II) tetrafluoroborate hydrate as metal source. An aqueous solution of copper(II) tetrafluoroborate hydrate, racemic 1,2-bis(1,2,4-triazol-4-yl)propane (*rac*-btrip) and benzene-1,4-dicarboxylic acid (H_2bdc) in approximately 2:2:1 molar ratio were mixed in a glass tube and then placed in a programmable heating oven at 125°C. NH_3 solution was used to deprotonate H_2bdc. The resulting crystals were filtered, washed with mother liquor. The reaction was repeated several times and found reproducible. The single crystals were manually separated and used for the subsequent characterization and analysis.

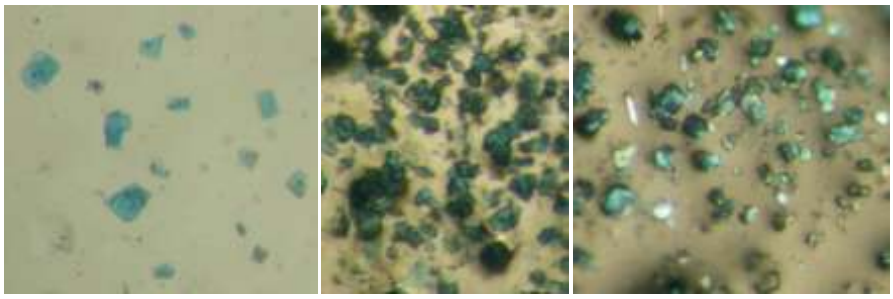

Fig. 6.3.1.1: Blue, square plate crystals of **17**.

Proton NMR analysis of a sample of **17** digested in DMSO-d_6 gave that Cu-atoms are only coordinated with btrip (see below). In compound **17** the methyl groups on the bis(triazolyl)propyl ligand could not be completely refined due to their disorder over four positions (Fig. 6.3.1.2), where the *R*-btrip and *S*-btrip configuration (see section 7.3.4) are coordinated to the Cu(II) atoms in statistically alternating orientation and direction. In addition, The BF_4^- anions were better refined as ClO_4^- in a disordered position due to free rotation and different location inside the lattice of the 3D-cationic net. Possibly the $Cu(BF_4)_2.xH_2O$ salt was not pure and contained a little $Cu(ClO_4)_2.xH_2O$ salt. Also, the chosen crystal did only diffract until 2theta = 50.22°. The methyl groups of the propyl part of the btrip ligands have been located as in other similar structures **16** and **19**.

Compound **17** crystallized in the tetragonal crystal system with the *I4/mmm* space group and a cell volume of 3214.9(6) $Å^3$. The crystallographic asymmetric unit consists of one Cu(II) ion with a quarter *rac*-btrip ligand, a quarter BF_4^-/ ClO_4^- anion, one Cl-atom in center SBU, one coordinated aqua ligand and some lattice water molecules. The propyl moiety of btrip ligand lies on a mirror plane and glide plane (analysis with the program Mercury [117]), the trans-bent btrip ligand has C_{2v}-symmetry, O-Cu-Cl bonds of the SBU lie on a 2-fold rotation axes and mirror planes. The center of SBU lies on a 4-fold rotation axes. The extended unit building of 3D-$\{[Cu_4(\mu_4\text{-}Cl)(\mu_4\text{-}rac\text{-}btrip)_4(H_2O)_4]\ (BF_4/ClO_4/OH)^-_7 \cdot xH_2O\}_n$ is represented in Figure 6.3.1.2. Selected bond lengths and angles are summarized in Table 6.3.1.1.

Table 6.3.1.1: Selected bond lengths [Å] and angles [°] for **17**.

Cu-N1	2.008(5)	O1-Cu-N1	90.36(15)
Cu-O1	2.255(9)	N1-Cu-N1^{i}	179.3(2)
Cu-Cl1	2.420(1)	N1-Cu-N1^{ii}	88.63(18)
Cl1-Cu-O1	179.98	N1-Cu-N1^{iii}	91.37(18)
Cl1-Cu-N1	89.64(15)		

Symmetry transformations used to generate equivalent atoms: i = x, 1-y, -z; ii = x, y, -z; iii = x, 1-y, z.

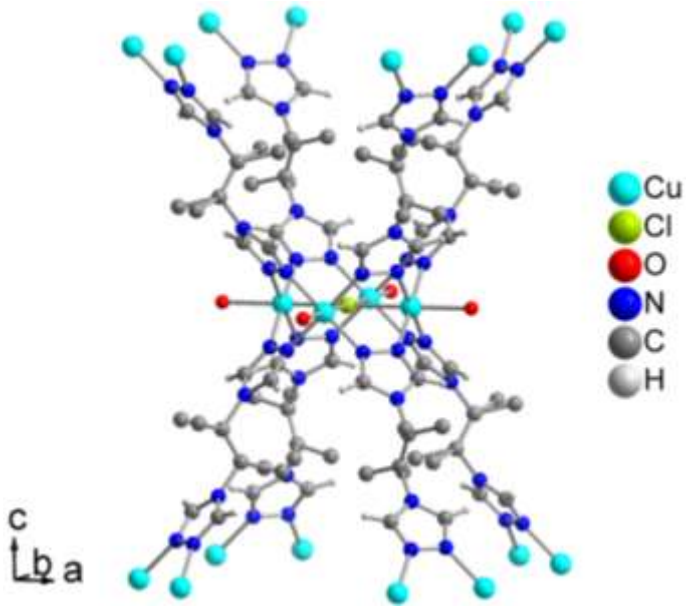

Figure 6.3.1.2: Extended unit building of compound **17**. The bis(triazolyl)propyl ligands sit on special positions. The methyl groups of the propyl moiety, anions and lattice water molecules are disordered. Anions and lattice water molecules are omitted for clarity.

The structure contains isolated tetranuclear copper cluster $[Cu_4(\mu_4\text{-}Cl)(triazolyl)_8(H_2O)_4]^{7+}$ (Fig. 6.3.1.3) as secondary building unit (SBU). In SBU, each Cu(II) center is coordinated to four N atoms from four different *rac*-btrip ligands in equatorial postion, one Cl-atom from center of tetranuclear coper cluster with one oxygen atom an aqua ligand in axial position to complete the Jahn-Teller-distorted octahedral coordination environment of Cu-atoms. Bond distances between Cu(II) ions in SBU are Cu…Cu = 3.4224(14) and 4.8399(20) Å, respectively. In the structure, the SBUs are stacked parallel to each other along ***c*** axis (Fig. 6.3.1.4 and Fig. 6.3.1.5).

Overall, six SBUs and eight *R*-,*S*-btrip ligands define the six vertices and eight edges, respectively of an octahedral cage (Figure 6.3.1.4) with distances between the Cl…Cl vertices = 13.0141(8), 18.4047(8) and 18.982(3) Å. Each octahedral cage shares its vertices and edges with eight other neighboring octahedron cavities, defining a 3D-network structure identical to the sodium halide structure (NaCl) or isopolyanions like $[W_6O_{19}]^{2-}$, $[Ta_6O_{19}]^{8-}$ [118], where tetrahedral holes are occupied between vertex-sharing octahedral (Figure 6.3.1.5).

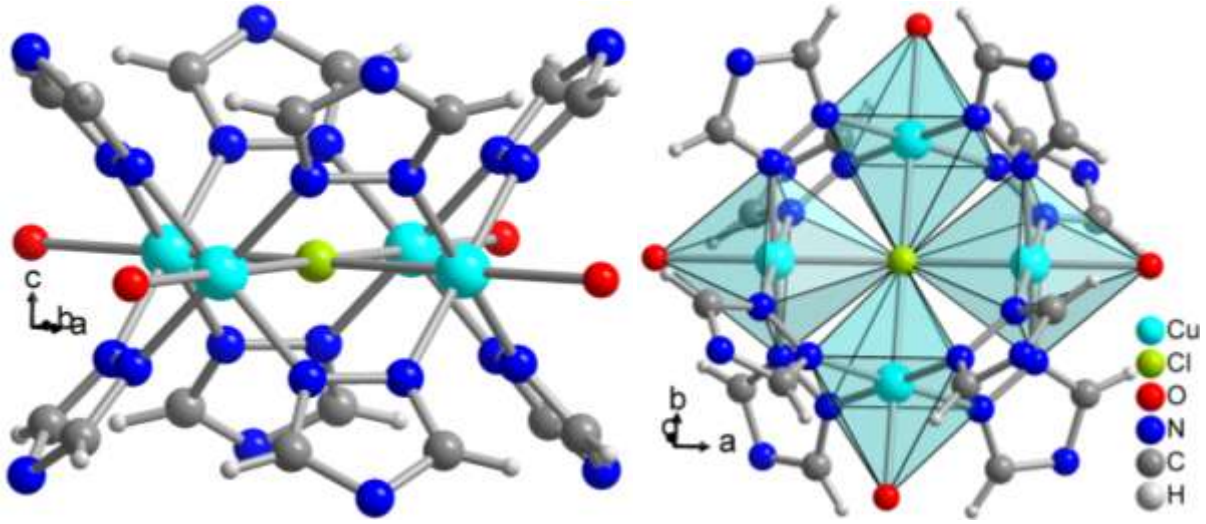

Figure 6.3.1.3: Structure of secondary building unit $[Cu_4(\mu_4\text{-}Cl)(triazolyl)_8(H_2O)_4]^{7+}$ for **17** in two different directions and representations.

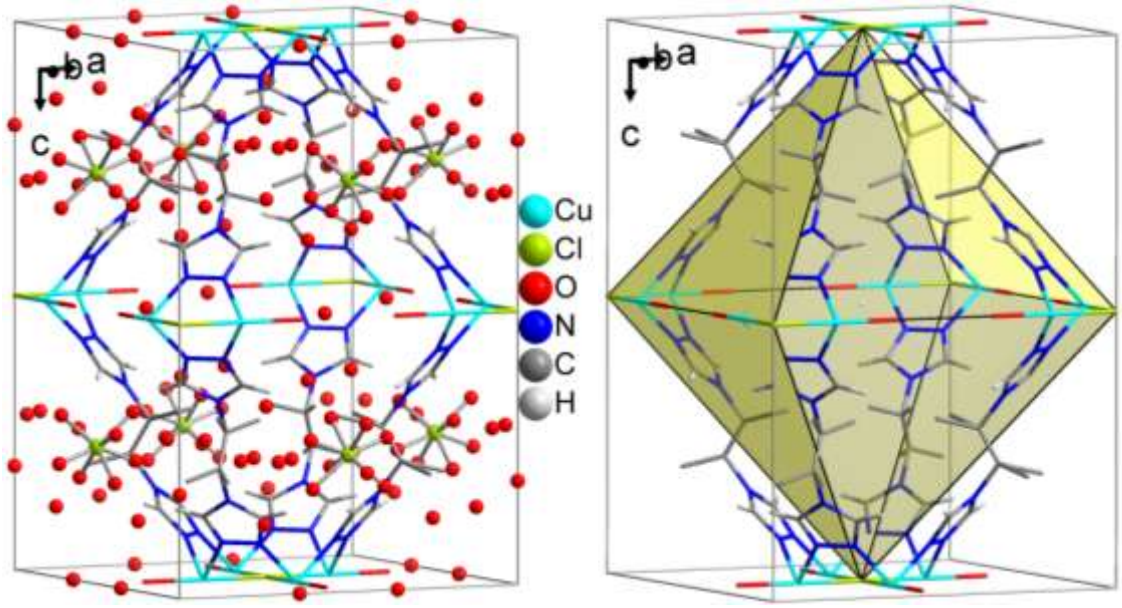

Figure 6.3.1.4: Representation of the octahedral cage in compound **17** with anions and lattice molecules in ball-stick model (left) and without guest molecules (right). Ligands and SBUs are showing in stick model.

Each trans-bent *rac*-btrip ligand is coordinated with four Cu(II) atoms as μ_4-tetradentate ligand in κN1:N1` mode and bridged between two SBUs.

Cu(II) atoms in the SBU are bridged by eight triazole rings above and below the plane of metal cluster $[Cu_4(\mu_4\text{-}Cl)(H_2O)_4]^{7+}$, such that each SBU is surrounded by eight *rac*-btrip ligands and connected *via* trans-bent *rac*-btrip ligands with eight neighboring SBUs, which

form a 3D-cationic network with rhombic channels (Figure 6.3.1.5) along ***a*** and ***b*** axis and square channels along ***c*** axis (Figure 6.3.1.6).

Topologically, each $[Cu_4(\mu_4\text{-}Cl)(triazolyl)_8(H_2O)_4]^{7+}$ can be simplified as a 8-connected unit, and the ligand as a linker. So that a 3D-cationic framework is defined as 3D-(2,8)-connected network.

There are two ClO_4^- anions per $\{Cu_4(\mu_4\text{-}Cl)\}^{7+}$ SBU. Within the 3D-cationic framework disordered ClO_4^-,-anions and possibly other disordered anions like BF_4^-, F^-, Cl^- and OH^- will equal the positive charge of 3D-cationic network.

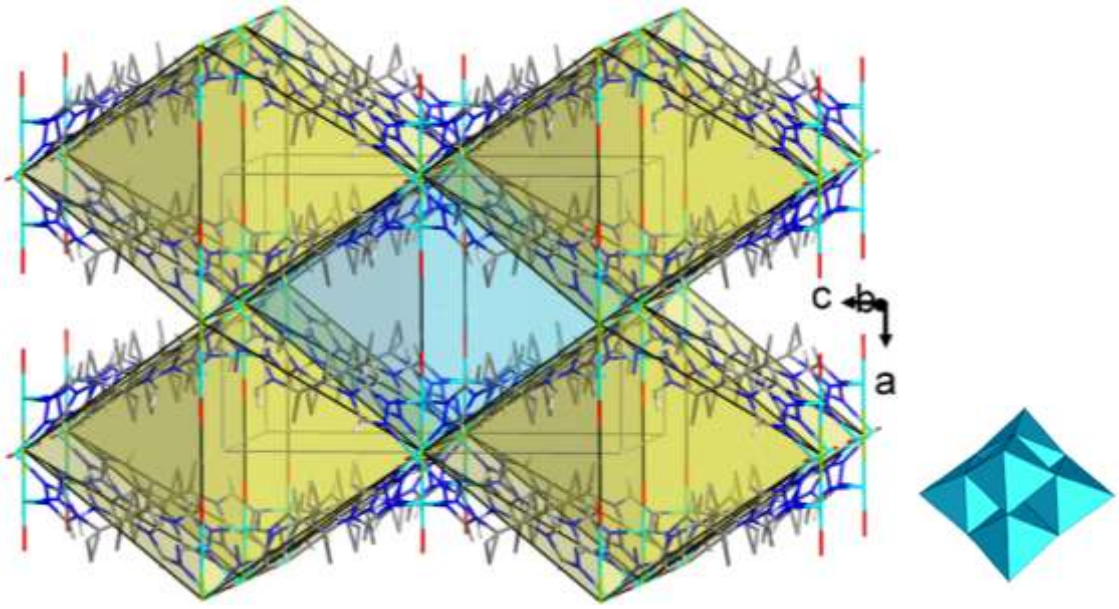

Figure 6.3.1.5: Representation of nine octahedral cavities in compound **17**, which are sharing through their edges and vertices. Tetrahedral holes are formed between neighboring shared octahedral cavities. Ligands and SBUs are presented in wire model. Channels along ***a*** and ***b*** axis are formed. Guest molecules and anions are omitted for clarity.

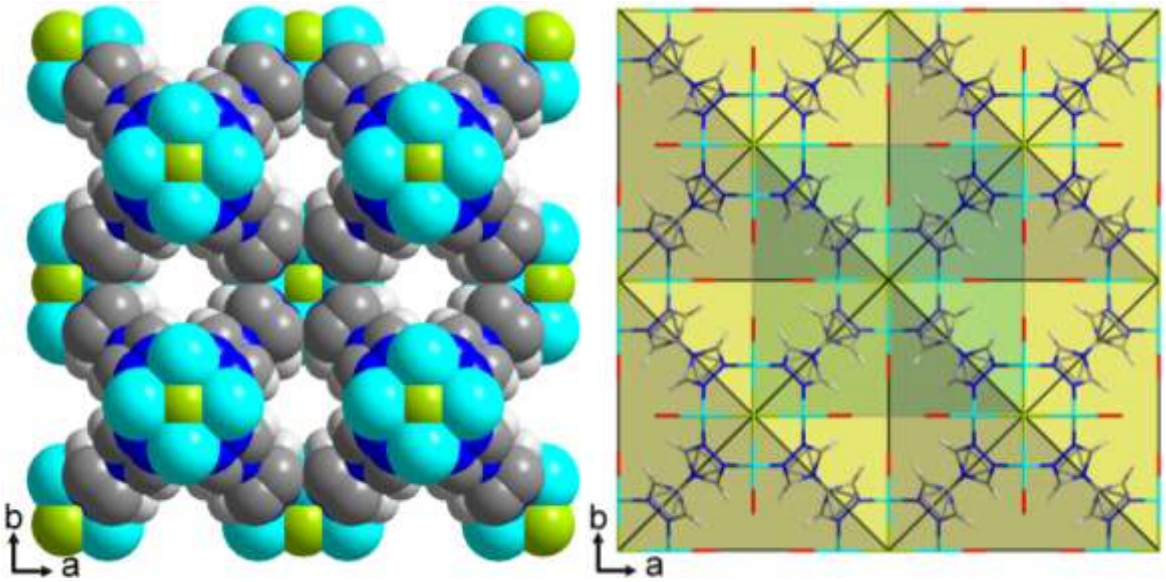

Figure 6.3.1.6: Representation of compound 3D-{[$Cu_4(\mu_4\text{-}Cl)(\mu_4\text{-}rac\text{-}btrip)_4(H_2O)_4$] $(BF_4/ClO_4/OH)^-_7 \cdot xH_2O\}_n$ in space filling model, coordinated aqua ligands are omitted for clarity (left) and stick model with polyhedral (right) shows the square channels along *c* axis. Guest molecules and anions are omitted for clarity.

For **17** a total of 642 electrons per potential solvent accessible void volume of 1271.8 $Å^3$ in the unit cell (3214.9 $Å^3$) with formula unit 3D-$[Cu_4(\mu_4\text{-}Cl)(\mu_4\text{-}rac\text{-}btrip)_4(H_2O)_4](anion)_x(solvent)_y\}_n$ and Z = 2 was squeezed. PLATON [119] calculates a total potential solvent area volume of 1271.8 $Å^3$ per unit cell volume of 3214.9 $Å^3$ [39.6%].

For formula 3D-$\{[Cu_4(\mu_4\text{-}Cl)(\mu_4\text{-}rac\text{-}btrip)_4(H_2O)_4](7BF_4^-, \sim 3H_2O)\}_n$, the void area also contains the BF_4^- anions. One BF_4^- anion has 42 electrons. Fourteen BF_4^- anions per unit cell (with Z = 2) then account for 588 electrons leaving about 60 electrons for solvent molecules in the unit cell. If the solvent molecules are taken as mostly H_2O molecules with 10 electrons each, then about 6 crystal water molecules reside in the unit cell. This translates into 3 solvent water molecules per $Cu_4(\mu_4\text{-}Cl)$ formula unit.

For formula 3D-$\{[Cu_4(\mu_4\text{-}Cl)(\mu_4\text{-}rac\text{-}btrip)_4(H_2O)_4](7ClO_4^-)\}_n$, the void area also contains the ClO_4^- anions. One ClO_4^- anion has 50 electrons. Fourteen ClO_4^- anions per unit cell then account for 700 electrons leaving no electrons for solvent molecules.

To the best of our knowledge, 3D-$\{[Cu_4(\mu_4\text{-}Cl)(\mu_4\text{-}rac\text{-}btrip)_4(H_2O)_4](\sim BF_4^-/ClO_4^-, \sim OH^-/H_2O)\}_n$ is the first example of a sodium halide or isopoly-anion structure constructed by 3D-cationic network $[Cu_4(\mu_4\text{-}Cl)(\mu_4\text{-}rac\text{-}btrip)_4(H_2O)_4]^{7+}$. The $[Cu_4(\mu_4\text{-}Cl/O)(triazolyl/tetrazolate/carboxylate)_8(H_2O)_4]^{n\pm}$ SBU is rare, and there are only a few known examples, such as reported sodalite-type MOFs, which are constructed from $[Cu_4(\mu_4\text{-}$

Cl)(L)$_x$(Solvent)$_y$]$^{n\pm}$ as part of SBU and ligands as triangle node like BTC [120], TTCA [121], BTTri, [122] BTT, [28e,f] TPB [123] and TPT [123] (Figure 6.3.1.7), or ligand TBA as linear linker [124] (Scheme 6.3.1.1). When tetrahedral tetrazolate ligands like Ad(TtH)$_4$, Ad(PhTtH)$_4$ [26] and C(PhTtH)$_4$ [125] as tetraangle node were used to synthesize MOFs with the SBU [Cu$_4$(μ_4-Cl)(L)$_x$]$^{n\pm}$, MOFs with fluorite net are formed (Figure 6.3.1.8).

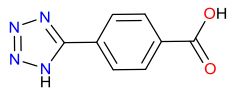

4-(1*H*-tetrazol-5-yl)benzoic acid

Scheme 6.3.1.1: Struktur of linear ligand TBA.

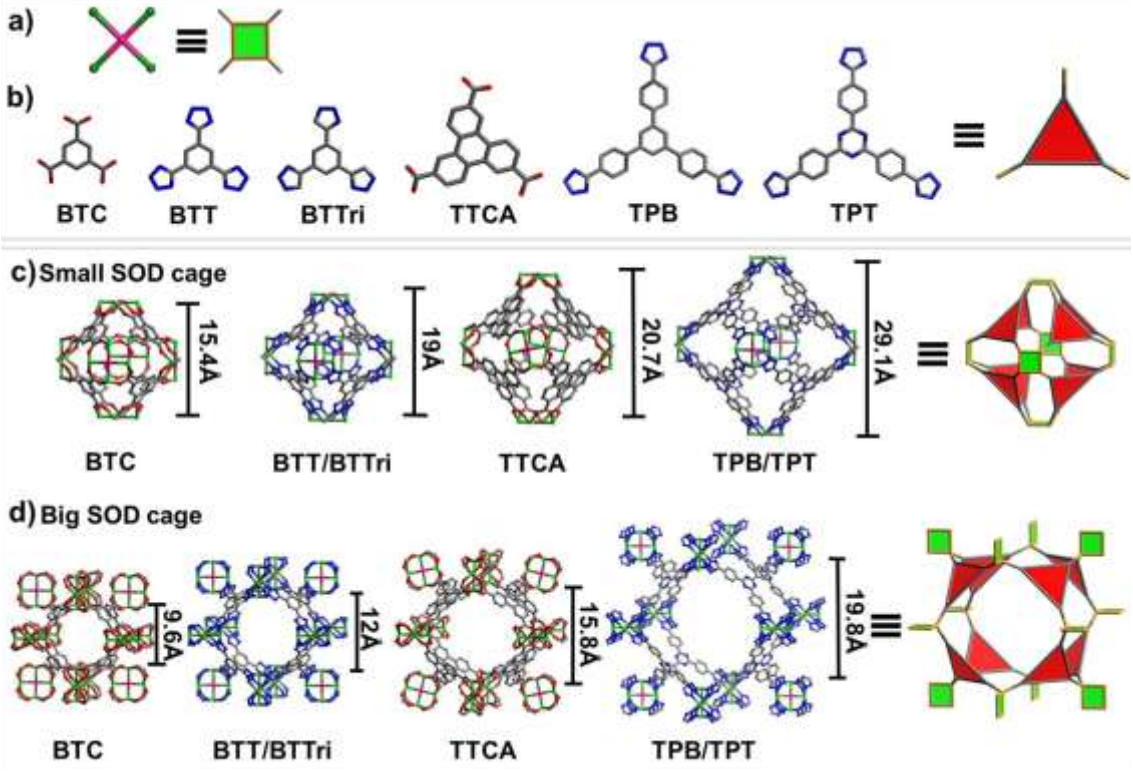

Figure 6.3.1.7: (a) Representation of SBU. (b) Structure of different used ligands as a triangle node. (c) octahedral cage, (d) cuboctahedral cage in MOFs with sodalite net and different size (Figure was reprinted from ref. [124], Copyright The Royal Society of Chemistry 2014).

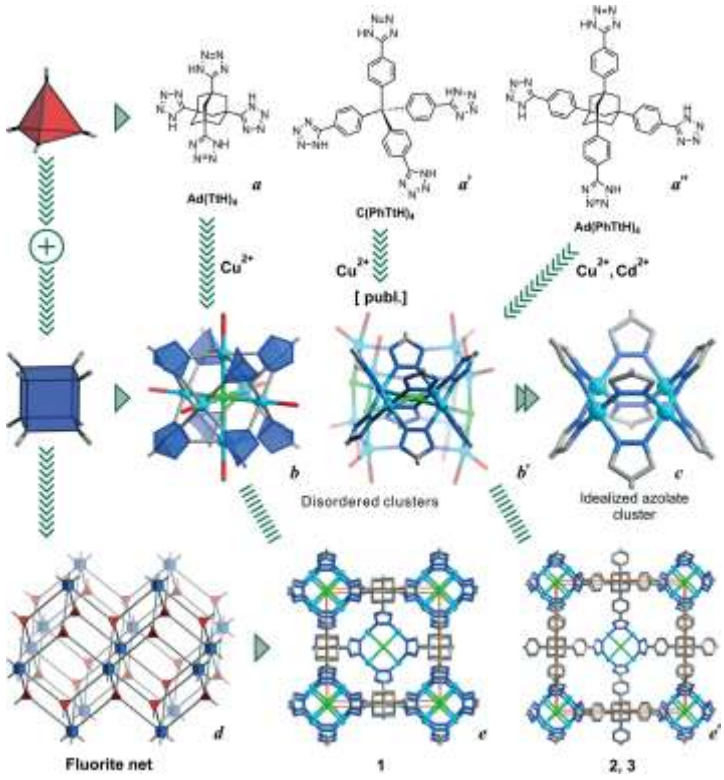

Figure 6.3.1.8: Representation of SBU, structure of different tetrahedral tetrazolate ligands as a tetrahedral node and crystal packing of MOFs with fluorite net (Figure was taken from ref. [26], Copyright The Royal Society of Chemistry 2014).

Comparison of the measured and simulated PXRD patterns, which is calculated from obtained X-ray single crystal structure data for the copper compound, shows some impurities but confirms the X-ray structure as the major crystalline phase. A typical agreement between the measured and simulated PXRD patterns is presented in Figure 6.3.1.9. The crystals were dried in a vacuum furnace for *ca.* 2-3h at temperature 40-45 °C before PXRD measurement.

NaCN was added to the sample to change the magnetic properties of the copper atoms from paramagnetic to diamagnetic by forming the Cu(I) d^{10} complex $Na_3[Cu(CN)_4]$ in the deuterated solvent. After centrifugation, the pipette-separated supernatant was measured. The ^{1}H NMR spectrum (Figure 6.3.1.10) of compound **17** shows the signals of the btrip ligand.

The comparison between the IR spectrum (ATR) for compound **17** and for the *rac*-btrip ligand (Figure 6.3.1.11) shows that the btrip ligand is coordinated to Cu-atoms. The band around 3124 cm^{-1} can attributable to the C–H stretching vibrations of the propyl group. The BF_4^-/ClO_4^- was observed as a strong band in the spectrum of **17** at 1060 cm^{-1} [126]. The M–Cl vibrations are observed as a strong band at 710 cm^{-1}. In the IR spectrum, the out-of-plane

ring torsion vibration of the 1,2,4-triazole for **17** is observed at 646 cm^{-1} [23h],[115]. Thus, the IR and ^1H NMR spectra are in agreement with the results from single-crystal X-ray diffraction.

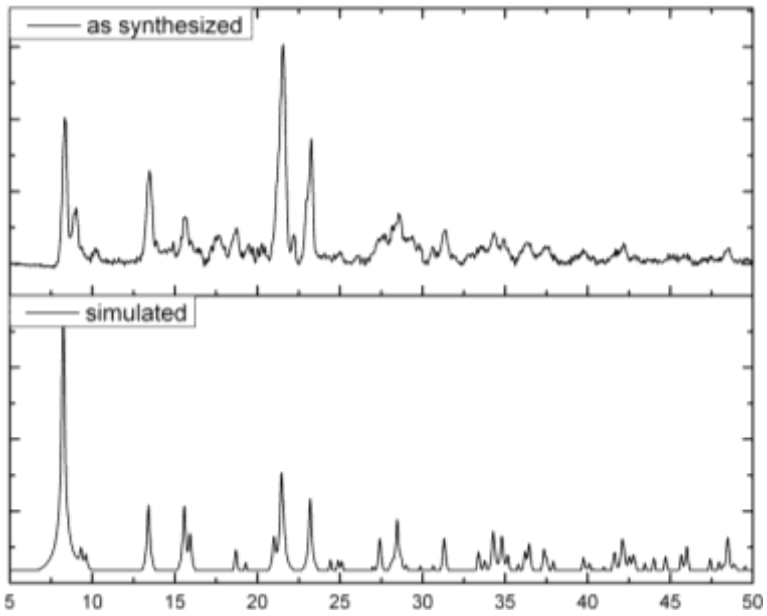

Fig. 6.3.1.9: Combination of the experimental powder X-ray diffractogram of compound **17** (top) at Cu-Kα wavelength 1.54184 Å with the theoretical pattern calculated from the single crystal data (bottom). The measured PXRD is smoothed and baseline corrected.

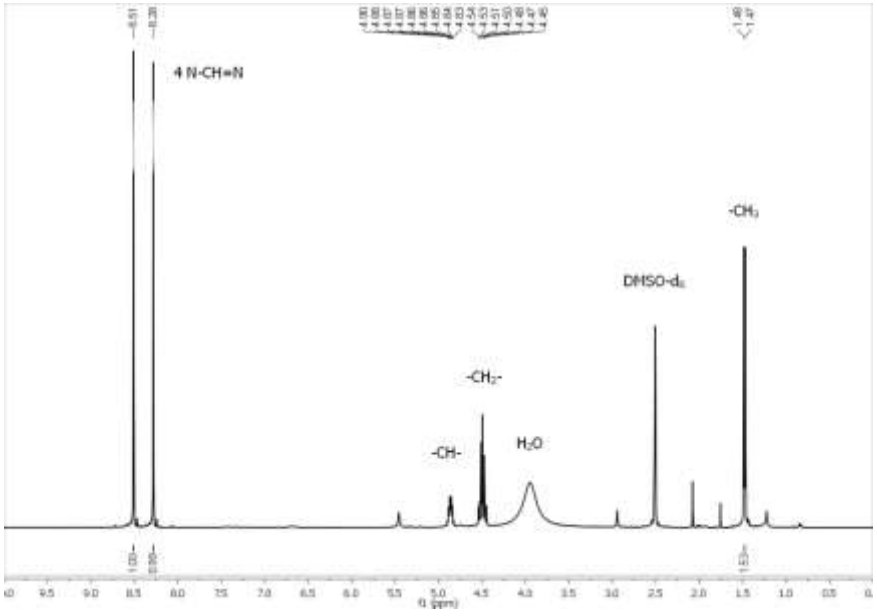

Fig. 6.3.1.10: ^1H NMR Spectrum (500 MHz) of **17** in DMSO-d_6.

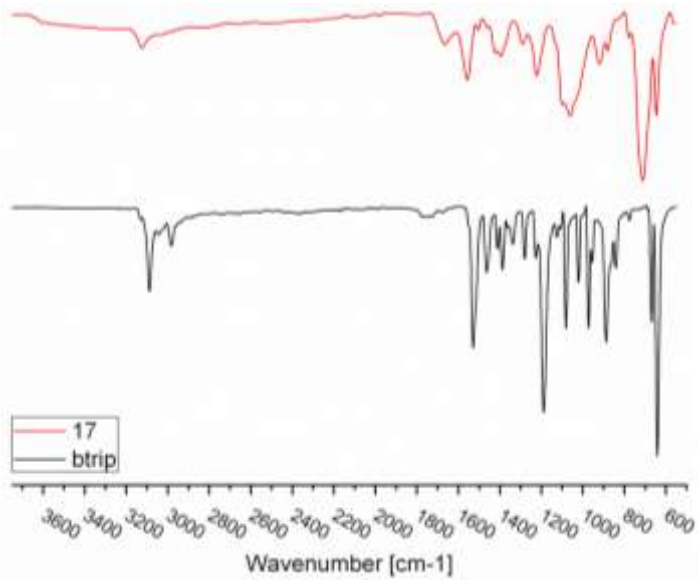

Fig. 6.3.1.11: IR Spectra (ATR) for comparison between the compound **17** and the btrip ligand.

The TG-DTG experiment (Figure 6.3.1.12) of compound **17** was carried out in the temperature range 27-600 °C to examine its thermal stability. The lattice water molecules were released in the temperature range of 60-100 °C. After that, the coordinated aqua ligands were released in multi weightloss steps on further heating in the temperature range of 100-~200 °C. The dehydrated compound **17** is thermally stable up to ~240°C and then the complex begins to decompose in multi weightloss steps on further heating. The final residual mass of black precipitate is mostly assigned as CuO and Cu_2O.

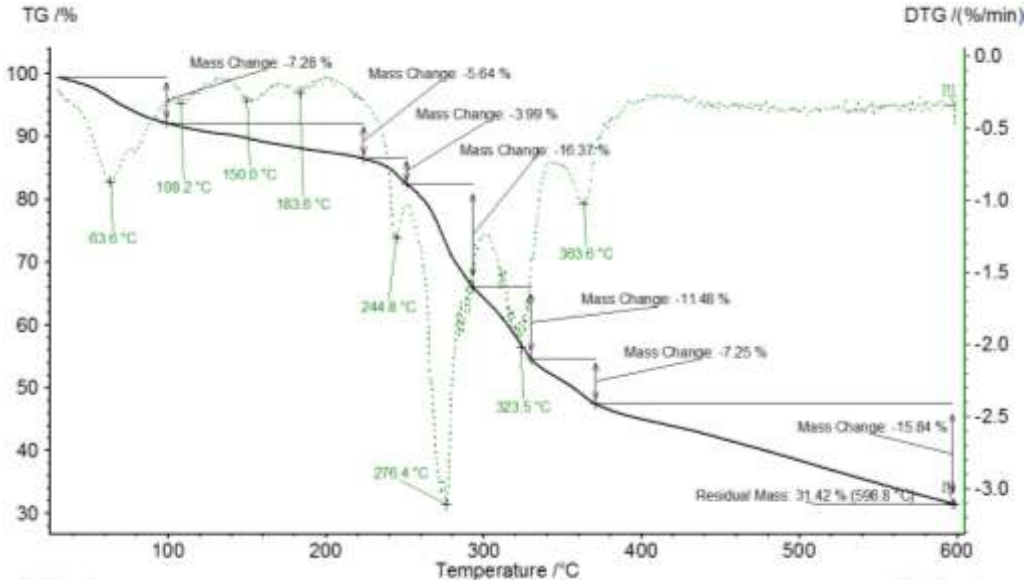

Fig. 6.3.1.12: Experimental TGA and derived DTG curves for the decomposition of **17**, in N_2 atmosphere, gas flow 10 ml/min at a heating rate of 5 °C/min and sample mass of 14.04 mg. TGA curve (black) together with the DTG curve (green, dotted line).

N_2 adsorption study: The potential permanent porosity of **17** was studied by gas sorption measurement. The porosity and BET surface area was evaluated by N_2 adsorption at 77 K. For activation the sample of **17** was heated at 150 °C under vacuum for 3 h to free the pores from solvent molecules (degassed). The result reveal an isotherm of type III accompanied by a type-H1 hysteresis loop according to the International Union of Pure and Applied Chemistry (IUPAC). This type of isotherms is distinctive of mesoporous materials [127] with a pore diameter of 20-500 Å and a high energy of adsorption, while the H1-type hysteresis is generally associated to regular pores with interconnecting channels [128]. Furthermore, the experimental data were fitted using the Barrett, Joyner and Halenda (BJH) model [129]. The pore size distribution (PSD) curve obtained using density functional theory (DFT) is displayed in the inset of Figure 6.3.1.13. One region can be confirmed as mesopores (20-500 Å) with PSD peaks at 29, 32, 41, 47, 62, 74, 89 and 107 Å. A Brunauer–Emmett–Teller (BET) calculation [130] gives the BET surface area for **17** equal to 102 m^2/g; and the Langmuir method gives the surface area of mesopores equal to 245 m^2/g. Moreover, the total pore volume is calculated and found to be 0.14 cm^3/g according to the amount adsorbed at a relative pressure P/P_0 of 0.954. The low value of BET surface area for **17** could be explained that the pores of 3D-cationic network are still occupied by BF_4^-/ClO_4^- anions to neutralize the positive charge 3D-framework Thus, the N_2 adsorption-desorption isotherm is in agreement with its single-crystal X-ray diffraction. PXRD patterns were measured before and after N_2 adsorption to verify structure stability upon activation (Figure 6.3.1.14). Crystal images before and after N_2 adsorption are shown in Figure 6.3.1.15.

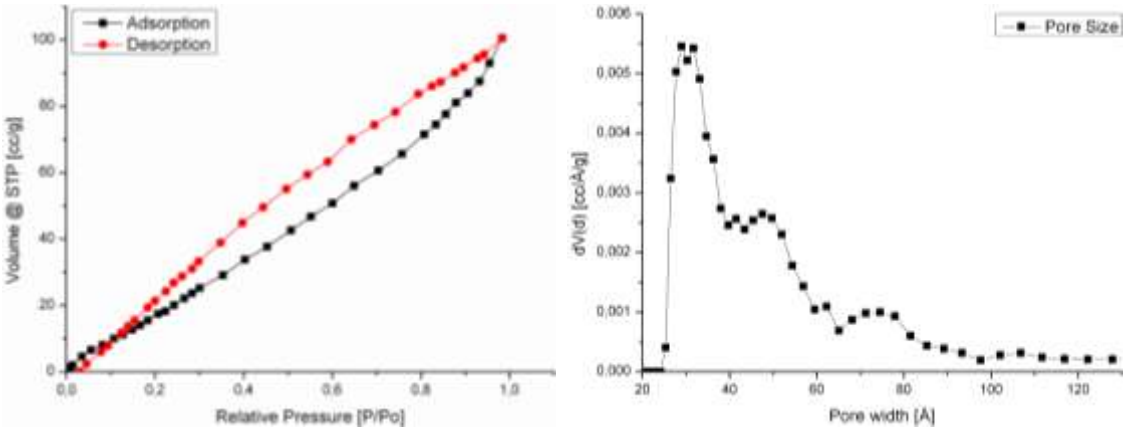

Fig. 6.3.1.13: Nitrogen adsorption-desorption isotherms at 77 K of **17** (left), The BJH pore-size distributions (right).

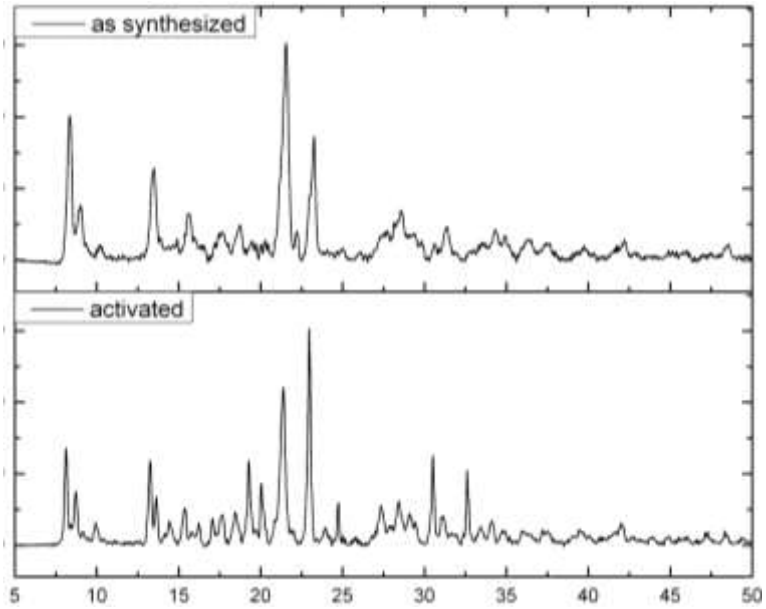

Fig. 6.3.1.14: Combination of the experimental powder X-ray diffractogram of compound **17** as synthesized (top) with activated (bottom) at Cu-Kα wavelength 1.54184 Á. The measured PXRD curves are smoothed and baseline corrected.

Fig. 6.3.1.15: Images of sample **17** as synthesized (left) and activated (right).

7.3.2 Structure analysis and characterization of 3D-{[Cu(μ_4-*rac*-btrip)(SO_4)] H_2O}$_n$ (18)

Light blue, thin needle-shaped single crystals of compound 3D-{[Cu(μ_4-*rac*-btrip)(SO_4)]·H_2O}$_n$ **18** (Figure 6.3.2.1) were obtained using a hydrothermal reaction with the same conditions for coordination polymer **16** and **17**, but by using copper(II) sulfate as metal resource. An aqueous solution of copper(II) sulfate, racemic 1,2-bis(1,2,4-triazol-4-yl)propane (*rac*-btrip) and benzene-1,4-dicarboxylic acid (H_2bdc) in approximately 2:2:1 molar ratio were mixed in a glass tube and then placed in a programmable heating oven at 125°C. NH_3 solution was used to deprotonate H_2bdc. The resulting crystals were filtered and washed with mother liquor. The reaction was repeated several times and found to be reproducible. The single

crystals were manually separated and used for the subsequent characterization and analysis.

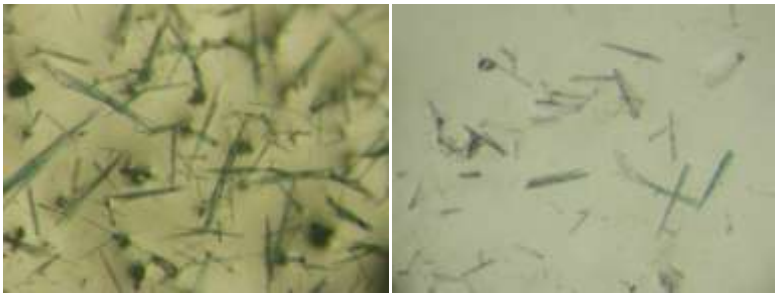

Fig. 6.3.2.1: Crystal images of compound **18**.

Proton NMR analysis of sample **18** digested in DMSO-d_6 gave that Cu-atoms are only coordinated with btrip (see below) Compound **18** crystallizes in the orthorhombic crystal system with the *Imma* space group and a crystallographic asymmetric unit consists of Cu(II) ions with half a btrip ligand, half a sulfate anion and lattice water molecule(s). The propyl part of btrip ligand lies on mirror plane (analysis with the program Mercury [117]), the trans-bent btrip ligand has C_{2h}-symmetry. The Cu atom lies on 2-fold screw axes and the bridging O-atom of SO_4^{2-} lies on a mirror plane. A 2-fold rotation lies along the bond S-O_{coord} of SO_4^{2-}. The extended asymmetric unit of 3D-{[Cu(μ_4-*rac*-btrip)(SO_4)]·H_2O}$_n$ with atom labeling is represented in Figure 6.3.2.3. Selected bond lengths and angles are summarized in Table 6.3.2.1. In compound **18** the methyl group of the bis(triazolyl)propyl ligand could not be well refined due to their disorder over four positions (see section 7.3.4) (Fig. 6.3.2.2). Also, the SO_4^{2-} anions are disordered due to the free rotation of the SO_3 part around the Cu-coordinated O-atom of the SO_4^{2-} anion. Furthermore, the chosen crystal did only diffract until 2theta = 40.34°.

Table 6.3.2.1: Selected bond lengths [Å] and angles [°] for **18**.

Cu1-N1	2.000(15)	$N1^{iii}$-Cu1-N1	180.0(6)
Cu1-O1	2.407(16)	$N1^{i}$-Cu1-O1	84.0(6)
$N1^{i}$-Cu1-$N1^{ii}$	180.0	$N1^{ii}$-Cu1-O1	96.0(6)
$N1^{i}$-Cu1-$N1^{iii}$	91.6(9)	O1-Cu1-$O1^{iii}$	180.0
$N1^{ii}$-Cu1-$N1^{iii}$	88.4(9)		

Symmetry transformations used to generate equivalent atoms: i = x, -y+3/2, z; ii = -x+1/2, y, -z+1/2; iii = -x+1/2, -y+3/2, -z+1/2.

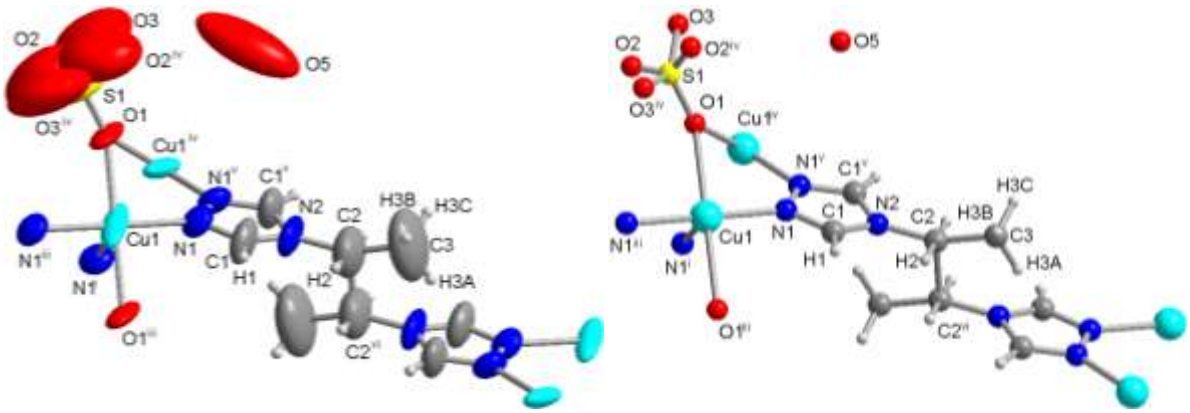

Figure 6.3.2.3: Extended asymmetric unit of compound 3D-{[Cu(μ_4-*rac*-btrip)(SO_4)]·H_2O}$_n$ with 50% thermal ellipsoids for non-hydrogen atoms (left) and ball-stick representation (right). The bis(triazolyl)propyl ligands sits on special positions. The methyl group of the propyl moiety and sulfate anion is disordered. Symmetry codes: i = x, -y+3/2, z; ii = -x+1/2, y, -z+1/2; iii = -x+1/2, -y+3/2, -z+1/2; iv = -x+1, -y+3/2, z; v = -x+1, y, z; vi = -x+1, -y+1, -z.

Each Cu(II) atom displays a Jahn-Teller-distorted octahedral coordination environment, formed by four nitrogen atoms from four *rac*-btrip ligands located in the equatorial plane and axial O-atoms belong to two different sulfate anions. The neighboring octahedral fashions are vertex-shared together *via* O-atoms and Cu(II) atoms are bridged through nitrogen atoms of *rac*-btrip ligands to form a 1D-chain with a Cu…Cu distance 3.5138 Å along the ***a*** axis (see Figure 6.3.2.4).

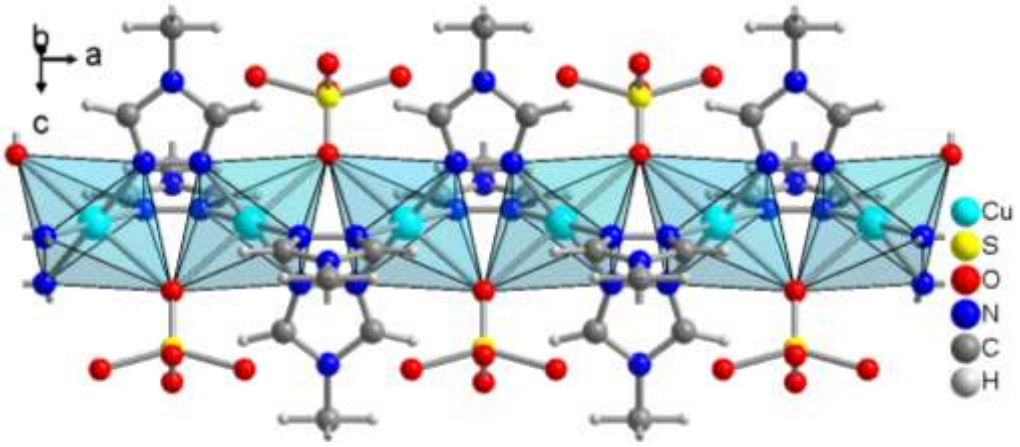

Figure 6.3.2.4: Formation of Cu strands along ***a*** axis by the bridging action of the *rac*-btrip ligand and sulfate anions in **18**.

Each trans-bent *rac*-btrip ligand coordinates four Cu(II) atoms as a μ_4-tetradentate ligand, in κN1:N1`:N2:N2' mode. So each Cu(II) chain connects to four neighboring Cu(II) chains through the trans-bent *rac*-btrip ligands, which lead to formation of a 3D network with square channels (Figure 6.3.2.5) along the ***a*** axis and distances of ca. 15.02 Å x 15.67 Å between Cu(II) atoms. The microporous channels are occupied with lattice water molecules,

For **18** a total of 76 electrons per potential solvent accessible void volume of 597 $Å^3$ in the unit cell (1653.6 $Å^3$) with formula unit 3D-$[Cu(\mu_4\text{-}rac\text{-btrip})(SO_4)]_n$ and Z = 4 was squeezed. PLATON [119] calculates a total potential solvent area volume of 596.9 $Å^3$ per unit cell volume of 1653.6 $Å^3$ [36.1%]. The void area contains mostly the H_2O molecules. One H_2O molecule has 10 electrons. About eight H_2O molecules per unit cell then account for 80 electrons. This translates into about 2 solvent water molecules per formula unit 3D-$\{[Cu(\mu_4\text{-}rac\text{-btrip})(SO_4)]\cdot 2H_2O\}_n$.

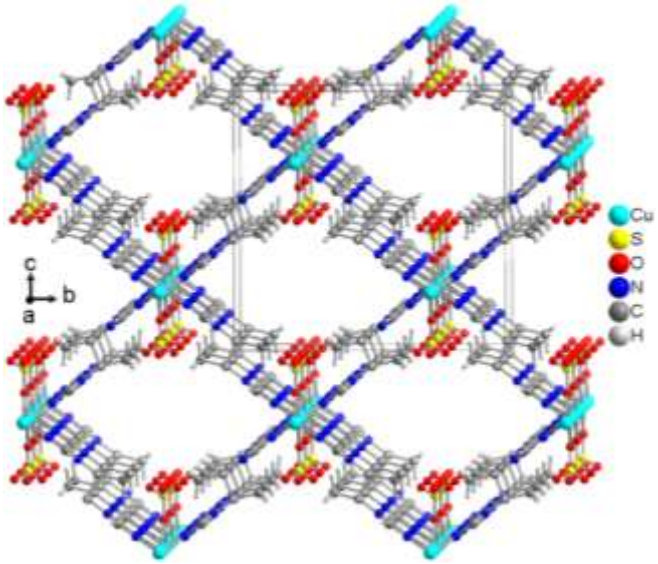

Figure 6.3.2.5: 3D framework in **18**. Crystal water molecules in channels are omitted. The methyl groups of the propyl moiety are disordered.

The phase purity of the copper compound **18** is confirmed by the comparison of the measured and simulated PXRD pattern, with the latter calculated from the single-crystal X-ray structure data. A typical agreement between measured and simulated PXRD pattern is presented in Figure 6.3.2.6. The crystals were dried in vacuum furnace for *ca.* 2-3h at temperature 40-45 °C before PXRD measurement.

NaCN was added to the sample to change the magnetic properties of copper atoms from paramagnetic to diamagnetic by forming the Cu(I) d^{10} complex $Na_3[Cu(CN)_4]$ in the

deuterated solvent. After centrifugation, the pipette-separated supernatant was measured. The ^{1}H NMR spectrum (Fig. 6.3.2.7) of compound **18** shows the signals of the btrip ligand. The amount of NaCN was not enough to reduction the oxidation state of Cu-atoms. The sample contains small amount of Cu(II).

The comparison between the IR spectrum (ATR) for compound **18** and for the *rac*-btrip ligand (Fig. 6.3.2.8) shows that the btrip ligand with sulfate anion is coordinated with Cu-atoms. The band around 3103 cm^{-1} is assigned to the C–H stretching vibrations of the propyl part of *rac*-btrip. Sulfate bands are observed at 1194 cm^{-1} (terminal S–O) and strong bands at 1087, 1036 (coordinated S–O) [131]. In the IR spectrum, the out-of-plane ring torsion vibrations of the 1,2,4-triazole for **18** are observed at 643 and 608 cm^{-1}, respectively [23h],[115]. Thus, the IR and ^{1}H NMR spectra are in agreement with the structure from single-crystal X-ray diffraction.

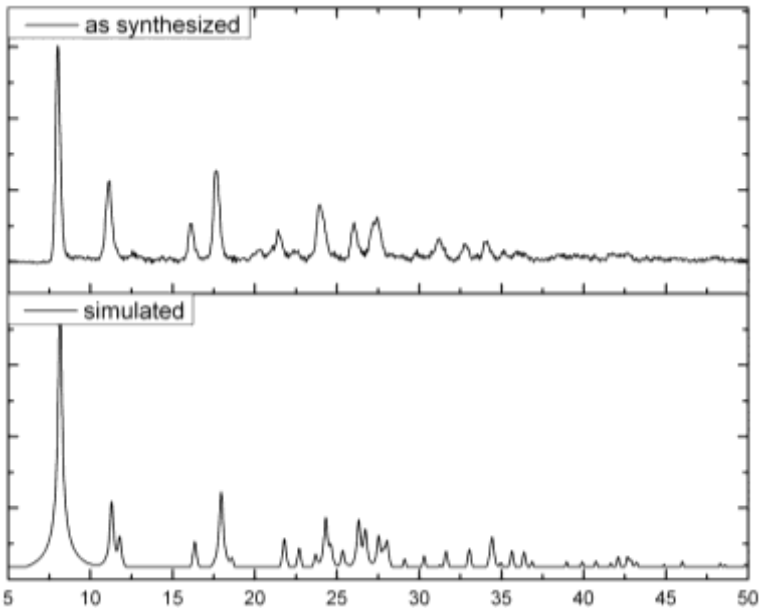

Fig. 6.3.2.6: Combination of the experimental powder X-ray diffractogram of compound **18** (top) at Cu-Kα wavelength 1.54184 Å with the theoretical pattern calculated from the single crystal data (bottom). The measured PXRD curve is smoothed and baseline corrected.

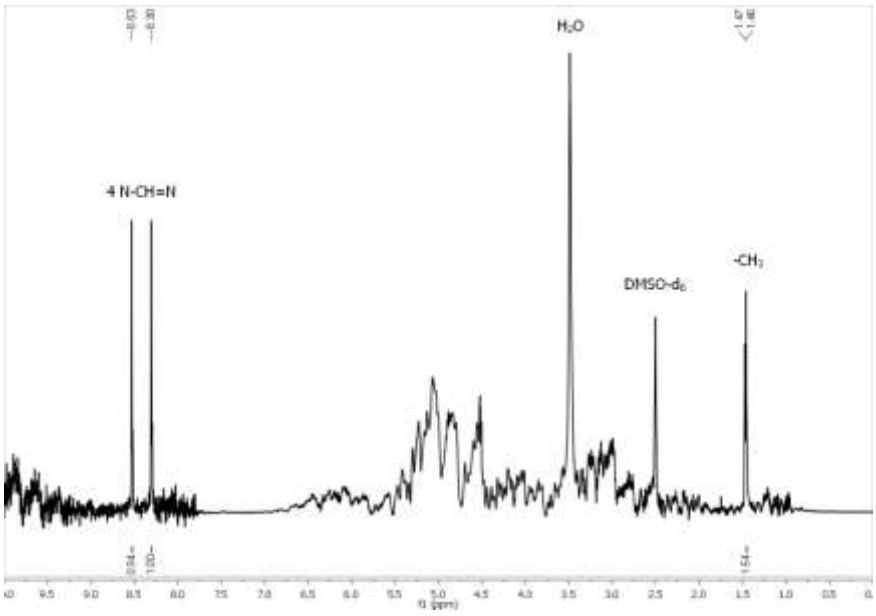

Fig. 6.3.2.7: ^{1}H NMR Spectrum (500 MHz) of **18** in DMSO-d_6.

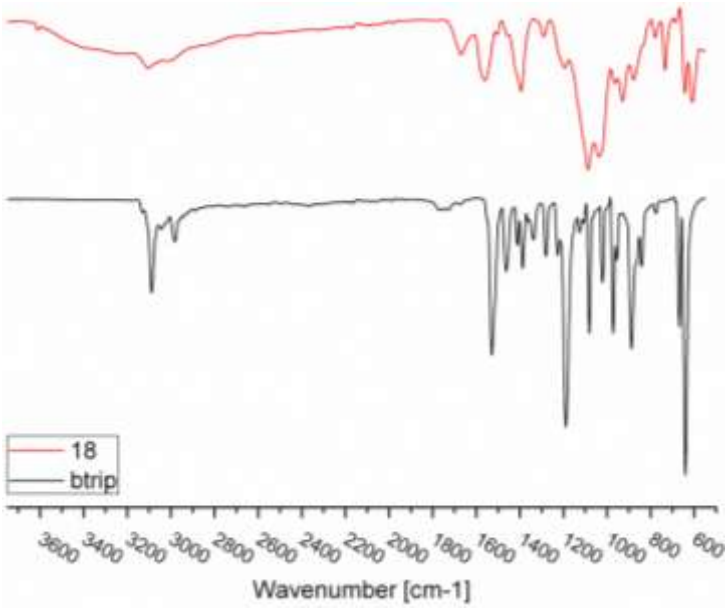

Fig. 6.3.2.8: IR Spectra (ATR) for comparison between the compound **18** and the ligand btrip.

The TG-DTG experiment (Figure 6.3.2.9) of compound **18** was carried out in the temperature range 27-600 °C to examine its thermal stability. The lattice water molecules were released in the temperature range of 40-120 °C. The dehydrated compound **18** is thermally stable up to ~240°C and then the complex begins to decompose in two weight loss steps on further heating. The final residual mass of the black precipitate is mostly assigned to CuO and Cu_2O.

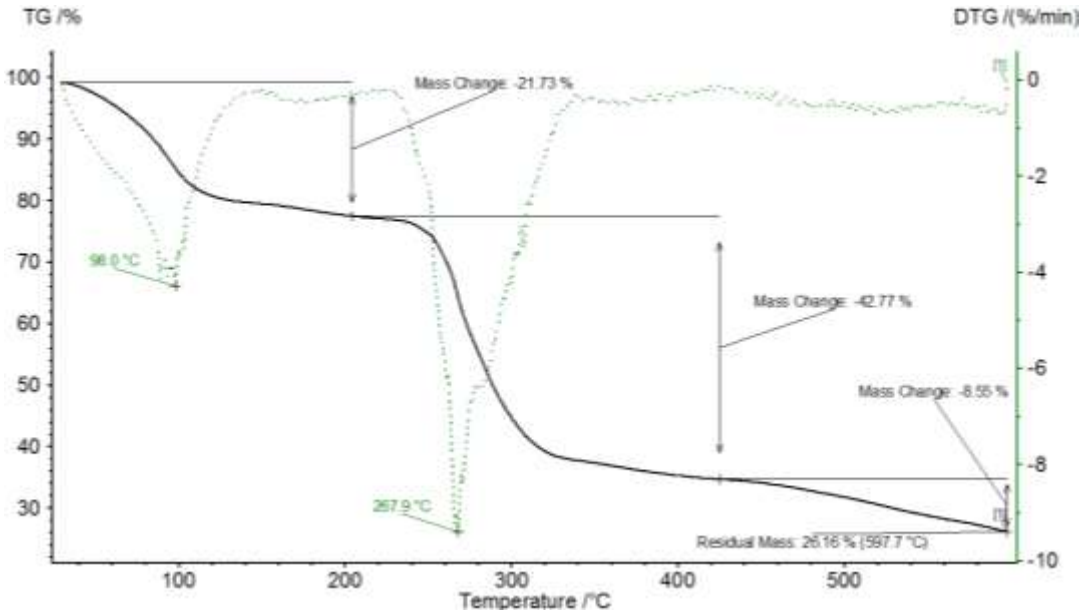

Fig. 6.3.2.9 : The experimental TGA and DTG curves for the decomposition of **18**, in N_2 atmosphere, gas flow 30 ml/min at a heating rate of 10 °C/min in Al-crucible and a sample mass of 7.51 mg. Common presentation of the TGA curve (black) together with the DTG curve (green, dotted line).

7.3.3 Structure analysis and characterization of 2D-{[Cu_2(μ-Br)$_2$(μ$_4$-*rac*-btrip)]·H_2O/MeOH}$_n$ (27)

Light green plate crystals (Fig. 6.3.3.1) of formula 2D-{[Cu_2(μ-Br)$_2$(μ$_4$-*rac*-btrip)]·H_2O/MeOH}$_n$ **27**, are obtained from the solvothermal reaction of copper(II) bromide, *rac*-btrip ligand and H_3btc ligand. The resulting single crystals were separated and washed with the mother liquor. The reaction was repeated several times and found to be reproducible.

Fig. 6.3.3.1: Light green needle-shaped crystals of 2D-{[Cu_2(μ-Br)$_2$(μ$_4$-*rac*-btrip)]·H_2O/MeOH}$_n$ **27** (left) and **27-1** (right).

Table 6.3.3.1: Selected bond lengths [Å] and angles [°] for **27**.

Br1-Cu	2.4791(14)	N3-Cu-N1	111.0(2)
Br2-Cu	2.5530(13)	N3-Cu-Br1	110.91(19)
Cu-N3	2.013(6)	N1-Cu-Br1	115.47(17)
Cu-N1	2.014(6)	N3-Cu-Br2	112.3(2)
Cu^{i}-Br1-Cu	80.33(6)	N1-Cu-Br2	105.62(18)
Cu-Br2-Cu^{i}	77.56(6)	Br1-Cu-Br2	101.04(4)

Symmetry transformations used to generate equivalent atoms: i = x, y, -z.

Proton NMR analysis of sample **27** digested in DMSO-d_6 gave that Cu-atoms are only coordinated with btrip (see below). This compound crystallizes in the orthorhombic crystal system with the *Pbam* space group and a crystallographic asymmetric unit consists of Cu(I) ion with half a btrip ligand, two bromide anions and lattice water or methanol molecule. The Br1 and Br2 anions lie on a mirror plane and a part of btrip ligand (N2, C2, C3, C4 and N4) lies on the next mirror plane (analysis with the program Mercury [117]). The extended asymmetric unit of 2D-{[Cu_2(μ-Br)$_2$(μ$_4$-*rac*-btrip)]·H_2O/MeOH}$_n$ with 50% thermal ellipsoids for non-hydrogen atoms and atom labeling is represented in Figure 6.3.3.2. Selected bond lengths and angles are summarized in Table 6.3.3.1.

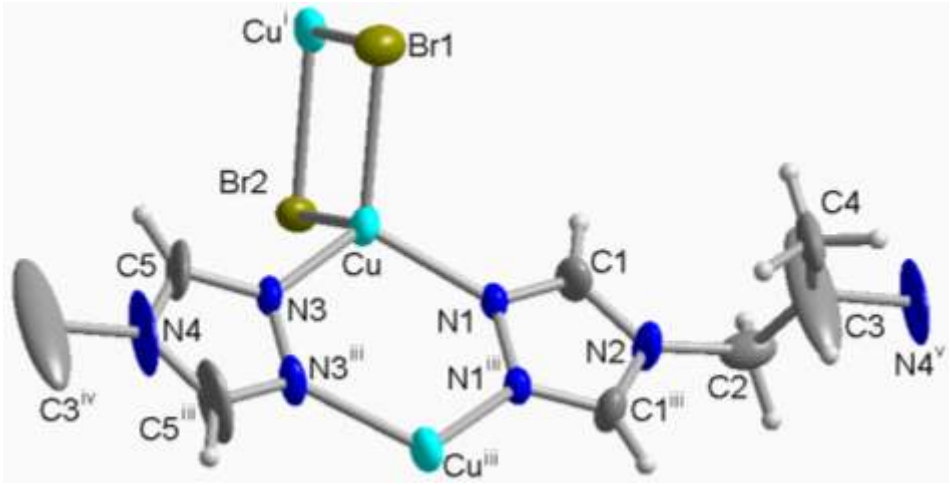

Fig. 6.3.3.2: Coordination environment of Cu(I) ion in 2D-{[Cu_2(μ-Br)$_2$(μ$_4$-*rac*-btrip)]·H_2O/MeOH}$_n$ **27** showing the bridging action of the ligands in this extended asymmetric unit with 50% thermal ellipsoids for non-hydrogen atoms. Crystal water or methanol molecule is omitted for clarity. Symmetry operations: i = x, y, -z; iii = x, y, -z+1; iv = x-1, y, z; v = x+1, y, z.

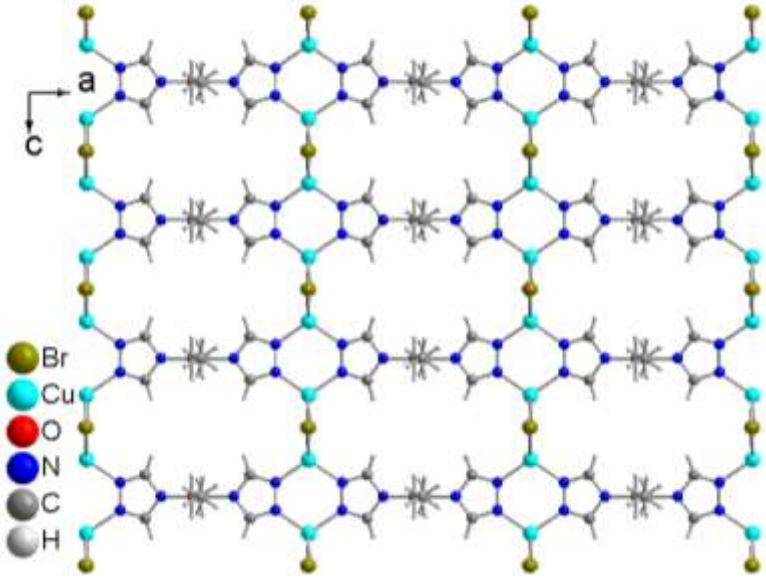

Fig. 6.3.3.3: Packing diagram structure of **27** shows a layer in **ac** lattice plane. Crystal water or methanol molecule is omitted for clarity.

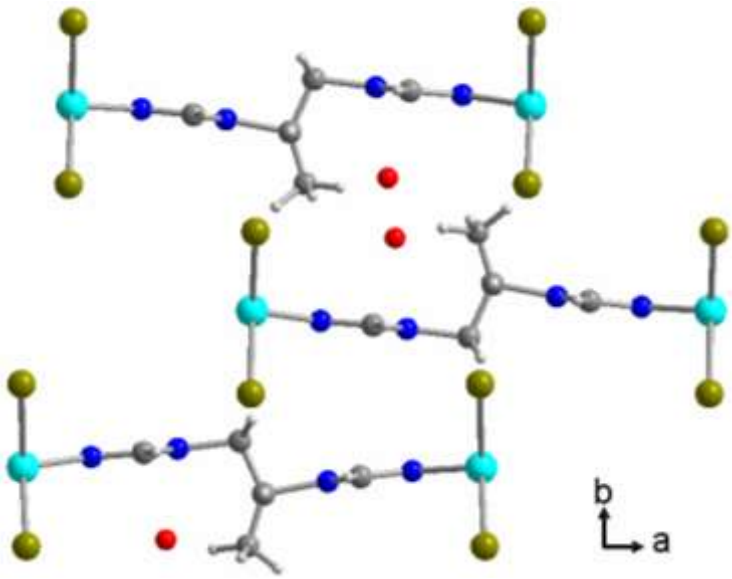

Fig. 6.3.3.4: Packing diagram structure of **27** for three adjacent layers in lattice planes **ab**.

The unique Cu atom is coordinated in a distorted tetrahedral fashion by two nitrogen atoms of two different *rac*-btrip ligand and two bromide ions. The Cu…Cu distance in the Cu-$(N\text{-}N)_2$-Cu ring is 3.660(1) Å, in the Cu-$(Br)_2$-Cu ring 3.198(1) Å. These "Cu-corner-sharing" Cu-$(N\text{-}N)_2$-Cu and Cu-$(Br)_2$-Cu rings alternate along the crystallographic ***c*** axis to form a Cu-ligand-bridged chain. Each bromide anion bridges between two Cu atoms. Each trans-bent *rac*-btrip ligand coordinates four Cu(I) atoms in κN1:N1`:N2:N2` mode and links between two

neighboring chains to form extend 2D-networks parallel to the ***ac*** lattice plane as shown in Figure 6.3.3.3. The structure is overall neutral. The 2D-networks are stacked parallel to each other along the lattice ***b*** axis. The remaining spaces between the neighboring 2D-networks are occupied by lattice water or methanol molecules as shown in Figure 6.3.3.4 as red balls. Furthermore, the structure of compound **27** may contains hydrogen bonds (Table 6.3.3.2) between the C-H of *rac*-btrip and the Br-atoms.

Table 6.3.3.2: Possible C-H...Br hydrogen bonds in **27** (Å, °).

D-H…A	d(D-H)	d(H…A)	d(D…A)	<(D-H…A)
C1-H1…Br2^{vi}	0.95	3.05	3.765(8)	133.5
C2-H2A…Br2$^{vii, vi}$	0.99	2.70	3.621(4)	155.0

Symmetry transformation used to generate equivalent atoms: vi = x+1/2, -y+1/2, -z; vii = x+1/2, -y+1/2, -z+1.

The representative nature of the investigated crystal of the copper compound **27** is supported by the comparison of the measured and simulated PXRD pattern. A typical agreement between measured and simulated PXRD patterns is shown in Figure 6.3.3.5. The crystals were dried in vacuum furnace for *ca.* 2-3h at temperature 40-45 °C before PXRD measurement.

For NMR studies the sample was dissolved in the deuterated solvent. After centrifugation, the pipette-separated supernatant was measured. The ^{1}H NMR spectrum (Figure 6.3.3.6) of compound **27** shows the signals of the btrip ligand.

The comparison between the IR spectrum (ATR) for compound **27** and *rac*-btrip ligand (Fig. 6.3.3.7) shows that ligand is coordinated with Cu-atoms. The band around 3115-2985 cm^{-1} is assigned to the C–H stretching vibrations of the propyl part of the *rac*-btrip ligand. The M–Br vibrations and the out-of-plane ring torsion vibrations of the 1,2,4-triazole for **27** are observed at 669-634 cm^{-1}, respectively [23h], [115]. Thus, the IR and ^{1}H NMR spectra are in agreement with the results from single-crystal X-ray diffraction.

A TG-DTG experiment (Figure 6.3.3.8) of compound **27** was carried out in the temperature range 27-600 °C shows that the lattice water molecules were released in the high temperature range of 100-~240 °C due to hydrogen bonds inside structure. The dehydrated compound **27** is thermally stable up to ~280 °C and then the complex begins to decompose in multi weight-loss steps on further heating. The final residual mass of precipitate is mostly assigned to a mixture of $CuBr_2$ and CuBr.

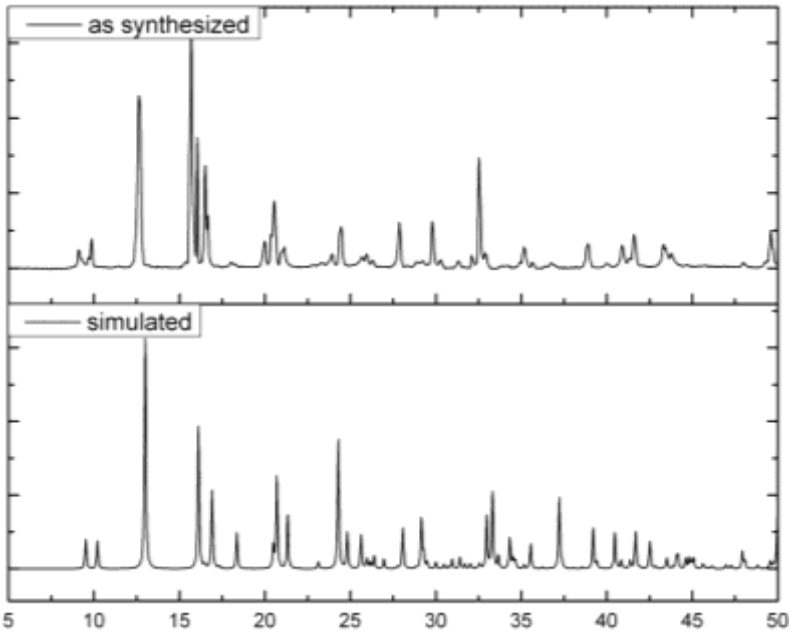

Fig. 6.3.3.5: Combination of the experimental powder X-ray diffractogram of compound **27** (top) at Cu-Kα wavelength 1.54184 Å with the theoretical pattern calculated from the single crystal data (bottom). The measured PXRD curve is smoothed and baseline corrected.

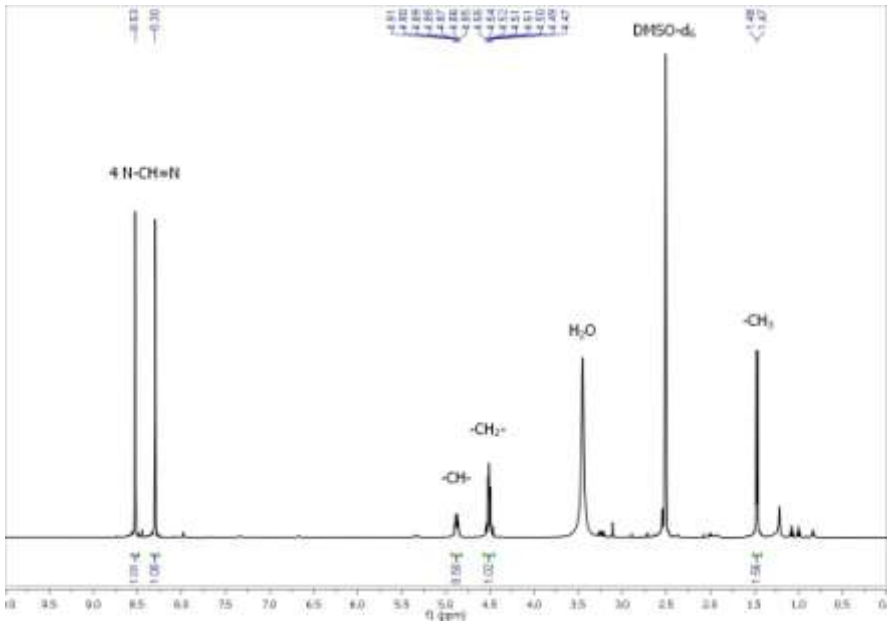

Fig. 6.3.3.6: ^{1}H NMR Spectrum (500 MHz) of **27** in DMSO-d_6.

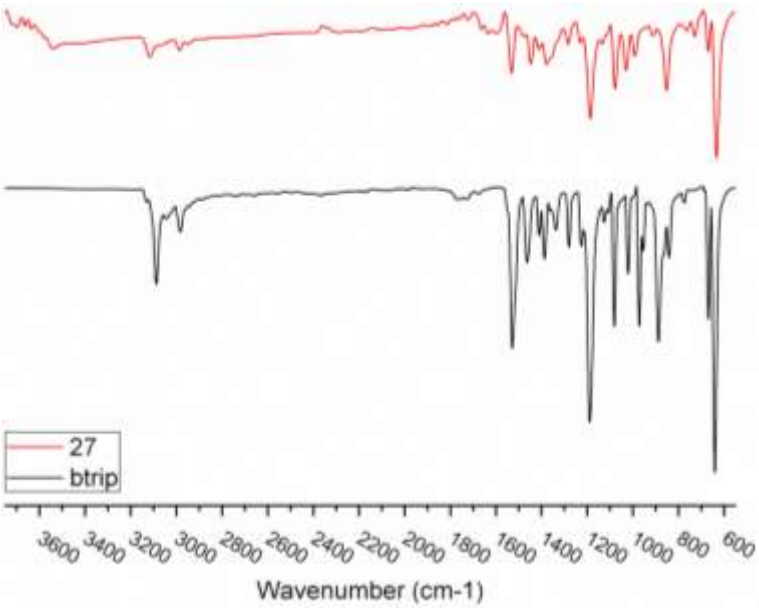

Fig. 6.3.3.7: IR Spectra (ATR) for comparison between the compound **27** and the ligand btrip.

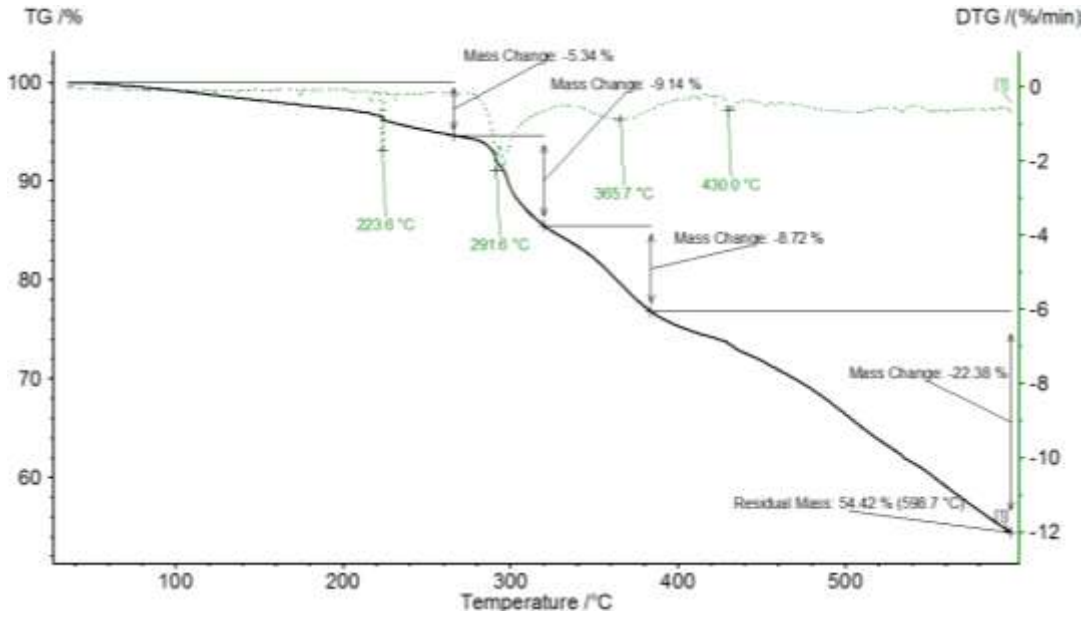

Fig. 6.3.3.8: The experimental TGA and DTG curves for the decomposition of **27**, in N_2 atmosphere, gas flow 20 ml/min at a heating rate of 5 °C/min and sample mass of 12.94 mg. Common presentation of the TGA curve (black) together with the DTG curve (green, dotted line). (The image is generated by the instrument's software).

7.3.4 Structure analysis and characterization of 3D-{[$Cu_2(\mu_4$-*rac*-btrip$)_2$] $SO_4 \cdot xH_2O\}_n$ (28) and 3D-{[$Cu(\mu_4$-*rac*-btrip)] $CH_3COO \cdot xH_2O\}_n$ (29)

Light green, needle-shaped, iridescent single crystals of compounds **28** and **29** (Figure 6.3.4.1) were obtained from the solvothermal reaction in the same condition of synthesis for compound **27**, but by using copper(II) sulfate hydrate for **28** or copper(II) acetate hydrate for **29** as metal resource, *rac*-btrip ligand and H_3btc ligand in approximately 2:3:1 molar ratio. The resulting crystals were filtered and washed with mother liquor. The reaction was repeated several times and found reproducible. The single crystals were manually separated and used for the subsequent characterization and analysis.

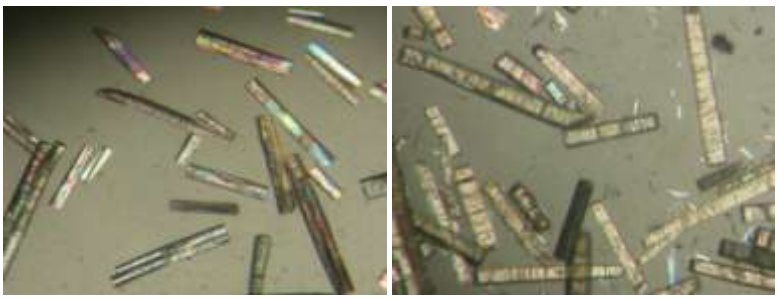

Fig. 6.3.4.1: Light green crystals of **29** (left), **28** (right).

Proton NMR analysis of samples **28** and **29** digested in DMSO-d_6 gave that Cu-atoms are only coordinated with btrip (see below). Compound **29** crystallizes in the orthorhombic crystal system with the *Cccm* space group and a crystallographic asymmetric unit consists of Cu(I) ions with half a btrip ligand, and a lattice water molecule. The propyl part of btrip ligand lies on a mirror plane, the trans-bent btrip ligand has C_2-symmetry and the Cu atom lies on a 2-fold rotation axis (analysis with the program Mercury [117]). The extended asymmetric unit of 3D-{[$Cu(\mu_4$-*rac*-btrip)] $CH_3COO \cdot xH_2O\}_n$ with atom labeling is represented in Figure 6.3.4.2. Selected bond lengths and angles are summarized in (Table 6.3.4.1).

In compound **29** the methyl groups on the bis(triazolyl)propyl ligand could not be located on the electron density maps due to their disorder over four positions (Fig. 6.3.4.2), together with an orientational disorder of the -CH-CH_2- moiety as depicted in scheme 6.3.4.1 Also, the crystal chosen for **29** did only diffract until 2theta = 47.2°.

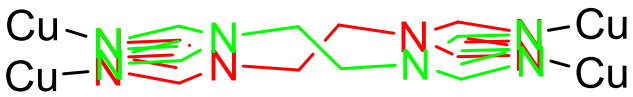

Scheme 6.3.4.1: Suggested orientational disorder of the bis(triazolyl)propyl ligand in structure of **29**. This orientational disorder of the bridging ligand is based on the orientation and the magnitude of the thermal ellipsoids of N-4 and the ethandiyl C atom(s) (see Fig. 6.3.4.2). The methyl groups of the methyl-ethandiyl moiety are not indicated for clarity but it is obvious that the methyl group will be disordered over eight positions.

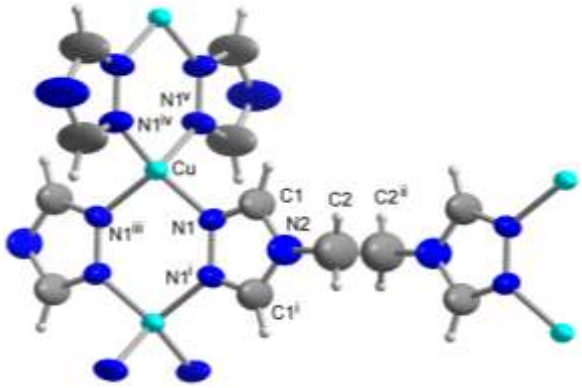

Figure 6.3.4.2: Extended asymmetric unit of compound **29**. The bis(triazolyl)propyl ligands sits on special positions. The methyl group of the propyl moiety has not been found due to its disorder (cf. Scheme 6.3.4.1). Symmetry codes: i = x, y, -z; ii = -x+1/2, -y+1/2, -z; iii = -x+1, -y+1, z; iv = x, -y+1, -z+1/2; v = -x+1, y, -z+1/2.

Table 6.3.4.1: Selected bond lengths [Å] and angles [°] for **29**.

Cu-N1	1.991(3)	$N1^{II}$-Cu-N1	112.5(3)
$N1^{I}$-Cu-N1	109.9(2)	$N1^{III}$-Cu-N1	106.1(2)

Symmetry transformations used to generate equivalent atoms for **29**: i = -x+1, -y+1, z; ii = x, -y+1, -z+1/2; iii = -x+1, y, -z+1/2.

For compound **29** a total of 266 electrons per 906 $Å^3$ and formula unit (Z = 4) was squeezed. PLATON calculates a total potential solvent area volume of 910.0 $Å^3$ per unit cell volume 1633.4 $Å^3$ [55.7%]. The total potential solvent area volume must be judged on the basis of the squeezed electron density of the acetate anion and methyl group which were not found. Hence, any real void volume (if any) which is present after solvent removal under the assumption of a stable framework will be much smaller.

The d^{10} copper(I) metal atom is tetrahedrally coordinated by four nitrogen atoms from four bridging btrip ligands (Fig. 6.3.4.2). Symmetry related neighboring copper atoms are bridged by two triazolyl rings to give metal strands along *c* (Fig. 6.3.4.3). There is only one crystallographically different btrip ligand in this structure. The trans-bent ligand has C_2-symmetry related triazolyl moieties and the triazolyl ring is further bisected by a plane of symmetry. This leaves only N1, C1, N2 and C2 as unique ligand atoms of which the latter two are half occupied. The btrip ligand connects four metal atoms in the typical κ*N*1:*N*2:*N*1':*N*2' mode, as seen before, and gives rise to a 3D framework (Fig. 6.3.4.4). The open 3D framework with rhombic channels contains the squeezed acetate ions and crystal solvent.

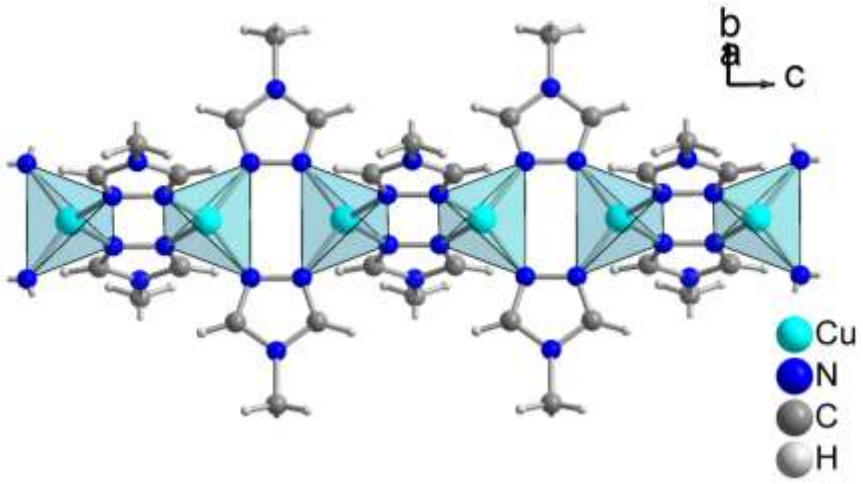

Figure 6.3.4.3: Formation of Cu strands along *c* by the bridging action of the btrip ligand in **29**.

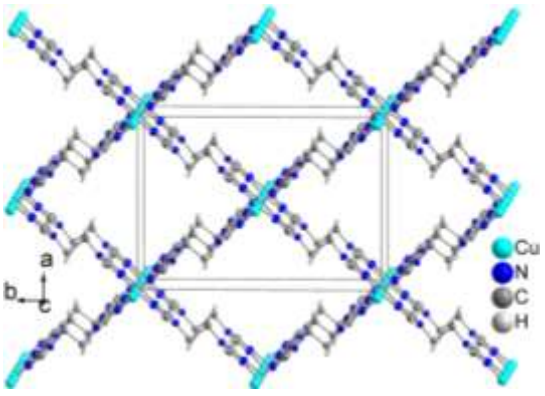

Figure 6.3.4.4: 3D framework in **29**, disordered acetate anions and crystal water in channels are not shown for clarity. The methyl groups of the propyl moiety have not been found due to disorder (cf. Scheme 6.3.4.1).

Compound **28** (1. SCXRD) crystallized in the orthorhombic crystal system with the *Ama2* space group while **28** (2. SCXRD) crystallize in the monoclinic crystal system with the *C2/c* space group. The crystallographic asymmetric unit consists of two Cu(I) ions with just two *rac*-btrip ligands and disordered sulfate anion. The extended asymmetric unit of 3D-{[Cu_2(μ_4-*rac*-btrip)$_2$] $SO_4 \cdot xH_2O$}$_n$ with atom labeling for compound **28** (1. SCXRD) is represented in Figure 6.3.4.5a,b. Selected bond lengths and angles are summarized in (Table 6.3.4.2). In compounds **28** (1. & 2. SCXRD), the methyl groups on the bis(triazolyl)propyl ligand could be located on the electron density maps by single crystal X ray diffraction (SCXRD) with disorder positions, where the crystal chosen for **28** (1. SCXRD) did only diffract until 2theta = 47.6° while **28** (2. SCXRD) until 2theta = 40°. The methyl groups of propyl part of btrip ligands have been located in the first SCXRD better than second measurment. Therefore, the structure discussion is outlined for the first SCXRD.

Compound 3D-{[Cu_2(μ_4-*rac*-btrip)$_2$] $SO_4 \cdot xH_2O$}$_n$ is isomorphous to the previously discussed compound **29**, where Cu(I) atoms display a distorted tetrahedral environment and are connected *via* N-atoms of *rac*-btrip ligands to form 1D-chain with the Cu…Cu distance 3.6381-3.6653 Å along the ***a*** axis (Figure 6.3.4.6). The neighboring Cu(I) chains are linked together *via* trans-bent *rac*-btrip ligands, which leading to form a 3D cationic network with rhombic channels (Figure 6.3.4.7) along *a* axis and distances of ca. 12.14 Å x 18.26 Å between Cu(I) atoms, respectively. The microporous channels are occupied with crystal solvent and disordered sulfate anions, which matches the positive charge of 3D-network.

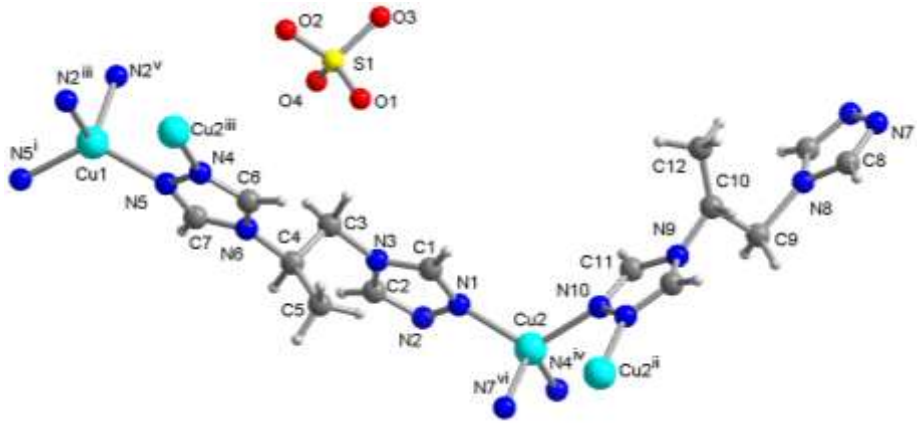

Figure 6.3.4.5a: Extended asymmetric unit of compound **28**. The bis(triazolyl)propyl ligands sits on special positions. The propyl moiety has disordered positions, therefore the extended asymmetric unit was represented as ball-stick. Symmetry codes: i =1-x, -y, z; ii =1/2-x, y, z; iii =x, -1/2+y, -1/2+z; iv =x, 1/2+y, 1/2+z; v =1-x, 1/2-y, -1/2+z; vi = 1/2-x, -1/2+y, 1/2+z.

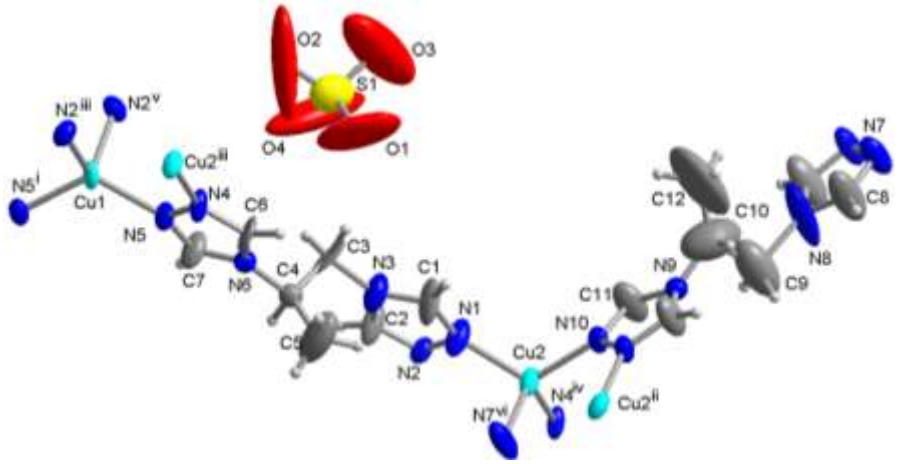

Figure 6.3.4.5b: Extended asymmetric unit of compound **28**. C4, N6 and N9 were represented as ball-stick. The other non-hydrogen atoms were represented as 50% thermal ellipsoids.

Table 6.3.4.1: Selected bond lengths [Å] and angles [°] for **28**.

Cu1-N5	1.992(7)	$N2^{v}$-Cu1-N5	102.5(3)
Cu1-$N2^{i}$	2.059(8)	$N2^{i}$-Cu1-$N2^{v}$	103.0(3)
Cu2-N1	1.994(9)	N1-Cu2-N10	118.8(4)
Cu2-N10	1.990(7)	N1-Cu2-$N4^{ii}$	110.4(3)
Cu2-$N4^{ii}$	2.035(8)	N1-Cu2-$N7^{iii}$	102.3(4)
Cu2-$N7^{iii}$	2.016(10)	$N4^{ii}$-Cu2-N10	105.3(3)
N5-Cu1-$N5^{iv}$	124.5(3)	$N7^{iii}$-Cu2-N10	111.0(3)
$N2^{i}$-Cu1-N5	111.3(3)	$N4^{ii}$-Cu2-$N7^{iii}$	108.8(4)

Symmetry transformations used to generate equivalent atoms: i = x, -1/2+y, -1/2+z; ii = x, 1/2+y, 1/2+z, iii = 1/2-x, -1/2+y, 1/2+z; iv = 1-x, -y, z; v = 1-x, 1/2-y, -1/2+z.

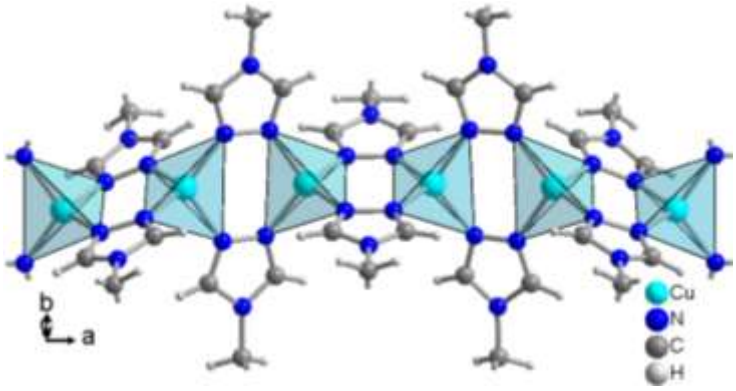

Figure 6.3.4.6: Formation of Cu strands along *a* by the bridging action of the btrip ligand in **28**.

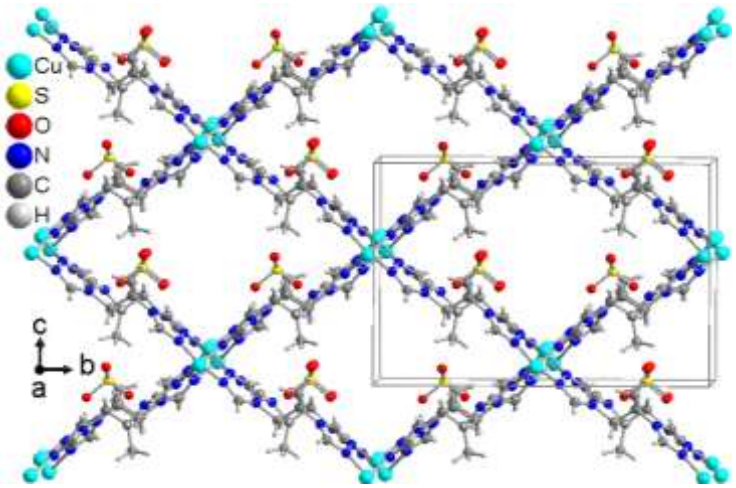

Figure 6.3.4.7: 3D framework in **28**. Disordered solvents and crystal water in channels are not shown for clarity.

For compound (first SCXRD) **28** a total of 531 electrons per 1678.3 $Å^3$ and formula unit (Z = 4) was squeezed. PLATON calculates a total potential solvent area volume of 1678.3 $Å^3$ per unit cell volume 4757.8 $Å^3$ [35.3%].

Copper(I) 3D-{[Cu(μ_4-btre)]SO_4~xH_2O} [132] and silver(I) 3D-{[Ag(μ_4-btre)](ClO_4)}$_n$ [23j] coordination polymers with the bis(1,2,4-triazol-4-yl)ethane (btre) exhibit a structure like compound **29**.

The representative nature of the investigated crystal of the copper compounds **28** and **29** is supported by the comparison of the measured and simulated PXRD pattern. A typical agreement between measured and simulated PXRD patterns is presented in Figures 6.3.4.8 and 6.3.4.9. The crystals were dried in vacuum furnace for *ca.* 2-3h at temperature 40-45 °C before PXRD measurement.

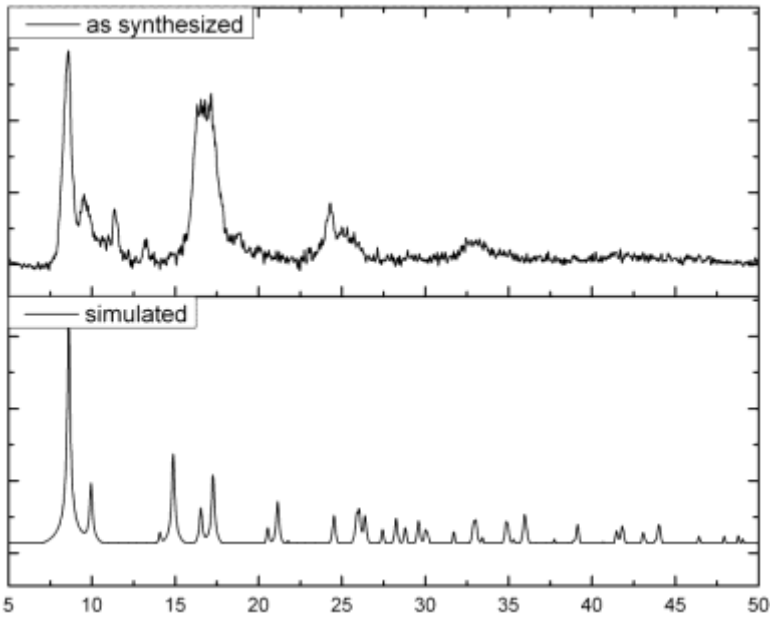

Fig. 6.3.4.8: Combination of the experimental powder X-ray diffractogram of compound **28** at Cu-Kα wavelength 1.54184 Å (top) with the theoretical pattern calculated from the single crystal data (bottom). The measured PXRD curve is smoothed and baseline corrected.

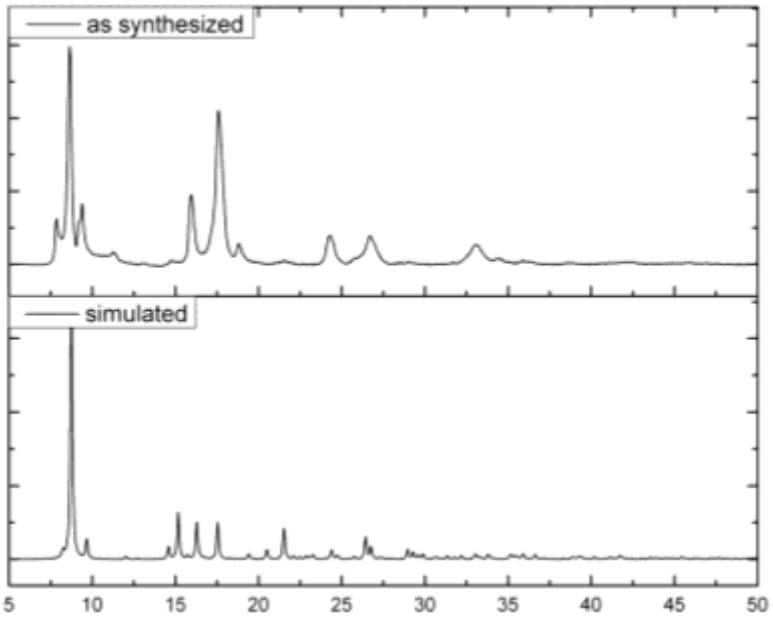

Fig. 6.3.4.9: Combination of the experimental powder X-ray diffractogram of compound **29** at Cu-Kα wavelength 1.54184 Å (top) with the theoretical pattern calculated from the single crystal data (bottom). The measured PXRD is smoothed and baseline corrected.

For NMR studies the samples were digested by addition of NaCN to extract the copper atoms as the complex $Na_3[Cu(CN)_4]$ and thereby dissolve the 3D network in the deuterated

solvent. After centrifugation, the pipette-separated supernatant was measured. The ^{1}H NMR spectra of compounds **28** and **29** shows (Figure 6.3.4.10) the signals of the btrip ligand.

The comparison between the IR spectrum (ATR) for compound **28** and **29** and *rac*-btrip ligand (Fig. 6.3.4.11) shows that ligand is coordinated with Cu-atoms. The bands around 3091-2992 and 3085-2986 cm^{-1} are assigned to the C–H stretching vibrations of the propyl part of *rac*-btrip. Sulfate anions are observed at 1077 cm^{-1} as strong bands for **28** [131b],[133]. Absorption bands of the typical asymmetric and symmetric stretching vibration of carboxylate groups of acetate anions are observed at 1657-1603 cm^{-1} as strong bands for **29**. In the IR spectra, the out-of-plane ring torsion vibrations of the 1,2,4-triazole are observed at 641-608 cm^{-1} [23h],[115]. Thus, the IR and ^{1}H NMR spectra are in agreement with the results from the single-crystal X-ray diffraction.

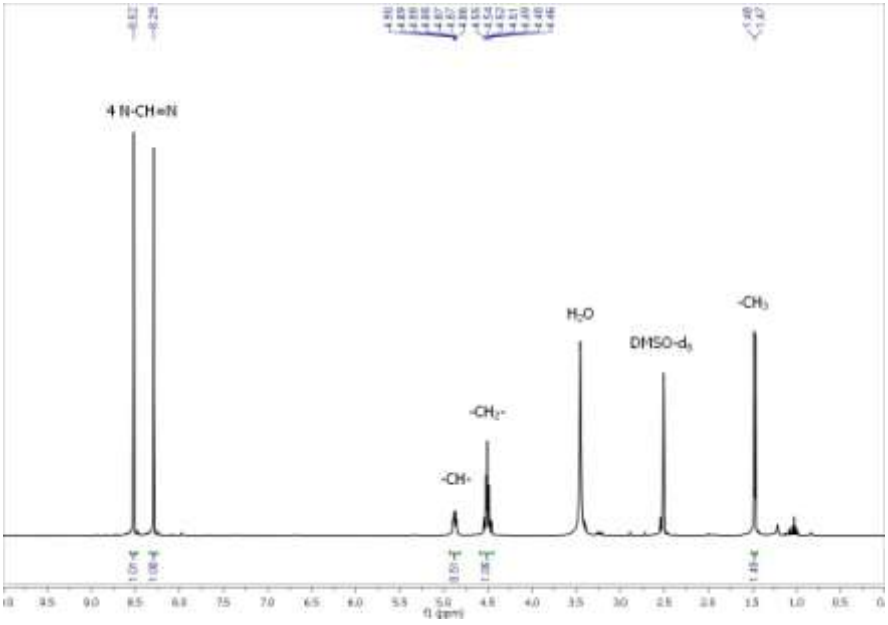

Fig. 6.3.4.10: ^{1}H NMR Spectrum (500 MHz) of **29** in DMSO-d_6.

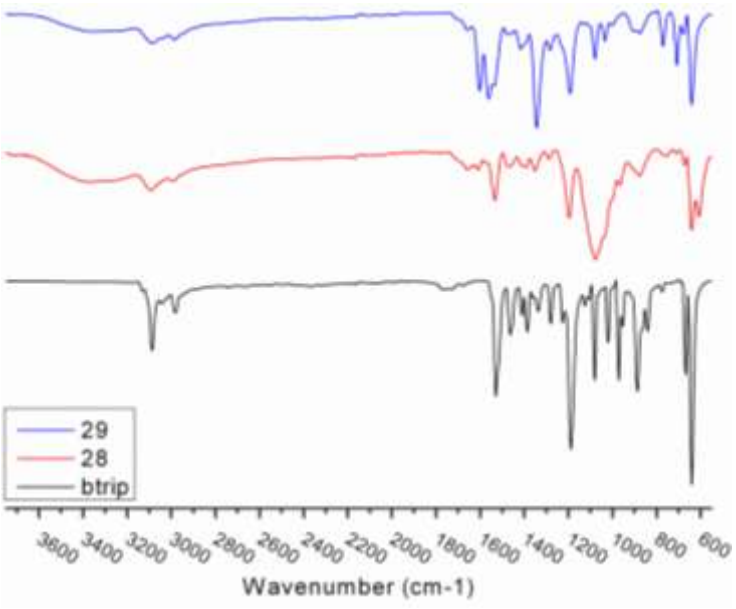

Fig. 6.3.4.11: IR Spectra (ATR) for comparison between btrip ligand, **28** and **29**.

A TG-DTG experiment (Figure 6.3.4.12) of compound **28** was carried out in the temperature range 27-600 °C shows that the lattice water molecules were released in the temperature range of 40-100 °C. After that, a mixture of gases (SO_2, SO_3) from decomposed SO_4^{2-} anions were released in two weight loss steps on further heating in the temperature range of 100-~180 °C. The dehydrated compound **28** is thermally stable up to ~220°C and then the complex begins to decompose in multi weight-loss steps on further heating. The final residual mass of black precipitate is mostly assigned to a mixture of CuO and Cu_2O.

A TG-DTG experiment (Figure 6.3.4.13) of compound **29** was carried out in the temperature range 27-600 °C. The lattice water molecules and a part of decomposed acetate anions were released in the temperature range of 40-140 °C. The dehydrated compound **29** is thermally stable up to ~200°C and then the complex begins to decompose in multi weight loss steps on further heating. The final residual mass of black precipitate is mostly assigned to a mixture of CuO and Cu_2O.

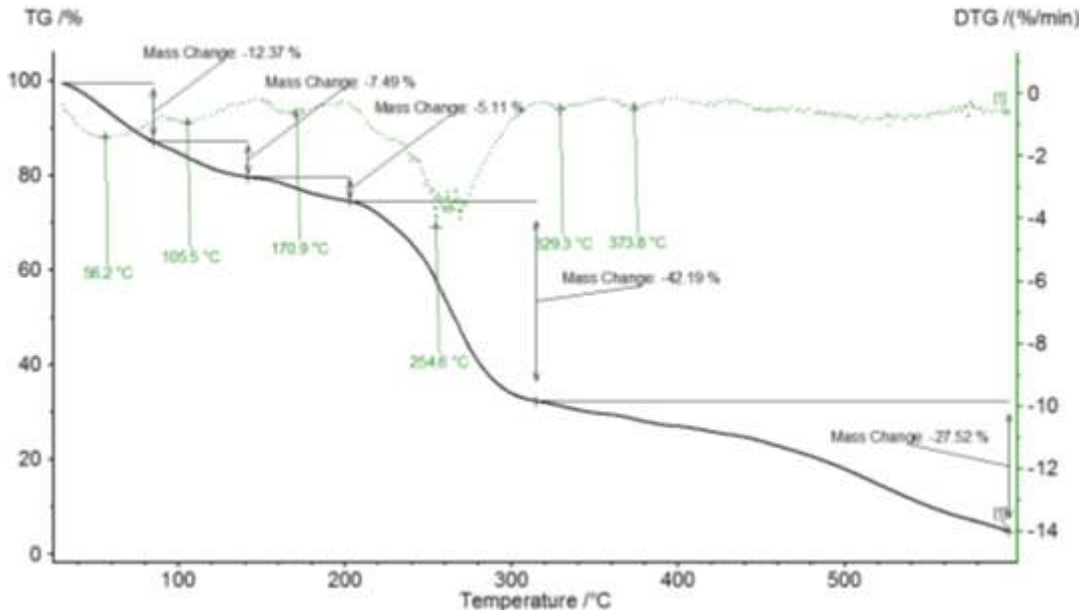

Fig. 6.3.4.12: The experimental TGA and DTG curves for the decomposition of **28**, in N_2 atmosphere, gas flow 20 ml/min at a heating rate of 5 °C/min and sample mass 6.08 mg. Common presentation of the TGA curve (black) together with the DTG curve (green, dotted line).

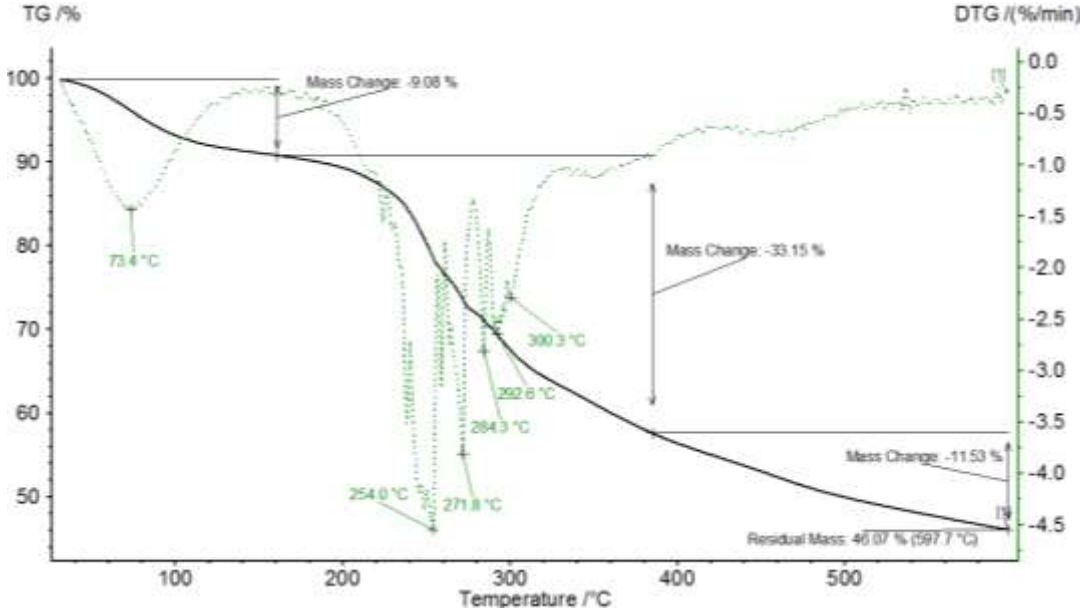

Fig. 6.3.4.13: The experimental TGA and DTG curves for the decomposition of **29**, in N_2 atmosphere, gas flow 30 ml/min at a heating rate of 10 °C/min in Al-crucible and the sample mass 10.05 mg. Common presentation of the TGA curve (black) together with the DTG curve (green, dotted line).

7.3.5 Synthesis and characterization the products of (30, 31 and 32)

Light yellow green plate prisma single crystals **30**, dark green needle shape single crystals **31** and light green needle shape single crystals **32** were obtained from the solvothermal reaction (Figure 6.3.4.1.1) in the same condition of synthesis the compound **27**, but by using other copper(II) salts, copper(II) nitrate hydrate for **30** or copper(II) tetrafluoroborate hydrate for **31** or copper(II) chloride for **32** as metal resource, *rac*-btrip ligand and H_3btc ligand in approximately 2:3:1 molar ratio. The resulting crystals were filtered, washed with mother liquor. The reaction was repeated several times and found reproducible. The single crystals were manually separated and used for the subsequent characterization and analysis. The crystals were not investigated by single-crystal XRD.

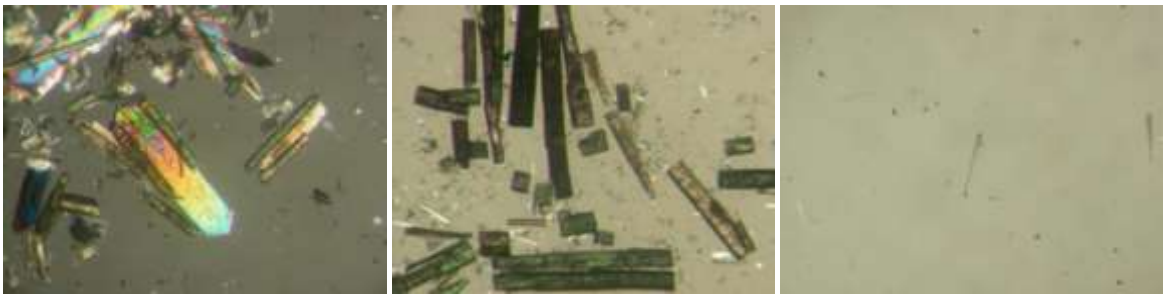

Fig. 6.3.4.1.1: Crystals image of **30** (left), **31** (middle), and **32** (right).

For NMR studies the sample was digested by addition of NaCN to extract the copper atoms as the complex $Na_3[Cu(CN)_4]$ and thereby dissolve the crystals in the deuterated solvent. After centrifugation, the pipette-separated supernatant was measured. The crystals were dissolved in DMSO-d_6 *via* heating in an ultrasonic bath at 50°C.

The ^{1}H NMR spectra of copper compounds **30**, **31** and **32** show only the signals of *rac*-btrip ligand Fig. 6.3.4.1.2.

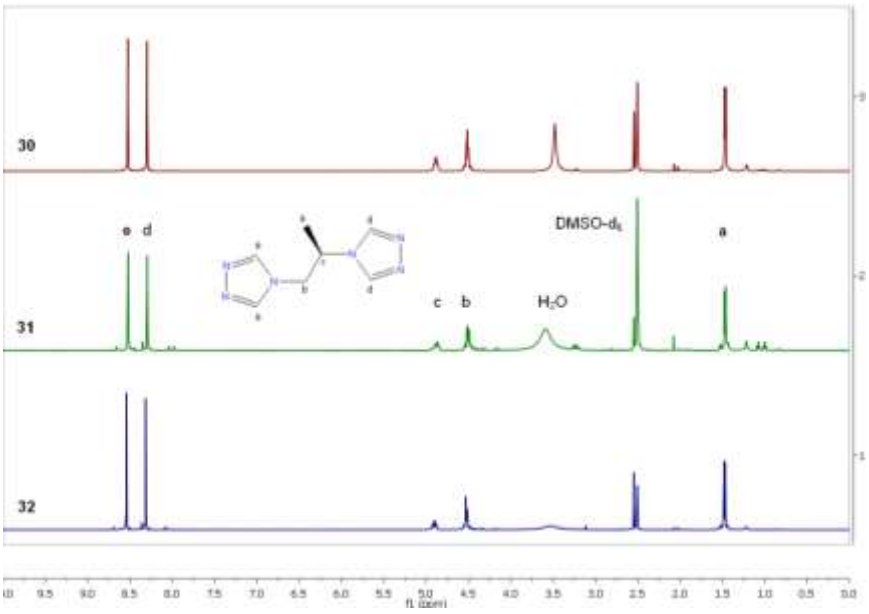

Fig. 6.3.4.1.2: ^{1}H NMR Spectra (500 MHz) of copper compounds **30-32** in DMSO-d_6 showing the signals of the btrip ligand.

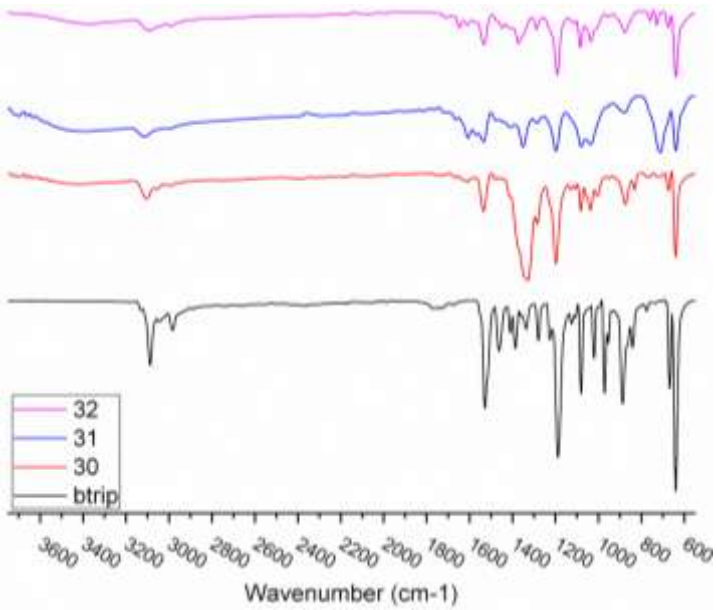

Fig. 6.3.4.1.3: IR Spectra (ATR) for comparison between btrip and copper compounds **30**, **31**, **32**.

The comparison of FT-IR Spectra (ATR) for the Cu-compounds obtained from solvothermal reactions of different copper(II) salts ($Cu(NO_3)_2 \cdot 2.5H_2O$, $Cu(BF_4)_2 \cdot 6H_2O$ and $CuCl_2$) and *rac*-btrip ligand show identical infrared spectra (ATR). The copper ions are mostly coordinated only with the ligand btrip and probably anions of metal salts as negative charge to make the

coordination polymer neutral, because the *rac*-btrip is a neutral ligand. The comparison of FT-IR spectra are presented in Fig. 6.3.4.1.3.

The measured PXRD patterns of the different copper compounds are not identical (Fig. 6.3.4.1.4).

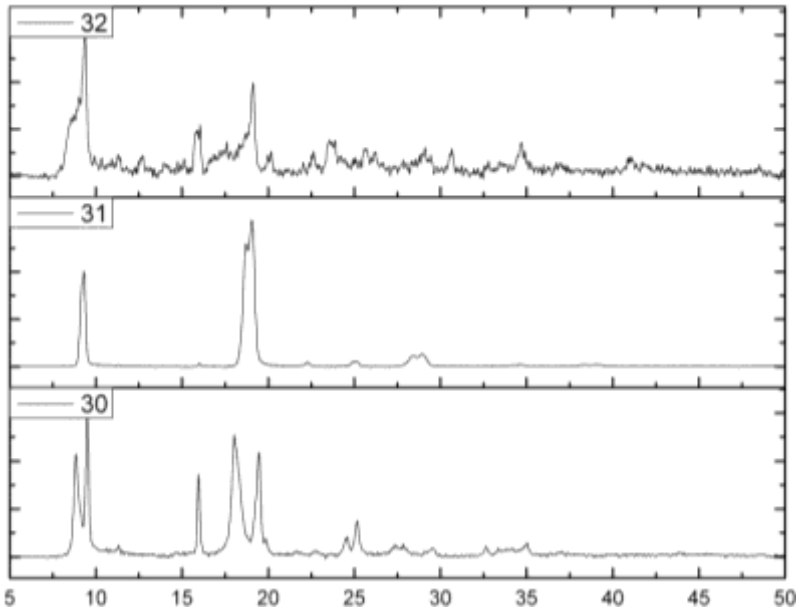

Fig. 6.3.4.1.4: Combination of the experimental PXRD of **30**, **31** & **32** from different copper salts at Cu-Kα wavelength 1.54184 Å. The measured PXRDs are smoothed and baseline corrected.

7.4 Coordination polymers constructed from aromatic carboxylate ligands

7.4.1 Structure analysis and characterization of 3D-{$[Cu(CH_3CN)_4][Cu_3(\mu_6\text{-}btc)_2]_2(NO_3/O_2CCH_3)\cdot(H_2O, CH_3CN)_x\}_n$ (33 and 34)

An acetonitrile solution of copper(II)nitrate hydrate, a solution of *rac*-btrip ligand and a solution of H_3btc ligand were mixed in a glass tube and then placed in a programmable furnace at 125°C. A solution of Et_3N (3 eq. to H_3btc) was used as base to deprotonate H_3btc.The resulting blue crystals (**33,** Fig. 6.4.1.1) were filtered, washed with the same solution of sample reaction (mother liquor). The reactions were repeated several times, found to be reproducible, and their crystals are insoluble in water and organic solvents such as ethanol or methanol. The crystals were crystallographically measured several weeks after their synthesis. Blue single crystals (**34,** Figure 6.4.1.2) were also obtained under the same conditions but by using copper(II)acetate hydrate as source for metal salt.

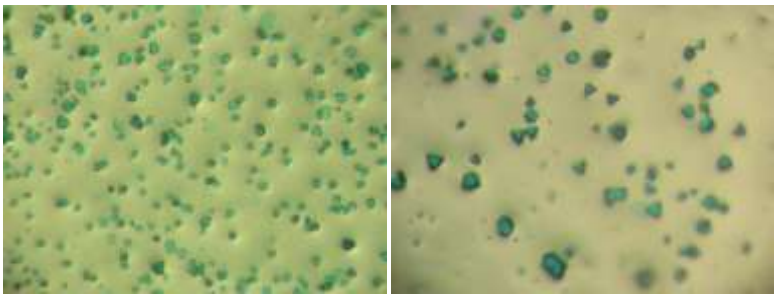

Fig. 6.4.1.1: Crystals image of **33**.

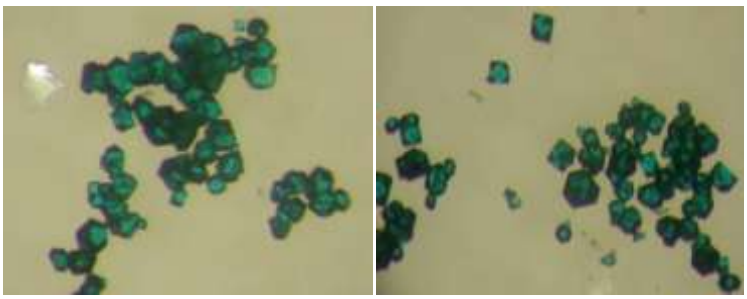

Fig. 6.4.1.2: Crystals image of **34**.

From single-crystal X-ray diffraction analysis both compounds **33** and **34** are isostructural and most likely have the identical composition of a 3D porous coordination polymer 3D-{$[Cu(CH_3CN)_4][Cu_3(\mu_6\text{-}btc)_2]_2(NO_3/O_2CCH_3)\cdot(H_2O, CH_3CN)_x\}_n$. The data set of **34** led to a

better refinement and forms the basis of the following structure discussion. The compounds crystallize in the cubic crystal system with the centrosymmetric space group *F m-3m* (a = 26.446 Á, V = 18496 Á^3) and eight formula units per unit cell. The asymmetric unit consists of one copper atom coordinated by a third of a btc ligand and an axial ligand and a seond copper atom with one acetonitrile ligand. X-ray diffraction analysis reveals that, both the framework in compounds **33** and **34** is isostructural with the previously literature compound 3D-$[Cu_3(\mu_6\text{-btc})_2(H_2O)_3]_n$ (better known as HKUST-1 or Cu-btc) reported by Williams [41].

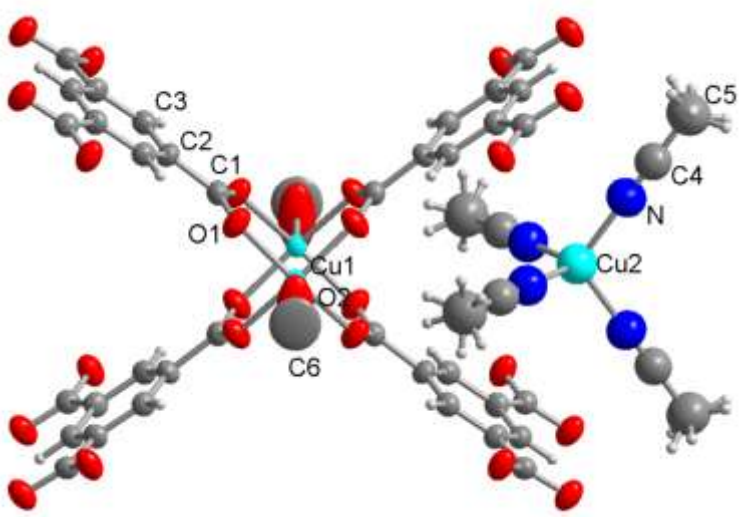

Figure 6.4.1.3: Representation of the Cu paddlewheel in the unit building of the 3D-coordination polymer with the guest molecular complex of $[Cu(CH_3CN)_4]^+$ cation. The displacement ellipsoids are drawn at 50% probability level. The hydrogen atoms are drawn in ball-stick model.

The 3D-framework of compound **34** is constructed from Cu(II) paddle-wheel secondary building units (SBUs) and triangular btc ligands (Fig. 6.4.1.3). The SBUs are composed of four carboxylate groups from four different btc ligands in equatorial positions and an axial ligand. Each Cu center in a paddlewheel unit is surrounded by four O1 from four different btc, $(Cu_2(\mu\text{-}COO)_4(L))$ (L = $(NO_3/O_2CCH_3)\cdot(H_2O, CH_3CN)_x$), (Cu1–O1 = 1.9685 Á). The axial ligand on the Cu1 atom is either an aqua ligand or a partially occupied acetate ligand. For the one $[Cu(NCCH_3)_4]^+$ group one anion charge is needed. This anion can be an acetate ligand which is then distributed over the six Cu1 atoms per formula unit.

The occupancy of the C6 atom of the assumed carboxylate group was refined to 0.11503 which is higher than required for a 1/6 occupancy on each Cu atom (0.04167). Hence, this

C6 atom can also be part of an acetontrile group which then would make the O2 atom an N atom.

The CH_3 group and the second O atom of the acetate group were too diffuse to be satisfactorily localized. Hence, their electron densities have been treated as a diffuse contribution to the overall scattering without specific atom positions by SQUEEZE/PLATON. The short distance Cu1-Cu1 in the dinuclear cupric tetracarboxylate units is 2.6733 Å (Fig. 6.4.1.3). The dinuclear *tetracarboxylate units* (SBUs) are a common highly stable arrangement in 3D porous Cu-carboxylate coordination polymers with HKUST-1 being the most famous example.

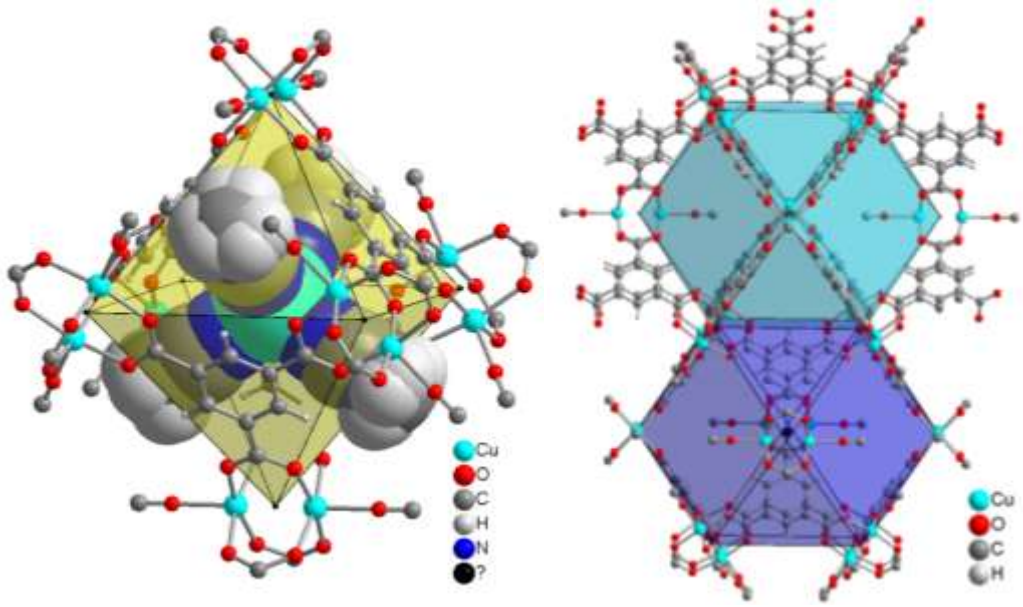

Figure 6.4.1.4: Representation of the $[Cu(CH_3CN)_4]^+$ cation as space-filling model in the octahedral pore A (left) and a cuboctahedral pore B and C (right) in the 3D-coordination polymer.

The tritopic btc linkers, positioned on the crystallographic C_3 axes, coordinate six Cu atoms at its three carboxylate groups and each paddlewheel unit ($Cu_2(\mu\text{-}COO)_4(L)$), positioned on the crystallographic C_4 axis, connects with four different btc ligands, that lead to the formation of an open extended porous 3D-framework with 3D-(3,4)-connected cubic network tbo-a [134] (Fig. 6.4.1.5). The 3D-structure of compound **34** extends to form a polymeric open framework identical like HKUST-1 possessing three kinds of pores A, B and C (Fig. 6.4.1.4 and 6.4.1.5).

Pore A, which accommodates the molecular complex cations $[Cu(CH_3CN)_4]^+$, has a octahedral shape in which the btc ligands define four of the eight triangular faces of the octahedron (Fig. 6.4.1.4, left). The other four triangular faces are occupied by methyl groups

of acetonitrile ligands from the molecular complex cation $[Cu(CH_3CN)_4]^+$. Paddlewheel units ($Cu_2(\mu\text{-}COO)_4(L)$) are located at the six vertices of the octahedron at a distance of 9.35 Å from each other. Opposite vertices are 13.22 Å apart. The distances are measured between the centers of the paddlewheel units.

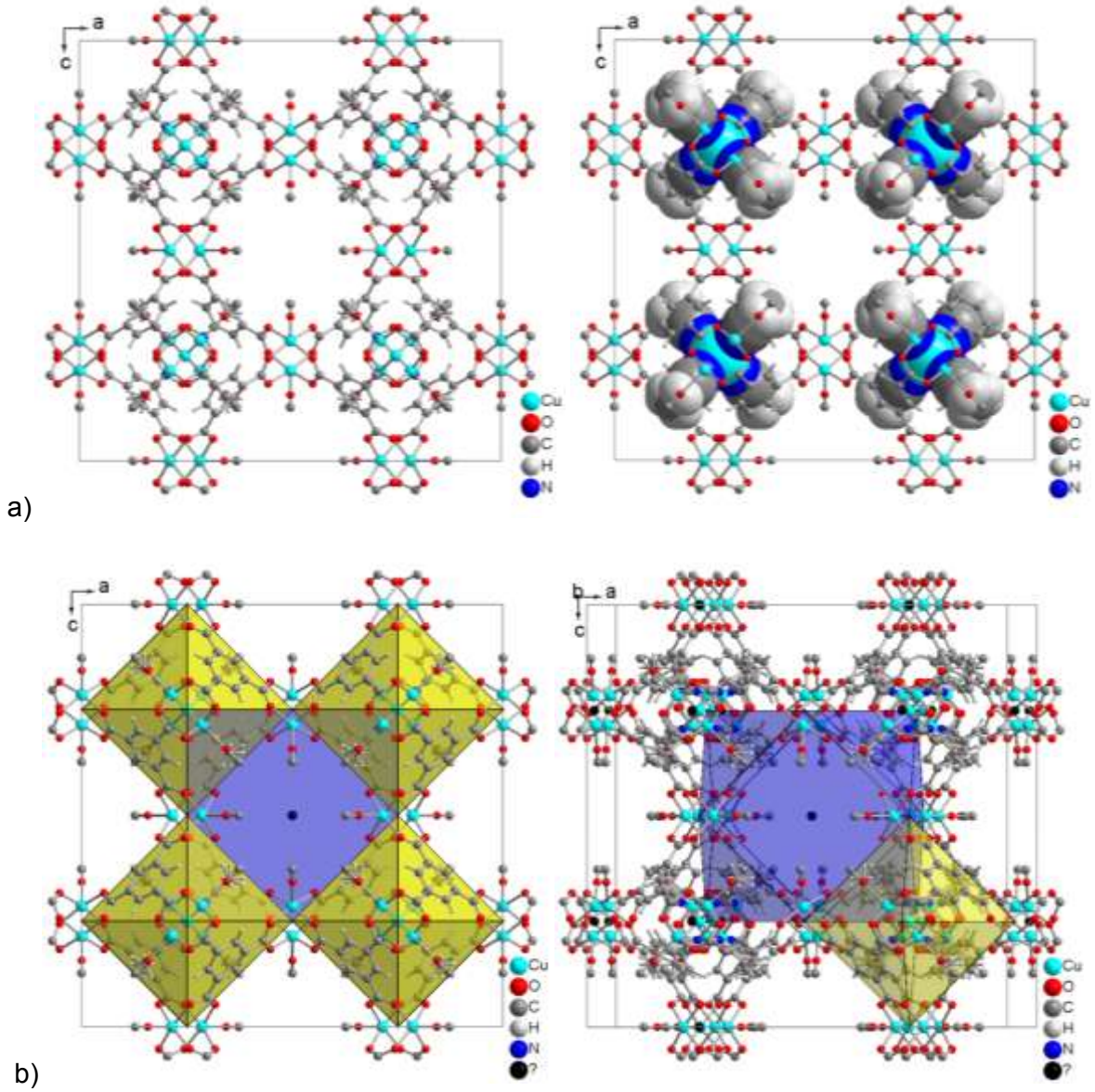

Figure 6.4.1.5: Representation of components of the unit cell of (3,4)-connected framework **34** along b-axis: **a-left)** View of 3D-framework and molecular complex cation $[Cu(CH_3CN)_4]^+$ represented as ball-stick model, showing one channel with four fold symmetry. **a-right)** guest molecular complex cation $[Cu(CH_3CN)_4]^+$ is represented as space-filling model. **b-left)** polyhedral model with two kinds of pores, the octahedral pore A and cuboctahedral pore B, the pore A accommodating guest cation $[Cu(CH_3CN)_4]^+$ (yellow octahedral). **b-right)** polyhedral models showing the face sharing between the octahedral pore A and cuboctahedral pore B.

Pore B and C have a cuboctahedral shape and are formed in a space between octahedral pores A as shown in Fig. 6.4.1.5b, right. The btc ligands define the eight triangular planes of the cuboctahedron of pore B and 12 Cu_2 SBUs define its 12 vertices. The eight triangular planes of pore C are interconnected with eight octahedral pores A but without sharing btc ligands. Pore B and C measures 18.70 Å between opposite vertices, 9.35 and 13.22 Å measured from the center of one paddlewheel unit to the adjacent center of paddlewheel unit, respectively [136],[139],[141].

The framework can be thought of being built by connecting the octahedral pores in a corner-sharing mode or the cuboctahedral pores in a square-face-sharing mode through the paddlewheel SBUs at the vertices as shown in Fig. 6.4.1.5b. Also, the octahedral pore A is surrounded by four cuboctahedral pores B or C and both share the triangular face. Each pore B is interconnected with six adjacent C pores through the square faces of cuboctahedron and with eight pores A through its triangular planes as shown in (Fig. 6.4.1.5). Pores B and C are arranged alternately in the face-centered cubic lattice. Pores A are connected to each other *via* their vertices and trianuglare-face-sharing mode with cuboctahedral pores. Eventually, the structure of 3D-coordination polymers has the same structure as perovskite [136],[139],[141].

The channels of 3D-framework **34** are arranged along the crystallographic a-, b- and c-axis with four fold symmetry, and are connected to each other, which lead to the formation of a 3D porous network as shown in (Figure 6.4.1.5). The size of the channels can be considered as result from the formation of larger paddlewheel units (SBUs) [136],[139],[141].

For **34** a total of 1131 electrons per 8925 $Å^3$ and formula unit (Z = 8) was squeezed. PLATON [103] calculates a total potential solvent area volume of 8998.4 $Å^3$ per unit cell volume of 18496 $Å^3$ [48.7%].

Single-crystal structure study reveals that **33** and **34** are isomorphous and that molecular complex $[Cu(CH_3CN)_4]^+$ with positive charge as guests has been introduced into the closed octahedral (Pore A) as shown in (Fig. 6.4.1.4, left).

To our knowledge, isomorphous compounds with paddle-wheel as secondary building units (SBUs) and triangular btc ligands have been reported with copper, iron, molybdenum, chromium, nickel and zinc [41],[135]. Other isostructural HKUST-1 compounds with paddle-wheel and triangular btc ligands have been reported with guest molecules or ions in pores B as anion $[HPW_{12}O_{40}]^{2-}$ [136], molecules like $FeTMPyPCl_5$, $CoTMPyPCl_4$, $MnTMPyPCl_5$, NiTMPyP, MgTMPyP and ZnTMPyP, where TMPyP is *meso*-tetra(*N*-methyl-4-pyridyl)porphine tetratosylate [137], anions like $[H_2SiW_{12}O_{40}]^{2-}$, $[H_2GeW_{12}O_{40}]^{2-}$, $[HPW_{12}O_{40}]^{2-}$, $[H_2SiMo_{12}O_{40}]^{2-}$, $[HPMo_{12}O_{40}]^{2-}$ and $[HAsMo_{12}O_{40}]^{2-}$ [138], anions as $[SiMo_{12}O_{40}]^{4-}$,

$[PW_{12}O_{40}]^{3-}$ and $[PMo_6W_6O_{40}]^{4-}$ [139], solvent molecules (DMF and H_2O) [135c] and anion $[PMo_{11}VO_{40}]^{4-}$ [140]. In pore B and C as Zn(II)-tetrakis(4-methylpyridyl)porphyrin (ZnT4MPyP) [141]. The paddle-wheel units have been used as building blocks for the construction of metal-organic frameworks with different ligands [42],[142]. In HKUST-1, it was reported that the compound exhibited enhanced hydrogen-storage capacity when the axial water ligands of SBUs were removed [143]. A great research interest in 3D-$[Cu_3(\mu_6\text{-btc})_2]_n$ are reported on functionalization of the H_3btc ligand. The copper frameworks constructed from H_3btc ligand that has been functionalized with methyl or ethyl groups and with amino group [144].

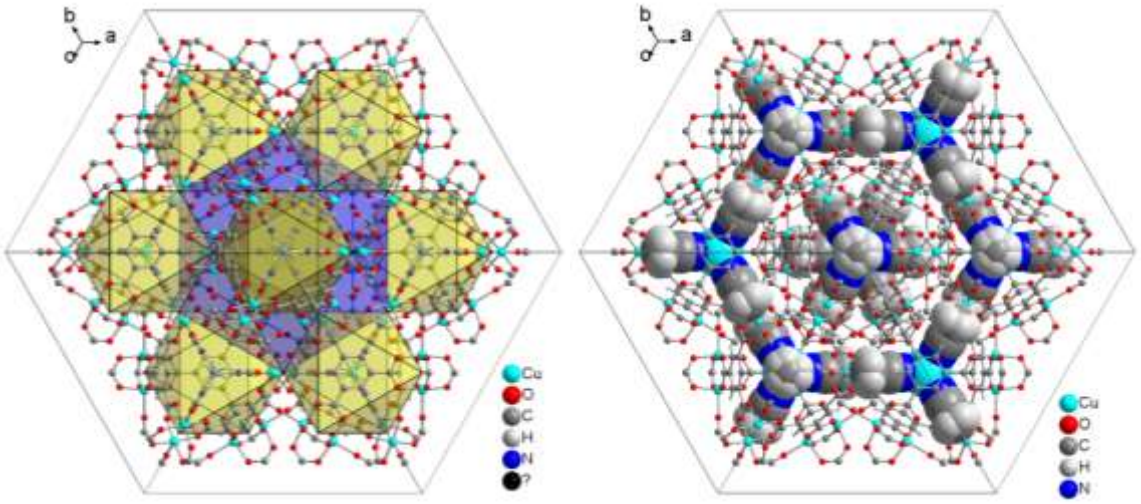

Figure 6.4.1.6: Representation of components of the unit cell of 3D-(3,4)-connected framework of **34** is viewed along the cell body diagonal [111], showing a hexagonal shaped window (**honeycomb**) from guest molecular complex cation $[Cu(CH_3CN)_4]^+$: **left)** polyhedral model with two kinds of pores, the octahedral pore A (yellow) and cuboctahedral pore B (blue), the pore A accommodating guest molecular complex cation $[Cu(CH_3CN)_4]^+$. **right)** View of 3D-framework is represented as ball-stick model, guest molecular complex cation $[Cu(CH_3CN)_4]^+$ is represented as space-filling model. The disordered water molecules in the pores are not shown, nor are the H atoms on the axial ligands.

The phase purity of the 3D-porous coordination polymer, 3D-$\{[Cu(CH_3CN)_4][Cu_3(\mu_6\text{-btc})_2]_2(NO_3/O_2CCH_3)\cdot(H_2O, CH_3CN)_x\}_n$ for **34** and **33** (Figure 6.4.1.7) are confirmed by the comparison of the measured and simulated PXRD pattern. The sample was dried in vacuum furnace for *ca.* 3h at temperature 40°C before PXRD measurement. The comparison of the measured PXRD patterns for both copper compounds **34** and **33** is presented in Figure

6.4.1.7 after peak at 2θ ~10°. Both PXRD patterns are mostly identical, which means both compounds **33** and **34** are mostly isomorphous.

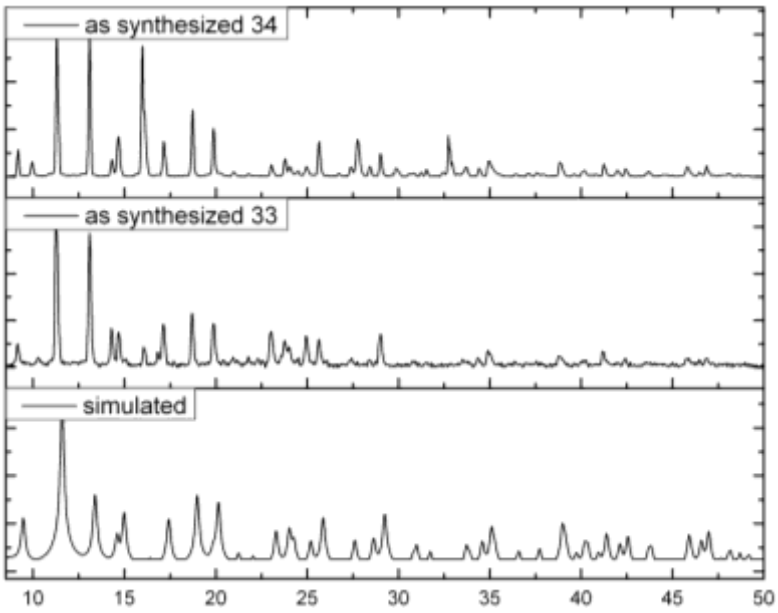

Fig. 6.4.1.7: Combination of the experimental powder X-ray diffractogram of compound **34** (top) and **33** (middle) with the theoretical pattern calculated from the single crystal data (bottom). Diffractograms were obtained with Cu-Kα-radiation wavelength 1.54184 Å on flat layer probes where at low angle the beam spot is strongly broadened so that only a fraction of the reflected radiation reaches the detector, hence, the low relative intensities measured at $2\theta < 10°$. The measured PXRD curves are smoothed and baseline corrected.

The formula unit after SQUEEZE in **34** is C46.76 H24 Cu7 N4 O30 which corresponds to $[Cu(NCCH_3)_4][Cu_3\{C_6H_3(CO_2)_3\}_2(L)_3]_2$ with L being H_2O, CH_3CN or $CH_3CO_2^-$ according to $2L_3$ = $(NO_3/O_2CCH_3)\cdot(H_2O, CH_3CN)_x$ Notably, the sample was washed with water for **34**, with mother liquor for **33** and after then dried in vacuum furnace for *ca.* 3 h at temperature 40°C before PXRD measurement.

To examine the thermal stability of 3D-$\{[Cu(CH_3CN)_4][Cu_3(\mu_6\text{-btc})_2]_2(NO_3/O_2CCH_3)\cdot(H_2O, CH_3CN)_x\}_n$ for **34**, TG-DTG experiment of **34** was carried out in the temperature range 27-600°C. Guest molecules and axial ligands were released at temperature range 64-200°C (obs. 20.63%). The compound is thermally stable up to ~250 °C and then the complex begin to decompose in one weight loss step on further heating(obs. 44.05%). In the last decomposition step a redox-reaction probably was happened, where the copper atom of

guest cation $[Cu(CH_3CN)_4]^+$ was oxidized to (2+). The final residual mass of black precipitate is mostly assigned to CuO and (obs. 34.84%) (Figure 6.4.1.8).

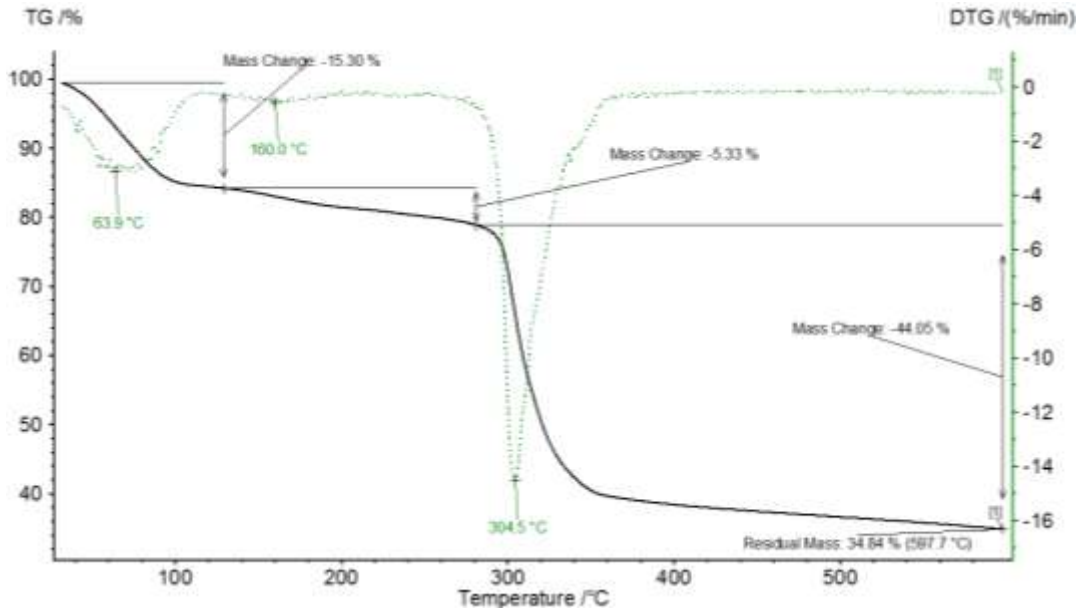

Fig. 6.4.1.8: The experimental TGA and DTG curves for the decomposition of **34**, in N_2 atmosphere, gas flow 30 ml/min at a heating rate of 10 °C/min and sample mass 9.82 mg. Common presentation of the TGA curve (black) together with the DTG curve (green, dotted line).

To examine the thermal stability of **33** is isostructural compound to **34**, TG-DTG experiment of **33** was carried out in the temperature range 27-600 °C. Guest molecules and axial ligands were released at temperature ~230 °C (obs. 13.52%). The dehydrated 3D-network is thermally stable up to ~260°C and then the complex begin to decompose in one weight-loss step on further heating (obs. 52.66%). In the last decomposition step a redox-reaction probably was happened, where the copper atom of guest cation $[Cu(CH_3CN)_4]^+$ was oxidized to state (2+). The final residual mass of black precipitate is mostly assigned to CuO (obs. 33.80%) (Figure 6.4.1.9).

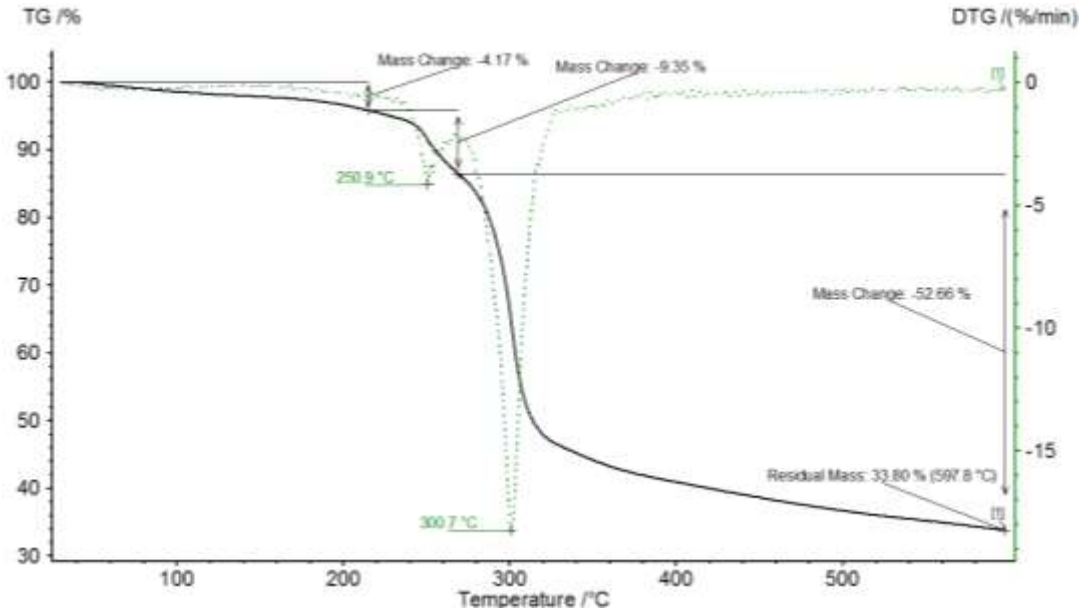

Fig. 6.4.1.9: The experimental TGA and DTG curves for the decomposition of **33**, in N_2 atmosphere, gas flow 30 ml/min at a heating rate of 10 °C/min and sample mass 6.59 mg. Common presentation of the TGA curve (black) together with the DTG curve (green, dotted line). (The image is generated by the instrument's software).

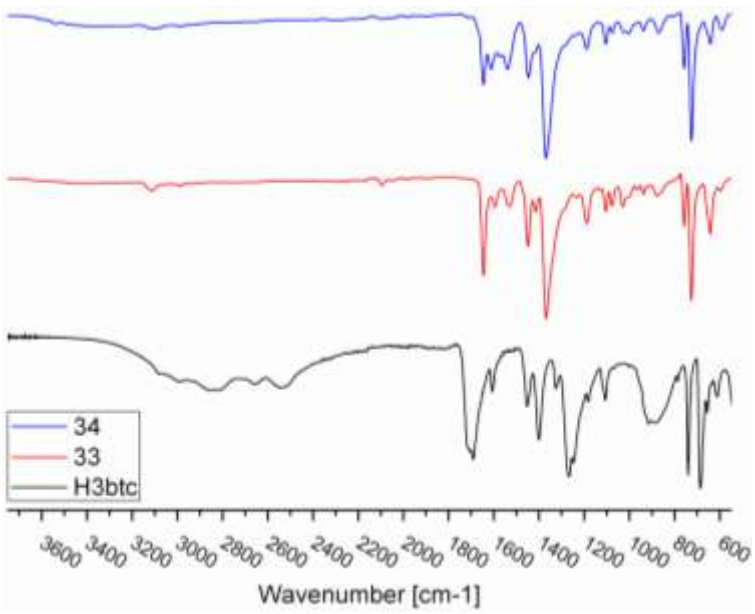

Fig. 6.4.1.10: IR Spectra (ATR) for comparison between **33**, **34** and H_3btc in range 550-3750 cm^{-1}.

The comparison between the FT-IR spectra (ATR) of compounds **33**, **34** and the mixture of the *rac*-btrip and H_3btc ligands shows that, both spectra of **33** and **34** are mostly identical, which were confirmed by their bands width and position matching. The characteristic bands of the coordinated carboxylate group (C=O) of btc ligand appeared at 1646 cm^{-1} for the

asymmetric stretching vibration and 1594-1612 cm^{-1} for the symmetric stretching vibration. The other characteristic bands of the carboxylate group (C-O) of btc ligand appeared at 1234 cm^{-1} for the asymmetric stretching vibration and 1190 cm^{-1} for the symmetric stretching vibration [105],[106],[107]. The absence of characteristic band of protonated carboxyl group (COOH) of H_3btc proves that, the carboxylate group is completely deprotonated [105],[108]. Weak sharp bands at 3111 and 2988 cm^{-1} are attributed to C–H stretching vibrations of H_3btc ligand. Band at 726 cm^{-1}, in the fingerprint region, for **33** and **34** is due to 1,3,5-trisubstituted benzene [109]. Band at 642 cm^{-1} is attributed to triazole ring of *rac*-btrip ligand in pore B of compounds **33** and **34**. This comparison of FT-IR spectra is presented in Figure 6.4.1.10.

When the NMR samples are prepared, an excess NaCN was added to each sample to change the magnetic properties of copper atoms from paramagnetic to diamagnetic by forming the Cu(I) d^{10} complex $Na_3[Cu(CN)_4]$ in the deuterated solvent. After centrifugation, the pipette-separated supernatant was measured.

The ^{1}H NMR spectrum of 3D-$\{[Cu(CH_3CN)_4][Cu_3(\mu_6\text{-btc})_2]_2(NO_3)\cdot(H_2O, CH_3CN)_x\}_n$ **33** shows that both *rac*-btrip and btc ligands are present in the compound. But there are problems associated with dissolving the network in deuterated NMR solvents. The peaks expected for the three equivalent protons of the benzene ring in btc ligand did not appear in the ^{1}H NMR spectrum, when the sample was dissolved in DMSO-d_6 *via* heating in an ultrasonic bath at 50°C. On the other hand, the peaks of the four protons of the two different triazole rings in the *rac*-btrip ligand did not show in the ^{1}H NMR spectrum, if a mixture of NaOD/D_2O was used as a solvent again by heating at 50°C and using ultrasonic bath for 15-30 min. The former is explained by the still present coordination of btc^{3-} to Cu in DMSO-d_6 which apparently was only able to displace and solubilize the btrip ligand. In the latter case, the slightly acidic C-H protons on the triazolyl ring are exchanged by C-D in NaOD/D_2O as was proven by measuring the H_2btc ligand in DMSO-d_6 and btrip ligand in NaOD/D_2O. (Figure 6.4.1.11a,b).

The ^{1}H NMR spectrum of **33** in DMSO-d_6 suggest that btrip molecules are located in the cuboctahedral pores B and C as guest molecules noncoordinated with metal atoms. But their high disorder in pores B and C makes these btrip molecules unobservable by X-ray single-crystal structure analysis. The signal at chemical shift 2.1 ppm could be assigned to the protons of acetonitrile molecules from cation $[Cu(CH_3CN)_4]^+$, which is occupied in octahedral pore A. The integration between CH_3- of btrip for three protons and three protons of CH_3CN show, that molar ratio between the both guest molecules (*rac*-btrip:CH_3CN) in pores is closely to ~1:2 in DMSO-d_6 as shown in Figure 6.4.1.11a but 1:4 in NaOD/D_2O (Fig.

6.4.1.11b). The latter would match the formula suggestion $\{[Cu(CH_3CN)_4][Cu_3(\mu_6\text{-btc})_2]_2(NO_3)(\textit{rac}\text{-btrip})_{1.1}\}$

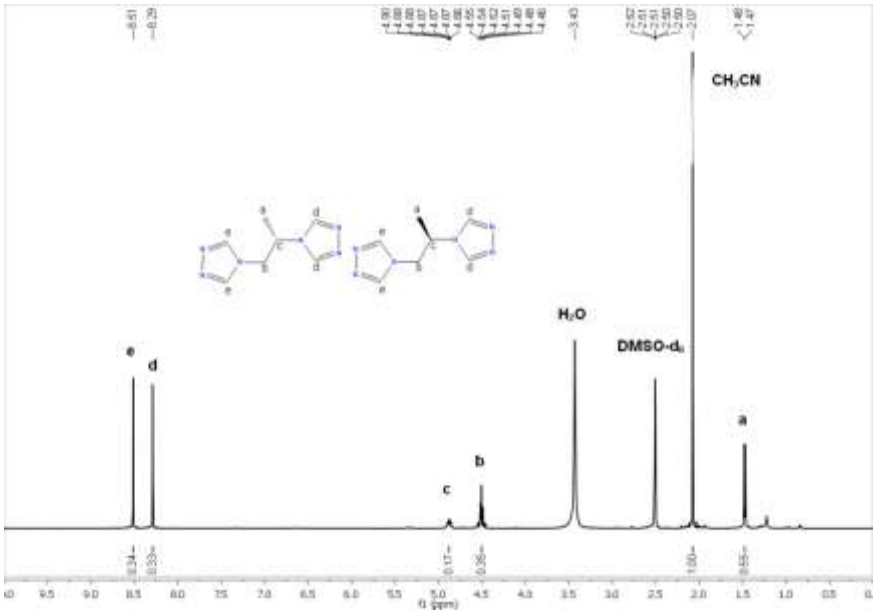

Fig. 6.4.1.11a: ^{1}H NMR Spectrum (500 MHz) of **33** in DMSO-d_6.

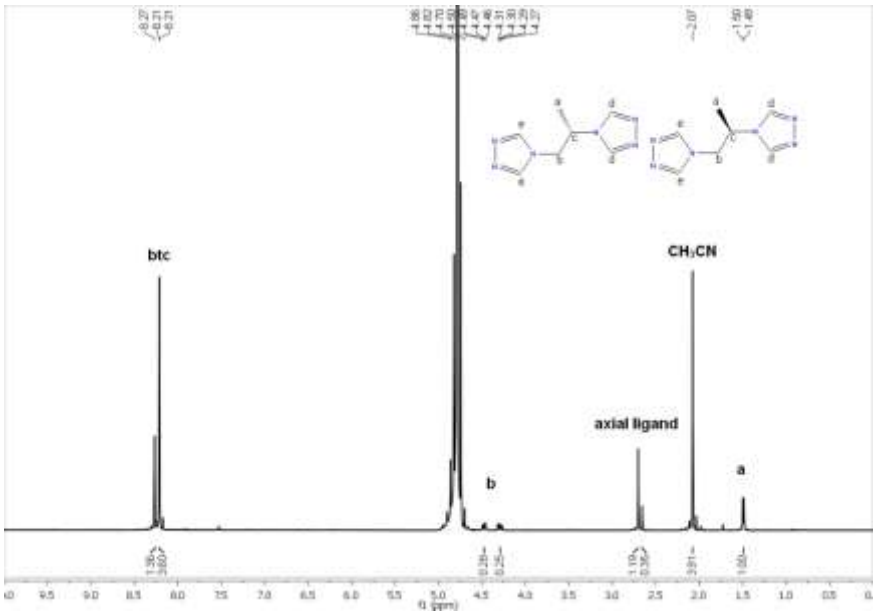

Fig. 6.4.1.11b: ^{1}H NMR Spectrum (500 MHz) of **33** in NaOD/D_2O.

The crystals are dissolved completely in NaOD/D_2O, because the NaOD can react with copper atoms, which lead to dissociation of the coordination polymer. In Figure 6.4.1.11b, the

signal at chemical shift 8.2 ppm could be assigned to the protons of btc ligands. The integration between CH_3CN and three protons of btc^{3-} show, that molar ratio between the both in compound is close to CH_3CN: btc, ~1:1 which would match the formula part $[Cu(CH_3CN)_4][Cu_3(\mu_6\text{-btc})_2]_2$. A slight excess of CH_3CN can be explained by either axially coordinated CH_3CN to Cu or by noncoordinated CH_3CN solvent.

For compound 3D-$\{[Cu(CH_3CN)_4][Cu_3(\mu_6\text{-btc})_2]_2(O_2CCH_3)\cdot(H_2O, CH_3CN)_x\}_n$ **34**, the ^1H NMR spectra (Fig. 6.4.1.12a,b) shows that, the signals of btrip ligands and CH_3CN at chemical shift 1.5 and 2.1 ppm are appearing in deuterated solvent DMSO-d_6, such the btrip ligands are occupied in cuboctahedral pore B and C. For signal at 2.1 ppm could be assigned to the protons of acetonitrile molecules of noncoordinated molecules as solvent molecules in pore B and C and as cation $[Cu(CH_3CN)_4]^+$, which is occupied in octahedral pore A. The integration between CH_3- of btrip and CH_3CN show, that molar ratio between the both is closely to ~1:1 as show in Figure 6.4.1.12b. The ^1H NMR spectra of compound **33** and **34** (Fig. 6.4.1.11b and 12b, respectively) in NaOD/D_2O show, that the integration between CH_3- of btrip for three protons and the three protons of btc is close to the molar ratios of 1:3.60 and 1:2.73. It is assumed that the *rac*-btrip ligand is located in pores B and C as non-coordinated guest molecule.

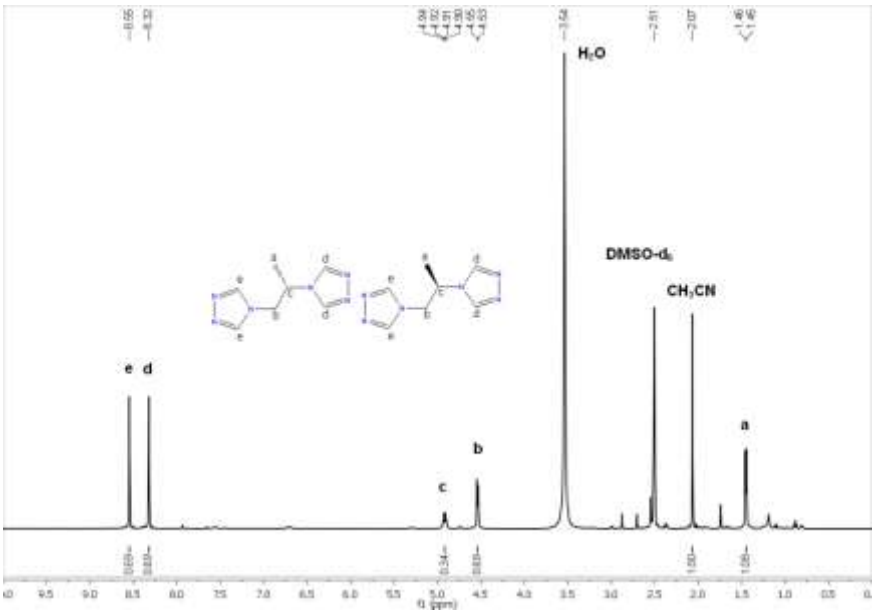

Fig. 6.4.1.12a: ^1H NMR Spectrum (500 MHz) of **34** in DMSO-d_6.

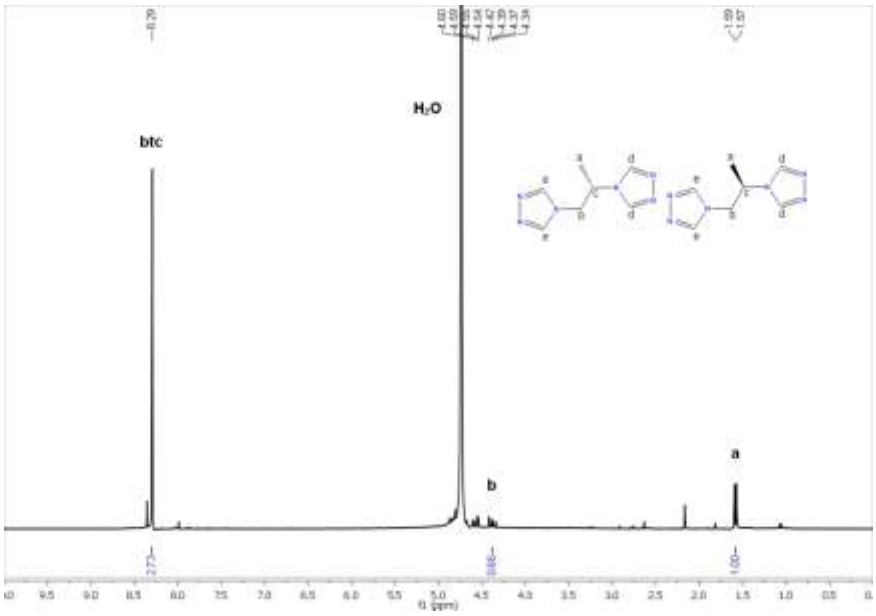

Fig. 6.4.1.12b: ^{1}H NMR Spectrum (300 MHz) of **34** in NaOD/D_2O.

N_2 adsorption study: The potential permanent porosity was studies by gas sorption measurements. The porosity and BET surface area was evaluated by N_2 adsorption at 77 K. For activation the samples of **33** and **34** were heated at 200 °C under vacuum for 3 h to free the pores from solvent molecules (degassed). Both N_2 isotherms of **33** and **34** (Fig. 6.4.1.13 and 6.4.1.14) show, that the both samples are of microporous structures [127]. Brunauer–Emmett–Teller (BET) surface areas for **33** and **34** were calculated as 170.9 and 128 m^2 g^{-1} [130] and the Langmuir method gives the surface area of mesopores equal to 1256.4 m^2/g for **33** and 675.9 m^2/g for **34**. The isotherm data show that the pore widths are distributed narrowly around 32, 45, 54, 62 and maximum peak at 68 Å for **33** and 15, 18, 27, 33 and maximum peak at 38 Å for **34**. The low value of BET surface area could be explained as follow, that pores are occupied by btrip ligands and $[Cu(CH_3CN)_4]^+$ complexes. Thus, the N_2 adsorption-desorption isotherm is in agreement with its single-crystal X-ray diffraction and proton NMR. Experimental.PXRD pattern were measured before and after N_2 adsorption for both samples of **33** and **34**, to verify structure stability upon activation. (Fig. 6.4.1 17). Crystal images before and after N_2 adsorption for both samples of **33** and **34** are shown in Fig. 6.4.1.15 and 6.4.1.16.

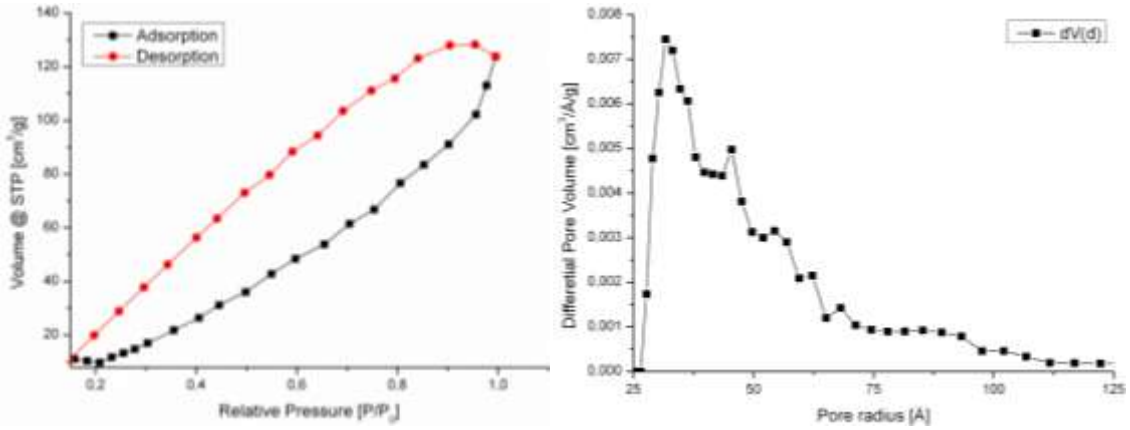

Fig. 6.4.1.13: Nitrogen adsorption-desorption isotherms (left) at 77 K of **33**. The BJH pore-size distributions (right).

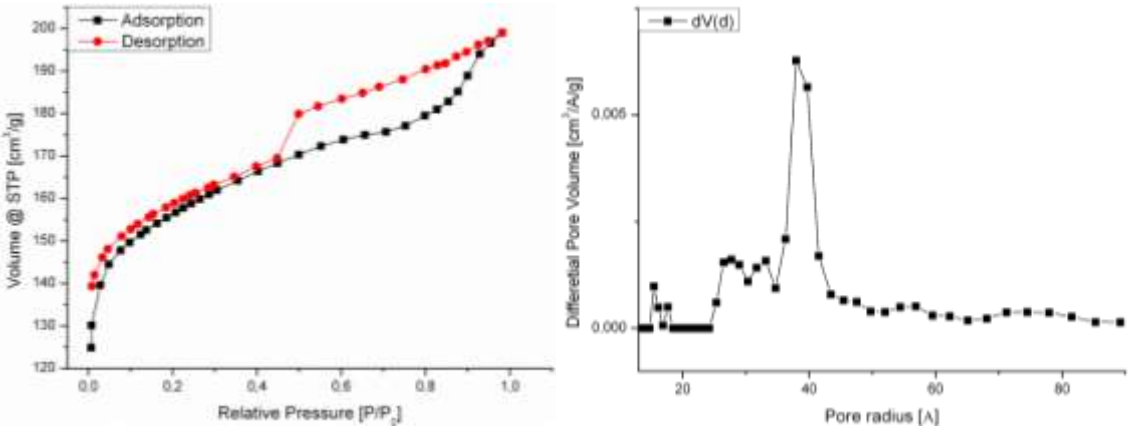

Fig. 6.4.1.14: Nitrogen adsorption-desorption isotherms (left) at 77 K of **34**. The BJH pore-size distributions (right).

Fig. 6.4.1.15: Sample images of 33 as synthesized (as) measurement (blue, left) activated (act) measurement (dark green, right).

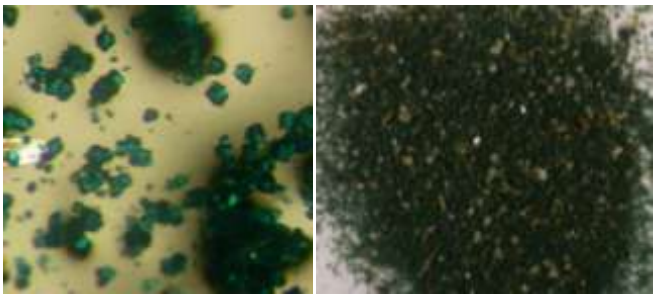

Fig. 6.4.1.16: Sample images of **34** as synthesized (as) measurement (dark blue, left) activated (act) measurement (dark red, right).

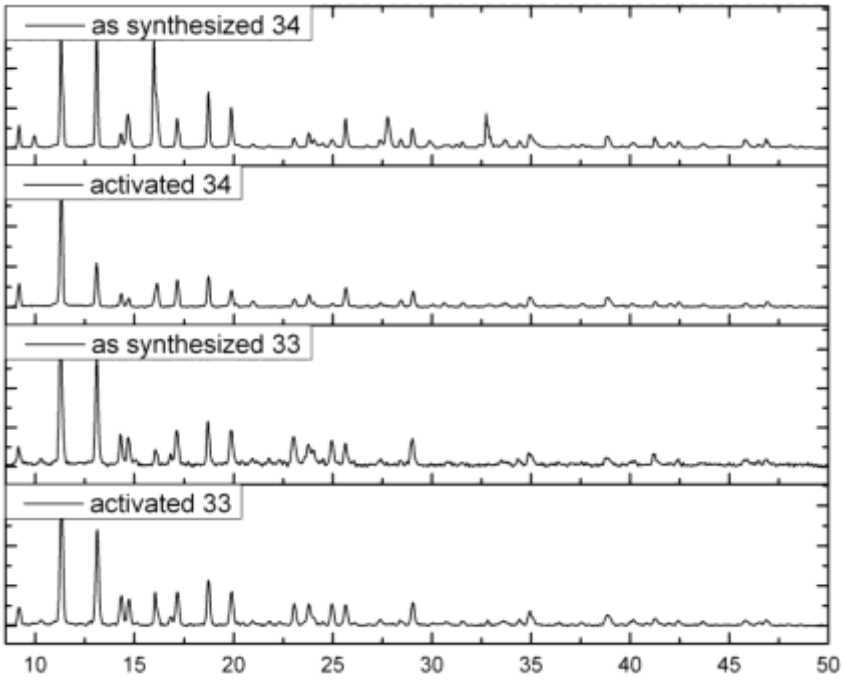

Fig. 6.4.1.17: Combination of the experimental powder X-ray diffractogram of compounds **33** and **34** as synthesized and activated. The measured PXRD is smoothed and baseline corrected.

7.4.2 Structure analysis and characterization of 2D-[Cd(μ_3-Hbtc)(H_2O)$_2$]$_n$ (26)

This compound has been synthesized by Mr. Ümit Köc in his Diploma work [113]. Colorless crystals (Fig. 6.4.2.1) of formula 2D-[Cd(μ_3-Hbtc)(H_2O)$_2$]$_n$ **26**, are obtained from the hydrothermal reaction of Cd(OAc)$_2$.2H_2O, 4,4`-bis(1,2,4-triazol-4-yl) (btr) and benzene-1,3,5-tricarboxylic acid (H_3btc). Triethylamine (Et_3N) is used as base to deprotonate the carboxylate groups of H_3btc. The synthesis is almost identical to those of complex **25**. Except, the synthesis was carried out at higher temperature 140°C instead of 125 °C, in an attempt to get better crystals for x-ray diffraction measurements.

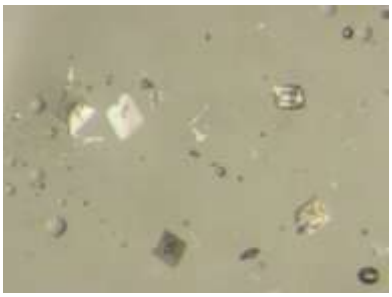

Figure 6.4.2.1: Colorless crystals of 2D-[Cd(μ_3-Hbtc)(H_2O)$_2$]$_n$, **26**.

The product and its structure has been reported before in the references given in [145]. The synthesis conditions were however different (see Scheme 6.4.2.1). The synthesis of 2D-[Cd(μ_3-Hbtc)(H_2O)$_2$]$_n$ was repeated several times and found to be reproducible. The obtained crystals are insoluble in water and organic solvents such as ethanol, methanol or acetone. The space group *C2/c* and refinement parameters R = 0.02 are as found before in the reported structures [145]. Therefore, only a short structure description is given here. The structure 2D-[Cd(μ_3-Hbtc)(H_2O)$_2$]$_n$ features a two-dimensional network, which consist of Cd-atoms, $Hbtc^{2-}$ and aqua ligands. The ligand 4,4`-bis(1,2,4-triazol-4-yl) (btr) is not incorporated into the network at 140°C probably due to decomposition.

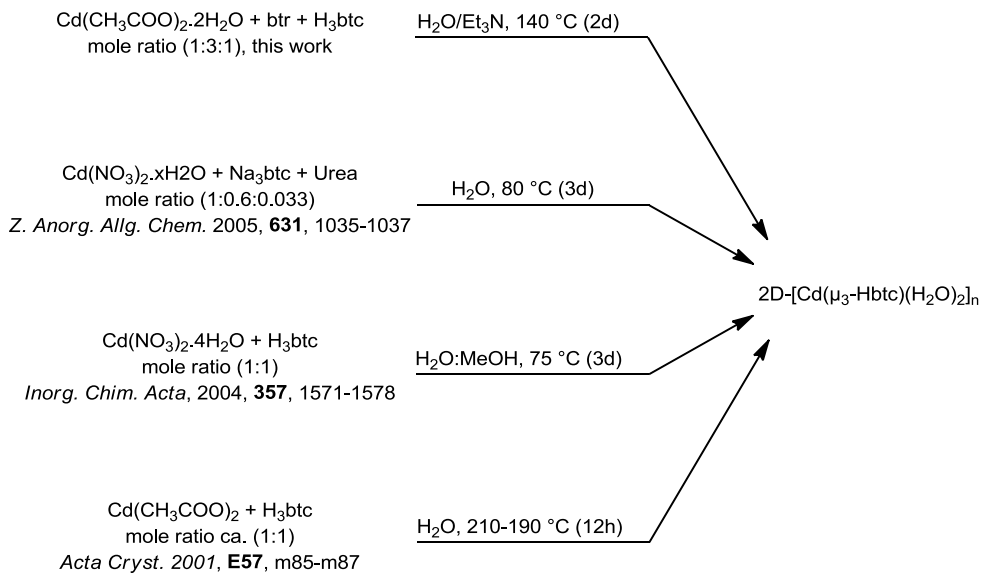

Scheme 6.4.2.1: Synthesis of 2D-[Cd(μ_3-Hbtc)(H_2O)$_2$]$_n$ under different conditions, **26**.

The Cd atom is coordinated in a distorted pentagonal bipyramidal fashion by seven oxygen atoms; two of them belong to axial aqua ligands. The other O atoms belong to three different ($Hbtc^{2-}$) monohydrogen benzene tricarboxylate anions, two of these are bonded *via* bidentate chelating carboxylate groups (O1-Cd-O2 and O5-Cd-O6), whilst the third ligand is coordinated in a monodentate fashion through its carboxylic group (Cd-O4). The O atoms of

($Hbtc^{2-}$) ligands are located in the equatorial plane. Bond distances and angles around Cd are as found before in the reported structures [145]. Cd-O bond lengths vary in the range 2.2462-2.5560 Á (Fig. 6.4.2.2, Table 6.4.2.1), which are in good agreement with the previously reported Cd-O values.

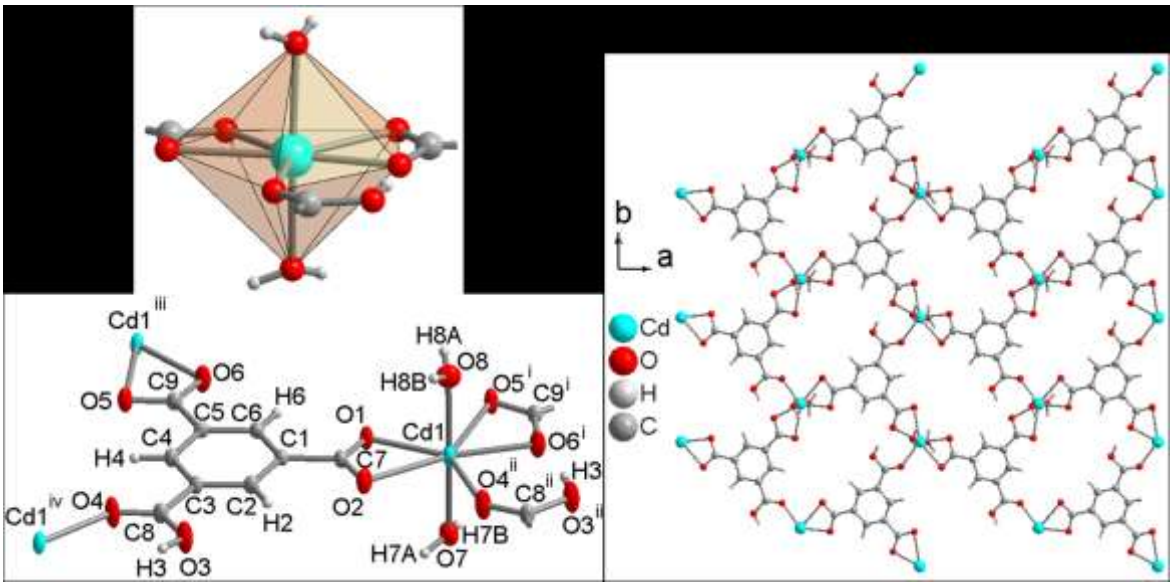

Figure 6.4.2.2: Coordination environment of the cadmium atom in **26** (top-left) and the extended asymmetric unit of 2D-$[Cd(\mu_3\text{-}Hbtc)(H_2O)_2]_n$ (bottom-left with 50% thermal ellipsoids for non-hydrogen atoms) and 2D network (right). Symmetry transformation: i = x-1/2,-y+1/2,z-1/2; ii = x-1/2,-y+3/2,z-1/2; iii = x+1/2,-y+1/2,z+1/2; iv = x+1/2,-y+3/2,z+1/2.

Table 6.4.2.1: Selected bond lengths [Å] and angles [°] for **26**.

Cd1-O1	2.2462(17)	O7-Cd1-O2	93.02(7)
Cd1-O6^{i}	2.2827(17)	O6^{i}-Cd1-O5^{i}	53.28(6)
Cd1-O4^{ii}	2.2983(17)	O8-Cd1-O5^{i}	84.54(7)
Cd1-O8	2.315(2)	O2-Cd1-O5^{i}	146.45(6)
Cd1-O7	2.383(2)	O1-Cd1-O4^{ii}	134.14(6)
Cd1-O2	2.5240(19)	O1-Cd1-O8	89.14(8)
Cd1-O5^{i}	2.5560(18)	O4^{ii}-Cd1-O8	94.94(9)
O1-Cd1-O6^{i}	145.74(6)	O6^{i}-Cd1-O7	90.81(7)
O6^{i}-Cd1-O4^{ii}	80.10(6)	O8-Cd1-O7	175.98(7)
O6^{i}-Cd1-O8	88.67(8)	O6^{i}-Cd1-O2	159.55(6)
O1-Cd1-O7	89.04(7)	O8-Cd1-O2	88.84(8)
O4^{ii}-Cd1-O7	88.89(8)	O1-Cd1-O5^{i}	92.48(6)
O1-Cd1-O2	54.49(6)	O4^{ii}-Cd1-O5^{i}	133.37(6)
O4^{ii}-Cd1-O2	79.90(7)	O7-Cd1-O5^{i}	91.96(6)

Symmetry transformations used to generate equivalent atoms: i = x-1/2,-y+1/2,z-1/2; ii = x-1/2,-y+3/2,z-1/2

The elemental analysis data for the complex is consistent with the proposed formula, ($CdC_9H_8O_8$) of 2D-[Cd(μ_3-Hbtc)(H_2O)$_2$]$_n$ **26**.

The phase purity of the cadmium compound is confirmed by positive matching of the measured and simulated PXRD pattern (Figure 6.4.2.3).

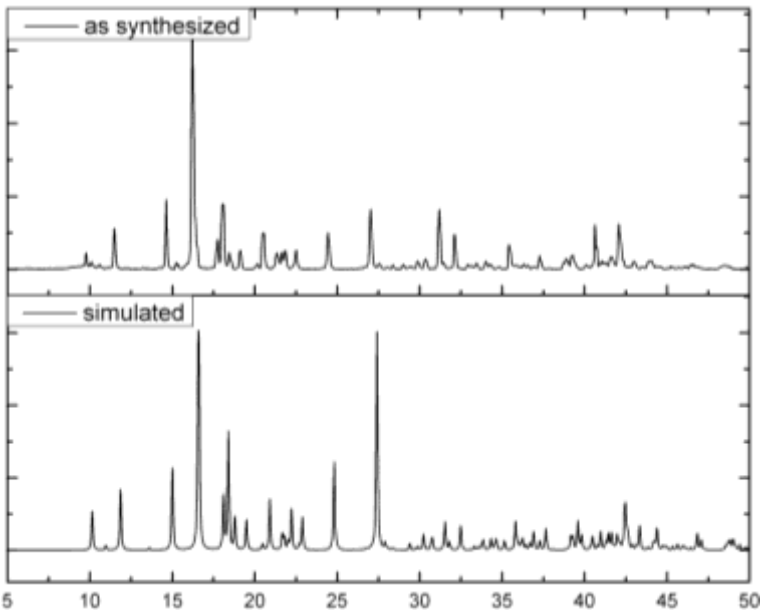

Fig. 6.4.2.3: Combination of the experimental powder X-ray pattern of **26** (top) at Cu-Kα wavelength 1.54184 Å with the theoretical pattern, which is calculated from the single crystal data (bottom). The measured PXRD is smoothed and baseline corrected.

The FT-IR spectra (ATR) of this 2D-coordination polymers, 2D-[Cd(μ_3-Hbtc)(H_2O)$_2$]$_n$ **26**, shows the characteristic bands of the coordinated carboxylate group of Hbtc ligand appearing at 1616 cm^{-1} for the asymmetric stretching vibration and 1549 cm^{-1} for the symmetric stretching vibration [105],[106],[107]. The characteristic band of protonated carboxyl group –COOH of Hbtc ligand is observed at 1680 and 1277 cm^{-1} [105]. The broad bands at 3295-3223 cm^{-1} and 3090 cm^{-1} are attributed to the O–H stretching vibrations of coordinated water molecules with the Cd-atoms which indicate the presence of inter-layer hydrogen bonding in the lattice [112]. Bands at 741 and 687 cm^{-1} for **26** are due to 1,3,5-trisubstituted benzene in the fingerprint region [109],[146].

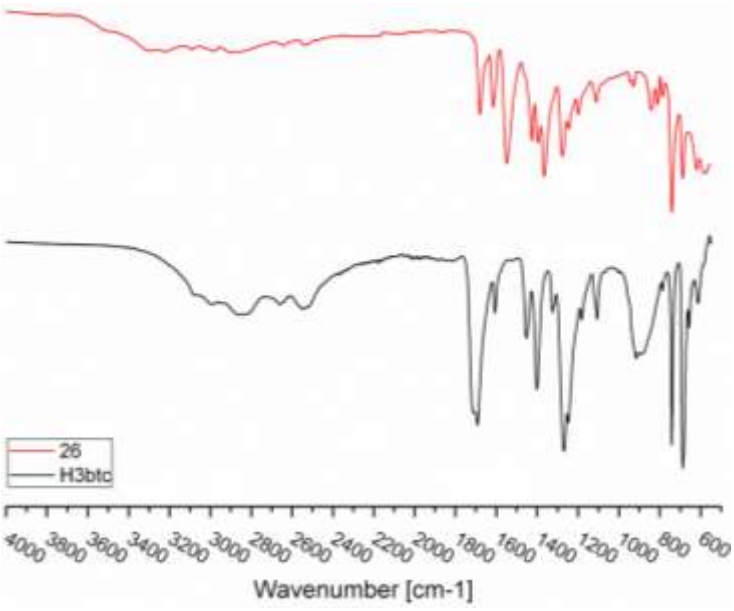

Fig. 6.4.2.4: FT-IR Spectra (ATR) for comparison between compound **26** and H_3btc ligand.

7.4.3 Structure analysis and characterization of 1D-$[M_3(\mu_3\text{-btc})(\mu_2\text{-btc})(H_2O)_{12}]_n$ (M = Co and Zn) (39, 35)

Red crystals (Fig. 6.4.3.1, left) of coordination polymer 1D-$[Co_3(\mu_3\text{-btc})(\mu_2\text{-btc})(H_2O)_{12}]_n$ **39** are obtained by the hydrothermal reaction of $Co(NO_3)_2{\cdot}6H_2O$, 1,4-di(1H-tetrazol-5-yl)benzene (H_2bdt) and benzene-1,3,5-tricarboxylic acid (H_3btc) in approximately 4:1:1 molar ratio at 150°C. Ammonia solution (NH_4OH) is used as base to deprotonate the tetrazolate and carboxylate groups of both ligands (H_2bdt, H_3btc).

The compound **35** has been synthesized by Mr. Ümit Köc in his Diploma work [113]. Colorless crystals (Fig. 6.4.3.1, right) of 1D-$[Zn_3(\mu_3\text{-btc})(\mu_2\text{-btc})(H_2O)_{12}]_n$ **35** are obtained after 30 min. at room temperature *via* the reaction of $Zn(NO_3)_2{\cdot}4H_2O$, 4,4`-bis(1,2,4-triazol-4-yl) (btr) and benzene-1,3,5-tricarboxylic acid (H_3btc) in approximately 2:3:1 molar ratio. Triethylamine (Et_3N) is used as base to deprotonate the carboxylate groups of (H_3btc). The same product was obtained by the same conditions but using other zinc salts such as ($Zn(NO_3)_2.6H_2O$, $Zn(ClO_4)_2.6H_2O$,$ZnCl_2$ and $ZnBr_2$).

Figure 6.4.3.1: Red crystals of **39** (left), colorless crystals of **35** (right).

The crystals isolated from the hydrothermal reaction for **39**, or the room temperature reaction for **35**, crystallize in the monoclinic crystal system with the *C2* space group and consist of infinite zigzag chains of alternating $[M(H_2O)_4]^{2+}$ ions and btc^{3-} ligands, which are connected by strong hydrogen-bonds and weak π-π interactions to each other. The 1D-polymeric chains of $[M_3(\mu_3\text{-btc})(\mu_2\text{-btc})(H_2O)_{12}]_n$ (M = Co and Zn) are analogous to a previously reported cobalt-polymer [5l],[147] and to zinc polymer [5a,l] (Scheme 6.4.3.1).

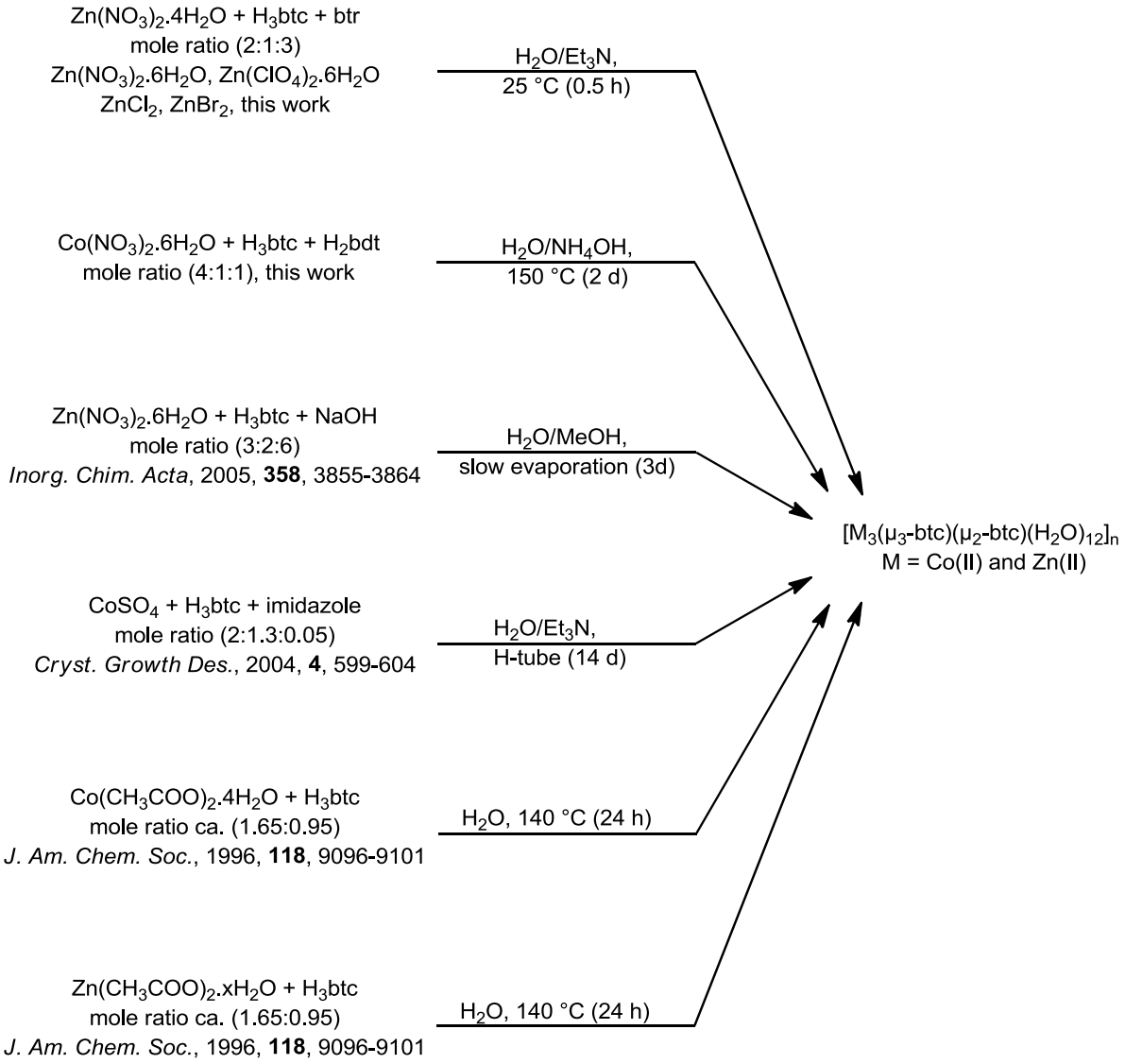

Scheme 6.4.3.1: Synthesis of $[M_3(\mu_3\text{-btc})(\mu_2\text{-btc})(H_2O)_{12}]_n$ (M = Co(II) and Zn(II)) through different routes, (**39** and **35**).

The crystallographic asymmetric unit of **35** contains two Zn(II) ions and two half of ligands. There are two fully deprotonated types of btc^{3-} anions in the structure. The structural representation of **35** with atom labeling Scheme is shown in (Fig. 6.4.3.2). Selected bond lengths and angles are summarized in (Table 6.4.3.1).

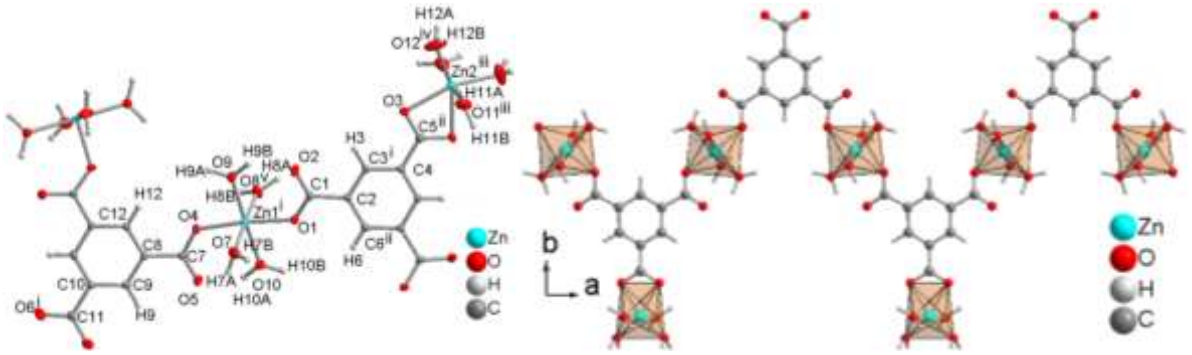

Figure 6.4.3.2: Part of the Zn-btc chain, including the asymmetric unit in $[Zn_3(\mu_3\text{-btc})(\mu_2\text{-btc})(H_2O)_{12}]_n$. The non-hydrogen atoms are represented by 50% thermal ellipsoids. The hydrogen atoms are drawn using an arbitrary sphere size. Ball-and-stick representation of part the polymeric zigzag chains of $[Zn_3(\mu_3\text{-btc})(\mu_2\text{-btc})(H_2O)_{12}]_n$ along the crystallographic ***a***-axis **35** (right). Symmetry transformation to generate the equivalent atoms in **35**: i =7 = -x,y,-z; ii = x-1,y,z-1; iii = x-1,y-1,z-1; iv = -x,y-1,-z; v = x-1/2,y-1/2,z-1: (Co instead Zn for **39**)

Table 6.4.3.1: Selected bond lengths [Å] and angles [°] for **35**.

Zn1-O1	2.038(4)	Zn1-O4	2.032(3)
Zn1-O7	2.162(4)	Zn1-O8^{i}	2.146(4)
Zn1-O9	2.098(3)	Zn1-O10	2.106(3)
O8-Zn1^{vi}	2.146(4)	O3-Zn2^{v}	2.154(4)
Zn2-O3^{iii}	2.154(4)	Zn2-O3^{iv}	2.155(4)
Zn2-O11^{ii}	2.141(4)	Zn2-O12^{ii}	1.993(4)
O4-Zn1-O1	173.64(10)	O4-Zn1-O9	89.83(15)
O1-Zn1-O9	94.06(15)	O4-Zn1-O10	90.66(15)
O1-Zn1-O10	85.80(15)	O9-Zn1-O10	176.08(11)
O4-Zn1-O8^{i}	94.39(13)	O1-Zn1-O8^{i}	90.72(13)
O9-Zn1-O8^{i}	88.71(15)	O10-Zn1-O8^{i}	87.37(15)
O4-Zn1-O7	86.11(13)	O1-Zn1-O7	88.65(13)
O9-Zn1-O7	93.14(15)	O10-Zn1-O7	90.78(15)
O8^{i}-Zn1-O7	178.09(11)	O12^{ii}-Zn2-O12	103.9(3)
O12^{ii}-Zn2-O11^{ii}	93.84(17)	O12^{ii}-Zn2-O11	84.24(17)
O11^{ii}-Zn2-O11	176.89(16)	O12^{ii}-Zn2-O3^{iii}	98.28(18)
O12-Zn2-O3^{iii}	156.44(14)	O11^{ii}-Zn2-O3^{iii}	86.59(13)
O11-Zn2-O3^{iii}	96.10(13)	O3^{iii}-Zn2-O3^{iv}	61.18(17)

Symmetry transformations used to generate equivalent atoms: i = -x+1/2,y-1/2,-z+1; ii = -x+1,y,-z+1; iii = x,y+1,z; iv = -x+1,y+1,-z+1; v = x,y-1,z; vi = -x+1/2,y+1/2,-z+1; vii = -x,y,-z.

Each Zn1 atom has a slightly distorted octahedral environment with four water molecules in the equatorial sites, while the axial sites are occupied by oxygen atoms of monodentate carboxylate groups from two different benzene tricarboxylate ligands. The Zn2 atoms have a distorted octahedral coordination sphere with *C2* symmetry. The coordination sphere around Zn2 contains four water molecules and one chelating carboxylate group. It is interesting to note that oxygen atoms from carboxylate are close bonded to Zn1 (average Zn–O = 2.035 Å), while they are weakly coordinated to Zn2 (average Zn-O = 2.154). The btc^{3-} anions coordinate to Zn centers in two different modes, the first type of btc^{3-} anion coordinates to two Zn1 atoms and one Zn2 atom, while the second type coordinates to two Zn1 atoms, with the third carboxylate group being uncoordinated (Fig. 6.4.3.2). These extended 1D-zigzag chains run along the crystallographic **a**-axis of the unit cell, which are composed from two constructed symmetry-nonequivalent tetra-aqua zinc(II) units and btc ligands as shown in (Fig. 6.4.3.2, right). The interchain distance between two Zn-atoms of the 1D zigzag chain is Zn1···Zn2 = 10.0902 Å and the shortest interchain distance is Zn1···Zn1 = 7.8072 Å. The chains overlap so that there are significant π-π interactions [116] between the benzene rings of the btc ligands (closest C···C distance is 3.2733 Å). In this structure, there are neither channels nor guest molecules in the remaining space between layers.

The measured PXRD patterns of zinc compounds show that, these compounds are isostructural, as they show identical PXRD patterns, which agree closely with their matched peaks width, position and intensity. The PXRD patterns are presented in Fig. 6.4.3.3.

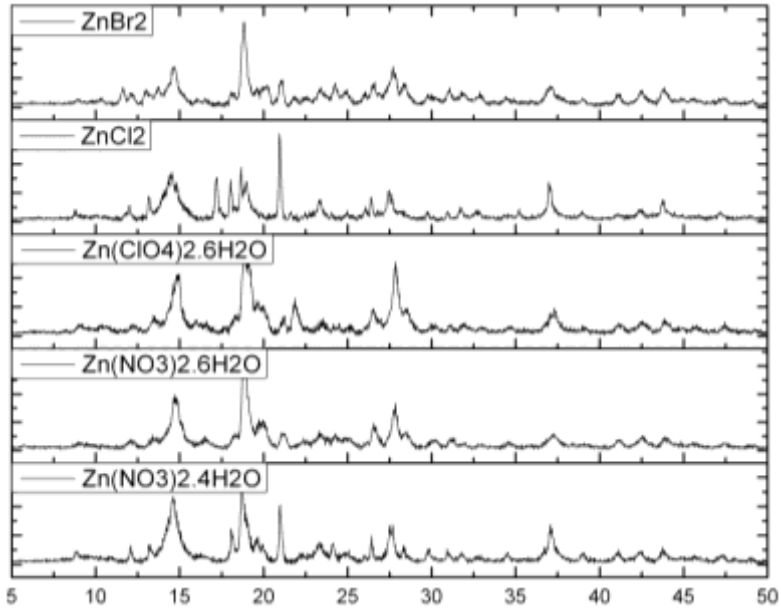

Fig. 6.4.3.3: Combination of the experimental PXRD of $[Zn_3(\mu_3\text{-btc})(\mu_2\text{-btc})(H_2O)_{12}]_n$ from different zinc salts at Cu-Kα wavelength 1.54184 Å.

The phase purity of the zinc compound and cobalt compound was checked by comparison of the measured with simulated PXRD pattern. A typical agreement between measured and simulated PXRD patterns is presented in Figure 6.4.3.4. It is evident that the crystal selected for **39** was not representative to the batch.

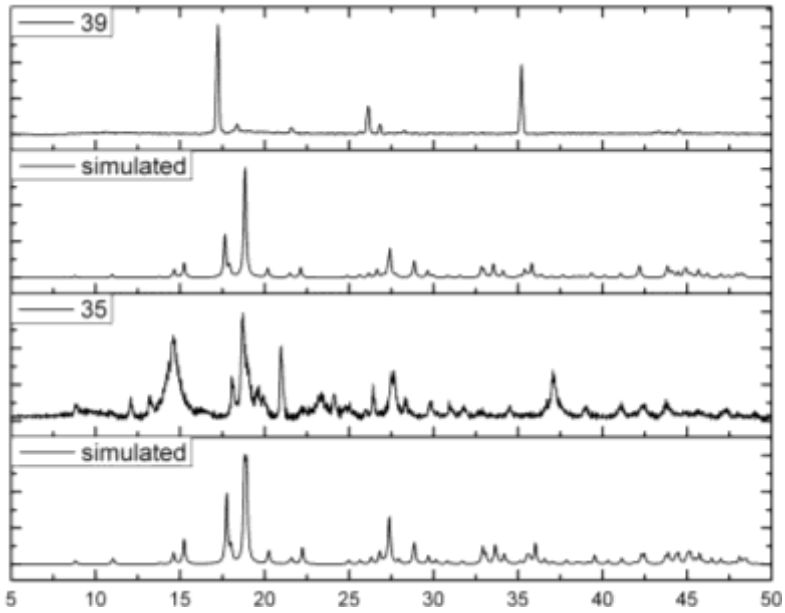

Fig. 6.4.3.4: Combination of the experimental powder X-ray pattern (top) at Cu-Kα wavelength 1.54184 Å with the theoretical pattern, which is calculated from the single crystal data (bottom) at Cu-Kα wavelength 1.540598 Å. Zinc compound **35**, cobalt compound **39**.

The 1D-coordination polymers of different Zn-salts (Figure 6.4.3.5 and 6.4.3.6) and Co-salt (Figure 6.4.3.5) show identical infrared spectra (ATR) with the absorption bands of the typical asymmetric and symmetric stretching vibration of coordinated carboxylate group of btc ligand respectively appearing at 1613 and 1550 cm^{-1} (for Co-compound at 1608 and 1514 cm^{-1}). The absence of absorption bands at 1750-1692 and 1269 cm^{-1}, where the –COOH of ligand is expected to appear, is indicative of the deprotonation of H_3btc upon its reaction with metal ions [105],[5a,l],[148]. The broad bands at 3444-3390 cm^{-1} and at 3101 cm^{-1} are indicative to O–H stretching vibrations of coordinated water molecules with the Zn-atoms (for Co-compound at 3392 and 3107 cm^{-1}) and indicate the presence of H-bonds between the layers in the lattice [112]. Bands at 714 and 613 cm^{-1} for **35** are due to the 1,3,5-trisubstituted benzene in the fingerprint region (for Co-compound at 710 and 655 cm^{-1}) [109],[146].

The infrared spectra (ATR) of zinc compounds show that, only the btc^{2-} anions are coordinated with zinc atoms in these compounds, as they show identical infrared spectra

(ATR), which agree mostly with their matched bands. The comparison of FT-IR spectra are presented in Fig. 6.4.3.6. The ^{1}H-NMR spectra of zinc compounds show signal of H_3btc ligand.

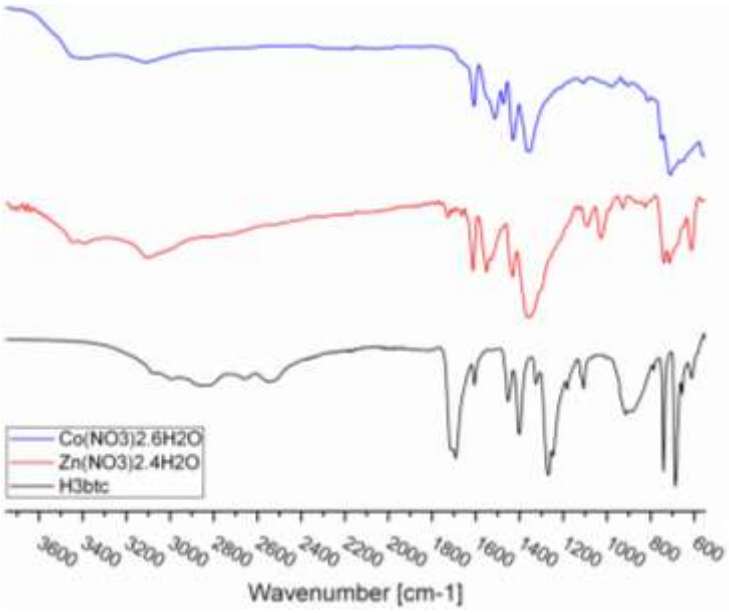

Fig. 6.4.3.5: FT-IR Spectra (ATR) for comparison between the zinc and cobalt compounds with the ligand H_3btc in range 550-3750 cm^{-1}.

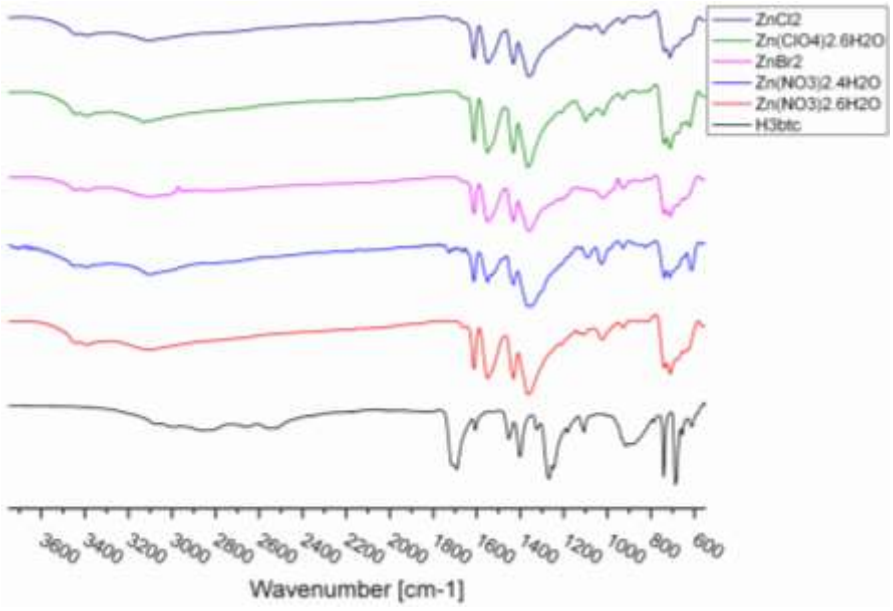

Fig. 6.4.3.6: FT-IR Spectra (ATR) for comparison between the zinc compounds and the ligand H_3btc.

7.4.4 Structure analysis and characterization of 2D-[Zn(μ_3-aip)(H_2O)]$_n$ (40)

Colorless crystals (Fig. 6.4.4.1) of the coordination polymer 2D-[Zn(μ_3-aip)(H_2O)]$_n$ **40** were obtained from the hydrothermal reaction of $Zn(NO_3)_2 \cdot 4H_2O$, 1,2-bis(1,2,4-triazol-4-yl)isopropanol (btrip) and 5-aminoisophthalic acid (H_2aip) in approximately (2:2:1) molar ratio at 125°C. Triethylamine (Et_3N) was used as base to deprotonate the carboxylate groups of the ligand H_2aip.

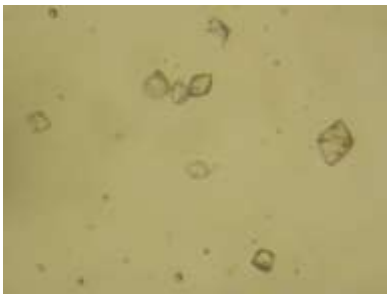

Figure 6.4.4.1: Colorless crystals of 2D-[Zn(μ_3-aip)(H_2O)]$_n$ **40**.

This compound crystallizes in the monoclinic crystal system with the *P* 2_1/c space group and consists of infinite layers of alternating Zn(II) ions and (aip) ligands which are hydrogen-bonded to each other. The obtained 2D-network polymer 2D-[Zn(μ_3-aip)(H_2O)]$_n$ is identical to the previously reported one in reference [149] which was synthesised under different conditions (Scheme 6.4.4.1). The synthesis of 2D-[Zn(μ_3-aip)(H_2O)]$_n$ was repeated three times and found it reproducible, crystals are insoluble in water and some organic solvents such as ethanol or methanol.

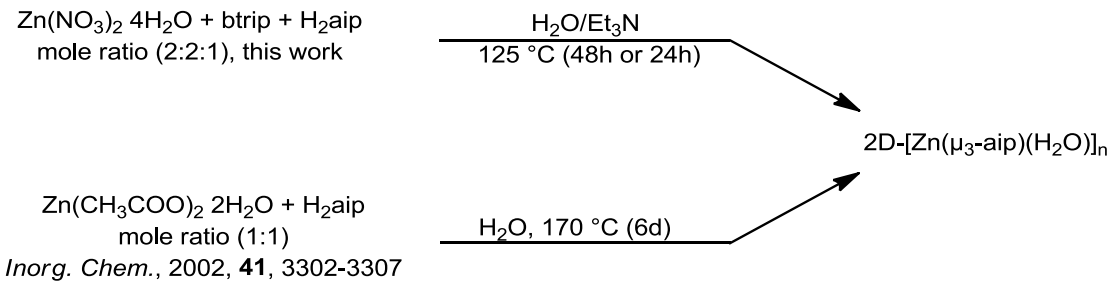

Scheme 6.4.4.1: Synthesis of 2D-[Zn(μ_3-aip)(H_2O)]$_n$ under different conditions, **40**.

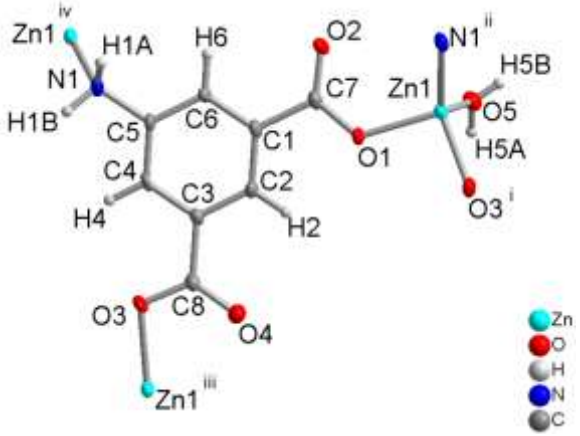

Figure 6.4.4.2: Coordination environment of the zinc atom in **40** and the building unit of the polymer 2D-$[Zn(\mu_3\text{-aip})(H_2O)]_n$. The nonhydrogen atoms are represented by 50% thermal ellipsoids. The hydrogen atoms are drawn using an arbitrary sphere size. Selected distances and angles are in (Table 6.4.4.1). Some atoms are related by symmetry codes, symmetry transformation to generate the equivalent atoms in (X): i = x+1,-y-1/2,z+1/2; ii = x+1,-y+1/2,z+1/2; iii = x-1,-y-1/2,z-1/2; iv = x-1,-y+1/2,z-1/2.

Table 6.4.4.1: Selected bond lengths [Å] and angles [°] for **40**.

Zn1-O1	1.963(3)	Zn1-O5	1.966(3)
Zn1-O3^{i}	1.982(3)	Zn1-N1^{ii}	2.036(3)
O1-Zn1-O5	109.72(13)	O1-Zn1-O3^{i}	94.72(11)
O5-Zn1-O3^{i}	110.13(12)	O1-Zn1-N1^{ii}	104.67(13)
O5-Zn1-N1^{ii}	118.19(13)	O3^{i}-Zn1-N1^{ii}	116.41(13)
C7-O1-Zn1	123.1(2)	C8-O3-Zn1^{iii}	108.8(2)

Symmetry transformations used to generate equivalent atoms: i = x+1,-y-1/2,z+1/2; ii = x+1,-y+1/2,z+1/2; iii = x-1,-y-1/2,z-1/2.

The crystallographic asymmetric unit of **40** consist of one Zn(II) ions, one aip^{2-} anion and an aqua ligand. The structure is overall neutral. In this polymer, each zinc ion is in a distorted tetrahedron environment defined by two carboxylate groups from two different aip^{2-} anions, one amino group of other aip^{2-} anion, and one water molecule. Each aip^{2-} anion in **40** is coordinated to three metal atoms (Fig. 6.4.4.2, Table 6.4.4.1). Thus, The Zn(II) cations and $aiph^{2-}$ anions form a two-dimensional infinite network (Fig. 6.4.4.3, left). The layers of 2D-network are parallel to each other and to lattice plane **ab** (Fig. 6.4.4.3, right). The distance between the planes of neighboring layers is more than 3 Å with possible weak π-π interactions [116] between the benzene rings of the neighboring layers. In the remaining space between the layers, there are not any guest molecules. The layers are linked together

in pairs through strong hydrogen bonding into a 3D supramolecular network as shown in Fig 6.4.4.4.

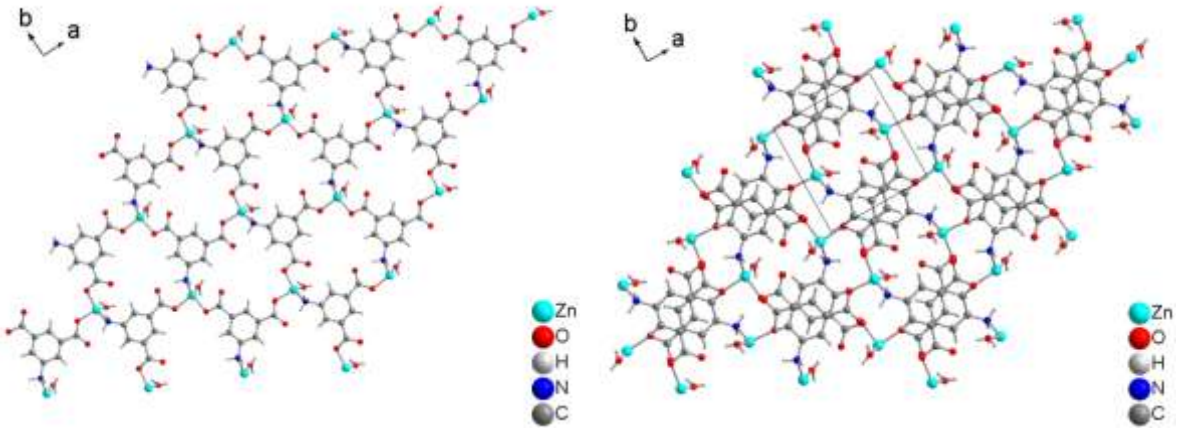

Figure 6.4.4.3: One 2D network of 2D-[Zn(μ_3-aip)(H_2O)]$_n$ (left), and two adjacent layers (right) showing how the layers are located in crystal packing in lattice plane **ab**.

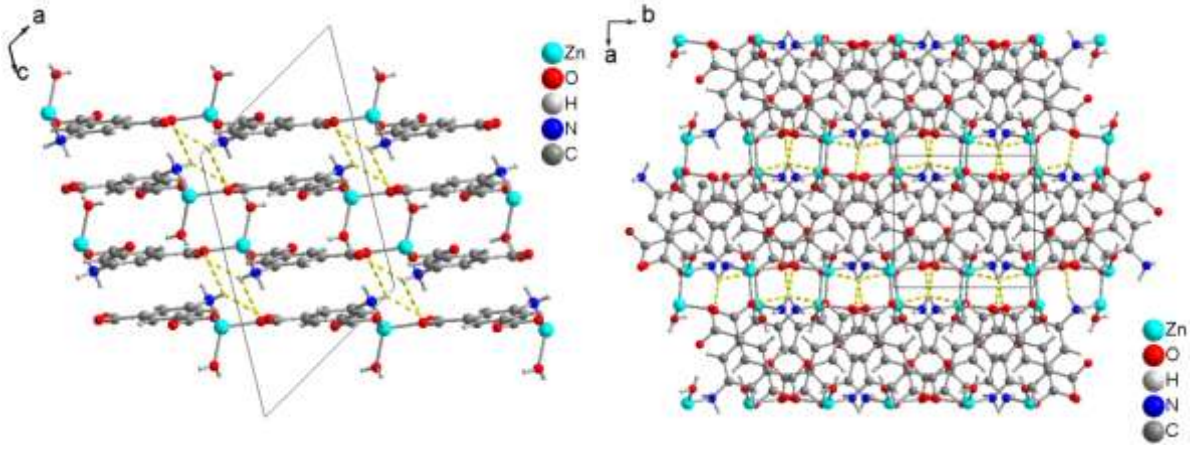

Figure 6.4.4.4: The hydrogen bond between the layers within the unit cell of 2D-[Zn(μ_3-aip)(H_2O)]$_n$ showing two neighboring layers connected through N–H···O hydrogen bonds as dashed lines. There are another O–H···O hydrogen. Note the layers are parallel to each neighboring layers.

The phase purity of the zinc compound is confirmed by the comparison of the measured and simulated PXRD pattern. A typical agreement between measured and simulated PXRD patterns is presented in Figure 6.4.4.5.

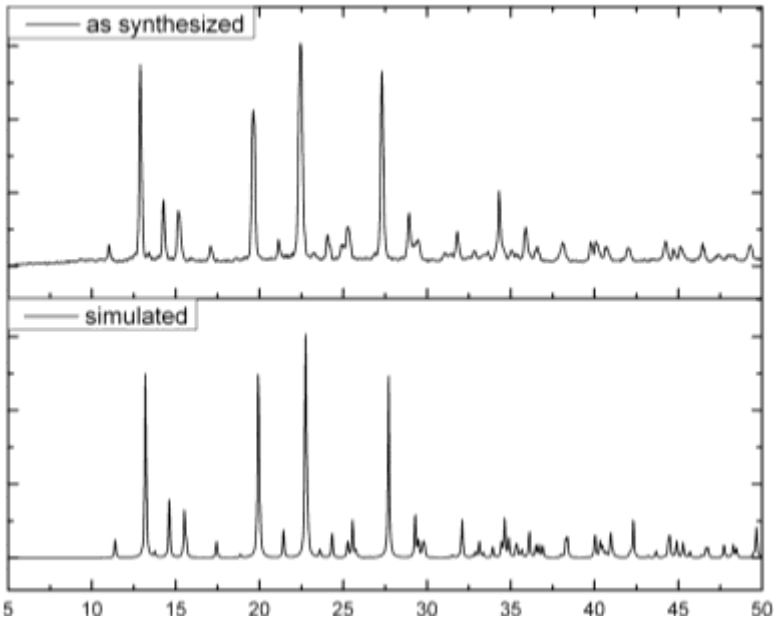

Fig. 6.4.4.5: Combination of the experimental PXRD of zinc compound (top) at Cu-Kα wavelength 1.54184 Á with the theoretical pattern, which is calculated from the single crystal data (bottom) at wavelength Cu-Kα 1.540598 Á. The measured PXRD is smoothed and baseline corrected.

The IR spectrum (ATR) of 2D-coordination polymer 2D-$[Zn(\mu_3\text{-aip})(H_2O)]_n$ (Figure 6.4.4.6) shows the characteristic bands of the typical asymmetric and symmetric stretching vibration of coordinated carboxylate group of the aip^{2-} ligand at 1622 and 1477 cm^{-1} for the asymmetric vibration and at 1544 and 1438 cm^{-1} for the symmetric vibration, The absence of the expected characteristic bands at 1690 cm^{-1}, which are attributed to the protonated carboxylate group, indicative of the complete deprotonation of aip^{2-} ligand [105], [106], [107]. Bands at 736 and 674 cm^{-1} for **40** are due to the 1,3,5-trisubstituted benzene in the fingerprint region [109], [146]. The broad bands of aqua ligand and amino group at 3257, 3095 and 3003 cm^{-1} are indicative to O–H and N–H bonds stretching vibrations of coordinated water and amino group of aip^{2-} molecules with the Cd-atoms. These indicate the presence of H-bonds between the layers in the lattice [112].

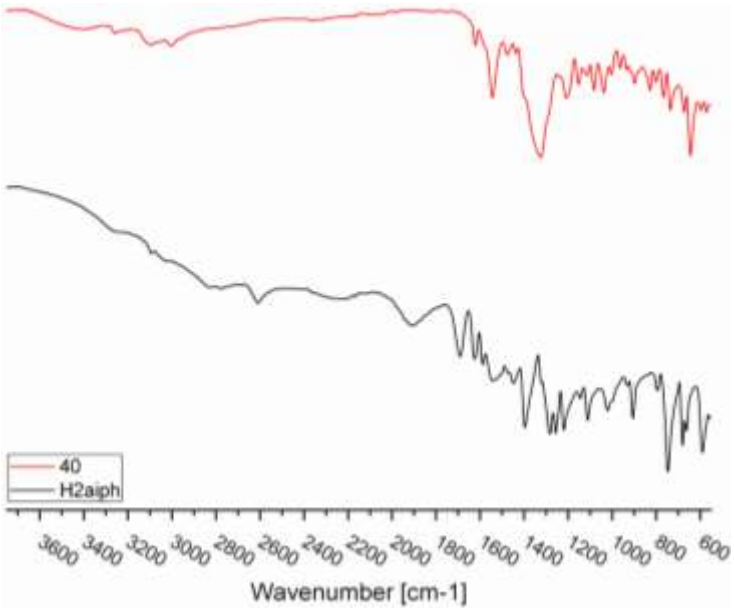

Fig. 6.4.4.6: FT-IR Spectra (ATR) for comparison between H_2aip and compound **40**.

7.4.5 Data analysis and characterization of compounds with other aromatic carboxylic ligand (H_2aip, H_2ip or dm-H_2aip)

We have described the 2D-coordination polymer of zinc(II) atoms with btrip ligand and $Hbtc^{2-}$ ligand **19** and **20** in section 7.2.3 and 7.2.4 (Figure 6.4.5.1). It was noted that, in the structure of compound **19**, the third carboxyl group of $Hbtc^{2-}$ ligand stayed protonated and was not coordinated to a zinc atom.

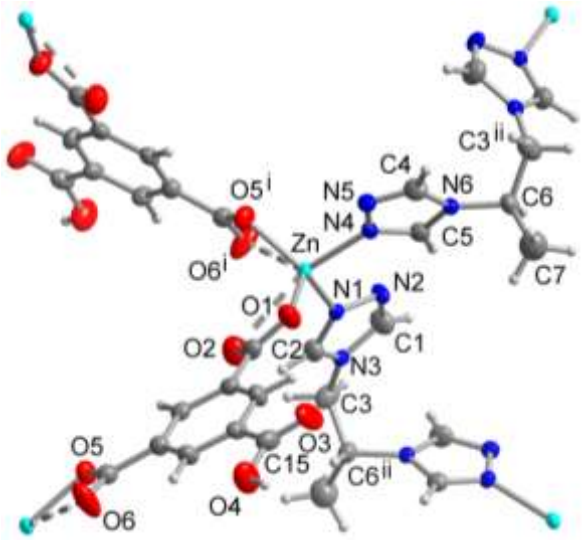

Fig. 6.4.5.1: Building unit for compound **19** repeated from section 7.2.3.

Therefore we planed to obtain similar structures to compound **19**, by using aromatic dicarboxylic acids like isophthalic acid (H_2ip), 5-amino isophthalic acid (H_2aip) and 4,6-dimethyl-5-aminoisophthalic acid (dm-H_2aip), akin to the doubly deprotonated $Hbtc^{2-}$ ligand.

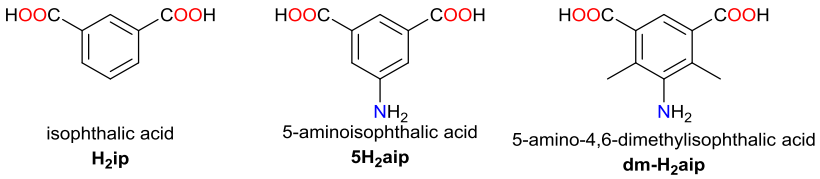

Scheme 6.4.5.1: Structure of used aromatic ligands.

7.4.5.1 5-amino isophthalic acid (5H_2aip)

To an aqueous solution of different zinc(II) salts, a methanolic solution of ligand btrip and an aqueous solution of 5-aminoisophthalic acid of (5H_2aip), which was deprotonated by triethylamine (Et_3N) as base, were added in a glass tube, which was sealed, stirred for 10 min and then placed in a programmable furnace. The mixture was heated to 125°C during 3h and held at this temperature for 24h or 48h, then cooled at 5°C/h rate to room temperature. The resulting crystals were filtered, washed with the mother liquor. Only single crystal of sample **40** was measured. The other samples were not measured.

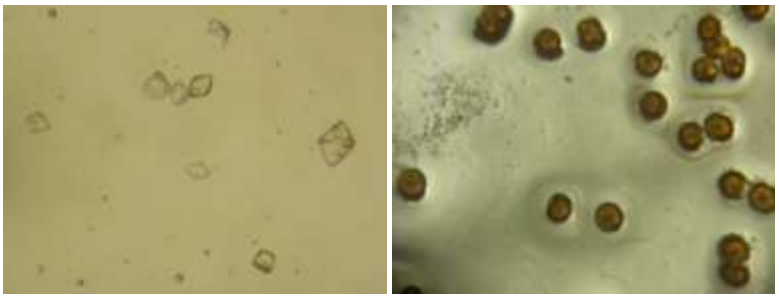

Fig. 6.4.5.2: Crystals image of **40** (left) (Crystals form and color of **41** are like **40**). Crystals image of **42** (right) (Crystals form and color of **43** are like **42**).

The measured PXRD patterns of different zinc compounds show that, some isolated compounds are isostructural, Their PXRD patterns are presented in (Fig. 6.4.5.3). Also the measured PXRD patterns zinc complexes obtained using $Zn(NO_3)_2.4H_2O$ **40**, $Zn(OAc)_2.2H_2O$

41 as Zn(II) ions source (Figure 6.4.5.3) show that, they are mostly isostructural. The other matched PXRD patterns for other zinc compounds were produced by $ZnCl_2$ **42**, $ZnBr_2$ **43** as Zn(II) ions source (Figure 6.4.5.3) show that they are also mostly isostructural.

Comparison of the FT-IR Spectra (ATR) for the Zn-complexes show which ligand is coordinated with metal ion. FT-IR spectra revealed that, only one ligand was coordinated with the zinc(II) ions. The comparison of FT-IR spectra for the Zn-complexes isolated from the hydrothermal reactions of two different salts ($Zn(NO_3)_2.4H_2O$ and $Zn(OAc)_2.2H_2O$) with a mixture of ligands *rac*-btrip and H_2aip show that, the Zn(II) ions are mostly coordinated only to H_2aip ligand (Figure 6.4.5.4, left) like compound 2D-$[Zn(\mu_3\text{-aip})(H_2O)]_n$. On the other side, the result for the comparison of FT-IR spectra for the different Zn-complexes prepared through the hydrothermal reactions of $ZnBr_2$ and $ZnCl_2$ with a mixture of ligands *rac*-btrip and H_2aip show that, the Zn(II) ions are mostly coordinated only with *rac*-btrip ligand (Figure 6.4.5.4, right). The slightly yellow crystals were not measured.

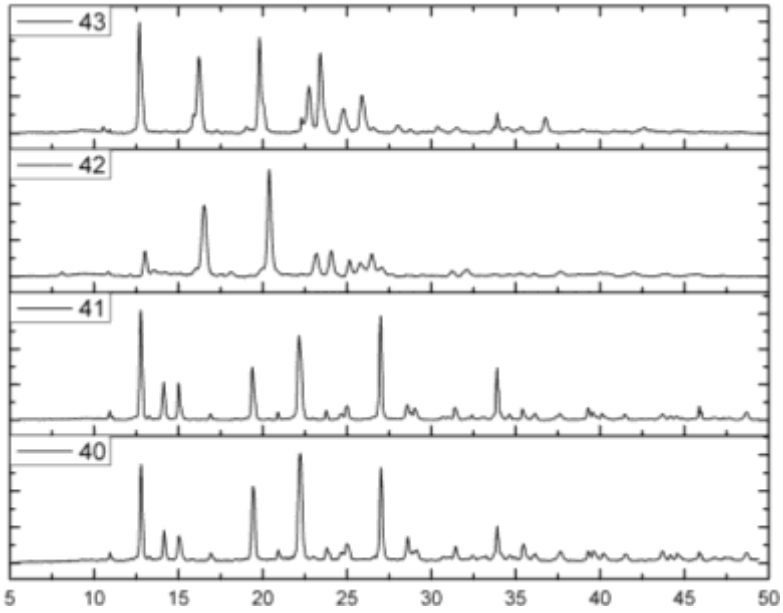

Fig. 6.4.5.3: Combination of the experimental powder X-ray pattern at Cu-Kα wavelength 1.54184 Å between the zinc compounds from two different zinc salts $Zn(NO_3)_2.4H_2O$ **40**, $Zn(OAc)_2.2H_2O$ **41**, and the other zinc compounds from two different zinc salts $ZnCl_2$ **42**, $ZnBr_2$ **43**.

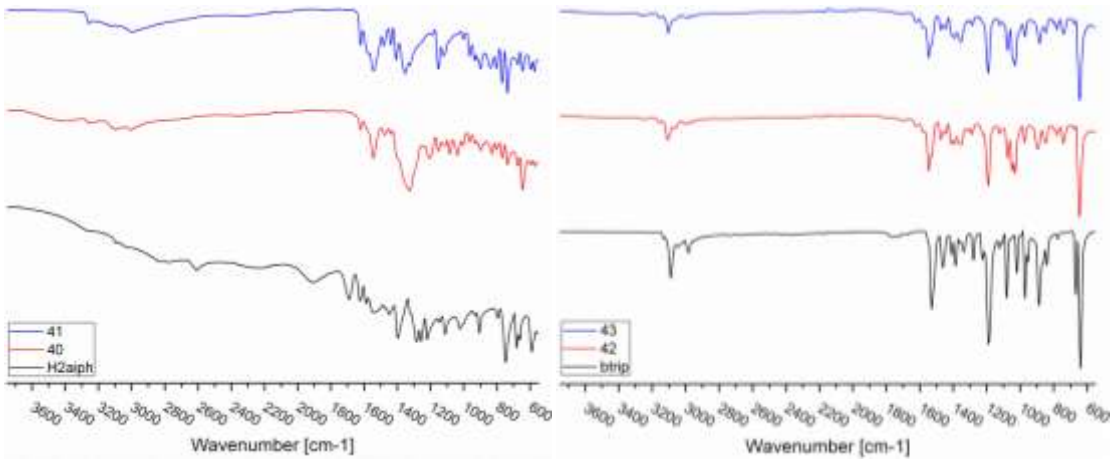

Fig. 6.4.5.4: FT-IR Spectra (ATR) for comparison between the Zn-compounds from two different salts $Zn(NO_3)_2.4H_2O$ **40**, $Zn(OAc)_2.2H_2O$ **41** and the ligand H_2aip (left), and the another Zn-compounds from two different salts $ZnCl_2$ **42**, $ZnBr_2$ **43** with the ligand btrip (right) in range 550-3750 cm^{-1}.

7.4.5.2 Isophthalic acid of (H_2ip)

An aqueous solution of different zinc salts $Zn(NO_3)_2.4H_2O$ **44**, $ZnCl_2$ **45** and $ZnBr_2$ **46**, a methanolic solution of ligand btrip and an aqueous solution of isophthalic acid of (H_2ip), which was deprotonated by using triethylamine (Et_3N) as base, were mixed in a glass tube, which was sealed, stirred for 10 min. and then kept in a programmable furnace. The mixture was heated to 125°C during 3h and held at this temperature for 24h or 48h, then cooled at 5°C/h rate to room temperature. The resulting crystals were filtered, washed with the mother liquor. The obtained single crystals were not measured.

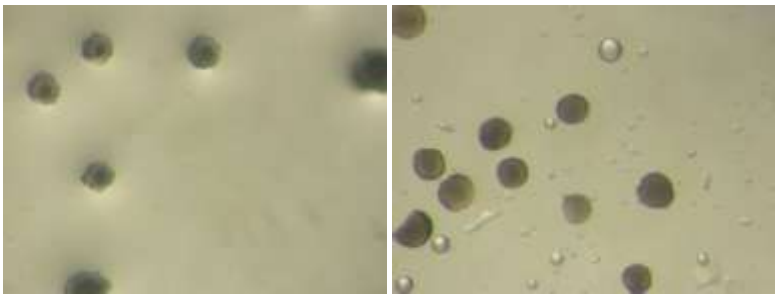

Fig. 6.4.5.5: Crystal image of **44** (left) and **46** (right) (Crystals form and color of **45** are like **46**).

The measured PXRD patterns of difference zinc compounds show that; PXRD patterns are not identical, which are different with their peaks width, position and relative intensity. The PXRD patterns are presented in (Fig. 6.4.5.6).

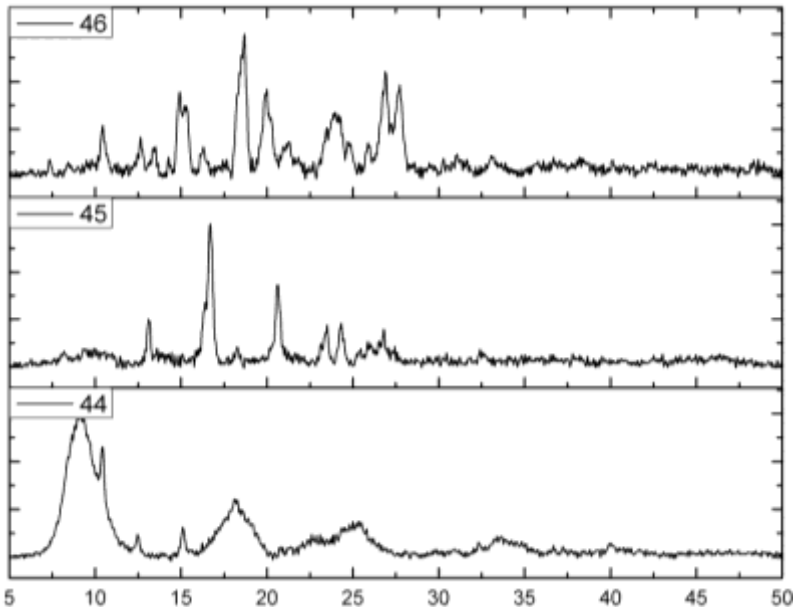

Fig. 6.4.5.6: Combination of the experimental powder X-ray patterns at Cu-Kα wavelength 1.54184 Å of different zinc salts $Zn(NO_3)_2.4H_2O$ **44**, $ZnCl_2$ **45** and $ZnBr_2$ **46**. The measured PXRD patterns are smoothed and baseline corrected.

The comparison of FT-IR Spectra (ATR) for the Zn-compounds obtained from hydrothermal reactions of different zinc salts $Zn(NO_3)_2.4H_2O$ **44**, $ZnCl_2$ **45** and $ZnBr_2$ **46**, a mixture of btrip and H_2ip show that, the zinc ion is mostly coordinated only with ligand btrip. The FT-IR Spectra is presented in (Fig. 6.4.5.7).

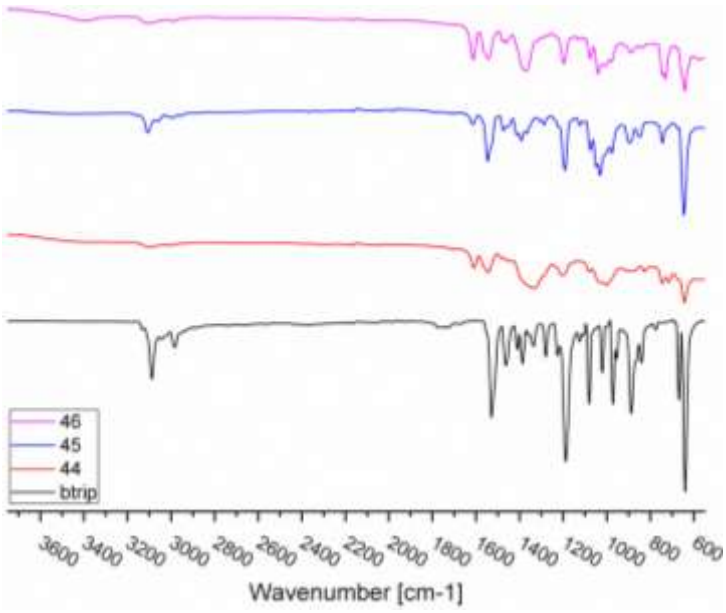

Fig. 6.4.5.7: FT-IR Spectra (ATR) for comparison between **44**, **45**, **46** and btrip ligand.

7.4.5.3 4,6-Dimethyl-5-amino isophthalic acid (dm-H_2aip)

An aqueous solution of zinc chloride, a methanolic solution of ligand btrip and an aqueous solution of 4,6 dimethyl-5-amino isophthalic acid (dm-H_2aip), which was deprotonated by using triethylamine (Et_3N) as base, were mixed in a glass tube, which was sealed, stirred for 10 min. and then kept in a programmable furnace. The mixture was heated to 125°C during 3h and held at this temperature for 24h or 48h, then cooled at 5°C/h rate to room temperature. The resulting crystals were filtered, washed with mother liquor. The obtained single crystals were not measured.

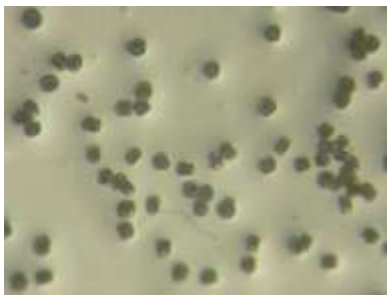

Fig. 6.4.5.8: Crystals image of **47**.

The measured PXRD patterns of zinc compound show that, PXRD pattern has identical pattern of compound **45**, which agree with their identical peaks width, position and relative intensity. But it has difference relative intensity in compared with compound **42**. PXRD pattern is presented in (Fig. 6.4.5.9, right) and (Fig. 6.4.5.10).

The comparison of FT-IR spectra (ATR) for the Zn-compounds isolated from the hydrothermal reaction of zinc chloride, btrip and dm-H_2aip show that, the zinc ion is mostly coordinated only to the btrip ligand. The FT-IR Spectra is presented in (Fig. 6.4.5.9, left).

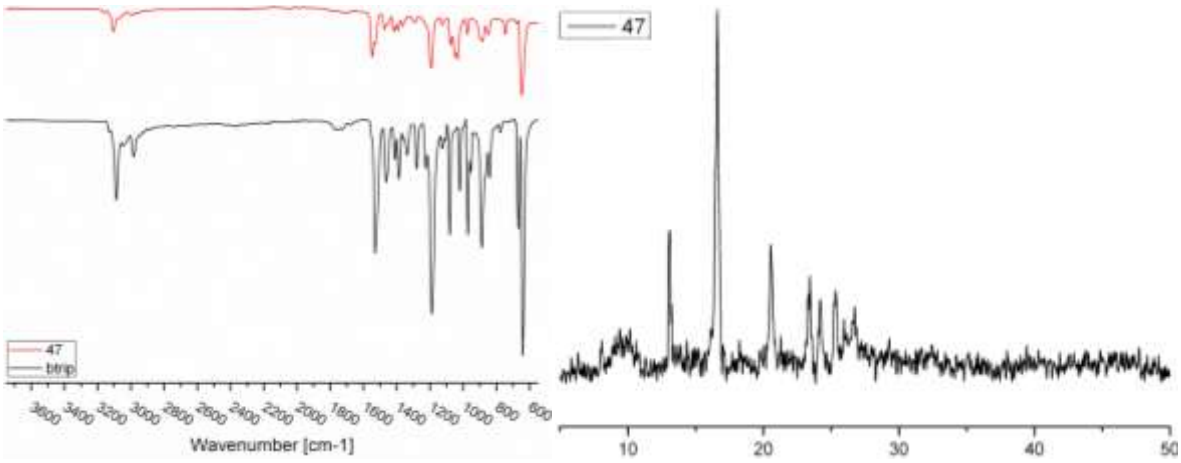

Fig. 6.4.5.9: FT-IR Spectra (ATR) for comparison between **47** and the btrip in range 550-3750 cm^{-1} (left), the measured powder X-ray patterns of **47** at Cu-Kα wavelength 1.54184 Å (right).

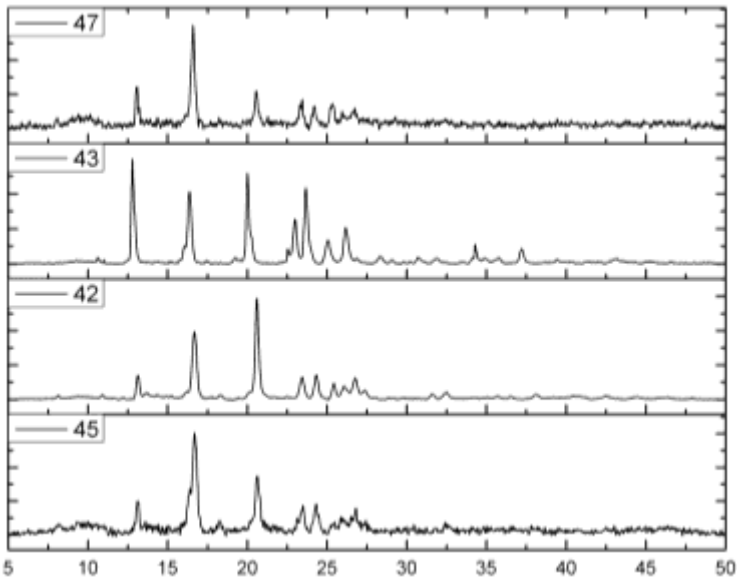

Fig. 6.4.5.10: Combination of the experimental powder X-ray patterns at Cu-Kα wavelength 1.54184 Å of difference zinc compounds. The measured PXRD patterns are smoothed and baseline corrected.

7.5 Coordination polymers constructed from aromatic azolate ligands

7.5.1 Introduction

Tetrazolate and carboxylate ligands are very interesting because they can induce different metal SBUs which lead to the construction of different (porous) coordination polymers.

The aim of this work in this section was to synthesize new coordination polymers with mixed ligand system of tetrazolate and carboxylate ligands, and after that to study their properties such as thermal stability and magnetism and their applications for heat transformation, non-linear optics, chirality, luminescence, etc. The structure of used tetrazolate and carboxylate ligands with their different possible mixed-ligand systems are presented in Scheme 6.5.1.1.

The preparation of new coordination polymers by using a mixture of ligands was not easy work, because only one of both ligands mostly will be coordinated with the metal ions with solvent molecules contribution.

In the following section, different methods for preparation of coordination polymers in different conditions were written, and the data analysis of crystallized compounds were discussed.

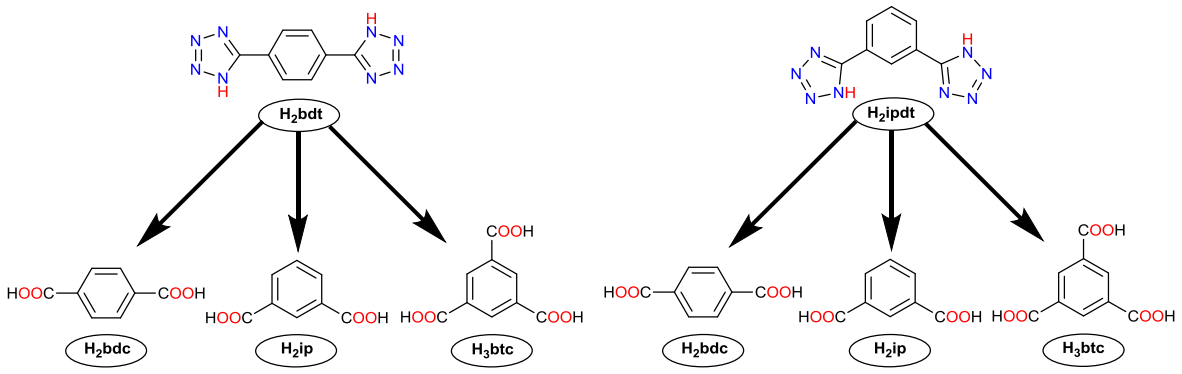

Scheme 6.5.1.1: Structure of used tetrazolate and carboxylate ligands with their different possible mixed-ligand systems.

7.5.2 Slow evaporation method (S.: MeOH, DMF)

A solution of metal nitrate hydrate in methanol, a solution of H_2bdc in DMF and a solution of H_2bdt in DMF were mixed, stirred for about 1 h, and then the sample was filtered and the filtrate was placed at ambient temperature for slow evaporation. The resulting single crystals were separated from the precipitate, washed with mother liquor, dried and after then measured by IR-spectra to examine the ligand content. Other experiments in the same condition with other metal chloride or metal nitrate of Cd^{2+}, Cu^{2+}, Zn^{2+}, Mn^{2+}, Fe^{2+} and Co^{2+} were carried out without successful. Comparison of IR spectra revealed that, H_2bdc ligand was coordinated to the metal ions by using slow evaporation method. The data analyses of crystalline products are summarized in Table 6.5.2.1.

Table 6.5.2.1: The data analyses of the crystallized compounds were as follows:

Product	Metal salt	Image	NMR	IR	PXRD	SCXRD
48	$Cd(NO_3)_2.4H_2O$:H_2bdt:H_2bdc, 2:1:1			H_2bdc		
49	$Cu(NO_3)_2.2.5H_2O$:H_2bdt:H_2bdc, 2:1:1			H_2bdc		
50	$Zn(NO_3)_2.4H_2O$:H_2bdt:H_2bdc, 4:1:1			x		

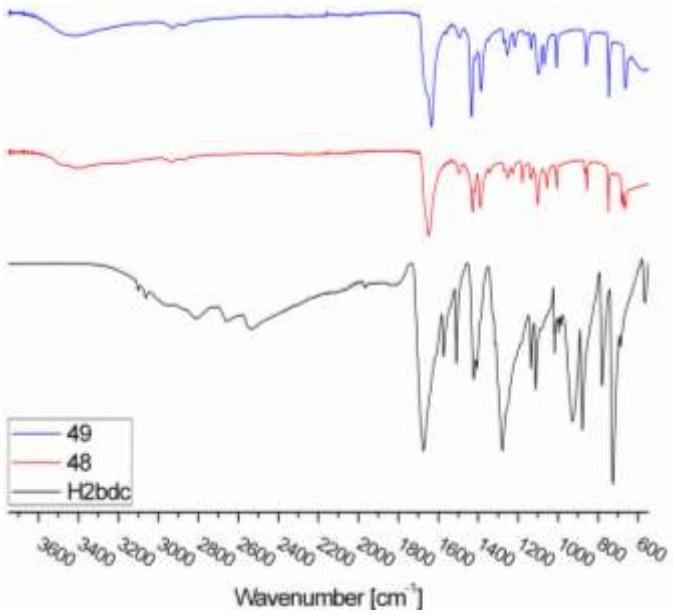

Fig. 6.5.2.1: IR Spectra (ATR) for comparison between crystallized compounds and H_2bdc-ligand.

7.5.3 Solvothermal method at low temperature (S.: MeOH, DMF)

A solution of metal chloride of Cd^{2+}, Zn^{2+} in H_2O or Mn^{2+} in MeOH, a solution of H_3btc in DMF and a solution of H_2ipdt in DMF were mixed, stirred for about 10 minutes and placed in the furnace at 70 °C for Mn^{2+}, Cd^{2+} and 100 °C for Zn^{2+}. Finally, the reaction mixtures were removed from furnace when the crystals were formed. The resulting single crystals were separated from the precipitate, washed with mother liquor, dried and after that NMR- or IR-spectra were measured to examine the ligand content. Other experiments in the same condition with other metal chloride or metal sulfate of Cd^{2+}, Zn^{2+}, Cu^{2+}, Ni^{2+}, Mn^{2+}, Fe^{2+} and Co^{2+} and metal nitrate of Cu^{2+} and Co^{2+} were carried out without successful. Comparison of IR and ^{1}H NMR spectra revealed, that H_3btc ligand was coordinated to the metal ions by using solvothermal reaction at low temperature. Comparison of ^{1}H NMR is not presented. The data analyses of crystalline products are summarized in Table 6.5.3.1.

Table 6.5.3.1: The data analyses of the crystallized compounds were as follows:

Product	Metal salt	Image	NMR	IR	PXRD	SCXRD
51	$MnCl_2.4H_2O$:H_2ipdt:H_3btc, 4:1:1			H_3btc		
53	$ZnCl_2$:H_2ipdt:H_3btc, 4:1:1					
54	$CdCl_2.H_2O$:H_2ipdt:H_3btc, 4:1:1		H_3btc	H_3btc		

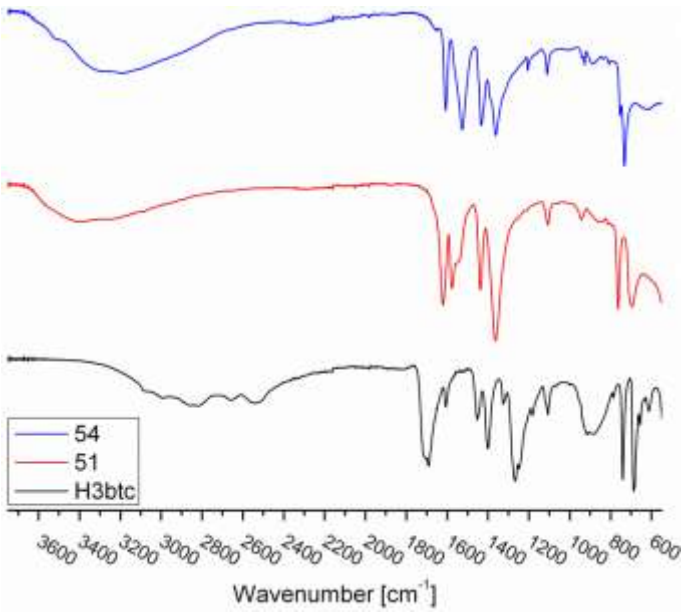

Fig. 6.5.3.1: IR Spectra (ATR) for comparison between **51**, **54** and H_3btc-ligand.

7.5.4 Solvothermal method at low temperature with mineral acid (S.: MeOH, DMF)

A solution of metal nitrate or metal chloride of Cd^{2+}, Zn^{2+} in H_2O or Mn^{2+} in MeOH, a solution of H_2bdc, H_2ip or H_3btc in DMF, and a solution of H_2bdt or H_2ipdt in DMF were mixed and stirred for about 10 minutes. After that concentrated acid (15 – 25 µl) was added for each sample (HCl acid for metal chloride, HNO_3 acid for metal nitrate). The sample was stirred again for about 5 minutes and placed in the furnace at 70 or 100 °C. Finally, the reaction mixtures were removed from furnace when the crystals were formed. The resulting single crystals were separated from the precipitate, washed with mother liquor, dried and after that NMR- or IR-spectra were measured. Other experiments in the same condition with other metal chloride or metal nitrate of Cd^{2+}, Zn^{2+} and Mn^{2+} carried out without successful. Comparison of IR and ^{1}H NMR spectra show that, either two ligands or single ligand with solvent molecules were coordinated with metal ions by using solvothermal reaction. The data analyses of the crystallized compounds are summarized in Table 6.5.4.1.

Fig. 6.5.4.1a: Crystal images of **57** (left), **58** (middle), **59** (right).

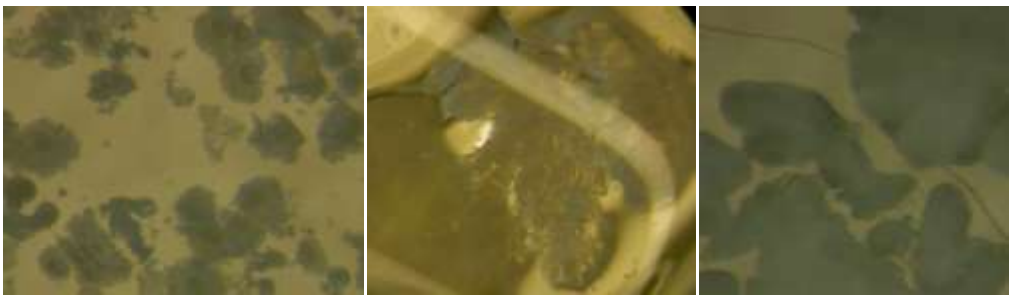

Fig. 6.5.4.1b: Crystal images of **63** (left), **62** (middle), **64** (right).

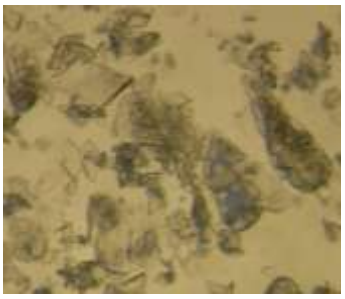

Fig. 6.5.4.1c: Crystal images of **69**.

Table 6.5.4.1: The data analyses of the crystallized compounds were as follows:

Product	Metal salt	Image	NMR	IR	PXRD	SCXRD
55	$CdCl_2.H_2O$:H_2bdt:H_2bdc, 4:1:1					
56	$Cd(NO_3)_2.4H_2O$:H_2bdt:H_2bdc, 4:1:1					
57	$MnCl_2.4H_2O$:H_2bdt:H_2bdc, 3:1:1	1	H_2bdt:DMF			
58	$Mn(NO_3)_2.4H_2O$:H_2bdt:H_2bdc, 4:1:1	3		H_2bdc		
59	$Cd(NO_3)_2.4H_2O$:H_2bdt:H_2ip, 4:1:1	2	H_2bdt:H_2ip, n:n, 0.7:1, DMF	H_2bdt:H_2ip		
60	$CdCl_2.H_2O$:H_2bdt:H_3btc, 4:1:1		H_2bdt:DMF			
61	$Cd(NO_3)_2.4H_2O$:H_2bdt:H_3btc, 4:1:1		H_2bdt:H_3btc, n:n, 1:1.3, DMF			
62	$MnCl_2.4H_2O$:H_2bdt:H_3btc, 3:1:1	1	H_3btc:DMF			
63	$Mn(NO_3)_2.4H_2O$:H_2bdt:H_3btc, 4:1:1	1		H_3btc		
64	$MnCl_2.4H_2O$:H_2ipdt:H_2bdc, 3:1:1	1		H_2bdc		
65	$Mn(NO_3)_2.4H_2O$:H_2ipdt:H_2bdc, 4:1:1					
66	$Cd(NO_3)_2.4H_2O$:H_2ipdt:H_2bdc, 4:1:1					
67	$Cd(NO_3)_2.4H_2O$:H_2ipdt:H_2ip, 4:1:1					
68	$Mn(NO_3)_2.4H_2O$:H_2ipdt:H_2ip, 4:1:1					
69	$MnCl_2.4H_2O$:H_2ipdt:H_3btc, 3:1:1	1		H_2ipdt:H_3btc		
70	$Mn(NO_3)_2.4H_2O$:H_2ipdt:H_3btc, 4:1:1					
71	$Cd(NO_3)_2.4H_2O$:H_2ipdt:H_3btc, 4:1:1		H_2ipdt:H_3btc, n:n, 1:1, DMF			

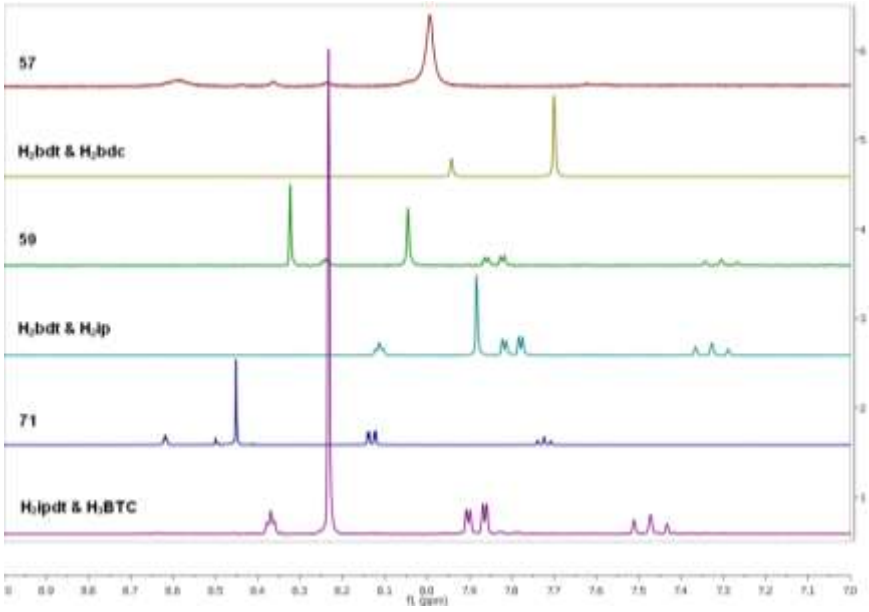

Fig. 6.5.4.2a: ^{1}H NMR Spectra (200 MHz) for comparison between signals of crystallized compounds and signals of different ligands in NaOD/D_2O solution (Compound **71** was measured at 500 MHz).

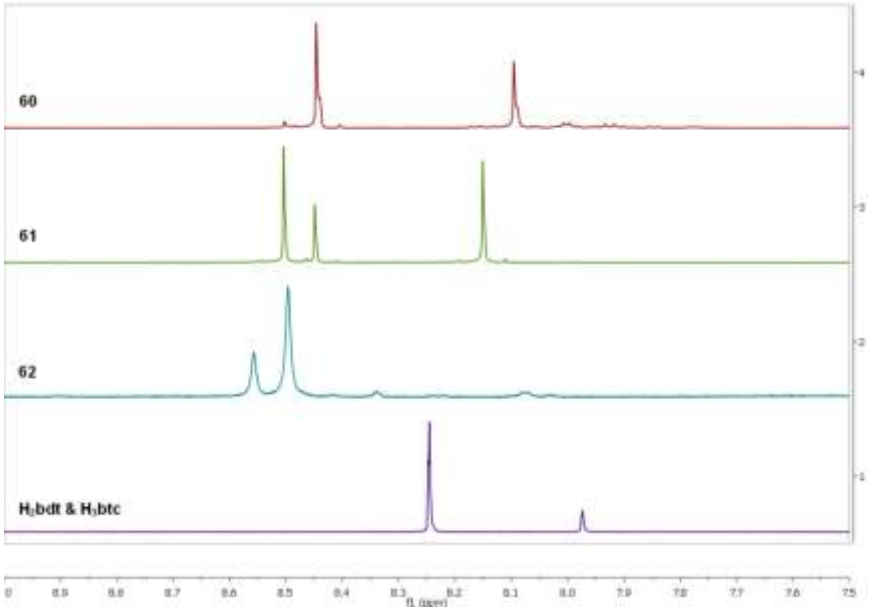

Fig. 6.5.4.2b: ^{1}H NMR Spectra (200 MHz) for comparison between signals of crystallized compounds and signals of ligands in NaOD/D_2O solution (Compounds **60** and **61** were measured at 500 MHz).

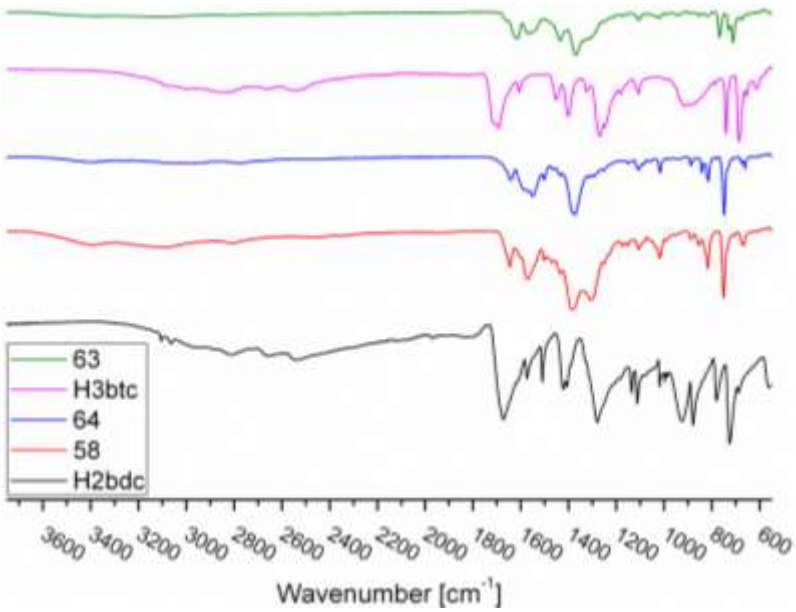

Fig. 6.5.4.3a: IR Spectra (ATR) for comparison between crystallized compounds and H_2bdc- or H_3btc-ligand in range 550-3750 cm^{-1}.

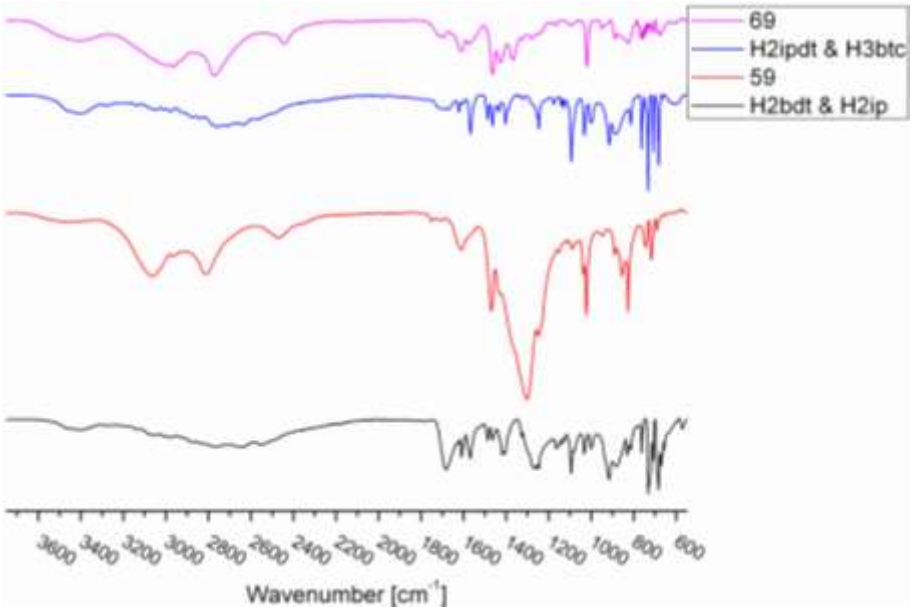

Fig. 6.5.4.3b: IR Spectra (ATR) for comparison between crystallized compound and mixed ligand system in range 550-3750 cm^{-1}.

7.5.5 Solvothermal method at low temperature without mineral acid (S.: MeOH, DMSO, DMF)

A solution of metal nitrate or metal chloride of Zn^{2+} in DMSO or Cd^{2+}, Mn^{2+} in MeOH or a mixture of MeOH:DMSO, a solution of H_2bdc, H_2ip or H_3btc in DMF, and a solution of H_2bdt or H_2ipdt in DMF were mixed and stirred for about 10 minutes. After that the sample was putted in furnace at 70, 90 or 125 °C. Finally, the reaction mixtures were removed from furnace when the crystals were formed. ^{1}H NMR- or IR-spectra of resulting single crystals were measured to examine the ligand content. Other experiments in the same condition with other metal chloride or metal nitrate of Cd^{2+}, Zn^{2+} and Mn^{2+} were carried out without successful. Comparison of IR and ^{1}H NMR spectra show, that mostly one ligand with solvent molecules were coordinated with metal ions by using this solvothermal reaction. The data analyses of the crystallized compounds are summarized in Table 6.5.5.1.

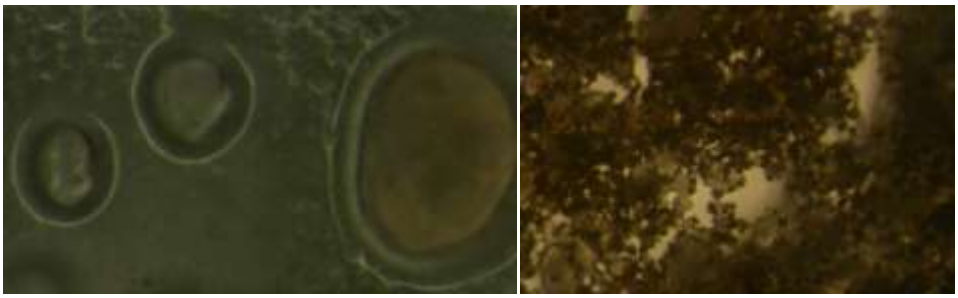

Fig. 6.5.5.1a: Crystal images of **73** (left), when the sample let in the ofen for long time (right).

Fig. 6.5.5.1b: Crystal images of **72** (left), **75** (middle), **75** after long time in the ofen (right).

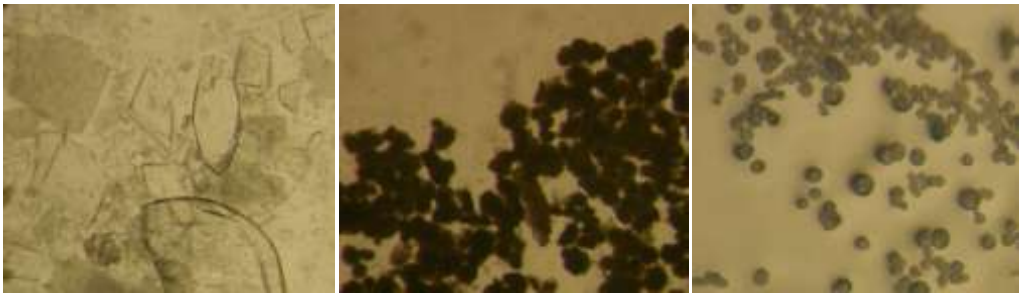

Fig. 6.5.5.1c: Crystal images of **76** (left), **78** (middle), **77** (right).

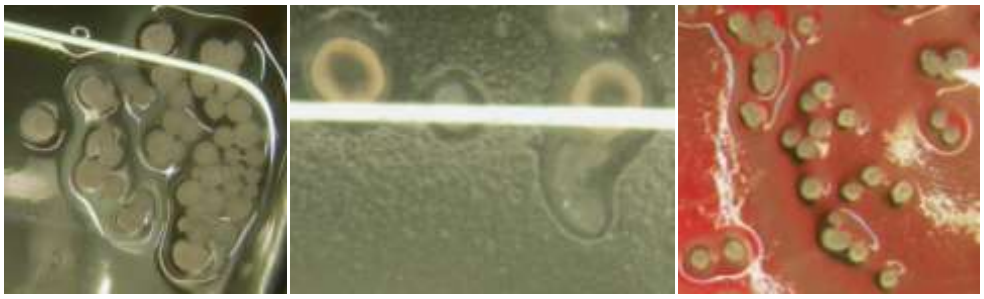

Fig. 6.5.5.1d: Crystal images of **81** (left), **83** (middle), **84** (right).

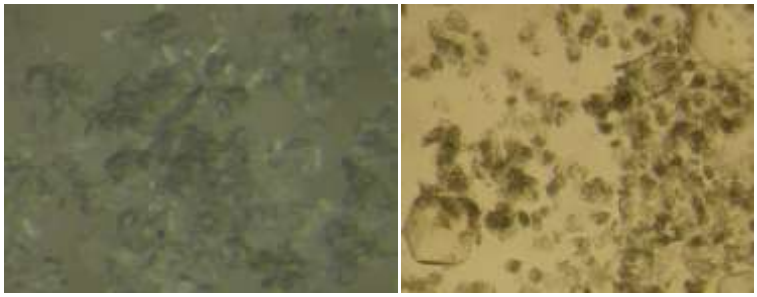

Fig. 6.5.5.1e: Crystal images of **85**.

Table 6.5.5.1: The data analyses of the crystallized compounds were as follows:

Product	Metal salt	Image	NMR	IR	PXRD	SCXRD
72	$MnCl_2.4H_2O$:H_2bdt:H_2bdc, 4:1:1	1	H_2bdc:DMF			
73	$Mn(NO_3)_2.4H_2O$:H_2bdt:H_2bdc, 4:1:1	2				
74	$Cd(NO_3)_2.4H_2O$:H_2bdt:H_2bdc, 4:1:1					
75	$Zn(NO_3)_2.4H_2O$:H_2bdt:H_2bdc, 4:1:1	1	H_2bdt	H_2bdt		
76	$Cd(NO_3)_2.4H_2O$:H_2bdt:H_2ip, 4:1:1	1	H_2ip:DMF: MeOH	H_2ip		
77	$MnCl_2.4H_2O$:H_2bdt:H_3btc, 4:1:1	1	H_3btc:DMF: MeOH			
78	$Mn(NO_3)_2.4H_2O$:H_2bdt:H_3btc, 4:1:1	1		H_3btc		
79	$CdCl_2.H_2O$:H_2bdt:H_3btc, 4:1:1					
80	$Cd(NO_3)_2.4H_2O$:H_2bdt:H_3btc, 4:1:1					
81	$Mn(NO_3)_2.4H_2O$:H_2ipdt:H_2bdc, 4:1:1	1	H_2bdc:DMF			
82	$Cd(NO_3)_2.4H_2O$:H_2ipdt:H_2bdc, 4:1:1					
83	$Mn(NO_3)_2.4H_2O$:H_2ipdt:H_2ip, 4:1:1	1	DMF			
84	$Mn(NO_3)_2.4H_2O$:H_2ipdt:H_3btc, 4:1:1	1				
85	$ZnCl_2$:H_2ipdt:H_3btc, 4:1:1	1	H_3btc:DMF	H_3btc		

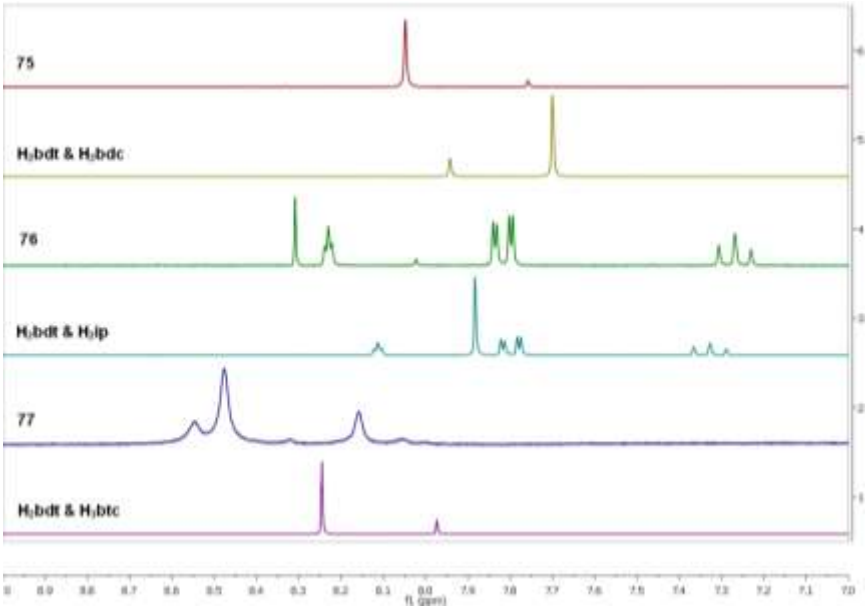

Fig. 6.5.5.2: ^{1}H NMR Spectra (200 MHz) for comparison between signals of crystallized compounds and signals of different ligands in $NaOD/D_2O$ solution.

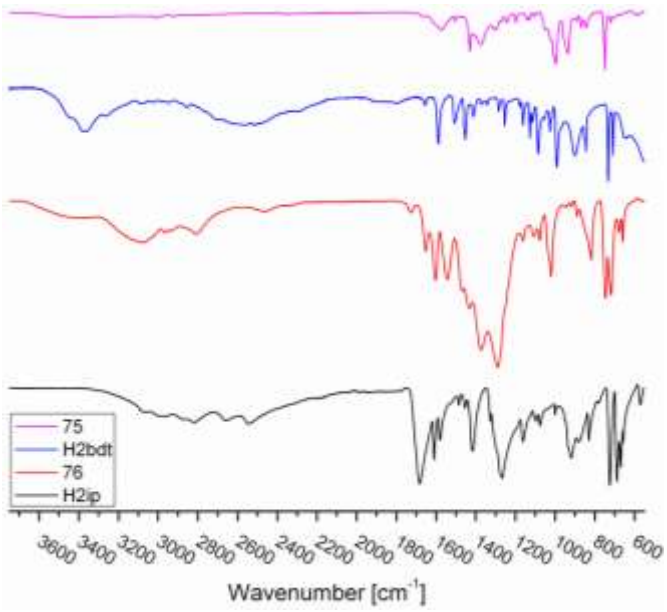

Fig. 6.5.5.3a: IR Spectra (ATR) for comparison between crystallized compound and H_2bdt- or H_2ip-ligand in range 550-3750 cm^{-1}.

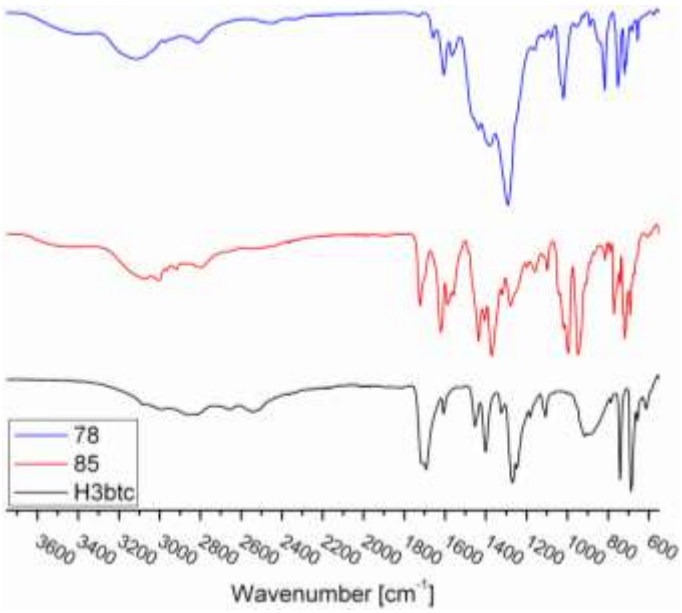

Fig. 6.5.5.3b: IR Spectra (ATR) for comparison between **78**, **85** and H_3btc-ligand.

7.5.6 Solvothermal method at high temperature (S.: H_2O, DMF)

An aqueous solution of metal salts, a solution of H_2bdc and a solution of H_2bdt dissolved in a mixture of H_2O:DMF (v:v, 1:1) were mixed in a glass tube, which was sealed and stirred for about 5 min. and then placed in a programmable furnace at 150°C. The resulting single crystals were analyzed by ^{1}H NMR- or IR-spectra to examine the ligand content. Other experiments in the same condition with other metal chloride or metal nitrate of Cd^{2+}, Zn^{2+}, Mn^{2+}, Cr^{3+}, Cu^{2+}, Co^{2+}, Ni^{2+}, Fe^{2+}, and Al^{3+} were carried out without successful. It was noticed that, the reaction conditions were good to obtain more suitable crystals. But it is better to use lower temperature as 120 °C, to obtain more suitable crystals and lower precipitate amount. Comparison of IR and ^{1}H NMR spectra of **89** and **91** show, that mostly two ligands were coordinated with metal ions. Comparison of IR and ^{1}H NMR spectrum of crystallized Al-compound **90** with IR and ^{1}H NMR spectrum of H_2bdt ligand shows, that mostly H_2bdt ligand with solvent molecules were coordinated with metal ions. The measured PXRD patterns of different crystalline compounds show that, the isolated compounds are not isostructural. The data analyses of the crystallized compounds are summarized in Table 6.5.6.1.

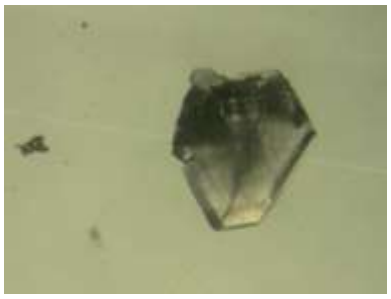

Fig. 6.5.6.1a: Crystal images of **87** (left), (For compound **86** , the crystals looking samelary to **87**).

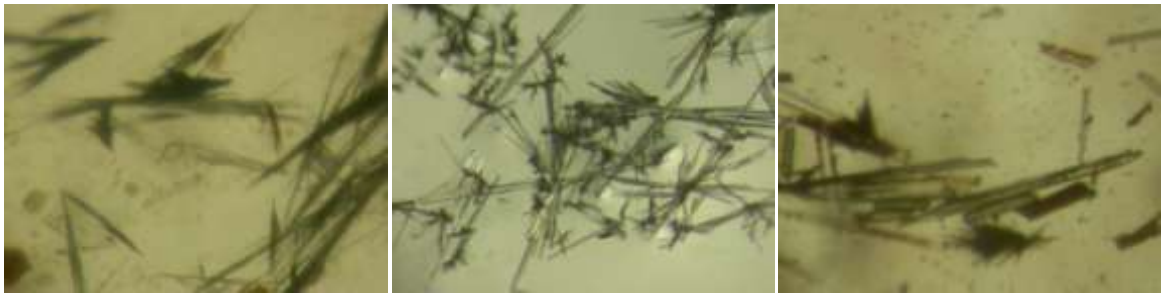

Fig. 6.5.6.1b: Crystal images of **90** (left), **91** (middle), **89** (right).

Table 6.5.6.1: The data analyses of the crystallized compounds were as follows:

Product	Metal salt	Image	NMR	IR	PXRD	SCXRD
86	$MnCl_2$:H_2bdt:H_2bdc, 4:1:1					
87	$Mn(NO_3)_2.4H_2O$:H_2bdt:H_2bdc, 4:1:1	1				
88	$Ni(NO_3)_2.6H_2O$:H_2bdt:H_2bdc, 4:1:1				x	
89	$Fe(NO_3)_3.9H_2O$:H_2bdt:H_2bdc, 4:1:1	1	H_2bdt:H_2bdc , n:n, 1:0.85	H_2bdt:H_2bdc	x	x
90	$Al(NO_3)_3.9H_2O$:H_2bdt:H_2bdc, 4:1:1	1	H_2bdt	H_2bdt	x	x
91	$CrCl_3.6H_2O$:H_2bdt:H_2bdc, 4:1:1	1	H_2bdt:H_2bdc , n:n, 1:1	H_2bdt:H_2bdc	x	x

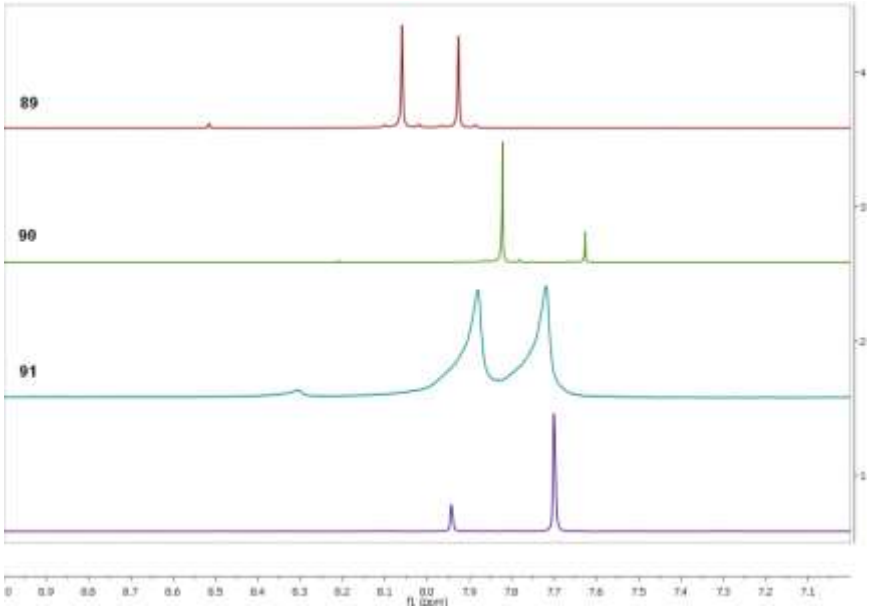

Fig. 6.5.6.2: ^{1}H NMR Spectra (500 MHz) for comparison between signals of crystallized compounds and signals of a mixture of ligands in NaOD/D_2O solution (mixed-ligands was measured at 200 MHz).

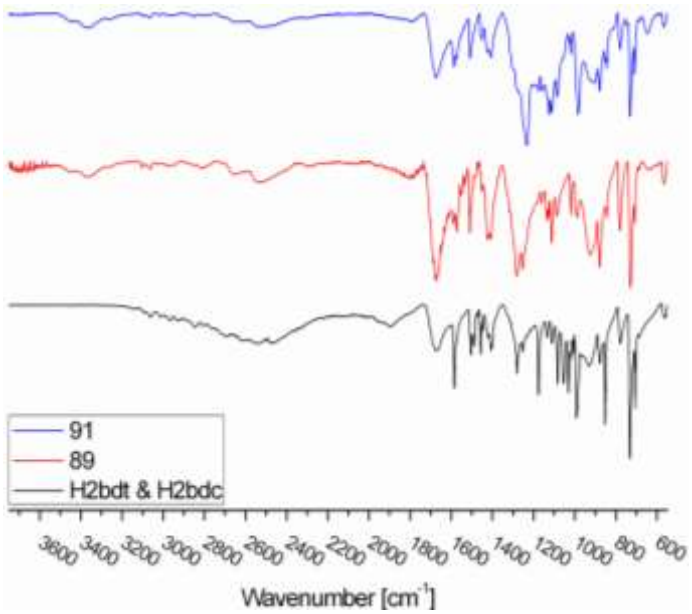

Fig. 6.5.6.3a: IR Spectra (ATR) for comparison between **89**, **91** and a mixture of ligands.

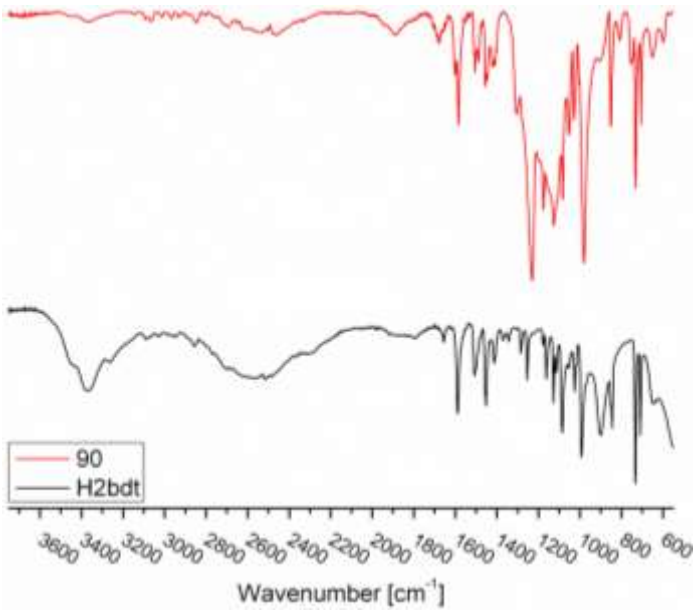

Fig. 6.5.6.3b: IR Spectra (ATR) for comparison between **90** and H_2bdt-ligand.

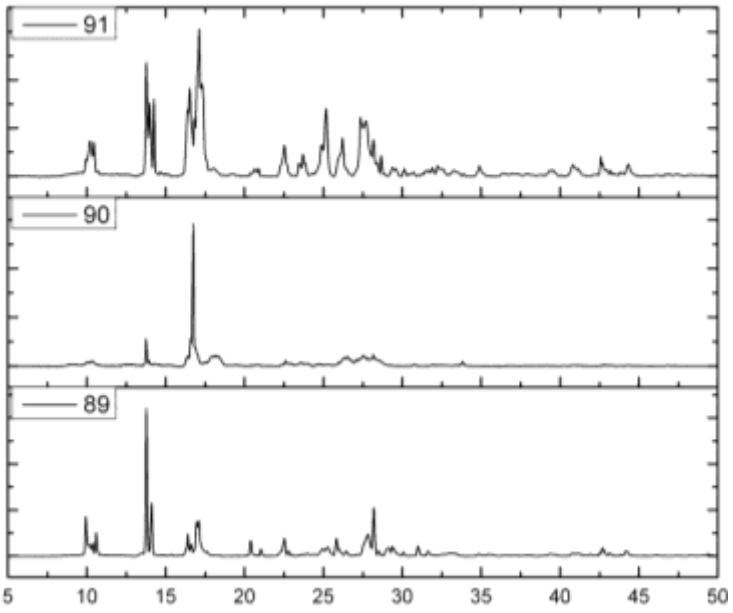

Fig. 6.5.6.4: Combination of the experimental powder X-ray patterns at Cu-Kα wavelength 1.54184 Å of different crystallized compounds. The measured PXRD patterns are smoothed and baseline corrected.

7.5.7 Hydrothermal method at low temperature (S.: NaOH or NH_4OH)

NaOH or NH_4OH solution (0.08 mmol/l) as base was used to deprotonate the used ligands (H_2bdc, H_2ip, H_3btc or H_2bdt) by using ultrasonic bath at 40-50°C. The metal salts were dissolved in water, H_2bdc, H_2ip or H_3btc and H_2bdt were dissolved either in NaOH or NH_4OH solution as base (For H_3btc was dissolved in 0.75 ml of NaOH or NH_4OH solution to deprotonate their three carboxyl groups). The solutions were mixed in a glass tube, stirred for about 10 minutes, and then placed in a furnace at 75 or 100 °C. The sample was removed from the furnace when suitable single crystals were formed. The resulting single crystals were analyzed by ^1H NMR- or IR-spectra. Other experiments in the same condition with other metal chloride or halogen (Br^- for Cu^{2+}) or metal nitrate of Cr^{3+}, Cu^{2+}, Co^{2+}, Ni^{2+}, Fe^{3+} and Al^{3+} (ClO_4^- for Ni^{2+}) were carried out without successful. Comparison of ^1H NMR spectrum of crystallized compound shows, that mostly one ligand was coordinated with metal ions. The data analyses of the crystallized compounds were summarized in Table 6.5.7.1.

Table 6.5.7.1: The data analyses of the crystallized compounds were as follows:

Product	Metal salt	Image	NMR	IR	PXRD	SCXRD
92	$CoCl_2.6H_2O$:H_2bdt:H_2bdc, 4:1:1		H_2bdc			
93	$Co(NO_3)_2.6H_2O$:H_2bdt:H_2bdc, 4:1:1		H_2bdc			
94	$CoCl_2.6H_2O$:H_2bdt:H_2bdc, 4:1:1		H_2bdc			
95	$FeCl_2.4H_2O$:H_2bdt:H_2bdc, 4:1:1		H_2bdt:H_2bdc, n:n, 1.1:1			
96	$CoCl_2.6H_2O$:H_2bdt:H_2ip, 4:1:1					
97	$FeCl_2.4H_2O$:H_2bdt:H_2ip, 4:1:1		H_2bdt:H_2ip, n:n, 2.6:1			
98	$CoCl_2.6H_2O$:H_2bdt:H_3btc, 4:1:1		H_3btc			
99	$Co(NO_3)_2.6H_2O$:H_2bdt:H_3btc, 4:1:1		H_3btc			
100	$Ni(NO_3)_2.6H_2O$:H_2bdt:H_3btc, 4:1:1		H_3btc			
101	$Ni(ClO_4)_2.6H_2O$:H_2bdt:H_3btc, 4:1:1		H_3btc			
102	$CuBr_2$:H_2bdt:H_3btc, 4:1:1		H_3btc			
103	$Cu(NO_3)_2.2.5H_2O$:H_2bdt:H_3btc, 4:1:1		H_3btc			
104	$CoCl_2.6H_2O$:H_2bdt:H_3btc, 4:1:1		H_3btc			
105	$Co(NO_3)_2.6H_2O$:H_2bdt:H_3btc, 4:1:1		H_3btc			
106	$Ni(NO_3)_2.6H_2O$:H_2bdt:H_3btc, 4:1:1		H_3btc			
107	$Ni(ClO_4)_2.6H_2O$:H_2bdt:H_3btc, 4:1:1		H_3btc			
108	$CuBr_2$:H_2bdt:H_3btc, 4:1:1		H_3btc			
109	$Cu(NO_3)_2.2.5H_2O$:H_2bdt:H_3btc, 4:1:1		H_3btc			
110	$FeCl_2.4H_2O$:H_2bdt:H_3btc, 4:1:1		H_2bdt:H_3btc, n:n, 1:0.5			

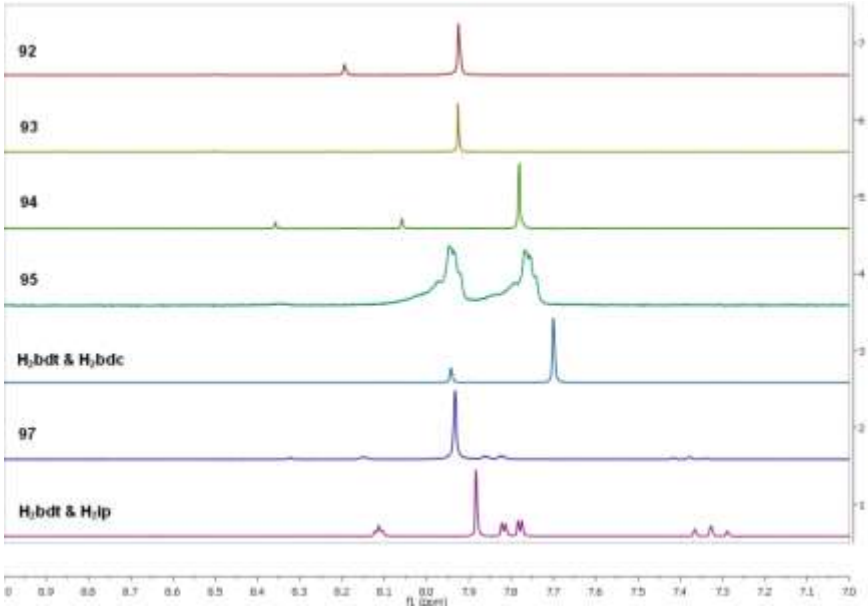

Fig. 6.5.7.2a: ^{1}H NMR Spectra (200 MHz) for comparison between signals of crystallized compounds and signals of ligands in NaOD/D_2O solution (Compounds **92** and **93** were measured at 500 MHz).

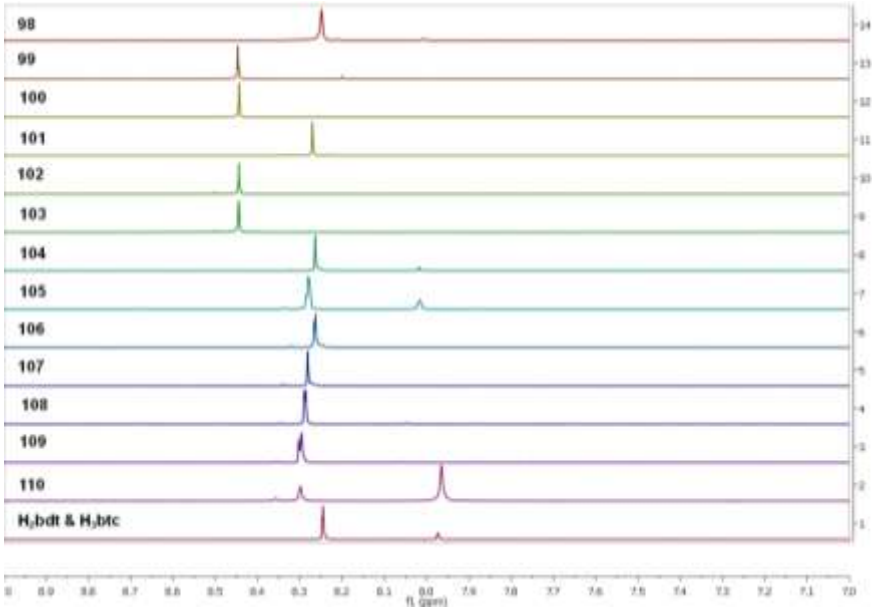

Fig. 6.5.7.2b: ^{1}H NMR Spectra (200 MHz) for comparison between signals of crystallized compounds and signals of ligands in NaOD/D_2O solution (Compounds **98**, **99**, **100**, **101**, **102** and **103** were measured at 500 MHz).

7.5.8 Hydrothermal method at high temperature (S.: NaOH)

Part (a): NaOH solution (0.16 mmol/l) as base was used to deprotonate the used ligands (H_2bdc or H_2bdt) *via* ultrasonic bath at 40-50°C. An aqueous solution of metal salts, an aqueous solution of H_2bdc and an aqueous solution of H_2bdt were mixed in a glass tube, stirred for about 5 minutes and then placed in a programmable furnace at 150°C. The resulting single crystals were dried in vacuum furnace for *ca*. 2-3h at 40°C. ^{1}H NMR- or IR-spectra were measured to examine the ligand content. Unfortunately, our attempts to obtain coordination architectures with other metal chloride or metal nitrate of Cd^{2+}, Zn^{2+}, Mn^{2+}, Cr^{3+}, Cu^{2+}, Co^{2+}, Ni^{2+}, Fe^{2+} (Fe^{3+} For nitrate), and Al^{3+} using the same conditions were unsuccessful. Comparison of IR and ^{1}H NMR spectrum of the isolated crystalline compound revealed that, either mixed-ligands or single ligand with solvent molecules were coordinated with metal ions by using hydrothermal reaction at high temperature. In this reaction condition, some samples contain two different crystal forms or more. The measured PXRD patterns of different crystallized compounds show that, some isolated compounds (**112**, **114**, **116**, **118** and **123**) or (**113**, **115**, **117** and **120**) are isostructural. While the other isolated compounds (**119**, **121**, **111** and **122**) are not isostructural. Single-crystal X-ray structure analysis at room temperature revealed that, H_2bdt ligand was crystallized with water molecule for compound **111** [27i] while without water molecules for compounds **115** and **120** [93g],[27q] (Figure 6.5.8.5). The data analyses of the crystallized compounds were summarized in Table 6.5.8.1.

Fig. 6.5.8.1a: Crystal images of **123** (left), **111** (middle), **121** (right).

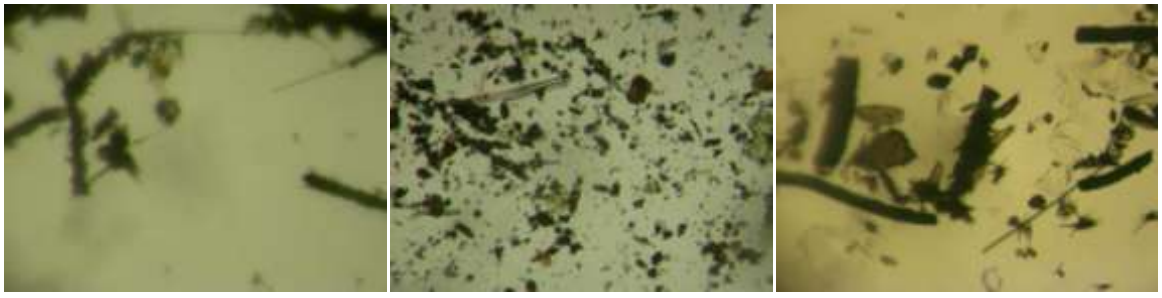

Fig. 6.5.8.1b: Crystal images of **120** (left), **118** (middle), **117** (right).

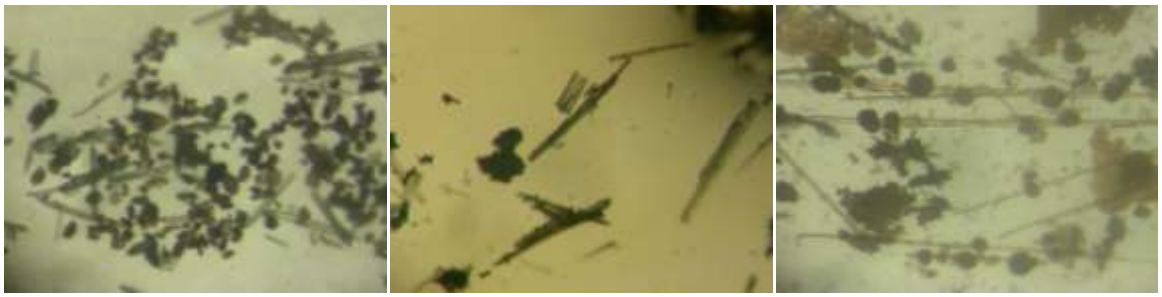

Fig. 6.5.8.1c: Crystal images of **119** (left), **113** (middle), **122** (right).

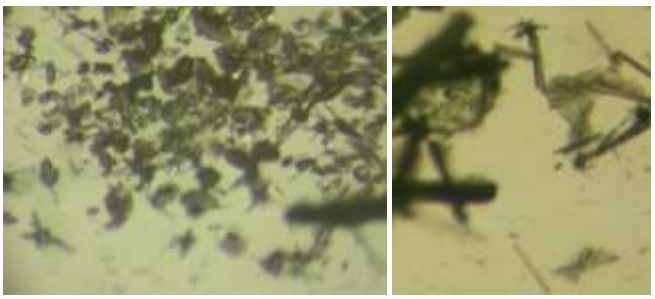

Fig. 6.5.8.1d: Crystal images of **116** (left), **115** (right).

Table 6.5.8.1: The data analyses of the crystallized compounds were as follows:

Product	Metal salt	Image	NMR	IR	PXRD	SCXRD
111	$CdCl_2$:H_2bdt:H_2bdc, 4:1:1	2	H_2bdt:H_2bdc, n:n, 1:0.64	H_2bdt:H_2bdc	x	H_2bdt:H_2O
112	$Cd(NO_3)_2.4H_2O$:H_2bdt:H_2bdc, 4:1:1		H_2bdt	H_2bdt	x	
113	$MnCl_2$:H_2bdt:H_2bdc, 4:1:1	1	H_2bdt:H_2bdc, n:n, 1:0.7	H_2bdt:H_2bdc	x	
114	$Mn(NO_3)_2.4H_2O$:H_2bdt:H_2bdc, 4:1:1		H_2bdt	H_2bdt	x	
115	$ZnCl_2$:H_2bdt:H_2bdc, 4:1:1	2	H_2bdt	H_2bdt	x	H_2bdt
116	$Zn(NO_3)_2.6H_2O$:H_2bdt:H_2bdc, 4:1:1	2	H_2bdt:H_2bdc, n:n, 0.8:1	H_2bdt	x	
117	$CrCl_3.6H_2O$:H_2bdt:H_2bdc, 4:1:1	3	H_2bdt:H_2bdc, n:n, 0.6:1	H_2bdt:H_2bdc	x	
118	$Cr(NO_3)_3.9H_2O$:H_2bdt:H_2bdc, 4:1:1	1	H_2bdt	H_2bdt	x	
119	$Cu(NO_3)_2.2.5H_2O$:H_2bdt:H_2bdc, 4:1:1	2	H_2bdc	H_2bdc	x	
120	$CoCl_2.6H_2O$:H_2bdt:H_2bdc, 4:1:1	2	H_2bdt:H_2bdc, n:n, 2.25:1	H_2bdt:H_2bdc	x	H_2bdt
121	$Co(NO_3)_2.6H_2O$:H_2bdt:H_2bdc, 4:1:1	1	H_2bdt	H_2bdt	x	
122	$NiCl_2.6H_2O$:H_2bdt:H_2bdc, 4:1:1	2	H_2bdt:H_2bdc	H_2bdt:H_2bdc	x	
123	$Al(NO_3)_3.9H_2O$:H_2bdt:H_2bdc, 4:1:1	2	H_2bdt	H_2bdt	x	

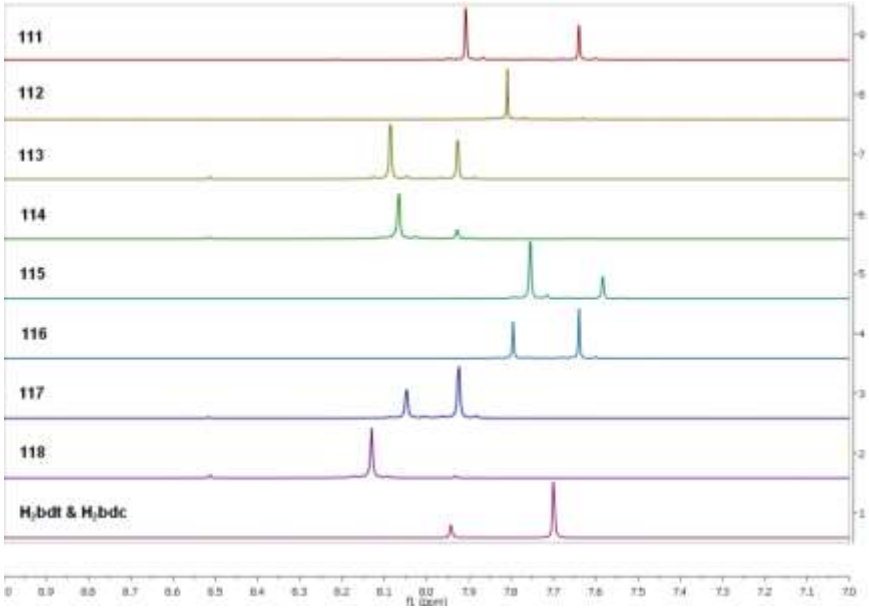

Fig. 6.5.8.2a: ^{1}H NMR Spectra (500 MHz) for comparison between signals of crystallized compounds and signals of ligands in NaOD/D_2O solution (mixture of ligands was measured at 200 MHz).

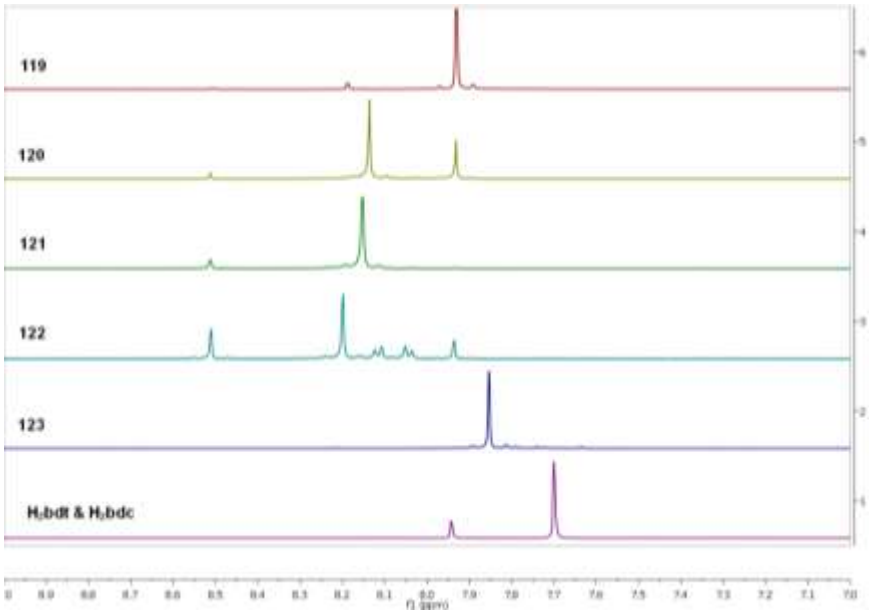

Fig. 6.5.8.2b: ^{1}H NMR Spectra (500 MHz) for comparison between signals of crystallized compounds and signals of ligands in NaOD/D_2O solution (mixture of ligands was measured at 200 MHz).

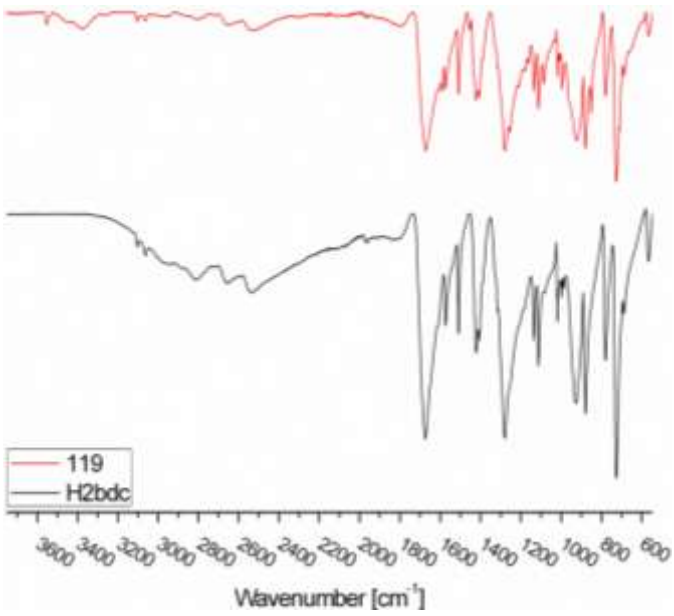

Fig. 6.5.8.3a: IR Spectra (ATR) for comparison between **119** and H_2bdc-ligand.

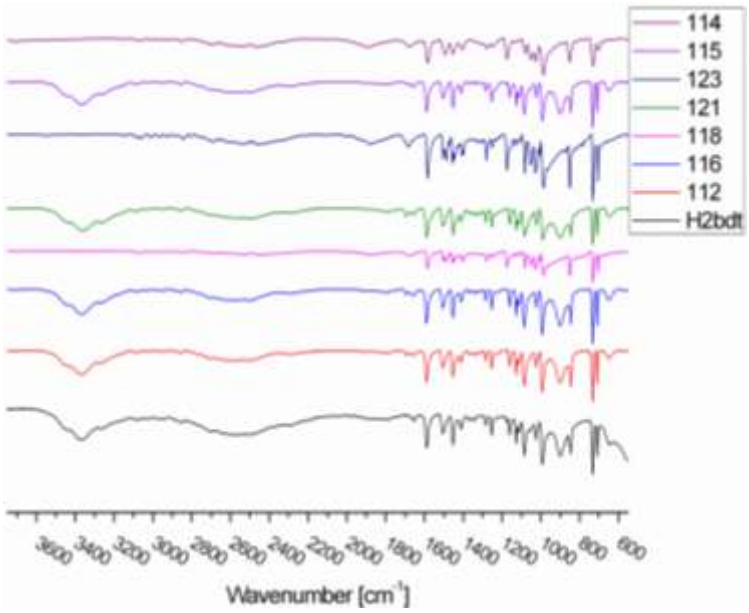

Fig. 6.5.8.3b: IR Spectra (ATR) for comparison between crystallized compounds and H_2bdt-ligand.

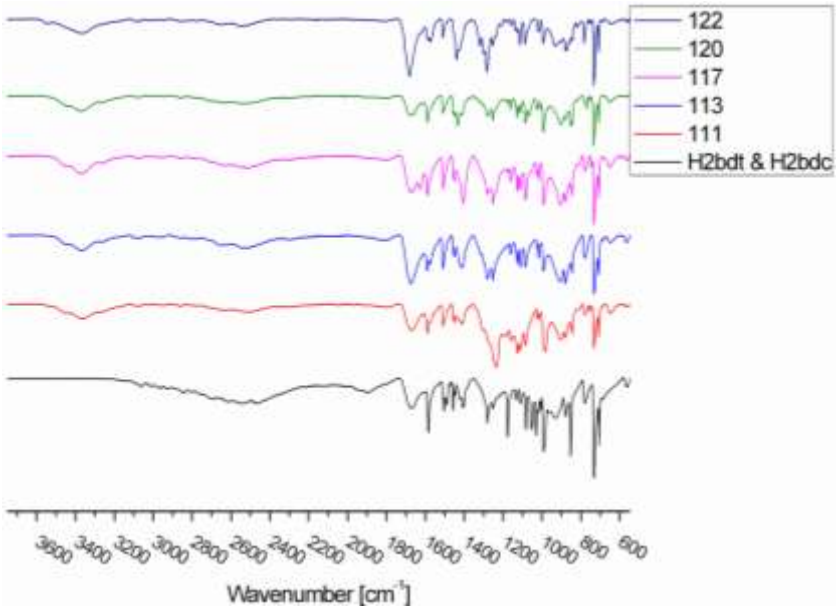

Fig. 6.5.8.3c: IR Spectra (ATR) for comparison between crystallized compounds and a mixture of ligands in range 550-3750 cm^{-1}.

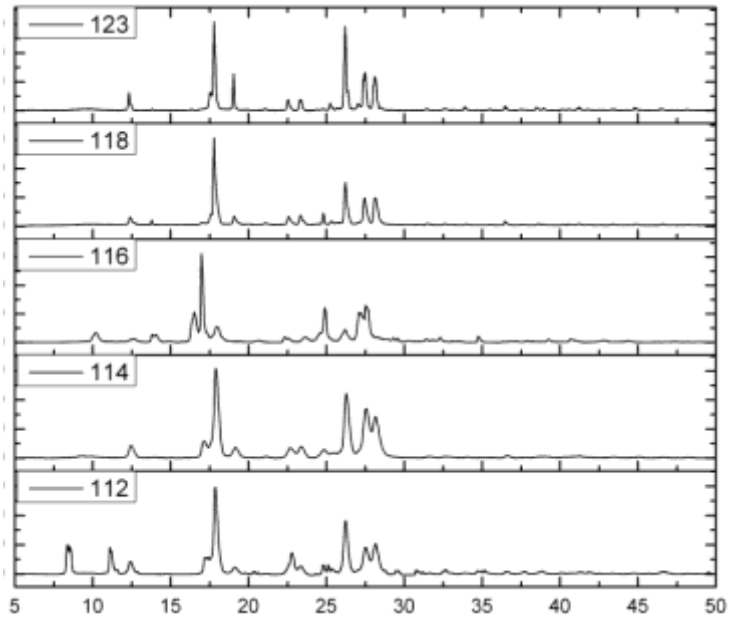

Fig. 6.5.8.4a: Combination of the experimental powder X-ray patterns at Cu-Kα wavelength 1.54184 Å of different crystallized compounds. The measured PXRD patterns are smoothed and baseline corrected.

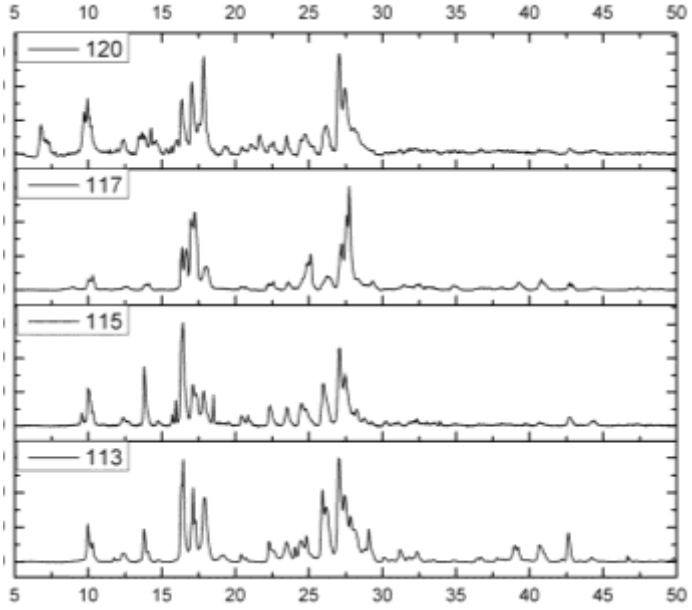

Fig. 6.5.8.4b: Combination of the experimental powder X-ray patterns at Cu-Kα wavelength 1.54184 Å of different crystallized compounds. The measured PXRD patterns are smoothed and baseline corrected.

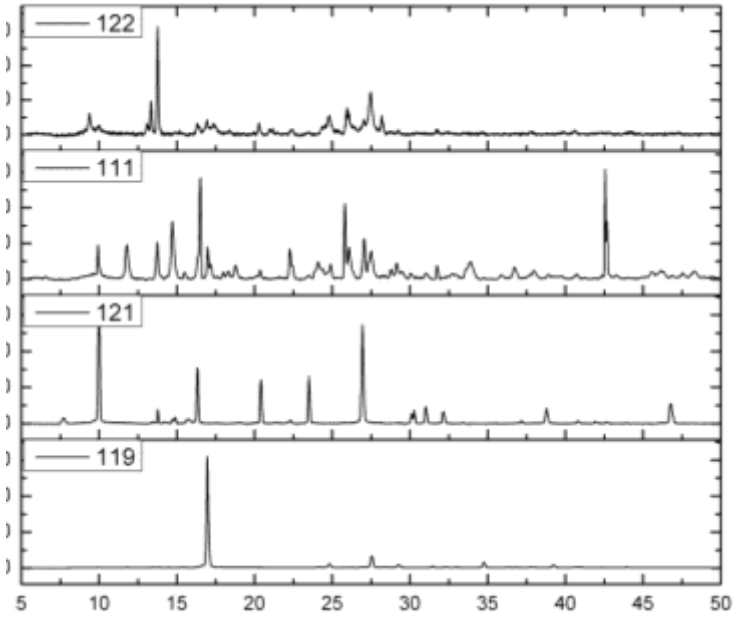

Fig. 6.5.8.4c: Combination of the experimental powder X-ray patterns at Cu-Kα wavelength 1.54184 Å of different crystallized compounds. The measured PXRD patterns are smoothed and baseline corrected.

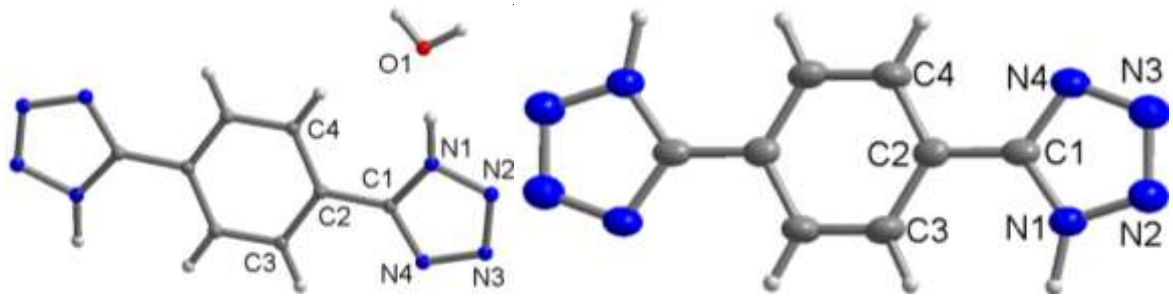

Fig. 6.5.8.5: The molecular structure of H_2bdt ligand for compounds **111** (left) [27i], **120** and **115** (right) [93g],[27q].

Part (b): NaOH solution (0.16 mmol/l) as base was used to deprotonate the used ligands (H_2bdc, H_2ip, H_3btc or H_2ipdt) using ultrasonic bath at 40-50°C. An aqueous solution of different metal salts, an aqueous solution of H_2bdc, H_2ip or H_3btc and an aqueous solution of H_2ipdt (For H_3btc was dissolved in 0.75 ml of NaOH to deprotonate their three carboxyl groups) were mixed in glass tube, stirred for about 5 minutes, and then placed in a programmable furnace at 150°C. ^{1}H NMR- or IR-spectra of resulting single crystals were measured to examine the ligand content. Unfortunately, our attempts to obtain coordination polymers with other metal nitrates of Cd^{2+}, Zn^{2+}, Mn^{2+}, Cr^{3+}, Cu^{2+}, Co^{2+}, Ni^{2+}, Fe^{3+}, and Al^{3+} using the same conditions were unsuccessful. Comparison of IR and ^{1}H NMR spectrum of the isolated crystalline compound revealed that either two ligands or one were/was coordinated with metal ions. In this reaction condition, some samples contain different crystal forms. The measured PXRD patterns of different crystallized compounds show that, some isolated compounds **124** and **133** or **125** and **127** are isostructural. While the other isolated compound **126** are not isostructural. Single-crystal X-ray structure analysis at room temperature revealed that, H_2bdc ligand was crystallized for compounds **124** [10],[150] and **126** [151] as needle-shaped crystals while H_2ip ligand was crystallized for compound **129** [152] as plate crystals (Figure 6.5.8.10). The needle-shaped crystal of compound **129** revealed a novel binuclear Cd complex with H_2bdt ligand and solvent molecules. But the structure could not refine completely, because the crystals were damaged at the end of single-crystal measurement, when the crystal was measured at ambient temperature. The data analyses of crystallized compounds were summarized in Table 6.5.8.2.

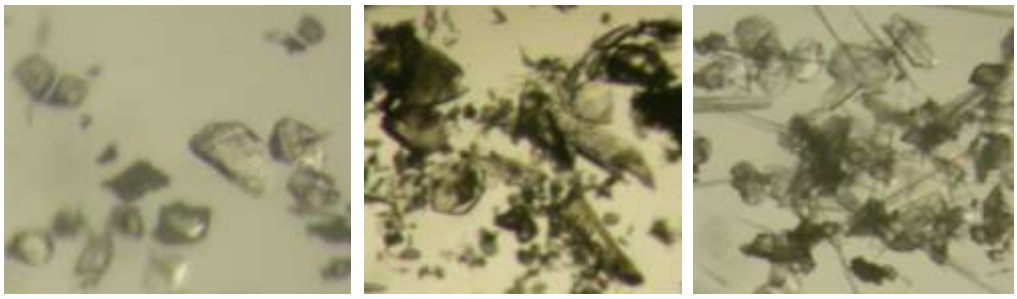

Fig. 6.5.8.6a: Crystal images of **127** (left), **125** (middle), **126** (right).

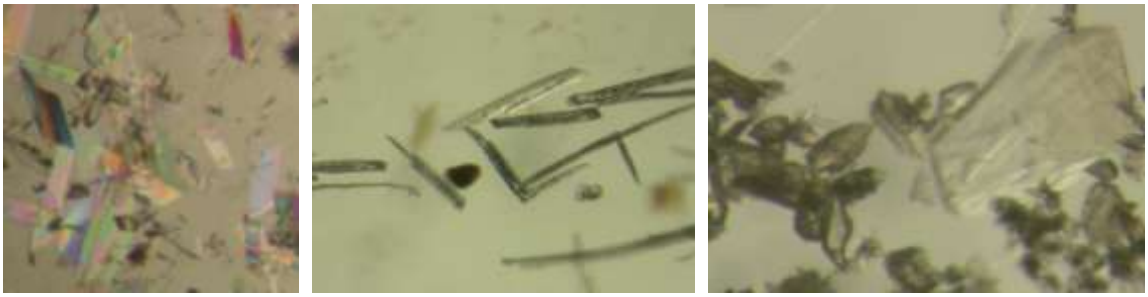

Fig. 6.5.8.6b: Crystal images of **129a & b** (left), **133** (middle), **124** (right).

Table 6.5.8.2: The data analyses of the crystallized compounds were as follows:

Product	Metal salt	Image	NMR	IR	PXRD	SCXRD
124	$Cd(NO_3)_2.4H_2O$:H_2ipdt:H_2bdc, 4:1:1	3	H_2ipdt:H_2bdc, n.n, 1:0.925	H_2ipdt:H_2bdc	x	H_2bdc
125	$Mn(NO_3)_2.4H_2O$:H_2ipdt:H_2bdc, 4:1:1	2	H_2ipdt:H_2bdc, n.n, 1:1.54	H_2ipdt:H_2bdc	x	
126	$Zn(NO_3)_2.6H_2O$:H_2ipdt:H_2bdc, 4:1:1	2	H_2ipdt:H_2bdc, n.n, 1:0.53	H_2ipdt	x	H_2bdc
127	$Cr(NO_3)_3.9H_2O$:H_2ipdt:H_2bdc, 4:1:1	1	H_2ipdt:H_2bdc, n.n, 1:0.8	H_2ipdt:H_2bdc	x	
128	$Ni(NO_3)_2.6H_2O$:H_2ipdt:H_2bdc, 4:1:1		H_2ipdt:H_2bdc, n.n, 1:1.7			
129	$Cd(NO_3)_2.4H_2O$:H_2ipdt:H_2ip, 4:1:1	2		H_2ipdt:H_2ip	x	H_2ip and complex
130	$Ni(NO_3)_2.6H_2O$:H_2ipdt:H_2ip, 4:1:1		H_2ipdt:H_2ip, n:n, 0.33:1			
131	$Al(NO_3)_2.9H_2O$:H_2ipdt:H_2ip, 4:1:1		H_2ipdt:H_2ip, n:n, x:x			
132	$Mn(NO_3)_2.4H_2O$:H_2ipdt:H_3btc, 4:1:1		H_2ipdt:H_3btc, n:n, 1:1.1			
133	$Cr(NO_3)_3.9H_2O$:H_2ipdt:H_3btc, 4:1:1	1			x	
134	$Cu(NO_3)_2.2.5H_2O$:H_2ipdt:H_3btc, 4:1:1					
135	$Co(NO_3)_2.6H_2O$:H_2ipdt:H_3btc, 4:1:1					
136	$Ni(NO_3)_2.6H_2O$:H_2ipdt:H_3btc, 4:1:1					
137	$Fe(NO_3)_3.9H_2O$:H_2ipdt:H_3btc, 4:1:1		H_2ipdt			

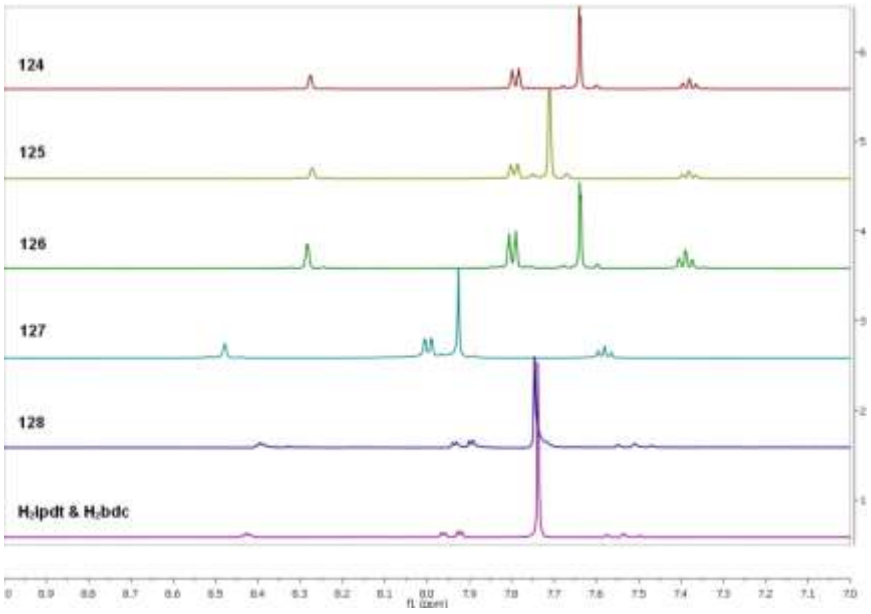

Fig. 6.5.8.7a: ^{1}H NMR Spectra (200 MHz) for comparison between signals of crystallized compounds and signals of a mixture of ligands in NaOD/D_2O solution (Compounds **124**, **125**, **126** and **127** were measured at 500 MHz).

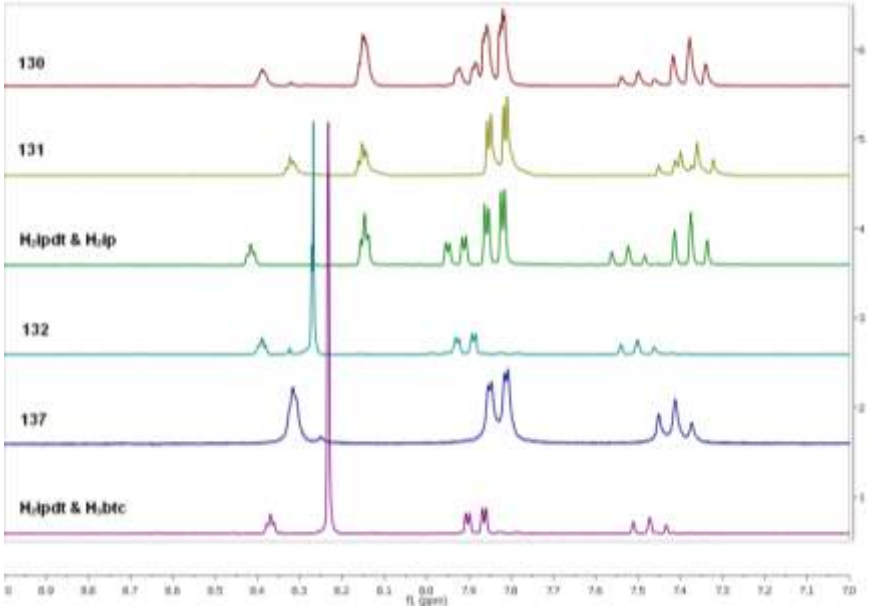

Fig. 6.5.8.7b: ^{1}H NMR Spectra (200 MHz) for comparison between signals of crystallized compounds and signals of different mixtures of ligands in NaOD/D_2O solution.

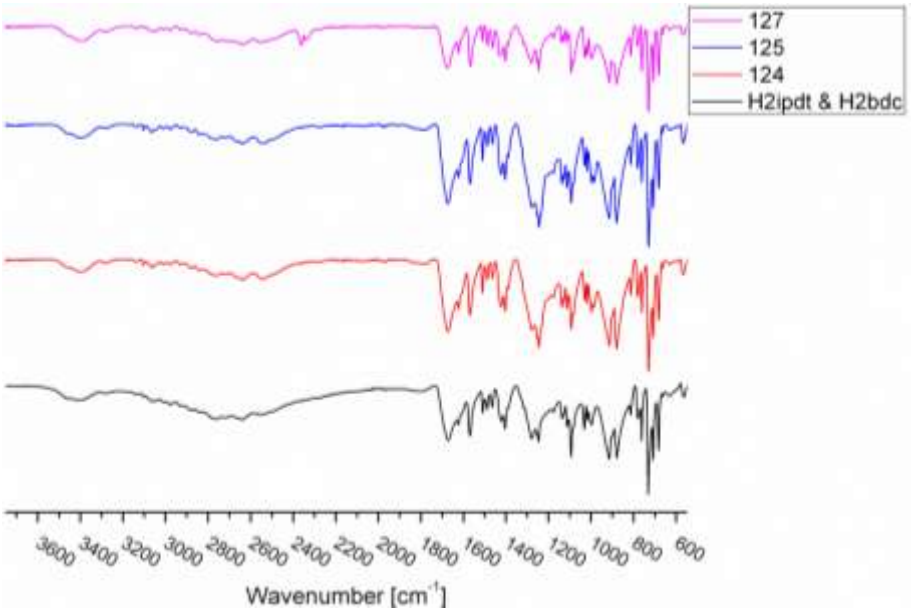

Fig. 6.5.8.8a: IR Spectra (ATR) for comparison between **124**, **125**, **127** and a mixture of ligands.

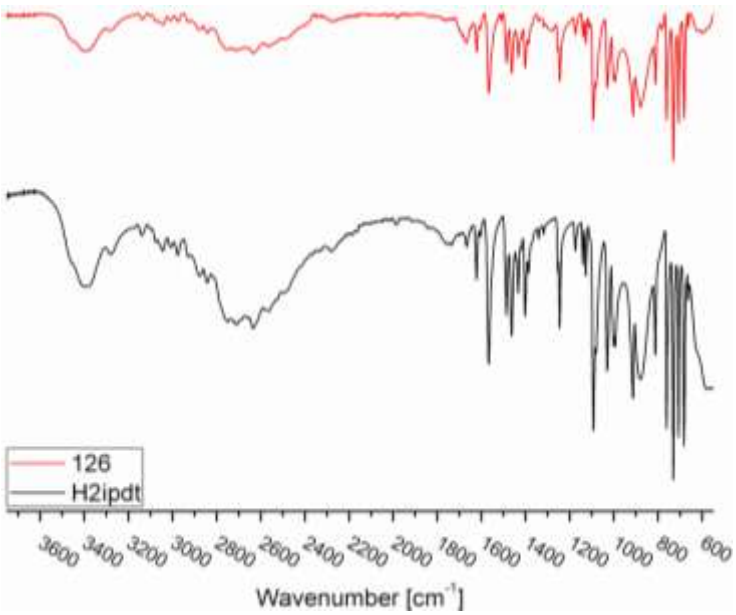

Fig. 6.5.8.8b: IR Spectra (ATR) for comparison between **126** and H_2ipdt-ligand.

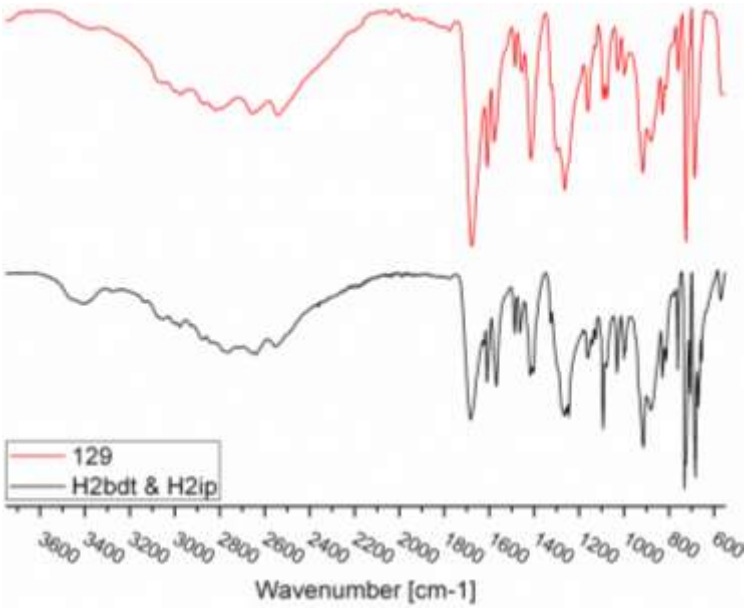

Fig. 6.5.8.8c: IR Spectra (ATR) for comparison between **129** and the mixture of ligands H_2bdt and H_2ip.

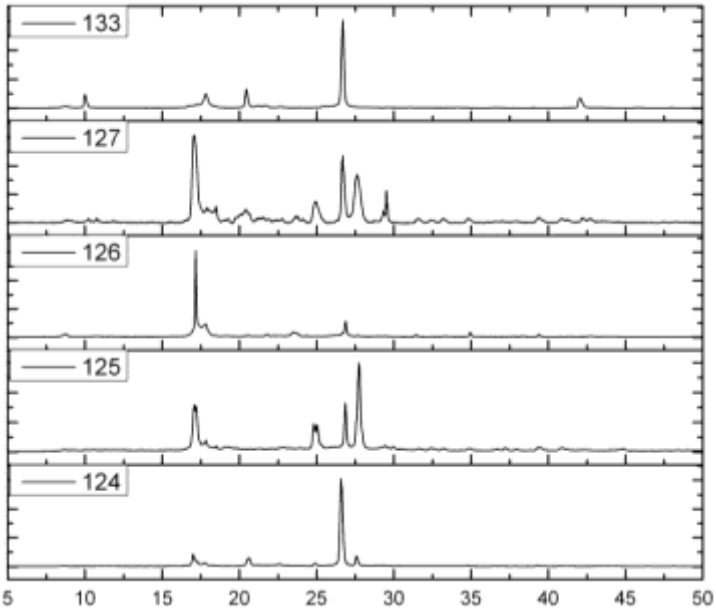

Fig. 6.5.8.9: Combination of the experimental powder X-ray patterns at Cu-Kα wavelength 1.54184 Å of different crystallized compounds. The measured PXRD patterns are smoothed and baseline corrected.

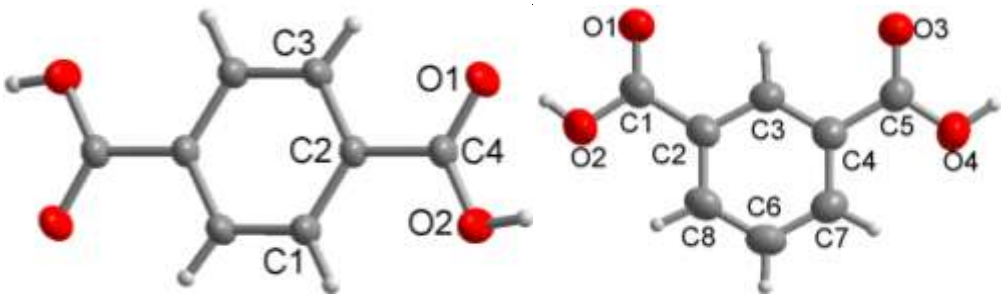

Fig. 6.5.8.10: The molecular structure of H_2bdc ligand for compounds **124** [10],[150] and **126** [151] (left), and H_2ip ligand for compound **129** [152] of plate crystals (right).

7.5.8.1 Structure analysis and characterization of $[Cd_2(Hipdt)_2(\mu\text{-}OH)_2(H_2O)_6]$ ~10(H_2O) (129b)

Colorless crystals (Fig. 6.5.8.6b, left) of formula $[Cd_2(Hipdt)_2(\mu\text{-}OH)_2(H_2O)_6]$ ~10(H_2O) **129b**, are obtained from the hydrothermal reaction, at 150 °C, of $Cd(NO_3)_2{\cdot}4H_2O$, H_2ipdt and H_2ip in approximately 4:1:1 molar ratio. A solution of NaOH was used as base to deprotonate the ligands. The resulting single crystals were washed with water. The reaction was repeated several times and found to be reproducible. Single-crystal X-ray structure analysis at room temperature revealed that, H_2ip ligand was crystallized for compounds **129a** [151] as plate crystals. The needle-shaped crystal of compound **129b** revealed a novel binuclear Cd complex with H_2ipdt ligand and solvent molecules. But the structure could not refine completely, because the disorder positions of terminal ligand H_2ipdt and lattice water molecules. This compound crystallizes in the monoclinic crystal system with the *C2* space group, and the crystallographic asymmetric unit consists of one Cd(II) ions with terminal Hipdt ligand, two bridged OH, three coordinated aqua ligands and five lattice water molecules. The extended asymmetric unit of $[Cd_2(Hipdt)_2(\mu\text{-}OH)_2(H_2O)_6]{\cdot}$~10($H_2O$) in ball-stick model is represented in Figure 6.5.8.1.1. Selected bond lengths and angles are summarized in Table 6.5.8.1.1.

Table 6.5.8.1.1: Selected bond lengths [Å] and angles [°] for **129b**.

Cd1-O5	2.17(3)	O5-Cd1-O1	95.1(11)
Cd1-N2	2.201(10)	N2-Cd1-O1	94.8(6)
Cd1-O3	2.226(15)	O3-Cd1-O1	90.5(6)
Cd1-O4	2.24(3)	O4-Cd1-O1	161.0(11)
Cd1-O1	2.362(15)	O5-Cd1-O2	172.5(12)

Cd1-O2	2.46(2)	N2-Cd1-O2	90.0(6)
O5-Cd1-N2	92.7(10)	O3-Cd1-O2	85.4(7)
O5-Cd1-O3	92.6(11)	O4-Cd1-O2	84.2(13)
N2-Cd1-O3	172.1(14)	O1-Cd1-O2	77.6(5)
O5-Cd1-O4	102.8(10)	$Cd1^{i}$-O1-Cd1	105.3(9)
N2-Cd1-O4	90.6(12)	$Cd1^{i}$-O2-Cd1	99.4(13)
O3-Cd1-O4	82.5(13)		

Symmetry transformations used to generate equivalent atoms: i = -x, y, -z.

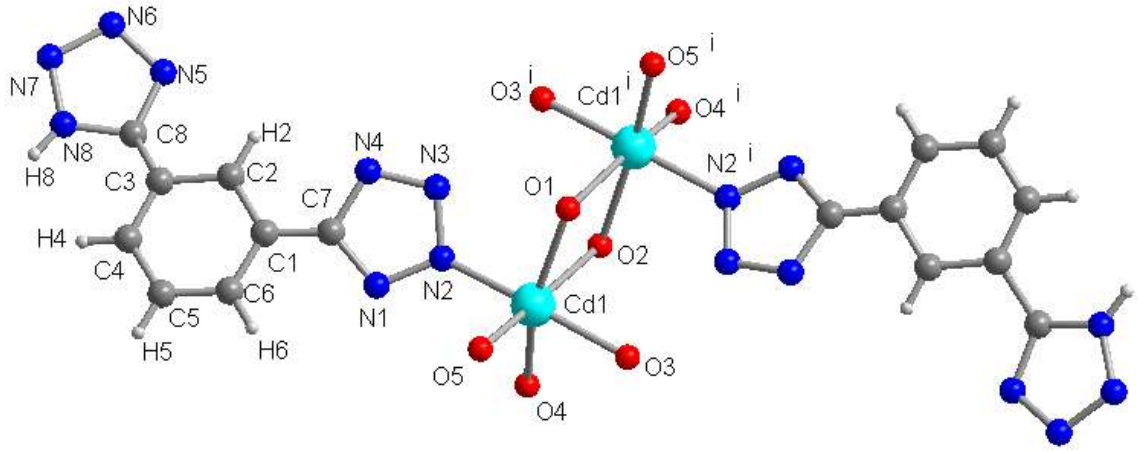

Fig. 6.5.8.1.1: The extended asymmetric unit showing the coordination environment of Cd(II) ions for compound **129b** with atom labeling. Symmetry operations: i = -x, y, -z.

The Cd atom is coordinated in a distorted octahedral environment by one nitrogen atom of terminal $Hipdt^{-}$ ligand, two bridged OH^{-} anions and three aqua ligands. The two bridged OH^{-} anions and two aqua ligands are located in the equatorial plane. The Hipdt ligand coordinates with Cd through N2-atom while the other N-atoms remain without coordination. Such a binuclear complex of $[Cd_2(Hipdt)_2(\mu\text{-}OH)_2(H_2O)_6]\cdot\sim10(H_2O)$ is formed. The positive charges of Cd-atoms neutralize the negative charges of terminal $Hipdt^{-}$ ligand and bridged OH^{-} anions so the structure is overall neutral. The $Hipdt^{-}$ ligands are stacked parallel to each other, so that there are significant π-π interactions [116] between the adjacent benzene or tetrazole rings of the $Hipdt^{-}$ ligands. In addition, the benzene and both tetrazole rings of the $Hipdt^{-}$ ligand form like left-handed helicity along ***c*** axis, which lead to form a chiral binuclear complex. The remaining spaces between the neighboring binuclear complexs are occupied by lattice water molecules as shown in Figure 6.5.8.1.2. Furthermore, the structure of compound **129b** contains mostly unusual strong hydrogen bonding between the aqua ligands of binuclear complexes and lattice water molecules. The π-π interactions between adjacent

$Hipdt^-$ ligands and the hydrogen bonds lead to stabile the Cd-complex in structure. The IR spectrum is in agreement with its single-crystal X-ray diffraction as shown in Figure 6.5.8.8c.

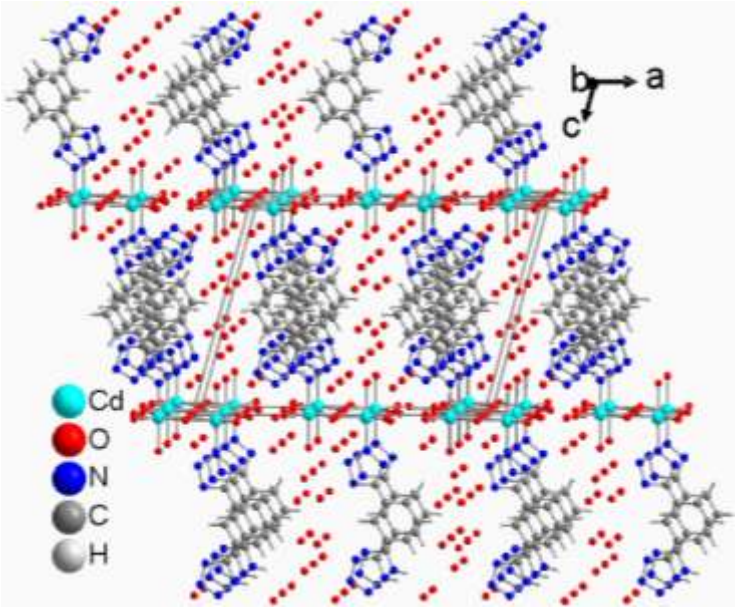

Figure 6.5.8.1.2: Packing diagram of **129b** shows the alternating complexes in ball-stick representation. Lattice water molecules are shown as red balls.

7.5.9 Hydrothermal method at high temperature (S.: NH_4OH)

NH_4OH solution (0.16 mmol/l) as base was used to deprotonate the used ligands (H_2bdc, H_2ip, H_3btc or H_2ipdt) using ultrasonic bath at 40-50°C. An aqueous solution of metal salt, an aqueous solution of H_2bdc, H_2ip or H_3btc and an aqueous solution of H_2ipdt were mixed in glass tube, stirred for about 5 minutes, and then placed in a programmable furnace at 150°C. ^{1}H NMR- or IR-spectrum of resulting single crystals was measured to examine the ligand content. Unfortunately, our attempts to obtain coordination polymers with other metal nitrate of Cd^{2+}, Zn^{2+}, Mn^{2+}, Cr^{3+}, Cu^{2+}, Co^{2+}, Ni^{2+}, Fe^{3+}, and Al^{3+} using the same conditions were unsuccessful. Comparison of IR and ^{1}H NMR spectrum of the isolated crystalline compound with those of used ligands revealed that either two ligands or one were/was coordinated with metal ions. In this reaction condition, some samples contain different crystal forms. The measured PXRD patterns of crystallized compounds show that, some isolated compounds are isostructural. While the other isolated compounds are not isostructural. Single-crystal X-ray structure analysis at room temperature revealed that, red crystals of isolated crystalline compound **39** was crystallized as 1D-$[Co_3(\mu_3\text{-btc})(\mu_2\text{-btc})(H_2O)_{12}]_n$. The 1D-polymeric chain is analogous to a previously reported cobalt-polymer [5l],[147] and to a zinc polymer [5a,l]. The

structure was discussed in previously section 7.4.3. The data analyses of the crystallized compounds were summarized in Table 6.5.9.1.

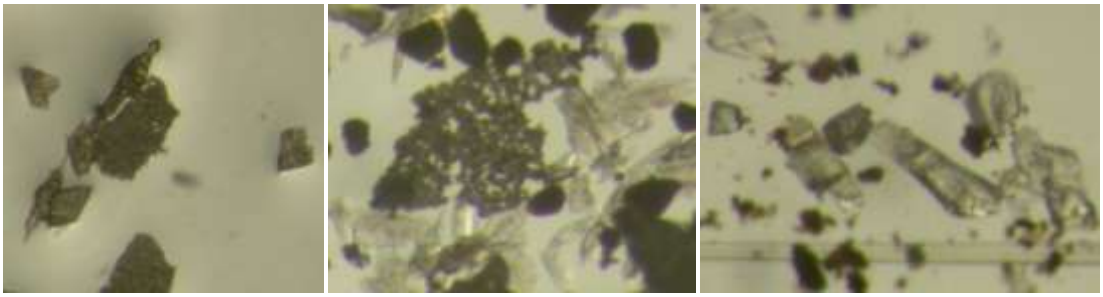

Fig. 6.5.9.1a: Crystal images of **146** (left), **138** (middle), **141** (right).

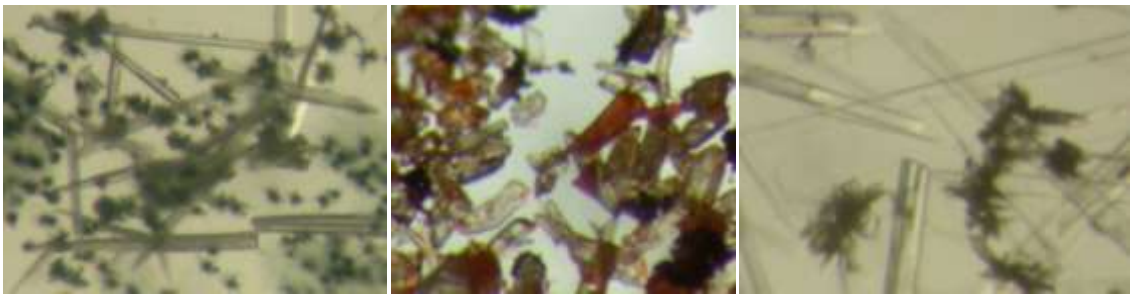

Fig. 6.5.9.1b: Crystal images of **142** (left), **145** (middle), **139** (right).

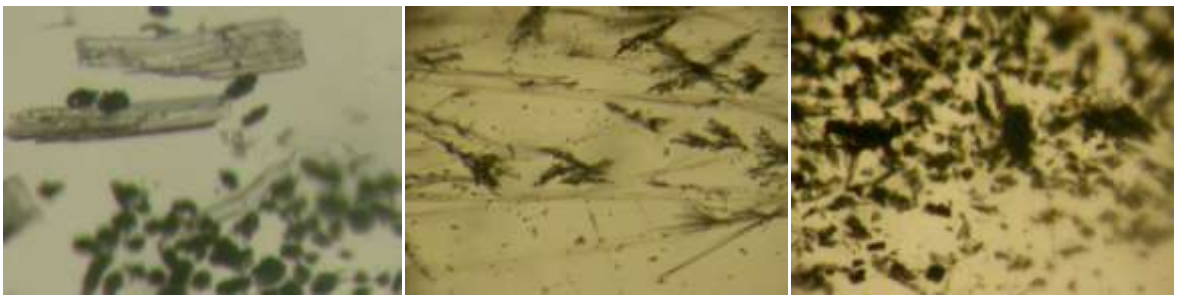

Fig. 6.5.9.1c: Crystal images of **144** (left), **151** (middle), **149** (right).

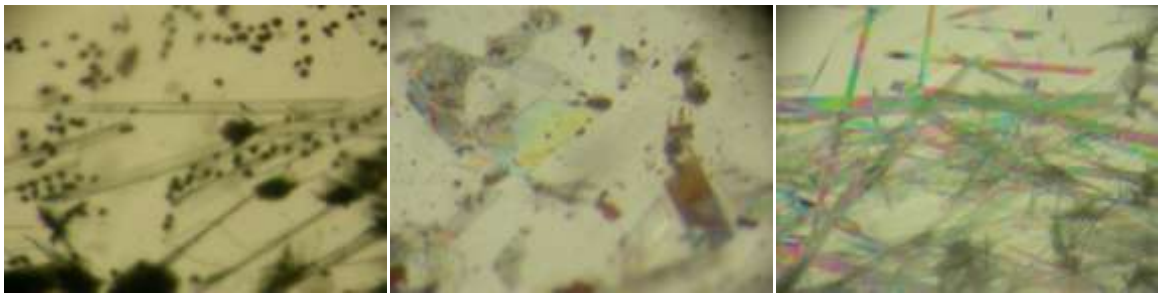

Fig. 6.5.9.1d: Crystal images of **150** (left), **153** (middle), **147** (right).

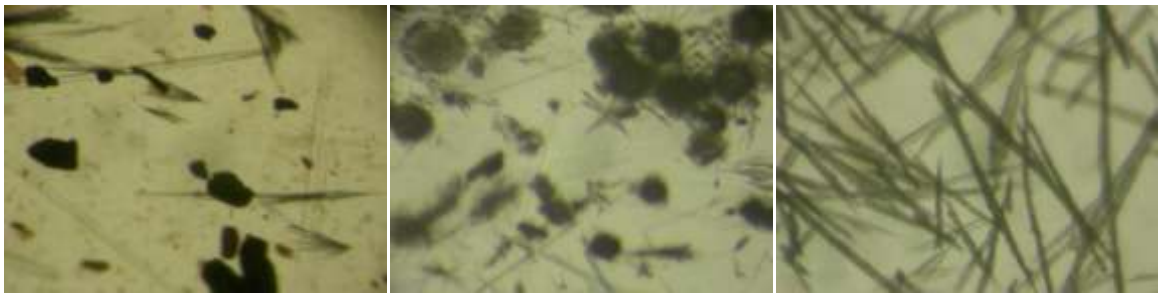

Fig. 6.5.9.1e: Crystal images of **152** (left), **148** (middle), **158** (right).

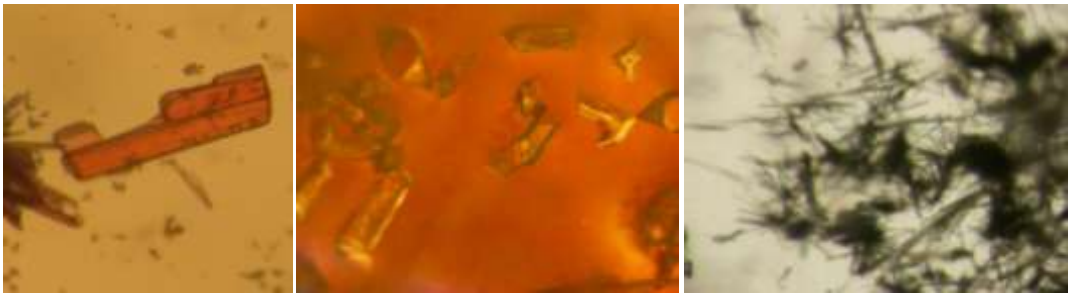

Fig. 6.5.9.1f: Crystal images of **39** (left), **157** (middle), **154** (right).

Table 6.5.9.1: The data analyses of the crystallized compounds were as follows:

Product	Metal salt	Image	NMR	IR	PXRD	SCXRD
138	$Cd(NO_3)_2.4H_2O$:H_2ipdt:H_2bdc, 4:1:1	1	H_2ipdt:H_2bdc, n:n, 1:1.45	H_2ipdt:H_2bdc	x	
139	$Mn(NO_3)_2.4H_2O$:H_2ipdt:H_2bdc, 4:1:1	2	H_2ipdt:H_2bdc	H_2ipdt:H_2bdc	x	
140	$Zn(NO_3)_2.6H_2O$:H_2ipdt:H_2bdc, 4:1:1		H_2ipdt:H_2bdc, n:n, 1:0.78	H_2ipdt:H_2bdc	x	
141	$Cr(NO_3)_3.9H_2O$:H_2ipdt:H_2bdc, 4:1:1	2	H_2ipdt:H_2bdc, n:n, 1:1	H_2ipdt:H_2bdc	x	
142	$Cu(NO_3)_2.2.5H_2O$:H_2ipdt:H_2bdc, 4:1:1	1	H_2bdc	H_2bdc	x	
143	$Co(NO_3)_2.6H_2O$:H_2ipdt:H_2bdc, 4:1:1	x	H_2bdc	H_2bdc	x	
144	$Ni(NO_3)_2.6H_2O$:H_2ipdt:H_2bdc, 4:1:1	1	H_2bdc	H_2bdc	x	
145	$Fe(NO_3)_3.9H_2O$:H_2ipdt:H_2bdc, 4:1:1	1	H_2ipdt:H_2bdc, n:n, 1:1.25	H_2ipdt:H_2bdc	x	
146	$Al(NO_3)_3.9H_2O$:H_2ipdt:H_2bdc, 4:1:1	1	H_2ipdt:H_2bdc, n:n, 1:0.25	H_2ipdt:H_2bdc	x	
147	$Mn(NO_3)_2.4H_2O$:H_2ipdt:H_2ip, 4:1:1	1			x	
148	$Zn(NO_3)_2.6H_2O$:H_2ipdt:H_2ip, 4:1:1	2			x	
149	$Cr(NO_3)_3.9H_2O$:H_2ipdt:H_2ip, 4:1:1	2			x	
150	$Cu(NO_3)_2.2.5H_2O$:H_2ipdt:H_2ip, 4:1:1	2			x	
151	$Co(NO_3)_2.6H_2O$:H_2ipdt:H_2ip, 4:1:1	2		x	x	
152	$Ni(NO_3)_2.6H_2O$:H_2ipdt:H_2ip, 4:1:1	1			x	

Product	Metal salt	Image	NMR	IR	PXRD	SCXRD
153	$Fe(NO_3)_2.9H_2O$:H_2ipdt:H_2ip, 4:1:1	1			x	
154	$Zn(NO_3)_2.6H_2O$:H_2ipdt:H_3btc, 4:1:1	1			x	
155	$Cu(NO_3)_2.2.5H_2O$:H_2ipdt:H_3btc, 4:1:1					
39	$Co(NO_3)_2.6H_2O$:H_2ipdt:H_3btc, 4:1:1	1			x	
157	$Fe(NO_3)_3.9H_2O$:H_2ipdt:H_3btc, 4:1:1	1			x	
158	$Al(NO_3)_3.9H_2O$:H_2ipdt:H_3btc, 4:1:1	1			x	

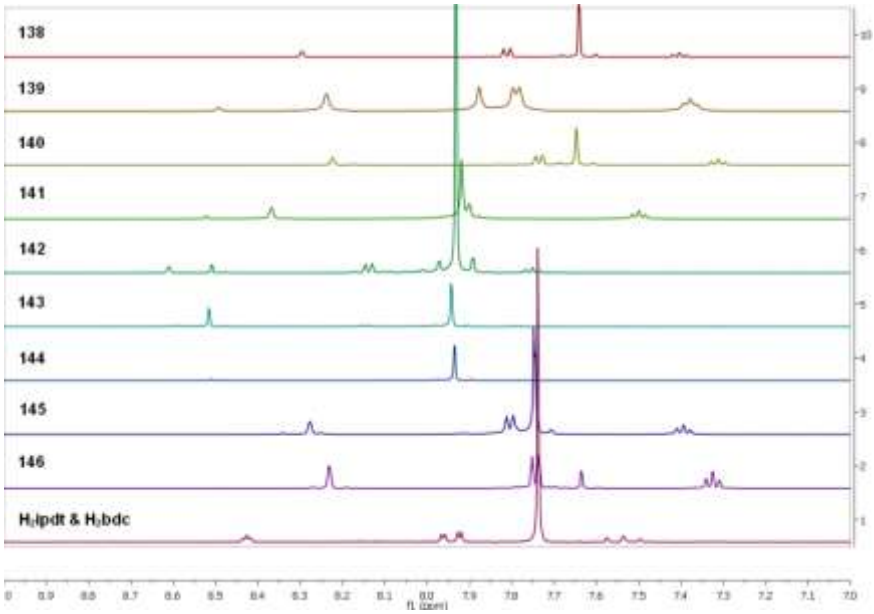

Fig. 6.5.9.2: ^{1}H NMR Spectra (500 MHz) for comparison between signals of crystallized compounds and signals of a mixture of ligands in NaOD/D_2O solution (mixture of ligands was measured at 200 MHz).

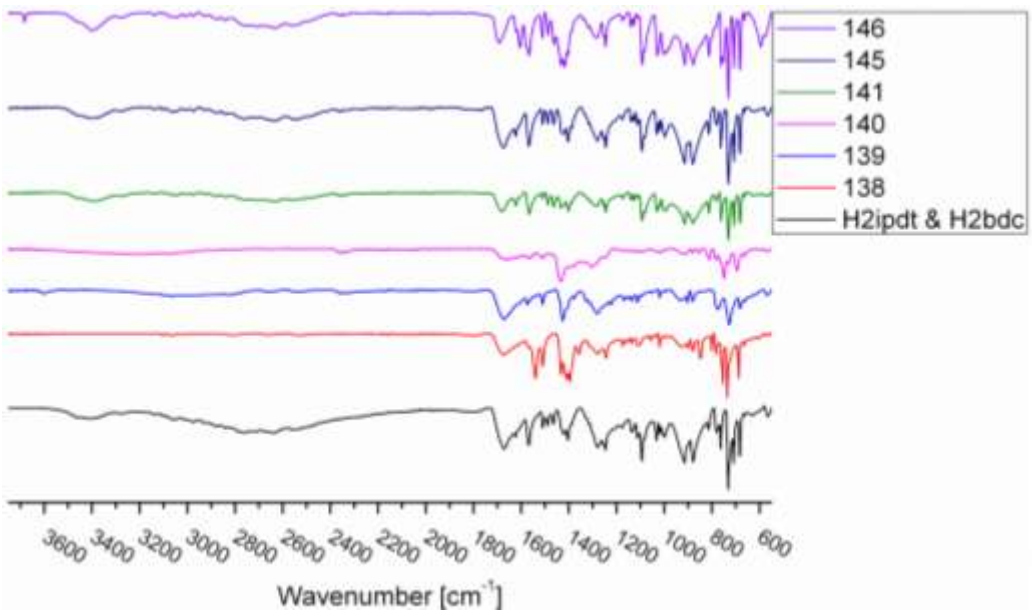

Fig. 6.5.9.3a: IR Spectra (ATR) for comparison between crystallized compounds and a mixture of ligands in range 550-3750 cm^{-1}.

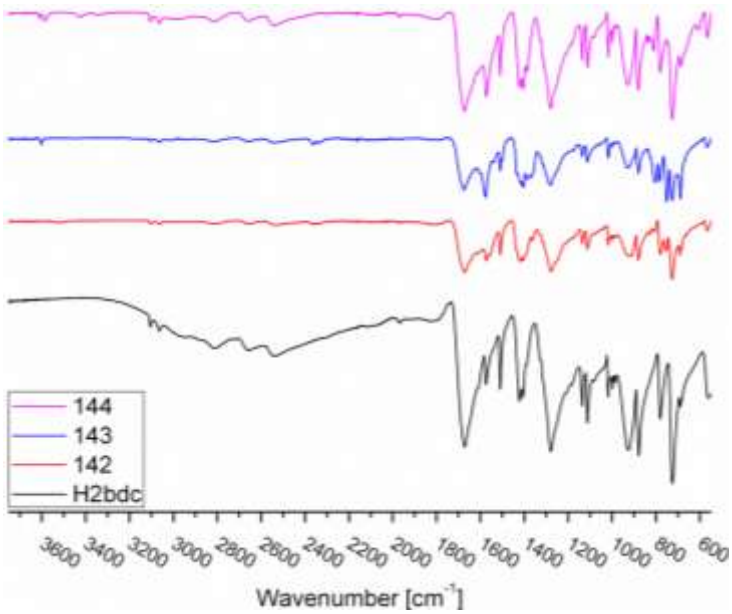

Fig. 6.5.9.3b: IR Spectra (ATR) for comparison between **142**, **143**, **144** and H_2bdc-ligand.

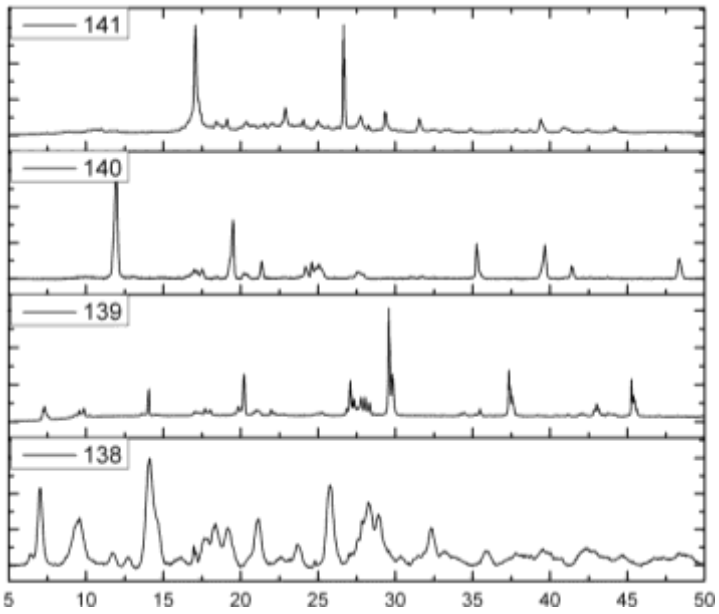

Fig. 6.5.9.4a: Combination of the experimental powder X-ray patterns at Cu-Kα wavelength 1.54184 Å of different crystallized compounds. The measured PXRD patterns are smoothed and baseline corrected.

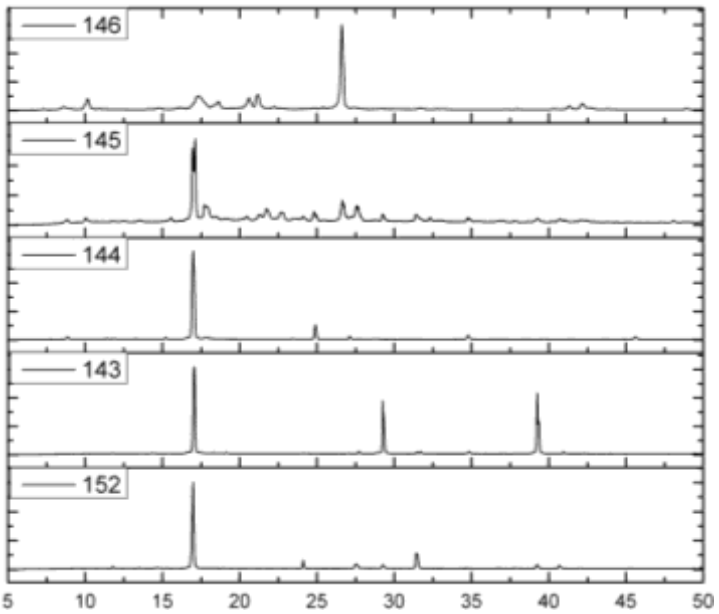

Fig. 6.5.9.4b: Combination of the experimental powder X-ray patterns at Cu-Kα wavelength 1.54184 Å of different crystallized compounds. The measured PXRD patterns are smoothed and baseline corrected.

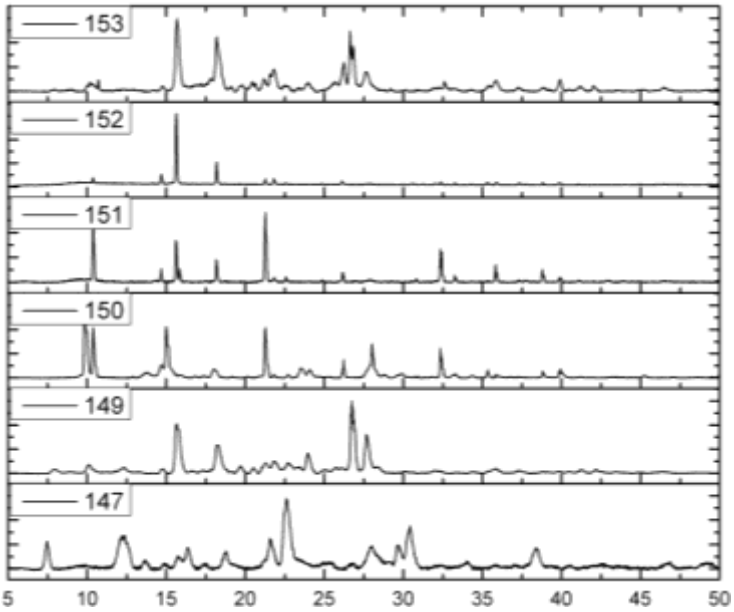

Fig. 6.5.9.4c: Combination of the experimental powder X-ray patterns at Cu-Kα wavelength 1.54184 Å of different crystallized compounds. The measured PXRD patterns are smoothed and baseline corrected.

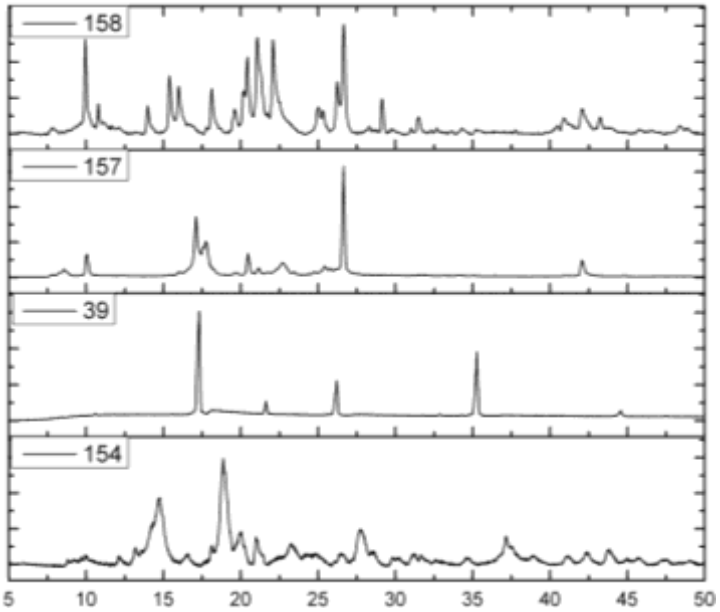

Fig. 6.5.9.4d: Combination of the experimental powder X-ray patterns at Cu-Kα wavelength 1.54184 Å of different crystallized compounds. The measured PXRD patterns are smoothed and baseline corrected.

7.5.10 Solvothermal method at low temperature (S.: H_2O, DMSO, DMF)

A solution of metal nitrate or metal chloride in H_2O, a solution of H_3btc in DMSO, and a solution of H_2bdt or H_2ipdt in DMF were mixed in glass tube. After that the sample was putted in furnace at 90 or 120 °C. Finally, the sample was taken out, when the crystals were formed. ^{1}H NMR- or IR-spectra of resulting crystals were measured to examine the ligand content. Other experiments in the same condition with other metal chloride and metal nitrate of Zn^{2+}, Mn^{2+}, Cr^{3+}, Cu^{2+}, Co^{2+}, Ni^{2+} and Fe^{2+} (Fe^{3+} for nitrate) were carried out without successful. Comparison of ^{1}H NMR spectra revealed, that one ligand with solvent molecules were coordinated with metal ions. The data analyses of the crystallized compounds were summarized in Table 6.5.10.1.

Table 6.5.10.1: The data analyses of the crystallized compounds were as follows:

Product	Metal salt	Image	NMR	IR	PXRD	SCXRD
159	$CoCl_2.6H_2O$:H_2bdt:H_3btc, 4:1:1					
160	$CuCl_2$:H_2bdt:H_3btc, 4:1:1		H_2bdt:H_3btc, n:n, 1:1.3, DMF			
161	$MnSO_4.H_2O$:H_2bdt:H_3btc, 4:1:1					
162	$Cu(NO_3)_2.2.5H_2O$:H_2bdt:H_3btc, 4:1:1		H_2bdt:H_3btc, n:n, 1:1.3, DMF			
163	$ZnCl_2$:H_2ipdt:H_3btc, 4:1:1		H_3btc:DMF: DMSO			
164	$Zn(NO_3)_2.6H_2O$:H_2ipdt:H_3btc, 4:1:1		H_2ipdt:H_3btc , n:n, 0.7:1, DMF:DMSO			
165	$MnCl_2$:H_2ipdt:H_3btc, 4:1:1		H_3btc:DMSO			
166	$MnSO_4.H_2O$:H_2ipdt:H_3btc, 4:1:1		H_3btc:DMSO			
167	$CoCl_2.6H_2O$:H_2ipdt:H_3btc, 4:1:1		H_3btc:DMF: DMSO			
168	$Co(NO_3)_2.6H_2O$:H_2ipdt:H_3btc, 4:1:1		H_3btc:DMF: DMSO			

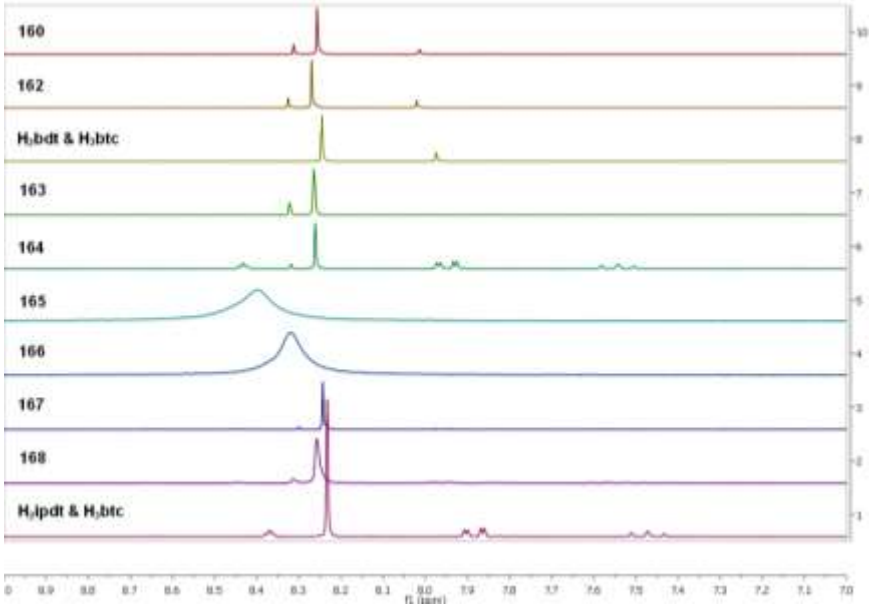

Fig. 6.5.10.2: ^{1}H NMR Spectra (200 MHz) for comparison between signals of crystallized compounds and signals of different mixtures of ligands in NaOD/D_2O solution.

7.5.11 Solvothermal method at high temperature (S.: H_2O, DMSO)

Ligand (H_2bdc, H_2ip, H_3btc or H_2ipdt) was dissolved in a mixture of DMSO and water in volume ratio (v:v, 1:1). An aqueous solution of different metal salts, a solution of H_2bdc, H_2ip or H_3btc and a solution of H_2ipdt were mixed in glass tube and then placed in a programmable furnace at 150°C. ^{1}H NMR- or IR-spectra of resulting single crystals were measured to examine the ligand content. Other experiments in the same condition with other metal chloride and metal nitrate of Cd^{2+}, Zn^{2+}, Mn^{2+}, Cr^{3+}, Cu^{2+}, Co^{2+}, Ni^{2+}, Fe^{3+} and Al^{3+} were carried out without successful. Comparison of IR and ^{1}H NMR spectrum of crystallized compound revealed, that mostly one ligand was coordinated with metal ions. The measured PXRD patterns of different crystallized compounds show that, some isolated compounds are partially isostructural. While the other isolated compounds are not isostructural. Single-crystal X-ray structure analysis at room temperature revealed that, H_2bdc ligand was crystallized for compound **171**. The data analyses of the crystallized compounds were summarized in Table 6.5.11.1.

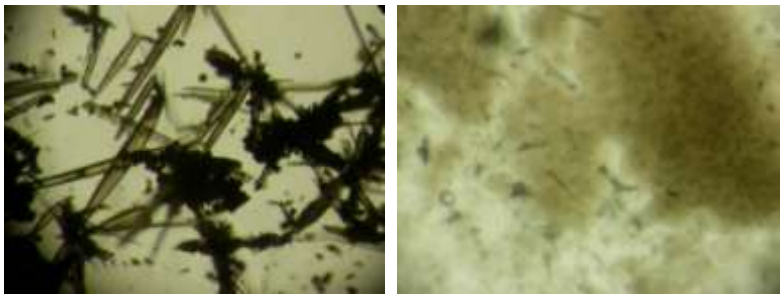

Fig. 6.5.11.1a: Crystal images of **170** (left), **169** (right).

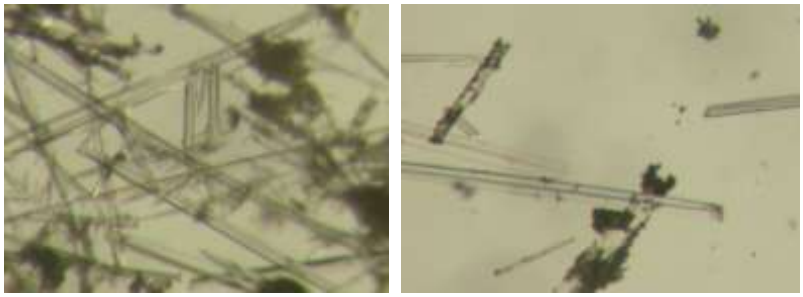

Fig. 6.5.11.1b: Crystal images of **171** (left), **172** (right).

Table 6.5.11.1: The data analyses of the crystallized compounds were as follows:

Product	Metal salt	Image	NMR	IR	PXRD	SCXRD
169	$Cr(NO_3)_3.9H_2O$:H_2ipdt:H_2bdc, 4:1:1	2	H_2ipdt:H_2bdc, n:n, 1:1.22		x	
170	$Co(NO_3)_2.6H_2O$:H_2ipdt:H_2bdc, 4:1:1	1	H_2bdc	H_2bdc	x	
171	$Ni(NO_3)_2.6H_2O$:H_2ipdt:H_2bdc, 4:1:1	1	H_2bdc	H_2bdc	x	
172	$Fe(NO_3)_3.9H_2O$:H_2ipdt:H_2bdc, 4:1:1	1	H_2bdc	H_2bdc	x	
173	$Cd(NO_3)_2.4H_2O$:H_2ipdt:H_3btc, 4:1:1					
174	$Mn(NO_3)_2.4H_2O$:H_2ipdt:H_3btc, 4:1:1					

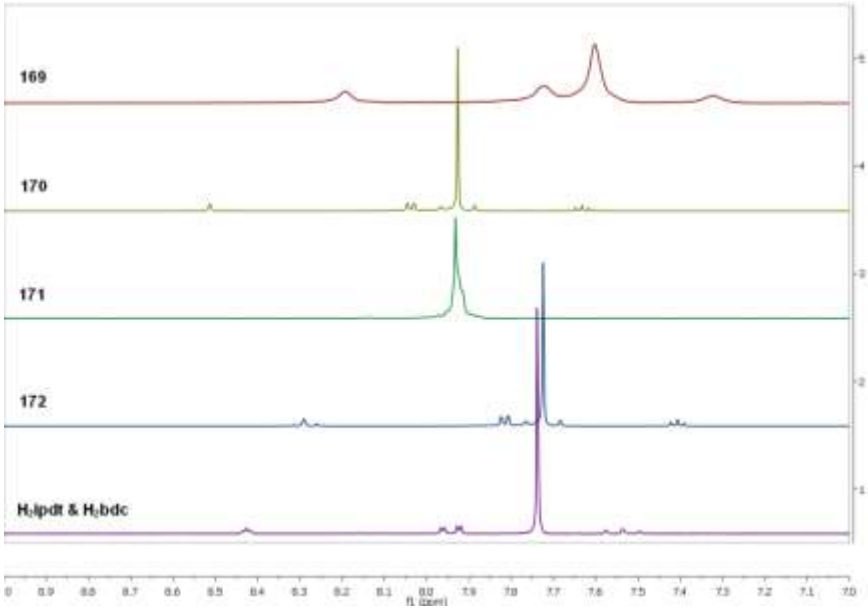

Fig. 6.5.11.2: ^{1}H NMR Spectra (500 MHz) for comparison between signals of crystallized compounds and signals of a mixture of ligands in NaOD/D_2O solution (mixture of ligands was measured at 200 MHz).

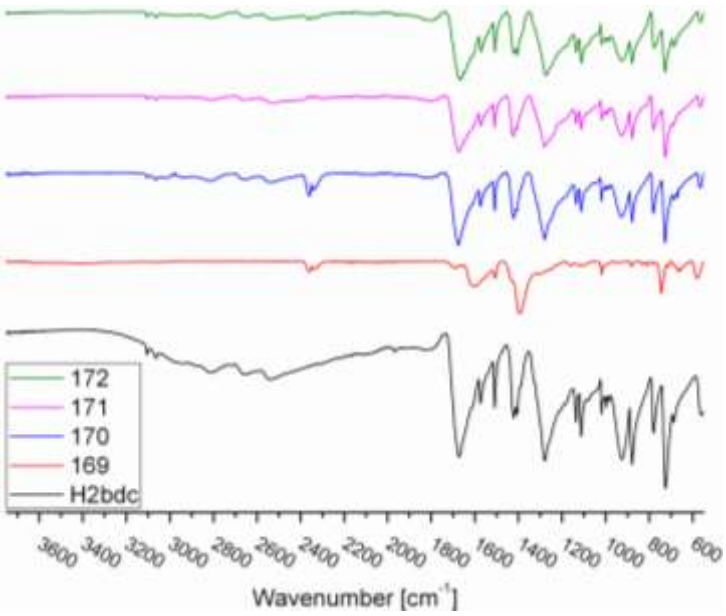

Fig. 6.5.11.3: IR Spectra (ATR) for comparison between **169**, **170**, **171**, **172** and H_2bdc-ligand.

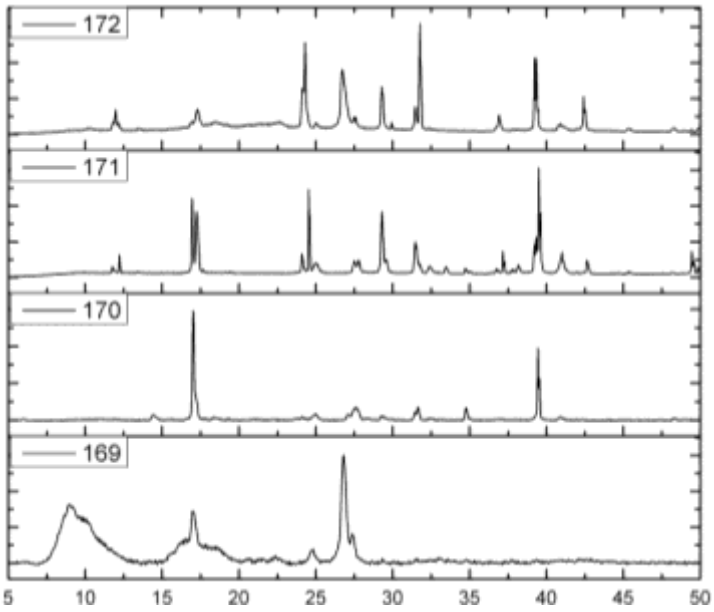

Fig. 6.5.11.4: Combination of the experimental powder X-ray patterns at Cu-Kα wavelength 1.54184 Å of different crystallized compounds. The measured PXRD patterns are smoothed and baseline corrected.

8 Conclusions and Summary

Supramolecular interactions, network interpenetration, construction of homo- and heterochains, cross-links between metal atoms and ligands, the metal atom geometry, number and type of coordinating groups of the ligand, coordination form of donor groups, different dimensional framework hydrogen bonds, van der Waals forces, topology of the layers and SBUs contribute to the dimensionality of the frameworks and the stability of their structures.

Generally, solvents, the pH value, structure of ligands and functional groups of used ligands have a very important influence in the formation of different coordination frameworks and there is the necessity of controlling the formation of such structures by a better understanding of the various influences.

When the ligands benzene-1,4-dicarboxylate (bdc^{2-}) and 1,2-bis(1,2,4-triazol-4-yl)propane (*rac*-btrip) were reacted with copper nitrate hydrate in the presence of NH_3 solution for deprotonation of the carboxylic acid under hydrothermal conditions 125 °C for 2 days the following products could be obtained as single crystals and structurally characterized 3D-$\{[Cu_4(\mu\text{-}OH)_2(\mu\text{-}bdc)_2(\mu_4\text{-}rac\text{-}btrip)_3]\cdot(NO_3)_2(H_2O)_{10}\}_n$ **16**. The novel three-dimensional coordination polymer is constructed from tetranuclear $Cu_4(\mu\text{-}OH)_2$ SBU, which are crossliked to each other through the both ligands bdc^{2-} and *rac*-btrip to form a complicated 3D coordination polymer based on mixed ligands with opened rhombic channels along **c** axis. *Rac-btrip* ligand exhibit disorder with methyl group; therefore it is not possible to investigate the chirality in this compound.

In the attempted synthesis of other mixed-ligand coordination polymers only one of the ligands was incorporated into the product as became evident from their single-crystal X-ray diffraction analysis. When bdc^{2-} and *rac*-btrip were tried to combine with $Cu(BF_4)_2\cdot 6H_2O$ for **17** or $CuSO_4$ for **18** in the presence of NH_3 solution under identical hydrothermal conditions for **16** the successfully crystallized products only contained the *rac*-btrip ligand in 3D-$\{[Cu_4(\mu_4\text{-}Cl)(\mu_4\text{-}rac\text{-}btrip)_4(H_2O)_4]$ $(BF_4/ClO_4/OH)^-_7\cdot xH_2O\}_n$ **17**, and in 3D-$\{[Cu(\mu_4\text{-}rac\text{-}btrip)(SO_4)]\cdot H_2O\}_n$ **18**. The inorganic anion of different copper salts has an important influence to change the structure of resulting crystallized products.

In 3D-$\{[Cu_4(\mu_4\text{-}Cl)(\mu_4\text{-}rac\text{-}btrip)_4(H_2O)_4]$ $(BF_4/ClO_4/OH)^-_7\cdot xH_2O\}_n$ **17**, the structure contains tetranuclear copper cluster $[Cu_4(\mu_4\text{-}Cl)(triazolyl)_4(H_2O)_4]^{7+}$ as secondary building unit SBU. Topologically, each $[Cu_4(\mu_4\text{-}Cl)(triazolyl)_4(H_2O)_4]^{7+}$ SBU can be simplified as a 8-connected unit, and the ligand as a linker. So that a 3D-cationic framework is defined as 3D-(2,8)-

connected network. In 3D-{[Cu(μ_4-*rac*-btrip)(SO_4)]·H_2O}$_n$ **18**, Each trans-bent *rac*-btrip ligand coordinates four Cu(II) atoms as μ_4-tetradentate ligand and extend in four different directions, which lead to formation of a 3D network with square channels along ***a*** axis.

Benzene-1,3,5-tricarboxylate btc^{3-} and *rac*-btrip were reacted with zinc nitrate hydrate for **19** or zinc bromide for **20** in the presence of Et_3N solution for deprotonation of the carboxylic acid under hydrothermal conditions 125 °C for 2 days. The following chiral coordination polymers 2D-{[Zn(μ-Hbtc)(μ-*R*-btrip)]·H_2O}$_n$ **19** and 2D-{[Zn(μ-Hbtc)(μ-*S*-btrip)]·H_2O}$_n$ **20** could be obtained as single crystals, structurally characterized and they are examples of spontaneous resolution as a racemic conglomerate. The homochiral crystals contain only one of the enantiomers from the *rac*-btrip ligand. The zinc atom shows a pseudo-tetrahedral environment from both ligands *R* or *S*-btrip and $Hbtc^{2-}$ anions. The compounds **19** and **20** are constructed as 2D 4,4-net. The coordination mode of ligands lead to two fold interpenetrative 2D-4,4 rhombic helical chiral networks.

The reaction of other zinc salts ($ZnBr_2$, $Zn(ClO_4)_2·6H_2O$ and $Zn(OAc)_2·2H_2O$) with btc^{3-} and *rac*-btrip in the same condition for compounds **19** and **20** lead to obtain single crystals which are characterized by ^{1}H NMR, IR and PXRD. The results show that the new compounds **21**, **22** and **23** are isomorphous to compounds **19** and **20**. The inorganic anion of different zinc salts do not has any influence to change the structure of resulting coordination polymer.

It was noted that, in the previous structure of compounds **19** and **20**, the third carboxyl group of $Hbtc^{2-}$ ligand stayed protonated and not coordinated therefore, a same synthetic procedure was used to prepare new 2D-coordination polymer of zinc(II) atom with new mixed ligands. Such as isophthalic acid (H_2ip), 5-amino isophthalic acid (H_2aip) and 4,6-dimethyl-5-aminoisophthalic acid (dm-H_2aip) instead of monohydrogen 1,3,5-benzenetricarboxylic acid ($Hbtc^{2-}$) with *rac*-1,2-bis(1,2,4-triazol-4-yl)propane (*rac*-btrip). 2D-[Zn(μ_3-aip)(H_2O)]$_n$ **40**, previously reported [149], consists of infinite layers of alternating three-coordinated Zn(II) cations and aip^{2-} anions to yield $(Zn)_3(aip)_3$ rings.

Attempts to incorporate the 4,4`-bis(1,2,4-triazol-4-yl) (btr) ligand under identical hydrothermal conditions for compounds **19** and **20** lead to its decomposition with formation of 4-amino-1,2,4-triazol-4-yl (atr) as evidenced by the structural charactization of 2D-[Cu_3(μ_6-btc)(μ-btc)(μ-atr)(H_2O)$_5$]$_n$ **24**, previously reported in reference [114] as 2D-waved layers, where 2D-layers are polycatenated along ***b*** axis to form 3D-network, and novel 1D-{[Cd_2(μ_2-btc)$_2$(atr)$_2$(H_2O)$_4$][Cd(H_2O)$_6$]·$2H_2O$}$_n$ **25** was obtained under the same hydrothermal conditions for compounds **24** as an infinite 1D-anionic chains, where cationic aqua complexes are located between chains and equal its negative charge.

2D-$[Cd(\mu_3\text{-Hbtc})(H_2O)_2]_n$ **26**, previously reported in reference [145], was obtained under just identical hydrothermal synthesis conditions for compound **25**, but 140 °C was used intead 125 °C. The 4,4`-bis(1,2,4-triazol-4-yl) (btr) ligand was not appeared in the structure due to its complectly decomposition at high temperature. In 2D-$[Cd(\mu_3\text{-Hbtc})(H_2O)_2]_n$, the Cd atoms and $Hbtc^{2-}$ anions form a 2D-network. The layers are parallel to each other.

Novel 2D-$\{[Cu_2(\mu\text{-Br})_2(\mu_4\text{-}rac\text{-btrip})]\cdot H_2O/MeOH\}_n$ **27**, 3D-$\{[Cu_2(\mu_4\text{-}rac\text{-btrip})_2]\ SO_4\cdot xH_2O\}_n$ **28** and 3D-$\{[Cu(\mu_4\text{-}rac\text{-btrip})]\ CH_3COO\cdot xH_2O\}_n$ **29** are obtained under the solvothermal reaction, when the ligands H_3btc and *rac*-btrip are react with copper salts ($CuBr_2$ for **27**, $CuSO_4\cdot 5H_2O$ for **28** and $Cu(OAc)_2\cdot H_2O$ for **29**). In **27**, each bromide anion bridges between two Cu atoms. Each trans-bent *rac*-btrip ligand coordinates four Cu(I) atoms and linked between two neighboring chains to form extend 2D-networks parallel to **ac** plane. The 2D-networks are stacked paralleled to each other along the lattice **b** axis. **28** and **29** are isomorphous, the Cu(I) atoms display a distorted tetrahedral coordination geometry, coordinated by four nitrogen atoms from four *rac*-btrip ligands and each trans-bent *rac*-btrip ligand coordinates four Cu (I) atoms in a μ_4-tetradentate fashion and extend in four different directions alternatively, which leading to formation of a 3D cationic network with rhombic channels along ***c*** axis.

Other attempts through variation of the metal salt ($Cu(NO_3)_2\cdot 2.5H_2O$ for **30**, $Cu(BF_4)_2\cdot 6H_2O$ for **31**and $CuCl_2$ for **32**) lead to obtain single crystals which are characterized by ^{1}H NMR, IR and PXRD. The crystals were not determenated by SCXRD, because the aim of synthesis to obtain coordination polymers with mixed ligands. The inorganic anion of different copper salts has an influence to change the structure of resulting coordination polymer.

In the attempted synthesis of mixed-ligand coordination polymers with other metal only one of the ligands was incorporated into the product as became evident from their single-crystal X-ray diffraction analysis. When H_3btc and *rac*-btrip were tried to combine with $Cu(NO_3)_2\cdot 2.5H_2O$ for **33** or $Cu(OAc)_2\cdot H_2O$ for **34** in the presence of Et_3N solution under identical hydrothermal conditions for compounds **19** and **20**, the successfully crystallized products only contained the btc ligand in 3D-$\{[Cu(CH_3CN)_4][Cu_3(\mu_6\text{-btc})_2]_2(NO_3/O_2CCH_3)\cdot(H_2O,\ CH_3CN)_x\}_n$ **33** and **34,** Both compounds crystallize isomorphous consisting of a nanoporous framework (HKUST-1) 3D-$[Cu_3(\mu_6\text{-btc})_2(H_2O)_3]_n$ accommodating molecular complexes cations $[Cu(CH_3CN)_4]^+$, which were occupied as noncoordinating guests in the octahedral cages of HKUST-1. Thermogravimetric analysis indicates that, the framework is stable up to ~300°C.

Two isomorphous 1D-coordination polymers 1D-$[M_3(\mu_3\text{-btc})(\mu_2\text{-btc})(H_2O)_{12}]_n$ (M = Zn, **35** and Co, **39**) have been synthesized in different conditions with mixed-ligand, which previously

analogous reported Co-polymer [5a],[147] and Zn-polymer [5a,l]. The polymer exist as a zigzag chain with both bridging and terminal M^{2+} ions through bidentate chelating or monodentate fashion of carboxyl groups and each metal centre is coordinated to four water molecules.

The Reaction of other zinc salts ($ZnBr_2$ for **36**, $Zn(ClO_4)_2 \cdot 6H_2O$ for **37** and $ZnCl_2$ for **38**) with btc^{3-} and btr in the same condition for compounds **35** lead to obtain single crystals which are characterized by ^1H NMR, IR and PXRD. The results show that the new compounds **36**, **37** and **38** are isostructural to compounds **35** and **39**. The inorganic anion of different zinc salts do not has any influence to change the structure of resulting coordination polymer.

In the attempted synthesis of other mixed-ligand coordination polymers only one of the ligands was incorporated into the product or ligand was crystallized as became evident from their single-crystal X-ray diffraction analysis, when azolate ligands (benzene tetrazolate and carboxylate ligands) were tried to combine with different metal salts in different used base under hydrothermal or solvothermal synthesis.

As some literatures have been reported that the dimensionality of resulting coordination framework of topology constructed by metal ions and btc is extremely dependent on the deprotonation degree of H_3btc [145b],[148]. According of the dissociation constants of H_3btc (pKa_1 =2:12, pKa_2 = 3:89, pKa_3 = 5:20) [153], a reasonable for the success of the approach results of MOF-synthesis is, that the controlling of the deprotonation degree of H_3btc ligand to influence the high dimensionality coordination network. This can do it by using Et_3N as the base to deprotonate H_3btc. The deprotonation of H_3btc ligand lead to higher homogeneity in hydrothermal reaction and great probably to synthesis better crystals.

The successful controlling of the deprotonation degree of H_3btc resulted in a high dimensionality of resulting coordination topology. Other influence for coordination polymer synthesis is the reaction mechanism. It is not easy to exactly now and understand it, because there are many factors that can influence the structures of the frameworks and especially the complex redox reactions that could be happened around the Cu-atom in $[Cu(CH_3CN)_4]^+$ cations as in **33** and **34**.

Coordination polymers are mostly structurally characterized by single crystal X-ray diffraction, powder X-ray diffraction (PXRD), elemental analysis, thermogravimetric analysis (TGA), infrared (IR) and ^1H-NMR spectra.

9 Instruments, Chemicals and General crystallization methods

9.1 Instruments

9.1.1 Crystal Images

The light microscopy images were observed with a **Leica *MS5*** binocular eyepiece with transmitted light and polarization filter. The images were taken with a **Nikon *COOLPIX 4500*** digital camera through a special ocular connection.

9.1.2 Melting Point

Melting points of the synthesized ligands were measured by **BÜCHI B-540** in open glass capillaries with heating rate 3°C/min in a melting point regulation apparatus. The measured data are not corrected.

9.1.3 Elemental analyses

Elemental analyses were performed on a **Vario Micro Cube** from Elementar GmbH in Heinrich Heine University Düsseldorf.

9.1.4 Infrared spectroscopy

Infrared spectra were recorded by a **Bruker Optik TENSOR 37** spectrophotometer with a **Diamond ATR (Attenuated Total Reflection) unit**. Medium Infrared spectra (MIR) were measured from 4000 to 400 cm^{-1}. Opus was the software used to edit the IR spectra while Origin 8.1 was used to compare the IR spectra. The following abbreviations were used to classify spectral bands: br (broad), sh (shoulder), very weak (vw), w (weak), m (medium), s (strong) and vs (very strong).

9.1.5 Nuclear magnetic resonance (NMR) spectroscopy

The NMR spectra were recorded either on a **Bruker Advance DRX 200 MHz** NMR spectrometer or on a **Bruker Advance DRX 500 MHz** NMR spectrometer with calibration against solvent signal.

The paramagnetic d^9-copper(II) compounds, which were not suitable for NMR analysis must be reduced to diamagnetic d^{10}-sytem copper(I) by the sodium cyanide, which then could be analyzed by NMR. Therefore, the dry crystals of copper(II) complexes were dissolved in

DMSO-d_6 and sodium cyanide was added to this solution then heated briefly in an ultrasonic bath. The reaction was usually observed by a color change of the solution.

^{1}H-NMR: ^{1}H-NMR spectra were measured either at 200 MHz or 500 MHz and calibrated against the residual protonated solvent signals: D_2O (4.79 ppm), CD_2Cl_2 (5.47 ppm) and DMSO-d_6 (2.50 ppm). The multiplicity was specified with s (singlet), d (doublet), t (triplet), q (quartet) and m (multiplet).

^{13}C-NMR: ^{13}C-NMR spectra were measured either at 50 MHz or 125 MHz with ^{1}H-broadband decoupling and the calibration was carried out against the used solvent: DMSO-d_6 (39.52 ppm).

9.1.6 Thermogravimetric analyses

Thermogravimetric analysis was carried out in a simultaneous thermoanalysis apparatus **TG 209 F3** from **NETZSCH GmbH** under flowing nitrogen gas 10-30 ml/min with a heating rate 5-10°C min^{-1} in the temperature range from 26 °C to 600 °C using **Al crucible**.

9.1.7 Porosity measurement

A porosity measurement for a dry sample was carried out by **Quantachrome Autosorb NOVA 4000e** automated gas sorption system. The DFT calculations were made using the Nova Win 11.03 software employing the (N_2 at 77 K, slit pore, NL-DFT equilibrium) model. Theoretical porosity calculations for the potential solvent volume in the solvent-depleted single-crystal X-ray structures are carried out with PLATON calc void/solv [103],[154].

9.1.8 Structure determination

Suitable single crystals were carefully selected under a polarizing microscope. The single crystals were mounted in oil.

9.1.8.1 Data collection

The X-ray structure analyses for the single crystals were carried out by a **Bruker AXS** microsource with **APEX II CCD** area-detector diffractometer. Temperatures are specified in Crystal Data Tables, **appendix** 11.1, Mo-Kα radiation (λ = 0.71073 Å) microsource, multilayer mirror monochromator, double-pass method phi and ω-scans. Data collection with **APEX II** [155] and cell refinement were accomplished with **SMART**, data reduction with **SAINT** [156] and experimental absorption correction with **SADABS** [157].

9.1.8.2 Structure analysis and refinement

The structures were solved by direct methods, **SHELXS-97** [158]. The refinement was carried out by full-matrix least squares on F^2 using the SHELXL-97 software suite [159]. All non-hydrogen positions were found and refined with anisotropic temperature factors.

Hydrogen atoms on the aromatic rings and the carbon atoms were placed geometrically at calculated positions with an appropriate riding model (AFIX 43 for aromatic CH, AFIX 13 for aliphatic CH, AFIX 23 for CH_2 and AFIX 137 for CH_3) and an isotropic temperature factor of $U_{iso}(H) = 1.2\ U_{eq}(CH, CH_2)$ and $1.5\ U_{eq}(CH_3)$. Hydrogen atoms on nitrogen atoms and on oxygen atoms were refined with $U_{iso}(H) = 1.5\ U_{eq}(N)$ and $U_{iso}(H) = 1.2\ U_{eq}(O)$. In case they were not found, they were placed at calculated positions with an appropriate riding model (AFIX 13 for NH, AFIX 23 for NH_2). The hydrogen atoms of protonated amine/ammonium ligands were calculated as an idealized NH_3 group with tetrahedral angles in a rotating group refinement (AFIX 137) with $U_{iso}(H) = 1.5\ U_{eq}(N)$. Hydrogen atoms of OH-groups were calculated as idealized OH-group in a rotating group refinement (AFIX 147) with $U_{iso}(H) = 1.2\ U_{eq}(O)$.

Details of the X-ray structure determinations and refinements are provided in the tables in **Appendix** 11.1 crystal data and structure refinement. Void volumes and residual electrons in voids were carried out with PLATON for Windows.

Graphics were drawn by **DIAMOND (Version 3.2)** [160]. Displacement ellipsoids were drawn at the 50% probability level and H atoms were shown as spheres of arbitrary radii.

9.1.9 X-ray powder diffractometry

Powder X-ray diffraction patterns were measured at ambient temperature by using a **Bruker AXS D2 PHASER** with transmission image-plate, Cu-Kα radiation (λ = 1.54184 Å) and stationary flat panel samples. The **D2 PHASER** uses X-ray powder diffraction (in the classic Bragg Brentano configuration) to obtain high quality data for applications , **LYNXEYE™** compound silicon-strip X-ray detector technology (monochromator) to collect high quality data with unprecedented speed and nickel filter in the range 2θ = 5–50° (step 0.02° in 2θ). Simulated powder patterns were based on single-crystal data and calculated using the **STOE Win^{XPOW}** software package [161].

9.2 Chemicals

Reagents and solvents were obtained from commercial sources and used without any further purification. *N,N`*-dimethylformamide has been dried for 2 days over $MgSO_4$, distilled and stored under inert gas. The used chemicals and their source are listed in Table 8.2.1.

Table 8.2.1: Manufacturer data of the used chemicals.

Chemicals	**Source**
1,3,5-benzenetricarboxylic acid	Merck, Aldrich
1,3-benzendicarbxylic acid	Aldrich
1,4-benzendicarbxylic acid	Aldrich, Acros
4-aminopyridine	Acros Organics
acetonitrile	Sigma-Aldrich
activated carbon	Sigma-Aldrich
cadmium(II) nitrate hexahydrate	Merck
cadmium(II) nitrate tetrahydrate	Merck
cadmium(II) acetate dihydrate	Fluka
cadmium(II) bromide tetrahydrate	Aldrich
cadmium(II) chloride	Merck, Fluka
cadmium(II) nitrate tetrahydrate	Merck
cadmium(II) perchlorate hexahydrate	Aldrich
cadmium(II) sulfate hydrate	Acros
chloroform	Aldrich, Merck
chloroform-d	Sigma-Aldrich
copper(II) acetate monohydrate	Fluka
copper(II) bromide (anhydrous)	Janssen
copper(II) chloride (anhydrous)	Sigma-Aldrich, Merck
copper(II) chloride dehydrate	Merck
copper(II) perchlorate hexahydrate	Sigma-Aldrich
copper(II) sulfate pentahydrate	Aldrich, Acros
copper(II) tetrafluoroborate hexahydrate	Uni. Freiburg, Alfa

Chemicals	Source
deuterium oxide	Deutero GmbH
dichloromethane	Sigma-Aldrich, Acros
diethyl ether	Merck, Sigma-Aldrich
dimethyl sulfoxide-d_6	Deutero GmbH
dimethylsulfoxide	Roth
ethanol (synthesis grade)	VWR
hydrazine monohydrate	Sigma-Aldrich, Merck
iron(III) nitrate nonahydrate	Fluka
propane-1,2-diamine	Aldrich
isopropanol (p.a.)	Aldrich
magnesium(II) sulphate	Aldrich
manganese(II) chloride	Alfa Aesar
manganese(II) nitrate tetrahydrate	Roth
manganese(II) perchlorate hexahydrat	Aldrich
methanol (abs.)	Aldrich, H2O < 0.01%
methanol (Uvasol)	Merck
N,N-dimethylacetamide	VWR
N,N-dimethylformamide	Roth, Alfa Aesar
nickel(II) bromide	Aldrich
nickel(II) chloride	Uni. Freiburg
nickel(II) perchlorate hexahydrate	Aldrich
nickel(II) nitrate hexahydrate	Uni. Freiburg
potassium carbonate	Uni. Duesseldorf
p-toluenesulfonic acid monohydrate	Merck, Acros
silica gel	Sigma-Aldrich
sodium carbonate	Uni. Duesseldorf
sodium chloride	Carl Roth GmbH
sodium cyanide	Fluka
sodium hydrogen carbonate	Merck

Chemicals	Source
sodium sulfat	Grüssing
terephthalonitrile	Aldrich
thionyl chloride	Merck, Acros
toluene	Merck
triethylamine (synthesis grade)	Uni. Duesseldorf
water	deionized, Uni. Duesseldorf
zinc(II) nitrate hexahydrate	Merck
zinc(II) nitrate tetrahydrate	Merck
zinc(II) bromide	Fluka
zinc(II) chloride	Merck
zinc(II) perchlorate hexahydrate	Aldrich
zinc(II) sulfate heptahydrate	Uni. Freiburg
zink(II) acetate dihydrat	Uni. Freiburg
copper(II) nitrate 2.5 hydrate	Aldrich, Riedel-de Haën

9.3 General crystalization methods [162]

Practically, every chemist knows the necessity of re-crystallization as a method of purification. For structure determination of a compound using single crystal X-ray diffraction, it is essential to obtain good quality single crystals with as less defects as possible. The crystal should be sufficiently large, a true single crystal of good regularity and low mosaicity. Crystals quality is usually better if the crystals grow slowly at low temperatures and as undisturbed as possible from shocks, vibrations or other movements. Crystal growing is an art and there are as many variations to the basic crystal growing recipes as there are crystallographers. The chosen techniques will largely depend on the chemical properties of the compound of interest:

Is the compound air sensitive, moisture sensitive? Is it hygroscopic? etc.

A common problem with coordination polymer crystallization is that once the polymer is formed, dissolution leads to dissociation of the metal-lgand bonds and a true re-crystallization as for molecular compounds is not possible. The following methods (Figure 8.3.1) were used or attempted in order to obtain a good regularity single crystal suitable for X-ray diffraction study directly upon formation of the coordination polymer compound. The first four methods are quite common for molecular compounds, whereas the next methods were more successful for coordination polymers.

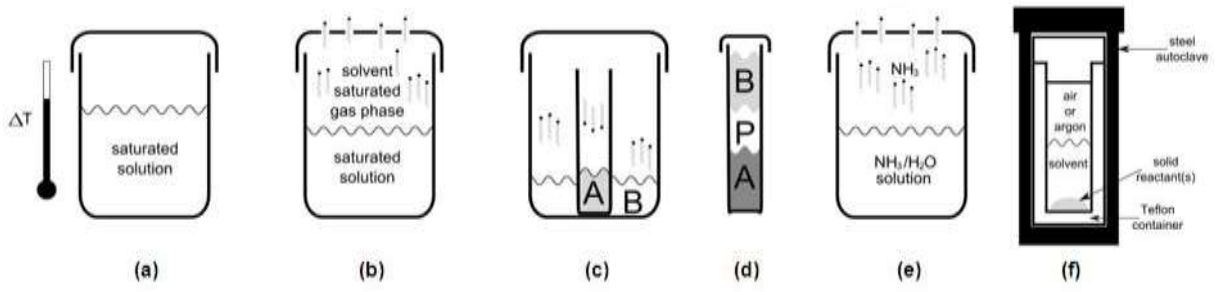

Fig. 8.3.1: Schematic description of the different crystallization methods: (a) by slowly cooling; (b) by slow evaporation; (c) by vapour diffusion; (d) by liquid diffusion; (e) evaporation of a volatile ligand; (f) Hydrothermal-, Solvothermal-synthesis [162a].

9.3.1 Crystallization by cooling (classical re-crystallization)

To obtain crystals with this method, all reactants should be completely dissolved (or soluble). The product was dissolved then the solution is filtered or a saturated solution is produced directly from the reactants. The obtained saturated solution is placed in a refrigerator. Better crystals may form or be induced from single solvent solution.

Another possibility is to allow the warm solution to cool slowly to room temperature. A saturated solution of the compound was prepared where the solvent was heated to about its boiling point. The solution was transferred to a test tube and sealed. Then the test tube was transferred to a Dewar flask in hot water (heated to a temperature below the solvent boiling point). The water level should exceed the solvent level in the test tube, but should not exceed the height of the test tube. The Dewar should be capped and left for several days. (Fig. 8.3.1a).

9.3.2 Slow solvent evaporation

This method is the simplest technique for air stable samples to obtain crystals through solvent evaporation with complete solubility of the reactants and the product. The solution of the reactants is filled in a vial or a test tube, which was covered with parafilm. A thin wire is used to make small holes in the cover where the solvent can slowly evaporate. The rate of the evaporation can be varied though the size or the number of holes. After a few days, the solution is saturated then the crystals start growing on the side of the vial or the test tube (Fig. 8.3.1b). Another variation by using this method with two solvents. A requirement for this variant is that the product is more soluble in a volatile first solvent and less or non-soluble in the second solvent. A saturated solution of the product is prepared and the second solvent is added. The mixed solvent solution is left for slow solvent evaporation as described above. The more volatile solvent evaporates first and as the solvent rate changes crystal growth sets in.

9.3.3 Slow vapour diffusion

This method is applicable to mg quantities of the sample. To obtain crystals through solvent evaporation, it is important that, the complete solubility of the reactants and the product in

one solvent but the insolubility of the product in a volatile solvent. The method works best if the solution solvent of sample is the less volatile and the second solvent vapor diffuses into the sample solution. Therefore, a small vessel is filled with a solution of the reactants or product. This vessel is placed in a second larger vessel containing the second solvent. The whole system is sealed. The second solvent evaporates and gets resolved in the solution containing the product to give a mixed solvent system. Over time crystals start growing slowly (Fig. 8.3.1c).

9.3.4 Slow liquid diffusion

This method is applicable to mg quantities of air or solvent sensitive samples. A solution of the reactants or product is filled into a vessel and the second solvent is carefully added to the top of the solution. But if the solubility of the product is very low in the second solvent, precipitation can occur on the transition phase between the layers. A good solvent combination is CH_2Cl_2/EtOH. The vessels should not be moved until diffusion is complete. This will only be successful if the density of the second solvent smaller than the first solvent and care is exercised in creating the solvent layer. Different forms of vessels are common for slow liquid diffusion (Fig. 8.3.1d).

9.3.5 Evaporation of volatile ligand

Ammonia (NH_3) forms labile amine complexes with some transition metals (such as Ag^+, Cd^{2+}, Co^{2+}, Cu^{2+}, Ni^{2+} and Zn^{2+}). Due to this, it is possible to solve a metal-organic framework in aqueous ammonia solution. By slowly evaporation of the ammonia, the metal-organic framework can re-crystallize (Fig. 8.3.1e).

9.3.6 Hydrothermal-, Solvothermal-synthesis

The hydrothermal-, solvothermal synthesis can be used when one, or both, of the reactants do not dissolve well. A mixture of the reactants and the solvent are filled into a Teflon container with Teflon lid. This Teflon container is placed into a steel autoclave, which keeps the Teflon container sealed at high pressures (Fig. 8.3.1f). The reaction mixture is heated up

to a temperature ~10-30% above the boiling point of the solvent. This temperature is kept for 2 to 4 days and then it is slowly cooled to room temperature.

The cooling rate has a main influence on the crystal growth. Different rate can lead to different crystal sizes or even different structures and compounds with different stoichiometry. We used in this work mostly hydrothermal-, solvothermal-synthesis, to obtain a good regularity single crystal suitable for X-ray diffraction measurements by using a suitable DURAN® culture glass tube for coordination polymer synthesis up to 150°C instead autoclave.

DURAN® culture glass tubes with PTFE-faced sealing wad, diameter 12 mm, height 100 mm and DIN thread 14 GL, which can were closed with red PBT screw cap, so that the tubes are suitable for the cultivation of microorganisms, substance storage, or hydro- solvothermal synthesis etc. The contents only come into contact with the glass and PTFE seal.

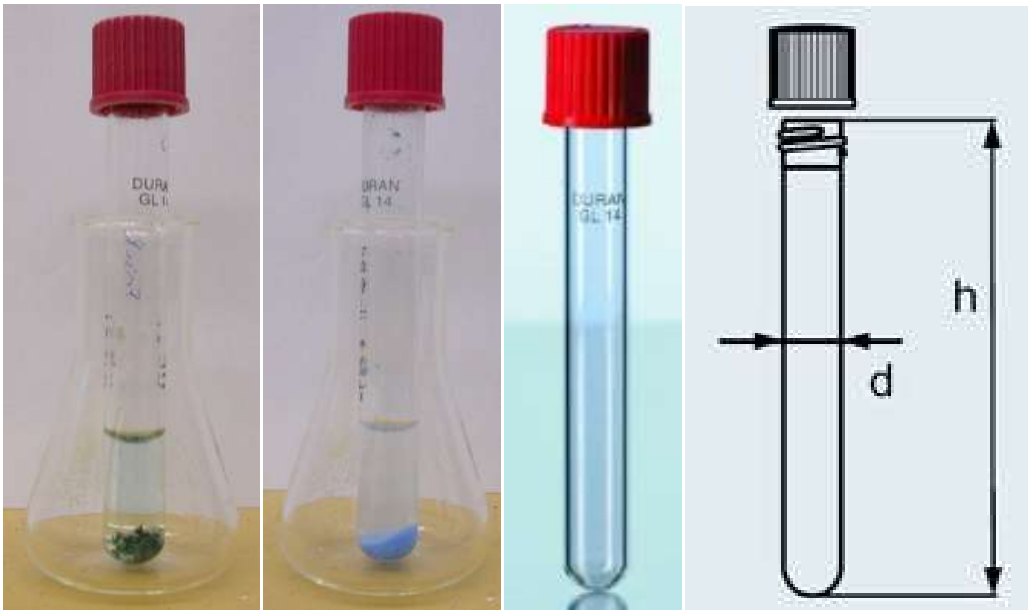

10 Experimental section (Synthesis of ligands and coordination polymers)

10.1 Synthesis of ligands

10.1.1 Synthesis of *N,N`*-dimethylformamide azine (1)

a) Synthesis of *N,N`*-dimethylformamide azine dihydrochloride [85],[87].

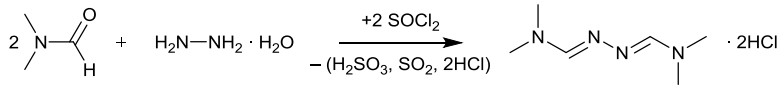

Thionyl chloride (v = 57 ml, 99.7%, n = 0.78 mol) was added slowly dropwise to freshly dried DMF (v = 300 ml, 99.8%, n = 3.85 mol) at 0 °C in ice bath, after then the reaction mixture was stirred for 24 h at RT. A solution of hydrazine monohydrate (v = 16 ml, 98%, n = 0.32 mol, 0.5 eq) in dried DMF (40 ml) was added dropwise to the resulted yellow solution, after then the mixture was stirred for 1-2 days at RT. The formed white precipitate was filtered off, washed with dried DMF (3 x 40 ml) and dried under vacuum.

Molecular formula ($C_6H_{16}Cl_2N_4$), M_w: 215.12 g mol^{-1}, yield: 66.3 g, 0.3 mol, 93 %, based on hydrazine monohydrate.

^{1}H NMR (200 MHz, MeOD-d_4): δ/ppm = 2.75 (s, 12H, 4CH_3), 7.7 (s, 2H, 2CH)

IR (ATR) v/cm^{-1}: 408.5(w), 436.4(m), 484.9(m), 532.8(w), 715.7(m), 759.2(s), 876(w), 1030,8(m), 1051.4(m), 1131.4(m), 1227.8(w), 1258.7(w), 1297.5(s), 1400.5(w), 1448.2(m), 1503(m), 1703.2(s), 2576.8(s), 2939.9(w).

b) Neutralization of *N,N`*-dimethylformamide azine DMFA [87a]

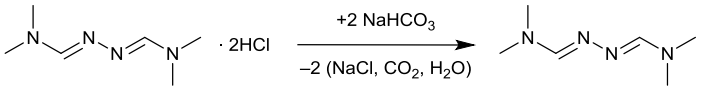

A solution of *N,N`*-dimethylformamide azine dihydrochloride (m = 66.3 g, n = 0.3 mol) in water 100 ml was added, for neutralization, to a solution of sodium hydrogen carbonate (m = 63 g, n = 0.75 mol, 2.5 eq) in water 100 ml. After stirring for 2 h at RT, the reaction mixture was extracted with dichloromethane (13 x 20 ml). The organic phase was dried over anhydrous sodium sulfate 5 g for 3 h with stirring. The solvent was removed under reduced pressure by using rotatory evaporator at 40-50 °C. The obtained product was allowed to stand in air for drying.

Molecular formula ($C_6H_{14}N_4$), M_w: 142.2 g mol^{-1}, yield: 92 %

^{1}H NMR (200 MHz, DMSO-d_6): δ/ppm = 2.75 (s, 12H, 4CH_3), 7.7 (s, 2H, 2CH)

IR (ATR) ν/cm^{-1}: 668.3(w), 879.9(w), 962.5(m), 1093.4(s), 1144(w), 1252.7(m), 1322.7(m), 1365.8(s), 1411.7(m), 1430.2(m), 1477.7(m), 1616.3(s), 1692.2(w), 1930.1(w), 1988.3(w), 2006.2(w), 2026.2(w), 2034.2(w), 2130.7(w), 2288.9(w), 2806.2(m), 2890.6(m).

10.1.2 Synthesis of *5*-(1,2,4-triazol-4-yl)isophthalic acid (5H_2iptr) (2)

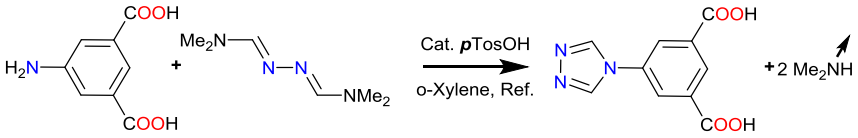

a) Synthesis [88],[29a,b]: The reaction was carried out under inert conditions. *5*-Aminoisophthalic acid (m = 9:53 g, 95%, n = 49.98 mmol), *N,N`*-dimethylformamide azine (m = 8.60 g, n = 60.47 mmol, 1.2 eq) and *p*-toluenesulfonic acid monohydrate as catalyst (m = 1,022 g, n = 5.26 mmol, 0.1 eq) were mixed and refluxed in dried *o*-xylene 50 ml for 2 d. until the solid color change from brown to white (light gray), and no more *N,N`*-dimethylamine gas formation could be detected by using wet pH paper which exposed to the exhaust gas (color change to basic). After refluxing, the solvent was decanted.

b) Purification: *5*-(1,2,4-Triazol-4-yl)isophthalic acid (5H_2iptr) was purified by dissolving in KOH solution (m = 5.92 g, n = 105 mmol, 2 eq) in water 75 ml pH > 10, stirred for 10 min. and filtered. After then diluted HCl solution (100 ml, 1M) was added to filtrate up to no more white precipitate was formed pH < 2. The product was filtered and washed several times with the water until the pH filtrate value has the same pH of deionized water. At the end, the obtained leight brown precipitate was dried in vacuum oven at 40 °C.

Molecular formula ($C_{10}H_7N_3O_4$), M_w: 233.18 g mol^{-1}, yield: 7.9 g, 33.8 mmol, 68 %, based on 5-aminoisophthalic acid.

^{1}H NMR (200 MHz, DMSO-d_6): δ/ppm = 8.4 (s, 2H, arom. C-**H**), 8.5 (s, 1H, arom. C-**H**), 9.3 (s, 2H, triazol C-**H**), 13.6 (b, 2H, 2 COO**H**).

10.1.3 Synthesis of *n*-(1,2,4-triazol-4-yl)pyridine (npytr, n = 3 or 4, 3 & 4)

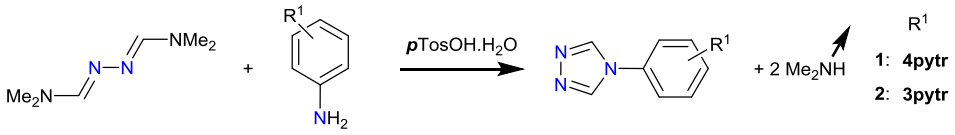

a) Synthesis: The reaction was carried out under inert conditions. *n*-aminopyridine (n = 3 or 4) (m = 1.88 g, 98%, n = 0.02 mol), *N,N`*-dimethylformamide azine (m = 3.13 g, n = 0.022 mol, 1.1 eq) and *p*-toluenesulfonic acid monohydrate as catalyst (m = 0.38 g, n = 0.002 mol, 0.1 eq) were mixed and refluxed in dried toluene 80 ml for 2-3 d. until no more *N,N`*-dimethylamine gas formation could be detected by using wet pH paper which exposed to the exhaust gas (color change to basic). After refluxing, the solvent was decanted.

b) Purification: *n*-(1,2,4-triazol-4-yl)pyridine (npytr, n = 3 or 4) was purified by washing with dichloromethane and after then dissolved in ethanol and the solution refluxed with active carbon for 0.5 h. After then it was filtered. The filtrate volume of the combined ethanol was reduced to ~10 ml after that was cooled to 0 °C in refrigerator. The white solid precipitate was separated by filtration, washed with cold diethyl ether or dichloromethane and dried in air.

Data analysis

For *3*-(1,2,4-triazol-4-yl)pyridin (3pytr, 3)

Molecular formula ($C_7H_6N_4$), M_w: 146.15 g mol^{-1}, yield: 0.7 g, 4.72 mmol, 23.6 % based on *3*-aminopyridine.

^{1}H NMR (200 MHz, D_2O-d_2): δ/ppm = 7.58 (dd, 1H, arom. C**H**), 8.00 (ddd, 1H, arom. C**H**), 8.57 (dd, 1H, arom. C**H**), 8.71 (d, 1H, arom. C**H**), 8.86 (s, 2H, triazole C**H**)

IR (ATR) v/cm^{-1}: 3121, 3098, 3066 (m), 3028, 2946 (m), 2536 (w), 1634 (m), 1586 (m), 1527 (s), 1515 (s), 1470 (m), 1436 (m), 1373 (m), 1304 (w), 1270, 1255 (s), 1241 (s), 1089 (s), 1011 (s), 947 (s), 868 (s), 812 (s), 702 (s), 632, 619 (s), 568 (w).

LR-MS (EI): m/z = 146 [M^+].

For *4*-(1,2,4-triazol-4-yl)pyridine (4pytr, 4)

Molecular formula ($C_7H_6N_4$), M_w: 146.15 g mol^{-1}, yield: 2.03 g, 13.8 mmol, 69.5 % based on *4*-aminopyridine.

^{1}H NMR (200 MHz, D_2O-d_2): δ/ppm = 7.6 (m, 2H, arom. C-**H**), 8.6 (m, 2H, arom. C-**H**), 9.0 (s, 2H, triazol C-**H**).

IR (ATR) v/cm^{-1}: 3096 (m), 3031 (m), 2323 (w), 1597 (s), 1525 (s), 1474 (w), 1426 (m), 1377 (m), 1353 (w), 1263 (m), 1246 (s), 1222 (m), 1091 (s), 1007 (w), 995 (m), 941 (w), 943 (m), 872 (m), 819 (s), 689 (s), 664 (m), 628 (s), 527 (s).

LR-MS (EI): m/z = 146 [M$^+$].

10.1.4 Synthesis of *rac*-1,2-bis(1,2,4-triazol-4-yl)propane (btrip, 5) and bis(1,2,4-triazol-4-yl) (btr, 6)

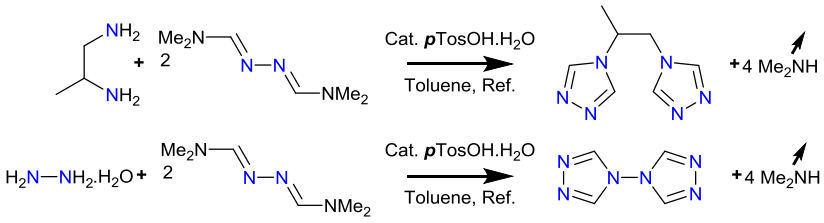

a) Synthesis: The reaction was carried out under inert conditions. Diamine derivates (*rac*-1,2-diaminopropane, hydrazinium hydroxid), *N,N`*-dimethylformamide azine (2.2 eq) and *p*-toluenesulfonic acid monohydrate as catalyst (0.2 eq) were mixed and refluxed in dried toluene 50-80 ml for 3-4 d. until no more *N,N`*-dimethylamine gas formation could be detected by using wet pH paper which exposed to the exhaust gas (color change to basic). After refluxing, the solvent was decanted.

Product	H_2N-R-NH_2	DMFA	*p*TosOH	Yield
rac-1,2-diaminopropane	v = 3.4 ml, ρ = 0.870, 99 %, n = 0.04 mol	m = 12.52 g, n = 0.088 mol, 2.2 eq	m = 1.52 g, n = 8 mmol, 0.2 eq	3.5 g, 19.55 mmol, 49 %
hydrazinium hydroxide (hydrazine monohydrate)	v = 1 ml, ρ = 1.03, 100 %, n = 0.02 mol	m = 6.26 g, n = 0.044 mol, 2.2 eq	m = 0.76 g, n = 4 mmol, 0.2 eq	0.7 g, 5 mmol, 25 %

b) Purification: *rac*-1,2-bis(1,2,4-triazol-4-yl)propane (btrip, **5**) or bis(1,2,4-triazol-4-yl) (btr, **6**) was purified by washing with dichloromethane and after then dissolved in ethanol and the solution refluxed with active carbon for 0.5 h. After then it was filtered. The filtrate volume of

the combined ethanol was reduced to ~10-15 ml after that was cooled to 0 °C. The white solid precipitate was separated by filtration, washed with cold diethyl ether or dichloromethane and dried in air.

Data analysis

For *rac*-1,2-bis(1,2,4-triazol-4-yl)propane (btrip, 5)

Molecular formula ($C_7H_{10}N_6$), M_w: 178.19 g mol^{-1}, yield: 3.5 g, 19.55 mmol, 49 % based on 1,2-diaminopropane.

^{1}H NMR (200 MHz, DMSO-d_6): δ/ppm = 1.50 (d, J = 6.9 Hz, 3H, C**H**$_3$), 4.48-4.42 (m, 1H, C**H**), 4.87-4.73 (m, 2H, C**H**$_2$), 8.25 (s, 2H, triazol C**H**), 8.48 (s, 2H, triazol C**H**).

IR (ATR) v/cm^{-1}: 3087 (m), 2982 (w), 1529 (s), 1463 (w), 1410 (w), 1386 (w), 1363 (w), 1336 (w), 1280 (w), 1226 (w), 1189 (s), 1125 (w), 1108 (m), 1020 (m), 971 (m), 887 (m), 841 (w), 668 (m), 641 (vs).

LR-MS (EI): m/z = 178 [M$^+$].

For bis(1,2,4-triazol-4-yl) (btr, 6)

Molecular formula ($C_4H_4N_6$), M_w: 136.11 g mol^{-1}, yield: 0.7 g, 5 mmol, 25 % based on hydrazinium hydroxide.

^{1}H NMR (500 MHz, DMSO-d_6): δ/ppm = 9.2 (s, 4H, triazole C**H**).

IR (ATR) v/cm^{-1}: 3144 (w), 3100 (m), 3079 (m), 3013 (w), 1492 (m), 1478 (m), 1290 (m), 1222 (w), 1199 (w), 1081 (s), 1058 (s), 979 (m), 924 (m), 876 (m), 870 (m), 684 (w), 606 (vs).

LR-MS (EI): m/z = 136 [M$^+$].

Elemental analysis (EA): calc.: C: 35.30 %, H: 2.96 %, N: 61.74 %, found C: 35.18 %, H: 3.12 %, N: 60.10 %.

10.1.5 Synthesis of 5-methyl-1H-tetrazolate (5met, 7)

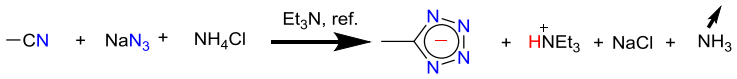

a) Synthesis [92e,f,j],[95a]: The reaction was carried out under inert conditions. Acetonitrile (v = 30 ml, ρ = 0.78, n = 0.5 mol), sodium azide (m = 16.3 g, n = 0.5 mol) and ammonium chloride as catalyst (m = 26.5 g, n = 0.5 mol) in molar ratio 1:1:1 eq were mixed, stirred and refluxed in concentration triethylamine 30 ml at 140-150°C for 2 d. After refluxing, the solvent was decanted.

b) Purification: The resulting precipitate consists of sodium chloride, the obtained product and non reacted sodium azide. To separate the product, the precipitate was washed with ethanol (4x20 ml) and filtered. The solvent of filtrate was removed at reduced pressure by using rotary evaporator. The product of triethylammonium-5-methyltetrazolate was dried in vacuum furnace.

Molecular formula ($C_8H_{19}N_5$), M_w: 185.27 g mol^{-1}, yield: 48.14 g, 0.26 mol, 52 % based on Acetonitrile.

^{1}H NMR (200 MHz, D_2O): δ/ppm = 1.2 (t, 3H, Et_3N, C**H$_3$**), 2.4 (s, 3H, 5met, C**H$_3$**), 3.1 (q, 2H, Et_3N, C**H$_2$**).

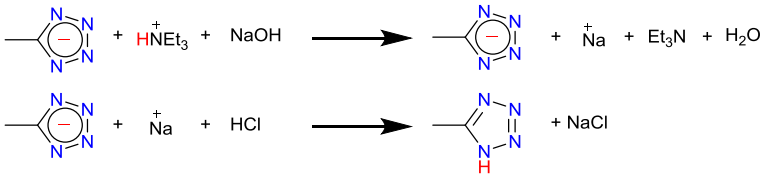

c) Neutralization [94]: The triethylammonium-5-methyltetrazolate (m = 48.14 g, n = 0,26 mol) was dissolved in water 100 ml, made basic with sodium hydroxide solution (m = 20.8 g in 100 ml, 1 eq) and evaporated to dryness at reduced pressure on a steam-bath by using rotary evaporator to remove amines like triethylamine and ammonia. The residue was redissolved in water 100 ml, acidified to pH 1-2 with diluted hydrochloric acid (24 ml, 37% in 100 ml water) and again evaporated to dryness at reduced pressure on a steam-bath by using rotary evaporator to remove the rest of hydrazoic acid (HN_3) and hydrochloric acid. The 5-methyl-1H-tetrazole was then extracted from the residue of sodium chloride with ethanol (4x20 ml) or methanol and recrystallized from toluol to give a white solid in a good purity.

Molecular formula ($C_2H_4N_4$), M_w: 84.08 g mol^{-1}, yield: 19.33 g, 0.23 mol, 88.4 % based on triethylammonium-5-methyltetrazolate.

^{1}H NMR (500 MHz, D_2O): δ/ppm = 2.5 (s, 3H, C**H$_3$**).

^{13}C{^{1}H}-NMR (125 MHz, D_2O): δ (ppm) = 8 (**C**H_3), 153,8 (**C**$_{tetrazole}$).

IR (ATR) v/cm^{-1}: 682,6(w), 807,4(w), 1036,8(m), 1058,2(m), 1172,5(m), 1256,9(m), 1390,7(s), 1443,2(w), 1475,5(sh), 1556,4(w), 1581,7(w), 1666,2(w), 1733,0(w), 2008,5(sh), 2496,0(w), 2800,7(m), 2978,0(m), 3116,4(m).

Elemental analysis (EA): calc.: C: 28.57 %, H: 4.80 %, N: 66.64 %, found C: 30.83 %, H: 4.68 %, N: 64.64 %.

LR-MS (GC-EI): m/z = 84 [M^{+}].

10.1.6 Synthesis of benzene-1,3-di(1H-tetrazol-5-yl) (H_2ipdt, 8) and benzene-1,4-di(1H-tetrazol-5-yl) (H_2bdt, 9)

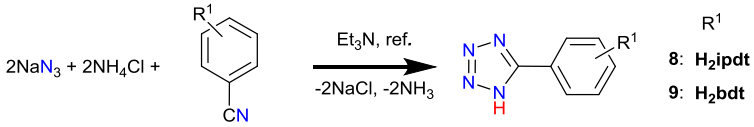

a) Synthesis [93]: The reaction was carried out under inert conditions. Benzene-1,3-dinitrile (m = 6.4 g, n = 0,05 mol), sodium azide (m = 6.6 g, n = 0.1 mol) and ammonium chloride as catalyst (m = 5.37 g, n = 0.1 mol) in molar ratio 1:2:2 eq were mixed, stirred and refluxed in concentration triethylamine as catalyst and solvent 50 ml at 140°C for 24 h. After refluxing, the solvent was removed at reduced pressure by using rotary evaporator.

The other ligand of **H_2bdt** was obtained as in the previous synthesis for **H_2ipdt**, where benzene-1,4-dinitrile was used as reagent instead of benzene-1,3-dinitrile and the reaction was refluxed for 48 h.

b) Purification: The resulting precipitate consists of sodium chloride, the obtained product and non reacted componentes. To separate the product, the reaction residue was dissolved in NaOH solution and filtered; the filtrate was acidified with diluted hydrochloric acid HCl to pH = 1-2. The product was stirred for 0.5 h and after then removed by filtration under low pressure, which was further purified by washing with several portions of distilled water and dried in vacuum furnace.

Data analysis

For benzene-1,3-di(1H-tetrazol-5-yl) (H_2ipdt, 8)

Molecular formula ($C_8H_6N_8$), M_w: 214,19 g mol^{-1}, yield: 10.94 g, 0.05 mol, 99.9 % based on benzene-1,3-dinitrile.

^{1}H NMR (200 MHz, DMSO-d_6): δ/ppm = 7.8 (t, 1H, arom. C-**H**), 8.1 (d, 1H, arom. C-**H**), 8.2 (d, 1H, arom. C-**H**), 8.7 (s, 1H, arom. C-**H**).

Elemental analysis (EA): calc.: C: 44.86 %, H: 2.82 %, N: 52.32 %, found C: 41.58 %, H: 3.29 %, N: 47.33 %.

LR-MS (EI): m/z = 214.07 [M^+].

For benzene-1,4-di(1H-tetrazol-5-yl) (H_2bdt, 9)

Molecular formula ($C_8H_6N_8$), M_w: 214,19 g mol^{-1}, yield: 8.9 g, 0.04 mol, 83 % based on benzene-1,4-dinitrile.

^{1}H NMR (200 MHz, DMSO-d_6): δ/ppm = 8.3 (s, 4H, arom. C-**H**).

Elemental analysis (EA): calc.: C: 44.86 %, H: 2.82 %, N: 52.32 %, Found C: 44.20 %, H: 2.54 %, N: 50.74 %.

LR-MS (EI): m/z = 214.07 [M^+].

10.1.7 Synthesis of *N,N`*-dimethylacetamide azine dihydrochloride (10)

a) General information: Toluene was dried by active molecular sieve. *N,N`*-dimethylacetamide (DMA) was dried with sodium sulfate anhydrous. It is important for synthesis, that to use more toluene, which forms a surface over the obtained product to protect it from moisture, because the product was hygroscopic. The *N,N`*-dimethylacetamide azine dihydrochloride is not well soluble in DMA and Et_2O, but very soluble in DCM, chloroform ($CHCl_3$) and DMF. *N,N`*-dimethylacetamide azine dihydrochloride can be obtain by using $POCl_3$ or $SOCl_2$ or by heating DMA with $N_2H_4.H_2O$.

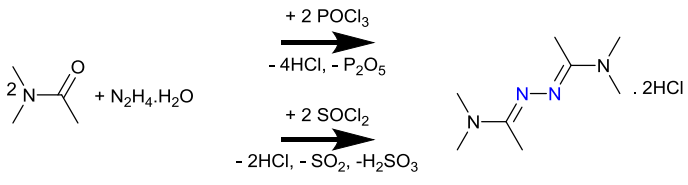

b) Synthesis: A solution of phosphorus oxychloride $POCl_3$ (v = 57 ml, n = 0.6 mol) in dried toluene (50 ml) was added dropwise to fresh dried DMA (v = 56 ml, n = 0.6 mol, 1 eq) in dried toluene (150 ml) at 0°C by using ice bath. Thereafter, the mixture was stirred overnight at room temperature. Thereafter, hydrazine monohydrate (v = 20 ml, n = 0.3 mol, 0.5 eq) was added slowly dropwise at RT. The reaction was then stirred further for 2 days at RT.

It is possible to obtain the *N,N`*-dimethylacetamide azine dihydrochloride by using thionyl chloride ($SOCl_2$) instead of phosphorus oxychloride $POCl_3$ under the same reaction conditions.

Fig. 9.1.7.1: The reaction flask after synthesis of *N,N`*-dimethylacetamide azine dihydrochloride by using $SOCl_2$ (left) or $POCl_3$ (right).

c) Purification: The *N,N`*-dimethylacetamide azine dihydrochloride was purified in $N_2$-atmosphere by using Schlenk technique. The toluene is first decanted. The yellow gel was suspended in *N,N`*-dimethylacetamide (4x20 ml). A heat development is happened. The yellow suspension is filtered off over a frit and in inert gas atmosphere. Thus, the product was separated from hydrochloric acid, residual phosphorus oxychloride, and other products. Then, the yellow solid was washed by diethyl ether (4x20 ml) to remove excess DMA. At the end, the product is dissolved in dichloromethane DCM (10x40 ml). Thus, the *N,N`*-dimethylacetamide azine dihydrochloride was separated from phosphorus pentaoxide P_2O_5. The dichloromethane is removed under high vacuum by using Schlenk technique.

Molecular formula ($C_8H_{20}Cl_2N_4$), M_w: 243.18 g mol^{-1}, yield: 40.73 g, 0.167 mol, 55.83 %, based on hydrazine monohydrate, when $POCl_3$ was used.

^{1}H NMR (500 MHz, $CDCl_3$): δ/ppm = 2.5 (s, 3H, -C**H$_3$**), 3.1 (s, 6H, -N-(C**H$_3$**)$_2$), 12.7 (s, 2H, N^+**H**Cl^-).

$^{13}C\{^{1}H\}$ NMR (125 MHz, $CDCl_3$): δ/ppm = 19 (s, 1C, -**C**H_3), 39 (s, 2C, -N-(**C**H_3)$_2$), 175 (s, 1C, N=**C**-N).

LR-MS (ESI): m/z = 171.16 [M+H^+], 172.0 [M+2H^+].

d) Neutralization: A red oil was obtained after neutralization, if the *N,N`*-dimethylacetamide azine dihydrochloride was neutralized in the same process as for *N,N`*-dimethylformamide azine dihydrochloride. Therefore, it is better to solve the *N,N`*-dimethylacetamide azine dihydrochloride in dried DCM and use the mixture of Na_2CO_3 with Na_2SO_4 or $MgSO_4$ anhydride for neutralization, because the neutralization reaction will give water molecules, which will be absorbed by Na_2SO_4 or $MgSO_4$ anhydride. All spectra are presented in Appendix 11.2.

10.1.8 Synthesis of *n*-acetamido-aromatic derivates (*n* = 3, 4 and 5)

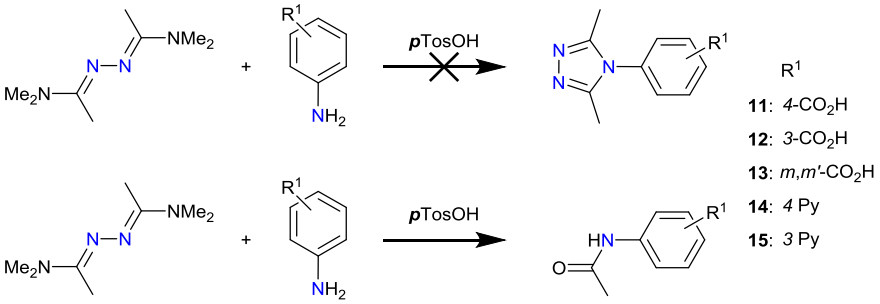

a) Synthesis: *n*-Amino aromatic derivates (*n* = 3, 4 and 5), *N,N`*-dimethylacetamide azine and *p*-toluenesulfonic acid monohydrate was mixed and refluxed in toluene or *o*-xylene (50-80 ml). in inert gas atmosphere for (2-3 d). Finally, the solvent was decanted.

Product	H_2N-R	DMAA	*p*TosOH	Yield
4-acetamido-benzoic acid	m = 4.56 g, n = 0.03 mol	m = 8.2 g, n = 0.03 mol, 1 eq	m = 0.585 g, n = 0.003 mol, 0.1 eq	m = 1.78 g, n = 0.01 mol, 30.1 %
3-acetamido-benzoic acid	m = 4.60 g, n = 0.03 mol	m = 8.48 g, n = 0.03 mol, 1 eq	m = 0.615 g, n = 0.003 mol, 0.1 eq	m = 3.918 g, n = 0.029 mol, 66.3 %
5-acetamido-isophthalic acid	m = 5.8 g, n = 0.03 mol	m = 8.14 g, n = 0.03 mol, 1 eq	m = 0.595 g, n = 0.003 mol, 0.1 eq	m = 3.531 g, n = 0.015 mol, 47.8 %
4-acetamido-pyridine	m = 3.115 g, n = 0.03 mol	m = 8.6 g, n = 0.03 mol, 1 eq	m = 0.668 g, n = 0.003 mol, 0.1 eq	m = 2.148 g, n = 0.015 mol, 47.8 %
3-acetamido-pyridine	m = 3.175 g, n = 0.03 mol	m = 8.204 g, n = 0.03 mol, 1 eq	m = 0.751 g, n = 0.003 mol, 0.1 eq	m = 1.381 g, n = 0.01 mol, 30.73 %

b) Recrystallization**:** For acetamido benzene carboxylic acid derivates, the obtained precipitate was dissolved in sodium hydroxide solution and filtered. To the filtrate, diluted HCl was added until the product completely has failed again. The suspension was stirred for (0.5 h) and then filtered under vacuum and washed several times with the water. The product was dried in vacuum furnace.

For acetamido pyridine derivates, the obtained residue was washed with dichloromethane and after then dissolved in ethanol and the solution refluxed with active carbon for 0.5 h. After then it was filtered. The filtrate volume of the combined ethanol was reduced to ~10 ml and the reduced solution was cooled to 0 °C in refrigerator. The white solid precipitate was separated by filtration, and dried in vacuum furnace.

All spectra are presented in Appendix 11.2.

Data analysis

For *4*-acetamido-benzoic acid (11)

^{1}H NMR (200 MHz, DMSO-d_6): δ (ppm) = 2.1 (s, 3H, C**H$_3$**), 7.7 (m, 2H, arom. C-**H**), 7.9 (m, 2H, arom. C-**H**), 10.5 (s, 1H, COO**H**), 12.5 (b, 1H, -CO-N**H**-).

LR-MS (EI): m/z = 179 [M^+].

For *3*-acetamido-benzoic acid (12)

^{1}H NMR (500 MHz, DMSO-d_6): δ (ppm) = 2.1 (s, 3H, C**H$_3$**), 7.4 (t, 1H, arom. C-**H**), 7.6 (d, 1H, arom. C-**H**), 7.8 (d, 1H, arom. C-**H**), 8.2 (s, 1H, arom. C-**H**), 10.1 (s, 1H, COO**H**), 13 (b, 1H, -CO-N**H**-).
^{13}C{^{1}H} NMR (125 MHz, DMSO-d_6): δ (ppm) = 24.4 (s, 1C, **C**H$_3$); 120 (s, 1C, arom. **C**-H); 123.4 (s, 1C, arom. **C**-H); 124.1 (s, 1C, arom. **C**-H); 129.3 (s, 1C, arom. **C**-H); 131.6 (s, 1C, arom. **C$_q$**-CO_2H); 139.9 (s, 1C, arom. **C$_q$**-NH); 167.5 (s, 1C, **C$_q$**O$_2$H); 168.9 (s, 1C, CH_3-**C**O-NH).

LR-MS (EI): m/z = 179 [M^+].

For *5*-acetamidoisophthalic acid (13)

^{1}H NMR (500 MHz, DMSO-d_6): δ (ppm) = 2.1 (s, 3H, C**H$_3$**), 8.1 (s, 2H, arom. C-**H**), 8.4 (s, 1H, arom. C-**H**), 10.3 (s, 2H, COO**H**), 13.3 (b, 1H, -CO-N**H**-).
^{13}C{^{1}H} NMR (125 MHz, DMSO-d_6): δ (ppm) = 24.4 (s, 1C, **C**H$_3$); 123.7 (s, 1C, arom. **C**-H); 124.7 (s, 2C, arom. **C**-H); 132.0 (s, 2C, arom. **C$_q$**-CO_2H); 140.3 (s, 1C, arom. **C$_q$**-NH); 166.8 (s, 2 C, **C$_q$**O$_2$H); 169.2 (s, 1C, CH_3-**C**O-NH).

LR-MS (EI): m/z = 223 [M^+].

For *4*-acetamido-pyridine (14)

^{1}H NMR (500 MHz, DMSO-d_6): δ (ppm) = 2.2 (s, 3H, C**H$_3$**), 8 (m, 2H, arom. C-**H**), 8.4 (m, 2H, arom. C-**H**).
^{13}C{^{1}H} NMR (125 MHz, DMSO-d_6): δ (ppm) = 24.3 (s, 1C, **C**H$_3$); 115.4 (s, 2C, arom. **C**-H); 141.9 (s, 2C, arom. **C**-H); 153.4 (s, 1C, arom. **C**-NH); 174.3 (s, 1C, CH$_3$-**C**O-NH).

LR-MS (EI): m/z = 136 [M^+], LR-MS (ESI): m/z = 137.1 [M+H^+].

For *3*-acetamido-pyridine (15)

^{1}H NMR (500 MHz, DMSO-d_6): δ (ppm) = 2.1 (s, 3H, C**H$_3$**), 7.9 (m, 1H, arom. C-**H**), 8.3 (m, 1H, arom. C-**H**), 8.4 (m, 1H, arom. C-**H**), 9.1 (s, 1H, arom. C-**H**).
^{13}C{^{1}H} NMR (125 MHz, DMSO-d_6): δ (ppm) = 23.5 (s, 1C, **C**H$_3$); 127.9 (s, 1C, arom. **C**-H); 132.9 (s, 1C, arom. **C**-H); 136.7 (s, 1C, arom. **C**-H); 136.8 (s, 1C, arom. **C**-H); 138.4 (s, 1C, arom. **C**-NH); 173.5 (s, 1C, CH$_3$-**C**O-NH).
LR-MS (ESI): m/z = 137.07 [M+H^+].

10.2 Synthesis of coordination polymers

10.2.1 General information about the synthesis of coordination polymers

For the synthesis of coordination polymers, hydrothermal or solvothermal synthesis were mostly used in different temperature programs (Scheme 9.2.1.1). The carboxylic or tetrazole ligands were deprotonated in a solution of ammonium hydroxide, sodium hydroxide or triethylamine as base (0.16 mmol/l) in an ultrasonic bath and heating at 45-50°C. Equal amount of base was used here to dissolve the carboxylate or tetrazolate ligands. The metal salt was dissolved in the first solvent noted in Table 9.2.1.1. The first ligand was dissolved in the second solvent and the second ligand was dissolved in the third solvent given in Table 9.2.1.1. These solutions were then mixed in a glass tube vessel (7 ml), stirred (hand shaked) for a few minutes, until homogeny suspension in some probes was formed. Finally, the sample was placed in a programmable furnace using temperature program. For example, the first temperature program (P1 in Scheme 9.2.1.1) means that the sample was heated to 125°C during 3 h and held at that temperature for 48 h, then cooled at temperature rate 5°C/h to ambient temperature.

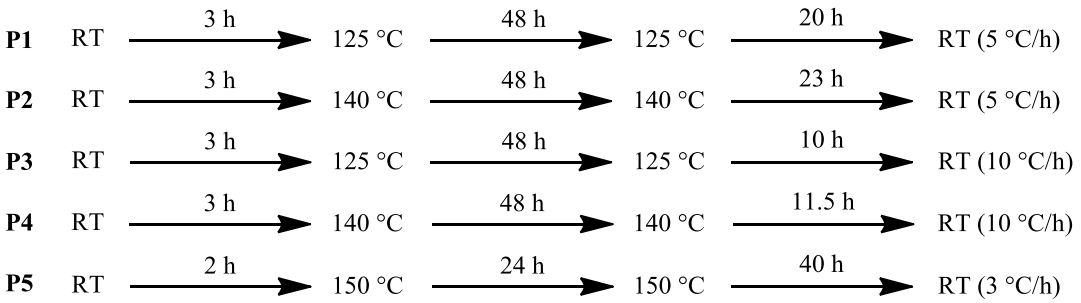

Scheme 9.2.1.1: The used temperature programs for synthesis of coordination polymers.

10.2.2 Synthesis of coordination compounds 16, 17 & 18

A mixture of an aqueous or an acetonitrile solution of different copper(II) salts and an aqueous solution of *rac*-btrip ligand were mixed in a glass tube, which was sealed and hand shaked for about 3 min. After that, an aqueous solution of H_2bdc ligand was added to this mixture, which was deprotonated in a glass tube by using an NH_3/H_2O solution (0.16 mmol/l, 2eq to H_2bdc) as base in ultrasonic bath and heating at 45-50°C. The solutions were mixed in

a glass tube, which was sealed, hand shaked for about 10 minutes and then placed in a programmable furnace. The sample was heated to 125°C during 3h and held at that temperature for 48h, then cooled at temperature rate 5°C/h to ambient temperature, (For compound **18**, the sample was placed in an ultrasonic bath for *ca.* 15 min until a slightly blue suspension was formed, before it was introduced to the furnace). The single crystals for compound **16** were grown completely after two weeks. The resulting crystals were separated from a light blue precipitate and washed with mother liquor (and methanol for **16** *ca.* 20 ml). Finally, the sample was dried in vacuum furnace for ca. 2-3h at 40°C. The synthesis of these compounds is summarized in Table 9.2.2.1.

Table 9.2.2.1: Synthesis conditions for products **16**, **17** & **18**:

Product	Metal salt	btrip	H_2bdc	Rate	Solvents	Result and remark
16 (P1)	$Cu(NO_3)_2{\cdot}2.5H_2O$ 18.4 mg, 0.08 mmol	14.24 mg, 0.08 mmol	6.6 mg, 0.04 mmol	2:2:1	$(H_2O$:MeCN):H_2O: NH_3/H_2O, (v:v):v:v, (0.5:0.5): 0.5:0.5, 2 ml	Hts, 125°C, light blue plate crystals.
16-1 (P1)	$Cu(NO_3)_2{\cdot}2.5H_2O$ 18.4 mg, 0.08 mmol	7.12 mg, 0.04 mmol	6.6 mg, 0.04 mmol	2:1:1	MeCN:H_2O:NH_3/H_2O , v:v:v, 0.5:0.5:0.5, 1.5 ml	Hts, 125°C, light blue plate crystals.
17 (P1)	$Cu(BF_4)_2{\cdot}6H_2O$ 18.4 mg, 0.08 mmol	14.24 mg, 0.08 mmol	6.6 mg, 0.04 mmol	2:2:1	MeCN:H_2O:NH_3/H_2O , v:v:v, 0.5:0.5:0.5, 1.5 ml	Hts, 125°C, light blue square plate crystals.
18 (P1)	$CuSO_4$ 12 mg, 0.08 mmol	14.24 mg, 0.08 mmol	6.6 mg, 0.04 mmol	2:2:1	($MeCN:H_2O$):H_2O: NH_3/H_2O, (v:v):v:v, (0.5:0.5):0.5:0.5, 2 ml	Hts, 125°C, light blue needle shaped crystals.

3D-$[Cu_4(\mu\text{-}OH)_2(\mu\text{-}bdc)_2(\mu_4\text{-}btrip)_3]_n$, M_w ($\mathbf{C_{37}H_{40}Cu_4N_{18}O_{10}}$) = 1151.02 g/mol, Yield: 11 mg, 0.0095 mmol (23.9 % based on H_2bdc; 11.9 % based on metal salt).

EA of 3D-$\{[Cu_4(\mu\text{-}OH)_2(\mu\text{-}bdc)_2(\mu_4\text{-}rac\text{-}btrip)_3]\ (NO_3)_2(H_2O)_{10}\}_n$ **16**:

Calc.: C: 30.54%, H: 4.16%, N: 19.25%.

Found: C: 30.38 %, H: 4.00 %, N: 20.93 %.

IR (ATR) for **16** ν**/cm^{-1}**: 3610 (w, sh, ν (O-H) of water), 3101 (w, br, ν_{asym} (C-H) of btrip), 3007 (w, br, ν_{sym} (C-H) of btrip), 2167, 2095, 1986 (w, H-bonds) 1567 (s, ν_{asym} C=O, C=N), 1500 (w, ν_{sym} C=O, C=N), 1291 (s, ν_{asym} C-O, C-N), 1209 (m, ν_{sym} C-O, C-N), 828 (m, sh, γ (C-H)), 734 (s, γ (1,4-disubstituted benzene ring) of bdc), 645 (m, γ (triazole ring) of btrip).

3D-[$Cu_4(\mu_4\text{-}Cl)(\mu_4\text{-}rac\text{-btrip})_4(H_2O)_4]_n$, M_w (**$C_{28}H_{48}ClCu_4N_{24}O_4$**) = 1074.48 g/mol, Yield: 10 mg, 0.0093 mmol (11.6 % based on metal salt).

IR (ATR) for **17 ν/cm^{-1}**: 3124 (w, sh, ν (C-H) of btrip), 1060 (w, ν BF_4^-/ClO_4^-), 1557 (s, ν_{asym} C=N), 1505 (m, ν_{sym} C=N), 1291 (s, ν_{asym} C-N), 1222 (s, ν_{sym} C-N), 880 (w, sh, γ (C-H)), 710 (s, ν Cu-Cl or -F), 646 (s, γ (triazole ring) of btrip).

3D-[$Cu(\mu_4\text{-}rac\text{-btrip})(SO_4)]_n$, M_w (**$C_7H_{10}CuN_6O_4S$**) = 337.80 g/mol, Yield: 12.1 mg, 0.0358 mmol (44.77 % based on metal salt).

IR (ATR) for **18 ν/cm^{-1}**: 3610 (w, sh, ν (S-O)), 3103 (w, sh, ν (C-H) of btrip), 1669 (m, ν (S=O)), 1560 (s, ν_{asym} C=N), 1504 (m, ν_{sym} C=N), 1393 (m, ν (S-O)), 1289 (w, ν_{asym} C-N), 1194 (m, ν_{sym} C-N), 878 (m, γ (C-H)), 643 (s, γ (triazole ring) of btrip).

10.2.3 Synthesis of coordination compounds 19, 20, 21, 22 & 23

A mixture of an aqueous solution of different zinc (II) salts and a methanol solution of *rac*-btrip ligand were mixed in a glass tube, which was sealed and hand shaked for about 3 minutes. After that, an aqueous solution of H_3btc ligand was added to glass tube, which was deprotonated by using Et_3N/H_2O solution (0.16 mmol/l, 3eq to H_3btc) as base in ultrasonic bath and heating at 45-50°C. The solutions were mixed in a glass tube, which was sealed, hand shaked for about 10 minutes, and then placed in a programmable furnace. The sample was heated to 125°C or 140°C during 3h and held at that temperature for 48h, then cooled at temperature rate 5°C/h to ambient temperature. The resulting colorless single crystals were separated from weight precipitate and washed with mother liquor. Finally, the sample was dried in vacuum furnace for ca. 3h at 40°C. The synthesis of the compounds is summarized in Table 9.2.3.1.

Table 9.2.3.1: Synthesis conditions for **19**, **20**, **21**, **22** & **23**:

Product	Metal salt	btrip	H_3btc	Rate	Solvents	Result and remark
19 (P1)	$Zn(NO_3)_2{\cdot}6H_2O$ 20.8 mg, 0.08 mmol	14.24 mg, 0.08 mmol	8.4 mg, 0.04 mmol	2:2:1	H_2O:MeOH: Et_3N/H_2O, v:v:v, 0.5:1:0.75, 2.25 ml	Hts, 125°C, colorless crystals.
19-1 (P1)	$Zn(NO_3)_2{\cdot}4H_2O$ 23.8 mg, 0.08 mmol	7.12 mg, 0.04 mmol	8.4 mg, 0.04 mmol	2:1:1	H_2O:MeOH: Et_3N/H_2O, v:v:v, 0.5:0.5:0.75, 1.75 ml	Hts, 125°C, colorless crystals.

Product	Metal salt	btrip	H_3btc	Rate	Solvents	Result and remark
19-2 (P4)	$Zn(NO_3)_2{\cdot}4H_2O$ 23.8 mg, 0.08 mmol	7.12 mg, 0.04 mmol	8.4 mg, 0.04 mmol	2:1:1	H_2O:H_2O:Et_3N/H_2O, v:v:v, 0.5:0.5:0.75, 1.75 ml	Hts, 140 °C, colorless crystals.
19-3 (P1)	$Zn(NO_3)_2{\cdot}6H_2O$ 20.8 mg, 0.08 mmol	7.12 mg, 0.04 mmol	8.4 mg, 0.04 mmol	2:1:1	H_2O:MeOH: Et_3N/H_2O, v:v:v, 0.5:0.5:0.75, 1.75 ml	Hts, 125°C, colorless crystals.
20 (P1)	$ZnBr_2$ 17.6 mg, 0.08 mmol	14.24 mg, 0.08 mmol	8.4 mg, 0.04 mmol	2:2:1	H_2O:MeOH: Et_3N/H_2O, v:v:v, 0.5:1:0.75, 2.25 ml	Hts, 125°C, colorless crystals.
21 (P1)	$ZnCl_2$ 10.4 mg, 0.08 mmol	14.24 mg, 0.08 mmol	8.4 mg, 0.04 mmol	2:2:1	H_2O:MeOH: Et_3N/H_2O, v:v:v, 0.5:1:0.75, 2.25 ml	Hts, 125°C, colorless crystals.
22 (P1)	$Zn(ClO_4)_2{\cdot}6H_2O$ 29.6 mg, 0.08 mmol	14.24 mg, 0.08 mmol	8.4 mg, 0.04 mmol	2:2:1	H_2O:MeOH: Et_3N/H_2O, v:v:v, 0.5:1:0.75, 2.25 ml	Hts, 125°C, colorless crystals.
23 (P1)	$Zn(OAc)_2{\cdot}2H_2O$ 17.6 mg, 0.08 mmol	14.24 mg, 0.08 mmol	8.4 mg, 0.04 mmol	2:2:1	H_2O:MeOH: Et_3N/H_2O, v:v:v, 0.5:1:0.75, 2.25 ml	Hts, 125°C, colorless crystals.

2D-{[Zn(μ-Hbtc)(μ-*R*-btrip)]·H_2O}$_n$, M_w (**$C_{16}H_{16}N_6O_7Zn$**) = 469.7 g.mol^{-1}.

Yield for **19**: 7 mg, 0.015 mmol (38.7% based on H_3btc).

Yield for **20**: 7.5 mg, 0.016 mmol (39.9% based on H_3btc).

Yield for **21**: 10.9 mg, 0.023 mmol (58% based on H_3btc).

Yield for **22**: 5.7 mg, 0.012 mmol (30.3% based on H_3btc).

EA for **19**: Calc.: C: 40.91%, H: 3.43%, N: 17.89%.

Found: C: 40.79%, H: 3.39%, N: 17.46%.

IR (ATR) for **19 ν/cm^{-1}**: 3643 (w, sh, ν (O-H) of water), 3113, 3110 (m, sh, ν (C-H) of btrip), 2485, 2056 (w, br, H-bonds), 1689 (s, ν COOH), 1630 (s, ν_{asym} C=O, C=N), 1561 (s, ν_{sym} C=O, C=N), 1259 (s, ν_{asym} C-O, C-N), 1187 (s, ν_{sym} C-O, C-N), 799 (m, sh, γ (C-H)), 736, 684 (s, γ (1,3,5-trisubstituted benzene ring) of Hbtc),640 (s, γ (triazole ring) of btrip).

EA for **20**: Calc.: C: 40.91%, H: 3.43%, N: 17.89%.

Found: C: 40.43%, H: 3.80%, N: 16.98%.

IR (ATR) for **20 ν/cm^{-1}**: 3643 (w, sh, ν (O-H) of water), 3128, 3113 (w, sh, ν (C-H) of btrip), 2483, 2051 (w, br, H-bonds), 1691 (m, ν COOH), 1627 (s, ν_{asym} C=O, C=N), 1567 (m, ν_{sym}

C=O, C=N), 1259 (s, ν_{asym} C-O, C-N), 1188 (s, ν_{sym} C-O, C-N), 799 (m, sh, γ (C-H)), 736, 685 (s, γ (1,3,5-trisubstituted benzene ring) of Hbtc),641 (s, γ (triazole ring) of btrip).

IR (ATR) for **21** ν**/cm^{-1}**: 3643 (w, sh, ν (O-H) of water), 3115, 2991 (m, sh, ν (C-H) of btrip), 2488 (w, br, H-bonds), 1691 (s, ν COOH), 1626 (s, ν_{asym} C=O, C=N), 1565 (m, ν_{sym} C=O, C=N), 1260 (s, ν_{asym} C-O, C-N), 1187 (s, ν_{sym} C-O, C-N), 799 (m, sh, γ (C-H)), 736, 684 (s, γ (1,3,5-trisubstituted benzene ring) of Hbtc), 641 (s, γ (triazole ring) of btrip).

IR (ATR) for **23** ν**/cm^{-1}**: 3643 (w, sh, ν (O-H) of water), 3125 (m, sh, ν (C-H) of btrip), 2485 (w, br, H-bonds), 1690 (s, ν COOH), 1631 (s, ν_{asym} C=O, C=N), 1560 (m, ν_{sym} C=O, C=N), 1259 (s, ν_{asym} C-O, C-N), 1188 (s, ν_{sym} C-O, C-N), 799 (m, sh, γ (C-H)), 737, 684 (s, γ (1,3,5-trisubstituted benzene ring) of Hbtc), 641 (s, γ (triazole ring) of btrip).

TG-DTG curves experiments of **21** (Figure 9.2.3.1) were carried out in the temperature range 27-600 °C. It is looking the same TG-DTC curves of sample **20**, which was discussed in previous section 7.2.4. TG analyses for compounds with other zinc salts were not measured, because the crystals were not synthesed more. Combination of the experimental TG analysis of zinc compounds **19**, **20** and **21** show that, these compounds have the same decomposition process, as they show identical weight loss steps, special for compounds **20** and **21**. TG curves are in Figure 9.2.3.2 presented.

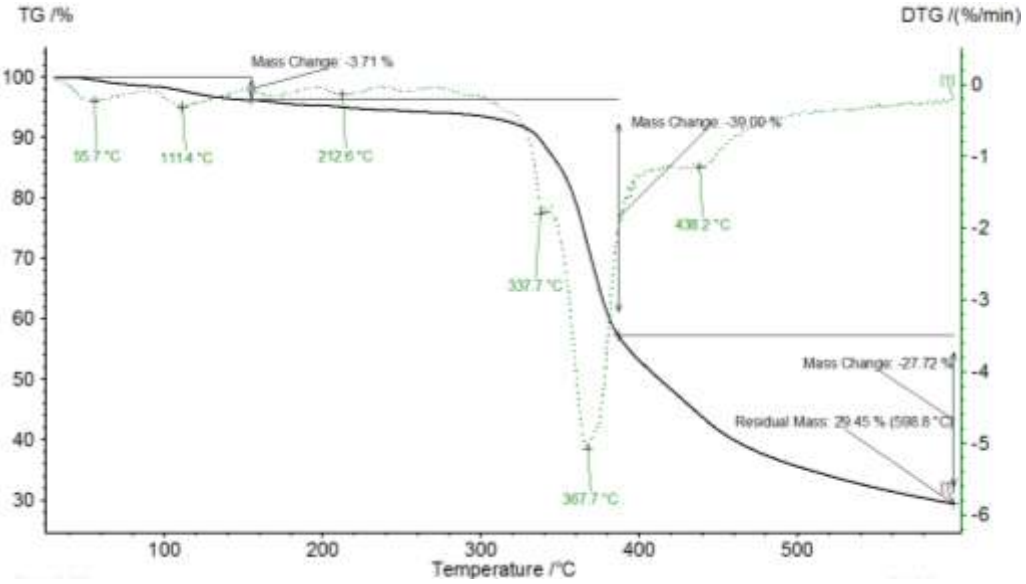

Fig. 9.2.3.1: The experimental TGA and DTG curves for the decomposition of **21**, in N_2 atmosphere, gas flow 10 ml/min at a heating rate of 5 °C/min and sample mass 15.04 mg. Common presentation of the TGA curve (black) together with the DTG curve (red, dotted line). (The image is generated by the instrument's software).

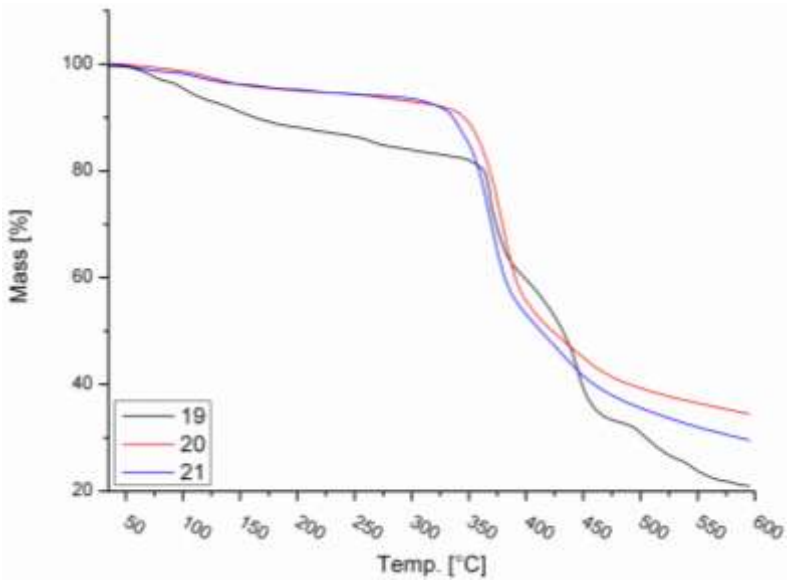

Fig. 9.2.3.2: Combination of the experimental TG analysis of zinc compounds **19**, **20** and **21**.

10.2.4 Synthesis of coordination compounds 24, 25 & 26

A mixture of an aqueous solution of metal salt and an aqueous solution of 4,4`-bis(1,2,4-triazol-4-yl) (btr) ligand was mixed in a glass tube, which was sealed and hand shaked for about 3 minutes. After that, an aqueous solution of benzene-1,3,5-tricarboxylic acid (H_3btc) ligand was added to previously mixture, which was deprotonated in a glass tube with Et_3N/H_2O solution (0.16 mmol/l, 3eq to H_3btc) as base by using ultrasonic bath and heating at 45-50°C. The solutions were mixed in a glass tube, which was sealed, hand shaked for about 10 min., and then placed in a programmable furnace. The sample was heated to 125°C (140°C for **26**, 2D-$[Cd(\mu_3\text{-Hbtc})(H_2O)_2]_n$) during 3h and held at that temperature for 48h, then cooled at temperature rate 5°C/h to ambient temperature. The resulting blue single crystals were separated from precipitate and washed with the mother liquor. Finally, the sample was dried in vacuum furnace for *ca.* 2h at 40°C. The synthesis of the compounds is summarized in Table 9.2.4.1.

Table 9.2.4.1: Synthesis conditions for **24**, **25** & **26**:

Product	Metal salt	btr	H_3btc	Rate	Solvents	Result
24 (P1)	$CuCl_2 \cdot 2H_2O$ 13.6 mg, 0.08 mmol	16.32 mg, 0.12 mmol	8.4 mg, 0.04 mmol	2:3:1	H_2O:H_2O:Et_3N/H_2O, v:v:v, 0.5:0.5:0.75, 1.75 ml	Hts, 125°C, green and blue crystals.

Product	Metal salt	btr	H_3btc	Rate	Solvents	Result
25 (P1)	$Cd(OAc)_2 \cdot 2H_2O$ 10.7 mg, 0.04 mmol	16.32 mg, 0.12 mmol	8.4 mg, 0.04 mmol	1:3:1	H_2O:H_2O:Et_3N/H_2O, v:v:v, 0.5:0.5:0.75, 1.75 ml	Hts, 125°C, colorless crystals.
26 (P2)	$Cd(OAc)_2 \cdot 2H_2O$ 10.7 mg, 0.04 mmol	16.32 mg, 0.12 mmol	8.4 mg, 0.04 mmol	1:3:1	H_2O:H_2O:Et_3N/H_2O, v:v:v, 1:1:0.75, 2.75 ml	Hts, 140°C, colorless crystals.

2D-$[Cu_3(\mu_6\text{-btc})(\mu\text{-btc})(\mu\text{-atr})(H_2O)_5]_n$, M_w ($\mathbf{C_{20}H_{20}Cu_3N_4O_{17}}$) = 779.0334 g.mol^{-1}, Yield for **24**: 11 mg, 0.014 mmol (35 % based on H_3btc).

EA for **24**: Calc.: C: 30.84 %, H: 2.59 %, N: 7.19 %.

Found: C: 31.15 %, H: 2.74 %, N: 10.44 %.

IR (ATR) for **24 ν/cm^{-1}**: 3374, 3304 (w, ν (N-H)), 3128 (w, ν (C-H)), 1715 (m, ν COOH), 1622 (s, ν_{asym} C=O, C=N), 1568 (m, ν_{sym} C=O, C=N), 1251 (s, ν_{asym} C-O, C-N), 1188 (s, ν_{sym} C-O, C-N), 793 (m, sh, γ (C-H)), 748, 724, 684 (s, γ (1,3,5-trisubstituted benzene ring) of Hbtc), 620 (s, γ (triazole ring)).

1D-$\{[Cd_2(\mu_2\text{-btc})_2(atr)_2(H_2O)_4][Cd(H_2O)_6]\cdot 2H_2O\}_n$, M_w ($\mathbf{C_{22}H_{38}Cd_3N_8O_{24}}$) = 1135.7829 g.mol^{-1}, Yield for **25**: 14 mg, 0.012 mmol (30 % based on H_3btc).

EA for **25**: Calc.: C: 23.27 %, H: 3.37 %, N: 9.87 %.

Found: C: 23.23 %, H: 2.97 %, N: 10.43 %.

Found: C: 23.35 %, H: 2.99 %, N: 10.35 %.

IR (ATR) for **25 ν/cm^{-1}**: 3100 (w, ν (C-H)), 1607 (s, ν_{asym} C=O, C=N), 1527 (m, ν_{sym} C=O, C=N), 1204 (s, ν_{asym} C-O, C-N), 1110 (s, ν_{sym} C-O, C-N), 871 (m, sh, γ (C-H)), 752, 731 (s, γ (1,3,5-trisubstituted benzene ring) of Hbtc), 612 (m, γ (triazole ring)).

2D-$[Cd(\mu_3\text{-Hbtc})(H_2O)_2]_n$, M_w ($\mathbf{C_9H_8CdO_8}$) = 356.5577 g.mol^{-1}, Yield for **26**: 13 mg, 0.036 mmol (91.15 % based on H_3btc or metal salt).

EA for **26**: Calc.: C: 30.32%, H: 2.26%.

Found: C: 30.14%, H: 2.58%.

IR (ATR) for **26 ν/cm^{-1}**: 3295, 3223 (w, ν (O-H)), 3091, 2985 (w, ν (C-H)), 1680 (m, ν COOH), 1615 (s, ν_{asym} C=O), 1549 (m, ν_{sym} C=O), 1277 (s, ν_{asym} C-O), 1198 (s, ν_{sym} C-O), 842 (m, sh, γ (C-H)), 740, 687 (s, γ (1,3,5-trisubstituted benzene ring) of Hbtc), 620 (s, γ (triazole ring)).

10.2.5 Synthesis of coordination compounds 27, 28, 29, 30, 31 & 32

A mixture of a methanol solution of different copper (II) salts and a methanol solution of *rac*-btrip ligand were mixed in a glass tube, which was sealed, and hand shaked for about 3 min. After then, an aqueous solution of H_3btc ligand, which was deprotonated in a glass tube, with Et_3N/H_2O solution (0.16 mmol/l, 3eq to H_3btc) as base by using ultrasonic bath and heating at 45-50°C, was added to previously mixture. The solutions were mixed in a glass tube, which was sealed, hand shaked for about 10 min., and then placed in a programmable furnace. The sample was heated to 125°C during 3h and held at that temperature for 48h, then cooled at temperature rate 5°C/h to ambient temperature. In the second part of synthesis, DMSO (0.5 ml) was added to each sample. After then each sample was hand shaked for about 10 minutes. The sample was heated to 140°C during 3h and held at that temperature for 48h, then cooled at temperature rate 5°C/h to the ambient temperature. The resulting single crystals were separated from precipitate and washed with the same mother liquor. Finally, the sample was dried in vacuum furnace for *ca.* 2-3h at 40°C. The synthesis of compounds is summarized in Table 9.2.5.1.

Table 9.2.5.1: Synthesis conditions for **27**, **28**, **29**, **30**, **31** & **32**:

Product	Metal salt	btrip	H_3btc	Rate	Solvents	Result
27 (P1 & P2)	$CuBr_2$ 17.6 mg, 0.08 mmol	14.24 mg, 0.08 mmol	8.4 mg, 0.04 mmol	2:2:1	MeOH:MeOH: Et_3N/H_2O, v:v:v, 0.5:1:0.75, 2.25 ml DMSO, v, 0.5 ml	Sts, 125°C/140°C light green plate prism crystals
27-1 (P1 & P2)	$CuBr_2$ 17.6 mg, 0.08 mmol	21.36 mg, 0.12 mmol	8.4 mg, 0.04 mmol	2:3:1	MeOH:MeOH: Et_3N/H_2O, v:v:v, 0.5:1:0.75, 2.25 ml DMSO, v, 0.5 ml	Sts, 125°C/140°C light green prism crystals.
28 (P1 & P2)	$CuSO_4 \cdot 5H_2O$ 20 mg, 0.08 mmol	14.24 mg, 0.08 mmol	8.4 mg, 0.04 mmol	2:2:1	MeOH:MeOH: Et_3N/H_2O, v:v:v, 0.5:1:0.75, 2.25 ml DMSO, v, 0.5 ml	Sts, 125°C/140°C light green needle shaped prism crystals.
28-1 (P1 & P2)	$CuSO_4 \cdot 5H_2O$ 20 mg, 0.08 mmol	21.36 mg, 0.12 mmol	8.4 mg, 0.04 mmol	2:3:1	MeOH:MeOH: Et_3N/H_2O, v:v:v, 0.5:1:0.75, 2.25 ml DMSO, v, 0.5 ml	Sts, 125°C/140°C light green needle shaped prism crystals.

Product	Metal salt	btrip	H_3btc	Rate	Solvents	Result
29 (P1 & P2)	$Cu(OAc)_2 \cdot H_2O$ 16 mg, 0.08 mmol	21.36 mg, 0.12 mmol	8.4 mg, 0.04 mmol	2:3:1	MeOH:MeOH: Et_3N/H_2O, v:v:v, 0.5:1:0.75, 2.25 ml DMSO, v, 0.5 ml	Sts, 125°C/140°C light green needle shaped prism crystals
30 (P1 & P2)	$Cu(NO_3)_2 \cdot 2.5H_2O$ 18.4 mg, 0.08 mmol	21.36 mg, 0.12 mmol	8.4 mg, 0.04 mmol	2:3:1	MeOH:MeOH: Et_3N/H_2O, v:v:v, 0.5:1:0.75, 2.25 ml DMSO, v, 0.5 ml	Sts, 125°C/140°C green plate crystals.
31 (P1 & P2)	$Cu(BF_4)_2 \cdot 6H_2O$ 18.4 mg, 0.08 mmol	21.36 mg, 0.12 mmol	8.4 mg, 0.04 mmol	2:3:1	MeOH:MeOH: Et_3N/H_2O, v:v:v, 0.5:1:0.75, 2.25 ml DMSO, v, 0.5 ml	Sts, 125°C/140°C light green needle shaped prism crystals.
32 (P1 & P2)	$CuCl_2$ 10.4 mg, 0.08 mmol	21.36 mg, 0.12 mmol	8.4 mg, 0.04 mmol	2:3:1	MeOH:MeOH: Et_3N/H_2O, v:v:v, 0.5:1:0.75, 2.25 ml DMSO, v, 0.5 ml	Sts, 125°C/140°C light green needle shaped prism crystals.

2D-$[Cu_2(\mu\text{-}Br)_2(\mu_4\text{-}rac\text{-btrip})]_n$, M_w ($\mathbf{C_7H_{10}Br_2Cu_2N_6}$) = 465.0966 g.mol^{-1}, Yield for **27**: 19.3 mg, 0.04 mmol (50 % based on metal salt).

EA for 2D-$[Cu_2(\mu\text{-}Br)_2(\mu_4\text{-}rac\text{-btrip})]_n$ **27**: Calc.: C: 18.08 %, H: 2.17 %, N: 18.07 %.

Found: C: 18.40 %, H: 2.33 %, N: 17.65 %.

Found: C: 18.32 %, H: 2.33 %, N: 17.74 %.

IR (ATR) for **27 ν/cm^{-1}**: 3538 (w, sh, ν (Cu-Br)), 3115, 2985 (w, sh, ν (C-H) of btrip), 1635 (s, ν_{asym} C=N), 1595 (m, ν_{sym} C=N), 1230 (m, ν_{asym} C-N), 1186 (s, ν_{sym} C-N), 852 (s, sh, γ (C-H)), 669 (w, ν (Br-Cu-Br)), 634 (s, γ (triazole ring) of btrip).

3D-$\{[Cu_2(\mu_4\text{-}rac\text{-btrip})_2]\ SO_4^{2-}\}_n$, M_w ($\mathbf{C_{14}H_{20}Cu_2N_{12}O_4S}$) = 579.55 g/mol, Yield: 10.6 mg, 0.018 mmol (22.8 % based on metal salt).

IR (ATR) for **28 ν/cm^{-1}**: 3377 (w, br, ν (S-O)), 3092, 2992 (m, sh, ν (C-H) of btrip), 1660 (w, ν (S=O)), 1610 (w, ν_{asym} C=N), 1533 (s, ν_{sym} C=N), 1351 (m, ν (S-O)), 1287 (w, ν_{asym} C-N), 1196 (m, ν_{sym} C-N), 878 (m, γ (C-H)), 642 (s, γ (triazole ring) of btrip).

3D-$\{[Cu(\mu_4\text{-}rac\text{-btrip})]\ CH_3COO^-\}_n$, M_w ($\mathbf{C_9H_{13}CuN_6O_2}$) = 300.78 g.mol^{-1}, Yield: 9 mg, 0.03 mmol (37.40 % based on metal salt).

EA for 3D-$\{[Cu(\mu_4\text{-}rac\text{-btrip})]\ CH_3COO^- \cdot 2H_2O\}_n$ **29**:

Calc.: C: 32.09 %, H: 5.09 %, N: 24.95 %.

Found: C: 32.20 %, H: 4.33 %, N: 21.23 %

IR (ATR) for **29 ν/cm^{-1}**: 3377 (w, br, ν (S-O)), 3085, 2986 (m, sh, ν (C-H) of btrip), 1658 (w, ν (S=O)), 1603 (s, ν_{asym} C=N), 1562 (s, ν_{sym} C=N), 1344 (s, ν (S-O)), 1284 (w, ν_{asym} C-N), 1193 (m, ν_{sym} C-N), 876 (m, γ (C-H)), 641 (s, γ (triazole ring) of btrip).

The mass for **30** is 18 mg, **31**: 18 mg, and **32**: 10 mg.

10.2.6 Synthesis of coordination compounds 33 & 34

A mixture of an acetonitrile solution of copper salt and an aqueous solution of *rac*-btrip ligand were mixed in a glass tube, which was sealed and hand shaked for about 3 min. After that, an aqueous solution of H_3btc ligand, which was deprotonated in a glass tube with Et_3N/H_2O solution (0.16 mmol/l, 3eq to H_3btc) as base by using ultrasonic bath and heating at 45-50°C, was added to previously mixture. The solutions were mixed in a glass tube, which was sealed again, hand shaked for about 10-15 min., and then placed in a programmable furnace. The sample was heated to 125°C during 3h and held at that temperature for 48h, then cooled at temperature rate 5 or 10°C/h to ambient temperature. The resulting single crystals were separated from precipitate and washed with the same mother liquor. Finally, the sample was dried in vacuum furnace for *ca.* 2-3h at 40°C. The synthesis of compounds is summarized in Table 9.2.6.1.

Table 9.2.6.1: Synthesis conditions for **33** & **34**:

Product	Metal salt	btrip	H_3btc	Rate	Solvents	Result
33 (P1)	$Cu(NO_3)_2{\cdot}2.5H_2O$ 18.4 mg, 0.08 mmol	14.24 mg, 0.08 mmol	8.4 mg, 0.04 mmol	2:2:1	MeCN:H_2O: Et_3N/H_2O, v:v:v, 0.5:1:0.75, 2.25 ml	Hts, 125°C, blue cubic crystals.
33-1 (P1)	$Cu(NO_3)_2{\cdot}2.5H_2O$ 18.4 mg, 0.08 mmol	7.12 mg, 0.04 mmol	8.4 mg, 0.04 mmol	2:1:1	MeCN:H_2O: Et_3N/H_2O, v:v:v, 0.5:0.5:0.75, 1.75 ml	Hts, 125°C, small light blue plate crystals.
33-2 (P3)	$Cu(NO_3)_2{\cdot}2.5H_2O$ 18.4 mg, 0.08 mmol	14.24 mg, 0.08 mmol	8.4 mg, 0.04 mmol	2:2:1	(MeCN:H_2O):H_2O: Et_3N/H_2O, (v:v):v:v, (0.5:0.5):1:0.75, 2.75 ml	Hts, 125°C, blue small prism crystals.
34 (P1)	$Cu(OAc)_2{\cdot}H_2O$ 16 mg, 0.08 mmol	14.24 mg, 0.08 mmol	8.4 mg, 0.04 mmol	2:2:1	(MeCN:H_2O): H_2O: Et_3N/H_2O, (v:v):v:v, (0.5:0.5):0.5:0.75, 2.25 ml	Hts, 125°C, blue small prism crystals.

Mass for **33**: 17 mg and for **34**: 16 mg.

IR (ATR) for **33** **ν/cm^{-1}**: 3112, 2988 (w, ν (C-H) of btrip), 2094, 1988 (w, H-bonds), 1646 (s, ν_{asym} C=O), 1594 (w, ν_{sym} C=O), 1234 (s, ν_{asym} C-O), 1189 (s, ν_{sym} C-O), 877 (w, γ C-H), 758, 726 (s, γ (1,3,5-trisubstituted benzene ring) of btc).

IR (ATR) for **34** **ν/cm^{-1}**: 3109 (w, ν (C-H) of btrip), 1646 (s, ν_{asym} C=O), 1612 (w, ν_{sym} C=O), 1240 (s, ν_{asym} C-O), 1190 (s, ν_{sym} C-O), 871 (w, γ C-H), 758, 726 (s, γ (1,3,5-trisubstituted benzene ring) of btc).

10.2.7 Synthesis of coordination compounds 35, 36, 37 & 38

A mixture of an aqueous solution of zinc salts and an aqueous solution of 4,4`-bi(1,2,4-triazol-4-yl) (btr) ligand were mixed in a glass tube, which was sealed, and hand shaked for about 3 min. After that, an aqueous solution of benzene-1,3,5-tricarboxylic acid (H_3btc) ligand, which was deprotonated in a glass tube with Triethylamine (Et_3N/H_2O) solution (0.16 mmol/l, 3eq to H_3btc) as base by using ultrasonic bath and heating at 45-50°C, was added to previously mixture. The solutions were mixed in a glass tube, which was sealed, hand shaked for about 2-3 minutes, and then kept for 30 min at ambient temperature. The resulting colorless single crystals were washed with the same mother liquor. Finally, the sample was dried in vacuum furnace for *ca.* 2-3h at 40°C. The synthesis of compounds is summarized in Table 9.2.7.1.

Table 9.2.7.1: Synthesis conditions for **35**, **36**, **37** & **38**:

Product	Metal salt	btr	H_3btc	Rate	Solvents	Result
35	$Zn(NO_3)_2{\cdot}6H_2O$ 23.8 mg, 0.08 mmol	16.32 mg, 0.12 mmol	8.4 mg, 0.04 mmol	2:3:1	H_2O:H_2O:Et_3N/H_2O, v:v:v, 0.5:0.5:0.75, 1.75 ml	colorless crystals after 30 min
35-1	$Zn(NO_3)_2{\cdot}4H_2O$ 20.8 mg, 0.08 mmol	16.32 mg, 0.12 mmol	8.4 mg, 0.04 mmol	2:3:1	H_2O:H_2O:Et_3N/H_2O, v:v:v, 0.5:0.5:0.75, 1.75 ml	colorless crystals after 30 min
36	$ZnBr_2$ 18 mg, 0.08 mmol	16.32 mg, 0.12 mmol	8.4 mg, 0.04 mmol	2:3:1	H_2O:H_2O:Et_3N/H_2O, v:v:v, 0.5:0.5:0.75, 1.75 ml	colorless crystals after 30 min
37	$Zn(ClO_4)_2{\cdot}6H_2O$ 29.6 mg, 0.08 mmol	16.32 mg, 0.12 mmol	8.4 mg, 0.04 mmol	2:3:1	H_2O:H_2O:Et_3N/H_2O, v:v:v, 0.5:0.5:0.75, 1.75 ml	colorless crystals after 30 min

Product	Metal salt	btr	H_3btc	Rate	Solvents	Result
38	$ZnCl_2$ 10.4 mg, 0.08 mmol	16.32 mg, 0.12 mmol	8.4 mg, 0.04 mmol	2:3:1	H_2O:H_2O:Et_3N/H_2O, v:v:v, 0.5:0.5:0.75, 1.75 ml	colorless crystals after 30 min

The mass of **35**: 8 mg, **36**: 9 mg, **37**: 10 mg and **38**: 6 mg.

1D-$[Zn_3(\mu_3\text{-btc})(\mu_2\text{-btc})(H_2O)_{12}]_n$, M_w ($\mathbf{C_{18}H_{30}O_{24}Zn_3}$) = 826.56 g.mol^{-1}, Yield for **35**: 8 mg, 0.009 mmol (24.2% based on H_3btc).

IR (ATR) for **35 ν/cm^{-1}**: 3443, 3389 (w, ν (O-H)), 3097 (w, ν (C-H)), 1612 (s, ν_{asym} C=O), 1548 (w, ν_{sym} C=O), 1212 (m, ν_{asym} C-O), 1127 (w, ν_{sym} C-O), 926 (w, γ C-H), 738, 711 (s, γ (1,3,5-trisubstituted benzene ring) of btc).

10.2.8 Synthesis of coordination compound 39

A mixture of an aqueous solution of $Co(NO_3)_2.6H_2O$ salt, an aqueous solution of benzene-1,3-di(1H-tetrazol-5-yl) (H_2ipdt) ligand and an aqueous solution of benzene-1,3,5-tricarboxylic acid (H_3btc) ligand were added to glass tube. The ligands were deprotonated by using ammonia (NH_3/H_2O) solution (0.16 mmol/l, 2eq. to H_2ipdt, 3eq. to H_3btc) as base by using ultrasonic bath and heating at 45-50°C, where the solutions were mixed in a glass tube, which was sealed, stirred for *ca.* 5 min, and then the sample was placed in a programmable furnace. The sample was heated to 150°C during 2h and held at that temperature for 24h, then cooled at temperature rate 3°C/h to ambient temperature. The resulting red single crystals were washed with the same mother liquor. Finally, the sample was dried in vacuum furnace for *ca.* 2-3h at 40°C. The synthesis of compounds is summarized in Table 9.2.8.1.

Table 9.2.8.1: Synthesis conditions for **39**:

Product	Metal salt	H_2ipdt	H_3btc	Rate	Solvents	Result
39 (P5)	$Co(NO_3)_2{\cdot}6H_2O$ 48 mg, 0.16 mmol	8.4 mg, 0.04 mmol	8.4 mg, 0.04 mmol	4:1:1	H_2O:NH_3/H_2O: NH_3/H_2O, v:v:v, 0.5:0.5:0.75, 1.75 ml	Hts.150°C red needle shaped crystals and small orange crystals.

1D-$[Co_3(\mu_3\text{-btc})(\mu_2\text{-btc})(H_2O)_{12}]_n$, M_w ($\mathbf{C_{18}H_{30}Co_3O_{24}}$) = 807.2214 g.mol^{-1}, Yield for **39**: 14 mg, 0.0173 mmol (43.35% based on H_3btc).

IR (ATR) for **39** **ν/cm^{-1}**: 3392 (m, br, ν (O-H)), 3107 (w, br, ν (C-H)), 1608 (s, ν_{asym} C=O), 1513 (s, ν_{sym} C=O), 1353 (s, ν C-O), 812 (m, γ C-H), 710, 655 (s, 1,3-disubstituted benzene ring).

10.2.9 Synthesis of coordination compound 40 with 41, 42 & 43

The zinc(II) compounds analogue were isolated as colorless or yellow single crystals using the same procedure, that described for the zinc(II) compounds **19** and **20**. A mixture of an aqueous solution of different zinc (II) salts and a methanol solution of bis-1,2,4-triazol-4-yl-isopropanol (*rac*-btrip) ligand were mixed in a glass tube vessel, which was sealed, and hand shaked for about 3 min. After that, an aqueous solution of 5-aminoisophtalic acid (H_2aip) ligand, which was deprotonated in a glass tube vessel with Et_3N/H_2O solution (0.16 mmol/l, 2eq. to H_2aip) as base by using ultrasonic bath and heating at 45-50°C, was added to previously mixture. The solutions were mixed in a glass tube, which was sealed again, stirred for *ca.* 15 min, and then placed in a programmable furnace. The sample was heated to 125°C during 3h and held at that temperature for 48h, then cooled at temperature rate 5°C/h to ambient temperature. The resulting colorless or yellow single crystals were separated from weight precipitate and washed with the same mother liquor. Finally, the sample was dried in vacuum furnace for *ca.* 3h at 40°C. The synthesis of compounds is summarized in Table 9.2.9.1.

Table 9.2.9.1: Synthesis conditions for **40**, **41**, **42** & **43**:

Product	Metal salt	btrip	H_2aip	Rate	Solvents	Result
40 (P1)	$Zn(NO_3)_2{\cdot}4H_2O$ 23.8 mg, 0.08 mmol	14.24 mg, 0.08 mmol	7.2 mg, 0.04 mmol	2:2:1	H_2O:MeOH: Et_3N/H_2O, v:v:v, 0.5:0.5:0.5, 1.5 ml	Hts, 125°C, colorless crystals.
41 (P1)	$Zn(OAc)_2{\cdot}2H_2O$ 17.6 mg, 0.08 mmol	14.24 mg, 0.08 mmol	7.2 mg, 0.04 mmol	2:2:1	H_2O:MeOH Et_3N/H_2O, v:v:v, 0.5:0.5:0.5, 1.5 ml	Hts, 125°C, colorless crystals.
42 (P1)	$ZnCl_2$ 10.4 mg, 0.08 mmol	14.24 mg, 0.08 mmol	7.2 mg, 0.04 mmol	2:2:1	H_2O:MeOH: Et_3N/H_2O, v:v:v, 0.5:0.5:0.5, 1.5 ml	Hts, 125°C, light yellow crystals.

Product	Metal salt	btrip	H_2aip	Rate	Solvents	Result
43 (P1)	$ZnBr_2$ 17.6 mg, 0.08 mmol	14.24 mg, 0.08 mmol	7.2 mg, 0.04 mmol	2:2:1	H_2O:MeOH: Et_3N/H_2O, v:v:v, 0.5:0.5:0.5, 1.5 ml	Hts, 125°C light yellow crystals.

IR (ATR) for **40 ν/cm^{-1}**: 3406, 3257 (w, ν O-H and N-H), 3095, 3003 (w, ν C-H), 1622 (w, ν_{asym} C=O), 1544 (m, ν_{sym} C=O), 1207 (w, ν_{asym} C-O, C-N), 1153 (w, ν_{sym} C-O, C-N), 829 (w, γ C-H), 736, 674 (m, 1,3,5-trisubstituted benzene ring of H_2aip).

10.2.10 Synthesis of compounds 44, 45 & 46

The zinc(II) compounds analogue were isolated as colorless or yellow single crystals using the same procedure, that described for the zinc(II) compounds **19** and **20**. A mixture of an aqueous solution of different zinc (II) salts and a methanol solution of bis-1,2,4-triazol-4-yl-isopropanol (*rac*-btrip) ligand were mixed in a glass tube vessel, which was sealed, and hand shaked for about 3 min. After that, an aqueous solution of isophtalic acid (H_2ip) ligand, which was deprotonated in a glass tube vessel with Et_3N/H_2O solution (0.16 mmol/l, 2eq. to H_2ip) as base by using ultrasonic bath and heating at 45°C, was added to previously mixture. The solutions were mixed in a glass tube, which was sealed again, stirred for *ca.* 15 min, and then placed in a programmable furnace. The sample was heated to 125°C during 3h and held at that temperature for 48h, then cooled at temperature rate 5°C/h to ambient temperature. The resulting colorless or yellow single crystals were separated from weight precipitate and washed with the mother liquor. Finally, the sample was dried in vacuum furnace for *ca.* 2-3h at 40°C. The synthesis of compounds is summarized in Table 9.2.10.1.

Table 9.2.10.1: Synthesis conditions for **44**, **45** & **46**:

Product	Metal salt	btrip	H_2ip	Rate	Solvents	Result
44 (P1)	$Zn(NO_3)_2{\cdot}4H_2O$ 23.8 mg, 0.08 mmol	14.24 mg, 0.08 mmol	6.6 mg, 0.04 mmol	2:2:1	H_2O:MeOH: Et_3N/H_2O, v:v:v, 0.5:0.5:0.5, 1.5 ml	Hts, 125 °C, light yellow crystals.
45 (P1)	$ZnCl_2$ 10.4 mg, 0.08 mmol	14.24 mg, 0.08 mmol	6.6 mg, 0.04 mmol	2:2:1	H_2O:MeOH: Et_3N/H_2O, v:v:v, 0.5:0.5:0.5, 1.5 ml	Hts, 125 °C, spherical light yellow crystals.

Product	Metal salt	btrip	H_2ip	Rate	Solvents	Result
46 (P1)	$ZnBr_2$ 17.6 mg, 0.08 mmol	14.24 mg, 0.08 mmol	6.6 mg, 0.04 mmol	2:2:1	H_2O:MeOH: Et_3N/H_2O, v:v:v, 0.5:0.5:0.5, 1.5 ml	Hts, 125 °C, spherical light yellow crystals.

10.2.11 Synthesis of compound 47

The zinc(II) compound **47** analogue was isolated as colorless single crystals using the same procedure, that described for the zinc(II) compounds **19** and **20**. A mixture of an aqueous solution of zinc(II)chloride and a methanol solution of bis-1,2,4-triazol-4-yl-isopropanol (*rac*-btrip) ligand were mixed in a glass tube, which was sealed, and hand shaked for about 3 min. After that, an aqueous solution of 4,6-dimethyl-5-aminoisophthalic acid (dm-H_2aip) ligand, which was added to glass tube. The solutions were mixed in a glass tube, which was sealed again, stirred for *ca.* 15 min, and then placed in a programmable furnace. The sample was heated to 125°C during 3h and held at that temperature for 48h, then cooled at temperature rate 5°C/h to ambient temperature. The resulting colorless single crystals were separated from weight precipitate and washed with the same mother liquor. Finally, the sample was dried in vacuum furnace for *ca.* 2-3h at 40°C (Table 9.2.11.1).

Table 9.2.11.1: Synthesis conditions for **47**:

Product	Metal salt	btrip	dm-H_2aip	Rate	Solvents	Result
47 (P1)	$ZnCl_2$ 10.4 mg, 0.08 mmol	14.24 mg, 0.08 mmol	8.37 mg, 0.04 mmol	2:2:1	H_2O:MeOH:H_2O, v:v:v, 0.5:1:0.5, 2 ml	Hts, 125 °C, colorless dark crystals.

10.3 Synthesis of coordination polymers constructed from aromatic azolate ligands

10.3.1 Slow evaporation method (S.: MeOH, DMF)

A solution of metal nitrate hydrate (0.08 or 0.16 mmol) in methanol (2 ml), a solution of terephthalic acid ligand H_2bdc (0.04 mmol, 6.6 mg) in DMF (1 ml) and a solution of benzene 1,4-ditetrazol-5-yl ligand H_2bdt (0.04 mmol, 8.4 mg) in DMF (1 ml) were mixed in mole ratio (4:1:1), stirred for about 1 hand then the reaction mixture was filtered and the filtrate was placed at ambient temperature to evaporate slowly for a few days. The resulting single crystals were separated from precipitate, washed with mother liquor, dried and after then measured by IR-spectra to examine either mixed-ligands or single-ligand were/was coordinated with the metal ions. Other experiments with other metal chloride or metal nitrate of Cd^{2+}, Cu^{2+}, Zn^{2+}, Mn^{2+}, Fe^{2+} and Co^{2+} under the same conditions were unsuccessful. The synthesis of compounds is summarized in Table 9.3.1.1.

Table 9.3.1.1: Synthesis conditions for crystallized compounds **48**, **49** & **50**:

Product	Metal salt	H_2bdt	H_2bdc	Rate	Solvents	Result and remark
48	$Cd(NO_3)_2{\cdot}4H_2O$ 24 mg, 0.08 mmol	8.4 mg	6.6 mg	2:1:1	MeOH:DMF:DMF, v:v:v, 2:1:1, 4 ml	Slow evap., crystals.
49	$Cu(NO_3)_2{\cdot}2.5H_2O$ 18.4 mg, 0.08 mmol	8.4 mg	6.6 mg	2:1:1	MeOH:DMF:DMF, v:v:v, 2:1:1, 4 ml	Slow evap., crystals.
50	$Zn(NO_3)_2{\cdot}4H_2O$ 23.3 mg, 0.16 mmol	8.4 mg	6.6 mg	4:1:1	MeOH:DMF:DMF, v:v:v, 2:1:1, 4 ml	Slow evap., crystals.

10.3.2 Solvothermal method at low temperature (S.: MeOH, DMF)

A solution of metal chloride of Cd^{2+}, Zn^{2+} (0.08 mmol) in H_2O (1 ml) or Mn^{2+} (0.08 mmol) in MeOH (1 ml), a solution of benzene-1,3,5-tricarboxylic acid H_3btc (0.02 mmol) in DMF (0.5 ml), and a solution of benzene-1,3-di(1H-tetrazol-5-yl) H_2ipdt (0.02 mmol) in DMF (0.5 ml) were mixed, stirred for about 10 minutes and palced in furnace at 70 °C for Mn^{2+}, Cd^{2+} and 100 °C for Zn^{2+}. Finally, the samples were removed from furnace when the crystals were formed, after a few days. The obtained single crystals were separated from precipitate, washed with mother liquor, dried and after that ^{1}H NMR- or IR-spectra were measured to examine either mixed-ligands or single-ligand were/was coordinated with the metal ions. Other experiments with other metal chloride or metal sulfate of Cd^{2+}, Zn^{2+}, Cu^{2+}, Ni^{2+}, Mn^{2+},

Fe^{2+} and Co^{2+} and metale nitrate of Cu^{2+} and Co^{2+} under the same conditions were unsuccessful. The synthesis of compounds is summarized in Table 9.3.2.1.

Table 9.3.2.1: Synthesis conditions for crystallized compounds **51**, **52**, **53** & **54**

Product	Metal salt	H_2ipdt	H_3btc	Rate	Solvents	Result and remark
51	$MnCl_2 \cdot 4H_2O$ 16 mg, 0.08 mmol	4.2 mg	4.2 mg	4:1:1	MeOH:DMF:DMF, v:v:v, 1:0.5:0.5, 2 ml	Sts, 70 °C crystals (4 d.)
52	$MnCl_2 \cdot 4H_2O$ 16 mg, 0.08 mmol	4.2 mg	4.2 mg	4:1:1	MeOH:DMF:DMF, v:v:v, 1:0.5:0.5, 2 ml (10 µl HCl)	Sts, 70 °C crystals (4 d.)
53	$ZnCl_2$ 10.4 mg, 0.08 mmol	4.2 mg	4.2 mg	4:1:1	H_2O:DMF:DMF, v:v:v, 1:0.5:0.5, 2 ml	Sts, 100 °C crystals
54	$CdCl_2 \cdot H_2O$ 16 mg, 0.08 mmol	4.2 mg	4.2 mg	4:1:1	H_2O:DMF:DMF, v:v:v, 1:0.5:0.5, 2 ml	Sts, 70 °C colorless crystals

10.3.3 Solvothermal method at low temperature with mineral acid (S.: MeOH, DMF)

A solution of metal nitrate or metal chloride of Cd^{2+}, Zn^{2+} (0.08 mmol) in H_2O (1 ml) or Mn^{2+} (0.06 mmol) in MeOH (1 ml), a solution of benzene carboxylate ligand H_2bdc, H_2ip or H_3btc (0.02 mmol) in DMF (0.5 - 0.75 ml), and a solution of benzene tetrazolate ligand H_2bdt or H_2ipdt (0.02 mmol) in DMF (0.5 - 0.75 ml) were mixed and stirred for about 10 minutes. After that concentrated acid (15 – 25 µl) was added for each sample (HCl acid for metal chloride, HNO_3 acid for metal nitrate). The reaction mixtures were stirred again for about 5 minutes and place in the furnace at 70 or 100 °C. Finally, the samples were removed from furnace when the crystals were formed. The formed single crystals were separated from precipitate, washed with mother liquor, dried and after that were measured by ^{1}H NMR- or IR-spectra to examine either mixed-ligands or single-ligand were/was coordinated with the metal ions. Other experiments with other metal chloride or metal nitrate of Cd^{2+}, Zn^{2+} and Mn^{2+} under the same conditions were unsuccessful. The synthesis of compounds is summarized in the following Tables.

Table 9.3.3.1: Synthesis conditions for crystallized compounds **55**, **56**, **57** & **58**

Product	Metal salt	H_2bdt	H_2bdc	Rate	Solvents	Result and remark
55	$CdCl_2 \cdot H_2O$ 16 mg, 0.08 mmol	4.2 mg	3.3 mg	4:1:1	H_2O:DMF:DMF, v:v:v, 1:0.5:0.5, 2 ml, (15 µl HCl)	Sts, 100 °C, small crystals

Product	Metal salt	H_2bdt	H_2bdc	Rate	Solvents	Result and remark
56	$Cd(NO_3)_2 \cdot 4H_2O$ 24 mg, 0.08 mmol	4.2 mg	3.3 mg	4:1:1	H_2O:DMF:DMF, v:v:v, 1:0.75:0.75, 2.5 ml, (25 µl HNO_3)	Sts, 100 °C, small crystals
57	$MnCl_2 \cdot 4H_2O$ 13 mg, 0,06 mmol	4.2 mg	3.3 mg	3:1:1	MeOH:DMF:DMF, v:v:v, 1:0.75:0.75, 2.5 ml, (25 µl HCl)	Sts, 100 °C, small crystals (4 d.)
58	$Mn(NO_3)_2 \cdot 4H_2O$ 20 mg, 0.08 mmol	4.2 mg	3.3 mg	4:1:1	MeOH:DMF:DMF, v:v:v, 1:075:0.75, 2.5 ml, (25 µl HNO_3)	Sts, 100 °C, acicular crystals

Table 9.3.3.2: Synthesis conditions for crystallized compound **55**

Product	Metal salt	H_2bdt	H_2ip	Rate	Solvents	Result and remark
59	$Cd(NO_3)_2 \cdot 4H_2O$ 24 mg, 0.08 mmol	4.2 mg	3.3 mg	4:1:1	H_2O:DMF:DMF, v:v:v, 0.5:0.75:0.75, 2 ml, (25 µl HNO3)	Sts, 100 °C small crystals (4 d.)

Table 9.3.3.3: Synthesis conditions for crystallized compounds **60**, **61**, **62** & **63**

Product	Metal salt	H_2bdt	H_3btc	Rate	Solvents	Result and remark
60	$CdCl_2 \cdot H_2O$ 16 mg, 0.08 mmol	4.2 mg	4.2 mg	4:1:1	H_2O:DMF:DMF, v:v:v, 0.5:0.5:0.5, 1.5 ml), (15 µl HCl)	Sts, 100 °C-small crystals after long time
61	$Cd(NO_3)_2 \cdot 4H_2O$ 24 mg, 0.08 mmol	4.2 mg	4.2 mg	4:1:1	H_2O:DMF:DMF, v:v:v, 0.5:0.5:0.5, 1.5 ml, (15 µl HNO3)	Sts, 70 °C poly crystals
62	$MnCl_2 \cdot 4H_2O$ 13 mg, 0.06 mmol	4.2 mg	4.2 mg	3:1:1	MeOH:DMF:DMF, v:v:v, 0.5:0.75:0.75, 2 ml, (25 µl HCl)	Sts, 70 °C poly crystals
63	$Mn(NO_3)_2 \cdot 4H_2O$ 20 mg, 0.08 mmol	4.2 mg	4.2 mg	4:1:1	MeOH:DMF:DMF, v:v:v, 0.5:0.75:0.75, 2 ml, (25 µl HNO3)	Sts, 70 °C poly crystals

Table 9.3.3.4: Synthesis conditions for crystallized compounds **64**, **65** & **66**

Product	Metal salt	H_2ipdt	H_2bdc	Rate	Solvents	Result and remark
64	$MnCl_2 \cdot 4H_2O$ 13 mg, 0.06 mmol	4.2 mg	3.3 mg	3:1:1	MeOH:DMF:DMF, v:v:v, 0.5:0.75:0.75, 2 ml, (25 µl HCl)	Sts, 70 °C crystals
65	$Mn(NO_3)_2 \cdot 4H_2O$ 20 mg, 0.08 mmol	4.2 mg	3.3 mg	4:1:1	MeOH:DMF:DMF, v:v:v, 0.5:0.75:0.75, 2 ml, (25 µl HNO_3)	Sts, 70 °C crystals

Product	Metal salt	H_2ipdt	H_2bdc	Rate	Solvents	Result and remark
66	$Cd(NO_3)_2{\cdot}4H_2O$ 24 mg, 0.08 mmol	4.2 mg	3.3 mg	4:1:1	MeOH:DMF:DMF, v:v:v, 0.5:0.5:0.5, 1.5 ml, (15 µl HNO_3)	Sts, 70 °C crystals

Table 9.3.3.5: Synthesis conditions for crystallized compounds **67** & **68**

Product	Metal salt	H_2ipdt	H_2ip	Rate	Solvents	Result and remark
67	$Cd(NO_3)_2{\cdot}4H_2O$ 24 mg, 0.08 mmol	4.2 mg	3.3 mg	4:1:1	H_2O:DMF:DMF, v:v:v, 0.5:0.5:0.5, 1.5 ml, (15 µl HNO_3)	Sts, 70 °C crystals
68	$Mn(NO_3)_2{\cdot}4H_2O$ 20 mg, 0.08 mmol	4.2 mg	3.3 mg	4:1:1	MeOH:DMF:DMF, v:v:v, 0.5:0.5:0.5, 1.5 ml, (15 µl HNO_3)	Sts, 100 °C crystals

Table 9.3.3.6: Synthesis conditions for crystallized compounds **69**, **70** & **71**

Product	Metal salt	H_2ipdt	H_3btc	Rate	Solvents	Result and remark
69	$MnCl_2{\cdot}4H_2O$ 13 mg, 0.06 mmol	4.2 mg	4.2 mg	3:1:1	MeOH:DMF:DMF, v:v:v, 0.5:0.75:0.75, 2 ml, (25 µl HCl)	Sts, 70 °C crystals
70	$Mn(NO_3)_2{\cdot}4H_2O$ 20 mg, 0.08 mmol	4.2 mg	4.2 mg	4:1:1	MeOH:DMF:DMF, v:v:v, 0.5:0.75:0.75, 2 ml, (25 µl HNO_3)	Sts, 70 °C crystals
71	$Cd(NO_3)_2{\cdot}4H_2O$ 24 mg, 0.08 mmol	4.2 mg	4.2 mg	4:1:1	H_2O:DMF:DMF, v:v:v, 0.5:0.5:0.5, 1.5 ml, (15 µl HNO_3)	Sts, 100 °C crystals

10.3.4 Solvothermal method at low temperature without mineral acid (S.: MeOH, DMSO, DMF)

A solution of metal nitrate or metal chloride of Zn^{2+} (0.08 mmol) in DMSO (0.5 ml) or Cd^{2+}, Mn^{2+} (0.08 mmol) in MeOH (0.5 ml) or mixture of MeOH:DMSO (v:v, 0.5:0.5, 1 ml), a solution of benzene carboxylate ligand H_2bdc, H_2ip or H_3btc (0.02 mmol) in DMF (0.5 ml), and a solution of benzene tetrazolate ligand H_2bdt or H_2ipdt (0.02 mmol) in DMF (0.5 ml) were mixed and stirred for about 10 minutes and place in furnace at 70, 90 or 125 °C. Finally, the samples were removed from furnace, when the crystals were formed after a few days. The resulting crystals were separated from precipitate, washed with mother liquor, dried and after that ^{1}H NMR- or IR-spectra were measured to examine either mixed-ligands or single-ligand were/was coordinated with the metal ions. Other experiments with other metal chloride or

metal nitrate of Cd^{2+}, Zn^{2+} and Mn^{2+} under the same conditions were unsuccessful. The synthesis of compounds is summarized in the following Tables.

Table 9.3.4.1: Synthesis conditions for crystallized compounds **72**, **73**, **74** & **75**

Product	Metal salt	H_2bdt	H_2bdc	Rate	Solvents	Result and remark
72	$MnCl_2 \cdot 4H_2O$ 16 mg, 0.08 mmol	4.2 mg	3.3 mg	4:1:1	MeOH:DMF:DMF, v:v:v, 0.5:0.5:0.5, 1.5 ml	Sts, 70 °C acicular poly crystals (3 d.)
73	$Mn(NO_3)_2 \cdot 4H_2O$ 20 mg, 0.08 mmol	4.2 mg	3.3 mg	4:1:1	(MeOH:DMSO):DMF :DMF, (v):v:v, (1):0.5:0.5, 2 ml	Sts, 90 °C yellow and colorless crystals
74	$Cd(NO_3)_2 \cdot 4H_2O$ 24 mg, 0.08 mmol	4.2 mg	3.3 mg	4:1:1	(MeOH:DMSO):DMF :DMF, (v):v:v, (1):0.5:0.5, 2 ml	Sts, 125 °C yellow crystals
75	$Zn(NO_3)_2 \cdot 4H_2O$ 20.8 mg, 0.08 mmol	4.2 mg	3.3 mg	4:1:1	DMSO:DMF:DMF, v:v:v, 0.5:0.5:0.5, 1.5 ml	Sts, 90 °C crystals (4 d.)

Table 9.3.4.2: Synthesis conditions for crystallized compound **76**

Product	Metal salt	H_2bdt	H_2ip	Rate	Solvents	Result and remark
76	$Cd(NO_3)_2 \cdot 4H_2O$ 24 mg, 0.08 mmol	4.2 mg	3.3 mg	4:1:1	(MeOH:DMSO):DMF :DMF, (v):v:v, (1):0.5:0.5, 2 ml	Sts, 70 °C acicular poly crystals (4 d.)

Table 9.3.4.3: Synthesis conditions for crystallized compounds **77**, **78**, **79** & **80**

Product	Metal salt	H_2bdt	H_3btc	Rate	Solvents	Result and remark
77	$MnCl_2 \cdot 4H_2O$ 16 mg, 0.08 mmol	4.2 mg	4.2 mg	4:1:1	MeOH:DMF:DMF, v:v:v, 0.5:0.5:0.5, 1.5 ml	Sts, 70 °C small colorless crystals (4 d.)
78	$Mn(NO_3)_2 \cdot 4H_2O$ 20 mg, 0.08 mmol	4.2 mg	4.2 mg	4:1:1	MeOH:DMF:DMF, v:v:v, 0.5:0.5:0.5, 1.5 ml	Sts, 90 °C crystals
79	$CdCl_2 \cdot H_2O$ 16 mg, 0.08 mmol	4.2 mg	4.2 mg	4:1:1	($MeOH:H_2O$):DMF:D MF, (v):v:v, (1):0.5:0.5, 2 ml	Sts, 125 °C small crystals
80	$Cd(NO_3)_2 \cdot 4H_2O$ 24 mg, 0.08 mmol	4.2 mg	4.2 mg	4:1:1	(MeOH:DMSO):DMF :DMF, (v):v:v, (1):0.5:0.5, 2 ml	Sts, 125 °C crystals

Table 9.3.4.4: Synthesis conditions for crystallized compounds **81** & **82**

Product	Metal salt	H_2ipdt	H_2bdc	Rate	Solvents	Result and remark
81	$Mn(NO_3)_2{\cdot}4H_2O$ 20 mg, 0.08 mmol	4.2 mg	3.3 mg	4:1:1	MeOH:DMF:DMF, v:v:v, 0.5:0.5:0.5, 1.5 ml	Sts, 70 °C crystals
82	$Cd(NO_3)_2{\cdot}4H_2O$ 24 mg, 0.08 mmol	4.2 mg	3.3 mg	4:1:1	(MeOH:DMSO):DMF :DMF, (v):v:v, (1):0.5:0.5, 2 ml	Sts, 125 °C yellow crystals

Table 9.3.4.5: Synthesis conditions for crystallized compound **83**

Product	Metal salt	H_2ipdt	H_2ip	Rate	Solvents	Result and remark
83	$Mn(NO_3)_2{\cdot}4H_2O$ 20 mg, 0.08 mmol	4.2 mg	3.3 mg	4:1:1	MeOH:DMF:DMF, v:v:v, 0.5:0.5:0.5, 1.5 ml	Sts, 70 °C yellow crystals

Table 9.3.4.6: Synthesis conditions for crystallized compounds **84** & **85**

Product	Metal salt	H_2ipdt	H_3btc	Rate	Solvents	Result and remark
84	$Mn(NO_3)_2{\cdot}4H_2O$ 20 mg, 0.08 mmol	4.2 mg	4.2 mg	4:1:1	MeOH:DMF:DMF, v:v:v, 0.5:0.5:0.5, 1.5 ml	Sts, 70 °C crystals
85	$ZnCl_2$ 10.4 mg, 0.08 mmol	4.2 mg	4.2 mg	4:1:1	DMSO:DMF:DMF, v:v:v, 0.5:0.5:0.5, 1.5 ml	Sts, 125 °C crystals (3 d.)

10.3.5 Solvothermal method at high temperature (S.: H_2O, DMF)

A mixture of DMF and water in volume ratio (v:v, 1:1) was prepared to obtain a solution of used ligands (H_2bdc and H_2bdt). An aqueous solution of metal salts (0.16 mmol), a solution of benzene-1,4-dicarboxylic acid H_2bdc (0.04 mmol) and a solution of benzene-1,4-di(1H-tetrazol-5-yl) H_2bdt (0.04 mmol) dissolved in a mixture of H_2O:DMF (v:v, 1:1) were mixed in mole ratio (4:1:1) into a glass tube, which was sealed and stirred for about 5 min. and then placed in a programmable furnace. The sample was heated to 150°C during 2h and held at that temperature for 48h, then cooled through temperature rate 5°C/h to ambient temperature. The formed crystals were separated from precipitate, washed with mother liquor, dried and after that ^{1}H NMR- or IR-spectra were measured to examine either mixed-ligands or single-ligand were/was coordinated with the metal ions. Other experiments with other metal chloride or metal nitrate of Cd^{2+}, Zn^{2+}, Mn^{2+}, Cr^{3+}, Cu^{2+}, Co^{2+}, Ni^{2+}, Fe^{2+}, and Al^{3+} under the same conditions were unsuccessful. Colorless crystals of **86** and **87** were obtained

by at the end of reaction without any crystals or precipitate, therefore the sample was putted to slow evaporation of their reaction solutions. Colorless crystals were formed after one week. The synthesis of resulting compounds is summarized in Table 9.3.5.1.

Table 9.3.5.1: Synthesis conditions for crystallized compounds **86**, **87**, **88**, **89**, **90** & **91**

Product	Metal salt	H_2bdt	H_2bdc	Rate	Solvents	Result and remark
86	$MnCl_2$ 21 mg, 0.16 mmol	8.4 mg	6.6 mg	4:1:1	H_2O:(H_2O:DMF):(H_2O:DMF), v:v:v, 0.5:0.5:0.5, 1.5 ml	Sts, 150 °C, slow evaporation, Cololess crystals.
87	$Mn(NO_3)_2{\cdot}4H_2O$ 40 mg, 0.16 mmol	8.4 mg	6.6 mg	4:1:1	H_2O:(H_2O:DMF):(H_2O:DMF), v:v:v, 0.5:0.5:0.5, 1.5 ml	Sts, 150 °C, slow evaporation, Cololess crystals.
88	$Ni(NO_3)_2{\cdot}6H_2O$ 48 mg, 0.16 mmol	8.4 mg	6.6 mg	4:1:1	H_2O:(H_2O:DMF):(H_2O:DMF), v:v:v, 0.5:0.5:0.5, 1.5 ml	Sts, 150 °C, a little amount of green crystals.
89	$Fe(NO_3)_3{\cdot}9H_2O$ 64 mg, 0.16 mmol	8.4 mg	6.6 mg	4:1:1	H_2O:(H_2O:DMF):(H_2O:DMF), v:v:v, 0.5:0.5:0.5, 1.5 ml	Sts, 150 °C, acicular crystals.
90	$Al(NO_3)_3{\cdot}9H_2O$ 60 mg, 0.16 mmol	8.4 mg	6.6 mg	4:1:1	H_2O:(H_2O:DMF):(H_2O:DMF), v:v:v, 0.5:0.5:0.5, 1.5 ml	Sts, 150 °C, acicular colorless crystals.
91	$CrCl_3{\cdot}6H_2O$ 42.6 mg, 0.16 mmol	8.4 mg	6.6 mg	4:1:1	H_2O:(H_2O:DMF):(H_2O:DMF), v:v:v, 0.5:0.5:0.5, 1.5 ml	Sts, 150 °C, acicular crystals.

10.3.6 Hydrothermal method at low temperature (S.: NaOH or NH_4OH)

Hydrothermal reaction at low temperature was carried out using NaOH or NH_4OH solution (0.08 mmol/l) to deprotonate the used ligands (H_2bdc, H_2ip, H_3btc or H_2bdt) using ultrasonic irradiation at 40-50°C. The metal salts (0.08 mmol) were dissolved in water (0.5 ml), benzene carboxylate ligand H_2bdc, H_2ip or H_3btc (0.02 mmol) and benzene-1,4-di(1H-tetrazol-5-yl) H_2bdt (0.02 mmol) were dissolved either in NaOH (0.5 ml) or NH_4OH (0.5 ml) using ultrasonic bath at 40-50°C (For H_3btc was dissolved in 0.75 ml of NaOH or NH_4OH solution to deprotonate their three carboxyl groups). These solutions were mixed in a glass tube, which was sealed, stirred for about 10 minutes, and then placed in a furnace at 75 or 100 °C. The samples were removed from furnace when suitable single crystals were formed, after a few days. The resulting single crystals were separated from precipitate, washed with mother liquor, dried and after that measured by ^{1}H NMR- or IR-spectra to examine either mixed-ligands or single-ligand were/ was coordinated with the metal ions. Other experiments in the

same condition with other metal chloride (Br^- for Cu^{2+}) or metal nitrate (ClO_4^- for Ni^{2+}) of Cr^{3+}, Cu^{2+}, Co^{2+}, Ni^{2+}, Fe^{2+} (Fe^{3+} for nitrate), and Al^{3+} under the same conditions were unsuccessful. The synthesis of compounds is summarized in the following Tables.

Table 9.3.6.1: Synthesis conditions for crystallized compounds **92**, **93**, **94** & **95**

Product	Metal salt	H_2bdt	H_2bdc	Rate	Solvents	Result and remark
92	$CoCl_2 \cdot 6H_2O$ 18.4 mg, 0.08 mmol	4.2 mg	3.3 mg	4:1:1	H_2O:NaOH:NaOH, v:v:v, 0.5:0.5:0.5, 1.5 ml	Hts, 75 °C small pink crystals (3 d.)
93	$Co(NO_3)_2 \cdot 6H_2O$ 24 mg, 0.08 mmol	4.2 mg	3.3 mg	4:1:1	H_2O:NaOH:NaOH, v:v:v, 0.5:0.5:0.5, 1.5 ml	Hts, 75 °C acicular pink crystals (3 d.)
94	$CoCl_2 \cdot 6H_2O$ 18.4 mg, 0.08 mmol	4.2 mg	3.3 mg	4:1:1	H_2O:NH_4OH:NH_4OH, v:v:v, 0.5:0.5:0.5, 1.5 ml	Hts, 100 °C small pink crystals
95	$FeCl_2 \cdot 4H_2O$ 16 mg, 0.08 mmol	4.2 mg	3.3 mg	4:1:1	H_2O:NH_4OH:NH_4OH, v:v:v, 0.5:0.5:0.5, 1.5 ml	Hts, 100 °C small acicular yellow crystals

Table 9.3.6.2: Synthesis conditions for crystallized compounds **96** & **97**

Product	Metal salt	H_2bdt	H_2ip	Rate	Solvents	Result and remark
96	$CoCl_2 \cdot 6H_2O$ 18.4 mg, 0.08 mmol	4.2 mg	3.3 mg	4:1:1	H_2O:NH_4OH:NH_4OH, v:v:v, 0.5:0.5:0.5, 1.5 ml	Hts, 100 °C small crystals
97	$FeCl_2 \cdot 4H_2O$ 16 mg, 0.08 mmol	4.2 mg	3.3 mg	4:1:1	H_2O:NH_4OH:NH_4OH, v:v:v, 0.5:0.5:0.5, 1.5 ml	Hts, 100 °C light yellow crystals.

Table 9.3.6.3: Synthesis conditions for crystallized compounds from **98** to **110**

Product	Metal salt	H_2bdt	H_3btc	Rate	Solvents	Result and remark
98	$CoCl_2 \cdot 6H_2O$ 18.4 mg, 0.08 mmol	4.2 mg	4.2 mg	4:1:1	H_2O:NaOH:NaOH, v:v:v, 0.5:0.5:0.75, 1.75 ml	Hts, 75 °C acicular pink crystals (2-3 d.)
99	$Co(NO_3)_2 \cdot 6H_2O$ 24 mg, 0.08 mmol	4.2 mg	4.2 mg	4:1:1	H_2O:NaOH:NaOH, v:v:v, 0.5:0.5:0.75, 1.75 ml	Hts, 75 °C acicular pink crystals (2-3 d.)
100	$Ni(NO_3)_2 \cdot 6H_2O$ 24 mg, 0.08 mmol	4.2 mg	4.2 mg	4:1:1	H_2O:NaOH:NaOH, v:v:v, 0.5:0.5:0.75, 1.75 ml	Hts, 75 °C acicular green crystals (2-3 d.)
101	$Ni(ClO_4)_2 \cdot 6H_2O$ 28.8 mg, 0.08 mmol	4.2 mg	4.2 mg	4:1:1	H_2O:NaOH:NaOH, v:v:v, 0.5:0.5:0.75, 1.75 ml	Hts, 75 °C acicular green crystals

Product	Metal salt	H_2bdt	H_3btc	Rate	Solvents	Result and remark
102	$CuBr_2$ 17.6 mg, 0.08 mmol	4.2 mg	4.2 mg	4:1:1	H_2O:NaOH:NaOH, v:v:v, 0.5:0.5:0.75, 1.75 ml	Hts, 75 °C blue crystals (2-3 d.)
103	$Cu(NO_3)_2{\cdot}2.5H_2O$ 18.4 mg, 0.08 mmol	4.2 mg	4.2 mg	4:1:1	H_2O:NaOH:NaOH, v:v:v, 0.5:0.5:0.75, 1.75 ml	Hts, 75 °C blue crystals (2-3 d.)
104	$CoCl_2{\cdot}6H_2O$ 18.4 mg, 0.08 mmol	4.2 mg	4.2 mg	4:1:1	H_2O:NH_4OH:NH_4OH, v:v:v, 0.5:0.5:0.75, 1.75 ml	Hts, 100 °C acicular pink crystals (2-3 d.)
105	$Co(NO_3)_2{\cdot}6H_2O$ 24 mg, 0.08 mmol	4.2 mg	4.2 mg	4:1:1	H_2O:NH_4OH:NH_4OH, v:v:v, 0.5:0.5:0.75, 1.75 ml	Hts, 100 °C crystals (2-3 d.)
106	$Ni(NO_3)_2{\cdot}6H_2O$ 24 mg, 0.08 mmol	4.2 mg	4.2 mg	4:1:1	H_2O:NH_4OH:NH_4OH, v:v:v, 0.5:0.5:0.75, 1.75 ml	Hts, 100 °C acicular green crystals (2-3 d.)
107	$Ni(ClO_4)_2{\cdot}6H_2O$ 28.8 mg, 0.08 mmol	4.2 mg	4.2 mg	4:1:1	H_2O:NH_4OH:NH_4OH, v:v:v, 0.5:0.5:0.75, 1.75 ml	Hts, 100 °C acicular green crystals (2-3 d.)
108	$CuBr_2$ 17.6 mg, 0.08 mmol	4.2 mg	4.2 mg	4:1:1	H_2O:NH_4OH:NH_4OH, v:v:v, 0.5:0.5:0.75, 1.75 ml	Hts, 100 °C light blue crystals (3 d.)
109	$Cu(NO_3)_2{\cdot}2.5H_2O$ 18.4 mg, 0.08 mmol	4.2 mg	4.2 mg	4:1:1	H_2O:NH_4OH:NH_4OH, v:v:v, 0.5:0.5:0.75, 1.75 ml	Hts, 100 °C small blue crystals (3 d.)
110	$FeCl_2{\cdot}4H_2O$ 16 mg, 0.08 mmol	4.2 mg	4.2 mg	4:1:1	H_2O:NH_4OH:NH_4OH, v:v:v, 0.5:0.5:0.75, 1.75 ml	Hts, 100 °C crystals

10.3.7 Hydrothermal method at high temperature (S.: NaOH)

Part (a): NaOH solution (0.16 mmol/l) was used to obtain solutions of deprotonated ligands (H_2bdc or H_2bdt). An aqueous solution of metal salts (0.16 mmol), an aqueous solution of benzene-1,4-dicarboxylic acid H_2bdc (0.04 mmol) and an aqueous solution of benzene-1,4-di(1H-tetrazol-5-yl) H_2bdt (0.04 mmol) deprotonated by NaOH (0.16 mmol/l, 0.5 ml)/ ultrasonication (45-50°C). The solutions were mixed in mole ratio (4:1:1) in glass tube, which was sealed, stirred for about 5 minutes, and then placed in a programmable furnace. The sample was heated to 150°C during 2h and held at that temperature for 48h, then cooled through temperature rate 5°C/h to ambient temperature. The resulting single crystals were separated from precipitate and washed with water. Finally, the sample was dried in vacuum furnace for ca. 2-3h at 40°C. ^{1}H NMR- or IR-spectra were measured to examine either mixed-ligands or single-ligand were/ was coordinated with the metal atoms. Other experiments with other metal chloride or metal nitrate of Cd^{2+}, Zn^{2+}, Mn^{2+}, Cr^{3+}, Cu^{2+}, Co^{2+},

Ni^{2+}, Fe^{2+} (Fe^{3+} For nitrate), and Al^{3+} under the same conditions were unsuccessful. The synthesis of compounds is summarized in Table 9.3.7.1.

Table 9.3.7.1: Synthesis conditions for crystallized compounds from **111** to **123**

Product	Metal salt	H_2bdt	H_2bdc	Rate	Solvents	Result and remark
111	$CdCl_2$ 29.3 mg, 0.16 mmol	8.4 mg	6.6 mg	4:1:1	H_2O:NaOH:NaOH, v:v:v, 0.5:0.5:0.5, 1.5 ml	Hts, 150 °C, acicular crystals.
112	$Cd(NO_3)_2{\cdot}4H_2O$ 48 mg, 0.16 mmol	8.4 mg	6.6 mg	4:1:1	H_2O:NaOH:NaOH, v:v:v, 0.5:0.5:0.5, 1.5 ml	Hts, 150 °C, acicular crystals.
113	$MnCl_2$ 20.2 mg, 0.16 mmol	8.4 mg	6.6 mg	4:1:1	H_2O:NaOH:NaOH, v:v:v, 0.5:0.5:0.5, 1.5 ml	Hts, 150 °C, acicular crystals.
114	$Mn(NO_3)_2{\cdot}4H_2O$ 40 mg, 0.16 mmol	8.4 mg	6.6 mg	4:1:1	H_2O:NaOH:NaOH, v:v:v, 0.5:0.5:0.5, 1.5 ml	Hts, 150 °C, small crystals.
115	$ZnCl_2$ 20.8 mg, 0.16 mmol	8.4 mg	6.6 mg	4:1:1	H_2O:NaOH:NaOH, v:v:v, 0.5:0.5:0.5, 1.5 ml	Hts, 150 °C, acicular crystals.
116	$Zn(NO_3)_2{\cdot}6H_2O$ 41.6 mg, 0.16 mmol	8.4 mg	6.6 mg	4:1:1	H_2O:NaOH:NaOH, v:v:v, 0.5:0.5:0.5, 1.5 ml	Hts, 150 °C, acicular crystals (not stabel).
117	$CrCl_3{\cdot}6H_2O$ 64 mg, 0.16 mmol	8.4 mg	6.6 mg	4:1:1	H_2O:NaOH:NaOH, v:v:v, 0.5:0.5:0.5, 1.5 ml	Hts, 150 °C, acicular crystals.
118	$Cr(NO_3)_3{\cdot}9H_2O$ 42.6 mg, 0.16 mmol	8.4 mg	6.6 mg	4:1:1	H_2O:NaOH:NaOH, v:v:v, 0.5:0.5:0.5, 1.5 ml	Hts, 150 °C, acicular crystals.
119	$Cu(NO_3)_2{\cdot}2.5H_2O$ 36.8 mg, 0.16 mmol	8.4 mg	6.6 mg	4:1:1	H_2O:NaOH:NaOH, v:v:v, 0.5:0.5:0.5, 1.5 ml	Hts, 150 °C, acicular crystals.
120	$CoCl_2{\cdot}6H_2O$ 36.8 mg, 0.16 mmol	8.4 mg	6.6 mg	4:1:1	H_2O:NaOH:NaOH, v:v:v, 0.5:0.5:0.5, 1.5 ml	Hts, 150 °C, acicular crystals.
121	$Co(NO_3)_2{\cdot}6H_2O$ 48 mg, 0.16 mmol	8.4 mg	6.6 mg	4:1:1	H_2O:NaOH:NaOH, v:v:v, 0.5:0.5:0.5, 1.5 ml	Hts, 150 °C, colorless crystals.
122	$NiCl_2{\cdot}6H_2O$ 36.8 mg, 0.16 mmol	8.4 mg	6.6 mg	4:1:1	H_2O:NaOH:NaOH, v:v:v, 0.5:0.5:0.5, 1.5 ml	Hts, 150 °C, light green acicular crystals.
123	$Al(NO_3)_3{\cdot}9H_2O$ 60 mg, 0.16 mmol	8.4 mg	6.6 mg	4:1:1	H_2O:NaOH:NaOH, v:v:v, 0.5:0.5:0.5, 1.5 ml	Hts, 150 °C, colorless crystals.

Part (b): NaOH solution (0.16 mmol/l) was used as base to obtain a solution of used ligands (H_2bdc, H_2ip, H_3btc or H_2ipdt). An aqueous solution of different metal salts (0.16 mmol), an aqueous solution of benzene carboxylate ligand H_2bdc, H_2ip or H_3btc (0.04 mmol) and an aqueous solution of benzene-1,3-di(1H-tetrazol-5-yl) H_2ipdt (0.04 mmol) deprotonated in basic solution NaOH (0.16 mmol, 0.5 ml) using ultrasonic bath at 45-50°C (For H_3btc was dissolved in 0.75 ml of NaOH or NH_4OH to deprotonate their three carboxyl groups). The solutions were mixed in mole ratio (4:1:1) in glass tube, which was sealed, stirred for about 5 minutes, and then placed in a programmable furnace. The sample was heated to 150°C during 2h and held at that temperature for 24h, then cooled at temperature rate 3°C/h to ambient temperature (30°C). The resulting crystals were separated from precipitate and washed with water. Finally, the sample was dried in vacuum furnace for ca. 2-3h at 40°C. ^{1}H NMR- or IR-spectra were measured to examine either mixed-ligands or single-ligand were/was coordinated with the metal ions. Other experiments in the same condition with other metal nitrate of Cd^{2+}, Zn^{2+}, Mn^{2+}, Cr^{3+}, Cu^{2+}, Co^{2+}, Ni^{2+}, Fe^{3+}, and Al^{3+} were unsuccessful. The synthesis of compounds is summarized in the following Tables.

Table 9.3.7.2: Synthesis conditions for crystallized compounds from **124** to **128**

Product	Metal salt	H_2ipdt	H_2bdc	Rate	Solvents	Result and remark
124	$Cd(NO_3)_2{\cdot}4H_2O$ 48 mg, 0.16 mmol	8.4 mg	6.6 mg	4:1:1	H_2O:NaOH:NaOH, v:v:v, 0.5:0.5:0.5, 1.5 ml	Hts, 150 °C, colorless crystals.
125	$Mn(NO_3)_2{\cdot}4H_2O$ 40 mg, 0.16 mmol	8.4 mg	6.6 mg	4:1:1	H_2O:NaOH:NaOH, v:v:v, 0.5:0.5:0.5, 1.5 ml	Hts, 150 °C, colorless crystals.
126	$Zn(NO_3)_2{\cdot}6H_2O$ 41.6 mg, 0.16 mmol	8.4 mg	6.6 mg	4:1:1	H_2O:NaOH:NaOH, v:v:v, 0.5:0.5:0.5, 1.5 ml	Hts, 150 °C, cubic and acicular colorless crystals.
127	$Cr(NO_3)_3{\cdot}9H_2O$ 64 mg, 0.16 mmol	8.4 mg	6.6 mg	4:1:1	H_2O:NaOH:NaOH, v:v:v, 0.5:0.5:0.5, 1.5 ml	Hts, 150 °C, light green crystals.
128	$Ni(NO_3)_2{\cdot}6H_2O$ 48 mg, 0.16 mmol	8.4 mg	6.6 mg	4:1:1	H_2O:NaOH:NaOH, v:v:v, 0.5:0.5:0.5, 1.5 ml	Hts, 150 °C, green crystals.

Table 9.3.7.3: Synthesis conditions for crystallized compounds from **129** to **131**

Product	Metal salt	H_2ipdt	H_2ip	Rate	Solvents	Result and remark
129	$Cd(NO_3)_2{\cdot}4H_2O$ 48 mg, 0.16 mmol	8.4 mg	6.6 mg	4:1:1	H_2O:NaOH:NaOH, v:v:v, 0.5:0.5:0.5, 1.5 ml	Hts, 150 °C color crystals

Product	Metal salt	H_2ipdt	H_2ip	Rate	Solvents	Result and remark
130	$Ni(NO_3)_2 \cdot 6H_2O$ 48 mg, 0.16 mmol	8.4 mg	6.6 mg	4:1:1	H_2O:NaOH:NaOH, v:v:v, 0.5:0.5:0.5, 1.5 ml	Hts, 150 °C green acicular crystals
131	$Al(NO_3)_2 \cdot 9H_2O$ 60 mg, 0.16 mmol	8.4 mg	6.6 mg	4:1:1	H_2O:NaOH:NaOH, v:v:v, 0.5:0.5:0.5, 1.5 ml	Hts, 150 °C colorless acicular crystals

Table 9.3.7.4: Synthesis conditions for crystallized compounds from **132** to **137**

Product	Metal salt	H_2ipdt	H_3btc	Rate	Solvents	Result and remark
132	$Mn(NO_3)_2 \cdot 4H_2O$ 40 mg, 0.16 mmol	8.4 mg	8.4 mg	4:1:1	H_2O:NaOH:NaOH, v:v:v, 0.5:0.5:0.75, 1.75 ml	Hts, 150 °C colorless acicular crystals
133	$Cr(NO_3)_3 \cdot 9H_2O$ 64 mg, 0.16 mmol	8.4 mg	8.4 mg	4:1:1	H_2O:NaOH:NaOH, v:v:v, 0.5:0.5:0.75, 1.75 ml	Hts, 150 °C colorless acicular crystals
134	$Cu(NO_3)_2 \cdot 2.5H_2O$ 36.8 mg, 0.16 mmol	8.4 mg	8.4 mg	4:1:1	H_2O:NaOH:NaOH, v:v:v, 0.5:0.5:0.75, 1.75 ml	Hts, 150 °C colorless acicular crystals
135	$Co(NO_3)_2 \cdot 6H_2O$ 48 mg, 0.16 mmol	8.4 mg	8.4 mg	4:1:1	H_2O:NaOH:NaOH, v:v:v, 0.5:0.5:0.75, 1.75 ml	Hts, 150 °C acicular crystals
136	$Ni(NO_3)_2 \cdot 6H_2O$ 48 mg, 0.16 mmol	8.4 mg	8.4 mg	4:1:1	H_2O:NaOH:NaOH, v:v:v, 0.5:0.5:0.75, 1.75 ml	Hts, 150 °C acicular crystals
137	$Fe(NO_3)_3 \cdot 9H_2O$ 64 mg, 0.16 mmol	8.4 mg	8.4 mg	4:1:1	H_2O:NaOH:NaOH, v:v:v, 0.5:0.5:0.75, 1.75 ml	Hts, 150 °C acicular crystals

10.3.8 Hydrothermal method at high temperature (S.: NH_4OH)

NH_4OH solution (0.16 mmol/l) was used as base to obtain a solution of used ligands (H_2bdc, H_2ip, H_3btc or H_2ipdt). An aqueous solution of different metal salts (0.16 mmol), an aqueous solution of benzene carboxylate ligand H_2bdc, H_2ip or H_3btc (0.04 mmol) and an aqueous solution of benzene-1,3-di(1H-tetrazol-5-yl) H_2ipdt (0.04 mmol) deprotonated in basic solution of NH_4OH (0.16 mmol/l, 0.5 – 0.75 ml) using ultrasonic bath at 45-50°C, the solutions were mixed in mole ratio (4:1:1) in glass tube, which was sealed, stirred for about 5 minutes, and then placed in a programmable furnace. The sample was heated to 150°C during 2h and held at that temperature for 24h, then cooled at temperature rate 3°C/h to ambient temperature (30°C). The resulting crystals were separated from precipitate, washed with mother liquor and water. Finally, the sample was dried in vacuum furnace for ca. 2-3h at

40°C. ^{1}H NMR- or IR-spectra were measured to examine either two ligands or one ligand were/was coordinated with the metal atoms. Other experiments in the same condition with other metal nitrate of Cd^{2+}, Zn^{2+}, Mn^{2+}, Cr^{3+}, Cu^{2+}, Co^{2+}, Ni^{2+}, Fe^{3+}, and Al^{3+} were unsuccessful. The synthesis of compounds is summarized in the following Tables.

Table 9.3.8.1: Synthesis conditions for crystallized compounds from **138** to **146**

Product	Metal salt	H_2ipdt	H_2bdc	Rate	Solvents	Result and remark
138	$Cd(NO_3)_2 \cdot 4H_2O$ 48 mg, 0.16 mmol	8.4 mg	6.6 mg	4:1:1	H_2O:NH_4OH:NH_4OH, v:v:v, 0.5:0.5:0.5, 1.5 ml	Hts, 150 °C, small colorless crystals.
139	$Mn(NO_3)_2 \cdot 4H_2O$ 40 mg, 0.16 mmol	8.4 mg	6.6 mg	4:1:1	H_2O:NH_4OH:NH_4OH, v:v:v, 0.5:0.5:0.5, 1.5 ml	Hts, 150 °C, acicular crystals.
140	$Zn(NO_3)_2 \cdot 6H_2O$ 41.6 mg, 0.16 mmol	8.4 mg	6.6 mg	4:1:1	H_2O:NH_4OH:NH_4OH, v:v:v, 0.5:0.5:0.5, 1.5 ml	Hts, 150 °C, small colorless crystals.
141	$Cr(NO_3)_3 \cdot 9H_2O$ 64 mg, 0.16 mmol	8.4 mg	6.6 mg	4:1:1	H_2O:NH_4OH:NH_4OH, v:v:v, 0.5:0.5:0.5, 1.5 ml	Hts, 150 °C, small light green crystals.
142	$Cu(NO_3)_2 \cdot 2.5H_2O$ 36.8 mg, 0.16 mmol	8.4 mg	6.6 mg	4:1:1	H_2O:NH_4OH:NH_4OH, v:v:v, 0.5:0.5:0.5, 1.5 ml	Hts, 150 °C, small and acicular green crystals.
143	$Co(NO_3)_2 \cdot 6H_2O$ 48 mg, 0.16 mmol	8.4 mg	6.6 mg	4:1:1	H_2O:NH_4OH:NH_4OH, v:v:v, 0.5:0.5:0.5, 1.5 ml	Hts, 150 °C, acicular crystals.
144	$Ni(NO_3)_2 \cdot 6H_2O$ 48 mg, 0.16 mmol	8.4 mg	6.6 mg	4:1:1	H_2O:NH_4OH:NH_4OH, v:v:v, 0.5:0.5:0.5, 1.5 ml	Hts, 150 °C, colorless plate crystals.
145	$Fe(NO_3)_3 \cdot 9H_2O$ 64 mg, 0.16 mmol	8.4 mg	6.6 mg	4:1:1	H_2O:NH_4OH:NH_4OH, v:v:v, 0.5:0.5:0.5, 1.5 ml	Hts, 150 °C, small colorless crystals.
146	$Al(NO_3)_3 \cdot 9H_2O$ 60 mg, 0.16 mmol	8.4 mg	6.6 mg	4:1:1	H_2O:NH_4OH:NH_4OH, v:v:v, 0.5:0.5:0.5, 1.5 ml	Hts, 150 °C, yellow acicular crystals.

Table 9.3.8.2: Synthesis conditions for crystallized compounds from **147** to **153**

Product	Metal salt	H_2ipdt	H_2ip	Rate	Solvents	Result and remark
147	$Mn(NO_3)_2 \cdot 4H_2O$ 40 mg, 0.16 mmol	8.4 mg	6.6 mg	4:1:1	H_2O:NH_4OH:NH_4OH, v:v:v, 0.5:0.5:0.5, 1.5 ml	Hts, 150 °C pink and colorless acicular crystals
148	$Zn(NO_3)_2 \cdot 6H_2O$ 41.6 mg, 0.16 mmol	8.4 mg	6.6 mg	4:1:1	H_2O:NH_4OH:NH_4OH, v:v:v, 0.5:0.5:0.5, 1.5 ml	Hts, 150 °C small white crystals

Product	Metal salt	H_2ipdt	H_2ip	Rate	Solvents	Result and remark
149	$Cr(NO_3)_3 \cdot 9H_2O$ 64 mg, 0.16 mmol	8.4 mg	6.6 mg	4:1:1	H_2O:NH_4OH:NH_4OH, v:v:v, 0.5:0.5:0.5, 1.5 ml	Hts, 150 °C green crystals
150	$Cu(NO_3)_2 \cdot 2.5H_2O$ 36.8 mg, 0.16 mmol	8.4 mg	6.6 mg	4:1:1	H_2O:NH_4OH:NH_4OH, v:v:v, 0.5:0.5:0.5, 1.5 ml	Hts, 150 °C different colorless crystals
151	$Co(NO_3)_2 \cdot 6H_2O$ 48 mg, 0.16 mmol	8.4 mg	6.6 mg	4:1:1	H_2O:NH_4OH:NH_4OH, v:v:v, 0.5:0.5:0.5, 1.5 ml	Hts, 150 °C colorless crystals
152	$Ni(NO_3)_2 \cdot 6H_2O$ 48 mg, 0.16 mmol	8.4 mg	6.6 mg	4:1:1	H_2O:NH_4OH:NH_4OH, v:v:v, 0.5:0.5:0.5, 1.5 ml	Hts, 150 °C white crystals
153	$Fe(NO_3)_2 \cdot 9H_2O$ 64 mg, 0.16 mmol	8.4 mg	6.6 mg	4:1:1	H_2O:NH_4OH:NH_4OH, v:v:v, 0.5:0.5:0.5, 1.5 ml	Hts, 150 °C white crystals

Table 9.3.8.3: Synthesis conditions for crystallized compounds from **154** to **158**

Product	Metal salt	H_2ipdt	H_3btc	Rate	Solvents	Result and remark
154	$Zn(NO_3)_2 \cdot 6H_2O$ 41.6 mg, 0.16 mmol	8.4 mg	8.4 mg	4:1:1	H_2O:NH_4OH:NH_4OH, v:v:v, 0.5:0.5:0.75, 1.75 ml	Hts, 150 °C colorless crystals
155	$Cu(NO_3)_2 \cdot 2.5H_2O$ 64 mg, 0.16 mmol	8.4 mg	8.4 mg	4:1:1	H_2O:NH_4OH:NH_4OH, v:v:v, 0.5:0.5:0.75, 1.75 ml	Hts, 150 °C different shape of colorless crystals
39	$Co(NO_3)_2 \cdot 6H_2O$ 48 mg, 0.16 mmol	8.4 mg	8.4 mg	4:1:1	H_2O:NH_4OH:NH_4OH, v:v:v, 0.5:0.5:0.75, 1.75 ml	Hts, 150 °C small orange crystals and red needle-shaped crystals
157	$Fe(NO_3)_3 \cdot 9H_2O$ 64 mg, 0.16 mmol	8.4 mg	8.4 mg	4:1:1	H_2O:NH_4OH:NH_4OH, v:v:v, 0.5:0.5:0.75, 1.75 ml	Hts, 150 °C small colorless crystals
158	$Al(NO_3)_3 \cdot 9H_2O$ 60 mg, 0.16 mmol	8.4 mg	8.4 mg	4:1:1	H_2O:NH_4OH:NH_4OH, v:v:v, 0.5:0.5:0.75, 1.75 ml	Hts, 150 °C white acicular crystals

10.3.9 Solvothermal method at low temperature (S.: H_2O, DMSO, DMF)

A solution of metal nitrate or metal chloride of different metals (0.08 mmol) in H_2O (0.5 ml), a solution of benzene-1.3,5-tricarboxylate ligand H_3btc (0.02 mmol) in DMSO (0.5 ml), and a solution of benzene tetrazolate ligand H_2bdt or H_2ipdt (0.02 mmol) in DMF (0.5 ml) were mixed and stirred for about 10 minutes in glass tube. After that, the samples placed in furnace at 90 or 120 °C. Finally, the sample was removed, when the crystals were formed.

The resulting crystals were separated from precipitate, washed with mother liquor, dried and after that ^{1}H NMR- or IR-spectra were measured to examine either two ligands or one ligand were/was coordinated with the metal atoms. Other experiments in the same condition with other metal chloride and metal nitrate of Zn^{2+}, Mn^{2+}, Cr^{3+}, Cu^{2+}, Co^{2+}, Ni^{2+} and Fe^{2+} (Fe^{3+} for nitrate) were unsuccessful. The synthesis of compounds is summarized in following Tables.

Table 9.3.9.1: Synthesis conditions for crystallized compounds from **159** to **162**

Product	Metal salt	H_2bdt	H_3btc	Rate	Solvents	Result and remark
159	$CoCl_2 \cdot 6H_2O$ 18.4 mg, 0.08 mmol	4.2 mg	4.2 mg	4:1:1	H_2O:DMF:DMSO, v:v:v, 0.5:0.5:0.5,1.5 ml	Sts, 90 °C small blue crystals
160	$CuCl_2$ 10.4 mg, 0.08 mmol	4.2 mg	4.2 mg	4:1:1	H_2O:DMF:DMSO, v:v:v, 0.5:0.5:0.5,1.5 ml	Sts, 90 °C small blue crystals
161	$MnSO_4 \cdot H_2O$ 13.6 mg, 0.08 mmol	4.2 mg	4.2 mg	4:1:1	H_2O:DMF:DMSO, v:v:v, 0.5:0.5:0.5,1.5 ml	Sts, 90 °C light pink crystals
162	$Cu(NO_3)_2 \cdot 2.5H_2O$ 18.4 mg, 0.08 mmol	4.2 mg	4.2 mg	4:1:1	H_2O:DMF:DMSO, v:v:v, 0.5:0.5:0.5,1.5 ml	Sts, 90 °C small blue crystals (3 d.)

Table 9.3.9.2: Synthesis conditions for crystallized compounds from **163** to **168**

Product	Metal salt	H_2ipdt	H_3btc	Rate	Solvents	Result and remark
163	$ZnCl_2$ 10.4 mg, 0.08 mmol	4.2 mg	4.2 mg	4:1:1	H_2O:DMF:DMSO, v:v:v, 0.5:0.5:0.5, 1.5 ml	Sts, 120 °C small colorless crystals
164	$Zn(NO_3)_2 \cdot 6H_2O$ 23.8 mg, 0.08 mmol	4.2 mg	4.2 mg	4:1:1	H_2O:DMF:DMSO, v:v:v, 0.5:0.5:0.5, 1.5 ml	Sts, 90 °C acicular crystals
165	$MnCl_2$ 10 mg, 0.08 mmol	4.2 mg	4.2 mg	4:1:1	H_2O:DMF:DMSO, v:v:v, 0.5:0.5:0.5, 1.5 ml	Sts, 90 °C small colorless crystals
166	$MnSO_4 \cdot H_2O$ 13.6 mg, 0.08 mmol	4.2 mg	4.2 mg	4:1:1	H_2O:DMF:DMSO, v:v:v, 0.5:0.5:0.5, 1.5 ml	Sts, 90 °C colorless crystals
167	$CoCl_2 \cdot 6H_2O$ 18.4 mg, 0.08 mmol	4.2 mg	4.2 mg	4:1:1	H_2O:DMF:DMSO, v:v:v, 0.5:0.5:0.5, 1.5 ml	Sts, 90 °C poly acicular dark blue crystals
168	$Co(NO_3)_2 \cdot 6H_2O$ 24 mg, 0.08 mmol	4.2 mg	4.2 mg	4:1:1	H_2O:DMF:DMSO, v:v:v, 0.5:0.5:0.5, 1.5 ml	Sts, 90 °C poly acicular dark blue crystals

10.3.10 Solvothermal method at high temperature (S.: H_2O, DMSO)

An aqueous solution of different metal salts (0.16 mmol), a solution of benzene carboxylate ligand H_2bdc, H_2ip or H_3btc (0.04 mmol) and a solution of benzene-1,3-di(1H-tetrazol-5-yl) H_2ipdt (0.04 mmol) dissolved in a mixture of H_2O:DMSO (v:v, 1:1), were mixed in mole ratio (4:1:1) in glass tube, which was sealed and stirred for about 5 min. and then placed in a programmable furnace. The sample was heated to 150°C during 2h and held at that temperature for 24h, then cooled at temperature rate 3°C/h to ambient temperature (30°C). The resulting single crystals were separated from precipitate, washed with mother liquor, dried and after that ^{1}H NMR- or IR-spectra were measured to examine either two ligands or one ligand were/was coordinated with the metal atoms. Other experiments in the same condition with other metal chloride and metal nitrate of Cd^{2+}, Zn^{2+}, Mn^{2+}, Cr^{3+}, Cu^{2+}, Co^{2+}, Ni^{2+}, Fe^{3+} and Al^{3+} were unsuccessful. The synthesis of compounds is summarized in the following Tables.

Table 9.3.10.1: Synthesis conditions for crystallized compounds from **169** to **172**

Product	Metal salt	H_2ipdt	H_2bdc	Rate	Solvents	Result and remark
169	$Cr(NO_3)_3 \cdot 9H_2O$ 64 mg, 0.16 mmol	8.4 mg	6.6 mg	4:1:1	H_2O:(DMSO:H_2O):(DMSO:H_2O), v:v:v, 0.5:0.5:0.5, 1.5 ml	Sts, 150 °C, green crystals and colorless crystals
170	$Co(NO_3)_2 \cdot 6H_2O$ 48 mg, 0.16 mmol	8.4 mg	6.6 mg	4:1:1	H_2O:(DMSO:H_2O):(DMSO:H_2O), v:v:v, 0.5:0.5:0.5, 1.5 ml	Sts, 150 °C, light red acicular crystals
171	$Ni(NO_3)_2 \cdot 6H_2O$ 48 mg, 0.16 mmol	8.4 mg	6.6 mg	4:1:1	H_2O:(DMSO:H_2O):(DMSO:H_2O), v:v:v, 0.5:0.5:0.5, 1.5 ml	Sts, 150 °C, light green acicular crystals
172	$Fe(NO_3)_3 \cdot 9H_2O$ 64 mg, 0.16 mmol	8.4 mg	6.6 mg	4:1:1	H_2O:(DMSO:H_2O):(DMSO:H_2O), v:v:v, 0.5:0.5:0.5, 1.5 ml	Sts, 150 °C, colorless acicular crystals

Table 9.3.10.2: Synthesis conditions for crystallized compounds **173** & **174**

Product	Metal salt	H_2ipdt	H_3btc	Rate	Solvents	Result and remark
173	$Cd(NO_3)_2 \cdot 4H_2O$ 48 mg, 0.16 mmol	8.4 mg	8.4 mg	4:1:1	H_2O:(DMSO:H_2O):(DMSO:H_2O), v:v:v, 0.5:0.5:0.5, 1.5 ml	Sts, 150 °C white acicular crystals
174	$Mn(NO_3)_2 \cdot 4H_2O$ 40 mg, 0.16 mmol	8.4 mg	8.4 mg	4:1:1	H_2O:(DMSO:H_2O):(DMSO:H_2O), v:v:v, 0.5:0.5:0.5, 1.5 ml	Sts, 150 °C white crystals

11 Appendix

11.1 Crystal structure data of compounds and structure refinement

Table 10.1.1: Crystal data and structure refinement for 3D-{[Cu_4(μ-OH)$_2$(μ-bdc)$_2$(μ$_4$-*rac*-btrip)$_3$]·(NO_3)$_2$(H_2O)$_{10}$}$_n$ **16***.

Identification code	**16***
Empirical formula	C37 H40 Cu4 N18 O10
Formula weight	1151.03
Temperature	173(2) K
Wavelength	0.71073 Å
Crystal system	Monoclinic
Space group	C 2/m
Unit cell dimensions	a = 16.183 Å, α = 90°
	b = 21.670 Å, β = 121.492°
	c = 14.085 Å, γ = 90°
Volume	4211.9(16) $Å^3$
Z	2
Density (calculated)	0.908 Mg/m^3
Absorption coefficient	1.037 mm^{-1}
F(000)	1168
Crystal size	0.20 x 0.20 x 0.10 mm^3
Theta range for data collection	1.70 to 25.80°.
Index ranges	-19<=h<=19, -26<=k<=26, -17<=l<=16
Reflections collected	13035
Independent reflections	4175 [R(int) = 0.0385]
Completeness to theta = 25.80°	99.9 %
Absorption correction	Semi-empirical from equivalents
Max. and min. transmission	0.9034 and 0.8194
Refinement method	Full-matrix least-squares on F^2
Data / restraints / parameters	4175 / 0 / 174
Goodness-of-fit on F^2	1.048
Final R indices [I>2sigma(I)]	R1 = 0.0392, wR2 = 0.1158
R indices (all data)	R1 = 0.0439, wR2 = 0.1189
Largest diff. peak and hole	0.878 and -0.435 $e.Å^{-3}$

*(Tahli09_tief\work\263_11_no3_ok = at263_11_NO3)

Table 10.1.2: Crystal data and structure refinement for 3D-{[$Cu_4(\mu_4\text{-}Cl)(\mu_4\text{-}rac\text{-}btrip)_4(H_2O)_4$] $(BF_4/ClO_4/OH)^-_7 \cdot xH_2O\}_n$ **17***.

Identification code	**17***
Empirical formula	C28 H16 Cl3 Cu4 N24 O28.24
Formula weight	1501.96
Temperature	153(2) K
Wavelength	0.71073 Å
Crystal system	Tetragonal
Space group	I 4/m m m
Unit cell dimensions	a = 13.0141(8) Å, α = 90°.
	b = 13.0141(8) Å, β = 90°.
	c = 18.982(3) Å, γ = 90°.
Volume	3214.9(6) $Å^3$
Z	2
Density (calculated)	1.552 Mg/m^3
Absorption coefficient	1.523 mm^{-1}
F(000)	1489.8
Crystal size	0.063 x 0.055 x 0.021 mm^3
Theta range for data collection	1.897 to 25.110°.
Index ranges	-15<=h<=15, -15<=k<=15, -22<=l<=22
Reflections collected	9457
Independent reflections	863 [R(int) = 0.0922]
Completeness to theta = 25.11°	98.3 %
Absorption correction	Semi-empirical from equivalents
Max. and min. transmission	0.969 and 0.909
Refinement method	Full-matrix least-squares on F^2
Data / restraints / parameters	863 / 0 / 88
Goodness-of-fit on F^2	1.350
Final R indices [I>2sigma(I)]	R1 = 0.0921, wR2 = 0.2694
R indices (all data)	R1 = 0.1029, wR2 = 0.2924
Extinction coefficient	n/a
Largest diff. peak and hole	1.538 and -1.805 $e.Å^{-3}$

*(At263_11_BF4\work\AT263_11_BF4_matrix_Tetra_I_OK renamed to AT263_11_BF4)

Table 10.1.3: Crystal data and structure refinement for 3D-{[Cu(μ_4-*rac*-btrip)(SO_4)]· ~H_2O}$_n$ **18***.

Identification code	**18***
Empirical formula	C8 H12 Cu N6 O7 S
Formula weight	399.84
Temperature	123(2) K
Wavelength	0.71073 Å
Crystal system	Orthorhombic
Space group	I m m a
Unit cell dimensions	a = 7.0276(9) Å, α = 90°.
	b = 15.6684(17) Å, β = 90°.
	c = 15.0172(15) Å, γ = 90°.
Volume	1653.6(3) $Å^3$
Z	4
Density (calculated)	1.606 Mg/m^3
Absorption coefficient	1.489 mm^{-1}
F(000)	812
Crystal size	0.150 x 0.080 x 0.030 mm^3
Theta range for data collection	1.878 to 20.171°.
Index ranges	-6<=h<=6, -15<=k<=15, -14<=l<=14
Reflections collected	11588
Independent reflections	459 [R(int) = 0.0507]
Completeness to theta = 20.171°	53.9 %
Absorption correction	Semi-empirical from equivalents
Max. and min. transmission	0.956 and 0.867
Refinement method	Full-matrix least-squares on F^2
Data / restraints / parameters	459 / 51 / 68
Goodness-of-fit on F^2	3.720
Final R indices [I>2sigma(I)]	R1 = 0.1942, wR2 = 0.6144
R indices (all data)	R1 = 0.1992, wR2 = 0.6223
Extinction coefficient	0.02(2)
Largest diff. peak and hole	1.529 and -1.674 $e.Å^{-3}$

*1. SCXRD (AK_Tahli_263_11_SO4\work\ AK_Tahli_263_11_SO4_OK renamed at263-11-SO4)

*2. SCXRD (GM_Tahli_263_11_SO4\work\at291_12_SO4_1M_0ma)

Table 10.1.4: Crystal data and structure refinement for 2D-{[Zn(μ-Hbtc)(μ-*R*-btrip)]·H_2O}$_n$ **19*** and 2D-{[Zn(μ-Hbtc)(μ-*S*-btrip)]·H_2O}$_n$ **20****.

Identification code	**19**	**20**
Empirical formula	C16 H14 N6 O7 Zn	C16 H14 N6 O7 Zn
Formula weight	467.72	467.70
Temperature	173(2) K	296(2) K
Wavelength	0.71073 Å	0.71073 Å
Crystal system	Orthorhombic	Orthorhombic
Space group	P 2_1 2_1 2_1	P 2_1 2_1 2_1
Unit cell dimensions	a = 6.9452 Å, α = 90°	a = 6.9247 Å, α = 90°
	b = 12.6049 Å, β = 90°	b = 12.7138 Å, β = 90°
	c = 21.171 Å, γ = 90°	c = 21.182 Å, γ = 90°
Volume	1853.4(3) $Å^3$	1864.8(4) $Å^3$
Z	4	4
Density (calculated)	1.676 Mg/m^3	1.666 Mg/m^3
Absorption coefficient	1.381 mm^{-1}	1.372 mm^{-1}
F(000)	952	952
Crystal size	0.100 x 0.100 x 0.050 mm^3	0.20 x 0.20 x 0.10 mm^3
Theta range for data collection	1.924 to 25.125°.	1.87 to 25.30°.
Index ranges	-8<=h<=8, -15<=k<=15, -25<=l<=25	-8<=h<=8, -15<=k<=15, -25<=l<=25
Reflections collected	10811	10656
Independent reflections	3324 [R(int) = 0.0375]	3352 [R(int) = 0.0443]
Completeness to theta = 25.242°/25.30°	98.8 %	99.0 %
Absorption correction	Semi-empirical from equivalents	Semi-empirical from equivalents
Max. and min. transmission	0.933 and 0.871	0.872 and 0.768
Refinement method	Full-matrix least-squares on F^2	Full-matrix least-squares on F^2
Data / restraints / parameters	3324 / 0 / 275	3352 / 0 / 270
Goodness-of-fit on F^2	1.071	1.047
Final R indices [I>2sigma(I)]	R1 = 0.0273, wR2 = 0.0656	R1 = 0.0375, wR2 = 0.0829
R indices (all data)	R1 = 0.0289, wR2 = 0.0662	R1 = 0.0450, wR2 = 0.0857
Absolute structure parameter	0.005(8)	-0.005(16)
Largest diff. peak and hole	0.431 and -0.304 e.$Å^{-3}$	0.509 and -0.496 e.$Å^{-3}$

*(Tahli01tief\work\Shlexl\264-12-tief-100c renamed at264-12-NO3), **(Tahli2\work\at264-12-Br)

Table 10.1.5: Crystal data and structure refinement for 2D-$[Cu_3(\mu_6\text{-btc})(\mu\text{-btc})(\mu\text{-atr})(H_2O)_5]_n$ **24***.

Identification code	**24**
Empirical formula	C20 H18 Cu3 N4 O17
Formula weight	777.03
Temperature	173(2) K
Wavelength	0.71073 Å
Crystal system	Orthorhombic
Space group	C m c a
Unit cell dimensions	a = 18.878(4) Å, α = 90°.
	b = 17.716(4) Å, β = 90°.
	c = 14.975(3) Å, γ = 90°.
Volume	5008.3(18) $Å^3$
Z	8
Density (calculated)	2.061 Mg/m^3
Absorption coefficient	2.622 mm^{-1}
F(000)	3112
Crystal size	0.150 x 0.150 x 0.050 mm^3
Theta range for data collection	2.082 to 25.448°.
Index ranges	-22<=h<=20, -21<=k<=21, -18<=l<=11
Reflections collected	17266
Independent reflections	2400 [R(int) = 0.0708]
Completeness to theta = 25.448°	100.0 %
Absorption correction	Semi-empirical from equivalents
Max. and min. transmission	0.877 and 0.682
Refinement method	Full-matrix least-squares on F^2
Data / restraints / parameters	2395 / 0 / 211
Goodness-of-fit on F^2	1.587
Final R indices [I>2sigma(I)]	R1 = 0.1270, wR2 = 0.3676
R indices (all data)	R1 = 0.1587, wR2 = 0.3914
Extinction coefficient	0.0038(10)
Largest diff. peak and hole	2.786 and -5.116 $e.Å^{-3}$

*1. SCXRD (Tahli_UK32-2\work\uk32-2_Cmca_01_ok\mo_scan_0m_cmca),

**2. SCXRD (HeeringUK21\work\mo_HeeringUK21_0ma_c)

Table 10.1.6: Crystal data and structure refinement for 1D-{[$Cd_2(\mu_2\text{-btc})_2(atr)_2(H_2O)_4$][$Cd(H_2O)_6$]·$2H_2O$}$_n$ **25***.

Identification code	**25**
Empirical formula	C22 H34 Cd3 N8 O24
Formula weight	1131.80
Temperature	100(2) K
Wavelength	0.71073 Å
Crystal system	Monoclinic
Space group	P 21/c
Unit cell dimensions	a = 10.1435(18) Å, α = 90°.
	b = 26.471(5) Å, β = 106.213(13)°.
	c = 7.0263(13) Å, γ = 90°.
Volume	1811.6(6) $Å^3$
Z	2
Density (calculated)	2.075 Mg/m^3
Absorption coefficient	1.849 mm^{-1}
F(000)	1116
Crystal size	? x ? x ? mm^3
Theta range for data collection	2.09 to 25.34°.
Index ranges	-12<=h<=12, -31<=k<=31, -8<=l<=8
Reflections collected	15909
Independent reflections	3316 [R(int) = 0.1449]
Completeness to theta = 25.34°	98.9 %
Absorption correction	Semi-empirical from equivalents
Refinement method	Full-matrix least-squares on F^2
Data / restraints / parameters	3316 / 0 / 259
Goodness-of-fit on F^2	1.044
Final R indices [I>2sigma(I)]	R1 = 0.0539, wR2 = 0.1347
R indices (all data)	R1 = 0.0756, wR2 = 0.1491
Largest diff. peak and hole	1.304 and -1.762 e.$Å^{-3}$

*(Tahli_UK23a\work\mo_scan_0m_2a renamed uk23a-lt)

Table 10.1.7: Crystal data and structure refinement for 2D-[Cd(μ_3-Hbtc)(H_2O)$_2$]$_n$ **26***.

Identification code	**26**
Empirical formula	C9 H8 Cd O8
Formula weight	356.56
Temperature	296(2) K
Wavelength	0.71073 Å
Crystal system	Monoclinic
Space group	C 2/c
Unit cell dimensions	a = 19.744 Å, α = 90°
	b = 9.1047 Å, β = 117.994°
	c = 13.3701 Å, γ = 90°
Volume	2122.2(5) Å^3
Z	8
Density (calculated)	2.232 Mg/m^3
Absorption coefficient	2.092 mm^{-1}
F(000)	1392
Crystal size	0.20 x 0.15 x 0.10 mm^3
Theta range for data collection	2.34 to 27.63°.
Index ranges	-25<=h<=25, -11<=k<=11, -17<=l<=17
Reflections collected	11226
Independent reflections	2463 [R(int) = 0.0531]
Completeness to theta = 27.63°	99.8 %
Absorption correction	Semi-empirical from equivalents
Max. and min. transmission	0.811 and 0.693
Refinement method	Full-matrix least-squares on F^2
Data / restraints / parameters	2463 / 0 / 172
Goodness-of-fit on F^2	1.069
Final R indices [I>2sigma(I)]	R1 = 0.0234, wR2 = 0.0587
R indices (all data)	R1 = 0.0262, wR2 = 0.0610
Largest diff. peak and hole	0.766 and -0.544 e.Å^{-3}

*(uk_72_2_Mo\work\mo_scan_0m_1 renamed uk23b or uk72-2)

Table 10.1.8: Crystal data and structure refinement for 2D-{[Cu_2(μ-Br)$_2$(μ$_4$-*rac*-btrip)]·H_2O/MeOH}$_n$ **27***.

Identification code	**27***
Empirical formula	C14 H20 Br4 Cu4 N12 O2
Formula weight	962.22
Temperature	140(2) K
Wavelength	0.71073 Å
Crystal system	Orthorhombic
Space group	P b a m
Unit cell dimensions	a = 11.0001(14) Å, α = 90°.
	b = 17.335(2) Å, β = 90°.
	c = 6.8582(8) Å, γ = 90°.
Volume	1307.8(3) $Å^3$
Z	2
Density (calculated)	2.444 Mg/m^3
Absorption coefficient	9.358 mm^{-1}
F(000)	920
Crystal size	0.020 x 0.010 x 0.010 mm^3
Theta range for data collection	2.193 to 24.242°.
Index ranges	-12<=h<=12, -19<=k<=20, -7<=l<=7
Reflections collected	22347
Independent reflections	1153 [R(int) = 0.0771]
Completeness to theta = 24.242°	88.9 %
Absorption correction	Semi-empirical from equivalents
Max. and min. transmission	0.911 and 0.894
Refinement method	Full-matrix least-squares on F^2
Data / restraints / parameters	1153 / 0 / 95
Goodness-of-fit on F^2	1.031
Final R indices [I>2sigma(I)]	R1 = 0.0457, wR2 = 0.0917
R indices (all data)	R1 = 0.0693, wR2 = 0.1011
Extinction coefficient	n/a
Largest diff. peak and hole	0.936 and -0.892 $e.Å^{-3}$

*(GM_Tahli_291_12_Br_1MMo\work\Tahli_291_12_Br\291_12_br_neu1) or (Tahli_1_291_12_Br2_21\work\Tahli_1_291_12_Br2_21_0ma_OK)

Table 10.1.9: Crystal data and structure refinement for 3D-{[$Cu_2(\mu_4$-*rac*-btrip$)_2$] $SO_4 \cdot xH_2O\}_n$ **28***.

Identification code	**28-1M***
Empirical formula	C21 H30 Cu3 N18 O8 S2
Formula weight	917.40
Temperature	173(2) K
Wavelength	0.71073 Å
Crystal system	Orthorhombic
Space group	A m a 2
Unit cell dimensions	a = 21.462(3) Å, α = 90°
	b = 18.264(3) Å, β = 90°
	c = 12.1379(19) Å, γ = 90°
Volume	4757.8(13) $Å^3$
Z	4
Density (calculated)	1.281 Mg/m^3
Absorption coefficient	1.469 mm^{-1}
F(000)	1860
Crystal size	? x ? x ? mm^3
Theta range for data collection	1.898 to 23.814°.
Index ranges	-21<=h<=24, -20<=k<=20, -13<=l<=13
Reflections collected	120366
Independent reflections	3674 [R(int) = 0.0316]
Completeness to theta = 23.814°	84.9 %
Absorption correction	Semi-empirical from equivalents
Max. and min. transmission	
Refinement method	Full-matrix least-squares on F^2
Data / restraints / parameters	3674 / 4 / 246
Goodness-of-fit on F^2	1.093
Final R indices [I>2sigma(I)]	R1 = 0.0527, wR2 = 0.1367
R indices (all data)	R1 = 0.0543, wR2 = 0.1376
Absolute structure parameter	0.49(5)
Extinction coefficient	n/a
Largest diff. peak and hole	1.118 and -0.446 $e.Å^{-3}$

*(AT291_12_SO4_21\work\AT291-12-SO4-21_OK_1M\ at291_12_so4_21_a-sr)

Table 10.1.10: Crystal data and structure refinement for 3D-{[Cu(μ_4-*rac*-btrip)] $CH_3COO \cdot xH_2O$}$_n$ **29***.

Identification code	**29-2. SCXRD**
Empirical formula	C6 H8 Cu N6
Formula weight	227.72
Temperature	123(2) K
Wavelength	0.71073 Å
Crystal system	Orthorhombic
Space group	C c c m
Unit cell dimensions	a = 12.583(3) Å, α = 90°
	b = 17.771(4) Å, β = 90°
	c = 7.3047(13) Å, γ = 90°
Volume	1633.4(6) $Å^3$
Z	4
Density (calculated)	0.926 Mg/m^3
Absorption coefficient	1.315 mm^{-1}
F(000)	460
Crystal size	0.200 x 0.150 x 0.100 mm^3
Theta range for data collection	1.983 to 23.661°.
Index ranges	-14<=h<=8, -20<=k<=19, -8<=l<=8
Reflections collected	3600
Independent reflections	680 [R(int) = 0.0388]
Completeness to theta = 23.661°	84.5 %
Absorption correction	Semi-empirical from equivalents
Max. and min. transmission	0.877 and 0.789
Refinement method	Full-matrix least-squares on F^2
Data / restraints / parameters	680 / 0 / 34
Goodness-of-fit on F^2	1.107
Final R indices [I>2sigma(I)]	R1 = 0.0532, wR2 = 0.1687
R indices (all data)	R1 = 0.0691, wR2 = 0.1746
Absolute structure parameter	
Extinction coefficient	n/a
Largest diff. peak and hole	0.457 and -0.339 $e.Å^{-3}$

*(AK_Tahli_291_12_OAc\work\ at291-12-OAc_ok renamed at291_12_OAc)

Table 10.1.11: Crystal data and structure refinement for 3D-{[Cu(CH_3CN)$_4$][Cu_3(μ_6-btc)$_2$]$_2$(NO_3/O_2CCH_3)·(H_2O, CH_3CN)$_x$}$_n$ **33*** and **34****.

Identification code	**34**
Empirical formula	C46.76 H24 Cu7 N4 O30
Formula weight	1566.48
Temperature	296(2) K
Wavelength	0.71073 Å
Crystal system	Cubic
Space group	F m -3 m
Unit cell dimensions	a = 26.446 Å, α = 90°
	b = 26.446 Å, β = 90°
	c = 26.446 Å, γ = 90°
Volume	18496(4) $Å^3$
Z	8
Density (calculated)	1.125 Mg/m^3
Absorption coefficient	1.638 mm^{-1}
F(000)	6204
Crystal size	0.10 x 0.10 x 0.10 mm^3
Theta range for data collection	2.55 to 23.89°.
Index ranges	-29<=h<=30, -30<=k<=30, -28<=l<=30
Reflections collected	24718
Independent reflections	780 [R(int) = 0.0648]
Completeness to theta = 23.89°	99.4 %
Absorption correction	Semi-empirical from equivalents
Max. and min. transmission	0.8534 and 0.8534
Refinement method	Full-matrix least-squares on F^2
Data / restraints / parameters	780 / 0 / 51
Goodness-of-fit on F^2	1.473
Final R indices [I>2sigma(I)]	R1 = 0.0333, wR2 = 0.1048
R indices (all data)	R1 = 0.0353, wR2 = 0.1059
Largest diff. peak and hole	0.255 and -0.771 $e.Å^{-3}$

*(Tahli 03 vv\work\ cu_scan_0m_r-3\ AT263-12-no3) or (Tahli03_tief_123K).

**(Tahli_1_263_12_OAc\work\ mo_scan_0m_at263_12_OAc_orginal)

Table 10.1.12: Crystal data and structure refinement 1D-$[M_3(\mu_3\text{-btc})(\mu_2\text{-btc})(H_2O)_{12}]_n$ (Co/Zn) **39***, **35****.

Identification code	**39**	**35**
Empirical formula	C18 H26 Co3 O24	C18 H30 O24 Zn3
Formula weight	803.18	826.59
Temperature	296(2) K	296(2) K
Wavelength	0.71073 Å	0.71073 Å
Crystal system	Monoclinic	Monoclinic
Space group	C 2	C 2
Unit cell dimensions	a = 17.494 Å, α = 90°	a = 17.39 Å, α = 90°
	b = 12.981 Å, β = 111.959°	b = 12.90 Å, β = 111.81°
	c = 6.573 Å, γ = 90°	c = 6.583 Å, γ = 90°
Volume	1384.4(18) $Å^3$	1371(4) $Å^3$
Z	2	2
Density (calculated)	1.927 Mg/m^3	2.002 Mg/m^3
Absorption coefficient	1.883 mm^{-1}	2.711 mm^{-1}
F(000)	814	840
Crystal size	0.20 x 0.15 x 0.10 mm^3	0.20 x 0.12 x 0.10 mm^3
Theta range for data collection	2.01 to 34.65°.	2.02 to 31.16°.
Index ranges	-27<=h<=27, -20<=k<=20, -10<=l<=10	-25<=h<=25, -18<=k<=18, -9<=l<=9
Reflections collected	6947	9612
Independent reflections	5961 [R(int) = 0.0288]	4447 [R(int) = 0.0596]
Completeness to theta = 34.65°/31.16°	62.8 %	99.7 %
Absorption correction	Semi-empirical from equivalents	Semi-empirical from equivalents
Max. and min. transmission	0.828 and 0.720	0.763 and 0.684
Refinement method	Full-matrix least-squares on F^2	Full-matrix least-squares on F^2
Data / restraints / parameters	3485 / 1 / 212	4399 / 1 / 216
Goodness-of-fit on F^2	1.075	1.034
Final R indices [I>2sigma(I)]	R1 = 0.0301, wR2 = 0.0764	R1 = 0.0396, wR2 = 0.0931
R indices (all data)	R1 = 0.0309, wR2 = 0.0768	R1 = 0.0458, wR2 = 0.0972
Absolute structure parameter	0.434(11)	0.515(12)
Largest diff. peak and hole	0.845 and -0.578 $e.Å^{-3}$	0.644 and -0.569 $e.Å^{-3}$

*(Duo_AnasTahli_255_6), **(Tahli04_(uk_42_2_NO3))

Table 10.1.13: Crystal data and structure refinement for 2D-[Zn(μ_3-aip)(H_2O)]$_n$ **40***.

Identification code	**40**
Empirical formula	C8 H7 N O5 Zn
Formula weight	262.54
Temperature	296(2) K
Wavelength	0.71073 Å
Crystal system	Monoclinic
Space group	P21/c
Unit cell dimensions	a = 9.048 Å, α = 90°
	b = 8.290 Å, β = 120.85°
	c = 13.299 Å, γ = 90°
Volume	856.4(6) $Å^3$
Z	4
Density (calculated)	2.036 Mg/m^3
Absorption coefficient	2.867 mm^{-1}
F(000)	528
Crystal size	0.15 x 0.12 x 0.10 mm^3
Theta range for data collection	2.62 to 25.77°.
Index ranges	-11<=h<=11, -9<=k<=10, -15<=l<=16
Reflections collected	5240
Independent reflections	1635 [R(int) = 0.0722]
Completeness to theta = 25.77°	99.4 %
Absorption correction	Semi-empirical from equivalents
Max. and min. transmission	0.7510 and 0.6680
Refinement method	Full-matrix least-squares on F^2
Data / restraints / parameters	1635 / 0 / 139
Goodness-of-fit on F^2	1.016
Final R indices [I>2sigma(I)]	R1 = 0.0388, wR2 = 0.0880
R indices (all data)	R1 = 0.0548, wR2 = 0.0971
Largest diff. peak and hole	0.523 and -0.898 $e.Å^{-3}$

*(Tahli_1_264_14_neu)

Table 10.1.14: Crystal data and structure refinement for H_2bdt·H_2O **111**.

Identification code	**111***
Empirical formula	C4 H5 N4 O
Formula weight	125.12
Temperature	296(2) K
Wavelength	0.71073 Å
Crystal system	Monoclinic
Space group	P2(1)/c
Unit cell dimensions	a = 3.7613(4) Å, α = 90°.
	b = 12.4786(15) Å, β = 93.649°.
	c = 11.7346(14) Å, γ = 90°.
Volume	549.66(11) $Å^3$
Z	4
Density (calculated)	1.512 Mg/m^3
Absorption coefficient	0.116 mm^{-1}
F(000)	260
Crystal size	0.60 x 0.10 x 0.10 mm^3
Theta range for data collection	2.39 to 32.24°.
Index ranges	-3<=h<=5,-18<=k<=18,-17<=l<=17
Reflections collected	7570
Independent reflections	1946 [R(int) = 0.0483]
Completeness to theta = 32.24°	99.5 %
Absorption correction	Semi-empirical from equivalents
Max. and min. transmission	0.9884 and 0.9334
Refinement method	Full-matrix least-squares on F^2
Data / restraints / parameters	1946 / 0 / 103
Goodness-of-fit on F^2	1.015
Final R indices [I>2sigma(I)]	R1 = 0.0506, wR2 = 0.1270
R indices (all data)	R1 = 0.0985, wR2 = 0.1541
Extinction coefficient	0.004(4)
Largest diff. peak and hole	0.329 and -0.250 $e.Å^{-3}$

*(AT-240-1 vv)

Table 10.1.15: Crystal data and structure refinement for H_2bdt (**115** & **120**).

Identification code	**115***	**120****
Empirical formula	C4 H3 N4	C4 H3 N4
Formula weight	107.10	107.10
Temperature	296(2) K	296(2) K
Wavelength	0.71073 Å	0.71073 Å
Crystal system	Monoclinic	Monoclinic
Space group	P2(1)/c	P2(1)/c
Unit cell dimensions	a = 4.5739 Å, α = 90°	a = 4.5799 Å, α = 90°
	b = 9.847 Å, β = 92.97°	b = 9.8813 Å, β = 92.881°
	c = 9.717 Å, γ = 90°	c = 9.7618 Å, γ = 90°
Volume	437.1(2) $Å^3$	441.22(10) $Å^3$
Z	4	4
Density (calculated)	1.628 Mg/m^3	1.612 Mg/m^3
Absorption coefficient	0.116 mm^{-1}	0.114 mm^{-1}
F(000)	220	220
Crystal size	? x ? x ? mm^3	0.40 x 0.30 x 0.30 mm^3
Theta range for data collection	2.95 to 25.20°.	2.94 to 34.68°.
Index ranges	-5<=h<=5, -11<=k<=11, -11<=l<=11	-7<=h<=7, -15<=k<=15, -15<=l<=15
Reflections collected	3548	7276
Independent reflections	786 [R(int) = 0.0434]	1804 [R(int) = 0.0287]
Completeness to theta = 25.20/34.68°	99.5 %	94.8 %
Absorption correction	Semi-empirical from equivalents	Semi-empirical from equivalents
Max. and min. transmission		0.877 and 0.789
Refinement method	Full-matrix least-squares on F^2	Full-matrix least-squares on F^2
Data / restraints / parameters	786 / 0 / 86	1804 / 0 / 85
Goodness-of-fit on F^2	1.092	1.037
Final R indices [I>2sigma(I)]	R1 = 0.0378, wR2 = 0.0965	R1 = 0.0474, wR2 = 0.1236
R indices (all data)	R1 = 0.0460, wR2 = 0.1032	R1 = 0.0669, wR2 = 0.1381
Absolute structure parameter		
Extinction coefficient	0.074(12)	n/a
Largest diff. peak and hole	0.167 and -0.167 $e.Å^{-3}$	0.323 and -0.303 $e.Å^{-3}$

*(AT-242-1 vv), **(AT-245-1 vv)

Table 10.1.16: Crystal data and structure refinement for H_2bdc (**124** & **126**).

Identification code	**124***	**126****
Empirical formula	C4 H3 O2	C8 H6 O4
Formula weight	83.06	166.13
Temperature	296(2) K	296(2) K
Wavelength	0.71073 Å	0.71073 Å
Crystal system	triclinic	triclinic
Space group	P-1	P-1
Unit cell dimensions	a = 5.0390 Å, α = 71.931°	a = 3.7522 Å, α = 83.179°
	b = 5.3753 Å, β = 76.138°	b = 6.4422 Å, β = 80.600°
	c = 7.0094 Å, γ = 87.321°	c = 7.4082 Å, γ = 88.579°
Volume	175.16(6) $Å^3$	175.42 $Å^3$
Z	2	1
Density (calculated)	1.575 Mg/m^3	1.573 Mg/m^3
Absorption coefficient	0.129 mm^{-1}	0.129 mm^{-1}
F(000)	86	86
Crystal size	0.30 x 0.20 x 0.20 mm^3	0.70 x 0.25 x 0.15 mm^3
Theta range for data collection	3.15 to 25.09°.	2.81 to 34.66°.
Index ranges	-5<=h<=5, -6<=k<=6, -8<=l<=8	-5<=h<=5, -9<=k<=10, -11<=l<=11
Reflections collected	1545	2843
Independent reflections	623 [R(int) = 0.0131]	1372 [R(int) = 0.0155]
Completeness to theta = 25.09/34.66°	99.7 %	91.6 %
Absorption correction	Semi-empirical from equivalents	Semi-empirical from equivalents
Max. and min. transmission	0.9747 and 0.9624	0.9810 and 0.9153
Refinement method	Full-matrix least-squares on F^2	Full-matrix least-squares on F^2
Data / restraints / parameters	623 / 0 / 66	1372 / 0 / 63
Goodness-of-fit on F^2	1.112	1.043
Final R indices [I>2sigma(I)]	R1 = 0.0337, wR2 = 0.0892	R1 = 0.0495, wR2 = 0.1461
R indices (all data)	R1 = 0.0390, wR2 = 0.0925	R1 = 0.0640, wR2 = 0.1600
Absolute structure parameter		
Extinction coefficient	n/a	n/a
Largest diff. peak and hole	0.127 and -0.275 $e.Å^{-3}$	0.444 and -0.255 $e.Å^{-3}$

*(AT-180-4 vv), **(AT-182-4 vv)

Table 10.1.17: Crystal data and structure refinement for H_2ip and {$[Cd_2(Hipdt)_2(\mu\text{-}OH)_2(H_2O)_6]\cdot\sim10(H_2O)$} **129***.

Identification code	**129a**	**129b**
Empirical formula	C8 H6 O4	C8 H5 Cd N8 O10.67
Formula weight	166.13	496.25
Temperature	296(2) K	296(2) K
Wavelength	1.54178 Å	0.71073 Å
Crystal system	monoclinic	Monoclinic
Space group	P2(1)/c	C 2
Unit cell dimensions	a = 3.7656 Å, α = 90°	a = 19.000 Å, α = 90°
	b = 16.4075 Å, β = 90.562°	b = 6.7784 Å, β = 105.464(9)°
	c = 11.7572 Å, γ = 90°	c = 14.270 Å, γ = 90°
Volume	726.37(7) $Å^3$	1771.3 $Å^3$
Z	4	4
Density (calculated)	1.519 Mg/m^3	1.861 Mg/m^3
Absorption coefficient	1.068 mm^{-1}	1.305 mm^{-1}
F(000)	344	969.3
Crystal size	0.15 x 0.15 x 0.01 mm^3	0.60 x 0.02 x 0.01 mm^3
Theta range for data collection	4.63 to 55.79°.	2.224 to 23.157°.
Index ranges	-4<=h<=3, -17<=k<=17, -12<=l<=12	-18<=h<=20, -6<=k<=7, -15<=l<=14
Reflections collected	2616	5255
Independent reflections	905 [R(int) = 0.0251]	2148 [R(int) = 0.0525]
Completeness to theta = 55.79/25.24°	97.6 %	72.2 %
Absorption correction	Semi-empirical from equivalents	Semi-empirical from equivalents
Max. and min. transmission	0.9894 and 0.8562	0.987 and 0.969
Refinement method	Full-matrix least-squares on F^2	Full-matrix least-squares on F^2
Data / restraints / parameters	905 / 0 / 130	2148 / 363 / 235
Goodness-of-fit on F^2	1.035	1.107
Final R indices [I>2sigma(I)]	R1 = 0.0421, wR2 = 0.1108	R1 = 0.0768, wR2 = 0.1870
R indices (all data)	R1 = 0.0555, wR2 = 0.1214	R1 = 0.0936, wR2 = 0.1987
Absolute structure parameter		
Extinction coefficient	n/a	n/a
Largest diff. peak and hole	0.277 and -0.120 $e.Å^{-3}$	1.838 and -1.402 $e.Å^{-3}$

*(AT180-5 and AT180-5b)

11.2 NMR-, IR- and MS-spectra for organic synthesis

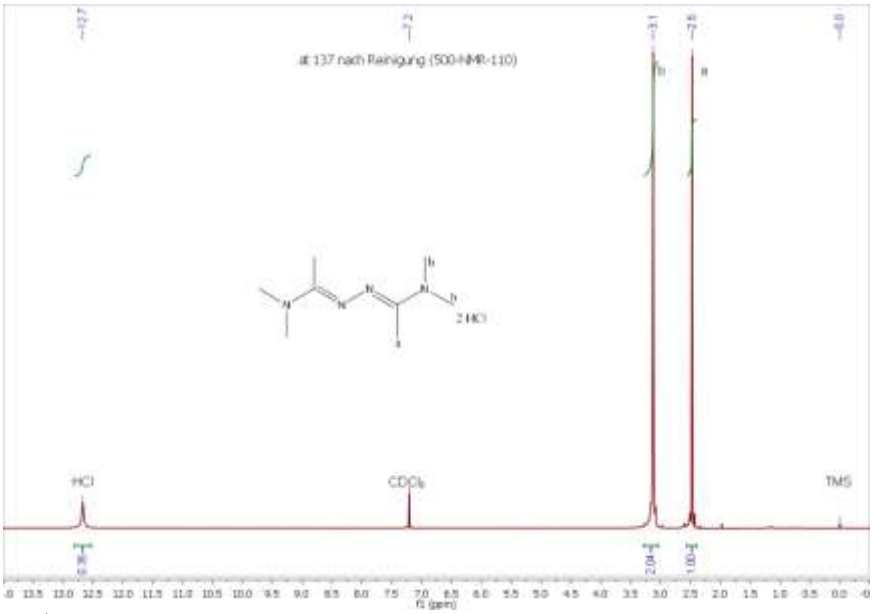

Fig. 10.2.1: ^{1}H NMR (500 MHz) of *N,N`*-dimethylacetamide azine dihydrochloride in $CDCl_3$.

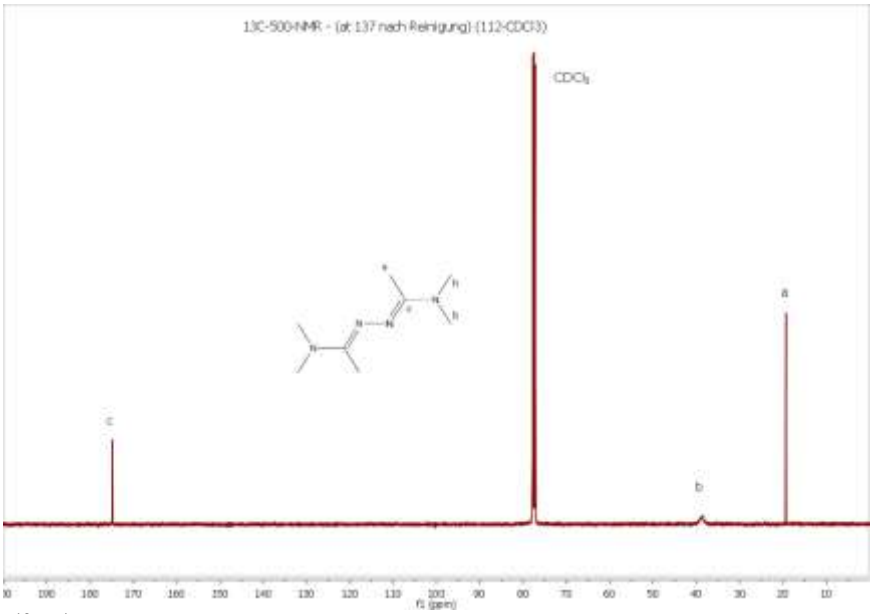

Fig. 10.2.2: $^{13}C\{^{1}H\}$ NMR (125 MHz) of *N,N`*-dimethylacetamide azine dihydrochloride in $CDCl_3$.

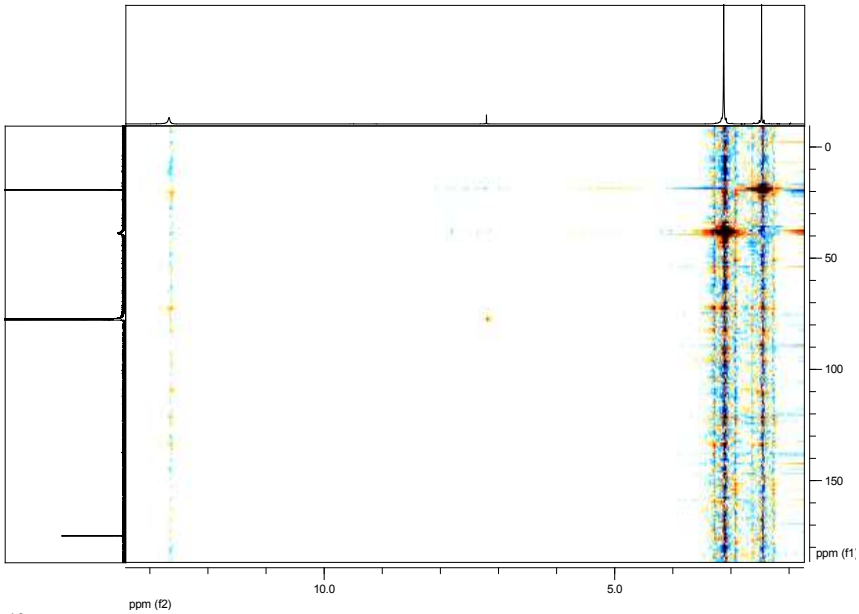

Fig. 10.2.3: ^{1}H-^{13}C COSY-NMR (500 MHz) of *N,N`*-dimethylacetamide azine dihydrochloride in $CDCl_3$.

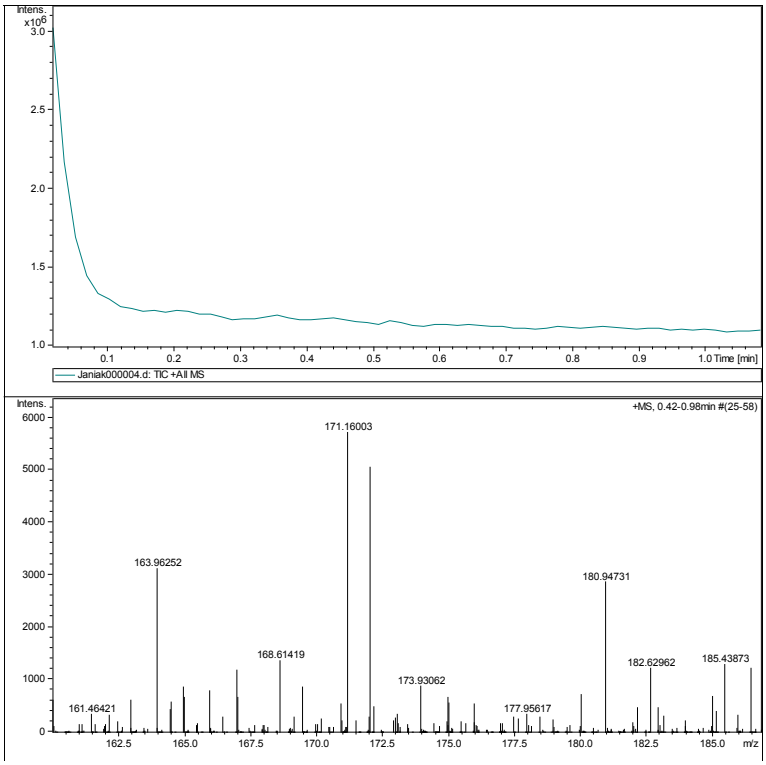

Fig. 10.2.4: Mass spectrum (ESI) of *3*-acetamidobenzoic acid in MeOH.

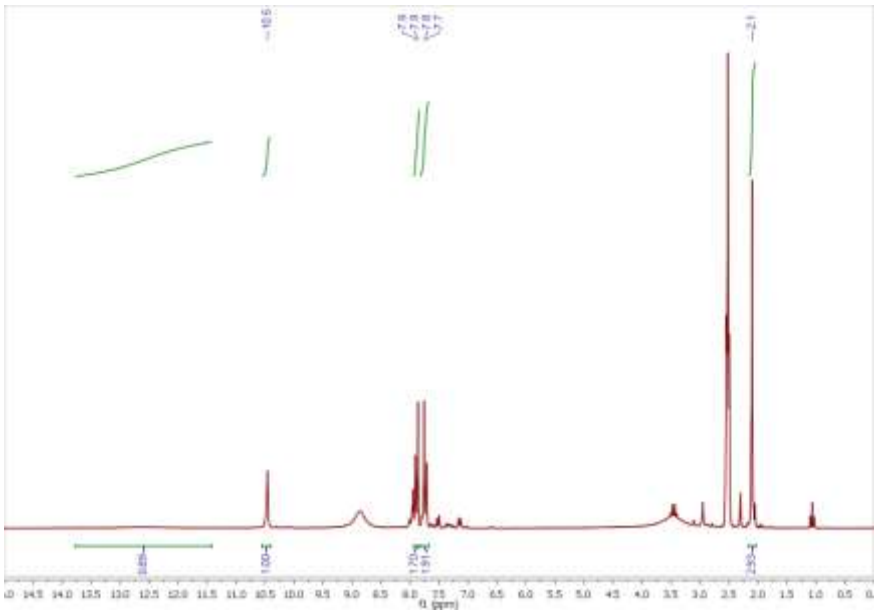

Fig. 10.2.5: ^{1}H NMR (200 MHz) of *4*-acetamidobenzoic acid in DMSO-d_6.

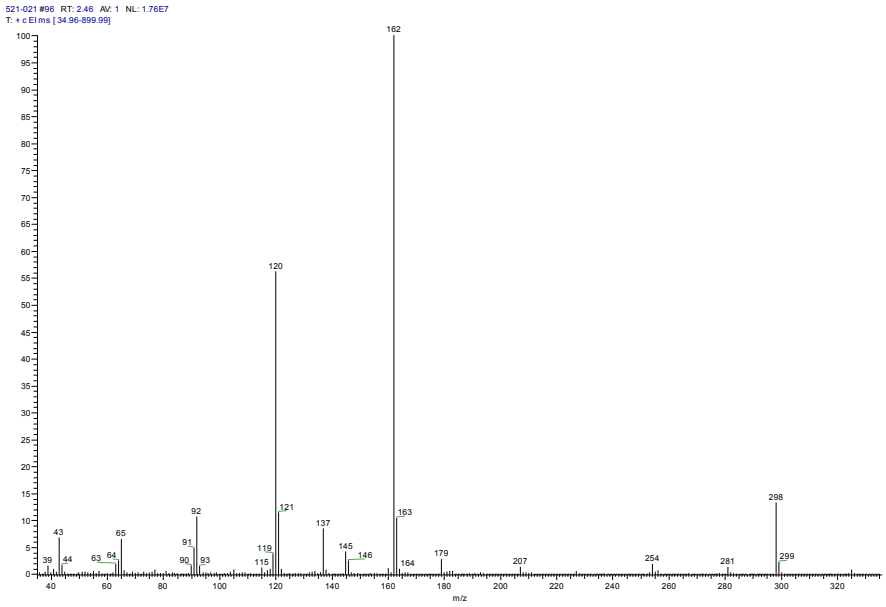

Fig. 10.2.6: Mass spectrum (EI) of *4*-acetamidobenzoic acid.

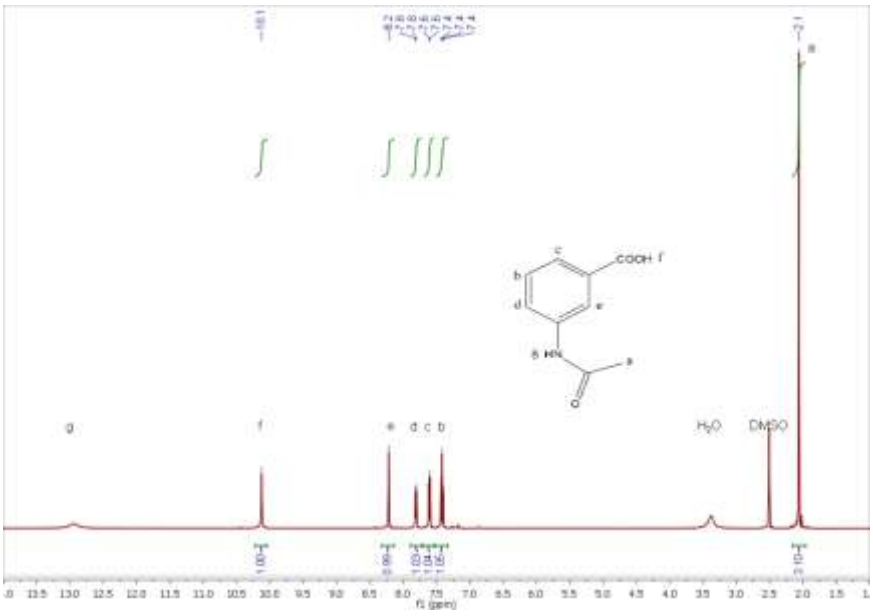

Fig. 10.2.7: ^{1}H NMR (500 MHz) of *3*-acetamidobenzoic acid in DMSO-d_6.

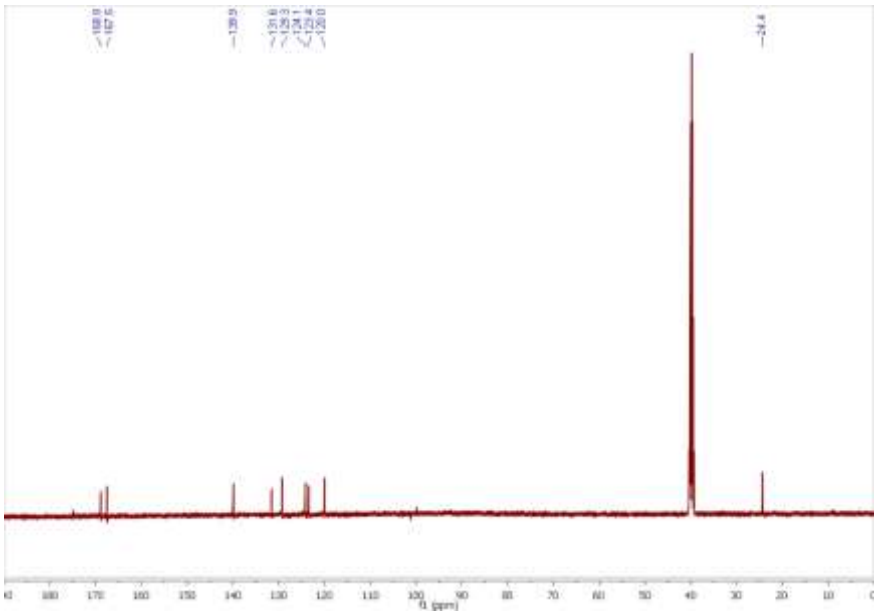

Fig. 10.2.8: $^{13}C\{^{1}H\}$ NMR (125 MHz) of *3*-acetamidobenzoic acid in DMSO-d_6.

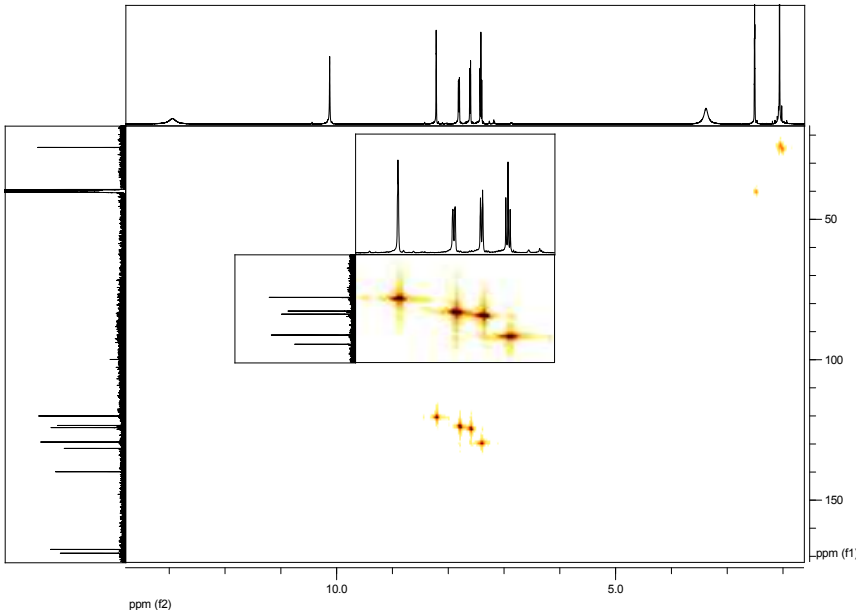

Fig. 10.2.9: ^{1}H-^{13}C COSY-NMR (500 MHz) of *3*-acetamidobenzoic acid in DMSO-d_6.

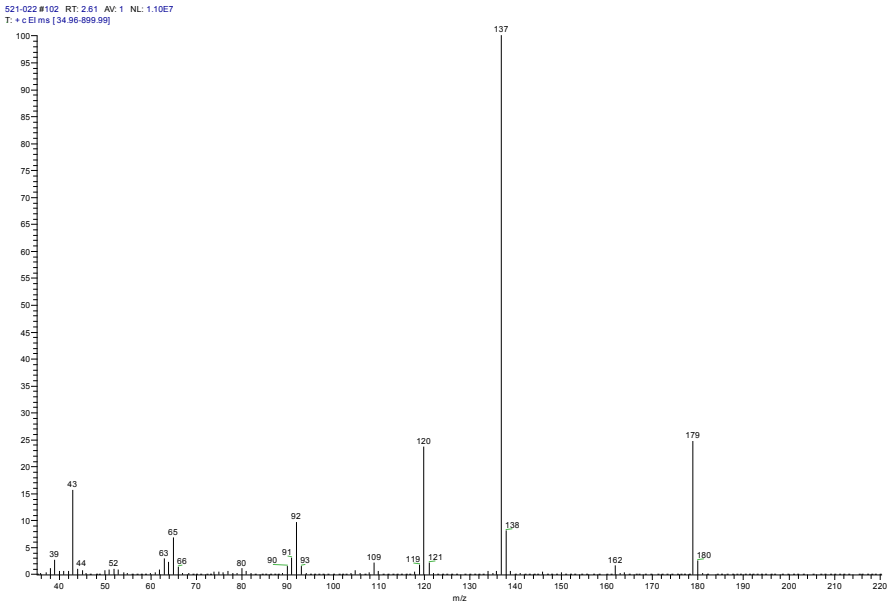

Fig. 10.2.10: Mass spectrum (EI) of *3*-acetamidobenzoic acid.

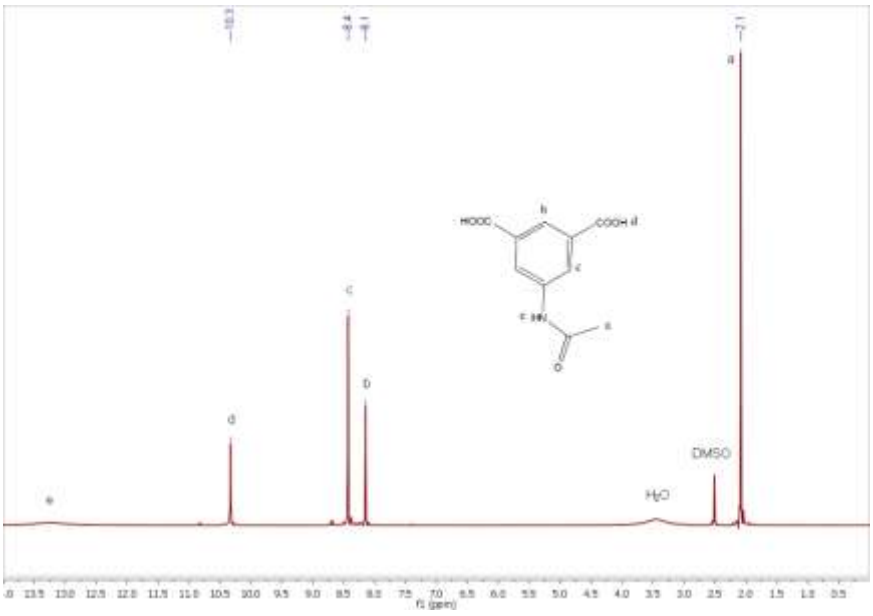

Fig. 10.2.11: ^{1}H NMR (500 MHz) of *5*-acetamidoisophthalic acid in DMSO-d_6.

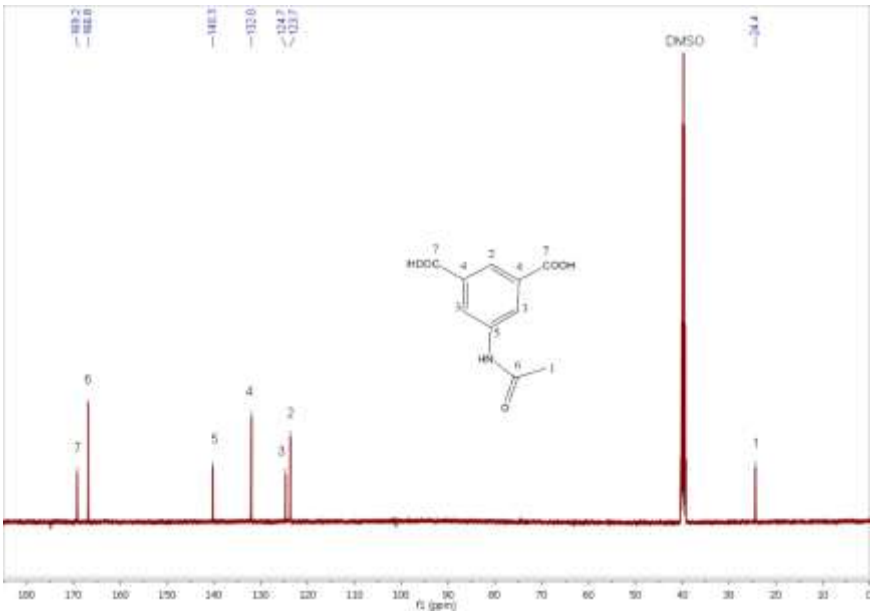

Fig. 10.2.12: ^{13}C{^{1}H} NMR (125 MHz) of *5*-acetamidoisophthalic acid in DMSO-d_6.

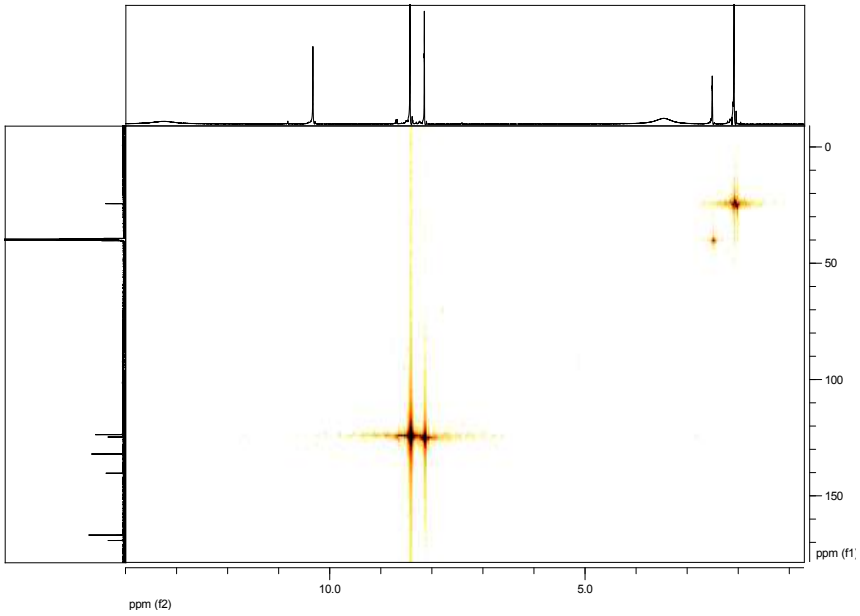

Fig. 10.2.13: ^{1}H-^{13}C COSY-NMR (500 MHz) of *5*-acetamidoisophthalic acid in DMSO-d_6.

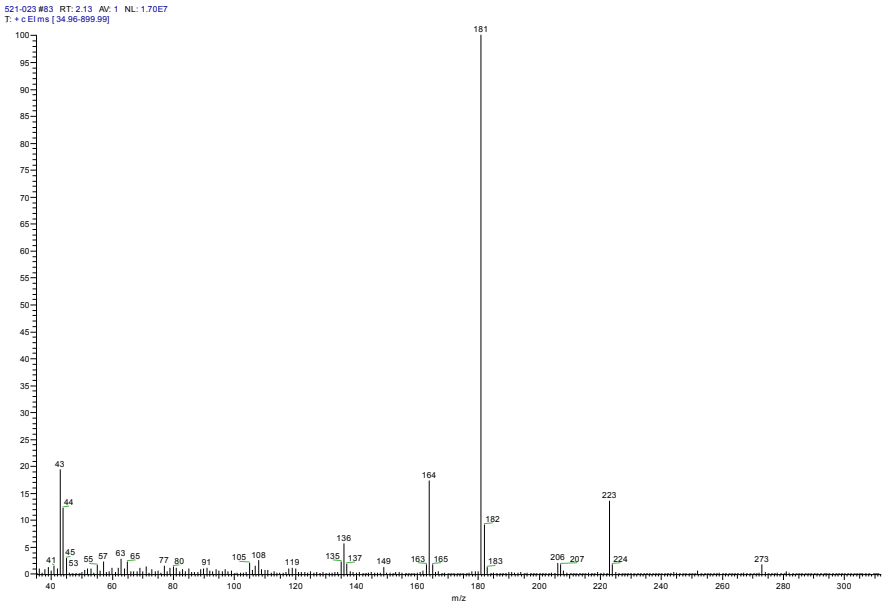

Fig. 10.2.14: Mass spectrum (EI) of *5*-acetamidoisophthalic acid (at139).

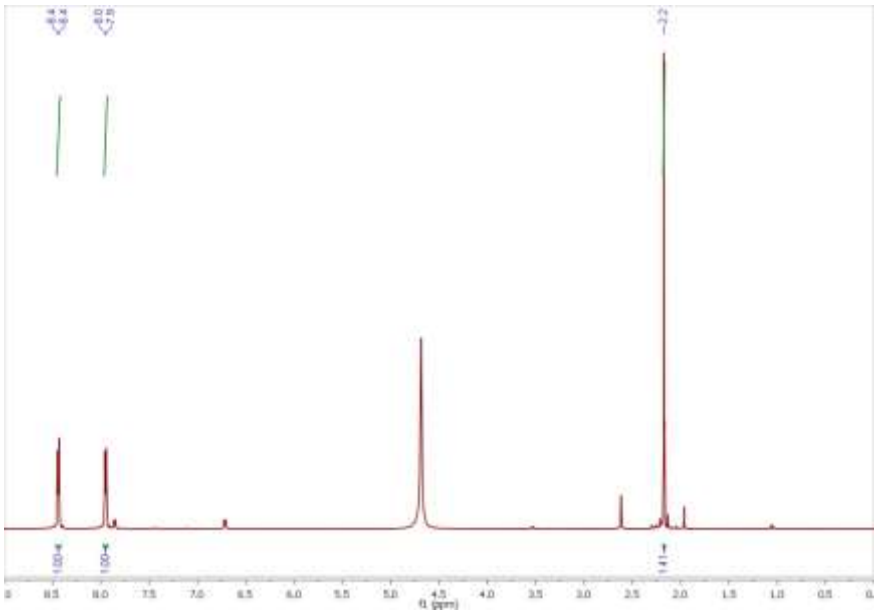

Fig. 10.2.15: ^{1}H NMR (500 MHz) of *4*-acetamido-pyridine in D_2O.

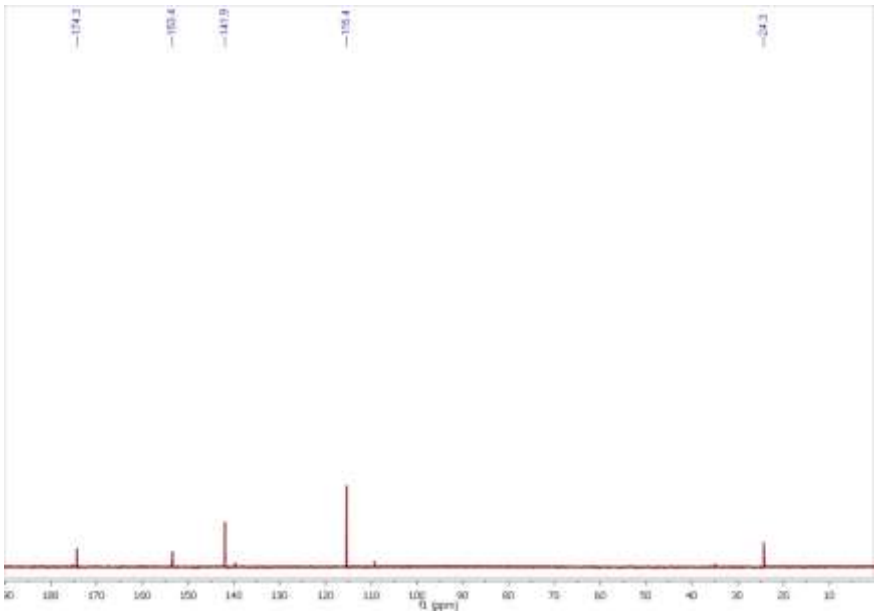

Fig. 10.2.16: $^{13}C\{^{1}H\}$ NMR (125 MHz) of *4*-acetamido-pyridine in D_2O.

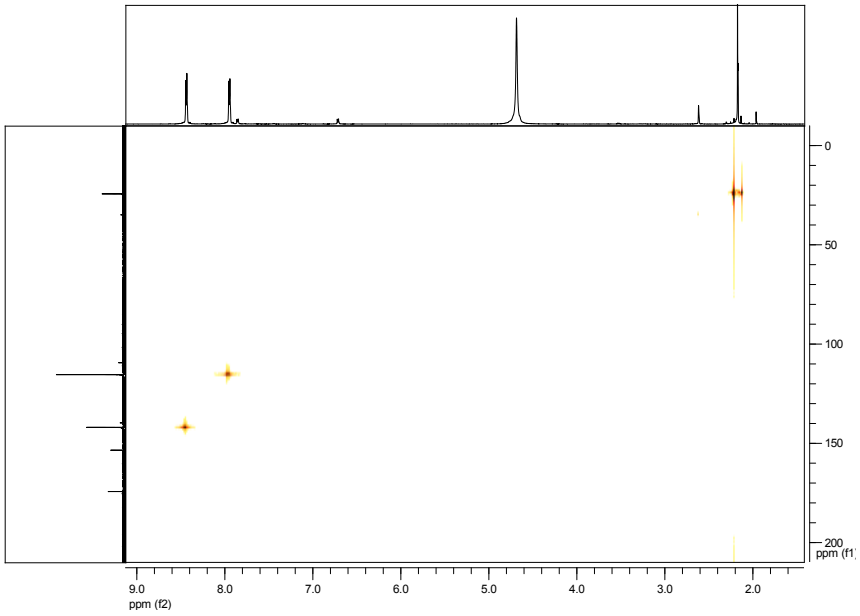

Fig. 10.2.17: ^{1}H-^{13}C COSY-NMR (500 MHz) of *4*-acetamido-pyridine in D_2O.

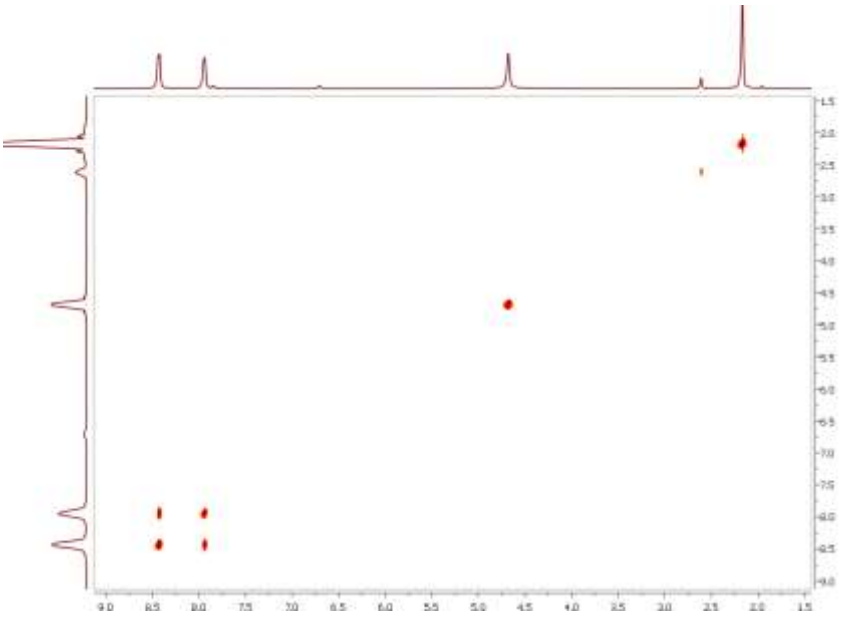

Fig. 10.2.18: ^{1}H-^{1}H COSY-NMR (500 MHz) of *4*-acetamido-pyridine in D_2O.

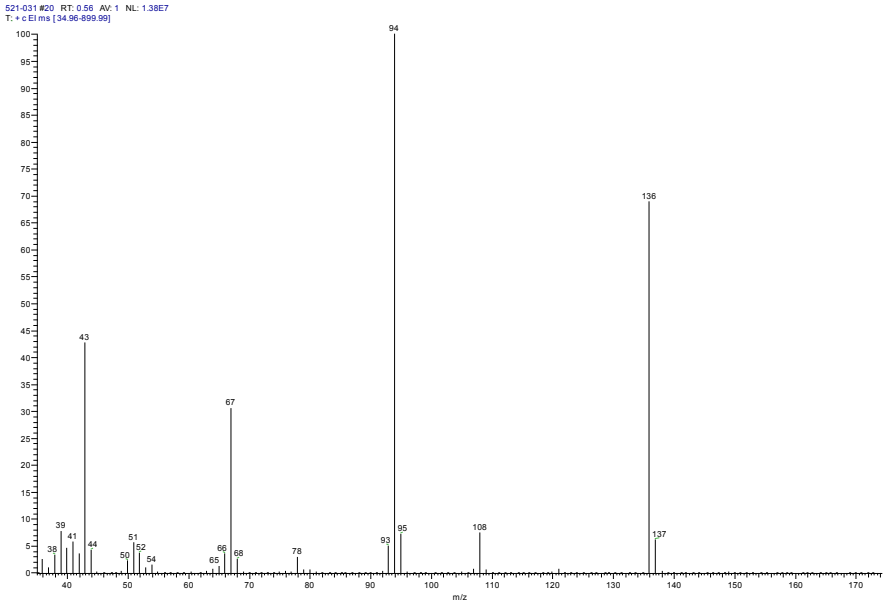

Fig. 10.2.19: Mass spectrum (EI) of *4*-acetamido-pyridine.

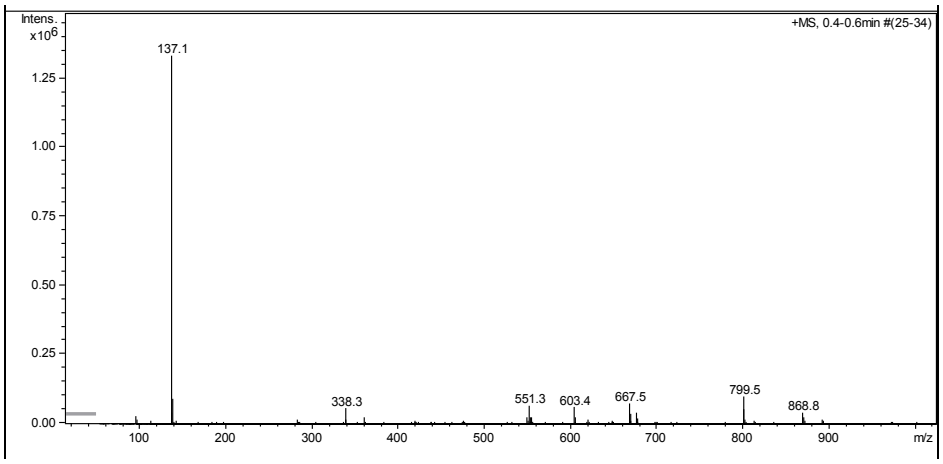

Fig. 10.2.20: Mass spectrum (ESI) of *4*-acetamido-pyridine.

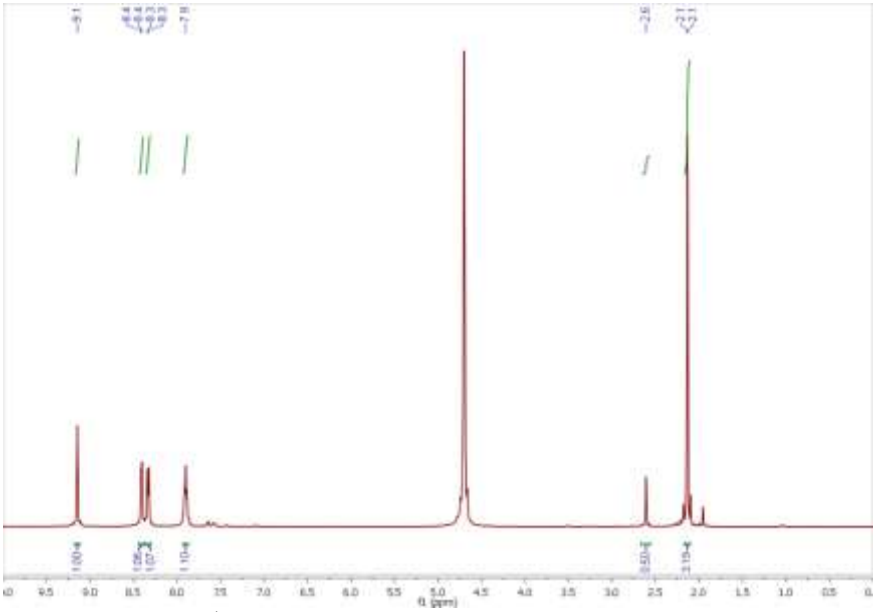

Fig. 10.2.21: ^{1}H NMR (500 MHz) of *3*-acetamido-pyridine in D_2O.

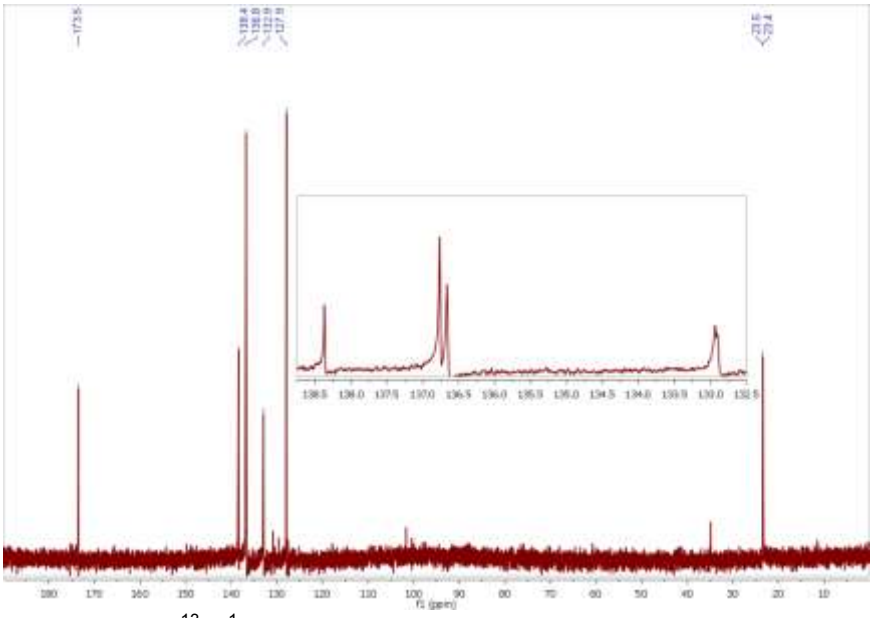

Fig. 10.2.22: $^{13}C\{^{1}H\}$ NMR (125 MHz) of *3*-acetamido-pyridine in D_2O.

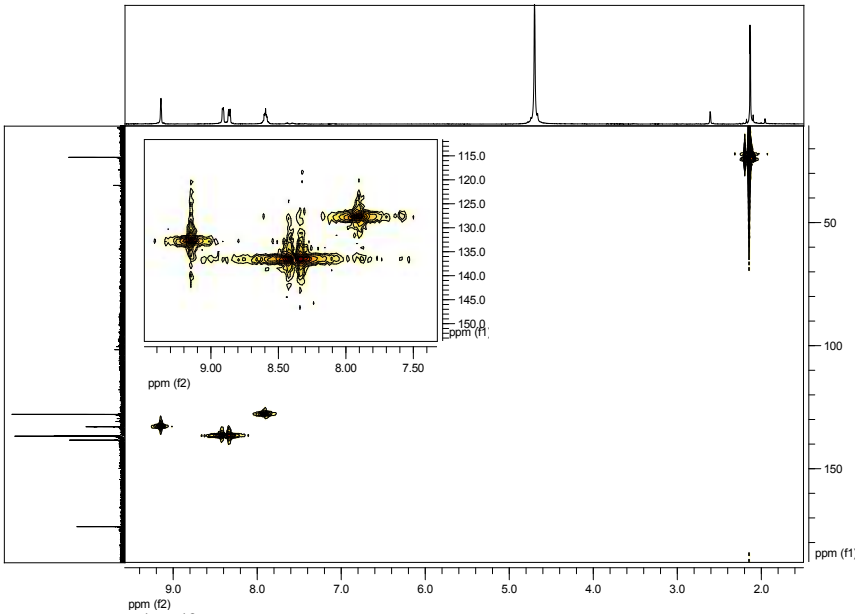

Fig. 10.2.23: ^{1}H-^{13}C COSY-NMR (500 MHz) of *3*-acetamido-pyridine in D_2O.

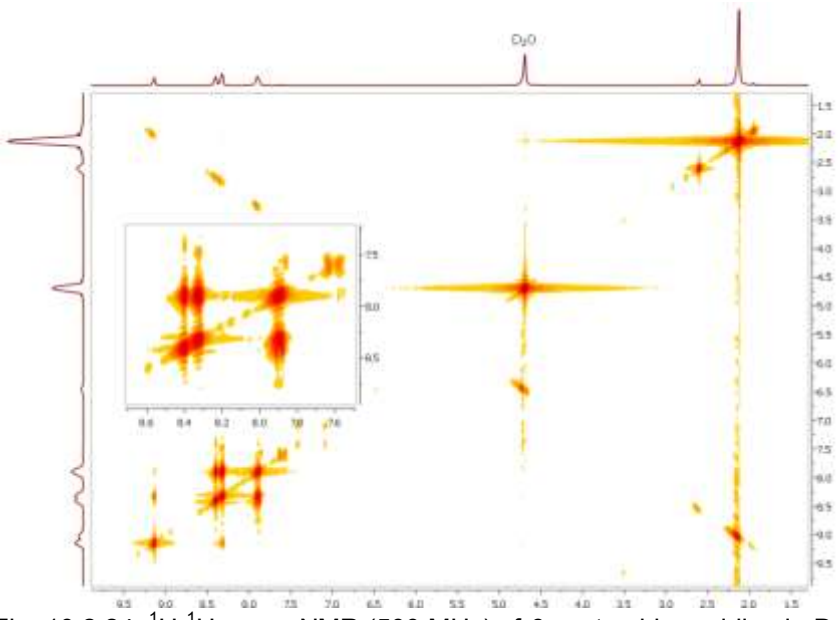

Fig. 10.2.24: ^{1}H-^{1}H COSY-NMR (500 MHz) of *3*-acetamido-pyridine in D_2O.

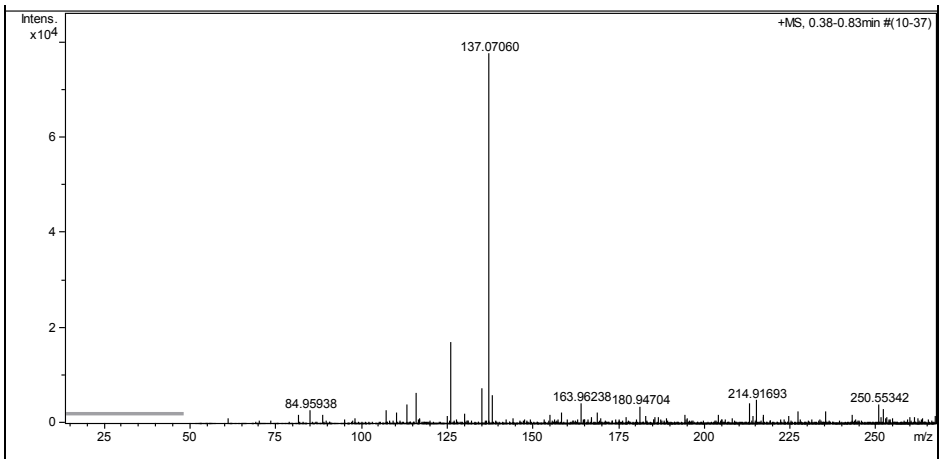

Fig. 10.2.25: Mass spectrum (ESI) of *3*-acetamido-pyridine.

12 References

[1] (a) C. Janiak, *Dalton Trans.*, 2003, **14**, 2781. (b) A.-K. Cheetham, C.-N.-R. Rao, and R. K. Feller, *Chem. Commun.*, 2006, **46**, 4780. (c) C. Janiak, and J. K. Vieth, *New J. Chem.*, 2010, **34**, 11, 2366. (d) S.-R. Batten, N.-R. Champness, X.-M. Chen, J. Garcia-Martinez, S. Kitagawa, L. Ohrstrom, M. O'Keeffe, M.-P. Suh and J. Reedijk, *Pure Appl. Chem.*, 2013, **85**, 1715.

[2] (a) M. O'Keeffe, *Chem. Soc. Rev.*, 2009, **38**, 5, 1215. (b) M.-J. Prakash, and M.-S. Lah, *Chem. Commun.* , 2009, **23**, 3326. (c) A. Mantion, L. Massuger, P. Rabu, C. Palivan, L.-B. McCusker, and A. Taubert, *J. Am. Chem. Soc.*, 2008, **130**, 8, 2517.

[3] (a) S. Banerjee, P.-G. Lassahn, C. Janiak, and A. Ghosh, *Polyhedron*, 2005, **24**, 18, 2963. (b) S.-C. Manna, E. Zangrando, J. Ribas, and N.-R. Chaudhuri, *Dalton Trans.*, 2007, **14**, 1383. (c) A. Carton, A. Mesbah, L. Perrin, and M. Francois, *Acta Cryst.*, Sect. E, 2007, **63**, 4, m948. (d) C.-S. Hong, and Y. Do, *Inorg. Chem.*, 1997, **36**, 25, 5684. (e) H.-X. Zhang, B.-S. Kang, A.-W. Xu, Z.-N. Chen, Z.-Y. Zhou, A.-S.-C. Chan, K.-B. Yu, and C. Ren, *Dalton Trans.*, 2001, **18**, 2559. (f) K.-Y. Choi, K.-M. Chun, K.-C. Lee, and J. Kim, *Polyhedron*, 2002, **21**, 19, 1913. (g) J. Cano, G.-De Munno, J.-L. Sanz, R. Ruiz, J. Faus, F. Lloret, M. Julve, and A. Caneschi, *Dalton Trans.*, 1997, **11**, 1915. (h) H.-K. Fun, S.-S.-S. Raj, R.-G. Xiong, J.-L. Zuo, Z. Yu, and X.-Z. You, *Dalton Trans.*, 1999, **12**, 1915.

[4] (a) B. Moulton, H. Abourahma, M.-W. Bradner, J. Lu, G.-J. McManus, and M.-J. Zaworotko, *Chem. Commun.*, 2003, **12**, 1342. (b) H. Abourahma, G.-J. Bodwell, J. Lu, B. Moulton, I.-R. Pottie, R.-B. Walsh, and M.-J. Zaworotko, *Cryst. Growth Des.*, 2003, **3**, 4, 513. (c) Y.-F. Zhou, F.-L. Jiang, D.-Q. Yuan, B.-L. Wu, R.-H. Wang, Z.-Z. Lin, and M.-C. Hong, *Angew. Chem.*, *Int. Ed.*, 2004, **43**, 42, 5665. (d) A.-C. Sudik, A.-P. Côté, and O.-M. Yaghi, *Inorg. Chem.*, 2005, **44**, 9, 2998. (e) Y.-H. Wen, J. Zhang, X.-Q. Wang, Y.-L. Feng, J.-k. Cheng, Z.-J. Li, and Y.-G. Yao, *New J. Chem.*, 2005, **29**, 8, 995. (f) A. Thirumurugan, and S. Natarajan, *Cryst. Growth Des.*, 2006, **6**, 4, 983.

[5] (a) A. Majumder, S. Shit, C.-R. Choudhury, S.-R. Batten, G. Pilet, D. Luneau, N. Daro, J.-P. Sutter, N. Chattopadhyay, and S. Mitra, *Inorg. Chim. Acta*, 2005, **358**, 13, 3855. (b) M.-J. Plater, M.-R. St. J. Foreman, E. Coronado, C.-J. Gómez-García, and A.-M.-Z. Slawin, *Dalton Trans.*, 1999, **23**, 4209. (c) M.-J. Plater, M.-R. St J. Foreman, R.-A. Howie, J.-M.-S. Skakle, E. Coronado, C.-J. Gómez- García, T. Gelbrich, and M.-B. Hursthouse, *Inorg. Chim. Acta*, 2001, **319**, 1-2, 159. (d) M. Du, X.-J. Jiang, and X.-J. Zhao, *Inorg. Chem.*, 2006, **45**, 10, 3998. (e) T.-J. Prior, and M.-J. Rosseinsky, *CrystEngComm*, 2000, **2**, 24, 128. (f) P. Wang,

C.-N. Moorefield, M. Panzer, and G.-R. Newkome, *Chem. Commun.*, 2005, **4**, 465. (g) Y.-F. Zhou, B.-Y. Lou, D.-Q. Yuan, Y.-Q. Xu, F.-L. Jiang, and M.-C. Hong, *Inorg. Chim. Acta*, 2005, **358**, 11, 3057. (h) Q. Wang, M.-J. Wu, X.-G. Wang, and X.-J. Zhao, *Acta Cryst.*, Sect. E, 2006, **62**, 10, m2496. (i) X. Shi, G. Zhu, Q. Fang, G. Wu, G. Tian, R. Wang, D. Zhang, M. Xue, and S. Qiu, Eur. *J. Inorg. Chem.*, 2004, **1**, 185. (j) M. Riou-Cavellec, C. Albinet, J.-M. Greneche, and G. Ferév, *J. Mater. Chem.*, 2001, **11**, 12, 3166. (k) B.-B. Ding, Y.-Q. Weng, Z.-W. Mao, C.-K. Lam, X.-M. Chen, and B.-H. Ye, *Inorg. Chem.*, 2005, **44**, 24, 8836. (l) O.-M. Yaghi, H. Li, and T. L. Groy, *J. Am. Chem. Soc.*, 1996, **118**, 38, 9096. (m) C.-J. Kepert, T.-J. Prior, and M.-J. Rosseinsky, *J. Am. Chem. Soc.*, 2000, **122**, 21, 5158. (n) S. Liang, H. Wang, Z. Wang, and J.-Y. Han, *Acta Cryst.*, Sect. E, 2006, **62**, 11, m3014. (o) K.-E. Holmes, P.-F. Kelly, and M.-R. J. Elsegood, *Dalton Trans.*, 2004, **21**, 3488. (p) H. Oshio, and H. Ichida, *J. Phys. Chem.*, 1995, **99**, 10, 3294. (q) J.-W. Ko, K.-S. Min, and M.-P. Suh, *Inorg. Chem.*, 2002, **41**, 8, 2151. (r) X. Li, D. Sun, R. Cao, Y. Sun, Y. Wang, W. Bi, S. Gao, and M. Hong, *Inorg. Chem. Commun.*, 2003, **6**, 7, 908. (s) J. Zhang, Y.-B. Chen, S.-M. Chen, Z.-J. Li, J.-K. Cheng, and Y.-G. Yao, *Inorg. Chem.*, 2006, **45**, 8, 3161. (t) S. Qin, S. Lu, Y. Ke, J. Li, S. Zhou, X. Wu, and W. Du, *Cryst. Res. Tech..*, 2006, **41**, 1, 98. (u) G. Smith, A.-N. Reddy, K.-A. Byriel, and C.-H. L. Kennard, *Dalton Trans.*, 1995, **22**, 3565. (v) B. Gómez-Lor, E. Gutiérrez-Puebla, M. Iglesias, M.-A. Monge, C. Ruiz-Valero, and N. Snejko, *Chem. Mater.*, 2005, **17**, 10, 2568.

[6] P.-S. Mukherjee, S. Konar, E. Zangrando, T. Mallah, J. Ribas and N.-R. Chaudhuri, *Inorg. Chem.*, 2003, **42**, 2545.

[7] O.-M. Yaghi, C.-E. Davis, G.-Li and H. Li, *J. Am. Chem. Soc.*, 1997, **119**, 2861.

[8] Q. Shi, L. Xu, J. Ji, Y. Li, R. Nang, Z. Zhau, R. Cao, M. Hong and A.-S.-C. Chan, *Inorg. Chem. Commun.*, 2004, **7**, 1254.

[9] (a) S.-R. Batten and R. Robson, *Angew. Chem., Int. Ed.*, 1998, **37**, 1460. (b) P.-J. Hagrman, D. Hagrman and J. Zubieta, *Angew. Chem., Int. Ed.*, 1999, **38**, 2639. (c) B. Moulton and M.-J. Zaworotko, *Chem. Rev.*, 2001, **101**, 1629. (d) D. Venkataraman, G.-B. Gardner, S. Lee and J.-S. Moore, *J. Am. Chem. Soc.*, 1995, **117**, 11600. (e) D.-M.-L. Goodgame, D.-A. Garchvogel and D.-J. Williams, *Angew. Chem., Int. Ed.*, 1999, **38**, 153. (f) K. Biradha, *Cryst. Eng. Commun..*, 2003, *5*, 274. (g) G.-S. Papaefstathiou and L.-R. MacGillivray, *Coord. Chem. Rev.*, 2003, **246**, 169. (h) M.-J. Rosseinsky, *Microporous Mesoporous Mater.*, 2004, **73**, 15. (i) L. Brammer, *Chem. Soc. Rev.*, 2004, **33**, 476. (j) R.-J. Hill, D.-L. Long, N.-R. Champness, P. Hubberstey and M. Schröder, *Acc. Chem. Res.*, 2005, **38**, 337. (k) M.-W. Hosseini, *Acc. Chem. Res.*, 2005, **38**, 313.

[10] M. Bailey and C.-J. Brown, *Acta Crystallogr.*, 1967, **22**, 387.

[11] R. Alcala and S. Martinez-Carrera, *Acta Crystallogr.*, 1972, **B28**, 1671.

[12] (a) D.-J. Duchamp and R.-E. March, *Acta Crystallogr.*, 1969, **B25**, 5. (b) M.-J. Zaworotko, *Chem. Commun.*, 2001, **1**, 1. (c) F.-H. Herbstein, *Top. Curr. Chem.*, 1987, **140**, 107.

[13] (a) M. I. H. Mohideen, B. Xiao, P. S. Wheatley, A. C. McKinlay, Y. Li, A. M. Z. Slawin, D. W. Aldous, N. F. Cessford, T. Düren, X. Zhao, R. Gill, K. M. Thomas, J. M. Griffin, S. E. Ashbrook and R. E. Morris, Nature Chemistry, 2011, **3**, 304. (b) S.-V. Kolotuchin, E.-E. Fenlon, S.-R. Wilson, C.-J. Loweth and S.-C. Zimmerman, *Angew. Chem., Int., Ed. Engl.*, 1996, **34**, 2654. (c) O. Ermer, *J. Am. Chem. Soc.*, 1988, **110**, 3747.

[14] R.-E. Melendez, C.-V. K. Sharma, M.-J. Zaworotko, C. Bauer and R.-D. Rogers, *Angew. Chem., Int. Ed. Engl.*, 1996, **35**, 2213.

[15] (a) N. Lin, A. Dmitriev, J. Weckesser, J.-V. Barth and K. Kern, *Angew. Chem., Int. Ed.*, 2002, **41**, 4779. (b) O.-M. Yaghi, G. Li, H. Li, *Nature*, 1995, **378**, 703. (c) S.-O.-H. Gutschke, M. Molinier, A.-K. Powell, R.-E.-P. Winpenny and P.-T. Wood, *Chem. Commun.*, 1996, 823.

[16] M. Dinca, A. F. Yu and J. R. Long, *J. AM. CHEM. SOC.*, 2006, **128**, 8904.

[17] (a) M. Pourayoubi, M.-R. Chaijan, T.-M. Percino and M.-A.-L. Ramirez, *Z. Kristallogr.-New Cryst. Struct.*, 2011, **226**, 115. (b) L. Yi, J.-Y. Du, S. Liu and X.-X. Wang, *J. Chem. Res.*, 2004, 29. (c) V.-N. Sinditskii, V.-I. Sokol, A.-E. Fogel'zang, M.-D. Dutov, V.-V. Serushkin and M.-A. Porai-Koshits, *Zh. Neorg. Khim. (Russ.) (Russ. J. Inorg. Chem.)*, 1987, **32**, 2726. (d) S. Cudzilo, W. Trzcinski, M. Nita, S. Michalik, S. Krompiec, R. Kruszynski, J. Kusz, *Propellants,Explos.,Pyrotech.*, 2011, **36**, 151. (e) D. Li, Y. Ren, F.-Q. Zhao, J.-H. Yi, J.-R. Song and K.-Z. Xu, *Wuji Huaxue Xuebao (Chin.) (Chin.J.Inorg.Chem.)*, 2010, **26**, 509. (f) M. Groessl, E. Reisner, C. G. Hartinger, R. Eichinger, O. Semenova, A.-R. Timerbaev, M.-A. Jakupec, V.-B. Arion and B.-K. Keppler, *J. Med. Chem.*, 2007, **50**, 2185. (g) A.-A. Udovenko, L.-A. Zemnukhova, E.-V. Kovaleva, Y.-E. Gorbunova, Y.-N. Mikhailov, *Koord. Khim. (Russ.) (Coord.Chem.)*, 2004, **30**, 587. (h) S.-W. Wang, L. Yang, J.-L. Feng, B.-D. Wu, J.-G. Zhang, T.-L. Zhang and Z.-N. Zhou, *Z. Anorg. Allg. Chem.*, 2011, 2215. (i) J.-A. Carpenter, J. Dshemuchadse, S. Busato, I. Braeunlich, A. Poethig, P. Smith and W. Caseri, *Z. Anorg. Allg. Chem.*, 2014, **640**, 724. (j) R.-L. Davidovich, M.-A. Pushilin, V.-B. Logvinova and A.-V. Gerasimenko, *Zh. Strukt. Khim. (Russ.) (J. Struct. Chem.)*, 2013, **54**, 696.

[18] (a) E.-N. Nfor, E.-A. Eno, J.-N. Foba-Tendo, G.-E. Iniama, E.-O. Duke and O.-E. Offiong, *Zh. Strukt. Khim. (Russ.) (J. Struct. Chem.)*, 2012, **53**, 1141. (b) M. Daszkiewicz and M.-K. Marchewka, *J. Mol. Struct.*, 2012, **90**, 1017. (c) Y.-Q. Huang, B. Ding, H.-L. Gao, P. Cheng, D.-Z. Liao, S.-P. Yan and Z.-H. Jiang, *J. Mol. Struct.*, 2005, **201**, 743. (d) L. Xuan-Wen, *Acta Crystallogr., Sect. E: Struct. Rep. Online*, 2005, **61**,m1777. (e) J.-H. Zhou, R.-M. Cheng, Y. Song, Y.-Z. Li, X.-T. Chen, Z.-L. Xue and X.-Z. You, *Inorg. Chem.*, 2005, **44**, 8011. (f) H.-S. Yoo, J.-H. Lim, J.-S. Kang, E.-K. Koh and C.-S. Hong, *Polyhedron*, 2007, **26**, 4383.

[19] (a) C.-W. Yeh, W.-J. Chang, M.-C. Suen, H.-T. Lee, H.-A. Tsai and C.-H. Tsou, *Polyhedron*, 2013, **61**, 151. (b) M.-M. Dirtu, C. Neuhausen, A.-D. Naik, A. Rotaru, L. Spinu and Y. Garcia, *Inorg.Chem.*, 2010, **49**, 5723. (c) J.-C. Liu, D.-G. Fu, J.-Z. Zhuang, C.-Y. Duan and X.-Z. You, *J. Chem. Soc., Dalton Trans.,* 1999, 2337. (d) H.-Y. Zhang, H. Li, G. Liu, T.-T. Liu, F. Yue and J.-D. Wang, *Koord. Khim. (Russ.) (Coord. Chem.)*, 2011, **37**, 409. (e) H.-Y. Zhang, H. Li, G. Liu, T.-T. Liu, F. Yue and J.-D. Wang, *Koord. Khim. (Russ.) (Coord. Chem.)*, 2011, **37**, 842. (f) Z.-Y. Liu, Y.-H. Su, E.-C. Yang and X.-J. Zhao, *Inorg. Chem. Commun.*, 2012, **26**, 56. (g) X.-Y. Wu, X.-F. Kuang, Z.-G. Zhao, S.-C. Chen, Y.-M. Xie, R.-M. Yu and C.-Z. Lu, *Inorg. Chim. Acta*, 2010, **363**, 1236. (h) Q.-L. Wang, H. Xu, H.-W. Hou and G. Yang, *Z. Naturforsch., B: Chem. Sci.*, 2009, **64**, 1143. (i) Q.-G. Zhai, X.-Y. Wu, S.-M. Chen, Z.-G. Zhao and C.-Z. Lu, *Inorg. Chem.*, 2007, **46**, 5046. (j) M.-M. Dirtu, A. Rotaru, D. Gillard, J. Linares, E. Codjovi, B. Tinant and Y. Garcia, *Inorg. Chem.*, 2009, **48**, 7838. (k) Q.-G. Zhai, X.-Y. Wu, S.-M. Chen, C.-Z. Lu and W.-B. Yang, *Cryst. Growth Des.*, 2006, **6**, 2126. (l) B. Ding, Y.-Q. Huang, Y.-Y. Liu, W. Shi and P. Cheng, *Inorg. Chem. Commun.*, 2007, **10**, 7. (m) G.-V. Romanenko, Z.-A. Savel'eva, N.-V. Podberezskaya and S.-V. Larionov, *Zh. Strukt. Khim. (Russ.) (J. Struct. Chem.)*, 1997, **38**, 207. (n) T. Mahenthirarajah and Y. Li, P. Lightfoot, *Dalton Trans.*, 2009 ,3280. (o) A. Grosjean, N. Daro, B. Kaufmann, A. Kaiba, J.-F. Letard and P. Guionneau, *Chem. Commun.*, 2011, **47**, 12382. (p) K. Drabent and Z. Ciunik, *Chem. Commun.*, 2001, 1254. (q) M.-A.-M. Abu-Youssef, A. Escuer, R. Vicente, F.-A. Mautner, L. Ohrstrom and M.-A.-S. Goher, *Polyhedron*, 2005, **24**, 557. (r) Y.-T. Gou, F. Yue, H.-M. Chen, G. Liu and D.-C. Sun, *J. Coord. Chem.*, 2013, **66**, 1889. (s) E.-C. Yang and X.-J. Zhao, *Sci. China. Chem.*, 2013, **56**, 465.

[20] (a) X.-L. Wang, W. Zhao, J.-W. Zhang and Q.-L. Lu, *J. S. S. Chem.*, 2013,**198**, 162. (b) E.-C. Yang, B. Ding, Z.-Y. Liu, Y.-L. Yang and X.-J. Zhao, *Cryst. Growth Des.*, 2012, **12**, 1185. (c) L.-Y. Qiao, J. Zhang, Z.-J. Li, Y.-Y. Qin, P.-X. Yin, J.-K. Cheng and Y.-G. Yao, *J. Mol. Struct.*, 2011, **994**,1. (d) E.-C. Yang, Z.-Y. Liu, C.-H. Zhang, Y.-L. Yang and X.-J. Zhao, *Dalton Trans.*, 2013, **42**, 1581. (e) E.-C. Yang, C.-H. Zhang, Z.-Y. Liu, N. Zhang, L.-N. Zhao and X.-J. Zhao, *Polyhedron*, 2012, **40**, 65. (f) E.-C. Yang, Z.-Y. Liu, L.-N. Zhao, Y.-L. Yang,

C.-H. Zhang and X.-J. Zhao, *Cryst. Eng. Commun.*, 2011, **13**, 5401. (g) U. Garcia-Couceiro, O. Castillo, A. Luque, J. P. Garcia-Teran, G. Beobide and P. Roman, *Eur. J. Inorg. Chem.*, 2005, 4280. (h) U. Garcia-Couceiro, D. Olea, O. Castillo, A. Luque, P. Roman, P. J. de Pablo, J. Gomez-Herrero and F. Zamora, *Inorg. Chem.*, 2005, **44**, 8343. (i) X.-L. Wang, W. Zhao, J.-W. Zhang and Q.-L. Lu, *J. Solid State Chem.*, 2013, **198**, 162. (j) Y. Zorlu, H. Can and F. Aksakal, *J. Mol. Struct.*, 2013, **368**, 1049. (k) B.-D. Wu, T.-L. Zhang, Y.-L. Li, S.-W. Wang, Z.-N. Zhou, J.-G. Zhang and L. Yang, *Z. Anorg. Allg. Chem.*, 2013, **639**, 2209.

[21] (a) E.-V. Govor, A.-B. Lysenko, E.-B. Rusanov, A.-N. Chernega, H. Krautscheid and K.-V. Domasevitch, *Z. Anorg. Allg. Chem.*, 2010, **636**, 209. (b) E.-V. Govor, A.-B. Lysenko and K.-V. Domasevitch, *Acta Crystallogr., Sect. C: Cryst. Struct. Commun.*, 2008 ,**64**, m201. (c) E.-V. Govor, A.-B. Lysenko, K.-V. Domasevitch, E.-B. Rusanov and A.-N. Chernega, *Acta Crystallogr., Sect. C: Cryst. Struct. Commun.*, 2008 , **64**, m117. (d) A.-B. Lysenko, E.-V. Govor and K.-V. Domasevitch, *Inorg. Chim. Acta*, 2007, **360**, 55. (e) A.-B. Lysenko, E.-V. Govor, H. Krautscheid and K.-V. Domasevitch, *Dalton Trans.*, 2006, 3772. (f) Y. Garcia, O. Kahn, L. Rabardel, B. Chansou, L. Salmon and J.-P. Tuchagues, *Inorg. Chem.*, 1999, **38**, 4663. (g) S. Pillet and C. Lecomte, *Acta Crystallogr., Sect. C: Cryst. Struct. Commun.*, 2007, **63**, m184. (h) C.-L. Zilverentant, W.-L. Driessen, J.-G. Haasnoot, J.-J.-A. Kolnaar and J. Reedijk, *Inorg. Chim. Acta*, 1998, **282**, 257. (i) M. Biagini-Cingi, A. M. Manotti-Lanfredi, F.-Ugozzoli, J.-G. Haasnoot and J. Reedijk, *Gazz. Chim. Ital.*, 1994, **124**, 509. (j) W. Vreugdenhil, J.-G. Haasnoot, R.-A.-G. de Graaff, H.-A. Nieuwenhuis, D. Reefman and J. Reedijk, *Acta Crystallogr., Sect. C: Cryst. Struct. Commun.*, 1987, **43**, 1527. (k) W. Vreugdenhil, S. Gorter, J.-G. Haasnoot and J. Reedijk, *Polyhedron*, 1985, **4**, 1769. (l) W. Vreugdenhil, J.-H. van Diemen, R.-A.-G. de Graaff, J. G. Haasnoot, J. Reedijk, A.-M. van der Kraan, O. Kahn and J. Zarembowitch, *Polyhedron*, 1990, **9**, 2971. (m) X.-C. Zhang, Y.-H. Chen and B. Liu, *Inorg. Chem. Commun.*, 2008, **11**, 446. (n) Y.-Q. Huang, X.-Q. Zhao, W. Shi, W.-Y. Liu, Z.-L. Chen, P. Cheng, D.-Z. Liao and S.-P. Yan, *Cryst. Growth Des.*, 2008, **8**, 3652. (o) X.-Y. Wang, L. Wang, Z.-M. Wang, G. Su and S. Gao, *Chem. Mater.*, 2005, **17**, 6369. (p) A. Ozarowski, Y. Shunzhong, B. R. McGarvey, A. Mislanker and J.-E. Drake, *Inorg. Chem.*, 1991, **30**, 3167. (q) V. Legrand, S. Pillet, C. Carbonera, M. Souhassou, J.-F. Letard, P. Guionneau and C. Lecomte, *Eur. J. Inorg. Chem.*, 2007, 5693. (r) Y.-Q. Huang and P. Cheng, *Inorg. Chem. Commun.*, 2008, **11**, 66.

[22] (a) A. Tahli, J.-K. Maclaren, I. Boldog and C. Janiak, *Inorg. Chim. Acta*, 2011, **374**, 506. (b) O.-G. Shakirova, D.-Y. Naumov, Y.-G. Shvedenkov, N.-I. Alferova, G.-V. Dolgushin and L.-G. Lavrenova, *Zh. Strukt. Khim. (Russ.) (J. Struct. Chem.)*, 2003, **44**, 701. (c) O.-G. Shakirova, A.-V. Virovets, D.-Yu. Naumov, Y.-G. Shvedenkov, V.-N. Elokhina and L.-G.

Lavrenova, *Inorg. Chem. Commun.*, 2002, **5**, 690. (d) Y. Wang, B. Ding, P. Cheng, D.-Z. Liao and S.-P. Yan, *Inorg. Chem.*, 2007, **46**, 2002. (e) Y. Wang, P. Cheng, Y. Song, D.-Z. Liao and S.-P. Yan, *Chem. Eur. J.*, 2007, **13**, 8131. (f) Y. Wang, X.-Q. Zhao, W. Shi, P. Cheng, D.-Z. Liao and S.-P. Yan, *Cryst. Growth Des.*, 2009, **9**, 2137. (g) B. Ding, L. Yi, P. Cheng, H.-B. Song and H.-G. Wang, *J. Coord. Chem.*, 2004, **57**, 771. (h) B. Ding, L. Yi, W.-Z. Shen, P. Cheng, D.-Z. Liao, S.-P. Yan and Z.-H. Jiang, *J. Mol. Struct.*, 2006, **784**, 138. (i) B. Ding, L. Yi, Y. Wang, P. Cheng, D.-Z. Liao, S.-P. Yan, Z.-H. Jiang, H.-B. Song and H.-G. Wang, *Dalton Trans.*, 2006, 665. (j) B. Ding, E.-C. Yang, X.-J. Zhao and X.-G. Wang, *J. Coord. Chem.*, 2008, **61**, 3793. (k) B. Ding and H.-A. Zou, *Acta Crystallogr., Sect. E: Struct. Rep. Online*, 2010, **66**, m933. (l) X.-G. Wang, X.-T. Han, Q. Zhou, Y. Wang and G.-Y. Liu, *Inorg. Chim. Acta*, 2012, **387**, 460. (m) J. Liu, Y. Song, J. Zhuang, X. Huang and X. You, *Polyhedron*, 1999, **18**, 1491. (n) J.-J. Liu, X. He, M. Shao and M.-X. Li, *J. Mol. Struct.*, 2009, **919**, 189. (o) Y.-H. Ma, P.-Z. Ma, H.-Q. Zhu and C.-C. Liu, *Acta Crystallogr., Sect. E: Struct. Rep. Online*, 2006, **62**, m1479. (p) L.-Y. Yuan and D. Bin, *J. Coord. Chem.*, 2007, **60**, 269. (q) H. Li, C.-J. Li and Z.-Q. Hu, *Acta Crystallogr., Sect. E: Struct. Rep. Online*, 2007, **63**, m407.

[23] (a) J.-G. Ding, X. Zhu, Y.-F. Cui, N. Liang, P.-P. Sun, Q. Chen, B.-L. Li and H.-Y. Li, *CrystEngComm*, 2014, **16**, 1632. (b) Y.-F. Cui, P.-P. Sun, Q. Chen, B.-L. Li and H.-Y. Li, *CrystEngComm*, 2012, **14**, 4161. (c) Y.-F. Cui, X. Qian, Q. Chen, B.-L. Li and H.-Y. Li, *CrystEngComm*, 2012, **14**, 1201. (d) H.-A. Habib, J. Sanchiz and C. Janiak, *Inorg. Chim. Acta*, 2009, **362**, 2452. (e) H.-A. Habib, A. Hoffmann, H.-A. Hoppe and C. Janiak, *Dalton Trans.*, 2009,1742. (f) H.-A. Habib, J. Sanchiz and C. Janiak, *Dalton Trans.*, 2008, **36**, 1734. (g) Y. Garcia, G. Bravic, C. Gieck, D. Chasseau, W. Tremel and P. Gütlich, *Inorg. Chem.*, 2005, **44**, 26, 9723. (h) Y. Garcia, P.-J. van Koningsbruggen, H. Kooijman, A.-L. Spek, J.-G. Haasnoot and O. Kahn, *Eur. J. Inorg. Chem.*, 2000, 307. (i) N. Liang, Y.-F. Cui, D.-Y. Yuan, B.-L. Li and H.-Y. Li, *Inorg. Chim. Acta*, 2011, **376**, 612. (j) N. Liang, J. Wang, D. Yuan, B. Li and H. Li, *Inorg. Chem. Commun.*, 2010, **13**, 844. (k) Y.-X. Zhang, J. Yang, W.-Q. Kann and J.-F. Ma, *CrystEngComm*, 2012, **14**, 6004. (l) G.-A. Senchyk, V.-A. Bukhan'ko, A.-B. Lysenko, H. Krautscheid, E.-B. Rusanov, A.-N. Chernega, M. Karboviak and K.-V. Domasevitch, *Inorg. Chem.*, 2012, **51**, 8025. (m) O.-V. Sharga, A.-B. Lysenko, H. Krautscheid and K.-V. Domasevitch, *Acta Crystallogr., Sect. C: Cryst. Struct. Commun.*, 2010, **66**, m269. (n) A.-B. Lysenko, G.-A. Senchyk, J. Lincke, D. Lassig, A.-A. Fokin, E.-D. Butova, P.-R. Schreiner, H. Krautscheid and K.-V. Domasevitch, *Dalton Trans.*, 2010, **39**, 4223. (o) Y. Feng, N. Liang, B. Li and H. Li, *Acta Crystallogr., Sect. E: Struct. Rep. Online*, 2010, **66**, m560. (p) R. Zhang, Q. Chen, J. Gao and X. Wu, *Acta Crystallogr. ,Sect. E: Struct.*

Rep. Online, 2010, **66**, m1208. (q) L. Yi, X. Yang, T. Lu and P. Cheng, *Cryst. Growth Des.*, 2005, **5**, 1215.

[24] (a) J. Lincke, D. Lassig, M. Kobalz, J. Bergmann, M. Handke, J. Mollmer, M. Lange, C. Roth, A. Moller, R. Staudt and H. Krautscheid, *Inorg. Chem.*, 2012, **51**, 7579. (b) L. Wen, W. Shi, X. Chen, H. Li and P. Cheng, *Eur. J. Inorg. Chem.*, 2012, 3562. (c) T. Panda, T. Kundu and R. Banerjee, *Chem. Commun.*, 2012, **48**, 5464. (d) T. Panda, P. Pachfule and R. Banerjee, *Chem. Commun.*, 2011, **47**, 7674. (e) M. Zhu, S.-Q. Su, X.-Z. Song, Z.-M. Hao, S.-Y. Song and H.-J. Zhang, *Dalton Trans.*, 2012, **41**, 13267. (f) M. Chen, Y. Lu, J. Fan, G.-C. Lv, Y. Zhao, Y. Zhang and W.-Y. Sun, *CrystEngComm.*, 2012, **14**, 2015. (g) M. Chen, M.-S. Chen, T. Okamura, M.-F. Lv, W.-Y. Sun and N. Ueyama, *CrystEngComm.*, 2011, **13**, 3801. (h) M. Chen, S.-S. Chen, T. Okamura, Z. Su, M.-S. Chen, Y. Zhao, W.-Y. Sun and N. Ueyama, *Cryst. Growth Des.*, 2011, **11**, 1901.

[25] S. Ma, D. Yuan, J.-S. Chang, and H.-C. Zhou, *Inorg. Chem.*, 2009, **48**, 12, 5398.

[26] I. Boldog, K. Domasevitch, J.-K. Maclaren, C. Heering,G. Makhloufi and C. Janiak, *CrystEngComm*, 2014, **16**,148.

[27] ref. for H_2bdt: (a) Q. Dang and H. Caiyun, *Acta Crystallogr.,Sect. E: Struct. Rep. Online*, 2013, **69**, m283. (b) W. Ouellette, K. Darling, A. Prosvirin, K. Whitenack, K.-R. Dunbar and J. Zubieta, *Dalton Trans.*, 2011, **40**, 12288. (c) W. Ouellette, A.-V. Prosvirin, K. Whitenack, K. R. Dunbar and J. Zubieta, *Angew. Chem., Int. Ed.*, 2009, **48**, 2140. (d) M.-S.-Y. Parast, A. Morsali and P. Ebrahimpour, *Dalton Trans.*, 2012, **41**, 5848. (e) Y.-W. Li, W.-L. Chen, Y.-H. Wang, Y.-G. Li and E.-B. Wang, *J. Solid State Chem.*, 2009, **182**, 736. (f) G. E. Kostakis, K. C. Mondal, C.-E. Anson and A.-K. Powell, *Polyhedron*, 2010, **29**, 24. (g) W.-T. Liu, J.-Y. Li, Z.-P. Ni, X. Bao, Y.-C. Ou, J.-D. Leng, J.-L. Liu and M.-L. Tong, *Cryst. Growth Des.*, 2012, **12**, 1482. (h) Z.-J. Ma, J. Tao, R.-B. Huang and L.-S. Zheng, *Acta Crystallogr., Sect. E: Struct. Rep. Online*, 2005, **61**, m361. (i) J. Tao, Z.-J. Ma, R.-B. Huang and L.-S. Zheng, *Inorg. Chem.*, 2004, **43**, 6133. (j) D.-C. Zhong, X.-L. Feng and T.-B. Lu, *CrystEngComm*, 2011, **13**, 2201. (k) C. Qiao, Q. Wei, Z. Xia, J. Liang and S. Chen, *Chin. J. Chem.*, 2011, **29**, 724. (l) J. Sun, D. Zhang, L. Wang, Y. Cao, D. Li, L. Zhang, W. Song, Y. Fan and J. Xu, *CrystEngComm*, 2012, **14**, 3982. (m) F. Yang, B. Li, W. Xu, G. Li, Q. Zhou, J. Hua, Z. Shi and S. Feng, *Inorg. Chem.*, 2012, **51**, 6813. (n) A. Maspero, S. Galli, V. Colombo, G. Peli, N. Masciocchi, S. Stagni, E. Barea and J. A. R. Navarro, *Inorg. Chim. Acta*, 2009, **362**, 4340.

(o) J. Lach, S.-V. Voitekhovich, V. Lozan, P.-N. Gaponik, O.-A. Ivanshkevich, J. Lincke, D. Lässig and B. Kersting, *Z. Anorg. Allg. Chem.*, 2010, **636**, 1980. (p) W.-T. Liu, Y.-C. Ou, Z.-j.

Lin and M.-L. Tong, *CrystEngComm*, 2010, **12**, 3487. (q) J.-H. Deng, X.-L. Yuan and G.-Q. Mei, *Inorg. Chem. Commun.*, 2010, **13**, 1585. (r) K. Sumida, M. L. Foo, S. Horike and J. R. Long, *Eur. J. Inorg. Chem.*, 2010, 3739. (s) Z. Yan, M. Li, H.-L. Gao, X.-C. Huang and D. Li, *Chem. Commun.*, 2012, **48**, 3960.

[28] ref for H_2ipdt and H_3btt: (a) T. Hu, L. Liu, X. Lv, X. Chen, H. He, F. Dai, G. Zhang and D. Sun, *Polyhedron*, 2010, **29**, 296. (b) G.-E. Kostakis, G. Abbas, C.-E. Anson and A.-K. Powell, *CrystEngComm*, 2008, **10**, 1117. (c) G.-E. Kostakis, C.-E. Anson and A.-K. Powell, *Bioinorg. Chem. Appl.*, 2010, 104329. (d) G.-E. Kostakis, G. Abbas, C.-E. Anson and A.-K. Powell, *CrystEngComm*, 2009, **11**, 82. (e) M. Dinca, A. Dailly, Y. Liu, C.-M. Brown, D.-A. Neumann and J.-R. Long, *J. Am. Chem. Soc.*, 2006, **128**, 16876. (f) M. Dinca, W.-S. Han, Y. Liu, A. Dailly, C.-M. Brown and J.-R. Long, *Angew. Chem., Int. Ed.*, 2007, **46**, 1419. (g) M.Hill, M.-F. Mahon and K.-C. Molloy, *J. Chem. Soc. ,Dalton Trans.*, 1996, 1857. (h) M. Hill, M.-F. Mahon, J.-M. Ginley and K.-C. Molloy, *J. Chem. Soc., Dalton Trans.*, 1996, 835. (i) C.-F. Qiao and C.-S. Zhou, *Acta Crystallogr., Sect. E: Struct. Rep. Online*, 2012, **68**, m173. (j) C.-F. Qiao, Q. Wei, Z.-Q. Xia, C.-S. Zhou and S.-P. Chen, *J. Thermal Analysis and Calorimetry*, 2012, **107**, 527. (k) M.-N. Li, G.-S. Yang, S.-L. Li, H.-Y. Zang, G.-J. Xu, K.-Z. Shao and Z.-M. Su, *Inorg. Chem. Commun.*, 2010, **13**, 1203. (l) J.-H. Liao, W.-T. Chen, C.-S. Tsai, C.-C. Yang and C.-C. Wang, *CrystEngComm*, 2010, **12**, 3033. (m) C. Jiang, Z. Yu, C. Jiao, S. Wang, J. Li, Z. Wang and Y. Cui, *Eur. J. Inorg. Chem.*, 2004, 4669. (n) K. Sumida, S. Horike, S. S. Kaye, Z. R. Herm, W. L. Queen, C. M. Brown, F. Grandjean, G. J. Long, A. Dailly and J. R. Long, *Chem. Sci.*, 2010, **1**, 184. (o) Y. Lu, *Acta Crystallogr., Sect. E: Struct. Rep. Online*, 2008, **64**, m1255.

[29] Synthesis of 2,5-dimethyloxadiazole from 1,2-diacetylhydrazine: (1) with thionyl chloride by heating: (a) M.-S. Skorobogatova, et al., *Chemistry of Heterocyclic Compounds* (New York, NY, United States), 1970, **6**, 1092. (b) M.-S. Skorobogatova, N.-P. Zolotareva, *Chem. Heter. Comp.*, 1968, **2**, 372. (c) K.-G. Soedinenii, 1970, **6**, 1171. (d) M. Golfier, M.-G. Guillerez, *Tetrahedron Letters*, 1976,267. (2) with acetic anhydride by heating: M. P. Hutt, et al., *Journal of Heterocyclic Chemistry*, 1970, **7**, 511. (3) with $BF_3.Et_2O$ by reflux: V. K. Tandon, R. B. Chhor, *Syn. commun.*, 2001, **31**, 11, 1727.

[30] Gamall Makhloufi, Diplom Thesis, Heinrich-Heine Universität Düsseldorf, 2012.

[31] Leif Römer, Bachelor Thesis, Heinrich-Heine Universität Düsseldorf, 2012.

[32] S. Baitalik and B. Dutta, *Polyhedron*, 2004, **23**, 913.

[33] Synthesis of 2,5-disubstituted oxadiazole from 5-substituted tetrazole: (a) B.-S. Jursic and Z. Zdravkovskif, Syn. Commun., 1994, **24**, 1575. (b) L.-I. Vereshchagin, A.-V. Petrov, V.-N. Kizhnyaev, F.-A. Pokatilov and A.-I. Smirnov, *Russ. J. Org. Chem.*, 2006, **42**, 1049. (c) G.-I. Koldobskii and S.-E. Ivanova, Russ. J. G. Chem., 1994, **64**, 1512. (d) Z.-O. Khimii, 1994, **64**, 10, 1698.

[34] Synthesis of 2,5-dimethyoxadiazole from acetylhydrazine and triethylortoacetate: C. Ainsworth and R.-E. Hackler, *J. Org. Chem.*, 1966, **31**, 3442.

[35] Jörg Linke, PhD Thesis, Universität Leipzig, 2012.

[36] T. Curtius, G. Schöfer and N.-J. Schwan, *Prakt. Chem.*, 1892, **51**, 180.

[37] (a) C.-J. Gerack and L. McElwee-White, *Molecules*, 2014, **19**, 7689. (b) H.-A. Saad, N.-A. Osman and A.-H. Moustafa, *Molecules*, 2011, **16**, 10187.

[38] R. Meyer, DRP No. 574944, 1933.

[39] S. L. James, Chem. *Soc. Rev.*, 2003, **32**, 5, 276.

[40] (a) A. Schoedel and M.-J. Zaworotko, *Chem. Sci.*, 2014, **5**, 1269. (b) D.-J. Tranchemontagne, J.-L. Mendoza-Cortes, M. O'Keeffe and O.-M. Yaghi, *Chem. Soc. Rev.*, 2009, **38**, 1257. (c) M. Eddaoudi, D.-B. Moler, H. Li, B. Chen, T.-M. Reineke, M. O'Keeffe and O.-M. Yaghi, *Acc. Chem. Res.*, 2001, **34**, 319.

[41] (Cu^{2+}) S.-S.-Y. Chui, S.-M.-F. Lo, J.-P.-H. Charmant, A.-G. Orpen and I.-D. Williams, *Science*, 1999, **283**, 1148.

[42] H. Chun, D.-N. Dybtsev, H. Kim and K. Kim, *Chem. Eur. J.*, 2005, **11**, 12, 3521.

[43] G. Férey, C. Mellot-Draznieks, C. Serre, F. Millange, J. Dutour, S. Surblé and I.Margiolaki, *Science*, 2005, **309**, 2040.

[44] P. Horcajada, S. Surble, C. Serre, D.-Y. Hong, Y.-K. Seo, J.-S. Chang, J.-M.Greneche, I. Margiolaki and G. Férey, *Chem. Commun.*, 2007, 2820.

[45] W.-X. Zhang, P.-Q. Liao, R.-B. Lin, Y.-S. Wei, M.-H. Zeng and X.-M. Chen, *Coord. Chem. Rev.*, 2014 in press.

[46] M. Francl, *Nature Chem.*, 2009, **1**, 334.

[47] (a) D.-M. Proserpio, *Nature Chem.*, 2010, **2**, 435. (b) L. Fang, M.-A. Olson, D. Benítez, E. Tkatchouk, W.-A. Goddard III and J.-F. Stoddart, *Chem. Soc. Rev.*, 2010, **39**, 17. (c) V.-A.

Blatov, L. Carlucci, G. Ciani and D.-M. Proserpio, *CrystEngComm*, 2004, **6**, 65, 377. (d) B. Xu, Z. Lin, L. Han and R. Cao, *CrystEngComm*, 2011, **13**, 440. (e) K.-A. Brown, D.-P. Martin and R.-L. LaDuca, *CrystEngComm*, 2008, **10**, 1305. (f) F. Luo, Y.-T. Yang, Y.-X. Che and J.-M. Zheng, *CrystEngComm*, 2008, **10**, 981.

[48] R. J. Kuppler, et al., *Coord. Chem. Rev.*, 2009, **253**, 3042.

[49] (a) R. I. Walton, *Chem. Soc. Rev.*, 2002, **31**, 4, 230. (b) S. Qiu and G. Zhu, *Coord. Chem. Rev.*, 2009, **253**, 2891.

[50] (a) S. Kitagawa, R. Kitaura and S. Noro, *Angew. Chem.*, Int. Ed. Engl., 2004, 43, 2334. (b) D. Zhao, D.-Q. Yuan and H.-C. Zhou, *Energy Environ. Sci.*, 2008, **1**, 222. (c) R. Robson, *Dalton Trans.*, 2008, 5113.

[51] N. Stock and S. Biswas, *Chem. Rev.*, 2012, **112**, 933.

[52] J. He, J.-X. Zhang, G.-P. Tan, Y.-G. Yin, D. Zhang, and M.-H. Hu, *Cryst. Growth Des.*, 2007, **7**, 1508.

[53] R. Mondal, M.-K. Bhunia and K. Dhara, *CrystEngComm*, 2008, **10**, 1167.

[54] X.-G. Guo, W.-B. Yang, X.-Y. Wu, Q.-K. Zhang, L. Lin, R. Yu, H.-F. Chen and C.-Z. Lu, *Dalton Trans.*, 2013, **42**, 15106.

[55] O. M. Nazarenko, E. B. Rusanov, A. N. Chernega and K. V. Domasevitch, *Acta Cryst.*, 2013. **C69**, 232.

[56] S.-W. Liang, M.-X. Li, M. Shao, H.-J. Liu, *Inorg. Chem. Commun.*, 2007, **10**, 1347.

[57] J. Hunger, H. Krautscheid and J. Sieler, *Crystal Growth & Design*, 2009, **9**, 4613.

[58] W. Kleist, F. Jutz, M. Maciejewski and A. Baiker, *Eur. J. Inorg. Chem.*, 2009, 3552.

[59] H. Deng, C. J. Doonan, H. Furukawa, R. B. Ferreira, J. Towne, C. B. Knobler, B. Wang and O. M. Yaghi, *Science*, 2010, **327,** 846.

[60] K. Koh, A. G. Wong-Foy and A. J. Matzger, *Chem. Commun.*, 2009, 6162.

[61] A. D. Burrows, CrystEngComm, 2011, 13, 3623.

[62] M. Du, C. P. Li, C. S. Liu and S. M. Fang, *Coord. Chem. Rev.*, 2013, **257**, 1282.

[63] K. Shen, M. Zhang and H. Zheng, *CrystEngComm*., 2015, **17**, 981.

[64] (a) J. Fielden, D. L. Long, A. M. Z. Slawin, P. Kögerler and L. Cronin, *Inorg. Chem.*, 2007, **46**, 9090; (b) H. K. Liu, X. H. Huang, T. H. Lu, X. J. Wang, W. Y. Sun and B. S. Kang, *Dalton Trans.*, 2008, 3178.

[65] B. Zheng, H. Dong, J. F. Bai, Y. Z. Li, S. H. Li and M. Scheer, *J. Am. Chem. Soc.*, 2008, **130**, 7778.

[66] Y. Q. Tian, Y. M. Zhao, Z. X. Chen, G. N. Zhang, L. H. Weng and D. Y. Zhao, *Chem. - Eur. J.*, 2007, **13**, 4146.

[67] Z. Yin, Y.-L. Zhou, M.-H. Zeng and M. Kurmoo, *Dalton Trans.*, 2015, **44**, 5258.

[68] (a) Q. Chen, J. B. Lin, W. Xue, M. H. Zeng and X. M. Chen, *Inorg. Chem.*, 2011, **50**, 2321.; (b) Q. Chen, W. Xue, J.-B. Lin, R. B. Lin, M. H. Zeng and X. M. Chen, *Dalton Trans.*, 2012, **41**, 4199.; (c) Q. Chen, W. Xue, B. Y. Wang, M. H. Zeng and X. M. Chen, *CrystEngComm*, 2012, **14**, 2009.

[69] (a) M. H. Zeng, Q. X. Wang, Y. X. Tan, S. Hu, H. X. Zhao, L. S. Long and M. Kurmoo, *J. Am. Chem. Soc.*, 2010, **132**, 2561.; (b) M. H. Zeng, Z. Yin, Y. X. Tan, W. X. Zhang, Y. P. He and M. Kurmoo, *J. Am. Chem. Soc.*, 2014, **136**, 4680.

[70] (a) M. H. Zeng, X. L. Feng, W. X. Zhang and X. M. Chen, *Dalton Trans.*, 2006, 5294.; (b) Y. L. Zhou, M. C. Wu, M. H. Zeng and H. Liang, *Inorg. Chem.*, 2009, **48**, 10146.; (c) M. H. Zeng, Y. L. Zhou, M. C. Wu, H. L. Sun and M. Du, *Inorg. Chem.*, 2010, **49**, 6436.

[71] J.-P. Zhang, P.-Q. Liao, H.-L. Zhou, R.-B. Lin and X.-M. Chen, *Chem. Soc. Rev.*, 2014, **43**, 5789.

[72] (a) V. Guillerm, D. Kim, J.-F. Eubank, R. Luebke, X. Liu, K. Adil, M.-S. Lah and M. Eddaoudi, *Chem. Soc. Rev.*, 2014, **43**, 6141. (b) J.-P. Zhang, Y.-B. Zhang, J.-B. Lin and X.-M. Chen, *Chem. Rev.*, 2012, **112**, 1001.

[73] S. Henke, A. Schneemann, A. Wütscher and R.A. Fischer, *J. Am. Chem. Soc.*, 2012, **134**, 9464.

[74] (a) G. Férey, *Dalton Trans.*, 2009, **23**, 4400. (b) M. P. Suh, Y. E. Cheon, and E. Y. Lee, *Coord. Chem. Rev.*, 2008, **252**, 8-9, 1007. (c) A.-M. Spokoyny, D. Kim, A. Sumrein, and C.-A. Mirkin, *Chem. Soc. Rev.*, 2009, **38**, 5, 1218. (d) U. Müller, M. Schubert, F. Teich, H. Puetter, K. Schierle-Arndt, and J. Pastre, *J. Mater. Chem.*, 2006, **16**, 7, 626. (e) G. Férey, *Chem. Soc. Rev.*, 2008, **37**, 191. (f) A.- U. Czaja, N. Trukhan and U. Müller, *Chem. Soc. Rev.*, 2009, **38**, 5, 1284. (g) T. Uemura, N. Yanai, and S. Kitagawa, *Chem. Soc. Rev.*, 2009,

38, 5, 1228. (h) K. Tanaka, and K.-I. Otani, *New J. Chem.*, 2010, **34**, 11, 2389. (i) A.-U. Czaja, N. Trukhan, and U. Müller, *Chem. Soc. Rev.*, 2009, **38**, 5, 1284. (j) J. Della Rocca, and W. Lin, *Eur. J. Inorg. Chem.*, 2010, **24**, 3725. (k) S. Kitagawa, R. Kitaura, and S. Noro, *Angew. Chem.*, Int. Ed., 2004, **43**, 18, 2334. (l) J.-R. Long, and O.-M. Yaghi, *Chem. Soc. Rev.*, 2009, **38**, 5, 1213.

[75] (a) L.-J. Murray, M. Dinca, and J.-R. Long, *Chem. Soc. Rev.*, 2009, **38**, 5, 1294. (b) S.-S. Han, J.-L. Mendoza-Cortes, and W.-A. Goddard III, *Chem. Soc. Rev.*, 2009, **38**, 5, 1460. (c) J. Sculley, D. Yuan, H.-C. Zhou, *Energy Environ. Sci.*, 2011, **4**, 2721. (d) Y. He, W. Zhou, G. Qian, B. Chen, *Chem. Soc. Rev.*, 2014, **43**, 5657.

[76] (a) H.-H. Wu, Q.-H. Gong, D.-H. Olson and J.-Li, *Chem. Rev.*, 2012, **112**, 836. (b) N. Nijem, H.-H. Wu, P. Canepa, A. Marti, K.-J. Balkus Jr., T. Thonhauser, J. Li and Y.-J. Chabal, *J. Am. Chem. Soc.*, 2012, **134**, 15201. (c) K.-H. Li, D.-H. Olson and J. Li, *Trends Inorg. Chem.*, 2010, **12**, 13. (d) J.-R. Li, R.-J. Kuppler, and H.-C. Zhou, *Chem. Soc. Rev.*, 2009, **38**, 5, 1477. (e) J.-R. Li, J. Sculley and H.-C. Zhou, *Chem. Rev.*, 2012, **112**, 869.

[77] S. Kitagawa, and K. Uemura, *Chem. Soc. Rev.*, 2005, **34**, 2, 109.

[78] (a) J.-A. Real, E. Andres, M.-C. Munoz, M. Julve, T. Granier, A. Bousseksou, and F. Varret, *Sci.*, 1995, **268**, 5208, 265. (b) L.-G. Beauvais, M.-P. Shores, and J.-R. Long, *J. Am. Chem. Soc.*, 2000, **122**, 12, 2763. (c) G.-J. Halder, C.-J. Kepert, B. Moubaraki, K.-S. Murray, and J.-D. Cashion, *Sci.*, 2002, **298**, 5599, 1762. (d) Z. Hu, B.-J. Deibert, J. Li, *Chem. Soc. Rev.*, 2014, **43**, 5815. (e) A. Bétard and R.-A. Fischer, *Chem. Rev.*, 2012, **112**, 1055.

[79] (a) J. Lee, O.-K. Farha, J. Roberts, K.-A. Scheidt, S.-T. Nguyen, and J.-T. Hupp, *Chem. Soc. Rev.*, 2009, **38**, 5, 1450. (b) L. Ma, C. Abney, and W. Lin, *Chem. Soc. Rev.*, 2009, **38**, 5, 1248. (c) J. Liu, L. Chen, H. Cui, J. Zhang, L. Zhang, C.-Y. Su, *Chem. Soc. Rev.*, 2014, **43**, 6011. (d) M. Yoon, R. Srirambalaji and K. Kim, *Chem. Rev.*, 2012, **112**, 1196. (e) J.-Y. Lee, O.-K. Farha, J. Roberts, K.-A. Scheidt, S.-T. Nguyen, J.-T. Hupp, *Chem. Soc. Rev.*, 2009, **38**, 1450. (f) D. Farrusseng, S. Aguado and C. Pinel, *Angew. Chem., Int. Ed.*, 2009, **48**, 7502.

[80] (a) M.-D. Allendorf, C.-A. Bauer, R.-K. Bhakta, and R.-J.-T. Houk, *Chem. Soc. Rev.*, 2009, **38**, 5,1330. (b) Y.-J. Cui, Y.-F. Yue, G.-D. Qian, B.-L. Chen, *Chem. Rev.*, 2012, **112**, 1126.

[81] (a) C. Janiak, T.-G. Scharmann, P. Albrecht, F. Marlow, and R. Macdonald, *J. Am. Chem. Soc.*, 1996, **118**, 26, 6307. (b) P. Ayyappan, G. Sirokman, O.-R. Evans, T.-H. Warren,

and W. Lin, *Inorg. Chim. Acta*, 2004, **357**, 13, 3999. (c) W.-W. Zhou, J.-T. Chen, G. Xu, M.-S. Wang, J.-P. Zou, X.-F. Long, G.-J. Wang, G.-C. Guo, and J.-S. Huang, *Chem. Commun.*, 2008, **24**, 2762. (d) C. Wang, T. Zhang and W. Lin, *Chem. Rev.*, 2012, **112**, 1084.

[82] (a) S. Horike, D. Umeyama and S. Kitagawa, *Acc. Chem. Res.*, 2013, **46**, 2376. (b) G. Givaja, P. Amo-Ochoa, C.-J. Gomez-Garcia and F. Zamora, *Chem. Soc. Rev.*, 2012, **41**, 115.

[83] (a) D.-W. Fu, W. Zhang, and R.-G. Xiong, *Dalton Trans.*, 2008, **30**, 3946. (b) M. Kurmoo, *Chem. Soc. Rev.*, 2009, **38**, 5, 1353. (c) D. Maspoch, D. Ruiz-Molina, and J. Veciana, *J. Mater. Chem.*, 2004, **14**, 18, 2713. (d) S.-R. Batten, and K.-S. Murray, *Coord. Chem. Rev.*, 2003, **246**, 1-2, 103. (e) E. Pardo, R. Ruiz-Garcia, J. Cano, X. Ottenwaelder, R. Lescouezec, Y. Journaux, F. Lloret, and M. Julve, *Dalton Trans.*, 2008, **21**, 2780. (f) M.-A.-M. Abu-Youssef, A. Escuer, F.-A. Mautner, and L. Öhrström, *Dalton Trans.*, 2008, **27**, 3553. (g) V.-H. Tran, and B. Swiatek-Tran, *Dalton Trans.*, 2008, **36**, 4860.

[84] (a) D. Fröhlich, S.-K. Henninger and C. Janiak, *Dalton Trans.*, 2014, **43**, 15300. (b) F. Jeremias, D. Fröhlich, C. Janiak and S.-K. Henninger, *New J. Chem.*, 2014, **38**, 1846. (c) F. Jeremias, D. Fröhlich, C. Janiak and S.-K. Henninger, *RSC Adv.*, 2014, **4**, 24073. (d) C. Janiak and S. K. Henninger, *Chimia*, 2013, **67**, 419. (e) M. Wickenheisser, F. Jeremias, S.-K. Henninger, C. Janiak, *Inorg. Chim. Acta*, 2013, **407**, 145. (f) F. Jeremias, V. Lozan, S.-K. Henninger and C. Janiak, *Dalton Trans.*, 2013, **42**, 15967. (g) A. Khutia, H.-U. Rammelberg, T. Schmidt, S. Henninger, and C. Janiak, *Chem. Mater.*, 2013, **25**, 790. (h) F. Jeremias, S.-K. Henninger and C. Janiak, *Chem. Commun.*, 2012, **48**, 9708. (i) S.-K. Henninger, F. Jeremias, H. Kummer, and C. Janiak, *Eur. J. Inorg. Chem.*, 2012, 2625. (j) F. Jeremias, A. Khutia, S.-K. Henninger and C. Janiak, *J. Mater. Chem.*, 2012, **22**, 10148. (k) J. Ehrenmann, S.-K. Henninger, and C. Janiak, *Eur. J. Inorg. Chem.*, 2011, 471. (l) S.-K. Henninger, H.-A. Habib, and C. Janiak, *J. Am. Chem. Soc.*, 2009, **131**, 8, 2776.

[85] R.-H. Wiley and A.-J. Hart, University of Louisville, Diformylhydrazine on Aminoheterocycles, *Org. Chem.*, 1953, **18**, 1368.

[86] H.-O. Bayer, R.-S. Cook and W.-C. von Meyer, US Patent 3, 821, 376, 1974.

[87] (a) R.-K. Bartlett and I.-R. Humphrey, *J. Chem. Soc.*, 1967, **C17**, 1664. (b) M.-C. Seidel, W.-C. von Meyer, S.-E. Greenflied, Rohm and Haas Company, US Patent 3 914 223, October 21, 1975. (c) A.-D. Naik, J. Marchand-Brynaert, and Y. Garcia, *Synthesis*, 2008, **1**, 149. (d) O.-A. Bondar, L.-V. Lukashuk, A.-B. Lysenko, H. Krautscheid, E.-B. Rusanov, A.-N. Chernega, and K.-V. Domasevitch, *CrystEngComm*, 2008, **10**, 9, 1216.

[88] D. Lässig, J. Lincke and H. Krautscheid, *Tetrahedron Letters*, 2010, **51**, 653-656.

[89] (a) H. Mayr and A.-R. Ofial. *Tetrahedron Letters*, 1997, **38**, 20, 3503. (b) O. Meth-Cohn, B. Narine and B. Tarnowski, *J. Chem. Soc., Perkin Trans I*, 1981, 1520. (c) O. Meth-Cohn, L. Platt, M. A. Kerry, G. W. Boyd and P. S.Mackay, *J. Chem. Soc., Perkin Trans I*, 1999, 315.

[90] A.-P. Railliet, D.-A. Safin, K. Robeyns and Y. Garcia, *CrystEngComm*, 2012, **14**, 4812.

[91] (a) C. Piguet, G. Bernardinelli and G. Hopfgartner, *Chem. Rev.*, 1997, **97**, 2005. (b) M. Albrecht, *Chem. Rev.*, 2001, **101**, 3457. (c) J.-S. Seo, D. Whang, H. Lee, S.-I. Jun, J. Oh, Y. J. Jeon and K. Kim, *Nature*, 2000, **404**, 982. (d) L.-J. Childs, N.-W. Alcock and M.-J. Hannon, *Angew. Chem., Int. Ed.*, 2001, **40**, 1097. (e) L.-J. Charbonniere, A.-F. Williams, C. Piguet, G. Bernardinelli and E. Rivara-Minten, *Chem.-Eur. J.*, 1998, **4**, 485. (f) R.-G. Xiong, X.-Z. You, B.-F. Abrahams, Z. Xue and C.-M. Che, *Angew. Chem., Int. Ed.*, 2001, **40**, 4422. (g) J.-Y. Sun, L.-H. Weng, Y.-M. Zhou, J.-X. Chen, Z.-X. Chen, Z.-C. Liu and D.-Y. Zhao, *Angew. Chem., int. Ed.*, 2002, **41**, 4471. (h) W.-B. Lin, *J. Solid State Chem.*, 2005, **178**, 2486.

[92] ref. for 5mt synthesis: (a) R. Shelkar, A. Singh and J. Nagarkar, *Tetrahedron Letters*, 2013, **54**, 1, 106. (b) V. Rama, K. Kanagaraj and K. Pitchumani, *J. Org. Chem.*, 2011, **76**, 21, 9090. (c) P.-Z. Demko and B.-K. Sharpless, *J. Org. Chem.*, 2001, **66**, 24, 7945. (d) Y. Qiu, H. Deng, J. Mou, S. Yang, M. Zeller, S.-R. Batten, H. Wu and J. Li, *Chem. Comm.*, 2009, **36**, 5415. (e) J. Roh, T.-V. Artamonova, K. Vavrova, G.-I. Koldobskii and A. Hrabalek, *Synthesis*, 2009, **13**, 2175. (f) X.-M. Zhang, Y.-F. Zhao, H.-S. Wu, S. R. Batten and S. W. Ng, *Dalton Trans.*, 2006, **26**, 3170. (g) A. Sinhamahapatra, A.-K. Giri, P. Pal, S.-K. Pahari, H.-C. Bajaj and A.-B. Panda, *J. Mat. Chem.*, 2012, **22**, 33, 17227. (h) A.-R. Katritzky, B.-E.-D. M. El-Gendy, B Draghici, C. D. Hall and P. J. Steel, *J. Org. Chem.*, 2010, **75**, 19, 6468. (i) B. Schmidt, D. Meid and D. Kieser, *Tetrahedron*, 2006, **63**, 2, 492. (j) W. Ogilvie and W. Rank, *Canad. J. Chem.*, 1987, **65**, 1, 166. (k) D.-P. Jiang, R.-X. Yao, F. Ji and X.-M. Zhang, *Eur. J. Inorg. Chem.*, 2013, **2013**, 4, 556. (l) Y. Qiu, Y. Li, G. Peng, J. Cai, L. Jin, L. Ma, H. Deng, M. Zeller and S.-R. Batten, *Crys. Growth Des.*, 2010, **10**, 3, 1332. (m) T. Wu, M. Chen and D. Li, *Eur. J. Inorg. Chem.*, 2006, **11**, 2132. (n) T. Wu, R. Zhou and D. Li, *Inorg. Chem. Comm.*, 2006, **9**, 3, 341. (o) X.-S. Wang, Y.-Z. Tang, X.-F. Huang, Z.-R. Qu, C.-M. Che, P.-W.-H. Chan and R.-G. Xiong, *Inorg. Chem.*, 2005, **44**, 15, 5278.

[93] ref. for H_2bdt and H_2ipdt synthesis: (a) H. Yoneyama, Y. Usami, S. Komeda and S. Harusawa, *Synthesis*, 2013, **45**, 8, 1051. (b) Y. Zhou, C. Yao, R. Ni and G. Yang, *Syn. Comm.*, 2010, **40**, 17, 2624. (c) J. He, B. Li, F. Chen, Z. Xu and G. Yin, *J. Mol. Cat. A: Chem.*, 2009, **304**, 1-2, 135. (d) M.-L. Kantam, V. Balasubrahmanyam and K.-B.-S. Kumar,

Syn. Comm., 2006, **36**, 12, 1809-1814. (e) A. Fleming, F. Kelleher, M.-F. Mahon, J. McGinley and V. Prajapati, *Tetrahedron*, 2005, **61**, 29, 7002. (f) J. Sauer, R. Huisgen and H.-J. Sturm, *Tetrahedron*, 1960, **11**, 241-51. (g) A. Maspero, S. Galli, N. Masciocchi and G. Palmisano, *Chem. Lett.*, 2008, **37**, 9, 956. (h) J.-H. Deng, X.-L. Yuan and G.-Q. Mei, *Inorg. Chem. Comm.*, 2010, **13**, 12, 1585. (i) E.-A. Popova, Y.-N. Pavlyukova, E.-V. Popov, V.-A. Ostrovskii and R.-E. Trifonov, *Russ. J. Org. Chem.*, 2009, **45**, 6, 890. (j) E.-A. Popova, A.-V. Ivanova, R.-E. Trifonov, E.-V. Popov, V.-Y. Zubarev, I.-V. Tselinskii and V.-A. Ostrovskii, *Russ. J. Org. Chem.*, 2007, **43**, 4, 591. (k) M. Koyama, N. Ohtani, F. Kai, I. Moriguchi and S. Inouye, *J. Med. Chem.*, 1987, **30**, 3, 552. (l) J. Tao, Z.-J. Ma, R.-B. Huang and L.-S. Zheng, *Inorg. Chem.*, 2004, **43**, 20, 6133. (m) K. Sumida, M. L. Foo, S. Horike and J. R. Long, *Euro. J. Inorg. Chem.*, 2010, **24**, 3739.

[94] W. G. Finnegan, R. A. Henry and R. Lofquist, *J. Am. Chem. Soc.*, 1958, **80**, 3908.

[95] (a) E.-H. Bret and A.-S. Michael, *Tetrahedron Letters*, 1993, **34**, 50, 8011. (b) P. scheiner, E. stockel, D. cruset and R. noto, *J. Org. Chem.*, 1972, **37**, 25, 4207.

[96] K.-V. Zelenin, V.-A. Khrustalev and V.-P. Sergutina, *Zh. Org. Khimii*, 1980, **16**, 276.

[97] A.-W. Addison, T.-N. Rao, J. Reedijk, J. van Rijn and G.-C. Verschoor, *J. Chem. Soc., Dalton Trans.*, 1984, 1349.

[98] V.-A. Blatov and D.-M. Proserpio, Acta Cryst., 2009, **A65**, 202. The three letter symbols, proposed by M. O'Keeffe, can be retrieved with examples and further information from the Reticular Chemistry Structure Resource database, http://rcsr.anu.edu.au/.

[99] V.-A. Blatov, M. O'Keeffe and D.-M. Proserpio, CrystEngComm, 2010, 12, 44.

[100] http://www.topos.ssu.samara.ru

[101] V.-A. Blatov, IUCr Compcomm. Newsletter 7 (2006) 4; http://www.iucr.org/iucr-top/comm/ccom/newsletters.

[102] X. López, J.-J. Carbó, C. Bo and J. M. Poblet, *Chem. Soc. Rev.*, 2012, **41**, 7537.

[103] (a) A. Spek, *Acta Crystallographica Section D*, 2009, **65**, 148. (b) A.-L. Spek, *PLATON - A multipurpose crystallographic tool*, Utrecht University: Utrecht, The Netherlands, 2005.

[104] K.-S.-W. Sing, D.-H. Everett, R.-A.-W. Haul, L. Moscou, R.-A. Pierotti, J. Rouquerol and T. Siemieniewska, *Pure Appl. Chem.*, 1985, **57**, 603.

[105] L.-J. Bellamy, *The Infrared Spectra of Comples Molecules*, Wiley, New York, 1958.

[106] C.-A. Téllez S., E. Hollauer, M.-A. Mondragon and V.-M. Castaño, *Spectrochimica Acta Part A*, 2001, **57**, 993.

[107] (a) F. Billes, H. Endredi and G. Keresztury, *J. Mol. Struc. (Theochem)*, 2000, **530**, 183. (b) D. Bougeard, N.-L. Calve, B. Saint Roch, and A. Novak, *J. Chem. Phys.*, 1976, **64**, 12.

[108] W.-Q. Kan, J. Yang, Y.-Y. Liu and J.-F. Ma, *Polyhedron*, 2011, **30**, 2113.

[109] G. Wu, X. Shi, Q. Fang, G. Tian, L. Wang, G. Zhu, A.-W. Addison, Y. Wei, S. Qiu, *Inorg. Chem. Commun.*, 2003, **6**, 4, 402.

[110] (a) H.-D. Flack, M. Sadki, A.-L. Thompson and D.-J. Watkin, *Acta Crystallogr., Sect. A*, 2011, **67**, 21. (b) H.-D. Flack and G. Bernardinelli, *Chirality*, 2008, **20**, 681. (c) H.-D. Flack and G. Bernardinelli, *Acta Crystallogr., Sect. A*, 1999, **55**, 908. (d) H.-D. Flack, *Acta Crystallogr., Sect. A*, 1983, **39**, 876.

[111] (a) C. Janiak, A.-C. Chamayou, A.-K. M.-R. Uddin, M. Uddin, K.-S. Hagen and M. Enamullah, *Dalton Trans.*, 2009, 3698. (b) M. Enamullah, A. Sharmin, M. Hasegawa, T. Hoshi, A.-C. Chamayou and C. Janiak, *Eur. J. Inorg. Chem.*, 2006, 2146.

[112] K. Nakamoto, Infrared and Raman Spectra of Inorganic and Coordination Compounds, Wiley, New York, 1970.

[113] Ümit Köc, Diplom Thesis, Heinrich-Heine Universität Düsseldorf, 2013.

[114] L.-Y. Qiao, J. Zhang, Z.-J. Li, Y.-Y. Qin, P.-X. Yin, J.-K. Cheng and Y.-G. Yao, *J. Mol. Struc.*, 2011, **994**, 1.

[115] Triazol ring: P.-M. Slangen, P.-J. van Koningsbruggen, K. Goubitz, J.-G. Haasnoot and J. Reedijk, *Inorg. Chem.*, 1994, **33**, 1121.

[116] π-π interactions: (a) B. Ma, S. Gao, T. Yi, C. Yan and G. Xu, *Inorg. Chem. Commun.*, 2000, **3**, 93. (b) R. Kiralj, B. Kojic-Prodic, I. Piantanida and M. Zinic, *Acta Crystallogr.*,1999, **B55**, 55.

[117] Mercury - Program for Crystal Structure Visualisation, Exploration and Analysis, The Cambridge Crystallographic Data Centre (CCDC), Version 3.3.1.

[118] X. López, J.-J. Carbó, C. Bo and J. M. Poblet, *Chem. Soc. Rev.*, 2012, **41**, 7537.

[119] (a) A. Spek, *Acta Crystallographica Section D*, 2009, **65**, 148. (b) A.-L. Spek, *PLATON - A multipurpose crystallographic tool*, Utrecht University: Utrecht, The Netherlands, 2005.

[120] (a) F.-J. Ma, S.-X. Liu, C.-Y. Sun, D.-D. Liang, G.-J. Ren, F. Wei, Y.-G. Chen and Z.-M. Su, *J. Am. Chem. Soc.*, 2011, **133**, 4178. (b) Y.-X. Tan, Y.-P. He and J. Zhang, *Chem. Commun.*, 2011, **47**, 10647.

[121] Y.-N. Gong, M. Meng, D.-C. Zhong, Y.-L. Huang, L. Jiang and T.-B. Lu, *Chem. Commun.*, 2012, **48**, 12002.

[122] A. Demessence, D.-M. D'Alessandro, M.-L. Foo and J.-R. Long, *J. Am. Chem. Soc.*, 2009, **131**, 8784.

[123] M. Dincă, A. Dailly, C. Tsay and J.-R. Long, *Inorg. Chem.*, 2007, **47**, 11.

[124] D. Wang, T. Zhao, G. Li, Q. Huo and Y. Liu; *Dalton Trans.*, 2014, **43**, 2365.

[125] M. Dincă, A. Dailly and J.-R. Long, *Chem. Eur. J.*, 2008, **14**, 10280.

[126] For (ClO_4^-): (a) O.-M. Yaghi, H. Li and T. L. Groy, *Inorg. Chem.*, 1997, **36**, 4292. (b) K.-S. Min and M.-P. Suh, *J. Am. Chem. Soc.*, 2000, **122**, 6834. For (BF_4^-): (a) O.-S. Jung, Y.-J. Kim, Y.-A. Lee, K.-M. Park and S.-S. Lee, *Inorg. Chem.*, 2003, **42**, 844. (b) O.-S. Jung, Y.-J. Kim, Y.-A. Lee, J.-K. Park and H.-K. Chae, *J. Am. Chem. Soc.*, 2000, **122**, 9921. (c) O.-S. Jung, Y.-J. Kim, Y.-A. Lee, H.-K. Chae and H.-G. Jang, *Inorg. Chem.*, 2001, **40**, 2105.

[127] F. Rouquerol, J. Roquerol and K. Sing, *Adsorption by Powders and Porous Solids*, Academic Press, London, 1999.

[128] J.-B. Condom, Surface Area and Porosity Determinations by Physisorption, Elsevier, Amsterdam, 2006, p. 6.

[129] E.-P. Barrett, L.-G. Joyner and P.-P. Halenda, *J. Am. Chem. Soc.*, 1951, **73**, 373.

[130] S.-J. Gregg and K.-S.-W. Sing, *Adsorption, Surface Area and Porosity*, Academic Press, London, 1982.

[131] (a) W. Clegg, R.-J. Errington, D.-C.-R. Hockless, A.-D. Glen and D.-G.-J. Richards, *Chem. Soc. Chem. Commun.*, 1990, 1565. (b) M. Du, Y.-M. Guo, S.-T. Chen and X.-H. Bu, *Inorg. Chem.*, 2004, **43**, 1287.

[132] H.-A. Habib, A. Hoffmann, H.-A. Höppe, G. Steinfeld and C. Janiak, *Inorg. Chem.*, 2009, **48**, 2166.

[133] W. Clegg, R.-J. Errington, D.-C.-R. Hockless, A.-D. Glen and D.-G.-J. Richards, *Chem. Soc. Chem. Commun.*, 1990, 1565.

[134] M. O'Keeffe, M.-A. Peskov, S.-J. Ramsden and O.-M. Yaghi, *Acc. Chem. Res.*, 2008, **41**, 1782.

[135] (a) (Fe^{2+}/Fe^{3+}) L. Xie, S. Liu, C. Gao, R. Cao, J. Cao, C. Sun and Z. Su, *Inorg. Chem.*, 2007, **46**, 7782. (b) (Cr^{3+}) L.-J. Murray, M. Dinca, J. Yano, S. Chavan, S. Bordiga, C.-M. Brown and J.-R.-J. Long, *Am. Chem. Soc.*, 2010, **132**, 7856. (c) (Ni^{2+}) P. Maniam and N. Stock, *Inorg. Chem.*, 2011, **50**, 5085. (d) (Zn^{2}+) J. Lu, R. Hajndl, S. Hariharan and M.-J. Zaworotko, *Angew. Chem.,Int. Ed.*, 2002, **41**, 2821.

[136] F.-J. Ma, S.-X. Liu, D.-D. Liang, G.-J. Ren, F. Wei, Y.-G. Chen and Z.-M. Su, *J. Solid State Chem.*, 2011, **184**, 3034.

[137] Z. Zhang, L. Zhang, L. Wojtas, M. Eddaoudi, and M.-J. Zaworotko, *J. Am. Chem. Soc.*, 2012, **134**, 928.

[138] C.-Y. Sun, S.-X. Liu, D.-D. Liang, K.-Z. Shao, Y.-H. Ren, and Z.-M. Su, *J. Am. Chem. Soc.*, 2009, **131**, 1883.

[139] L. Yang, H. Naruke and T. Yamase, *Inorg. Chem. Commun.*, 2003, **6**, 1020.

[140] H. Yang, J. Li, L. Wang, W. Dai, Y. Lv and S. Gao, *Catalysis Commun.*, 2013, **35**, 101.

[141] R.-W. Larsen, J. Miksovska, R.-L. Musselman, and L. Wojtas, *J. Phys. Chem. A.*, 2011, **115**, 11519.

[142] (a) B.-L. Chen, M. Eddaoudi, S.-T. Hyde, M. O'Keeffe and O.-M. Yaghi, *Science*, 2001, **291**, 5506, 1021. (b) M. Eddaoudi, J. Kim, M. O'Keeffe and O.-M. Yaghi, *J. Am. Chem. Soc.*, 2002, **124**, 376. (c) M. Eddaoudi, J. Kim, D. Vodak, A. Sudik, J. Wachter, M. O'Keeffe and O.-M. Yaghi, *Proc. Natl. Acad. Sci.*, U.S.A., 2002, **99**, 4900. (d) D.-N. Dybtsev, H. Chun and K. Kim, *Angew. Chem., Int. Ed.*, 2004, **43**, 5033. (e) Z.-Q. Wang, V.-C. Kravtsov and M.-J. Zaworotko, *Angew. Chem., Int. Ed.*, 2005, **44**, 2877.

[143] B.-L. Chen, N.-W. Ockwig, A.-R. Millward, D.-S. Contreras, O.-M. Yaghi, *Angew. Chem., Int. Ed.*, 2005, **44**, 30, 4745.

[144] (a) (Me, Et-) Y. Cai, Y. Zhang, Y. Huang, S.-R. Marder and K.-S. Walton, *Cryst. Growth Des.*, 2012, **12**, 7, 3709. (b) (NH_2-btc) K. Peikert, F. Hoffmann and M. Fröba, *Chem. Commun.*, 2012, **48**, 11196.

[145] (a) J.-M.-S. Skakle, M.-R. St J.Foreman, M.-J. Plater and C. Griffin, *Acta Cryst.*, 2001, **E57**, m85. (b) W. Zheng, X. Liu, J. Guo, L. Wu and D. Liao, *Inorg. Chim. Acta*, 2004, **357**, 1571. (c) R. Köferstein and C. Robl, *Z. Anorg. Allg. Chem.*, 2005, **631**, 1035.

[146] For IR-Spectra: Z. Shi, G. Li, L. Wang, L. Gao, X. Chen, J. Hua and S. Feng, *Cryst. Growth Des.*, 2004, **4**, 25.

[147] D. Cheng, M.-A. Khan, and R.-P. Houser, Cryst. Growth Des., 2004, 4, 3, 599.

[148] J.-C. Dai, X.-T. Wu, Z.-Y. Fu, C. Pcui, S.-M. Hu, W.-X. Du, L.-M. Wu, H.-H. Zhang, R.-Q. Sun, *Inorg. Chem.*, 2002, **41**, 1391.

[149] C.-D. Wu, C.-Z. Lu, W.-B. Yang, H.-H. Zhuang and J.-S. Huang, Inorg. Chem., 2002, 41, 12, 3302.

[150] (a) M. Colapietro, A. Domenicano, C. Marciante, G. Portalone, *Acta Crystallogr.,Sect.A: Found Crystallogr.*, 1984, **40**, 98. (b) A. Domenicano, G. Schultz, I. Hargittai, M. Colapietro, G. Portalone, P. George, C.-W. Bock, *Struct.Chem.*, 1990, **1**, 107. (c) R.-A. Zehnder, M. Zeller, B. Mouawad, D. Bonette, K. Olney, *Private Communication*, 2012.

[151] P. Fischer, P. Zolliker, B.-H. Meier, R.-R. Ernst, A.-W. Hewat, J.-D. Jorgensen, F.-J. Rotella; *J.Solid State Chem.*, 1986, **61**, 109.

[152] J.-L. Derissen, *Acta Crystallogr.,Sect.B:Struct.Crystallogr.Cryst.Chem.,* 1974, **30**, 2764. R. Alcala, S.-M. Carrera; *Acta Crystallogr.,Sect.B:Struct.Crystallogr.Cryst.Chem.,* 1972, **28**, 1671.

[153] Y.-B. Yao, T. Xie and Y.-M. Gao, *Handbook of Physical Chemistry*, Shanghai Science and Technology Publication of China, Shanghai, 1985.

[154] A.-L. Spek, *J. Appl. Cryst.*, 2003, **36**, 7.

[155] APEXII: Data collection program for the APEXII CCD area-detector system, Bruker Analytical Xray Systems, Madison, Wisconsin, USA 2010.

[156] SMART: Data Collection Program for the CCD Area-Detector System; SAINT: Data Reduction and Frame Integration Program for the CCD Area-Detector System. Bruker Analytical X-ray Systems, Madison, Wisconsin, USA, 1997.

[157] G. M. Sheldrick, Program SADABS: Area-detector absorption correction, University of Göttingen, Germany, 1996.

[158] G. M. Sheldrick, SHELXS-97, SHELXL-97, software for Crystal Structure Analysis, University of Göttingen, Germany, 1997.

[159] G. M. Sheldrick, SHELXL-97-Program for the refinement of crystal structur from diffraction data, university of Göttingen, Germany 1997.

[160] Diamond (Version 3.2k) for Windows, Crystal and Molecular Structure Visualization, Crystal Impact-K. Brandenburg and H. Putz GBr, Bonn, Germany 2009.

[161] STOE WinXPOW Version 1.10; STOE and Cie GmbH, Darmstadt, Germany, 2002.

[162] (a) Jana K. Maclaren, PhD Thesis, Albert-Ludwigs-Universität Freiburg im Breisgau, 2012. (b) Anne-Christine Chamayou, PhD Thesis, Albert-Ludwigs-Universität Freiburg im Breisgau, 2010. (c) Anas Tahli, Master Thesis, Albert-Ludwigs-Universität Freiburg im Breisgau, 2010. (d) Hesham Mena, PhD Thesis, Albert-Ludwigs-Universität Freiburg im Breisgau, 2008. (e) Barbara Wisser, PhD Thesis, Albert-Ludwigs-Universität Freiburg im Breisgau, 2007.